Analysis of Lubricant Film Thickness and Distribution along the Piston/Ring/Liner Interface in a Reciprocating Engine

by

Steven M. Casey

B.S., Mechanical Engineering
University of Illinois at Urbana-Champaign, 1995

Submitted to the Department of Mechanical Engineering
in Partial Fulfillment of the Requirements for the Degree of
Master of Science in Mechanical Engineering
at the

MASSACHUSETTS INSTITUTE OF TECHNOLOGY

February 1998

Signature of Author: _____
Department of Mechanical Engineering
December 16, 1997

Certified by: _____
Victor W. Wong
Lecturer, Department of Mechanical Engineering
Thesis Supervisor

Certified by: _____
Douglas P. Hart
Assistant Professor, Department of Mechanical Engineering
Thesis Supervisor

Certified by: _____
Ain A. Sonin
Professor, Department of Mechanical Engineering
Chairman, Committee for Graduate Students

(This page is intentionally left blank.)

Analysis of Lubricant Film Thickness and Distribution along the Piston/Ring/Liner Interface in a Reciprocating Engine

by

Steven M. Casey

Submitted to the Department of Mechanical Engineering
on December 16, 1997 in Partial Fulfillment of the Requirements for the
Degree of Master of Science in Mechanical Engineering

ABSTRACT

Acquired from a mono-cylinder, gasoline engine using Laser-Induced Fluorescence (LIF), lubricant film thickness and distribution data were analyzed along the piston/ring/liner interface. The magnitudes and trends are shown and interpreted for five selected lubricants tested at different engine operating conditions including liner temperatures, speeds, and firing and motoring operation. Effects along a stroke and azimuthally around midstroke were also captured by the four operable LIF windows within the liner. For model validation and assistance in interpretation, *FRICTION-OFT* and *RINGPACK-OC* models were applied where appropriate.

Oil film thickness (OFT) under the rings reveals only stroke-by-stroke differences for the oil-control (OC) ring. Along the free liner, only small stroke differences on the major-thrust side are observed and primarily caused by piston tilt effects on the scraper ring's relative profile. For the fired cases, OFT magnitudes and trends depend predominantly upon lubricant viscosity and agree both with approximate analytic scaling and more exact numerical predictions from the *FRICTION-OFT* model. Strong and weak exceptions include SAE-50 and SAE-10W/50n, respectively, whose OFTs start to decrease in the neighborhood of 30 cSt. (Although less clear and for more lubricants, motored data reveals this reversed OFT-viscosity trend starting around 30 cSt as well.) Speed effects from engine speeds from 1800 to 2500 rpm and instantaneous piston speeds along a stroke on the major-thrust side are characteristic of hydrodynamic lubrication where measured OFT increases with sliding speed comparable to analytical scaling with the square root of speed and more exact numerical calculations. For the multigrades, shear thinning is directly observed, and OFTs even near BC at window 6 are only dependent upon the high-shear viscosity (and insensitive to low-shear viscosity). Proper ring conforming to bore distortion is observed from azimuthal measurements.

Although oil distributions show no clear trends with lubricant viscosity within the ring pack, lubricant behavior along the piston skirt indicates significant thrust-side oil transport. Oil distributions increase with speed along all regions but only within the ring pack for load changes from firing to motoring. Results from speed and load effects as well as pattern similarity among the first three lands support first and second ring gap-and-groove oil transport between the regions. Oil dragging from gas flows, oil displacement from inertial effects, oil squeezing between rings and grooves, and ring scraping are also shown to affect the amount and spatial distributions of oil within regions.

Thesis Supervisors:

Victor W. Wong
Lecturer, Department of Mechanical Engineering

Douglas P. Hart
Assistant Professor, Department of Mechanical Engineering

(This page is intentionally left blank.)

ACKNOWLEDGMENTS

This thesis would have not been completed without the support of some very important people who I would like to thank and acknowledge. Dr. Victor Wong, who employed me as a research assistant in the Lubrication Consortium, provided helpful advice regarding technical issues and especially oral and written communication. Through our relationship, I have become a better leader and manager for future technical projects. Professor Douglas Hart, who is my other advisor and first introduced me to the Lubrication Consortium, provided specific technical guidance on certain experimental issues and looked out for my interests as a student here at MIT. To Doug and Dr. Wong, thank you.

In addition to their sponsorship, industrial participants of the Lubrication Consortium provided insightful feedback and input during my research. Consortium members include Dana Corporation, MAHLE GmbH, Peugeot, Renault, Shell Oil Company, and Volvo. Discussions with Dr. Richard Tucker from Shell Oil Company concerning lubricant behavior were valuable. In addition to giving important engineering advice, Remi Rabute from Dana Corporation provided detailed measurements of the new and worn ring geometries.

Fortunately, I have been able to work with some wonderful people who are very talented and have made my stay at MIT an enjoyable experience. A gifted engineer, Tian Tian taught me how to properly apply mathematical models and provided important insights to the experimental data. In addition to Tian, I would like to thank Bertrand Lecointe, Benoist Thirouard, and Bouke Noordzij for their friendship and good times as office mates. Goro Tamai answered my many detailed questions and provided valuable input concerning the experimental data and its acquisition. I would also like to thank Carlos Herrera, Peter Menard, Brian Corkum, and Mark Kiesel for their comradeship in and outside the lab and Norm Peralta whose positive and passionate attitude seemed to rub off on everyone. Additionally, the friendships with my buddies at the apartment including Michael Shelby, Brad VanDerWege, and Mark Dawson were encouraging and supportive.

I would like to thank the following list of fellow graduate students, undergraduate students, and visiting scholars in the Sloan Automotive Laboratory: Ertan Yilmaz, Jose Sanchez-Martinez, Kuo-Chun Wu, Helen Liu, Michaela Wiegel, David Kayes, Denis Artzner, Issam Lakkis, Robert Meyer, Chris O'Brien, Alan Shihadeh, Pierre Mulgrave, Wolf Bauer, Jon Fox, Peter Hinze, Younggy Shin, and John Rae. Additionally, I would like to thank Nancy Cook for all her help and pleasantness.

Finally, the wise advice and love from my parents back in Illinois cannot be understated. Their commitment to integrity and high standards have taught me many important lessons which have helped me become successful.

Steve Casey
November 1997

(This page is intentionally left blank.)

TABLE OF CONTENTS

Abstract 3
Acknowledgments 5
Table of Contents 7
List of Figures 11
List of Tables 16

Chapter 1 INTRODUCTION 17
1.1 Background 17
1.2 Previous Work 19
1.3 Project Objectives 21
1.3.1 Oil Film Thickness (OFT) under Rings and along Free Liner 21
1.3.2 Oil Distribution Along the PRL Regions within Ring Pack and along the Piston Skirt 22
1.3.3 Comprehensive Compilation of Accurate OFT Data 22

Chapter 2 TEST LUBRICANTS 24
2.1 Temperature Dependence of Viscosity 24
2.2 Shear Dependence of Viscosity 26
2.3 Oil Degradation 31

Chapter 3 ENGINE AND TEST MATRIX 32
3.1 Test Engine and Windows 32
3.2 Operating Conditions and Test Matrix 34

Chapter 4 OIL FILM THICKNESS (OFT) ALONG FREE LINER AND UNDER THE RING 35
4.1 Data Reduction for Ring Fitting and Free-Liner OFT 36
4.2 Baseline Results 41
4.2.1 Analysis of Film Thickness under Different Rings and Along the Free Liner 48
4.2.2 The Lubricant Effect 50
4.2.3 Stroke-by-Stroke Differences 55
4.2.3.1 The OC Ring -- the Upper and Lower OC Segments 56
4.2.3.2 The Top and Scraper Rings 62
4.2.3.3 The Free Liner 63
4.2.3.3.1 Piston Tilt Effects 63
4.2.3.3.2 Land Pressure and Twist Effects 72
4.2.3.4 Stroke-By-Stroke Summary 77
4.3 Results off Baseline -- Effects of Lubricants, Liner Temperature, and Load 78
4.3.1 Fired Cases for Different Lubricants at Moderate Liner Temperatures -- 60, 80, and 100°C 79
4.3.1.1 Lubricant Effect 79
4.3.1.1.1 1800 rpm 80
4.3.1.1.2 2500 rpm 81

4.3.1.2 Cylinder Liner Temperature Effect at 2500 rpm 85
4.3.1.3 Fired Viscosity Effect -- Combined Lubricant and Temperature Effects 92
4.3.2 Motored Cases for Different Lubricants at Low Liner Motored Temperatures -- 40 and 60°C at 2500 rpm 96
4.3.2.1 Lubricant Effect 96
4.3.2.2 Liner Temperature Effect 99
4.3.2.3 Motored Viscosity Effect -- Combined Lubricant and Temperature Effects 102
4.4 Speed Effects 104
4.4.1 Engine Speeds at 1800 and 2500 rpm 104
4.4.2 Instantaneous Piston Speed Along a Stroke 111
4.5 Shear Thinning and Thickening of Multigrade Lubricants 117
4.6 Azimuthal Effects at Midstroke from Bore Distortion 119
4.7 OFT Summary 126
4.7.1 Experimental Findings 126
4.7.2 Extent of Agreement between OFT Measurements and Predictions from the *FRICTION-OFT* Model 129

Chapter 5 OIL DISTRIBUTION WITHIN THE RING PACK AND ALONG THE PISTON SKIRT 135
5.1 A Detailed Oil Distribution Summary 136
5.1.1 Experimental Findings 137
5.1.2 Model Verification of Ring Boundary Conditions and Predicted Scraper Down-Scraping from the *FRICTION-OFT* Model and Predicted Top Ring Lift from the *RINGPACK-OC* Model 149
5.2 Data Reduction Along Different Regions of the Piston Assembly for Different Azimuthal and Axial Window Locations 150
5.3 Baseline Results 155
5.3.1 The Lubricant Effect 167
5.3.2 Stroke-by-Stroke Differences 178
5.3.2.1 Within the Ring Pack 178
5.3.2.1.1 Crown and Second Land Regions -- ARTs and Oil Squeezing in Grooves 180
5.3.2.1.2 Third Land Region 186
5.3.2.1.3 Region Between the Upper and Lower OC Rails 187
5.3.2.2 Below the OC Ring Including Oil Transport along the Skirt on the Major-Thrust Side 189
5.3.2.2.1 Major-Thrust Side -- Midstroke and Near Bottom Center (Windows 1 and 6) 190
5.3.2.2.2 Off the Major-Thrust Side at Midstroke (Windows 2 and 4) 199
5.4 Results of Parametric Studies -- Effects of Lubricants, Liner Temperature, and Load 199
5.4.1 Fired Cases for Different Lubricants at Moderate Liner Temperatures -- 60, 80, and 100°C 201
5.4.1.1 Lubricant Effect 201
5.4.1.1.1 1800 rpm 201

5.4.1.1.2 2500 rpm
5.4.1.2 Cylinder Liner Temperature Effect at 2500 rpm
5.4.2 Motored Cases for Different Lubricants at Low Liner Temperatures -- 40 and 60°C at 2500 rpm
5.4.2.1 Lubricant Effect
5.4.2.2 Liner Temperature Effect
5.4.3 Load Effects -- 2/3 Load versus Motored WOT at 60°C
5.5 Engine Speed Effects -- 1800 Versus 2500 rpm
5.6 Azimuthal Effects around Midstroke
5.7 Direct Observation of Oil Transport Mechanisms
5.7.1 Oil Squeezing between Top Ring and Groove
5.7.2 Down-Scraping of Scraper Ring along a Stroke
5.7.3 Lubricant Dragging from Gas Flow
5.7.4 Inertial Forces and Viscosity Restriction on Oil Flow
5.7.5 Oil Behavior along the Piston Skirt -- Thrust-Side Oil Transport

Chapter 6: CONCLUSIONS AND RECOMMENDATIONS

References

APPENDICES

Appendix A OVERVIEW OF PISTON-RING-LINER (PRL) SYSTEM AND GOVERNING MOTIONS OF LUBRICANT BEHAVIOR
A.1 Lubrication between Rings and Liner
A.2 Ring Axial and Angular Dynamics, Gas-Flow Oil Dragging, and Inertia of Oil Masses
A.3 Piston Secondary Motion

Appendix B EXPERIMENTAL APPARATUS
B.1 The Modified Engine
B.1.1 Window Location and Installation Procedure
B.1.2 Retrofitted Water Jacket
B.1.3 Thermocouples
B.1.4 Cylinder Pressure Transducer
B.1.5 Shaft Encoder
B.2 One-Dimensional (1-D) LIF Diagnostic System
B.2.1 Precision and Accuracy
B.2.2 Viscosity and Temperature Effects on Fluorescent Efficiency
B.3 The Data Acquisition System

Appendix C MEASUREMENTS OF ENGINE COMPONENTS
C.1 The Piston -- Macro-Geometry
C.2 Micro-Measurements -- The Bore and PRL System
C.2.1 The Rings
C.2.2 The Piston
C.2.2.1 Land Machining Mark Profiles on Major-Thrust Side
C.2.2.2 Upper Piston Machining Mark Profiles on Major-Thrust Side

C.2.3 Bore and Window-to-Liner Flushness 312
C.2.3.1 Bore Distortion 312
C.2.3.2 Window-to-Liner Flushness 313

Appendix D DATA PROCESSING 317
D.1 Engine Kinematics and Dynamics 318
D.2 Calibration 323
D.2.1 Method of Calibration 323
D.2.2 Calibration Coefficients for Cases Within Test Matrix 326
D.3 Piston Temperature Effects on Fluorescent Efficiency and Measured Oil 329

Appendix E NUMERICAL MODELS USED FOR DATA ANALYSIS AND INTERPRETATION 331
E.2 *FRICTION-OFT* 331
E.3 *RINGPACK-OC* 333

Appendix F: STANDARD DEVIATION AND UNCERTAINTY FORMULAS 334

Appendix G: ANALYTICAL ARGUMENT FOR MEASURED OFT HIERARCHY WITHIN ANY LUBRICANT CASE AND CRITERIA FOR LOCALLY FULLY-DEVELOPED FLOW, NEGLIGIBLE ENTRANCE LENGTH AND SQUEEZING, AND MOFT DEPENDENCE ON VISCOSITY AND SPEED FOR MIDSTROKE AND NEAR-BC LOCATIONS WITHIN THE KOHLER ENGINE 335

Appendix H: OFT-VISCOSITY EFFECT AT WINDOW 4 FOR THE FIRED CASES 343

Appendix I: ENGINE SPEED EFFECTS FOR CASES WITH LOW CALIBRATION ACCURACIES AT MIDSTROKE AND NEAR-BC 344

Appendix J: REFUTED ARGUMENTS FOR FREE-LINER STROKE-BY-STROKE TRENDS 349

Appendix K: STROKE-BY-STROKE DIFFERENCES IN OIL DISTRIBUTION BELOW THE OC RING OFF THE MAJOR-THRUST SIDE AT MIDSTROKE (WINDOWS 2 AND 4) 351

LIST OF FIGURES

Figure 2-1 Viscosity Versus Temperature for Four Selected Lubricants 25
Figure 2-2 Kinematic Viscosity Versus Average Shear Rate for SAE-10W/50n and -10W/50k from the Cross Equation 28
Figure 2-3 OFT Insensitivity to Low-Shear Viscosity of SAE-10W/50n. (a) Viscosity Versus Shear (b) Predicted OFT Insensitivity for Free Liner and Top Ring at Midstroke 30
Figure 3-1 LIF Probe/Window Locations and Number Convention of Kohler Engine 33
Figure 3-2 Test Matrix for Kohler Engine with Four Operable LIF Windows 34
Figure 4-1 Ring Fitting and Free-Liner OFT for Intake Stroke at Window 4. (a) Actual Ring and Segment Geometries Fit Within an OFT Trace (b) Free-Liner OFT and Ring MOFTs 37
Figure 4-2 Covariance Correlation: Standard Deviation Versus MOFT from Window 1 from Two Independent Studies (a) Lubricant Set One (the current test set) (b) Lubricant Set Two 40
Figure 4-3 Stroke-Averaged OFT for the Five Lubricants at the Baseline Condition from Windows (a) 1, (b) 2, (c) 4, and (d) 6 43
Figure 4-4 Intake Stroke OFT for the Five Lubricants at the Baseline Condition from Windows (a) 1, (b) 2, (c) 4, and (d) 6 44
Figure 4-5 Compression Stroke OFT for the Five Lubricants at the Baseline Condition from Windows (a) 1, (b) 2, (c) 4, and (d) 6 45
Figure 4-6 Expansion Stroke OFT for the Five Lubricants at the Baseline Condition from Windows (a) 1, (b) 2, (c) 4, and (d) 6 46
Figure 4-7 Exhaust Stroke OFT for the Five Lubricants at the Baseline Condition from Windows (a) 1, (b) 2, (c) 4, and (d) 6 47
Figure 4-3 Baseline OFT Measurements and Model Predictions from Windows (a) 1, (b) 2, (c) 4, and (d) 6 54
Figure 4-9 Stroke MOFTs at Baseline from Window 1 for (a) Upper OC Segment and (b) Lower OC Segment 57
Figure 4-10 Midstroke Window Locations: Stroke-Averaged Upstroke Versus Downstroke MOFTs of the Lower OC Rail at 1800 and 2500 rpm for (a) SAE -10W, (b) -10W/50n, (c) -50, and (d) -10W/50k 58
Figure 4-11 Window 6: Stroke-Averaged Upstroke Versus Downstroke MOFTs of the Lower OC Rail at 1800 and 2500 rpm for (a) SAE-10W, (b) -10W/50n, (c) -50, and (d) - 10W/50k 61
Figure 4-12 Stroke MOFTs at Baseline from Window 1 for (a) Top Ring and (b) Scraper Ring 63
Figure 4-13 Stroke Free-Liner OFT for the Baseline Condition at Window 1 for Highly Accurate Cases 64
Figure 4-14 Percent Increase in Free-Liner OFT from First Two to Last Two Strokes at Midstroke at Major-Thrust Side for Liner Temperatures of (a) 100, (b) 80, and (c) 60°C Measurements Off the Major-Thrust side at 100°C for windows (d) 2 and (e) 4 66
Figure 4-15 Piston, Ring, and Groove Interaction. (a) Effect of Piston Tilt on Scraper Ring Face Relative to Liner. (b) Possible Ring Tilt Relative to Groove 68
Figure 4-16 Percent Increase in Free-Liner OFT from First Two to Last Two Strokes from (a) Experiments and (b) Model Predictions for Five Lubricants at Major-Thrust Side 71
Figure 4-17 Ring Position with Exaggerated Twist at Midstroke Position During the Expansion Stroke -- 74° ATC (a) Axial Forces from Ring-Liner Friction, Land Pressures, and Inertia. (b) Radial Forces from Lubricant, Ring Tension, and Land and Groove Pressures 74
Figure 4-18 *RINGPACK-OC* Results for (a) Land Pressure Predictions and (b) Top and Scraper Ring Relative Lift within Their Grooves for 2/3 load, 2500 rpm, and 100°C Liner Midstroke Temperature 75
Figure 4-19 CA-Resolved Predicted MOFTs from *FRICTION-OFT* Model for Top, Scraper, and OC Ring 77
Figure 4-20 OFT Measurements and Model predictions for Lubricant Effect from Window 1 81

Figure 4-21 Free-Liner OFT and Ring MOFTs for the Lubricant Effect of SAE-10W, -10W/50n, -30, and -50 for the (a) Downstrokes of the Lower OC Segment, (b) Upstrokes of the Lower OC Segment, (c) Upper OC Segment, (d) Scraper Ring, (e) Top Ring, and (f) Free Liner 84
Figure 4-22 Free-Liner OFT and Ring MOFTs at Different Liner Temperatures at Window 1 for (a) SAE-10W, (b) -10W/50n, and (c) -50 87
Figure 4-23 Free-Liner OFT and Ring MOFTs for the Temperature Effect of SAE-10W, -10W/50n, and -50 for the (a) Downstrokes of the Lower OC Segment, (b) Upstrokes of the Lower OC Segment, (c) Upper OC Segment, (d) Scraper Ring, (e) Top Ring, and (f) Free Liner 91
Figure 4-24 Free-Liner OFT and Ring MOFTs for the Viscosity Effect of SAE-10W, -10W/50n, -30, and -50 for Liner Temperatures of 100, 80, and 60°C from (a) Window 1, (b) Window 2, and (c) Window 6 95
Figure 4-25 Free-Liner OFT and Ring MOFTs for the Motored Lubricant Effect for all Five Lubricants at 40 and 60°C for (a) Downstrokes of the Lower OC Segment, (b) Upstrokes of the Lower OC Segment, (c) Upper OC Segment, (d) Scraper Ring, (e) Top Ring, and (f) Liner 99
Figure 4-26 Free-Liner OFT and Ring MOFTs for the Lubricant Effect of SAE-10W, -10W/50n, -30, and -50 for (a) Downstrokes of the Lower OC Segment, (b) Upstrokes of the Lower OC Segment, (c) Upper OC Segment, (d) Scraper Ring, (e) Top Ring, and (f) Free Liner 102
Figure 4-27 Free-Liner OFT and Ring MOFTs for the Viscosity for the Five Lubricants for Liner Temperatures of 40 and 60°C 103
Figure 4-28 Engine Speed Effect from 1800 to 2500 rpm Measured from Window 1 for (a) SAE-10W, (b) -10W/50n, and (c) -50 106
Figure 4-29 Engine Speed Effect (1800 Vs. 2500 rpm) Measured from Window 6 for SAE-10W/50n 108
Figure 4-30 Instantaneous Speed Effect along a Stroke from Window 1 to Window for (a) SAE-10W, (b) -10W/50n, and (c) -50 114
Figure 4-31 Instantaneous Speed Effect along a Stroke from Window 1 to 6 for (a) SAE-10W (80°C, 2500 rpm), (b) -10W (60°C, 2500 rpm), and (c) -10W/50n 116
Figure 4-32 Top Ring MOFT for SAE-10W, -10W/50n, and -50 at Midstroke for (a) 1800 and (b) 2500 rpm 118
Figure 4-33 Top Ring MOFT for SAE-10W, -10W/50n, and -50 from Midstroke to near BC 119
Figure 4-34 Azimuthal OFT Measurements at Windows 1, 2, and 4 for Selected Lubricants and Operating Conditions for (a) Free Liner, (b) Top Ring, (c) Scraper Ring, (d) Upper OC Segment, (e) Lower OC Segment, Upstrokes, and (f) Lower OC Segment, Downstrokes 122
Figure 4-35 Bore Distortion with Non-Conformed Ring 124
Figure 4-36 Possible Local Ring Pressure Load on Lubricant Film 125
Figure 5-1 Region Assignments for the Free Liner and Ring Pack 151
Figure 5-2 Region Assignments below the OC Ring for the Azimuthal Locations at (a) Windows 1, (b) 4 (and 2), and the Near-BC Location at (c) Window 6 154
Figure 5-3 Baseline Average Region Thicknesses (Stroke-Averaged) for Regions 3 - 8 from Windows (a) 1, (b) 2, (c) 4, and (d) 6 157
Figure 5-4 Baseline Average Region Thicknesses (Stroke-Averaged) for Free Liner and First and Second Land Regions from Windows (a) 1, (b) 2, (c) 4, and (d) 6 158
Figure 5-5 Baseline Average Region Thicknesses for the Intake Stroke for Regions 3 - 8 from Windows (a) 1, (b) 2, (c) 4, and (d) 6 159
Figure 5-6 Baseline Average Region Thicknesses for the Intake Stroke for Free Liner and First and Second Land Regions from Windows (a) 1, (b) 2, (c) 4, and (d) 6 160
Figure 5-7 Baseline Average Region Thicknesses for the Compression Stroke for Regions 3 - 8] from Windows (a) 1, (b) 2, (c) 4, and (d) 6 161
Figure 5-8 Baseline Average Region Thicknesses for the Compression Stroke for Free Liner and

First and Second Land Regions from Windows (a) 1, (b) 2, (c) 4, and (d) 6 162
Figure 5-9 Baseline Average Region Thicknesses for the Expansion Stroke for Regions 3 - 8 from Windows (a) 1, (b) 2, (c) 4, and (d) 6 163
Figure 5-10 Baseline Average Region Thicknesses for the Expansion Stroke for Free Liner and First and Second Land Regions from Windows (a) 1, (b) 2, (c) 4, and (d) 6 164
Figure 5-11 Baseline Average Region Thicknesses for the Exhaust Stroke for Regions 3 - 8 from Windows (a) 1, (b) 2, (c) 4, and (d) 6 165
Figure 5-12 Baseline Average Region Thicknesses for the Exhaust Stroke for Free Liner and First and Second Land Regions Windows (a) 1, (b) 2, (c) 4, and (d) 6 166
Figure 5-13 Baseline Average Region Thicknesses (Stroke-Averaged) from Window 1 for Regions (a) 1, (b) 2, (c) 3, (d) 4, (e) 5, (f) 6, and (g) 7 170
Figure 5-14 Baseline Average Region Thicknesses (Stroke-Avg) from Window 4 for Regions 1 - 7 171
Figure 5-15 Baseline Average Region Thicknesses (Stroke-Averaged) from Window 6 for Regions (a) 2, (b) 3, (c) 4, (d) 5, (e) 6, (f) 7, and (g) 8 174
Figure 5-16 Stroke-By-Stroke, Average Region Thicknesses from the Ring Pack for the (a) Crown Land Region, (b) Second Land Region, (c) Third Land Region, and (d) Region between the Upper and Lower OC Rails 180
Figure 5-17 Oil Distribution Along Second Land Region During the Expansion Stroke for (a) SAE-50 and (b) -10W 181
Figure 5-18 Stroke-by-Stroke Top Ring Squeezing at Midstroke for (a) Bottom and (b) Top Channel Squeezing and near BC for (c) Bottom Channel Squeezing 183
Figure 5-19 Schematic of Oil Squeezing within Channels during an Latter Half of an (a) Expansion Stroke and (b) Intake Stroke 184
Figure 5-20 Top Ring Position within Its Groove at (a) Midstroke Windows, from (b) Predicted Top and Scraper Ring Lift from *RINGPACK-OC*, and at (c) Near-BC Window 6 185
Figure 5-21 Stroke-By-Stroke, Average Region Thicknesses for Region 4 from (a) Window 2 and (b) Window 4 188
Figure 5-22 Motored Stroke-By-Stroke, Average Region Thicknesses for Region 4 from Window 1 189
Figure 5-23 Oil Distribution along the Skirt as the Piston Translates throughout a Cycle for (a) Intake Stroke at midstroke, (b) Intake Stroke near BC, (c) Compression Stroke near BC, (d) Compression and Expansion Stroke at Midstroke, (e) Expansion Stroke near BC, (f) Exhaust Stroke near BC, and (g) Exhaust and Intake Strokes at Midstroke 193
Figure 5-24 Volumetric Oil Transport along Piston Skirt as Piston Reciprocates through TC from Compression to Expansion and Exhaust to Intake strokes 196
Figure 5-25 ARTs for Regions below the OC Ring on the Major-Thrust Side for (a) Groove and Chamfer Region -- Region 5, (b) Upper Piston Skirt Region -- Region 6, and (c) Lower Piston Skirt Region -- Region 7 198
Figure 5-26 ARTs along the Upper Piston Skirt Region -- Region 6 -- from Window 6 199
Figure 5-27 Average Region Thicknesses (Stroke-Averaged) at 1800 rpm from Window 1 for Regions (a) 1, (b) 2, (c) 3, (d) 4, (e) 5, (f) 6, and (g) 7 204
Figure 5-28 Average Region Thicknesses (Stroke-Averaged) at Moderate Temperatures of 60, 80, and 100°C from Window 1 for Regions (a) 1, (b) 2, (c) 3, (d) 4, (e) 5, (f) 6, and (g) 7 207
Figure 5-29 ARTs (Stroke-Averaged) for the Temperature Effect (Fired) at Moderate Temperatures of 60, 80, and 100°C from Window 1 for Regions (a) 1, (b) 2, (c) 3, (d) 4, (e) 5, (f) 6, and (g) 7 211
Figure 5-30 ARTs (Stroke-Averaged) for the Temperature Effect (Fired) at Moderate Temperatures of 60, 80, and 100°C from Window 6 for Regions (a) 2, (b) 3, (c) 4, (d) 5, (e) 6, (f) 7, and (g) 8 216
Figure 5-31 Average Region Thicknesses (Stroke-Averaged) for the Lubricant Effect (Motored) at Low Temperatures of 40 and 60°C from Window 1 for Regions (a) 1, (b) 2, (c) 3, (d) 4, (e) 5, (f) 6, and (g) 7 220
Figure 5-32 ARTs (Stroke-Averaged) for the Temperature Effect (Motored) at Low Temperatures

of 40 and 60°C from Window 1 for Regions (a) 1, (b) 2, (c) 3, (d) 4, (e) 5, (f) 6, and (g) 7 225
Figure 5-33 ARTs (Stroke-Averaged) for the Load Effect (Fired Versus Motored) from Window 1 for Regions (a) 1, (b) 2, (c) 3, (d) 4, (e) 5, (f) 6, and (g) 7 228
Figure 5-34 Ring-Pack Oil Distribution for SAE-10W for the Load Effect (Fired Versus Motored) for the (a) Intake and Compression Strokes and (b) Expansion and Exhaust Strokes 229
Figure 5-35 Ring-Pack Oil Distribution for SAE-10W/50n for the Load Effect (Fired Versus Motored) for the (a) Intake and Compression Strokes and (b) Expansion and Exhaust Strokes 230
Figure 5-36 Ring-Pack Oil Distribution for SAE-50 for the Load Effect (Fired Versus Motored) for the (a) Intake and Compression Strokes and (b) Expansion and Exhaust Strokes 231
Figure 5-37 Motored (WOT) *RINGPACK-OC* Results for (a) Land Pressure Predictions and (b) Top and Scraper Ring Relative Lift within Their Grooves 234
Figure 5-38 Predicted Mass Flow Rates through Channels between Rings and Grooves During a Cycle for Fired and Motored Conditions from (a) Crown Land to Region Behind Top Ring, (b) Region Behind Top Ring to Second Land, c) Second Land to Region Behind Second Ring, and (d) Region Behind Second Ring to Third Land 236
Figure 5-39 Predicted Gap Mass Flow Rates During a Cycle for Fired and Motored Conditions for the (a) Top and (b) Second Rings 236
Figure 5-40 Engine Speed Effect (1800 Versus 2500 rpm) at Midstroke on Major-Thrust Side (Window 1) for (a) SAE-10W, (b) -10W/50n, and (c) -50 241
Figure 5-41 Engine Speed Effect (1800 Versus 2500 rpm) near BC on Major-Thrust Side (Window 6) for SAE-10W/50n 242
Figure 5-42 Engine Speed Effect (1800 (adjusted) Versus 2500 rpm) at Midstroke Off Major-Thrust Side for SAE-10W/50n at (a) Window 2 and (b) 4 243
Figure 5-43 Ring-Pack Oil Distribution for SAE-10W for the Speed Effect (1800 Versus 2500 rpm) for the (a) Intake and Compression Strokes and (b) Expansion and Exhaust Strokes 246
Figure 5-44 Ring-Pack Oil Distribution for SAE-10W/50n for the Speed Effect (1800 Versus 2500 rpm) for the (a) Intake and Compression Strokes and (b) Expansion and Exhaust Strokes 247
Figure 5-45 Ring-Pack Oil Distribution for SAE-50 for the Speed Effect (1800 Versus 2500 rpm) for the (a) Intake and Compression Strokes and (b) Expansion and Exhaust Strokes 248
Figure 5-46 *RINGPACK-OC* Results at 1800 rpm for (a) Land Pressure Predictions and (b) Top and Scraper Ring Relative Lift within Their Grooves 249
Figure 5-47 Predicted Mass Flow Rates through Channels between Rings and Grooves During a Cycle for 1800 and 2500 rpm from (a) Crown Land to Region Behind Top Ring,, (b) Region Behind Top Ring to Second Land, (c) Second Land to Region Behind Second Ring, and (d) Region Behind Second Ring to Third Land 250
Figure 5-48 Predicted Gap Mass Flow Rates During a Cycle for 1800 and 2500 rpm for the (a) Top and (b) Second Rings 251
Figure 5-49 Azimuthal ARTs at Windows 1, 2, and 4 for Selected Lubricants and Operating Conditions for the Ring Pack Including the (a) Free Liner (reference), (b) Crown Land Region, (c) Second Land Region, (d) Third Land Region, (e) Region between OC Rails -- Upstrokes, and (f) Region between OC Rails -- Downstrokes 257
Figure 5-50 Azimuthal ARTs at Windows 1, 2, and 4 for Selected Lubricants and Operating Conditions for Regions Below the OC Ring Including the (a) Chamfer Region (Region 5) -- Upstrokes, (b) Region 5 -- Intake, (c) Region 5 -- Expansion, (d) Region 6 (Upper Piston Skirt for Major-Thrust Side) -- Upstrokes, (e) Region 6 -- Downstrokes, and (c) Region 7 259
Figure 5-51 Down-Scraping of the Second Ring from (a) an Illustrated Schematic and (b) Model Predictions of Approaching and Exiting Liner Oil Films 263
Figure 5-52 Measured Oil Down-Scraping Shown by (a) an Entire Oil Distribution Traces, (b) the Third Land Region, and (c) the ART in Third Land Region from Window 1 to Window 6 264

Figure 5-53 Oil Distribution Comparison at Midstroke -- Downstrokes Versus Upstrokes 271
Figure 5-54 Oil Distribution Comparison at Midstroke -- Downstrokes Versus Upstrokes 271
Figure 5-55 Oil Distribution Comparison at Midstroke -- Downstrokes Versus Upstrokes 272
Figure 5-56 Oil Distribution Comparison near BC-- Downstrokes Versus Upstrokes 272
Figure 5-57 Oil Distribution Comparison at Midstroke -- Downstrokes Versus Upstrokes 274
Figure 5-58 Oil Distribution Comparison near BC -- Downstrokes Versus Upstrokes 274
Figure A-1 The PRL System -- the Ring Pack and Piston 291
Figure A-2 Top Compression Ring 291
Figure A-3 Scraper Ring -- Scraping and Negative Twist 291
Figure A-4 Gap and Groove Oil Transport 294
Figure B-1 Schematic of the LIF System, Configured Engine, and Data Acquisition System 296
Figure C-1 Selected Piston Dimensions and Window Locations Relative to Skirt 304
Figure C-2 Micro-geometry of Ring Face Profiles 308
Figure C-3 Scraper Ring with Negative Static Twist under Tension with Minimum Point 309
Figure C-4 One Possible Configuration of the OC Ring Assembly Under Tension within Its Groove 309
Figure C-5 Micro-Measurements of Selected Piston Regions on Major-Thrust Side -- Top and Second Lands and Upper Piston Skirt (first five millimeters) 311
Figure C-6 Bore Distortion at Midstroke after Experiments 313
Figure C-7 Window 4 and Its Adjacent Liner (b) Before and (c) After Experiments 314
Figure D-1 Oil Film Thickness within the Ring Pack and Partially Along the Upper Skirt and Free Liner at Window 1 317
Figure D-2 Schematic of PRL System with Window Locations for Kinematic Evaluation 318
Figure D-3 Piston Region and Ring Position Versus Crank Angle with Reference To Midstroke Windows Along the Liner 319
Figure D-4 Instantaneous Piston Speed versus CA 319
Figure D-5 Piston Region and Ring Position Versus Crank Angle with Reference To Window Location Along the Liner 321
Figure D-6 Instantaneous Piston Speed versus CA for an Entire Stroke 321
Figure D-7 Oil Film Thickness near BC at Window 6 (a) Within the Ring Pack and Partially Along the Upper Skirt and (b) Along Entire Skirt and Free Liner Below Skirt 323
Figure D-8 Calibration to Upper Skirt Machining Marks During Compression Stroke 325
Figure D-9 Calibration to Upper OC Rail During Exhaust Stroke 325
Figure E Single-Piece Model Simplification of the Actual Three-Piece OC Ring 333
Figure G-1 Ring-Liner Lubrication with Sub-Ring Pressure Profile 336
Appendix H Free-Liner OFT and Ring MOFTs from Window 4 for the Viscosity Effect of SAE-10W, -10W/50n, -30, and -50 for Liner Temperatures of 100, 80, and 60°C 343
Appendix I Engine Speed Effects at Windows 2, 4, and 6 for Cases with Fair to Poor Calibration Coefficients 344
Figure K-1 Oil Distribution below the OC Ring from Window 2 for (a) Intake and Compression and (b) Expansion and Exhaust Strokes 352
Figure K-2 ARTs for Regions below the OC ring from Window 2 for (a) Groove and Chamfer Region -- Region 5, (b) Upper Piston Region -- Region 6, and (c) Lower Piston Region -- Region 7 354
Figure K-3 Oil Distribution below the OC Ring from Window 4 for (a) Intake and Compression and (b) Expansion and Exhaust Strokes 355
Figure K-4 ARTs for Regions below the OC Ring from Window 4 for (a) Groove and Chamfer Region -- Region 5, (b) Upper Piston Region -- Region 6, and (c) Lower Piston Region -- Region 7 356

LIST OF TABLES

Table 2.1 Kinematic Viscosity (cSt) Versus Temperature for All Five Lubricants 25
Table 4.1 Numbering Assignments for Lubricants 120
Table 4.2 Extent of Agreement between OFT Measurements and Predictions from the *FRICTION-OFT* Model 131
Table 5.1 Measured and Calculated Oil Travel along the Third Land for 1800 and 2500 rpm for SAE-10W, -10W/50n, and -50 253
Table 5.2 Numbering Assignments for Lubricants 255
Table 5.3 Scraper Down-scraping from Window 1 to 6 -- Measurements and Predictions with and without Expansion Tilt 265
Table B.1 Kohler Engine Specifications and Modifications 297
Table C.1 Surface Roughness and Protrusion of Operable LIF Windows Measured After the Experiments 315
Table D.1 Calibration Coefficients 328

CHAPTER 1: INTRODUCTION

The understanding of lubricant behavior within the piston/ring/liner (PRL) system as affected by oil properties, ring and piston geometry, and engine operation is crucial for improving engine performance while mitigating costs. Reducing midstroke friction, endstroke wear, and oil consumption is a challenge in view of the modern engine and the increasing lubricant requirements demanded by future engine designs.

To study the complex lubricant behavior, the Laser Induced Fluorescence (LIF) system has proven to be a reliable and accurate diagnostic tool for measuring the oil film thickness (OFT) within the PRL system. The focus of this project is to study LIF OFT measurements acquired from a production spark-ignition (SI) engine. OFT along the free liner and under the rings and the oil distribution between the rings and along the skirt for several lubricants are studied at different liner temperatures, engine speeds, and load conditions and from different locations along the cylinder liner. In addition, to aid in the data analysis and interpretation, predictions from the most recent OFT model developed at MIT are compared to OFT measurements along the free liner and under the rings.

1.1 BACKGROUND

Oil properties, ring and piston geometry, and engine operation influence lubricant behavior within the PRL system which is intimately related to engine performance including friction, wear, oil consumption, and emissions; thus, understanding lubricant behavior in the PRL system of the engine is imperative. Friction generated from lubrication between the piston assembly -- namely, the rings and skirt -- and the cylinder liner generally account for about fifty percent of the total engine mechanical loss [1]. Estimated by Coy *et al.* [2], viscometric and boundary friction effects can reduce fuel consumption by 3 - 5 percent.

Wear, especially that occurring at top center (TC) of the late compression and early expansion strokes because of high pressures and temperatures, has shown to change

the original unworn ring geometry [3]. Thus, the rings' function for lubricant control is affected as well.

In addition to the relatively thin oil films under the rings, large oil volumes exist along the piston assembly between the rings and along the piston skirt. In some cases, oil movement and transport between the different regions of the PRL system has been shown to account for 80 - 90 percent of the total oil consumed by the engine [4]. The remaining oil is consumed through other routes such as the engine overhead system and positive crankcase ventilation (PCV) [5]. Additionally, the amount of oil film left on the free liner and recirculation of oil flow within the piston assembly is crucial for studying oil absorption/desorption of hydrocarbons from fuel [6].

In view of the modern engine, reducing midstroke friction, endstroke wear, and oil consumption is a challenge. Improvement becomes even a tougher task as lubricant requirements for future engine designs increase. The trend toward higher power density, higher engine speeds, reduced oil consumption, extended maintenance periods, reduced quantity of oil in the sump, and longer oil drain intervals impose severe oil stress and require outstanding lubricant performance.

To facilitate the design of the PRL system for improving engine performance, model development is important as well. In addition to validating model accuracy with consistent, reliable, and accurate film thickness data, extending the understanding of the mechanisms and processes involved in lubricant behavior to improve and build more robust and comprehensive predictive tools is a high priority for those in the industry.

The lubricant behavior within the PRL system is complex. Although oil flow under a ring can often be approximately modeled as locally fully developed flow at midstroke and may appear quite simple at a first glance, the boundary conditions (which often depend upon other rings' behavior), ring dynamics (including effective ring pressure, twist, and flutter affected by gas flow, friction, and inertia), mixed (hydrodynamic and boundary) lubrication, and piston tilt creating azimuthal differences severely complicate the understanding of lubricant behavior under and around the rings. Along the lands, predicting oil transport between local regions of the PRL system and, subsequently, oil consumption is even more complicated and is most likely even coupled

to ring-liner lubrication, at least for the oil control (OC) ring. Therefore, lubricant behavior is very intricate and engine-specific.

To study the complex lubricant behavior the Laser Induced Fluorescence (LIF) system has proven to be reliable and accurate and is widely used in the industry for measuring the oil film thickness (OFT) within the PRL system. The nonintrusive fluorescence technique can accurately measure oil thicknesses from tenths of a micron up to 100 microns -- tailored quite nicely for oil under the rings and between the piston lands and liner.

1.2 PREVIOUS WORK

This project is a continuation of the work performed at MIT by Goro Tamai (MS, '95) [7]. His experiments were carefully and consistently conducted on a SI engine using the 1-D LIF system. Diligent attention was given to window-to-liner flushness and a strong and an accurate LIF signal. Very few researchers have taken LIF OFT measurements in an engine at multiple window locations. Although six quartz windows were installed, only four windows were proven operable -- three at midstroke and one near bottom dead center (BDC).

The five lubricants -- three monogrades and two multigrades -- were selected with particular emphasis placed on the oil set spanning a wide range of viscosities. If the viscosity range is not wide enough, effects of incremental viscosity differences of test lubricants on OFT can be masked by the uncertainty of the LIF measurement technique. This problem was just one of the difficulties encountered by Deutsch [8], Tamai's predecessor, and helped hinder conclusive results.

After developing the test engine -- a one-cylinder, SI Kohler engine -- steady-state experiments were conducted with selected lubricants. OFT measurements within the PRL system were taken at the four operable windows. Cylinder liner temperatures, lubricants, and engine speed were varied. In addition to the measurements taken during firing conditions at moderate temperatures of 100, 80, and 60°C, motored data was

collected at low temperatures of 60 and 40°C. After a quick MOFT analysis of a fraction of the data collected, Tamai concluded with the following fired MOFT results.

- MOFT differences were significant among the three LIF windows at midstroke. MOFTs were greatest on the thrust side where the cylinder wear was found to be most extensive. (He claimed differences were primarily caused by bore distortion.)
- MOFT differences were significant along a stroke from midstroke to near BDC -- a factor of 1.5 times higher at midstroke.
- MOFT under the rings increased with viscosity.
- The shear-thinning effect under the rings is noticeable between the monograde SAE-50 and the multigrade 10w50 oils.
- With decreasing cylinder liner temperature, MOFT increases with the decrease in viscosity except for SAE-50. For this high-viscosity lubricant, the MOFT-temperature relationship is reversed compared to the trends of the other lubricants. (Tamai conjectured that this trend reversal could be caused by "oil pumping difficulty" because of the lubricant's high viscosity.)
- As engine speed increases from 1800 to 2500 rpm, MOFT increases as well.

These MOFT results were compiled from only a fraction of the data set -- less than 20 percent; unfortunately, Tamai did not have sufficient time to reduce, show, and interpret the MOFT data in depth, let alone the oil distribution within the ring pack and along the skirt. Also, no quantitative comparisons with OFT modeling was performed. This thesis attempts to confirm Tamai's OFT findings for the entire database in a more comprehensive manner including analytical and numerical analyses. Additionally, the oil distribution along regions of the ring pack and skirt is another major subject of investigation.

1.3 PROJECT OBJECTIVES

The central focus of this project is to accurately reduce and conduct an in-depth analysis of all the oil film measurements acquired from the one-cylinder, Kohler gasoline engine. Emphasis is placed on showing and interpreting the magnitudes and trends of the oil behavior under the rings (MOFT) and along the PRL regions between the rings and along the piston skirt and cylinder free liner. Assisting with the interpretation, MIT's *RINGPACK-OC* and *FRICTION-OFT* models have been applied where appropriate, and their accuracy and range of applicability have been assessed as well.

1.3.1 Oil Film Thickness (OFT) under the Rings and along the Free Liner

The minimum oil film thickness (MOFT) under the rings -- top and scraper rings and the upper and lower segments (or rails) of the OC ring -- and the OFT left by the rings on the cylinder free liner are the focus of this section. The objectives for the MOFT study for the experimental results accompanied by the model predictions from the *FRICTION-OFT* model are to address the following topics.

1. Stroke-by-stroke differences
2. Cylinder liner temperature and lubricant effects
    a. Fired for moderate liner temperatures -- 60, 80, 100°C
    b. Motored for low liner temperatures -- 40 and 60°C
3. Speed effects
    a. Engine speeds from 1800 to 2500 rpm
    b. Midstroke (win-1) to near BC (win-6)
4. Shear Thinning and Thickening
5. Azimuthal effects at midstroke

To aid in the interpretation of the data, the current *FRICTION-OFT* model developed at MIT [9] is applied. (As an input to this model, results from the *RINGPACK-OC* model [10] which predict land pressures from the measured cylinder pressure is needed. Both of these models are described in further detail in Appendix E.)

As a natural outcome of the MOFT study, another objective is *FRICTION-OFT* model verification. Goals are to

1. confirm the physics captured by the model,
2. assess the model's accuracy -- both magnitudes and trends, and
3. assess the range of applicability.

1.3.2 Oil Distribution Along the PRL Regions within Ring Pack and along the Piston Skirt

A reasonable model predicting the oil distribution along the PRL system has not been developed yet. Thus, aside from applying an appropriate model, the objectives for the study of oil distribution along the PRL regions consist of those from the MOFT study and more. In addition to those MOFT topics 1-4, the objectives for oil distribution also include

6. Load effects between fired and motored at 60°C
7. Observing oil transport
    a. Oil squeezing between rings and grooves
    b. Down-scraping of scraper ring
    c. Oil behavior along the thrust-side of the piston skirt
    d. Inertial influences and viscosity restriction

Both models are applied to the oil distribution data where appropriate for interpretation and verification such as predicted ring lift from empirical oil squeezing in the grooves, gas flows on oil dragging (especially for oil movement within the grooves and along lands), and scraper down-scraping along a stroke.

1.3.3 Comprehensive Compilation of Accurate OFT Data

By careful record-keeping and comprehensive documentation, the author intends this thesis to be a valuable reference for current and future researchers in the field of engine lubrication. Especially for oil transport and consumption, the least understood

area in the PRL system, an explicit display of much of the data could assist the model developer to identify key oil transport and consumption routes and processes.

CHAPTER 2: TEST LUBRICANTS

Heavily influential on lubricant behavior within an engine are the lubricant properties. A lubricant within the PRL system is subjected to a the wide range of severe conditions. In addition to the high temperatures and their effects on viscosity variation and volatility, oils providing lubrication under the rings experience shear rates through a very wide range, from zero at the endstrokes up to magnitudes of 10^7 1/s at midstroke [11]. And depending on the lubricant formulation, a lubricant's behavior may not be Newtonian, but its viscosity may change above a critical shear rate. These special types of lubricants are called multigrades and are characterized by a less pronounced viscosity-temperature relationship compared to the monogrades.

The five tested lubricants consist of three monogrades and two multigrades. The three monograde lubricants are SAE-10W, -30, and -50 and cover an expansive kinematic viscosity range from 6.3 to 19.4 cSt at 100°C. The two multigrades, SAE-10w50n and SAE-10w50k, have slightly different viscosities; 'n' and 'k' represent 'thin' and 'thick' viscosities, respectively, and only differ by 1.5 cSt (9.9 - 8.4 high-shear kinematic viscosity) at 100°C. However, their large difference is their shear stabilities; SAE-10w50n and -10w50k have critical shear rates of 40,730 and 93,325 1/s, respectively.

2.1 TEMPERATURE DEPENDENCE OF VISCOSITY

Most fluids change viscosity as temperature changes. For the engine lubricants used in this experiment, kinematic viscosities change exponentially with temperature and can be curve fit by the Vogel Equation (eqn 2.1) [12].

$$\nu = K\exp\left(\frac{\theta_1}{\theta_2 + T}\right) \qquad (2.1)$$

ν is the kinematic viscosity (cSt). K (cSt) is an oil-dependent constant. Other oil-dependent constants include θ_1 and θ_2 with units of °C. Lastly, T (°C) is the lubricant temperature at which the viscosity is being evaluated.

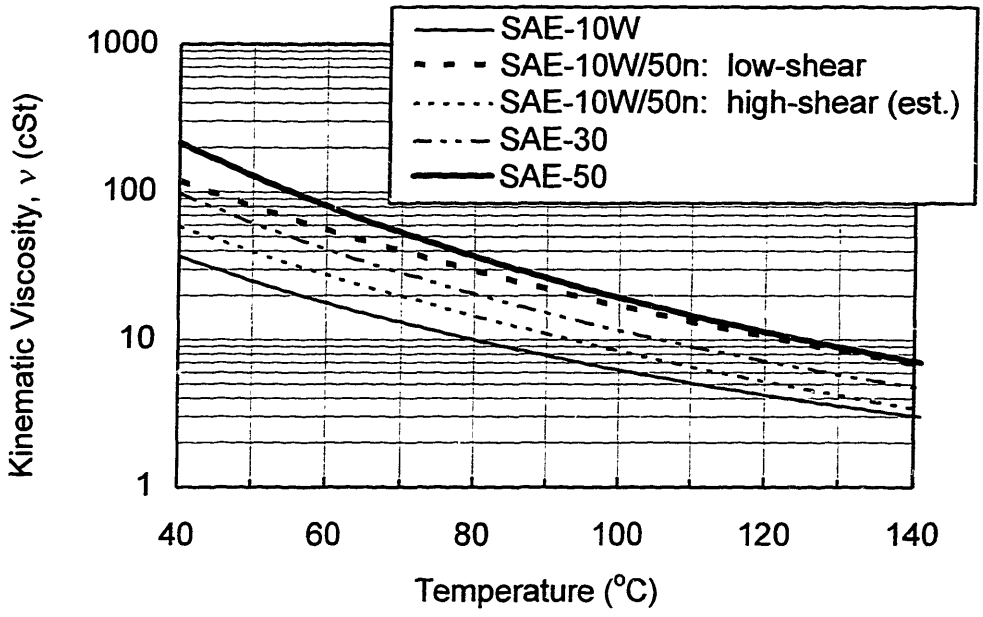

Figure 2-1 Viscosity Versus Temperature for Four Selected Lubricants.

Lubricant	*Temperature, T (°C)*			
	100°C	*80°C*	*60°C*	*40°C*
SAE-10W	6.3	10.0	17.9	37.0
SAE-10W/50n	8.4 (17.1)	14.6 (29.6)	27.7 (56.2)	58.9 (119.4)
SAE-10W/50k	9.9 (19.1)	(not tested)	35.8 (69.0)	80.2 (154.6)
SAE-30	11.6	(not tested)	41.3	98.6
SAE-50	19.4	36.9	81.1	216.1

Table 2.1 Kinematic Viscosity (cSt) Versus Temperature for All Five Lubricants. (For the multigrades, viscosities in parentheses are low-shear values.)

The viscosity-temperature relationship for four of the five oils is shown Figure 2-1. (SAE-10w50k was left out for clarity; its viscosity-temperature relationship is just slightly higher than SAE-10w50n. Furthermore, only high-shear viscosity measurements were made at 150°C; the remainder of the high-shear, viscosity-temperature curve is

estimated from the low-shear relationship.) Immediately following this figure is Table 2.1 showing all five lubricants and their high- and low-shear viscosities for all liner temperatures within the test matrix introduced in Chapter 3.

Several important observations can be made from this curve and corresponding table. First, for the multigrade 10W/50n at low-shear, notice the less pronounced viscosity-temperature relationship compared to SAE-50.

Secondly, over the array of lubricants at a particular temperature (defined as a lubricant effect), viscosities range from about 6 to 19 cSt at 100°C -- over a 200 percent increase from thin to thick lubricants; at 40°C, the range is 37 to 216 cSt -- slightly less than a 500 percent increase. Therefore, differences due to changes in viscosity should definitely be noticed in the OFT measurements.

Lastly, over the array of temperatures for a particular lubricant (defined as the temperature effect), viscosity increases more rapidly with each decreasing step in temperature necessitating the log scale for the ordinate in Figure 2-1. Thus, greater OFT differences should occur at temperature steps for lower temperatures compared to higher temperatures.

2.2 SHEAR DEPENDENCE OF VISCOSITY

Although the main difference between multigrade and monograde lubricants is their viscosity-temperature relationship, they also differ in their viscosity dependence upon high shear. When multigrades are subjected to a shear rate higher than their critical rate, they experience shear-thinning -- a decrease in viscosity.

The shear stability of multigrade lubricants differ depending upon the types of VI improvers added to them [12]. Although their viscosities do not differ much, the two multigrades, SAE-10W/50n and -10W/50k, have critical shear rates, β, of 40,730 and 93,325 1/s, respectively -- an increase over a factor of two. The critical shear rate is in the middle of the viscosity transition from low-to-high shear regime. Mathematically, the

local shear rate, $\dot{\gamma}$, is defined as the partial derivative of local fluid velocity with respect to the radial distance away from the cylinder liner.

$$\dot{\gamma} = \frac{\partial u}{\partial y} \tag{2.2}$$

For ring/liner lubrication, this local shear rate can be approximated by an average shear rate, $\bar{\dot{\gamma}}$, defined by the ring sliding speed divided by its MOFT. As the ring accelerates and the multigrade lubricant exceeds its critical shear rate, the oil experiences a decrease in viscosity. This viscosity transition to a lower viscosity is called shear-thinning which can be represented by the Cross Equation [12].

$$\nu = \nu_0 \frac{1 + \frac{\nu_\infty}{\nu_0}\left(\frac{\bar{\dot{\gamma}}}{\beta}\right)^m}{1 + \left(\frac{\bar{\dot{\gamma}}}{\beta}\right)^m} \tag{2.3}$$

The subscripts o and ∞ represent the low and high shears, respectively, and the exponent m is an oil-specific constant. As m increases, the viscosity transition from low to high shear decreases. This relationship between viscosity and shear rate for the two multigrades, SAE-10W/50n and -10W/50k, is shown in Figure 2-2.

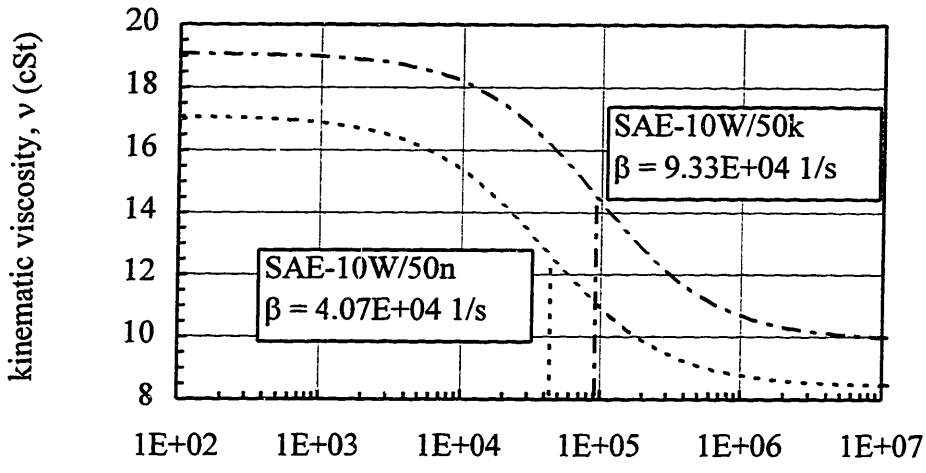

Figure 2-2 Kinematic Viscosity Versus Average Shear Rate for SAE-10W/50n and -10W/50k from the Cross Equation.

During most of the piston motion, except around the endstrokes, the piston rings experience high shear rates on the orders of 10^6 and 10^7 -- shear rates definitely in the high-shear viscosity regime. Figure 2-3 shows the OFT insensitivity to low-shear viscosity during the majority of a stroke including midstroke (at window 1) and near BC (at window 6) for the Kohler engine. Incurring the lowest speed near BC (at window 6), the top ring still subjects the multigrades to shear rates well above any significant change in viscosity due to shear ex ..nplified by SAE-10W/50n in Figure 2-3 (a). (The actual shear behavior of SAE-10W/50n corresponds to the solid curve for μ = 0.49 = (high-shear)/(low-shear viscosity). The dotted lines denote lower low-shear viscosities while keeping the high-shear value constant.) The lowest shear experienced near BC is 2.26×10^6 1/s -- well above any significant viscosity change from shear. (The top ring subjects SAE-10W/50n to the lowest shear when the top ring MOFT is high; the highest MOFT is 0.8 μm for 2/3 load at 60°C.)

Figure 2-3(b) shows the predicted OFT insensitivity of the free liner and top ring to the low-shear viscosity of SAE-10W/50n from the *FRICTION-OFT* model. For any practical purposes, OFTs change negligibly with very large changes in low-shear

viscosity. This fact remains true for the remaining rings (which induce even higher shear rates) and is why the high-shear viscosities are used to analyze OFT magnitudes and trends in Chapter 4.

This high-shear, low-viscosity behavior is desirable for reducing friction around midstroke where lubrication is mostly hydrodynamic, if not all, and wear is not a problem. However, as piston and ring sliding speed decreases around the endstrokes, mixed and pure boundary lubrication often occur, and, here, a higher viscosity is desirable to maximize ring lift and minimize squeezing under the ring to reduce endstroke wear. A multigrade can provide this function as it shear-thickens transitioning below its critical shear rate. So a multigrade provides the best of both worlds -- reducing midstroke friction and endstroke wear.

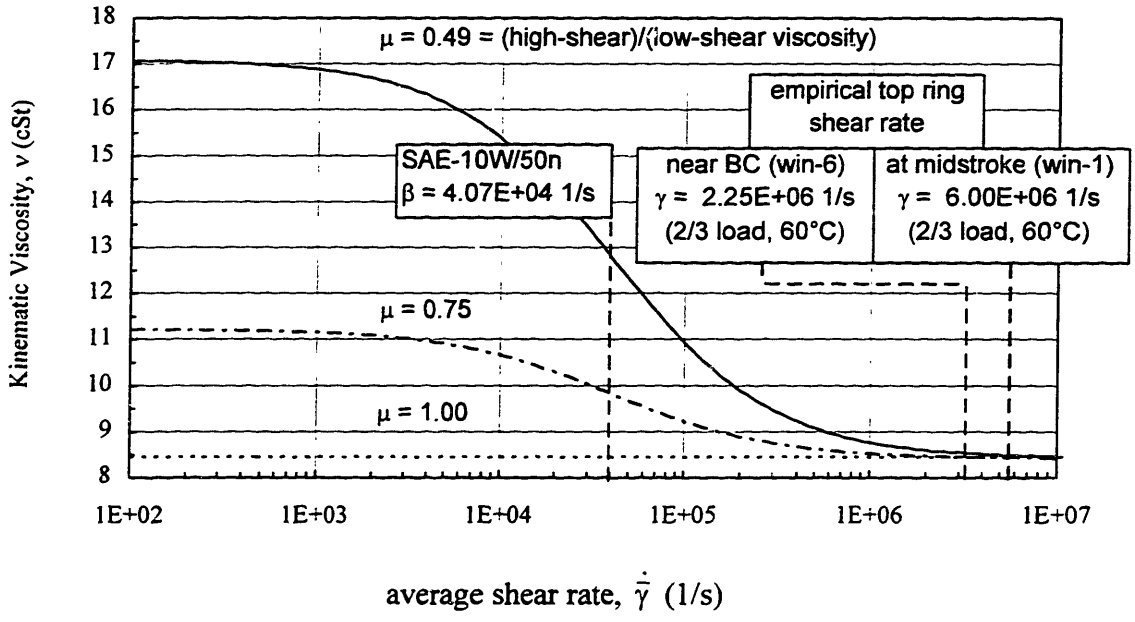

(a) Viscosity Versus Shear of SAE-10W/50n

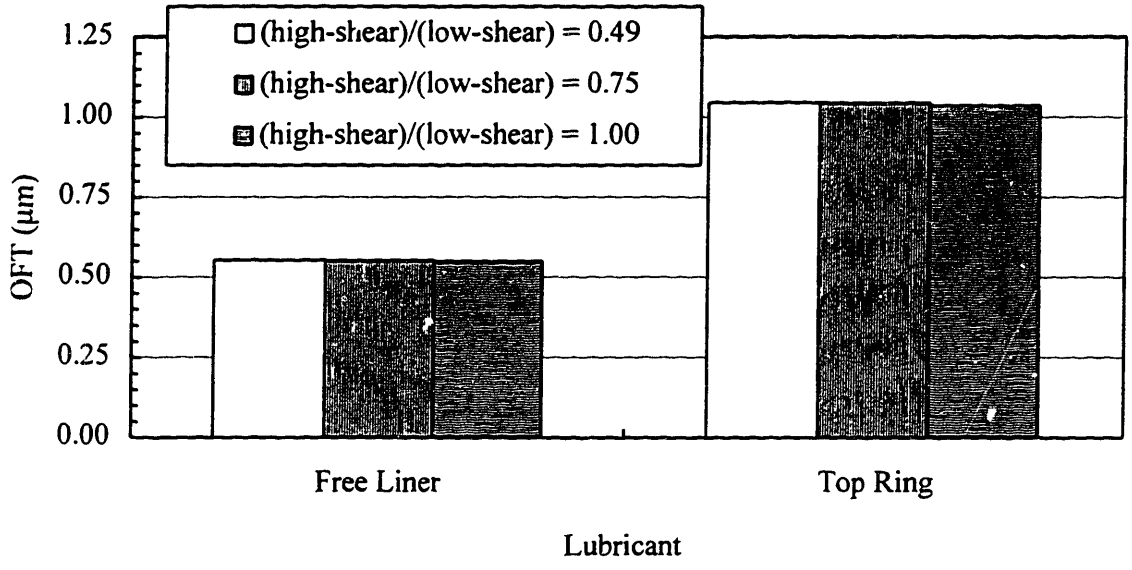

Figure 2-3 OFT Insensitivity to Low-Shear Viscosity of SAE-10W/50n. (a) Viscosity Versus Shear (b) Predicted OFT Insensitivity for Free Liner and Top Ring at Midstroke.

2.3 OIL DEGRADATION

Over extensive periods of engine operation, the quality of the oil deteriorates, whereby oil properties change and the oil's proper function to lubricate diminishes; this process is called oil degradation. Because of possible oil degradation -- from the harsh mechanical stresses and foreign debris such as fuel contamination and worn materials -- and LIF dye, the lubricant properties could have changed during our experiments. However, the lubricants were analyzed before and after the experiments, and no changes were evident.

CHAPTER 3: ENGINE AND TEST MATRIX

The production SI engine was modified to incorporate six LIF windows and instrumentation for data acquisition and engine control over the extensive test matrix.

3.1 TEST ENGINE AND WINDOWS

The Kohler CH-14 single-cylinder SI engine was only modified by installing six windows, a retrofitted water jacket, two thermocouples in the cylinder liner, and one cylinder pressure transducer, and a shaft encoder. To allow optical access of the LIF system, the cylinder liner was machined for six fused quartz/silica windows: four installed about 90° azimuthally around midstroke and one near each endstroke on the major-thrust side. Figure 3-1 shows the exact location of the windows azimuthally and along a stroke.

(Further description of the complete experimental apparatus may be found in Appendix B and other theses [7, 8]. Detailed geometry and microgeometry of the PRL system may be found in Appendix C. Detailed engine kinematics and dynamics for the Kohler engine may be found in Appendix D.1.)

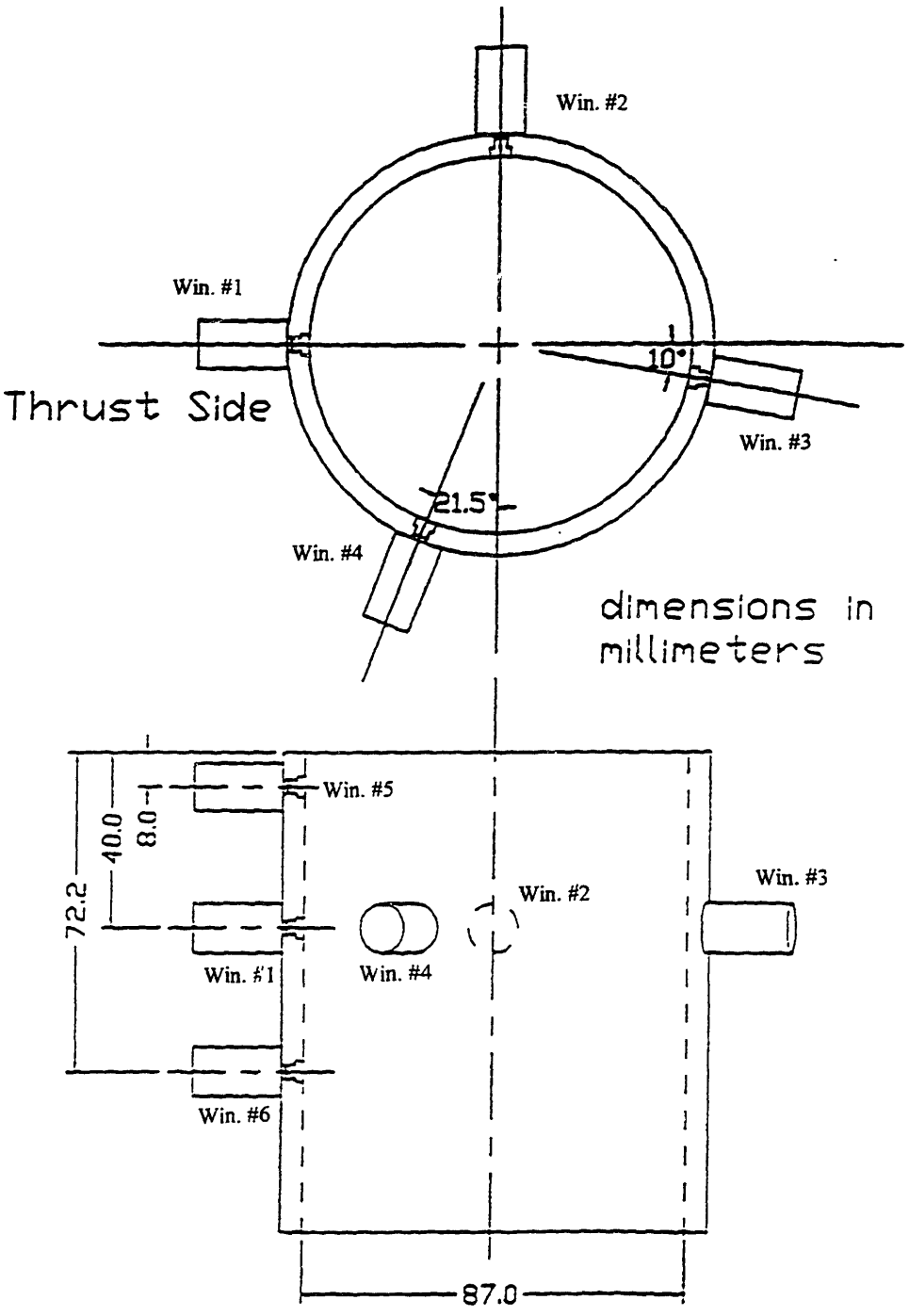

Figure 3-1 LIF Probe/Window Locations and Number Convention of Kohler Engine [8]

3.2 OPERATING CONDITIONS AND TEST MATRIX

The test matrix shown in Figure 3-2 was designed to study temperature, lubricant, and engine speed effects on oil film thickness for an array of five lubricants spanning a wide viscosity range. Additionally, the fired and motored conditions (the load effect) can be compared at 60°C. (Motored cases were run at wide-open throttle (WOT) for 2500 rpm.) For each test case, LIF measurements from the four operable windows also provide insight to azimuthal effects around midstroke and OFT differences along a stroke.

The baseline operating condition is fired at 20 N-m (approximately 2/3 of full load with a bmep of 631 kPa), 2500 rpm, and a midstroke liner temperature of 100°C. This load and speed were selected because the engine and dynamometer operated most smoothly and consistently at this condition. The midstroke temperature of 100°C was selected for two reasons. First, this temperature is representative of a typical engine in field use. Secondly, oil properties are conveniently measured at this temperature [7].

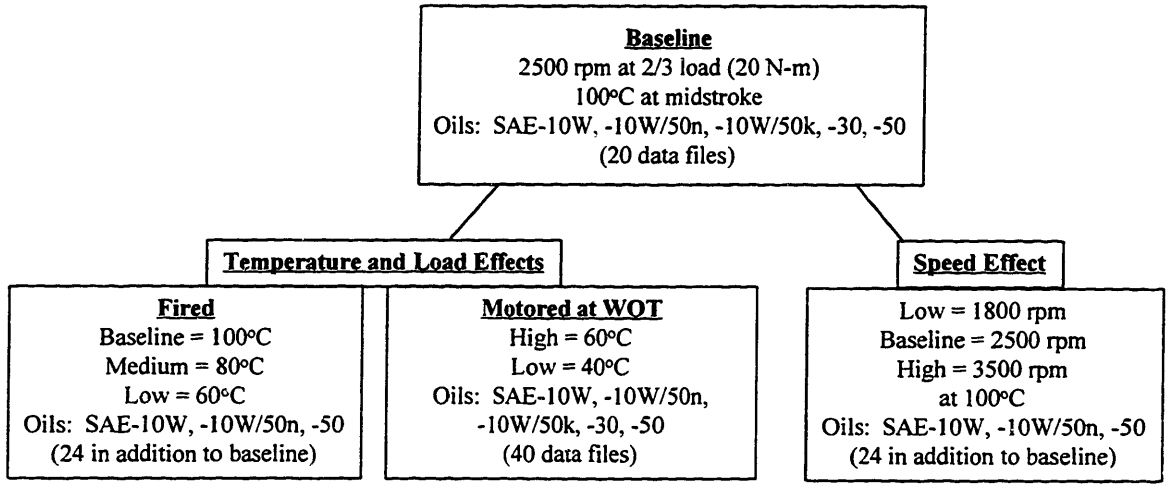

Figure 3-2 Test Matrix for Kohler Engine with Four Operable LIF Windows. (Three windows at midstroke and one near BDC.)

CHAPTER 4:
OIL FILM THICKNESS (OFT) ALONG THE FREE LINER AND UNDER THE RINGS

Lubrication under the rings not only generates close to half of the PRL-assembly friction and contributes to substantial wear but leaves an oil film on the free liner above the piston after it passes. The magnitudes and trends of the free-liner oil film thickness (OFT) and ring minimum oil film thicknesses (MOFTs) are the focus of this section.

First, a brief orientation of how the MOFTs are manually fitted from a 10 cycle-trace average is presented followed by a criterion from a covariance correlation used to help determine whether OFT differences are significant or not. Secondly, all of the baseline results from the four windows are shown and represented by stroke as well as a justified stroke-averaged representation. Shown both experimentally and theoretically, the OFT hierarchy along the ring pack to the free liner for any single lubricant case is explained and shown from inter-ring and free liner OFT dependence via lubricant behavior. Then, the effects of the different lubricants are investigated and an OFT-viscosity relationship is found characteristic of hydrodynamic lubrication. Additionally, any stroke-to-stroke differences (or lack thereof) within the cycle are shown and interpreted.

Thirdly, results off the baseline condition are addressed including effects from different liner temperatures, lubricants, load, and speeds are investigated. Related to piston speed, any shear thinning or thickening are studied along a stroke from window 1 to window 6. All results consider liner location azimuthally around midstroke and axially between midstroke and near bottom center (BC) in view of the calibration accuracy between cases addressed in Appendix D. The last section before the OFT summary directly addresses the bore distortion effects on OFT at midstroke.

Additionally, throughout this study, predictions from MIT's *FRICTION-OFT* model are compared with the results. A model verification summary for ring MOFTs and free-liner OFT is presented at the end of the chapter.

4.1 DATA REDUCTION FOR RING FITTING AND FREE-LINER OFT

Once proper calibration using individual LIF traces is completed (refer to appendix D), ten consecutive cycles from one case are averaged into one OFT trace called the 10 cycle-trace average exemplified in Figure 4-1(a). From cold piston-assembly geometry, the approximate ring locations are known along the piston. The top ring, scraper, and upper and lower OC segments are located about 6.0, 11.8, 14.7, and 17.0 millimeters, respectively, from the top of the crown land; the free-liner is calculated by taking the average OFT along the first five millimeters above the top of the crown.

Unlike the automated free-liner OFT calculation, the ring fitting is manual. Although very time consuming, a manual approach proves to be more accurate for the rings and is therefore favored over an automated approach. Although the approximate ring and segment distances are known from cold geometry of the piston assembly, the combination of ring and groove clearances, ring twist, piston tilt, and thermal expansion precludes exact determination of the minimum point along the piston or abscissa in Figure 4-1 (a). Secondly, noise in the signal, especially for the top ring, sometimes precludes a clear fit and requires experienced discretion from the experimenter in order to fit the ring properly to the trace. In this instance, an automated approach could just pick a high or low point in the signal which is just noise and provide a less accurate result. For these reasons and others [7], an automated approach for ring fitting was ruled out.

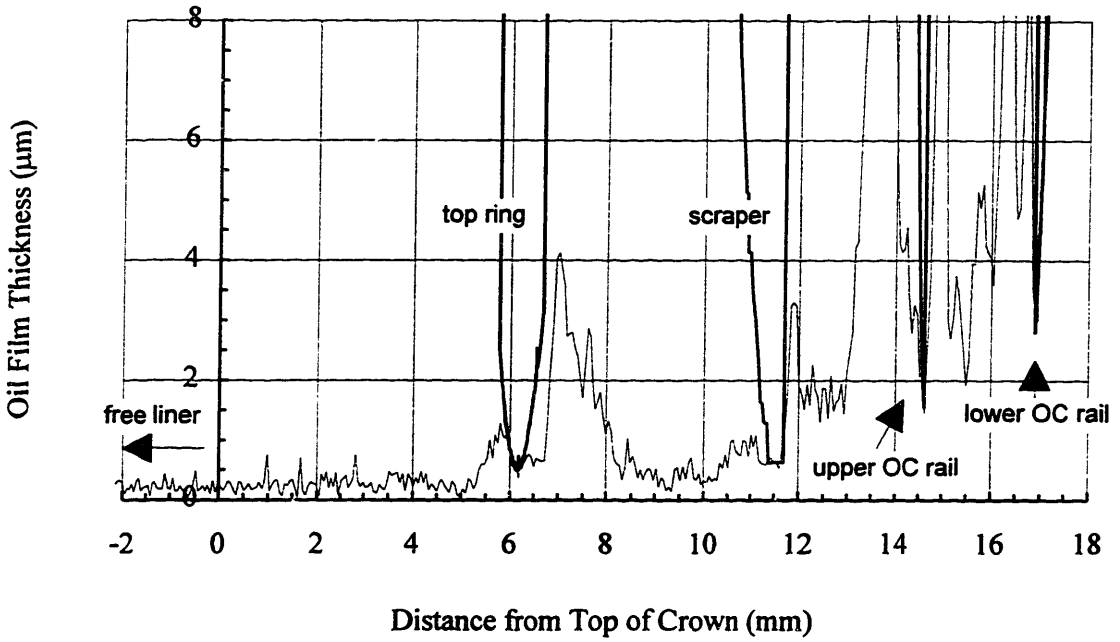

(a) Example of Actual Ring and Segment Geometries Fit Within an OFT Trace

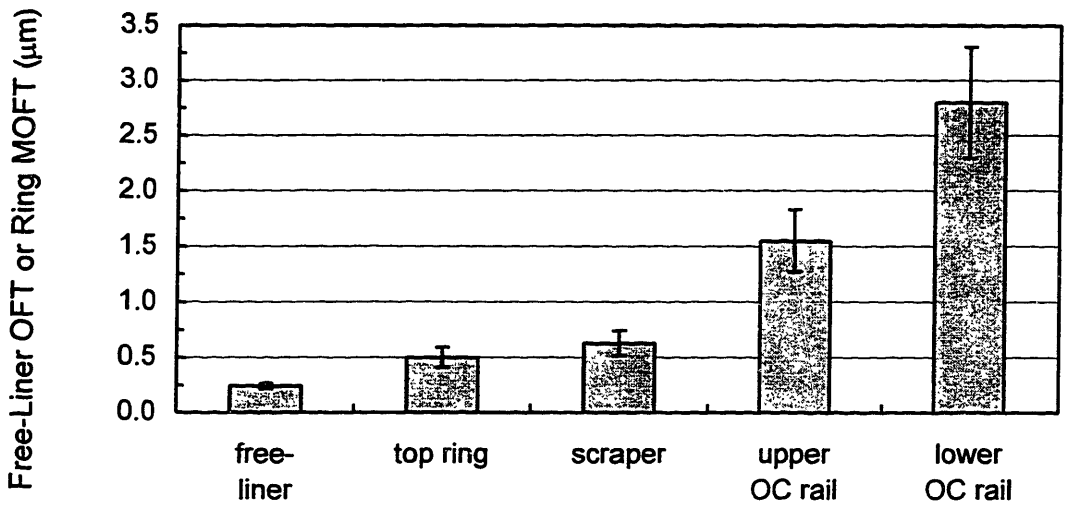

(b) Free-Liner OFT and Ring MOFTs Reduced from the Example Trace in Figure 4.1(a)

Figure 4-1 Ring Fitting and Free-Liner OFT for Intake Stroke at Window 4. (a) Actual Ring and Segment Geometries Fit Within an OFT Trace (b) Free-Liner OFT and Ring MOFTs
(SAE-10W/50k, 2/3 load @ 100°C, 40 mV/μm, 5 V)

Displaying OFT measurements from the example trace in Figure 4-1(a), Figure 4-1(b) shows the actual MOFTs of the ring pack, free-liner OFT, and their corresponding standard deviations which include human error for the manual ring fits, actual cycle-by-cycle variations, noise, and any small precision lost from the dynamic range of the data acquisition system (DAS) system (which includes a worst case of 0.08 mm increments determined in Appendix B). This measure of uncertainty provides an indication of the precision of the MOFTs and determines how significant differences are between two measured MOFTs; if standard deviations corresponding to two different MOFTs overlap, the significance of the MOFT difference is questionable. For example, in Figure 4-1(b) the MOFTs of the top and scraper rings are slightly different but the overlapping standard deviations suggest that this difference is suspect. In fact, soon to be explicitly shown for all of the results from the entire database, the MOFT difference between these two rings is insignificant in view of the standard deviation. Conversely, the MOFTs of the upper and lower OC segments are usually significantly different; lower segment MOFTs are greater than the upper segment MOFTs.

The standard deviations for the MOFTs are not determined directly for each case but indirectly from a covariance correlation

$$\text{Coefficient of Variation (COV)} = \frac{\sigma}{\text{MOFT}} = 0.18 \qquad (4.1)$$

The value of 0.18 was determined from some measurements from two independent data sets from the Kohler engine. (Standard deviation is calculated by the equation presented in Appendix F.) Figures 4-2 (a) and (b) show the linear regressions of the measurements from the two lubricant databases -- Lubricant Set One (the current database) and Lubricant Set Two (a previous database [7, 8]). Although this COV correlation was only determined from the major-thrust side at window 1, the measurements from Lubricant Set One span the extremes from the thin SAE-10W to the thick SAE-50, over cylinder liner temperatures from 40 to 100°C, and during different load conditions -- fired and motored. Each data point on the figure was calculated from ten manual fits from one ring or segment during a cycle for a particular stroke. Therefore, this COV correlation applies to the measured MOFTs for a particular stroke and ring. Each lubricant case represents 16

data points -- four per stroke from the rings and segments and four strokes per cycle. A total of 80 data points from Lubricant Set One make up Figure 4-2(a).

Instead of direct measurements of the standard deviation from the manually fitted MOFTs for all the cases in the current test matrix (Lubricant Set One), this COV correlation is used because the direct method for all the cases are too labor intensive and time consuming. Soon to be confirmed in the oil distribution analysis in Chapter 5 where an automated approach was used to average film thicknesses over regions along the piston assembly and free liner, the standard deviation for free-liner OFT is typically about half of that deduced from the MOFT COV correlation.

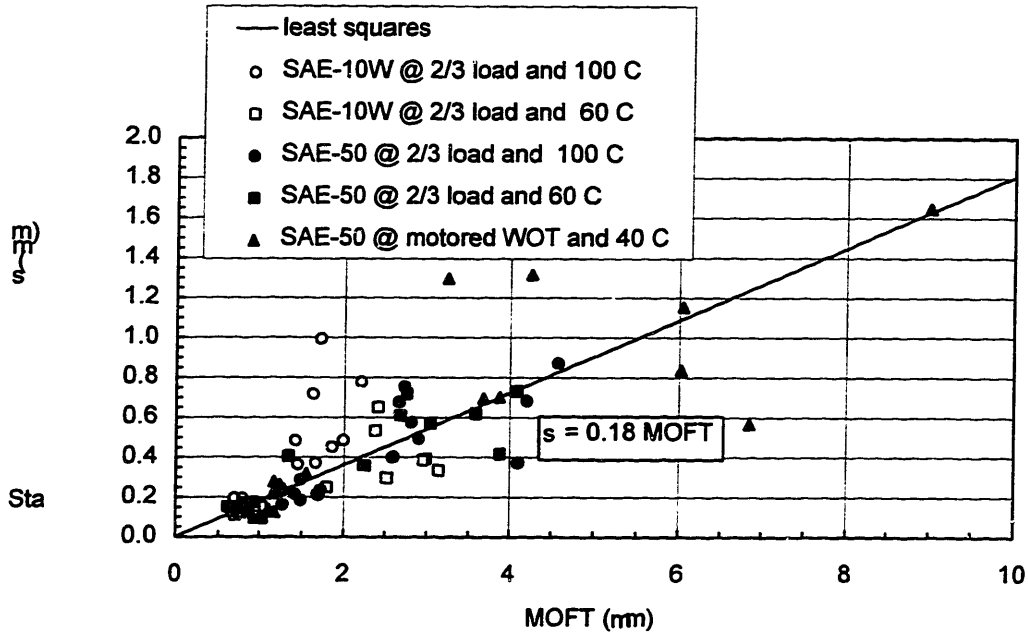

(a) Lubricant Set One (the Current Database)

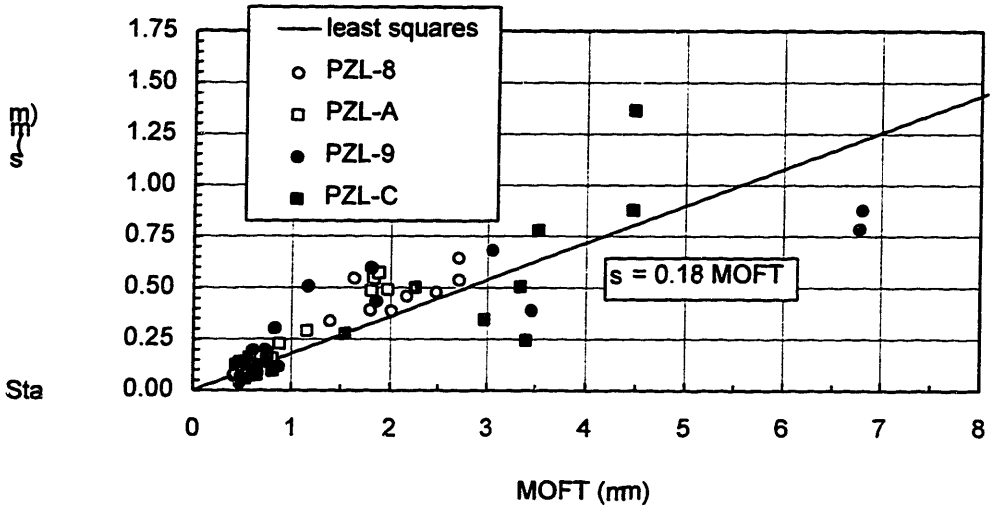

(b) Lubricant Set Two

Figure 4-2 Covariance Correlation: Standard Deviation Versus MOFT from Window 1 from Two Independent Studies (a) Lubricant Set One (the current test set from midstroke liner temperatures of 40 to 100°C using the thinnest and thickest lubricants spanning the viscosity range of 6.3 to 216.1 cSt and for fired and motored conditions) (b) Lubricant Set Two (2/3 load at 100°C liner temperature for lubricants spanning the viscosity range of 7 to 10 cSt)

4.2 BASELINE RESULTS

All of the OFT measurements are shown in this section for the baseline condition addressed within the test matrix in Figure 3-2. The five lubricants were tested within the engine operating at 2/3 load, 2500 rpm, and 100°C at midstroke, and LIF measurements were acquired from the four window locations -- three azimuthally around midstroke corresponding to windows 1, 2, and 4 and one window (6) near BC on the major-thrust side of the bore. In this order, the data corresponding to these windows are shown -- first, for the stroke-by-stroke averaged OFTs shown in Figures 4-3 (a) - (d) and second, for each stroke starting at the intake and corresponding to Figures 4-4, 4-5, 4-6, and 4-7, respectively. For each window (or figure) there are five clusters of data corresponding to the five lubricants. Each lubricant cluster displays OFTs starting with the free liner and continuing through the ring pack from the top ring to the lower OC segment.

Leading to the increasing OFT hierarchy observed within every lubricant cluster (or case), an analysis of film thickness under different rings (or effects of on ring on another) and along the free liner is addressed in the first subsection (section 4.2.1) which will facilitate understanding of stroke-by-stroke and stroke-averaged behavior for the remaining subsections.

Each lubricant cluster represents one calibrated case and, thus, one calibration coefficient. These calibration coefficients have three different levels of calibration accuracies, and, therefore, each cluster falls within one of three categories of calibration accuracy:

I. *Accuracy within plus or minus 5 percent of measured OFT.* These lubricant clusters are outlined with solid black lines.

II. *Questionable accuracy of plus or minus 5 percent of measured OFT.* Clusters are outlined with dotted black lines.

III. *Accuracy worse than 5 percent of measured OFT.* Clusters are outlined with solid light gray lines (which sometimes looks like no outlines at all).

The actual calibration coefficients and calibration accuracies for the entire test matrix are presented and explained in further detail in Table D.1 in Appendix D.

Consequently, when comparing different lubricant clusters (or cases), it is imperative to give more confidence to absolute magnitudes and trends for those cases with higher calibration accuracy and view the remaining cases as suspect. The second subsection (section 4.2.2) highlights the magnitudes and trends of these highly accurate cases for the ring pack and free liner and conducts comparisons with predictions from the *FRICTION-OFT* model. (Both the *FRICTION-OFT* and *RINGPACK-OC* models are described in Appendix E.) Since the different lubricant cases are compared with one another at the same engine operating condition, this type of effect on OFT is called the lubricant effect.

To provide a clear and succinct presentation, results are stroke-averaged -- a process justified by section 4.2.2 following the stroke-averaged results. In this section stroke-by-stroke differences (or lack thereof) are shown, interpreted, and explained through theory and numerical models applied to this specific engine and these lubricants.

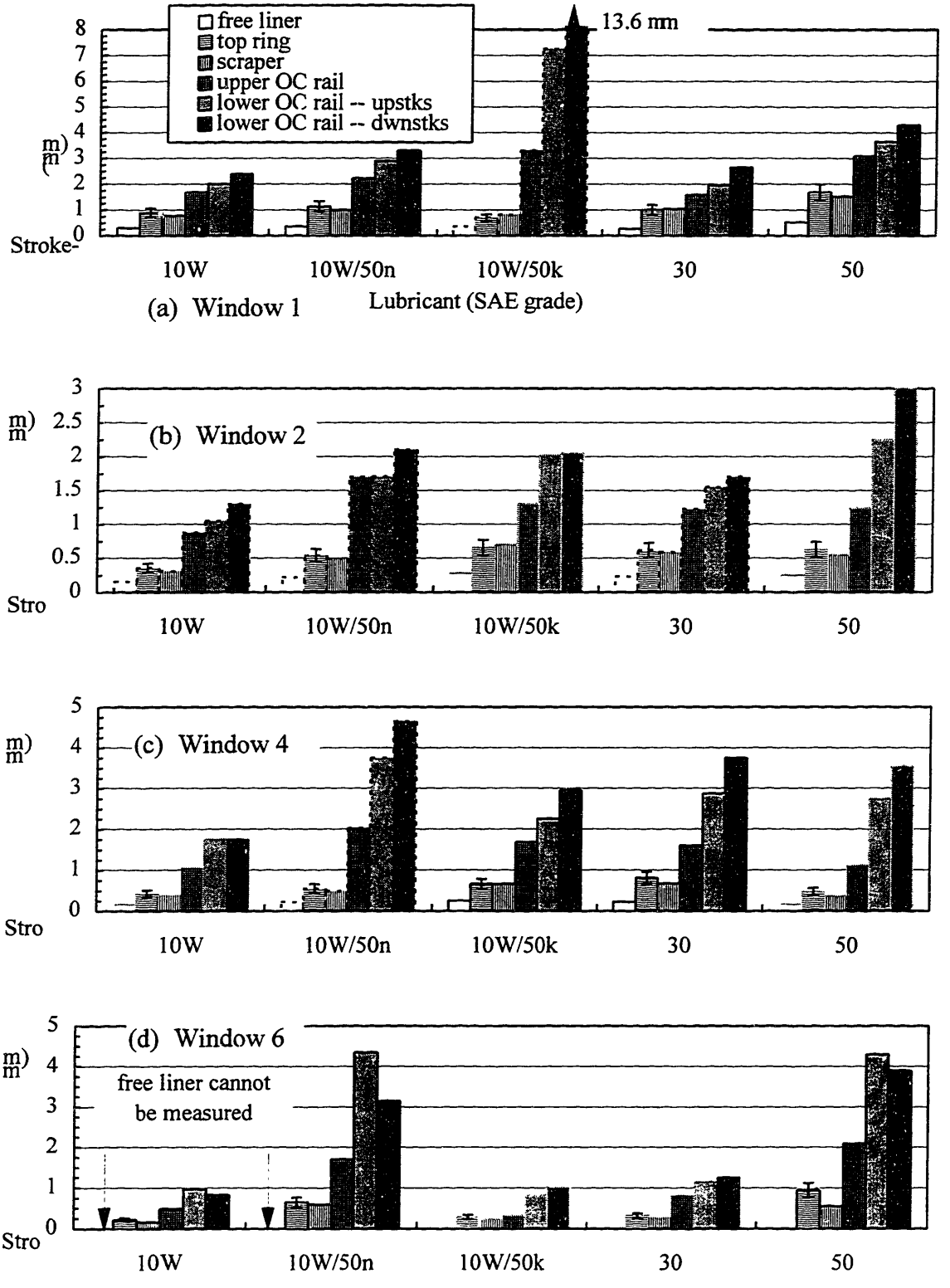

Figure 4-3 Stroke-Averaged OFT for the Five Lubricants at the Baseline Condition from Windows (a) 1, (b) 2, (c) 4, and (d) 6.
(2/3 Load, 2500 rpm, 100°C at midstroke)

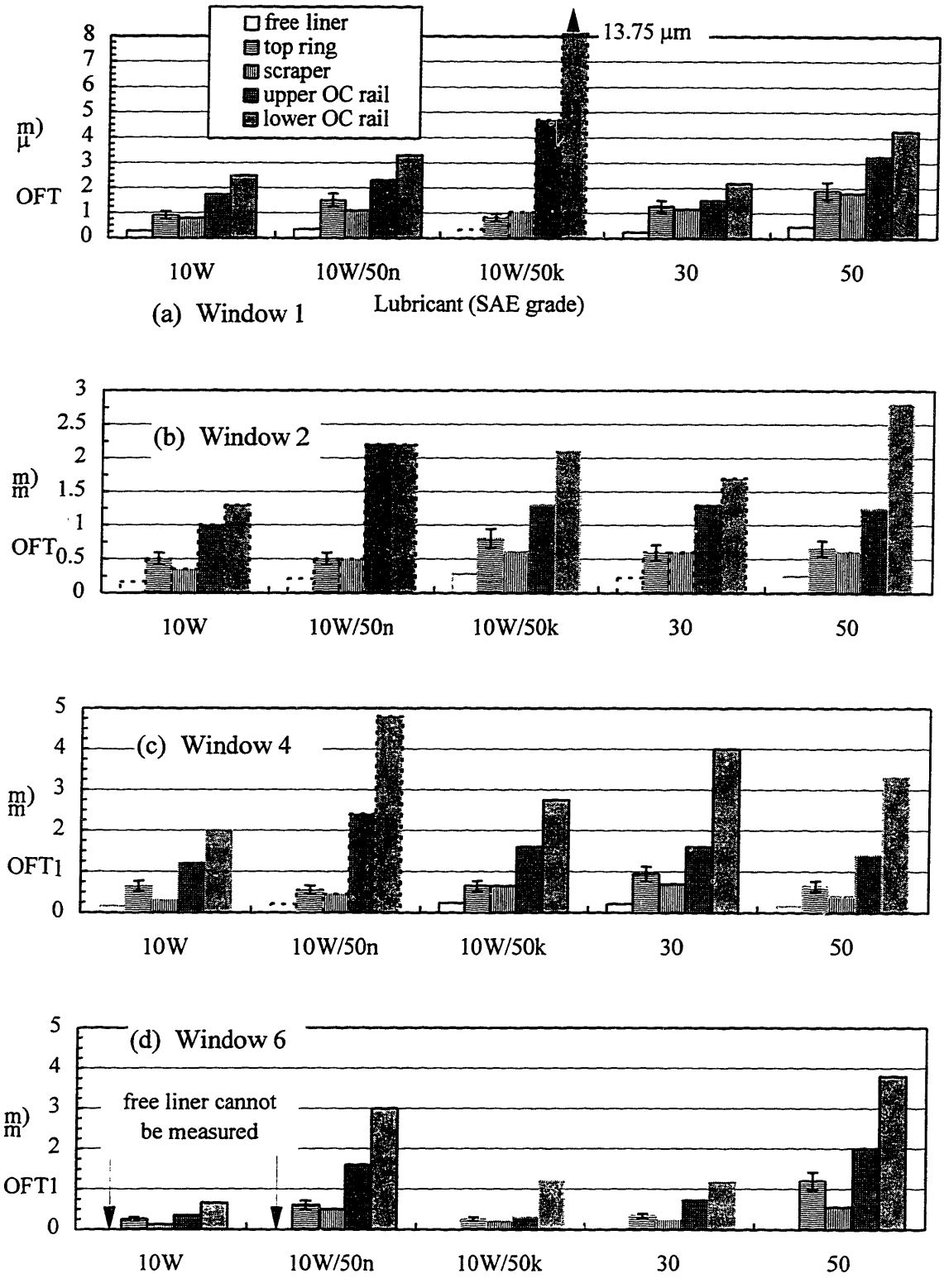

Figure 4-4 Intake Stroke OFT for the Five Lubricants at the Baseline Condition from Windows (a) 1, (b) 2, (c) 4, and (d) 6.
(2/3 Load, 2500 rpm, 100°C at midstroke)

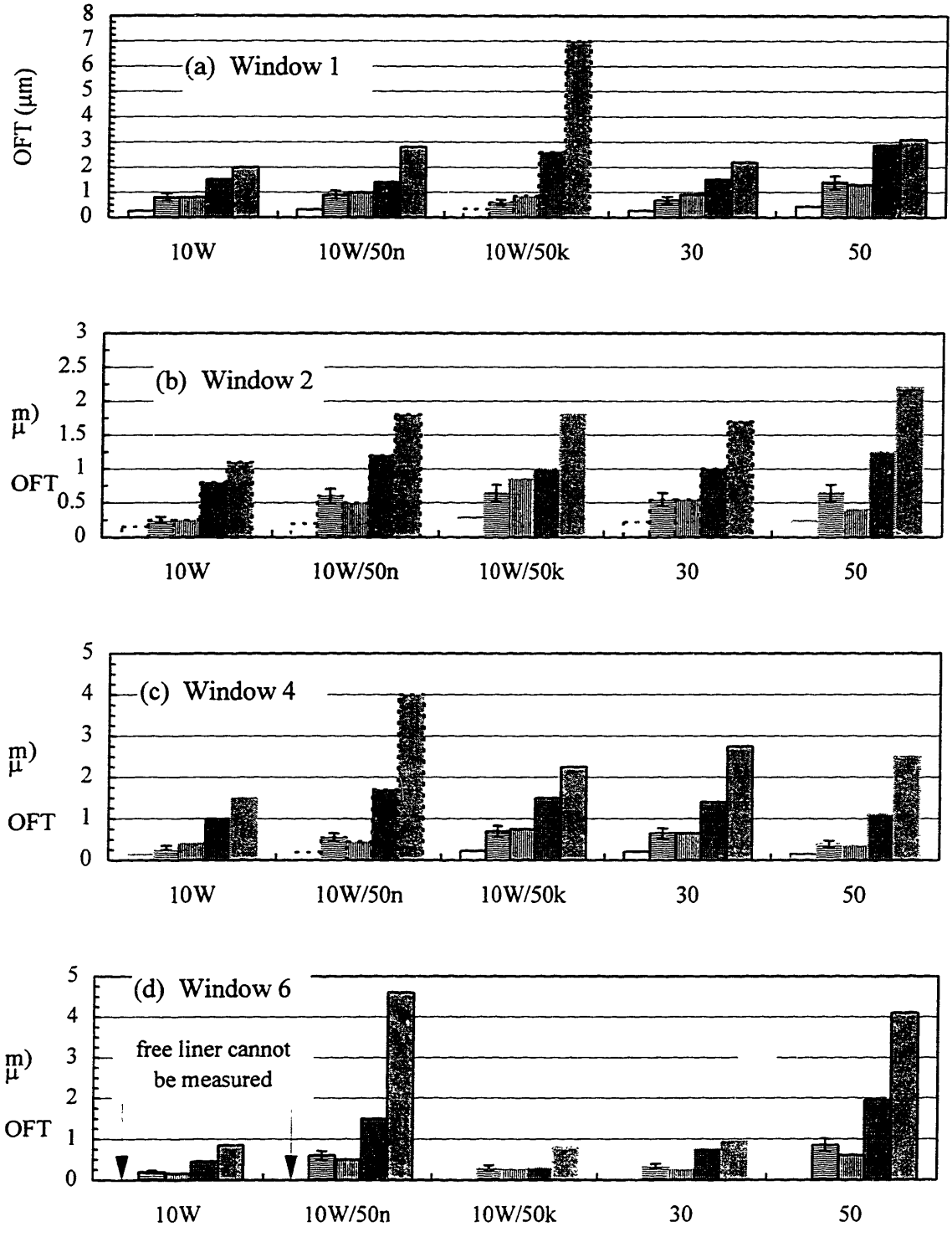

Figure 4-5 Compression Stroke OFT for the Five Lubricants at the Baseline Condition from Windows (a) 1, (b) 2, (c) 4, and (d) 6.
2/3 Load, 2500 rpm, 100°C at midstroke)

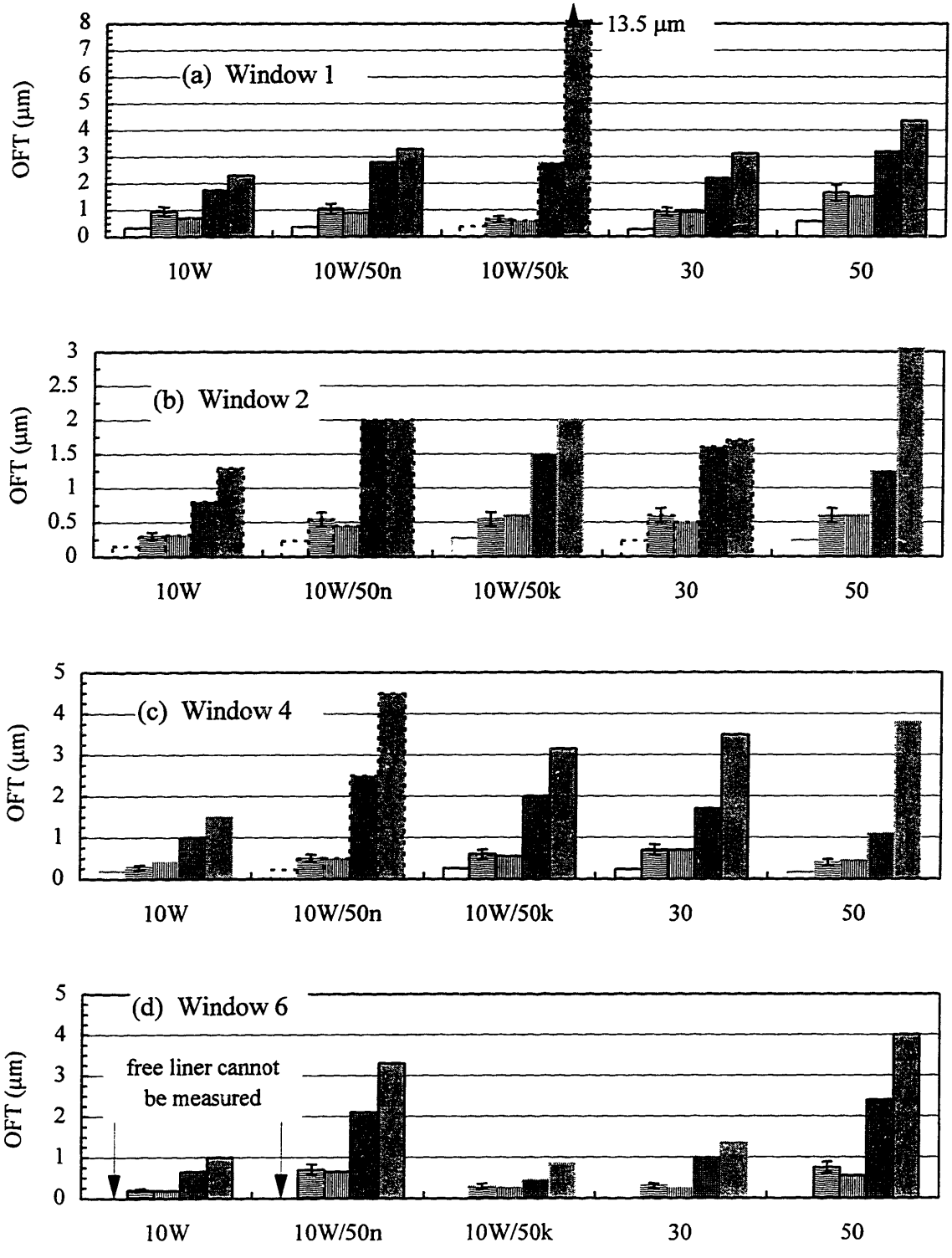

Figure 4-6 Expansion Stroke OFT for the Five Lubricants at the Baseline Condition from Windows (a) 1, (b) 2, (c) 4, and (d) 6.
2/3 Load, 2500 rpm, 100°C at midstroke)

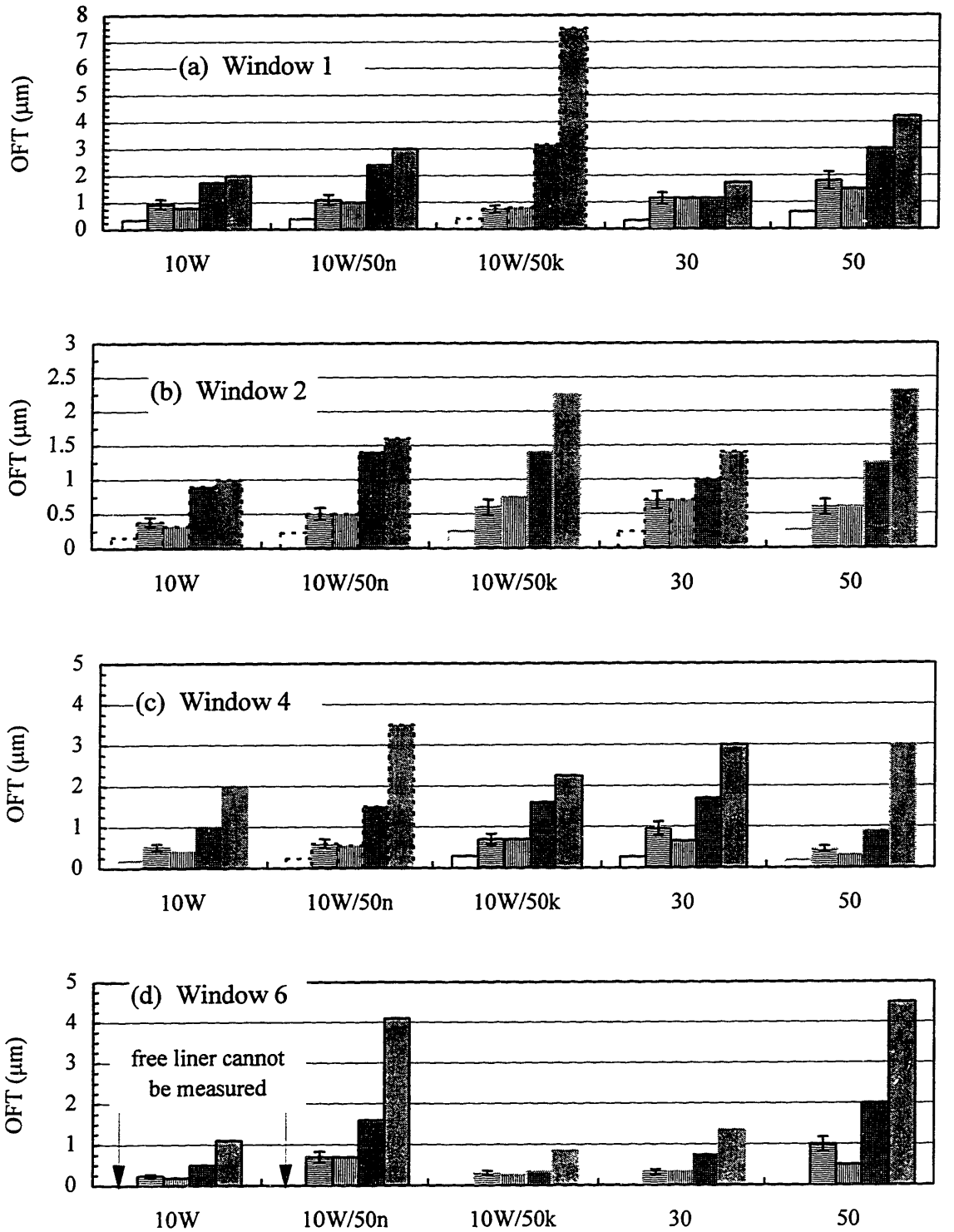

Figure 4-7 Exhaust Stroke OFT for the Five Lubricants at the Baseline Condition from Windows (a) 1, (b) 2, (c) 4, and (d) 6.
(2/3 Load, 2500 rpm, 100°C at midstroke)

4.2.1 Analysis of Film Thickness under Different Rings and along the Free Liner

Shown for any lubricant case in the baseline figures (Figures 4-1 - 4-7) or the off-baseline data (Figures 4-24(a) - (c)) for the individual strokes and the stroke-averaged results, a hierarchy of film thickness under different rings and along the free liner is evident. OFT increases in the following order: free liner, top and second rings (having the MOFTs), upper OC rail, and lower OC rail. Therefore, the ring pack is generally fulfilling one of its functions by controlling the vast oil supplies from the skirt regions and sump.

The top and scraper rings have approximately the same MOFTs, and the free-liner OFT is about half of this magnitude. Although the ring profiles, ring tensions, boundary conditions, lubricant properties, land pressures all influence the MOFTs of the rings and segments as their speed changes throughout a stroke, the free-liner OFT and MOFT of the top ring are mostly determined by the performance of the scraper ring if two conditions are satisfied. First, the top ring is starved, and no scraping occurs as shown in Figure 4-1 (a). Secondly, the sliding speed is fast enough so that ring squeezing is close to negligible.

Directly observed when manually fitting the top ring to the OFT trace, the first condition is always satisfied where the top ring is starved for all window locations -- midstroke and near BC. Additionally, all numerical calculations throughout this thesis confirm this finding as well.

The second criterion is satisfied even at the window 6 location -- near BC -- shown by both an analytical argument and numerical calculations. The analytical argument from order-of-magnitude scaling is presented in Appendix G and shows that the time-dependent terms of equation G.3 are negligible for the measured ring parameters, lubricant properties, and engine conditions from the Kohler engine provided near the end of the appendix. Again, the numerical calculations from the *FRICTION-OFT* model confirm negligible ring squeezing as well for the window locations along the liner.

Consequently, for a ring with a starved converging wedge which includes the top ring during all strokes and scraper during its upstroke, their MOFTs are slightly less than twice the liner OFT. This result agrees with a more rigorous studies. In a numerical

study by Tian [13], the MOFT is approximately 1.8 times the free-liner OFT. In a more general study including surface tension by Coyne *et al.* [14], ratios may vary from a little less than two to three for the window locations in the Kohler engine depending upon the nondimensional number, $N = (3\mu U/T)^{1/3}$.

Since during a downstroke the scraper ring always scrapes oil supplied by the OC ring, the MOFT of the scraper is always less than the MOFTs of the OC ring. Usually, the segments of the OC ring have different MOFTs as well. The lower OC segment always has the same or greater MOFT than the upper OC segment. The oil supply from the skirt regions always provides enough oil for the lower OC segment to be fully-flooded and, thus, generates maximum hydrodynamic lift.

However, the same cannot be said about the upper OC segment which has a similar but mirror-imaged geometry. Some segment fits of the upper OC rail showed only partial flooding despite the vast amount of oil in the third land region. A large fraction of this oil may be on the land and not contribute to fully-flooding conditions of the upper segment during the upstrokes.

Behavior of the OC ring has a marginal influence on the top and scraper ring behavior. In all the cases of the current database, the OC ring always allows enough oil supply for the converging wedge of the scraper to be fully-flooded during the downstrokes, and the behavior of a fully-flooded ring is not affected by the excess oil it scrapes.

In summary, for any lubricant case an OFT hierarchy exists for the free liner and rings; OFT increases in the following order: free liner, top and second rings (having the MOFTs), upper OC rail, and lower OC rail. To interpret the OFT hierarchy, the unsteady behavior in the lubricant flow under the rings including ring squeezing and inlet wetting variation can be neglected throughout most of the stroke including the liner location at window 6 (and, of course, not the varying ring speed affecting ring lift). Therefore, lubricant behavior above the scraper ring is predominantly affected by the scraper's behavior even through the near-BC window location. During a downstroke, the fully-flooded convergent wedge of the scraper allows leaves some oil on the liner available for

the starved top ring. This liner OFT is roughly one half of the MOFT magnitudes of the top and scraper rings. Once the top ring passes, it leaves the free-liner OFT -- the same magnitude as the liner OFT left by the scraper. On the return upstroke, the same free-liner OFT is now intercepted by the starved top ring leaving a liner OFT along the second land region which is the same magnitude as the free liner. Intercepting the liner OFT, the scraper MOFT is approximately twice this amount and equal to the MOFT of the top ring when it passed the same liner location. Thus, if effects on ring behavior from piston tilt and late-compression and expansion pressures are negligible, the MOFTs of the top and scraper rings and the free-liner OFT should be the same from stroke to stroke. (However, scraper behavior on OFT can be modestly affected from land pressure differences and piston tilt on the relative profile of the ring face to the liner. These effects on stroke-by-stroke variations of the top and scraper MOFTs and free-liner OFT are discussed in detail in section 4.2.3 as well as stroke-by-stroke differences of the segment MOFTs from the three-piece OC ring.)

Analytical and numerical theory confirm these experimental findings based on locally fully-developed flow throughout almost all of a stroke. Not only is the lubricant entrance length negligible, but ring squeezing and inlet wetting variation is negligible at midstroke and near-BC window locations. Through additional scaling shown in Appendix G, an analytically theoretical argument shows that the MOFT of a ring with a starved converging wedge is roughly twice the oil supplied from the liner; this finding is in agreement with a more general numerical studies by Coyne *et al.* [14] and Tian[13].

4.2.2 The Lubricant Effect

One logical and succinct way to extract general magnitudes and trends from the baseline measurements is to display the stroke-averaged OFTs from the different lubricant cases with high calibration accuracy as a function of kinematic viscosity shown in Figures 4-8 (a) - (d). Each figure corresponds to one of the four windows. Along the abscissa, lubricant viscosities correspond to the 100°C midstroke liner temperature and the high-shear values for the multigrades. (Section 2.2 shows that MOFTs are insensitive to the low-shear viscosities for the multigrades under all of the rings and at all window

locations and engine operating conditions within the test matrix.) For the same load condition, liner temperature, and speed, the resulting effect on OFT magnitudes and trends is called the lubricant effect. The hollow and shaded symbols correspond to the OC segment OFTs and the remaining OFTs, respectively, which include the top and scraper ring MOFTs and free-liner OFT.

Accompanying the measurements in the figures are numerical predictions from the *FRICTION-OFT* model. Predictions in the figures are symbolized with long dashed-dotted lines. At midstroke, the top ring MOFT is less than two percent greater than the scraper MOFT and, thus, is shown in the figures to represent both the top and scraper MOFTs. The one-piece OC ring from the model predictions have modestly different MOFTs between upstrokes and downstrokes; however, the average value is shown among the figures, and the MOFT percent differences from this average are less than five percent.

Uncertainty is included for the top ring and, again, roughly 20 percent of the MOFT for these cases of high accuracy. (Uncertainty bars for COV of 20 percent are implied for the remainder of the experimental MOFTs, only to avoid cluttering the figures. Uncertainty for the free liner is about half of this amount.) Here, this uncertainty not only includes the standard deviation but also the calibration accuracy of each respective case because two or more cases which were independently calibrated are being compared. These different components of uncertainty can be combined as proposed by Taylor [15] shown in Appendix F. However, because of the high calibration accuracy (or low calibration uncertainty), total uncertainty is still roughly 20 percent dominated by the standard deviation of our measurements. For cases with worse accuracy corresponding to accuracy categories II and III and noted in the figures, the 20 percent should be viewed as a lower limit to the actual uncertainty.

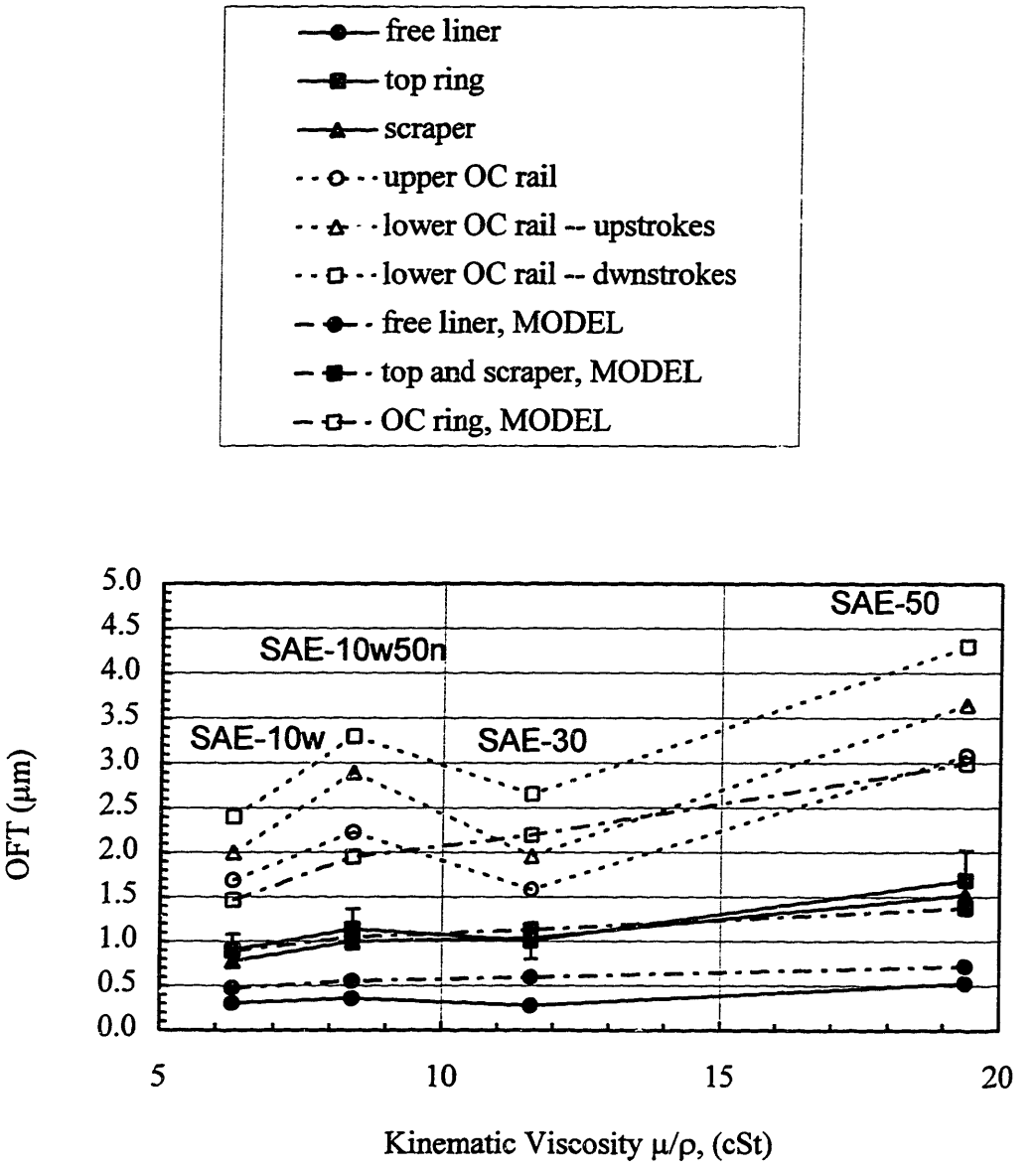
free liner
top ring
scraper
upper OC rail
lower OC rail -- upstrokes
lower OC rail -- dwnstrokes
free liner, MODEL
top and scraper, MODEL
OC ring, MODEL
SAE-50
SAE-10w50n
SAE-10w
SAE-30
OFT (μm)
5.0
4.5
4.0
3.5
3.0
2.5
2.0
1.5
1.0
0.5
0.0
5
10
15
20
Kinematic Viscosity μ/ρ, (cSt)

(a) Window 1

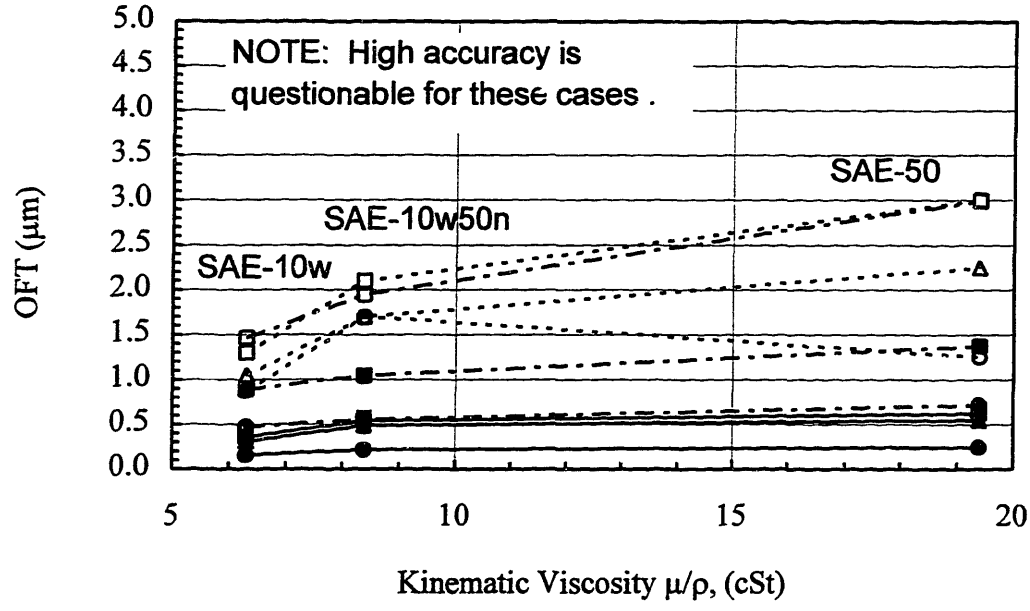

(b) Window 2

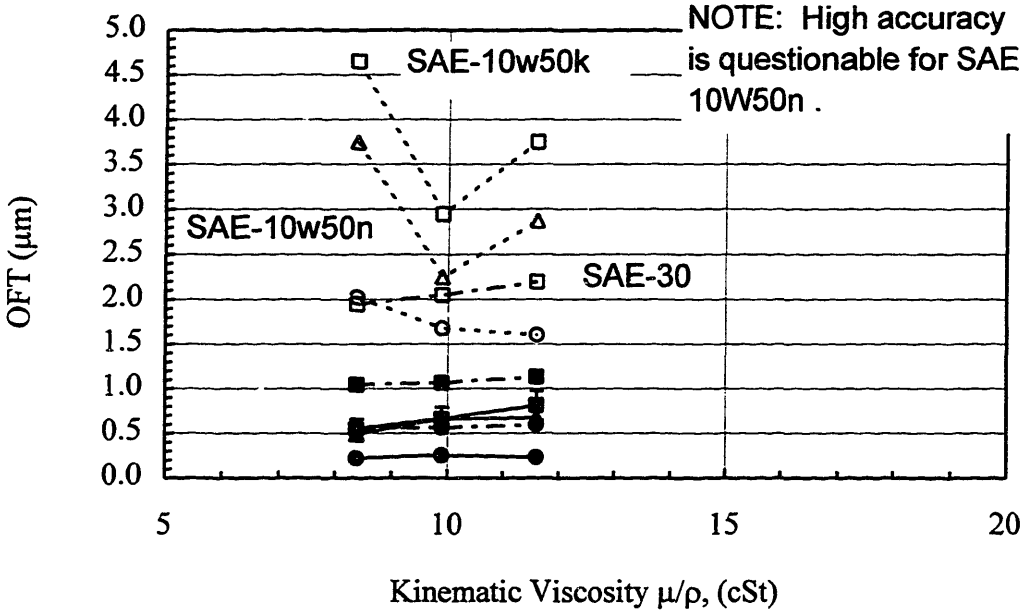

(c) Window 4

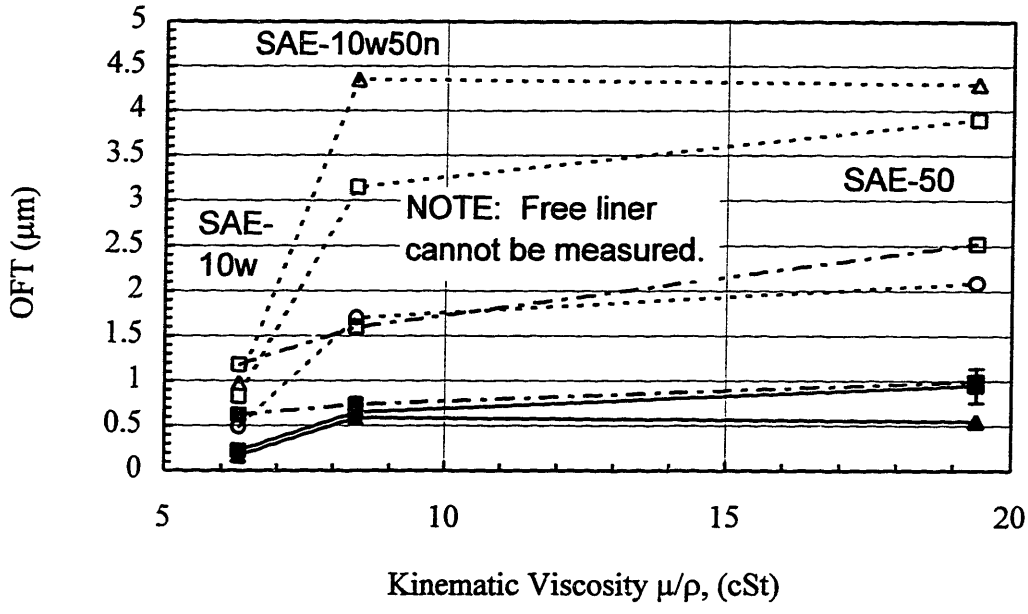

(d) Window 6

Figure 4-8 Baseline OFT Measurements and Model Predictions from Windows (a) 1, (b) 2, (c) 4, and (d) 6.
(2/3 Load, 2500 rpm, 100°C)

Although the OFT hierarchy of the liner and rings addressed in section 4.2.1 are further confirmed in the figures among the three lubricants, the magnitudes within this hierarchy change from lubricant to lubricant and from one window location to another. Overall trends show that the lubricant viscosities have a predominant effect on OFT; OFT increases with increasing viscosity -- characteristic of hydrodynamic lubrication.

Having the greatest number of OFT measurements with high calibration accuracy, window 1 shows good agreement for the OFT magnitudes and trends between the model and measured OFTs for the free liner and under the compression rings and rail. With the exception of the OC segments of SAE-30, the model predicts the magnitudes and trends of the MOFTs of the top ring, scraper, and upper OC segment within their standard deviations. However, the model overpredicts the measured free liner OFT but not more than a factor of two.

Although the calibration accuracies from window 2 are questionable (category II), the measured OFTs show the same increasing trend with viscosity and, therefore, are

consistent with the model trends. However, the model magnitudes overpredict by over a factor of two for the free liner and top and scraper rings. This overprediction may lend more to data calibration inaccuracy and/or effects of bore out-of-roundness (OOR) on the measured OFT than model magnitude inaccuracy. Effects of bore distortion on OFT are addressed later in section 4.6.

Magnitude overpredictions by a factor of two for the free liner and top and scraper rings also exist for the highly accurate cases at window 4. Near BC at window 6, the model predictions agree very well for the upper OC segment and top and scraper rings and typically within their standard deviations except for the overprediction of SAE-10W.

At the baseline condition, both the OFT measurements and theory from numerical calculations and analytical scaling from Appendix G show that lubricant viscosity has a predominant effect on OFT along the free liner and under the rings; OFT increases with lubricant viscosity -- behavior characteristic of hydrodynamic lubrication. However, other parameters besides viscosity may play a role in the more subtle differences. For instance, SAE-10W/50n has a high-shear viscosity much closer to SAE-10W than -50 and high-shear is definitely occurring for all windows (see sections 2.2 and 4.5). Yet, all too often the OFTs of SAE-10w/50n are closer to SAE-50's OFTs than SAE-10W's OFTs, and this behavior occurs in Figures 4-8 (a), (b), and (c). (Viscosity is the only lubricant parameter within the model, and model predictions do not show this behavior as well.) Thus, SAE-30 in Figure 4-8 (a) tends to have slightly less OFT than the less-viscous SAE-10W/50n making the pure OFT-viscosity relationship less clear. This slightly higher OFT behavior of multigrades implies lesser friction for multigrades. Friction reduction from multigrade lubricants has also been found by Azzola *et al.* [16]; however, the finding by Hoult suggests effects of surface tension which the current *FRICTION-OFT* model does not include.

4.2.3 Stroke-By-Stroke Differences

This section investigates the stroke-by-stroke differences and trends for the MOFTs within the ring pack and OFT along the free liner. Measured from a 10 cycle-trace average, the stroke-by-stroke differences in OFT are measured by comparing the

OFT from a particular window location along a stroke to other strokes in the cycle. Results will show the differences and trends for the lower OC segment between the upstrokes and downstrokes and justification for the four-stroke MOFT average for the top and scraper rings and the upper OC rail in view of the approximate 20 percent COV. Additionally, having greater precision and COVs about half of the MOFT COVs, the free-liner OFTs are shown to have some significant stroke-by-stroke differences and consistent trends. Plausible explanations include effects from piston tilt and land pressures and are investigated with *RINGPACK-OC* and *FRICTION-OFT* models. All results highlight the baseline measurements but also include some off-baseline data to further substantiate conclusions and point out the rare exceptions to the general and consistent trends found within the entire database.

4.2.3.1 The OC Ring -- the Upper and Lower OC Segments

Although only highlighting the highly-accurate baseline cases at window 1, Figure 4-9 (a) is typical of the random variations for upper rail MOFTs between lubricants over the entire database. For some random cases such as SAE-50 in the figure, the MOFT trends show greater MOFTs during the downstrokes than the upstrokes although the differences are suspect due to overlapping standard deviations. Other cases show no trends such as SAE-10W, -10W/50n, and -30 in the same figure. The cases with the trends are random, and no more of these cases are found for one condition versus another.

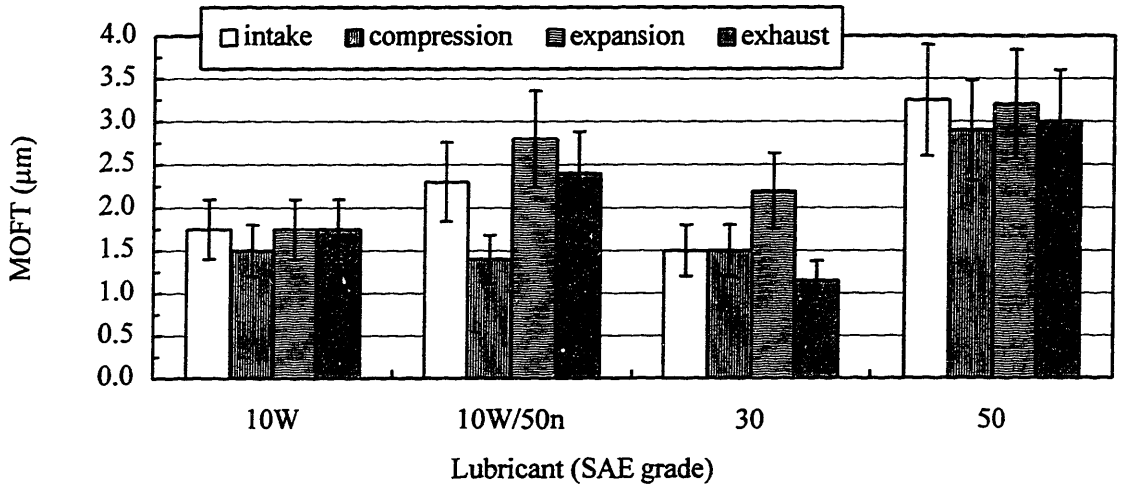

(a) Upper OC Segment

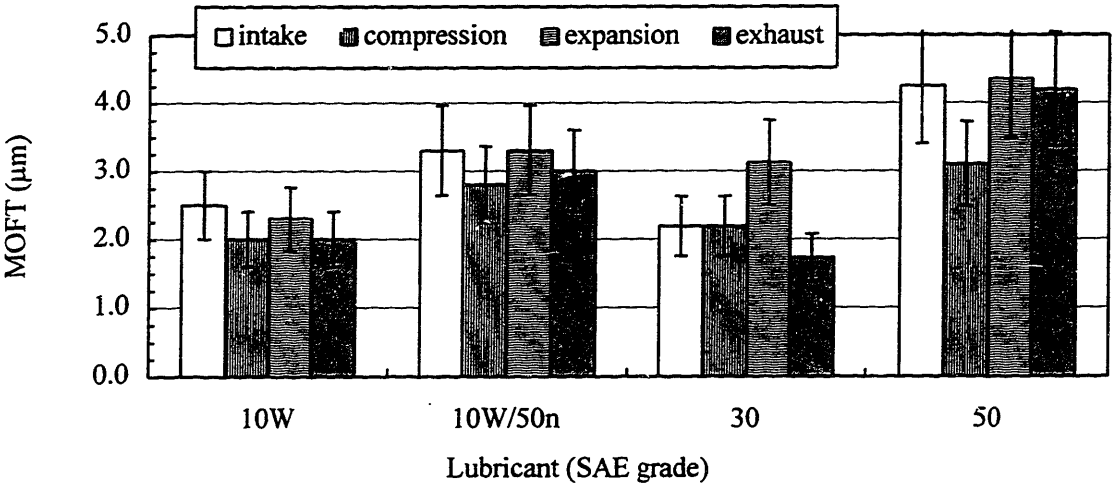

(b) Lower OC Segment

Figure 4-9 Stroke MOFTs at Baseline from Window 1 for (a) Upper OC Segment and (b) Lower OC Segment

However, for the lower OC segment for a high majority of the cases at midstroke, the downstroke MOFTs are greater than the upstroke MOFTs, and even non-overlapping standard deviations occur for a few cases. This pattern is illustrated in Figure 4-9 (b) taken from the baseline running condition at window 1.

From the clear majority of cases with this stroke-by-stroke trend for the lower OC segment, averages for the downstrokes and upstrokes were calculated as shown in the stroke-averaged results in the previous section for the baseline results. To illustrate that

this trend is found for different lubricants, azimuthal window locations at midstroke, and engine operating conditions including engine speeds of 1800 and 2500 rpm, liner temperatures from 40 to 100°C, and load conditions (2/3 load versus motored WOT), many cases are shown in Figures 4-10 (a) - (d).

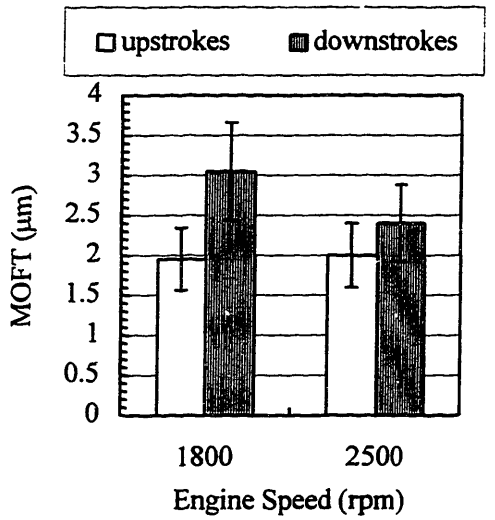

(a) SAE-10W
(Window 1, 2/3 Load at 100°C)

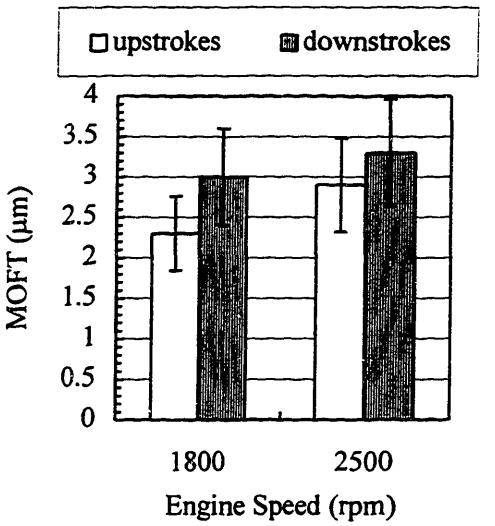

(b) SAE-10W/50n
(Window 1, 2/3 Load at 100°C)

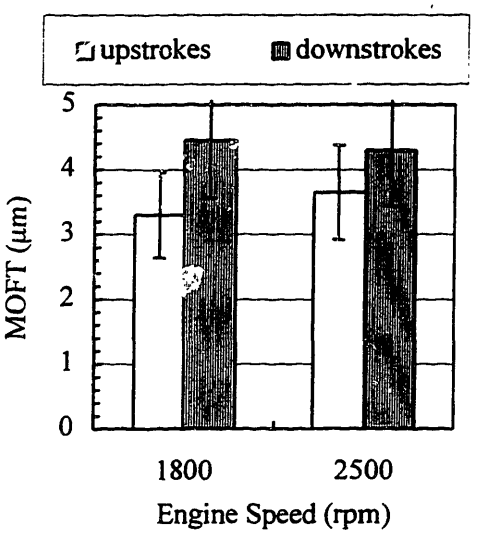

(c) SAE-50
(Window 2, 2/3 Load at 100°C)

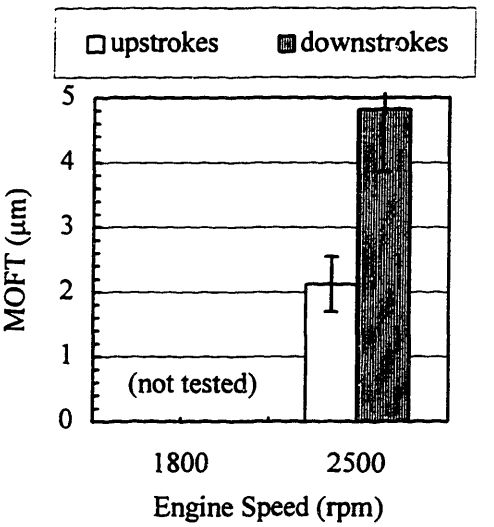

(d) SAE-10W/50k
(Window 4, motored WOT at 40°C)

Figure 4-10 Midstroke Window Locations: Stroke-Averaged Upstroke Versus Downstroke MOFTs of the Lower OC Rail at 1800 and 2500 rpm for (a) SAE -10W, (b) -10W/50n, (c) -50, and (d) -10W/50k.

Addressed in detail in Appendix C, the dynamic behavior of the three-piece oil control ring during a cycle is poorly understood which precludes accurate modeling. In view of the results from above, one possible and simplistic conceptual explanation is as follows. One may consider both the upper and lower OC segments to be narrow scrapers with their scraping edges facing each other separated by the expander shown in Figure C-4. (Detailed segment geometry is shown in Figures C-2 (c) and (d).) Additionally, consider the expander to be a restricted one-dimensional spring only allowing the segments to move radially with respect to each other. Since the large converging wedge of the lower OC rail during a downstroke is always fully-flooded, it should experience its greatest hydrodynamic force as opposed to its upstroke scraping with no convergent wedge. However, the lower OC segment is coupled via the expander to the upper OC rail which is experiencing its greatest hydrodynamic lift during the upstrokes due to its large convergent wedge. Thus, the lower rail is weakly supported by this lift through the expander (or spring).

Now, if both convergent wedges of the rings are fully-flooded throughout the cycle, have the same mirror-image profiles, and pressure conditions are the same on both sides of the ring (assuming negligible changes in segment and piston tilt as well throughout a stroke), one would expect the lower rail behavior during the downstrokes to be similar to the upper rail behavior during upstrokes; on the downstrokes the lower OC rail would experience greater MOFT than the upper OC rail, and on the upstrokes the upper OC rail would experience greater MOFT than the lower OC rail. In other words, the MOFT of the lower OC segment would be the same during the intake and expansion strokes and greater than the upper segment MOFT. Conversely, during the compression and exhaust strokes, the upper OC segment would have the larger MOFTs. The segment with the lower MOFT is scraping with no converging wedge; but its MOFT isn't zero because the expander (the radial spring) provides ring lift from the segment with the higher MOFT.

However, in most cases, contrary to the boundary conditions for the lower OC segment, the upper segment doesn't seem to be fully-flooded in the data, although the

actual profile-trace fit is often difficult to discern. Therefore, in these instances, the upper OC rail won't experience as much hydrodynamic lift on the upstrokes as previously experienced under fully-flooded conditions. It's plausible that this lesser lift is enough to cause approximately equal upper rail MOFTs on all strokes and still allow greater lower rail MOFTs during downstrokes than upstrokes. To make this simple conceptual model more complete, adding a radial spring offset between the upper and lower OC rails would cause a greater MOFT for the lower OC rail than the upper rail for all strokes as observed in the data.

This simple conceptual model is only intended as a starting point for developing a more comprehensive, numerically quantitative model and provide insight to how the segments may be interacting within the expander and with the lubricant boundary conditions at midstroke. By far, midstroke behavior is the easiest region to describe compared to regions around dead centers where the most complicated activity is occurring; time-dependent squeezing and high friction forces from boundary lubrication which changes rail angular position with expander and groove [17] are only two of many issues. Additionally, piston movement has shown to affect radial movement of the OC ring [17].

Near BC at window 6, results from MOFT measurements further confirm the complicated OC ring behavior. Although trends of the lower OC MOFTs at window 6 for 1800 rpm are the same as midstroke but less pronounced, the MOFT trend of the lower OC segment reverses at 2500 rpm; the upstroke MOFTs are now greater than downstroke MOFTs. Many cases are shown in Figures 4-11 (a) - (d) to illustrate that this trend is found for the same lubricants with opposite trends at midstroke and engine operating conditions including different liner temperatures from 40 to 100°C and load conditions (2/3 load versus motored WOT). Although these stroke-by-stroke trends at midstroke and near BC for the OC ring are highlighted within this section, these OC ring trends are also mentioned less explicitly but shown in additional data in sections 4.3 (off baseline results) and 4.4 (speed effects).

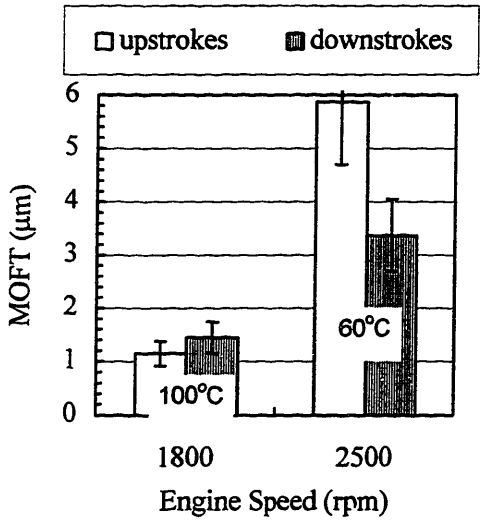

(a) SAE-10W
(Window 6, 2/3 Load)

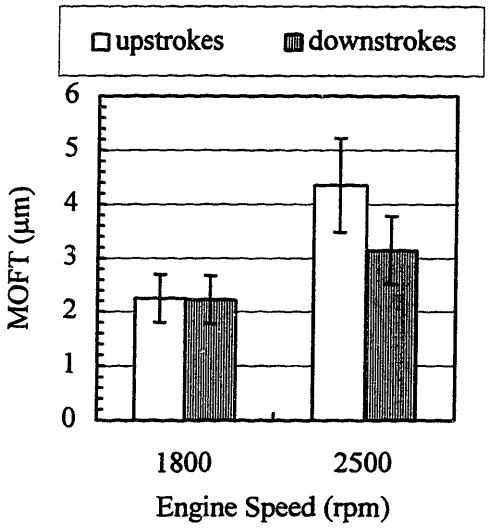

(b) SAE-10W/50n
(Window 6, 2/3 load at 100°C)

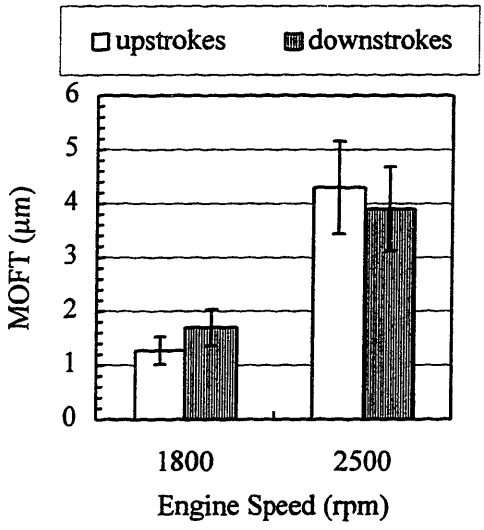

(c) SAE-50
(Window 6, 2/3 load at 100°C)

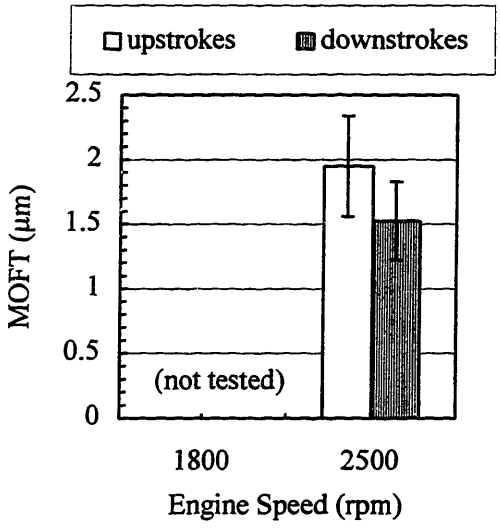

(d) SAE-10W/50k
(Window 6, motored WOT at 40°C)

Figure 4-11 Window 6: Stroke-Averaged Upstroke Versus Downstroke MOFTs of the Lower OC Rail at 1800 and 2500 rpm for (a) SAE-10W, (b) -10W/50n, (c) -50, and (d) -10W/50k.

4.2.3.2 The Top and Scraper Rings

Stroke-by-stroke differences in the MOFTs of the top and scraper rings during a cycle are found to be insignificant in view of the standard deviation exemplified by Figures 4-12 (a) and (b), respectively. However, for some random cases for the top ring, the MOFTs for the intake stroke tend to be higher than the remainder of the strokes. Whether this stroke-by-stroke trend is actually occurring is questionable because the OFT trace in the regions of the top and scraper rings were the most noisy regions and particularly so during the intake stroke. An exact MOFT is unclear, and only a good approximation may be determined by the discretion of an experienced ring-fitter. Therefore, in view of this fact and the standard deviations, one cannot conclude that significant stroke-by-stroke differences are occurring.

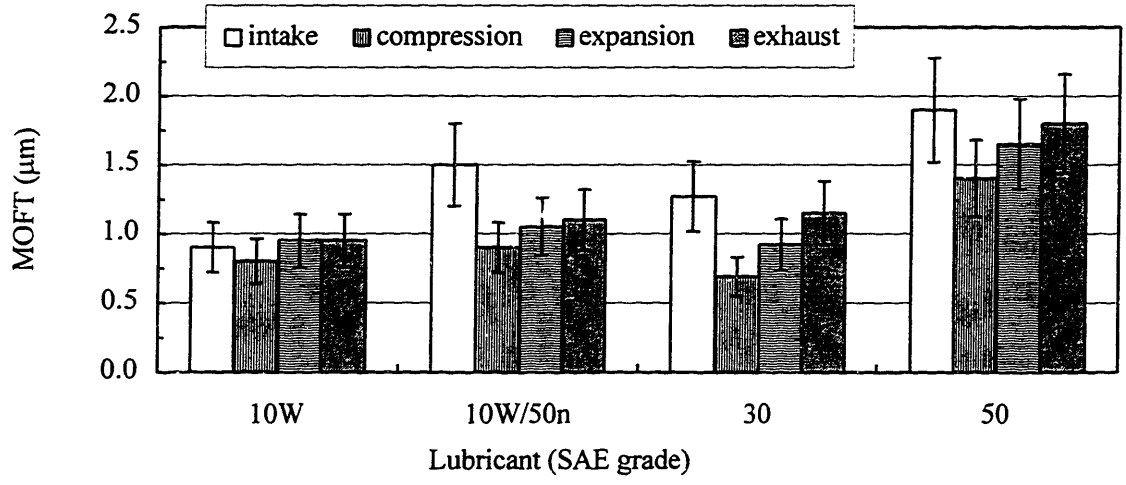

(a) Top Ring

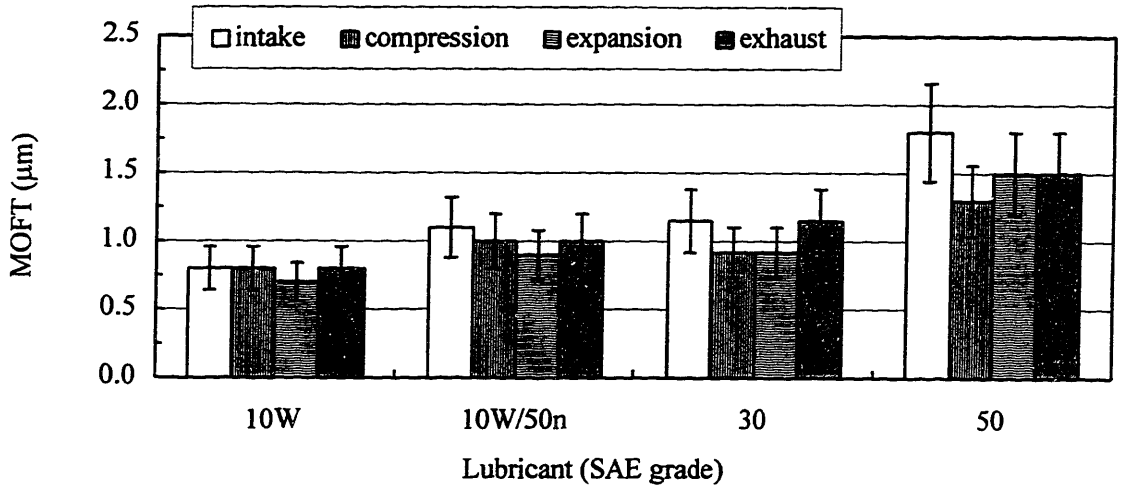

(b) Scraper Ring

Figure 4-12 Stroke MOFTs at Baseline from Window 1 for (a) Top Ring and (b) Scraper Ring

These results are consistent with the analytical arguments toward the end of section 4.2.1 and numerical predictions from the Friction OFT model which support approximately equality of MOFTs from stroke to stroke; MOFTs from stroke to stroke for the top and scraper rings are approximately equal provided that other secondary effects on MOFT are negligible. The other effects include late-compression and expansion pressures and piston tilt. The approximate equality of stroke-by-stroke MOFTs indicates that the secondary effects on MOFTs are relatively minor and don't show up in view of the precision of our measurements for the top and scraper rings.

The effects of land pressures, ring dynamics, and piston tilt on MOFT are addressed experimentally and numerically using *RINGPACK-OC* and *FRICTION-OFT* in the next section on the free-liner stroke-by-stroke differences where precision is much higher and significant differences and trends are observed.

4.2.3.3 The Free Liner

Although stroke-by-stroke differences in the MOFTs of the top and scraper rings are not detected, often the free-liner OFT is not the same among the four strokes; in some

cases, the standard deviation of the stroke OFTs do not overlap. At midstroke on the major-thrust side, the free-liner OFT corresponding to the intake and compression strokes are less than the expansion and exhaust strokes. Typical examples are given in Figure 4-13 from the baseline condition from window 1.

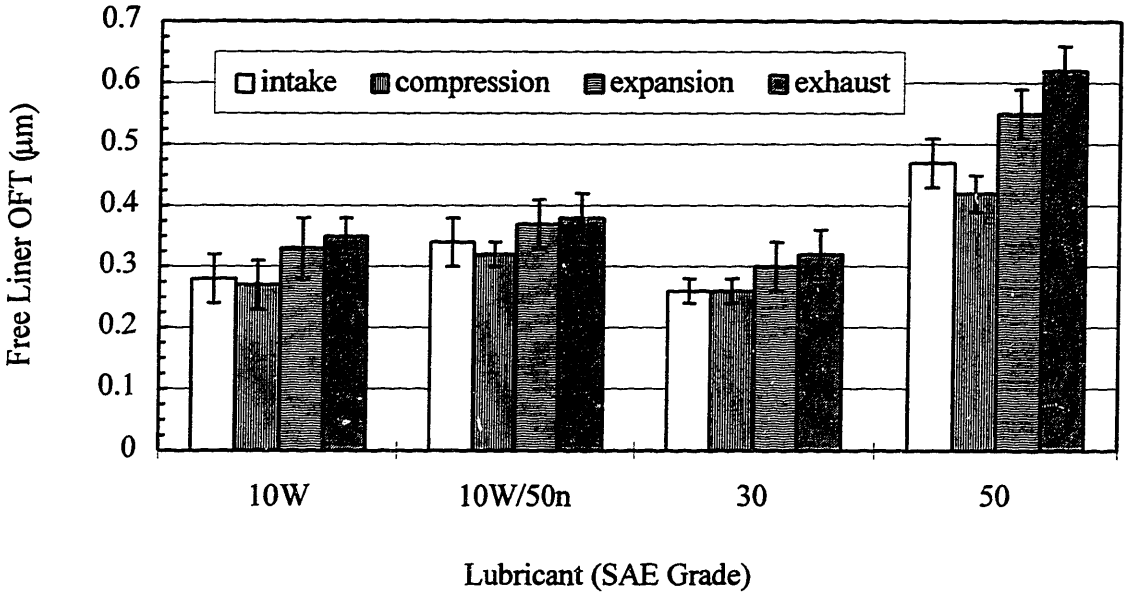

Figure 4-13 Stroke Free-Liner OFT for the Baseline Condition at Window 1 for Highly Accurate Cases.

The free-liner OFTs of the intake (expansion) and compression (exhaust) strokes are equivalent because the piston assembly does not pass over or disturb this oil film in front of the midstroke windows during this portion of piston reciprocation. Referring to Figure D-5, after about 92° ATC the LIF system measures the free-liner oil film continuously as the piston reciprocates through the latter half of the downstroke, BC, and the former half of upstroke ending at 268° ATC. Unless something disturbs the free liner OFT as the piston translates from 92 - 268° ATC through BC, the continuous free-liner OFT shouldn't change, and this result is, indeed, observed in the measurements. (One stroke measurement in Figure 4-13 is an average of the OFT trace over the first five millimeters above the top of the crown land corresponding to the first 9° after top of crown land passage.)

However, at midstroke on the major-thrust side the last two strokes corresponding to the expansion and exhaust strokes are reasonably greater than the first two strokes of the cycle between a 10 to 40 percent increase for most cases shown in Figures 4-13 and 4-14. Figures 4-14 (a) - (c) show the percent increase from the first two strokes to the last two strokes of the cycle for different midstroke liner temperatures. This trend is a common pattern among the fired cases although the motored cases are less clear. (This trend also occurs at the lower speed of 1800 rpm (at 100°C) but the effect is also not as severe. The percent increase is calculated by the percent change in OFT from averaged intake and compression strokes to averaged expansion and exhaust strokes. Standard deviations are adjusted according to equations in Appendix F.)

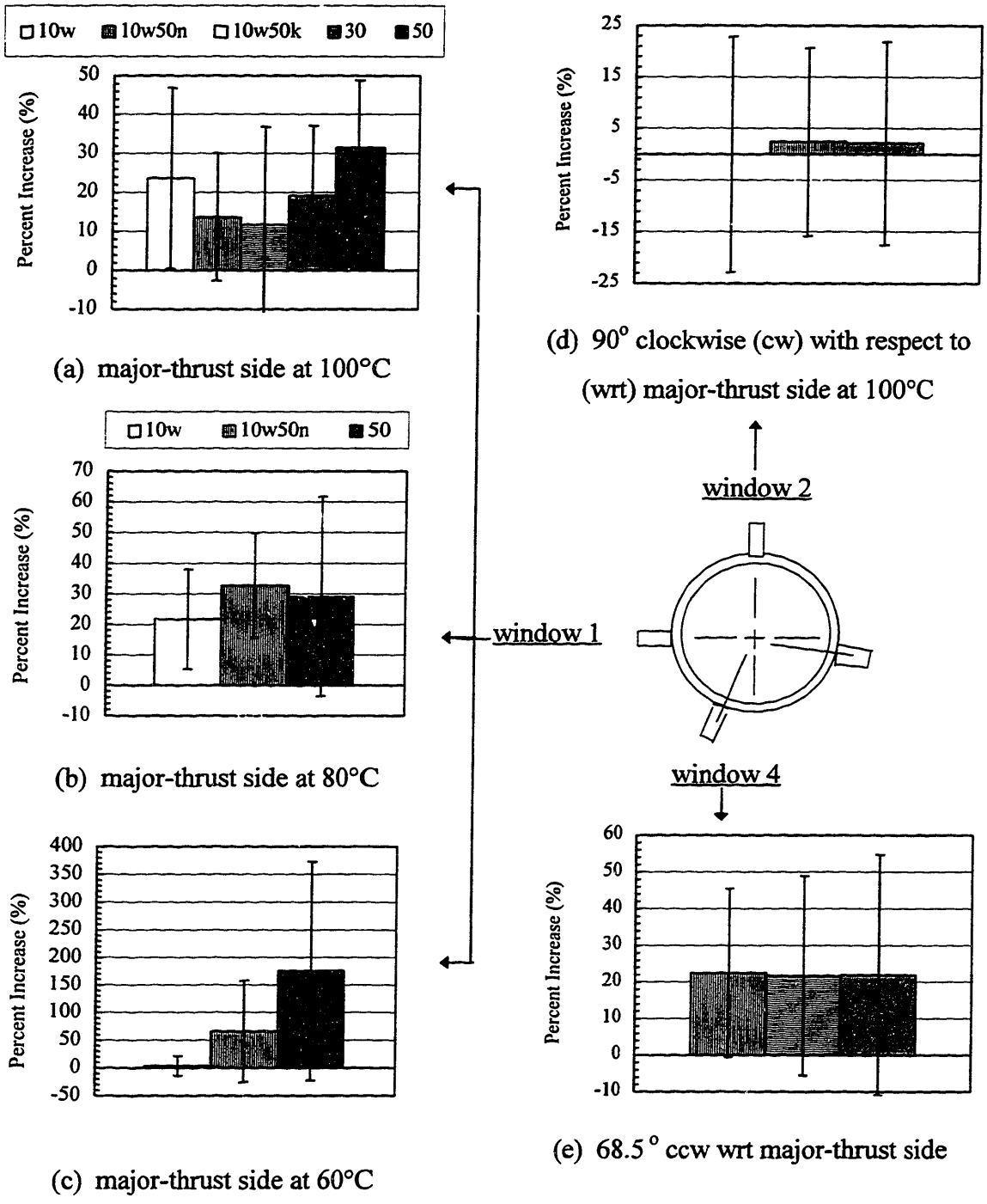

Figure 4-14 Percent Increase in Free-Liner OFT from First Two to Last Two Strokes at Midstroke at Major-Thrust Side for Liner Temperatures of (a) 100, (b) 80, and (c) 60°C. Measurements Off the Major-Thrust side at 100°C corresponding to windows 2 and 4 include (d) 90° cw and (b) 68.5 ° ccw wrt major-thrust side, respectively. (2/3 Load)

For some cases the percent increase in free-liner OFT is so great that the lower bound of standard deviation falls well above zero micrometers; this result implies that the percent change is certainly significant.

Before continuing, it is important to note that the precision of these measurements from stroke to stroke is extremely high. The automated free-liner measurements avoid the human error previously incurred in the MOFT measurements from the manual ring fitting. Additionally, the free-liner COVs are the exact values from the 10 cycles and not from a general COV correlation; free liner COVs are usually about half the MOFT COV value of approximately 20 percent. Consequently, although MOFTs from the top and scraper rings reveal no significant differences and trends in view of the poorer precision, the free-liner OFT with high precision reveals differences and trends among the strokes caused by secondary effects that are otherwise masked in the top and scraper MOFTs. (Although the free-liner magnitudes may seem rather small, they are at least twice as great as the liner surface roughness and an order of magnitude greater than the dynamic range of the LIF measurement system. Further details may be found in Appendix C and B, respectively.)

Since the scraper behavior governs the free-liner OFT as discussed in section 4.2.1, the equivalent free-liner OFTs of the intake (expansion) and compression (exhaust) strokes are governed by the scraper behavior during the intake (expansion) stroke. There are primarily two possible reasons why the expansion stroke leaves a higher free-liner OFT than the intake stroke, and both reasons depend on the behavior of the scraper ring. One reason is changes in the scraper's relative profile to the liner from piston tilt, and the other is changes in ring effective radial pressure caused by pressure differences. The focus of the remainder of this section is to quantify these effects and determine their relative contributions to stroke-by-stroke free-liner OFT differences.

Other arguments for the OFT trends have been investigated and include free-liner oil temperature variations throughout the cycle, stroke-by-stroke temperature effects on OFT calibration, and extraneous radiation from hot combustion gases during the expansion and exhaust strokes. However, all of these arguments are refuted in Appendix

J. In fact, two of the three arguments refuted in the appendix support a claim that the free-liner stroke-by-stroke trends are even more pronounced than those measured.

4.2.3.3.1 Piston Tilt Effects on Free-Liner OFT

Because the worn lower wedge of scraper rings for gasoline engines are so flat and only a fraction of a millimeter along the ring face (approximately 0.13 mm in this case), any small amount of tilt may significantly lengthen or shorten this wedge from the minimum contact point affecting its scraping function and, in turn, the OFT left on the free liner shown in Figure 4-15 (a).

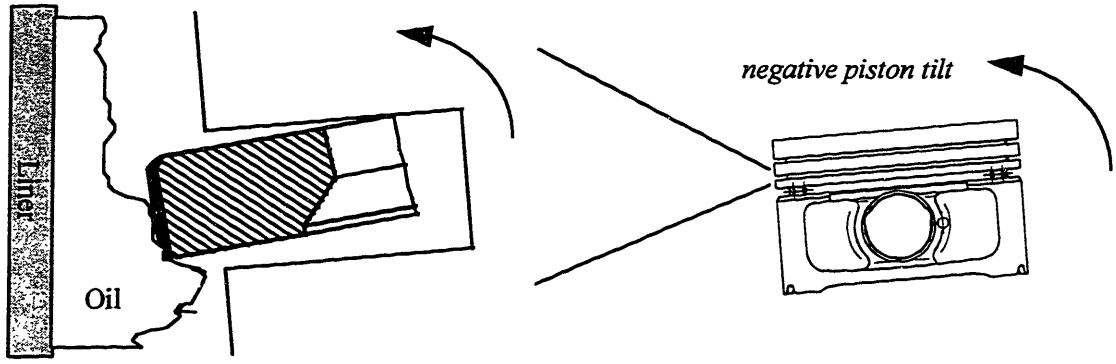

(a) Change in Scraper's Face Profile Relative to Liner Due to Piston Negative Tilt during the Expansion Stroke.

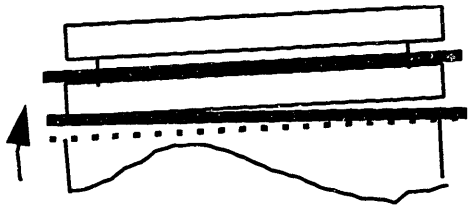

(b) Ring Tilt with Respect to Groove

Figure 4-15 Piston, Ring, and Groove Interaction. (a) Effect of Piston Tilt on Scraper Ring Face Relative to Liner. (b) Possible Ring Tilt Relative to Groove (Some features are exaggerated to highlight details.)

During the expansion stroke and unlike the intake stroke, piston tilt is highly negative and rotates the scraper's orientation with respect to the liner resulting in a greater lower wedge. This effect from piston tilt is greatest along the major- and minor-thrust sides of the cylinder bore. As the bore is azimuthally traversed from the thrust sides to 90° azimuthally off the thrust sides, the tilt effect on the orientation of the ring's relative profiles (and, in turn, OFT) diminishes. Since measurements were taken from the major-thrust side (window 1) and -67.5° (window 4) and 90° (window 2) azimuthally clockwise (cw) from the major-thrust side, the severity from tilt effects are able to be observed. Shown in Figures 4-14 (a) - (c), the percent increase is definitely significant at major-thrust side; for some cases the percent increase in free-liner OFT is so great that the lower bound of standard deviation falls well above zero micrometers.

At 90° azimuthally off the thrust side at window 2 where piston tilt effects are minimal, the percent increase is all but absent; in fact, standard deviation brackets zero percent quite well shown in Figure 4-14 (d).

Between these limiting tilt effects at window 1 and 2 lies window 4, 67.5° azimuthally counterclockwise (ccw) from the major-thrust side. The results are presented in Figure 4-14 (e). Although the percent increase in free-liner OFT is comparable to magnitudes at the major-thrust side (window 1), the corresponding standard deviations bracket zero percent increase. Thus, a lesser confidence should be placed on the significance of this percent increase.

Comparisons between experiments and predictions from the *FRICTION-OFT* model used to evaluate the piston tilt effects on free-liner OFT are shown in Figure 4-16(a) and (b), respectively. Although the model calculates along a line (or one dimension) and does not directly account for piston secondary motion, changes in ring face profiles due to piston tilt may be inputted to generate azimuthal, two-dimensional results. During the expansion stroke as the scraper passes the midstroke window on the major-thrust side, the change in the scraper face profile relative to the liner was calculated from a 10 minute negative piston tilt changing the lower wedge from 0.132 to 0.202 millimeters. During the intake stroke at 74.2° ATC as the scraper passes the midstroke

window, inertial forces change direction resulting in piston tilt transition from positive to negative tilts. Therefore, no tilt is assumed for the intake stroke at this CA position.

The predicted percentage increases from the first to last two strokes from piston tilt at the major-thrust side for the five lubricants are approximately 70 percent. Although this result is two- to three-times as large as the experimental results, the predictions qualitatively agree with the measurements that the mechanism of piston tilt's effect on ring relative profile can have a noticeable effect on free-liner OFT.

The tilt effect accounts for most of the percentage increase from intake to expansion. However, a small percentage increase (approximately 3 percent) is from a reduction of the scraper's effective radial pressure on the lubricant during the expansion stroke due to the land pressure difference and negative static ring twist. Not just at the major-thrust side, this small increase should occur at every azimuthal position and solely shows up at window 2 shown in Figure 4-14 (d) where tilt effects are absent. This phenomenon is explained in the next section, section 4.2.3.3.2.

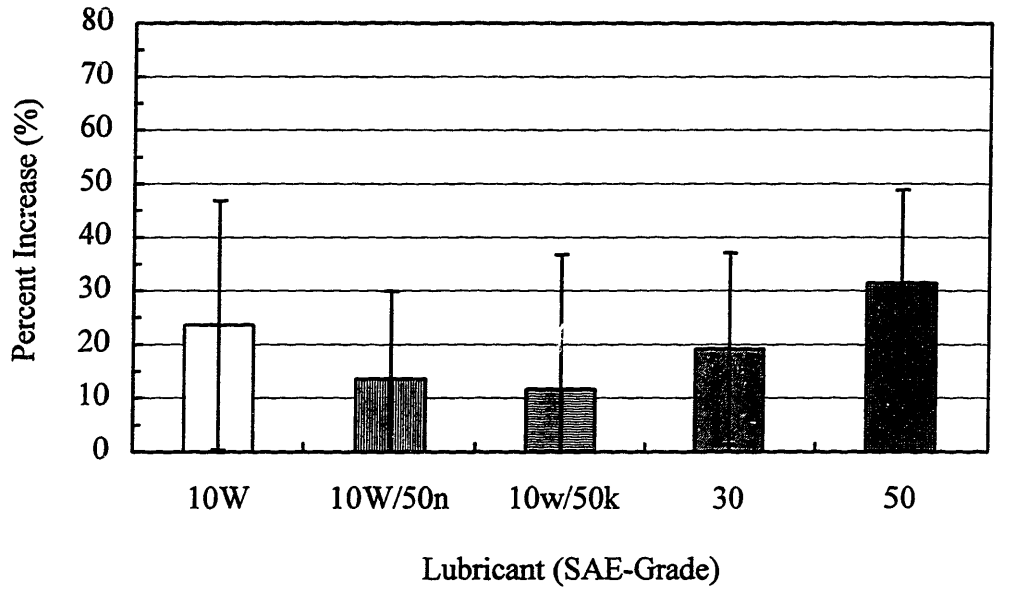

(a) Experiments

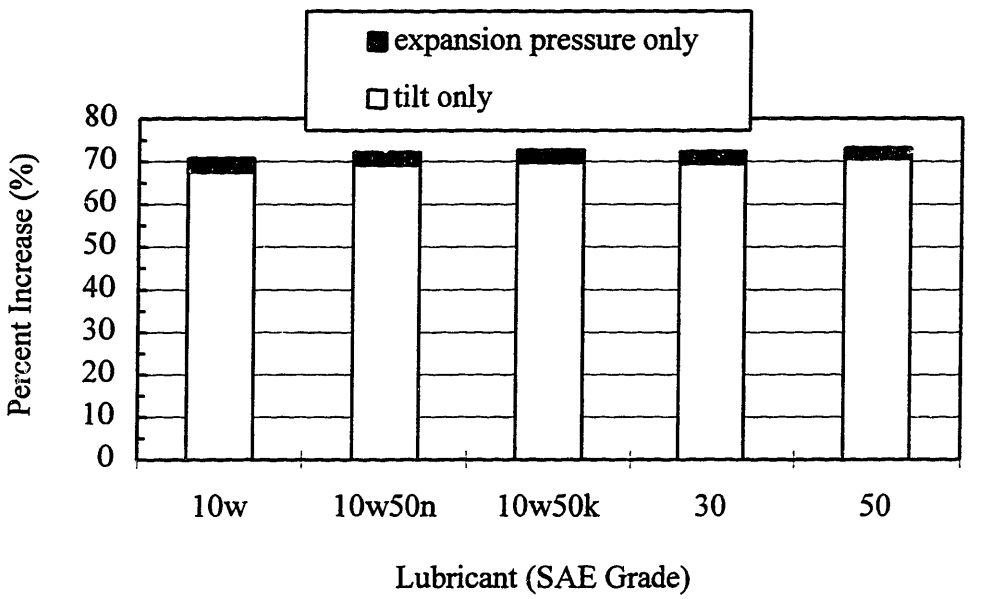

(b) Model Predictions -- Contributions of Piston Tilt and Expansion Pressures

Figure 4-16 Percent Increase in Free-Liner OFT from First Two to Last Two Strokes from (a) Experiments and (b) Model Predictions for Five Lubricants at Major-Thrust Side.
(Window 1, 2/3 Load, 100°C)

One possible explanation of this two- to three-fold difference between the predictions and experiments may be due to several reasons. First, the free-liner OFT differences and trends may be less pronounced than the actual magnitudes and trends due to the arguments posed in Appendix J. Secondly, the ring's orientation within its groove is not exactly known. The model assumes that the rings are flush with its groove represented by the dotted ring in Figure 4-15 (b). However, during a stroke the ring may not sit flush within its groove but tilt with respect to it shown by the solid line. Consequently, ring tilt within its groove may slightly change the scraper's relative profile to the liner and mitigate tilt effects.

In retrospect, piston tilt has a significant effect in stroke-by-stroke variations for the free-liner OFT shown experimentally and theoretically for a gasoline engine. As the bore is transversed azimuthally from the thrust sides to 90° from the thrust sides, the tilt effects on free-liner OFT diminish. In this study on the major-thrust side, the first two strokes are less than the last two strokes of the cycle. Although not verified experimentally in this study, the opposite trend should occur on the minor-thrust side where window 3 was inoperable.

4.2.3.3.2 Land Pressures and Twist Effects on Free-Liner OFT

In addition to the piston tilt, static and dynamic twist accompanied by high land pressures may change the way the scraper ring is orientated with respect to the liner and groove and, thus, affect the scraping function. Although the scraper dynamic twist is not high as the ring flutters past midstroke windows within the Kohler engine during the expansion stroke, the combination of negative static twist of the scraper and land pressures are enough to decrease the net ring pressure on the lubricant, decrease scraping, and, hereby, increase oil flow under the ring. The increased oil flow under the ring provides greater oil supply to the top ring and free liner and results in a percent increase from intake to expansion stroke of a few percent shown numerically and experimentally in Figures 4-16 and 4-14 (d), respectively. The purpose of this section is to describe this phenomenon in the context of the Kohler engine.

The scraper ring with exaggerated negative static twist has been drawn within its groove in Figure 4-17 (a). The governing axial forces for axial ring behavior are inertia, friction, and pressures from second and third land regions. During the first half of the expansion stroke, a net downward pressure difference from the second and third land pressures axially compete with the upward forces from friction and inertia. Upward inertial forces lift the ring towards the top of the groove tending to seal off gas flow between the ring and groove. This restricted flow raises the second land pressure slightly countering the upward inertial forces and pushing the ring down. The net result is ring suspension between the top and bottom of the groove and second ring fluttering occurs. Using *RINGPACK-OC* with the Kohler geometry and measured cylinder pressure, a numerical simulation of this fluttering behavior is shown in Figures 4-18 (a) and (b). Figure 4-18 (a) shows the measured cylinder and predicted second and third land pressures at 2/3 load for 2500 rpm as a function of crank angle. Figure 4-18 (b) indicates the amount of relative axial lift within the ring's groove. The black arrows correspond to the midstroke window locations at 74.2° ATC when the scraper ring passes.

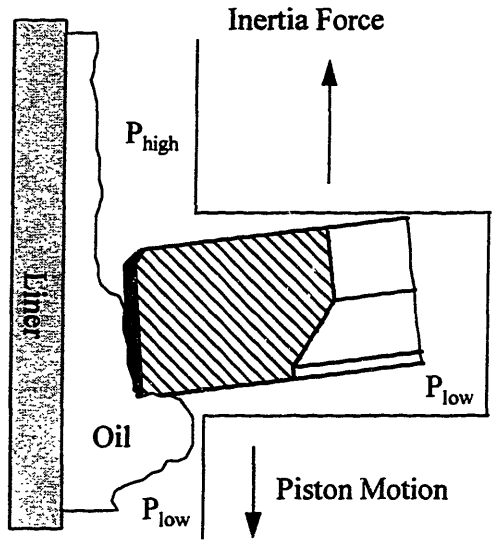

(a) Axial Forces -- Ring-Liner Friction, Inertia, and Land Pressures

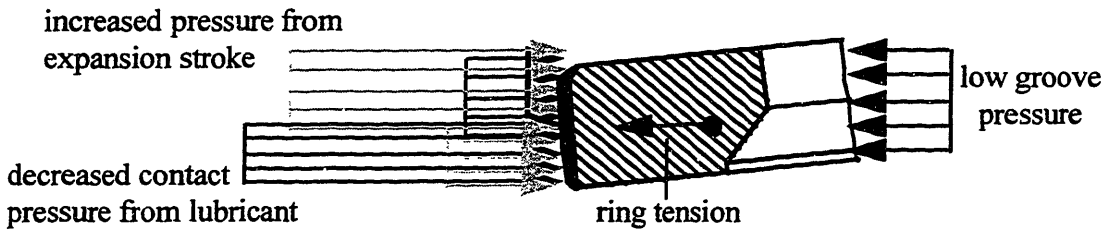

(b) Radial Forces -- Land and Groove Pressures, Lubricant Pressure, and Ring tension.

Figure 4-17 Ring Position with Exaggerated Twist at M[illegible]stroke Position During the Expansion Stroke -- 74° ATC (a) Axial Forces from Ring-Liner Friction, Land Pressures, and Inertia. (b) Radial Forces from Lubricant, Ring Tension, and Land and Groove Pressures.

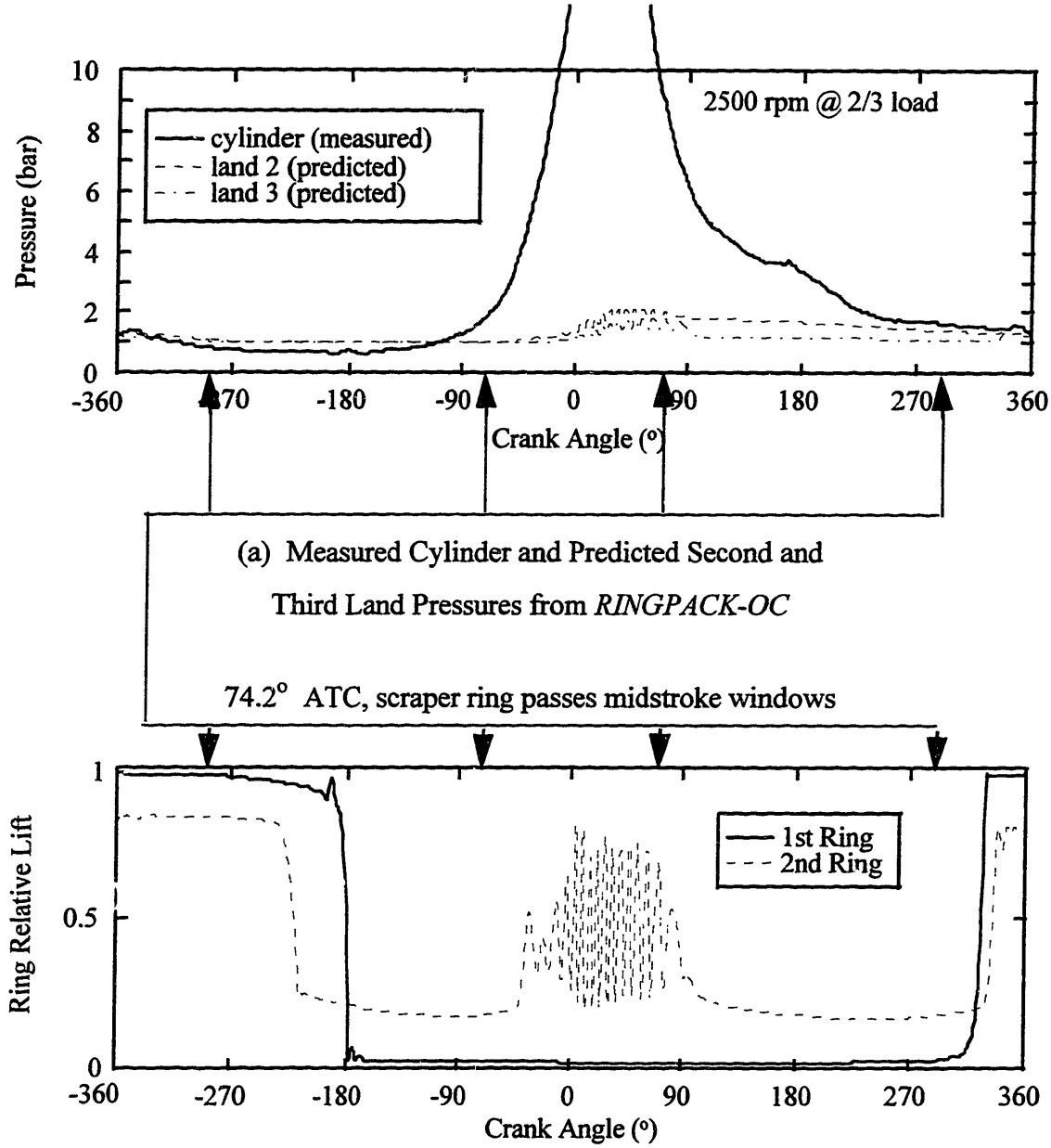

(b) First and Second Ring Relative Lift within Their Grooves

Figure 4-18 *RINGPACK-OC* Results for (a) Land Pressure Predictions and (b) Top and Scraper Ring Relative Lift within Their Grooves for 2/3 load, 2500 rpm, and 100°C Liner Midstroke Temperature.

According to the predictions, fluttering definitely occurs when the scraper ring passes the midstroke windows during the expansion stroke. Significant second land pressure develops which creates a net radial gas pressure difference between the back and front of the ring shown in Figure 4-17 (b). (This gas pressure difference is relatively negligible during the other strokes.) Because the first part of the expansion stroke is just ending at 74° ATC with an upward inertia force, the ring finds itself lifted much of the time during ring flutter shown in Figures 4-17 (a) and 4-18 (b). Therefore, a pressure lower than the second land pressure develops behind the ring. The higher pressure in front of the ring accompanied by a significant projected area increased by ring twist (both static and a little dynamic) reduces the effective ring force on the lubricant less than that of the other strokes; thus, the ring scrapes less and allows more oil to pass under it contributing to greater oil supply to the top ring and free liner during the expansion stroke than the intake stroke.

The 1-D *FRICTION-OFT* model (neglecting tilt effects) which calculates crank-angle resolved OFT accounts for pressure differences across the rings throughout the cycle. For an example, SAE-50 results for this engine are shown in Figure 4-19. Notice the higher MOFTs for the scraper during the expansion and exhaust strokes than the intake and compression strokes at approximately 74° from TC. In effect, the predicted intake and expansion free-liner OFTs correspond to 0.712 and 0.726 microns, respectively -- about a 2% increase in free-liner OFT. This small difference is very low compared to experimental precision of free-liner COVs typically between 5 and 10%. Nevertheless, at the location of window 2 where the tilt effects are minimal, the percent increase shown in Figure 4-14 (d) is greater (by just a few percent) or equal to zero -- a trend very consistent with this numerical analysis.

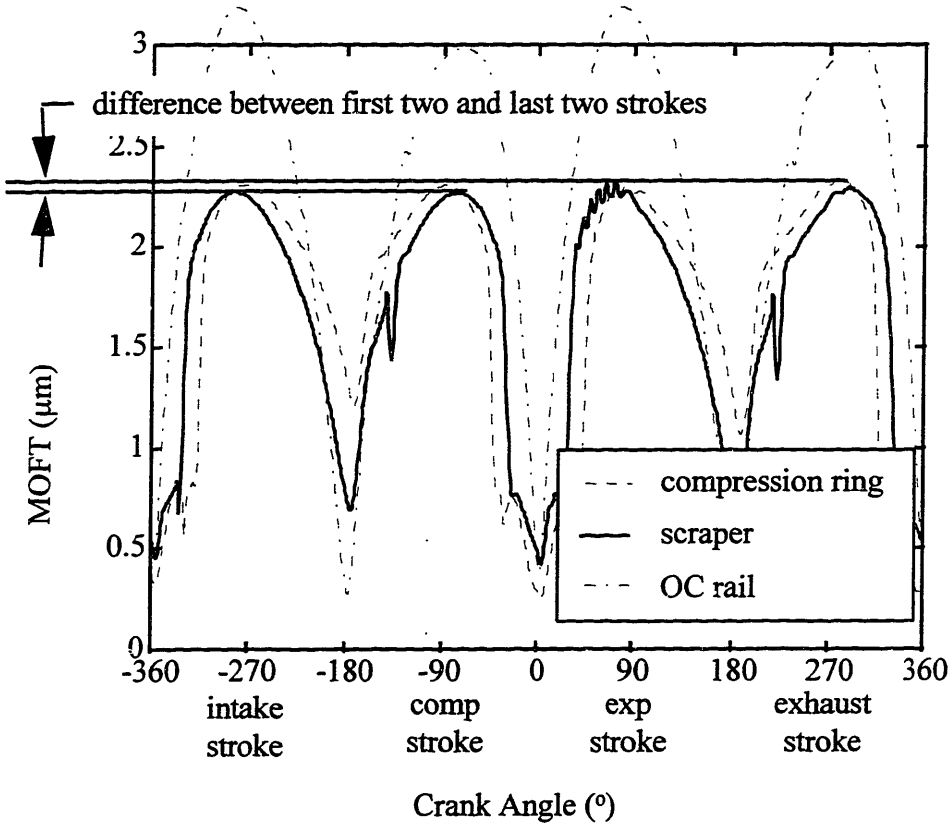

Figure 4-19 CA-Resolved Predicted MOFTs from *FRICTION-OFT* Model for Top, Scraper, and OC Ring. (SAE-50, 2/3 load, 2500 rpm, and 100°C Liner Midstroke Temperature.)

4.2.3.4 Stroke-By-Stroke Summary

The stroke-by-stroke differences and trends for the OFT under the rings and along the free liner were investigated to justify using stroke-averaged representation of the OFT measurements and confirm and improve understanding of ring behavior on OFT throughout a cycle.

For the MOFTs of the top, scraper, and OC rings, differences and trends are only significant for the lower OC segment between the upstrokes and downstrokes in view of the rough 20 percent COV. At midstroke for a majority of the cases, the lower OC MOFTs are greater during the downstrokes than upstrokes. For some random cases, the upper OC segment also shows this stroke-by-stroke trend, even near BC at window 6. A simplistic conceptual model for this three-piece OC ring was described and explained this

behavior. Although trends of the lower OC MOFTs at window 6 for 1800 rpm are the same as midstroke but less pronounced, the MOFT trend of the lower OC segment reverses at 2500 rpm; the upstroke MOFTs are now greater than downstroke MOFTs.

Having greater precision and a COV about half of the MOFT COV, the free-liner OFTs show some significant stroke-by-stroke differences and consistent trends. The intake and compression free-liner OFTs are approximately the same as well as the free-liner OFTs between the expansion and exhaust strokes. However, at the major-thrust side at midstroke, the expansion (exhaust) strokes are significantly greater than the intake (compression) strokes. Plausible explanations include effects from piston tilt and land pressures on scraper ring dynamics and are further supported with numerical calculations from *RINGPACK-OC* and *FRICTION-OFT* models. Although there are significant free-liner OFT differences from stroke to stroke, the stroke-averaged OFT over a cycle is still used to study the general OFT trends in other sections of this thesis but should not affect the results or interpretations.

4.3 RESULTS OF PARAMETRIC STUDIES -- EFFECTS OF LUBRICANT, LINER TEMPERATURE, AND LOAD

In addition to the extreme range of mechanical stresses a lubricant has to endure such as the very high and low shear stresses, extreme thermal and gaseous fluidic conditions from varying cylinder temperatures and loads during driving cycle subject lubricants to severe and extreme environments. This section investigates how the different lubricants behave when subjected to different cylinder liner temperatures and engine loads off the baseline shown in the test matrix in Figure 3-2. Two different loads are investigated separately because lubricant behavior has been found to behave differently under the different loads within different temperature ranges. Loading Conditions include the following:

- Fired conditions at 2/3 load include moderate liner temperatures of 60, 80, and 100°C.

- Motored conditions at WOT and 2500 rpm correspond to low cylinder liner temperatures of 40 and 60°C.

For each of the two loads, two different effects are studied. First, as a continuation from the baseline, the lubricant effects (the behavior between different lubricants at the same operating conditions) are studied off the baseline condition including 1800 rpm and the three moderate liner temperatures at 2500 rpm. Secondly, for the same lubricant, load condition, and speed, the cylinder liner temperature is varied, and the magnitudes and trends of ring MOFT and free-liner OFT are investigated. The resulting effect on OFT is defined as the temperature effect. Lastly, the final subsection for each load condition at 2500 rpm summarizes the results which turn out to be primarily a viscosity effect. For the sake of a concise and succinct representation, most model predictions and comparisons with the data are postponed until this last subsection where the condensed data may be shown all at once with the model predictions. Due to the high concentration of cases with high calibration accuracies at window 1, investigations start in this portion of Table D.1 and continue to the other windows which may include less accurate cases noted in the text or figures.

4.3.1 Fired Cases for Different Lubricants at Moderate Liner Temperatures – 60, 80, and 100°C

Fired at 2/3 load, the engine is operated at moderate cylinder liner temperatures of 60, 80, and 100°C. SAE-10W, -10W/50n, and -50 are tested at each temperature at 2500 rpm and 1800 rpm only at 100°C. Additionally at 2500 rpm and 100°C, SAE-10W/50k and -30 are tested as well. The lubricant and cylinder liner temperature effects provide the opportunity to observe the OFT measurements in two different ways.

4.3.1.1 Lubricant Effects off the Baseline

For the same cylinder liner temperature, load condition (and fired for this section), and speed, the lubricant is varied from very thin to thick lubricants ranging from SAE-

10W to -50, respectively. This lubricant study is continuing off the baseline investigation from section 4.2.2. The condition at 1800 rpm and 100°C is studied first followed by engine operation for 2500 rpm at the moderate liner temperatures of 60, 80, and 100°C.

4.3.1.1.1 1800 rpm at 100°C

Using the exact format as the baseline shown in Figures 4-8 (a) - (d) but for a different engine operating condition off the baseline, Figure 4-20 displays experimental and numerical OFT results for this same midstroke liner temperature but at 1800 rpm and only at window 1. Additionally, monogrades and multigrades correspond to the solid and hollow symbols respectively. (Due to poorer calibration accuracy, the cases from other windows are not explicitly shown.)

The trends from the data and model predictions agree at 1800 rpm as in the baseline at 2500 rpm; OFTs under the rings and along the free liner increase with lubricant viscosity. Although high for the lower OC segments, the predicted magnitudes for the upper OC segment and free liner are within a factor of two of the data. The top and scraper predictions fall within the standard deviation except for SAE-10W predictions which are a little high but still within a factor of two.

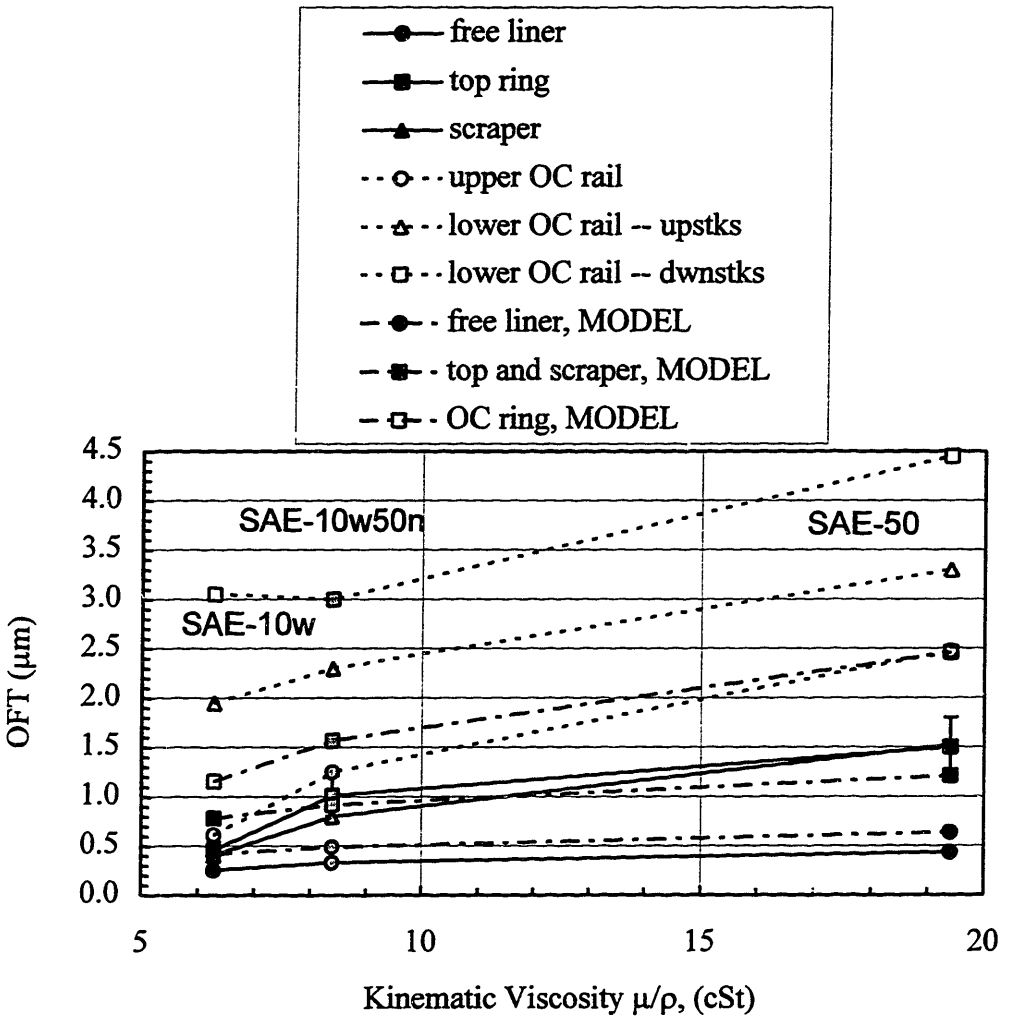

Figure 4-20 OFT Measurements and Model Predictions for Lubricant Effect from Window 1.
(2/3 Load, 1800 rpm, 100°C)

4.3.1.1.2 Moderate Liner Temperatures at 2500 rpm

Continuing off the baseline investigation from section 4.2.2, this section studies the lubricant effect as liner temperatures decrease off the 100°C baseline condition graphically represented in Figure 4-8 (a) for window 1. This type of representation for the measurements may be constructed for each liner temperature off the baseline as well. In order to further verify the OFT-viscosity relationship found at the baseline condition, overlaying these lubricant mappings corresponding to the different temperatures onto one figure provides further insight to the overall lubricant behavior for different liner

temperatures and are shown in Figures 4-21 (a) - (f); now, however, each figure containing measurements from different lubricants corresponds to a particular ring, segment, or free-liner OFT. Lines are used to connect the different lubricants at the same temperature. Additionally, monogrades and multigrades correspond to the solid and hollow symbols respectively. Again, as a reminder, the uncertainty of roughly 20 percent is shown only for 100°C but is implied for the rest of the temperatures.

Because the lubricant viscosities at a particular temperature span great widths but overlap viscosity ranges corresponding to other temperatures, OFTs may be directly compared. Revealing one of the clearest OFT-viscosity trends is the lower OC segment during the downstrokes in Figure 4-21 (a). MOFTs with viscosities close to one another from the different temperatures overlap one another in view of the uncertainty. 100°C overlaps 80°C; 80°C overlaps 60°C; and 80°C bridges the former and latter overlappings. Therefore, regardless of lubricants and chemically-formulated differences between the lubricants, the kinematic viscosity has a predominant effect on the MOFT; MOFTs for the lower OC segment primarily increase with increasing viscosity for SAE-50 which levels off at about 80°C and falls off at 60°C. A very similar trend exists for the segment's upstrokes in Figure 4-21 (b), although SAE-30 is slightly low.

As trends and magnitudes are studied closer to the top of ring pack, the trends become increasingly less clear. SAE-50 below 80°C (or above 30 cSt) falls off, and more scatter exists in the data. Nevertheless, it can still be argued that the kinematic viscosity has a predominant effect on OFT under the rings and along the free liner regardless of liner temperature and chemically formulated differences between the lubricants; OFTs primarily increase with increasing viscosity except above 30 cSt for SAE-50 corresponding to a liner temperature of 80 and 60°C.

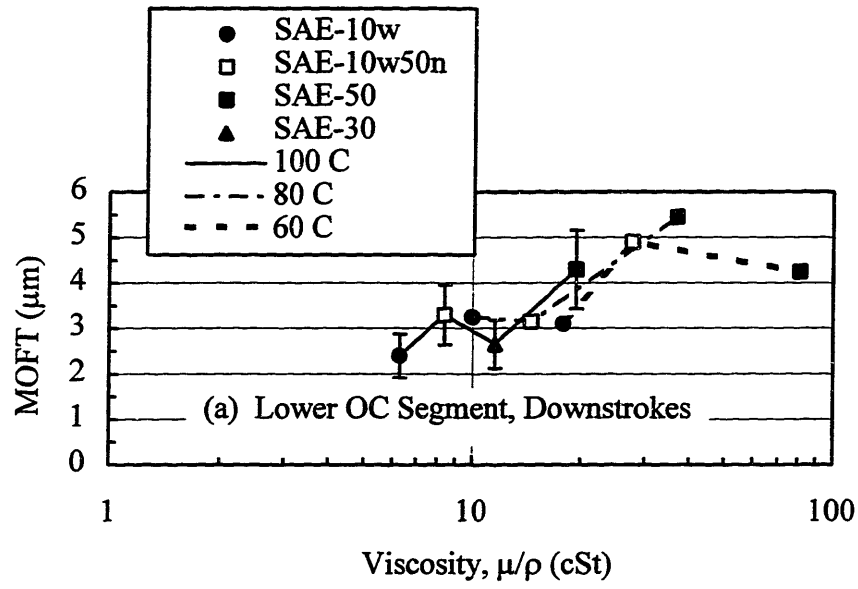
SAE-10w
SAE-10w50n
SAE-50
SAE-30
100 C
80 C
60 C
MOFT (μm)
(a) Lower OC Segment, Downstrokes
Viscosity, μ/ρ (cSt)

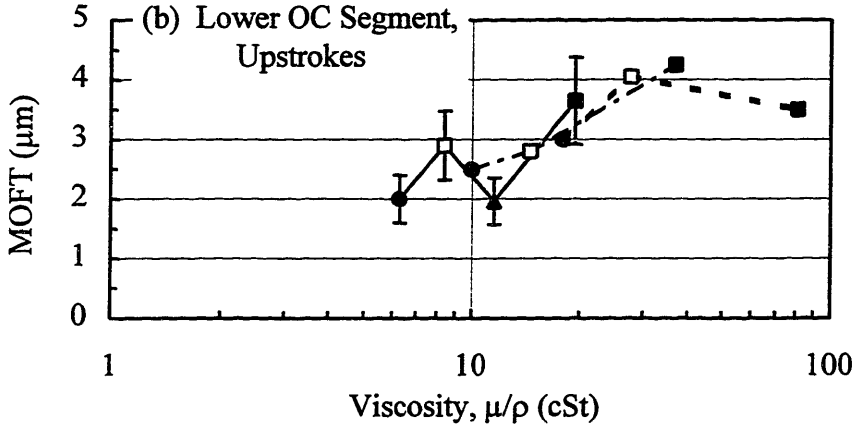
(b) Lower OC Segment, Upstrokes
MOFT (μm)
Viscosity, μ/ρ (cSt)

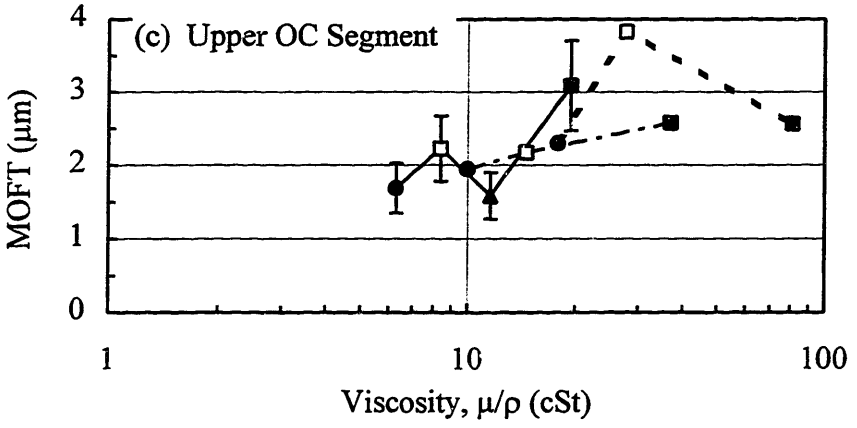
(c) Upper OC Segment
MOFT (μm)
Viscosity, μ/ρ (cSt)

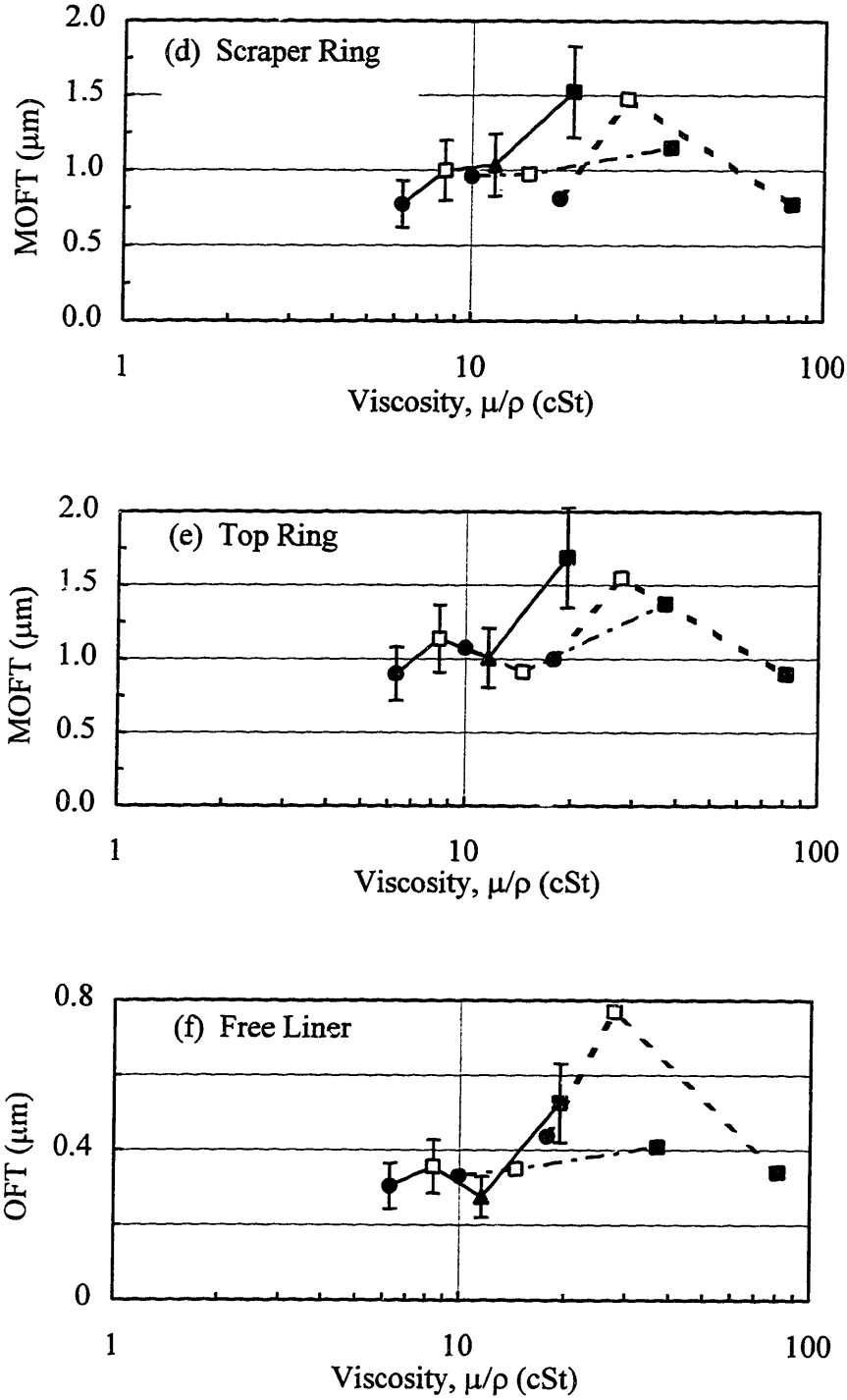

Figure 4-21 Free-Liner OFT and Ring MOFTs for the Lubricant Effect of SAE-10W, -10W/50n, -30, and -50 for the (a) Downstrokes of the Lower OC Segment, (b) Upstrokes of the Lower OC Segment, (c) Upper OC Segment, (d) Scraper Ring, (e) Top Ring, and (f) Free Liner.
(Window 1, 2/3 load at 2500 rpm)

Interestingly, the magnitudes and trends of these mappings become less consistent for OFTs closer to the top of the piston. This result is probably due to land pressures and gas flows which are more significant towards the upper portion of ring pack and, thus, more influenced by thermal expansions as well. However, lubricant viscosity still has a predominant influence.

The predominant viscosity influence also exists for the cases at the other windows as well. However, these results from both the lubricant and temperature effects are postponed and shown all together in section 4.3.1.3 -- the viscosity effect.

4.3.1.2 Cylinder Liner Temperature Effect at 2500 rpm

To further verify the OFT-viscosity relationship found in the lubricant effect on and off the baseline for the moderate liner temperatures at 2500 rpm, the measurements may be presented in a different way. For the same lubricant, load, and engine speed, ring MOFT and free-liner OFT varies with liner temperature. The resulting effect is called the temperature effect.

Including both experimental and numerical results for SAE-10W, -10W/50n, and -50, respectively, Figures 4-22 (a), (b), and (c) show results for the MOFT and free-liner OFT at the different liner temperatures of 60, 80, and 100°C. The hollow and shaded symbols correspond to the OC segments and the remaining OFTs, respectively, which include ring MOFTs and free-liner OFTs. Uncertainty is included for the top ring and, again, roughly 20 percent of the MOFT for these cases of high accuracy. (Uncertainty bars for COV of 20 percent are implied for the remainder of the experimental MOFTs, only to avoid cluttering the figures. Uncertainty for the free liner is about half of this amount.) Lastly, the dashed-dotted lines connecting certain data points correspond to the model predictions. At midstroke for numerical predictions, the top ring MOFT is only less than two percent greater than the scraper MOFT and, thus, is shown in the figures to represent both the top and scraper MOFTs. The one-piece OC ring from the model predictions have modestly different MOFTs between upstrokes and downstrokes;

however, the average value is shown among the figures, and the MOFT percent differences from the this average are less than five percent.

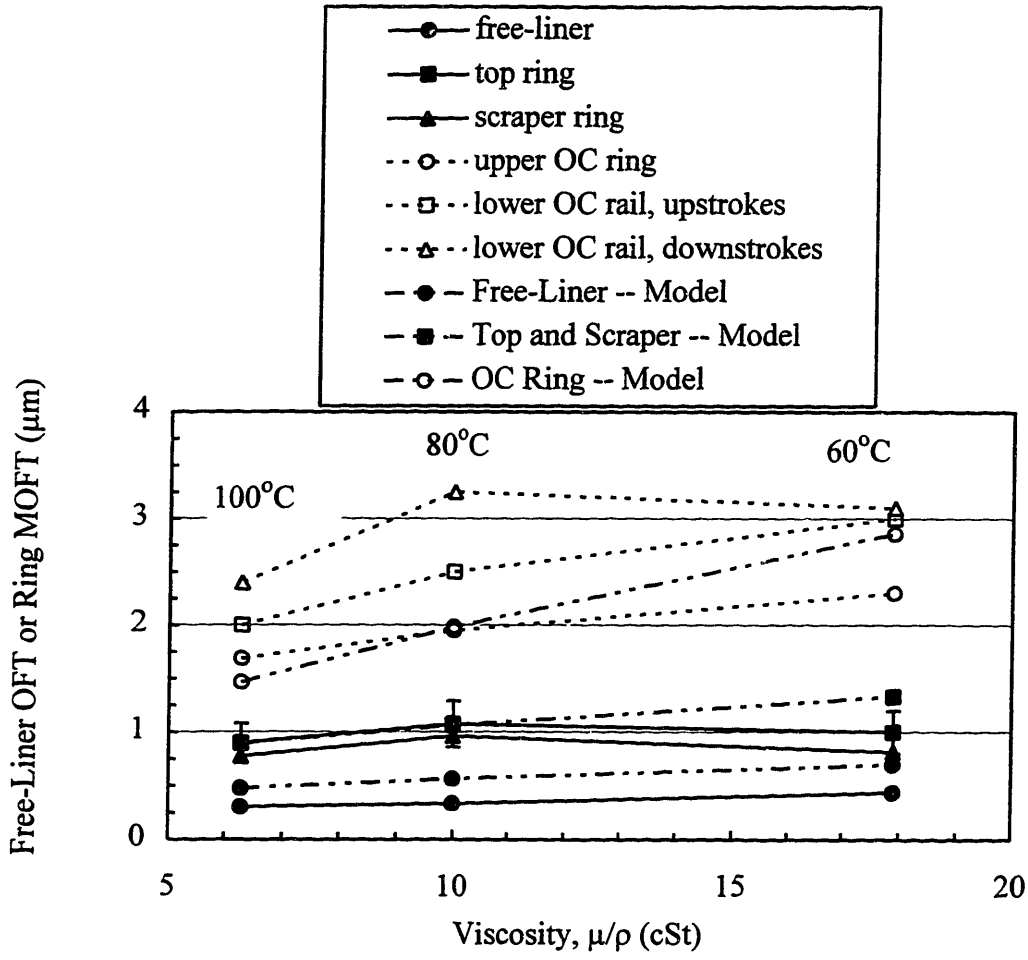

(a) SAE-10W

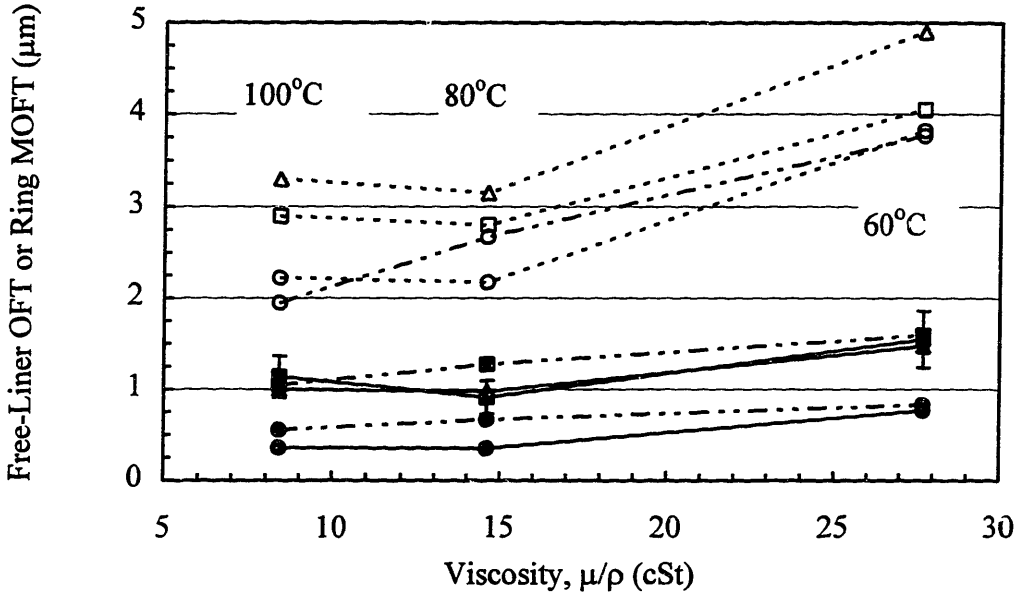

(b) SAE-10W/50n

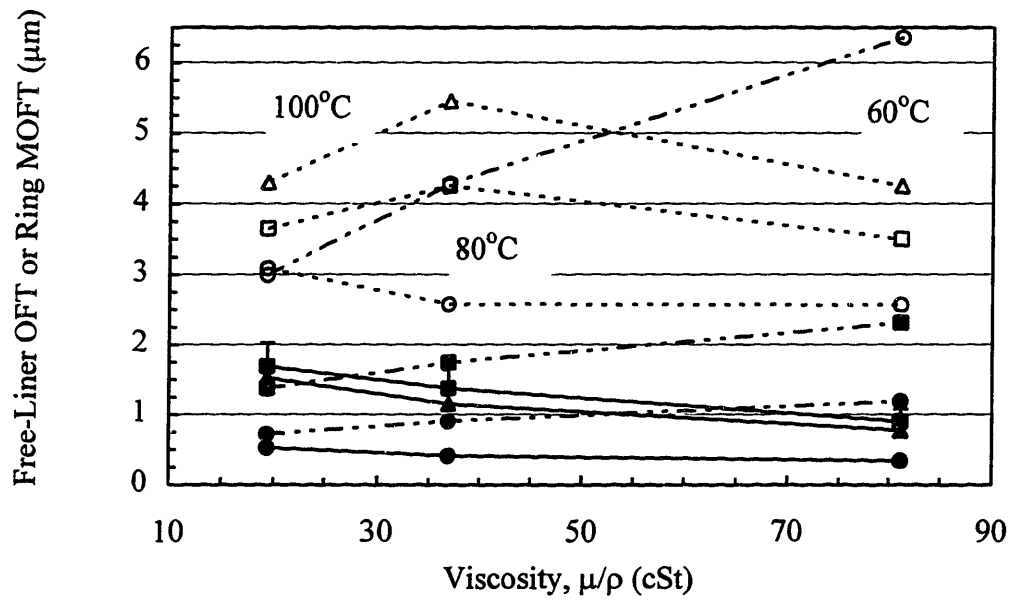

(c) SAE-50

Figure 4-22 Free-Liner OFT and Ring MOFTs at Different Liner Temperatures at Window 1 for (a) SAE-10W, (b) -10W/50n, and (c) -50 (2/3 load at 2500 rpm)

Although the OFT hierarchy of the liner and rings addressed in section 4.2.1 is further confirmed here shown in the figures among the three lubricants, the magnitudes within this hierarchy change among the lubricants for different liner temperatures corresponding to different lubricant viscosities. For SAE-10W in Figure 4-22(a), OFTs increase from 100 to 80°C but increase less, if at all for the lower OC downstrokes and top and scraper rings, as liner temperature decreases to 60°C. Also showing an OFT increase with decreasing liner temperatures, SAE-10W/50n doesn't show much of a difference between 100 and 80°C in view of uncertainty but then significantly increases from 80 to 60°C. For most of the data points for the top and scraper rings and the upper OC segment, the *FRICTION-OFT* model predicts within the uncertainty of the MOFTs; predictions for the free-liner OFT are a little high but still within a factor of two. The predicted increasing trend with decreasing liner temperature is also consistent with the data.

However, in terms of both magnitudes and trends, model predictions and measurements diverge for the highly-viscous SAE-50 shown in Figure 4-22 (c). Measurements continually decrease with decreasing temperature from 100 to 60°C except for the lower OC rail. But its MOFT, as well, eventually decreases for decreasing liner temperature from 80 to 60°C. Although magnitude predictions at 100°C lie on top of the measurements, the diverging magnitudes and opposite trends as temperatures decrease to 60°C result in model and experimental magnitudes which differ by factors greater than two at this temperature.

Overlaying these OFT mappings from the different lubricants for the temperature effect provides further insight to overall lubricant behavior and are shown in Figures 4-23 (a) - (f); now, however, each figure including three lubricants corresponds to a particular ring, rail, or free liner OFT.

Since wide ranges of viscosity for the different lubricants corresponding to the temperature range from 100 to 60°C spread and significantly overlap each other, the OFTs may be directly compared. For the lower OC segment in Figures 4-23 (a) - (b), MOFTs from different lubricants overlap one another at the same viscosity in view of uncertainty. SAE-10W overlaps with -10W/50n; -10W/50n overlaps with -50; and -

10W/50n bridges the former and latter overlappings. Therefore, regardless of liner temperature and chemically formulated differences between the lubricants, the kinematic viscosity has a predominant effect on MOFT; MOFTs for the lower OC segment primarily increase with increasing viscosity except for SAE-50 which falls off at 60°C.

For the upper OC segment in the next figure, the MOFTs hold to the same pattern as the lower OC segment except SAE-50 now starts decreasing at 80°C, roughly 30 cSt. With exception of different magnitudes, the other OFTs for the remainder of the rings and free liner have these same patterns and trends; OFTs for the free-liner and under the rings increase primarily with viscosity regardless of lubricant and liner temperature up to a certain threshold viscosity. This threshold occurs at roughly 30 cSt for SAE-50. Because no other lubricants span above this viscosity, it is difficult to say whether this threshold is due to high viscosities for any lubricant or only for SAE-50.

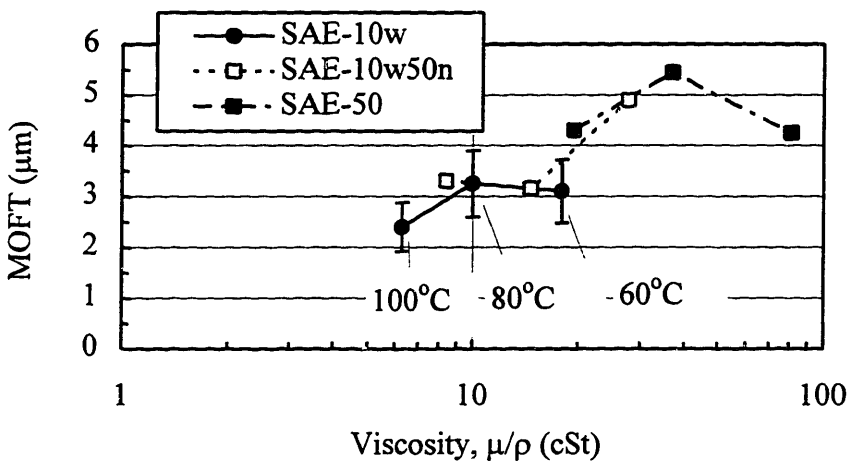

(a) Lower OC Segment, Downstrokes

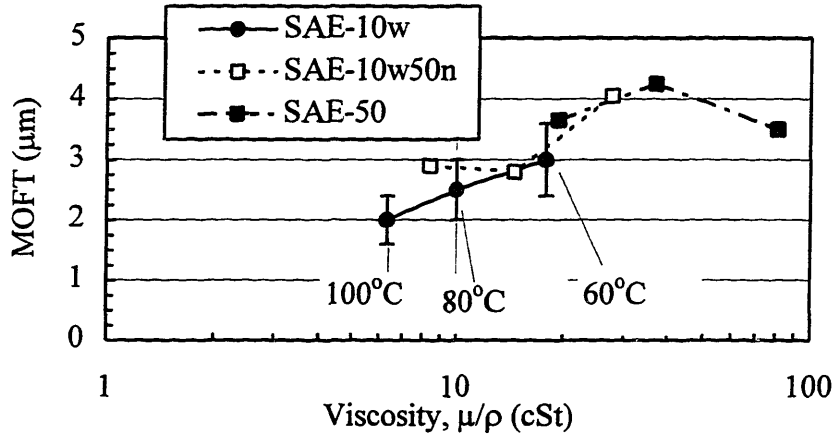

(b) Lower OC Segment, Upstrokes

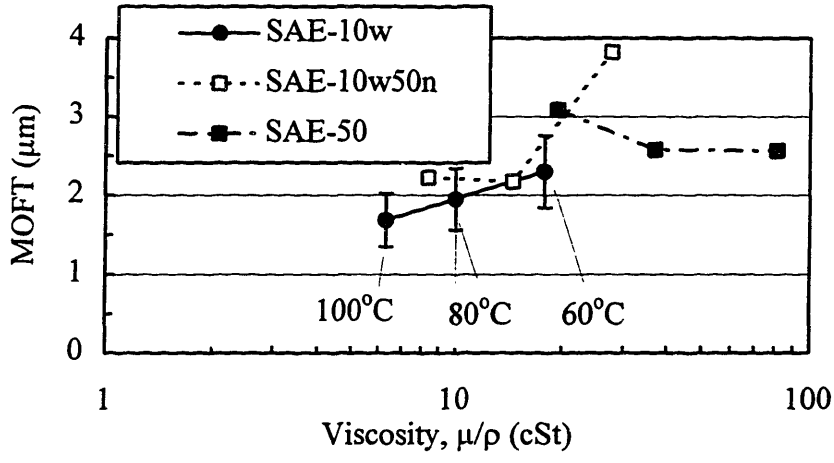

(c) Upper OC Segment

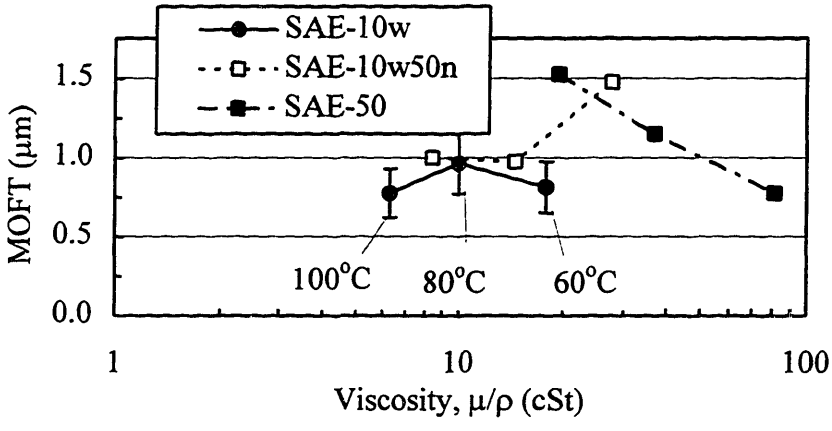

(d) Scraper Ring

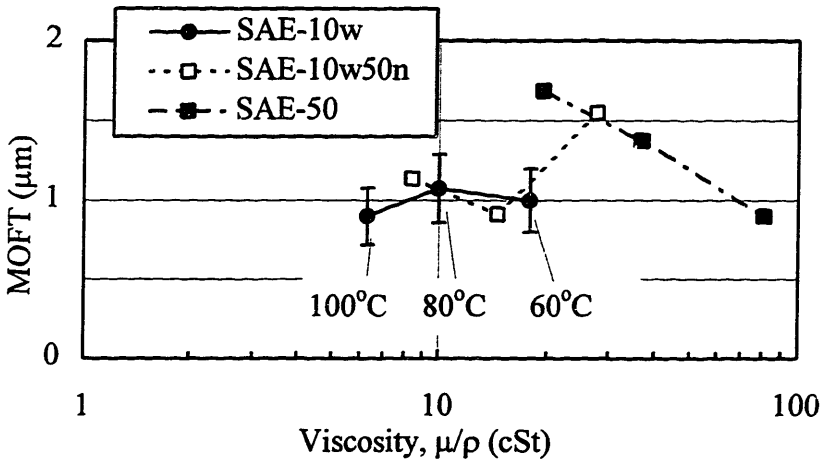

(e) Top Ring

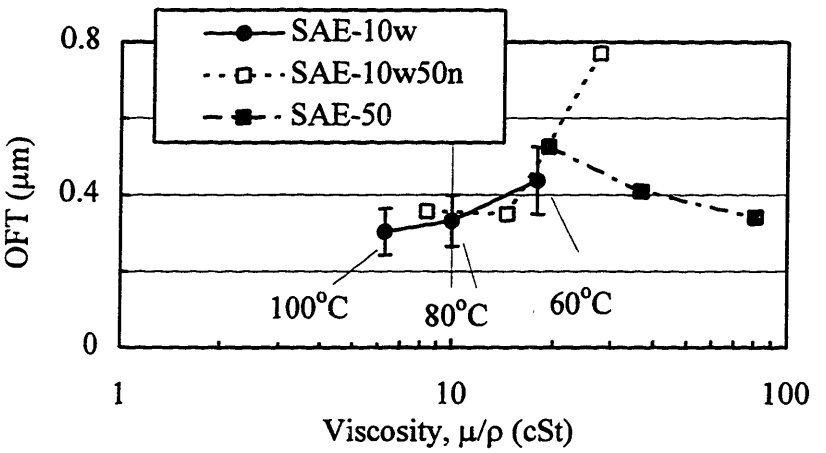

(f) Free Liner

Figure 4-23 Free-Liner OFT and Ring MOFTs for the Temperature Effect of SAE-10W, -10W/50n, and -50 for the (a) Downstrokes of the Lower OC Segment, (b) Upstrokes of the Lower OC Segment, (c) Upper OC Segment, (d) Scraper Ring, (e) Top Ring, and (f) Free Liner.
(Window 1, 2/3 load at 2500 rpm)

Again, as in the lubricant effect, the magnitudes and trends of these mappings become less consistent for OFTs closer to the top of the piston. Probably resulting from land pressures and gas flows which are more significant towards the upper portion of ring pack and, thus, more influenced by thermal expansions as well. However, lubricant viscosity still has a predominant influence.

4.3.1.3 Fired Viscosity Effect -- Combined Lubricant and Temperature Effects

Since viscosity has a predominant effect on OFTs under the rings and along the free liner, all of the fired OFT measurements at 2500 rpm from the liner, a ring, or segment are connected by lines and presented with the rest of the ring-pack and free-liner measurements shown in Figures 4-24 (a) - (c) for windows 1, 2, 6, respectively. Each case for a single lubricant and liner temperature corresponds to a single viscosity along the abscissa. Theoretical predictions for the free liner and rings are compared against the measurements.

Having the greatest number of OFT measurements with high calibration accuracy, window 1 shows good agreement for the OFT magnitudes and trends between the model and measured OFTs for the free liner and under the compression rings and rails up to the threshold viscosity of roughly 30 cSt; OFT along the free liner and under the rings increase with viscosity. Measured magnitudes from the top and scraper rings and the upper OC rail usually have uncertainty bars which include the model predictions. Free-liner OFT and lower rail MOFT is easily within a factor of two of the predicted values. But for viscosities in the neighborhood of 30 cSt of greater, both trends and magnitudes between the measurements and predictions sharply diverge; measured OFT now decreases with increasing viscosity for SAE-50.

Although magnitudes differ by roughly a factor of two for most cases at window 2, the same trends at window 1 are observed at window 2 shown in Figure 4-24 (b); OFT increases with increasing viscosity, and this trend reverses for viscosities roughly equal to or higher than 30 cSt. SAE-10W/50n now shows a marked decrease as well which may indicate trend reversals may include other lubricants other than SAE-50. (Absolute magnitude differences should not be of grave concern at this window. From Table D.1, all this data was calibrated using the upper OC rail; addressed in more detail in Appendix C, the accuracy of this method is questionable due to the unknown angular orientation of the segment within the OC ring. However, relative trends and magnitudes are probably reliable assuming the orientation of the upper OC rail is about the same as it passes the window between each case.)

For the last window around midstroke -- window 4 -- shown in Appendix H, both the absolute and relative magnitudes are questionable due to the calibration uncertainties greater than +/- 5 percent except for the cases of SAE-10W/50k and -30 at 100°C. For these two cases behaving consistent with the predictions, OFT does generally increase with viscosity; however, the upper rail MOFT doesn't change much. Model predictions are about a factor of two greater for the free liner and compression rings but closer to the OC rails. Although less accurate, the remainder of the data at window 4 echoes the resulting trends of windows 1 and 2.

Near BC at window 6 in Figure 4-24 (c), OFT trends are the same as found at midstroke windows with the measured trend reversal and deviation from model predictions for viscosities roughly equal to or greater than 30 cSt. For the compression rings, predictions usually fall within a factor of two of the data if not within the uncertainty. For the OC ring, the model predicts are in between the upper and lower segment MOFTs.

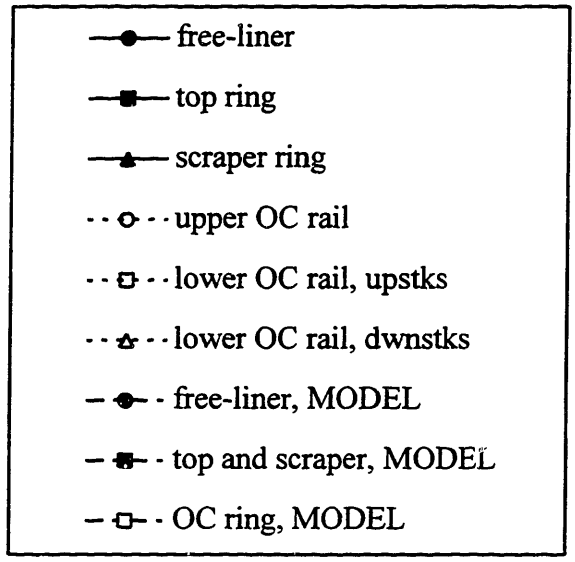

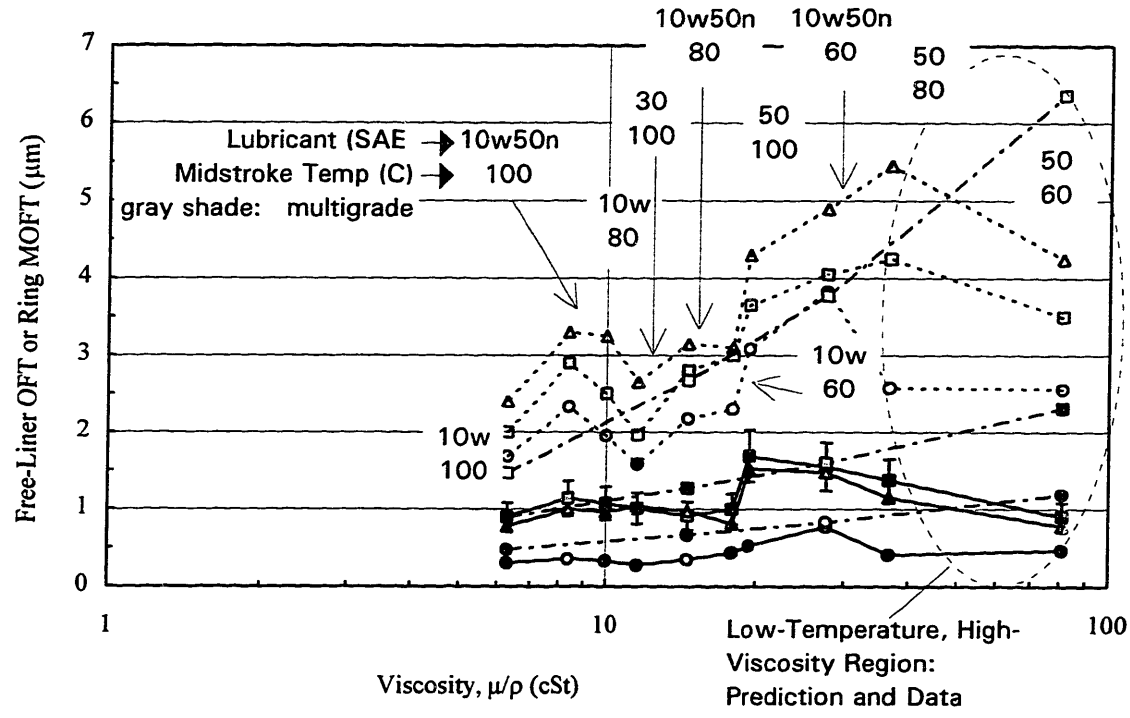

(a) Window 1

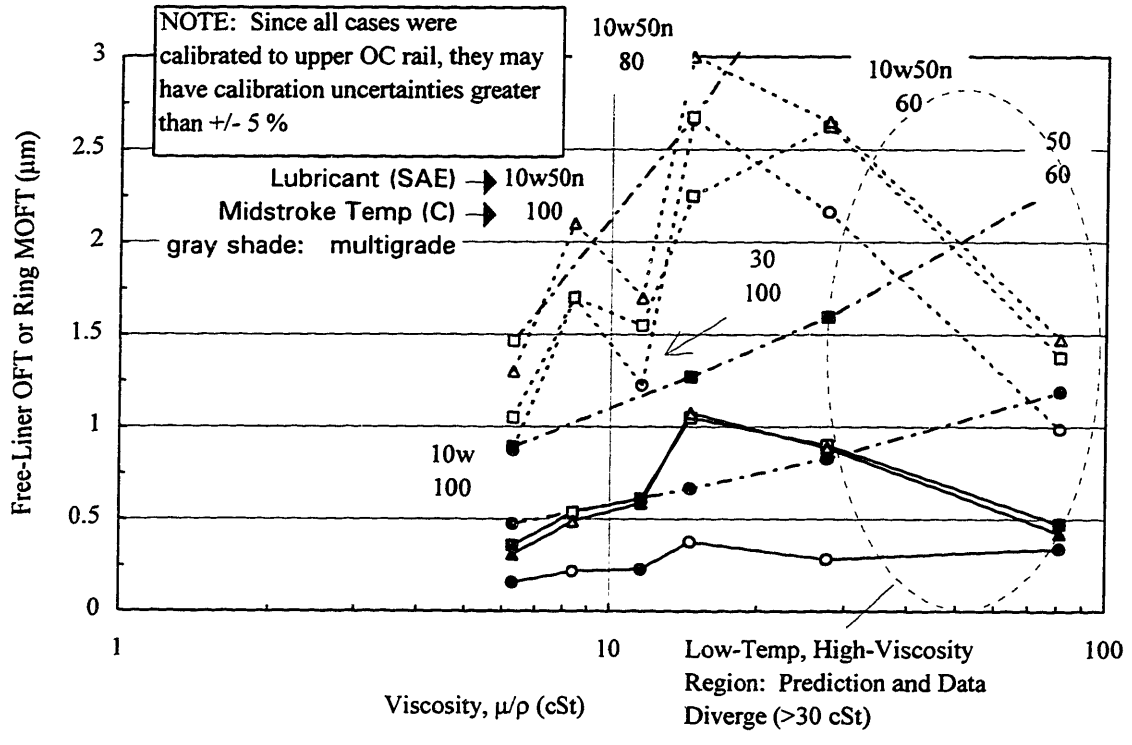

(b) Window 2

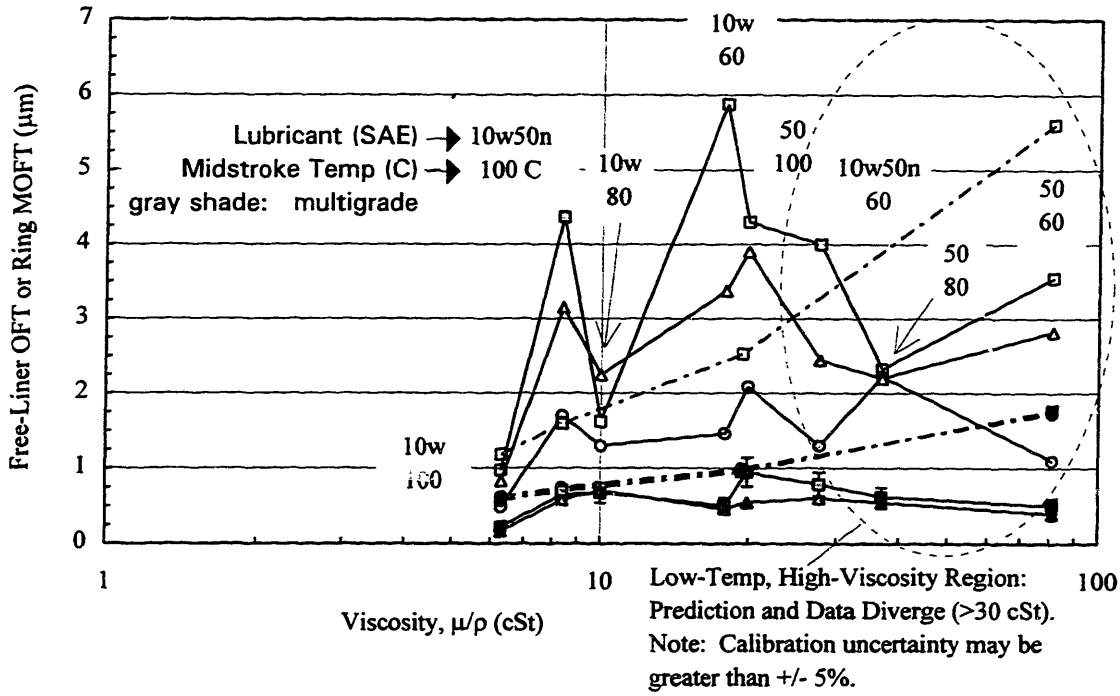

(c) Window 6

Figure 4-24 Free-Liner OFT and Ring MOFTs for the Viscosity Effect of SAE-10W, -10W/50n, -30, and -50 for Liner Temperatures of 100, 80, and 60°C from (a) Window 1, (b) Window 2, and (c) Window 6
(2/3 load at 2500 rpm)

This trend reversal of the OFT-viscosity relationship for highly-viscous lubricants have been observed in other works as well. Moore[18] found this inversed relationship between OFT and viscosity for the top compression ring near top center for several lubricants and not just those with high viscosity. He argues that the non-hydrodynamic oil flow routes through the second ring gap and groove shown in Figure A-4 are responsible for this inversed OFT-viscosity relationship; lubricants with higher viscosity are transported less to the starved top ring through the second ring gap and groove and supply less oil causing lower top ring MOFTs.

This explanation for SAE-50's behavior in this thesis isn't very convincing because our second land region is relatively dry as addressed in Chapter 5. Additionally, the inverse OFT-viscosity relationship in this thesis holds for all the rings, not just for the

top ring, and some increasing trends of oil distribution and accumulation between the rings for decreasing temperatures are not consistent with this explanation.. Further investigation of this topic and specific details on the oil distribution in view of gap-and-groove oil transport may be found in Chapter 5.

4.3.2 Motored Cases for Different Lubricants at Low Liner Temperatures -- 40 and 60°C at 2500 rpm

The motored cases at wide-open-throttle (WOT) for the low liner temperatures of 40 and 60°C at 2500 rpm include all five lubricants. Since almost all of the accurate motored cases are at window 1, results are only shown from this window. The approach for analyzing the motored data is comparable to the approach used for the fired measurements which include analyzing the lubricant and cylinder liner temperature effects from overlaying lubricant mappings from different temperatures.

4.3.2.1 Lubricant Effect

The overall motored behavior of different lubricants at the same low temperatures of 40 and 60°C are shown in Figures 4-25 (a) - (f). Each figure containing measurements from different lubricants corresponds to a particular ring, segment, or free-liner OFT. Lines are used to connect the different lubricants at the same temperature. Additionally, monogrades and multigrades correspond to the solid and hollow symbols, respectively. Again, as a reminder, the uncertainty of roughly 20 percent is shown only for 60°C but is implied for 40°C as well.

Revealing one of the clearest OFT-viscosity trends is the upper and lower OC segments in Figures 4-25 (a) - (c). At 60°C there really isn't any real trend except for the higher SAE-50 MOFTs. At 40°C OFT decreases with viscosity except for the sharp increase again from SAE-50. Additionally, if SAE-50 is left out of these figures, 40 and 60°C profiles overlap, and the 40°C decreasing trend starting at roughly 35 cSt appears to continue from the level 60°C trend. The OFT trends for the compression rings and free-liner are much less clear especially at 60°C, but the 40°C trends resemble the findings from the OC ring although less pronounced.

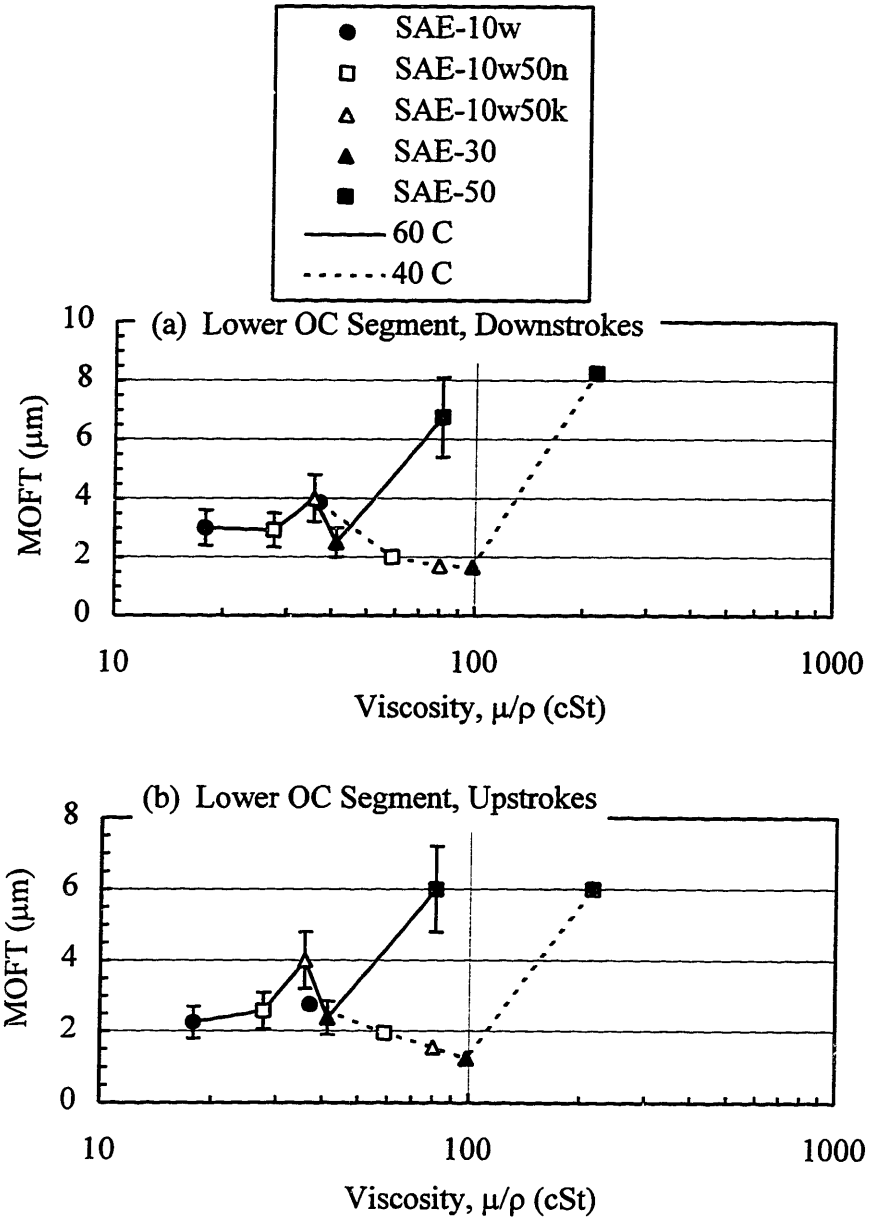
SAE-10w
SAE-10w50n
SAE-10w50k
SAE-30
SAE-50
60 C
40 C
(a) Lower OC Segment, Downstrokes
MOFT (μm)
Viscosity, μ/ρ (cSt)
(b) Lower OC Segment, Upstrokes
MOFT (μm)
Viscosity, μ/ρ (cSt)

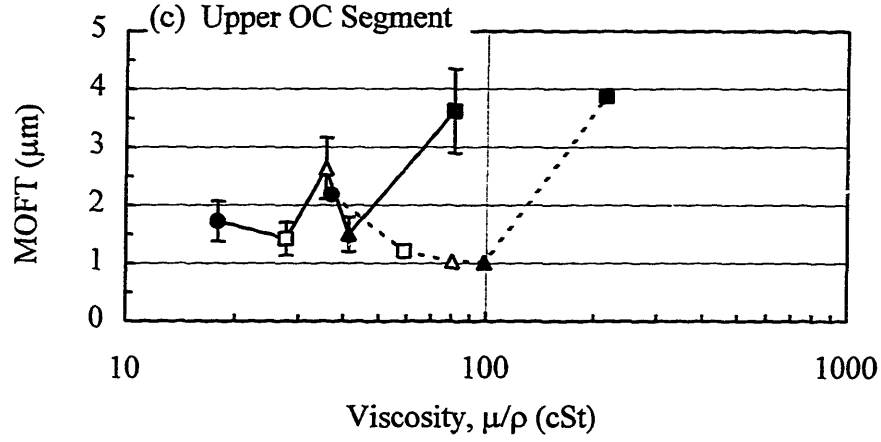
(c) Upper OC Segment
MOFT (μm)
5
4
3
2
1
0
10
100
1000
Viscosity, μ/ρ (cSt)

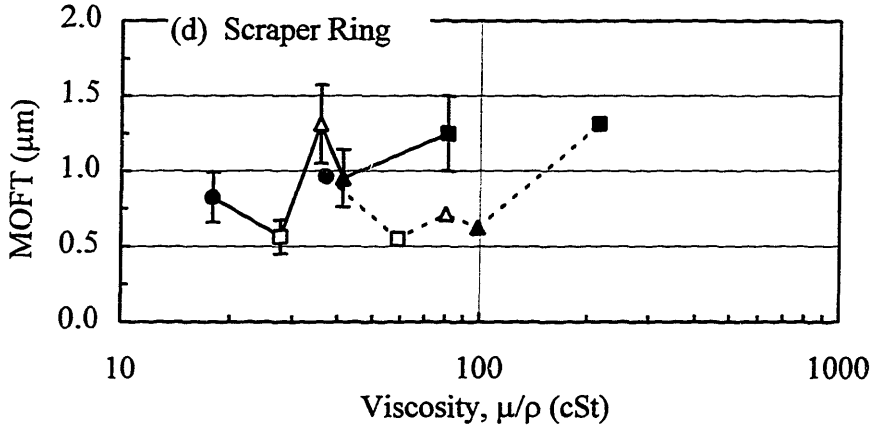
(d) Scraper Ring
MOFT (μm)
2.0
1.5
1.0
0.5
0.0
10
100
1000
Viscosity, μ/ρ (cSt)

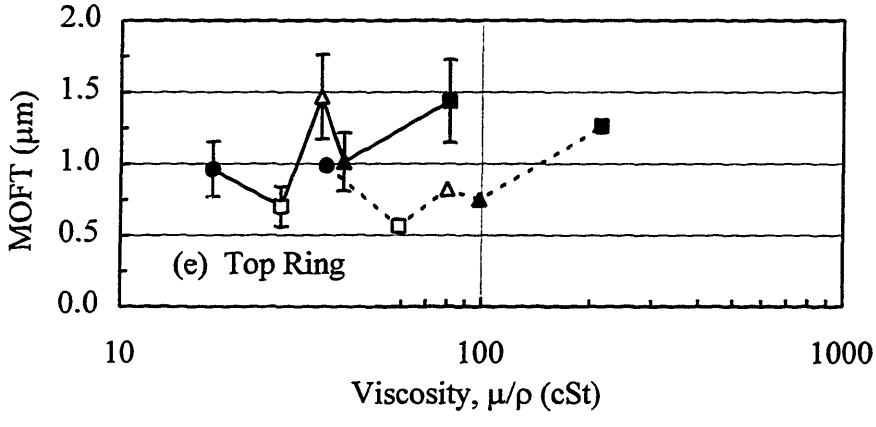
MOFT (μm)
2.0
1.5
1.0
0.5
0.0
(e) Top Ring
10
100
1000
Viscosity, μ/ρ (cSt)

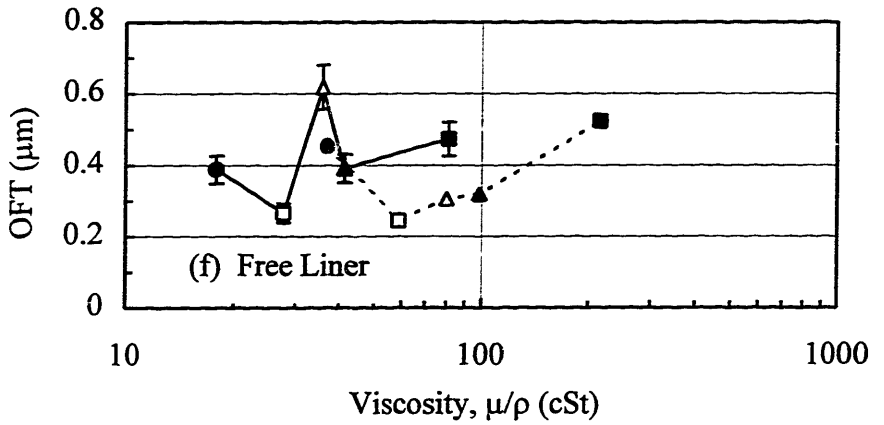

Figure 4-25 Free-Liner OFT and Ring MOFTs for the Motored Lubricant Effect for all Five Lubricants at 40 and 60°C for the (a) Downstrokes of the Lower OC Segment, (b) Upstrokes of the Lower OC Segment, (c) Upper OC Segment, (d) Scraper Ring, (e) Top Ring, and (f) Free Liner.
(Window 1, Motored WOT at 2500 rpm)

4.3.2.2 Liner Temperature Effect

The data representation used to investigate the liner temperature effects isolates the different lubricants from one another and provides additional insight to the motored trends. Shown in Figures 4-26 (a) - (f), OFTs within the entire ring pack and free liner definitely decrease with decreasing temperature between 30 and 100 cSt for the three moderate lubricants not including the thinnest and thickest lubricants corresponding to SAE-10W and -50, respectively. These two lubricants usually show a very slight OFT increase with decreasing temperature. Interestingly, the rough 30 cSt is the same threshold viscosity after which the fired cases decrease as well. Therefore, this finding further supports that the fired OFT-viscosity trend reversal after 30 cSt is due to the viscosity range independent of the particular lubricant and not solely for SAE-50. Perplexingly though, for the motored cases SAE-50 now does not decrease with viscosity.

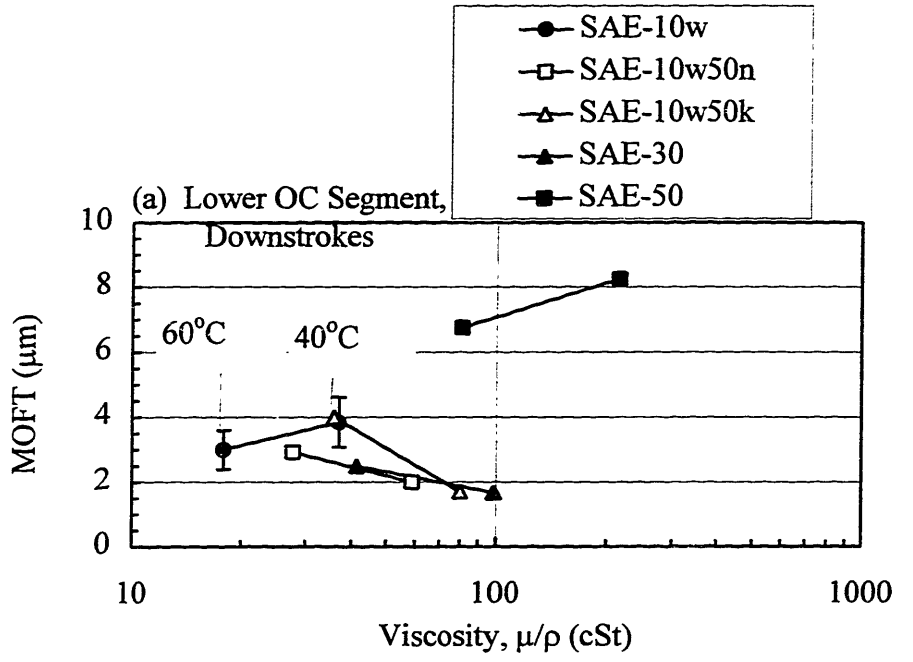
SAE-10w
SAE-10w50n
SAE-10w50k
SAE-30
SAE-50
(a) Lower OC Segment, Downstrokes
60°C
40°C
MOFT (μm)
Viscosity, μ/ρ (cSt)
0
2
4
6
8
10
10
100
1000

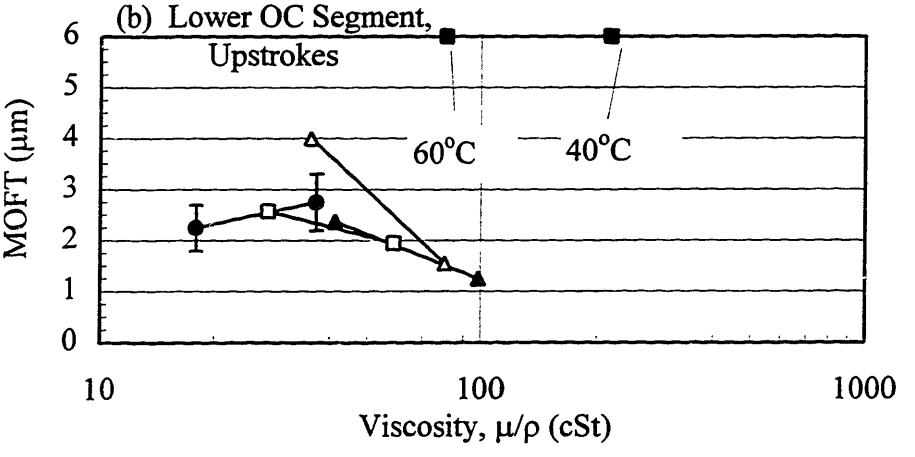
(b) Lower OC Segment, Upstrokes
60°C
40°C
MOFT (μm)
Viscosity, μ/ρ (cSt)
0
1
2
3
4
5
6
10
100
1000

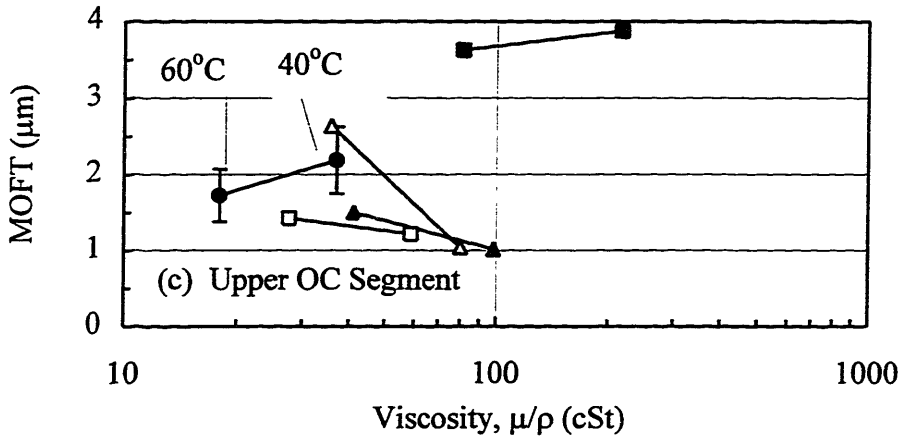
4
3
2
1
0
MOFT (μm)
60°C
40°C
(c) Upper OC Segment
10
100
1000
Viscosity, μ/ρ (cSt)

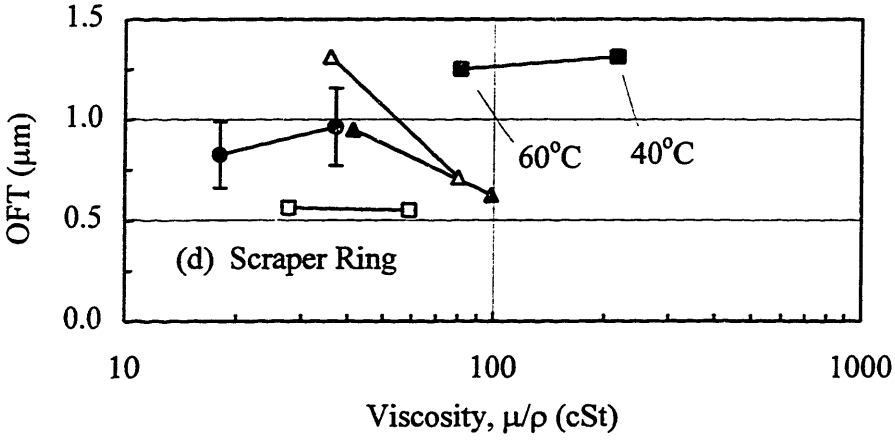
1.5
1.0
0.5
0.0
OFT (μm)
60°C
40°C
(d) Scraper Ring
10
100
1000
Viscosity, μ/ρ (cSt)

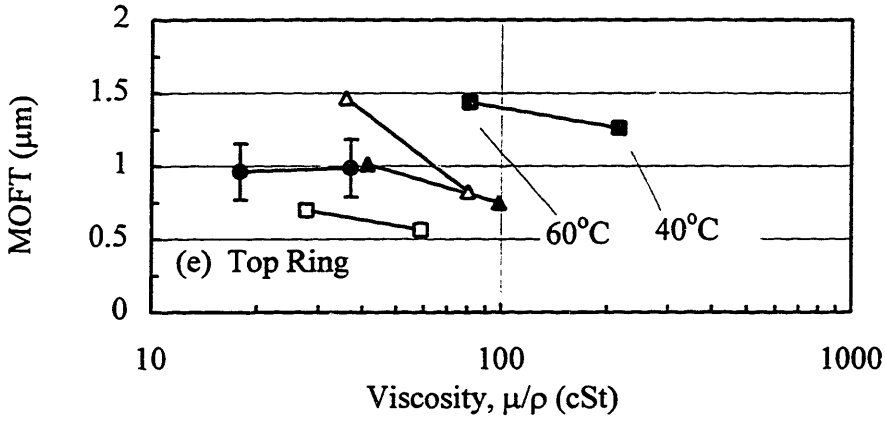
2
1.5
1
0.5
0
MOFT (μm)
60°C
40°C
(e) Top Ring
10
100
1000
Viscosity, μ/ρ (cSt)

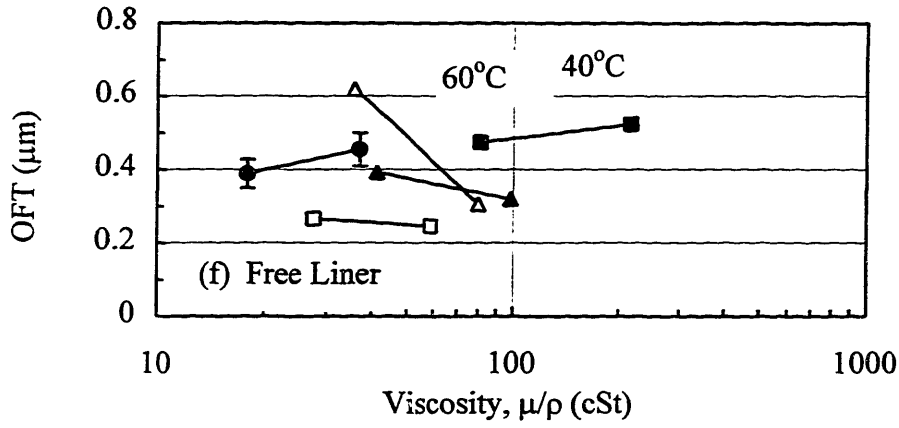

Figure 4-26 Free-Liner OFT and Ring MOFTs for the Lubricant Effect of SAE-10W, -10W/50n, -30, and -50 for the (a) Downstrokes of the Lower OC Segment, (b) Upstrokes of the Lower OC Segment, (c) Upper OC Segment, (d) Scraper Ring, (e) Top Ring, and (f) Free Liner.
(Window 1, Motored WOT at 2500 rpm)

4.3.2.3 Motored Viscosity Effect -- Combined Lubricant and Temperature Effects

After approaching the motored data similar to the fired data by evaluating the temperature and lubricant effects, an OFT-viscosity relationship is less clear. However, from 60 to 40°C, OFTs within the entire ring pack and free liner definitely decrease between 30 and 100 cSt for the three moderate lubricants not including the thinnest and thickest lubricants corresponding to SAE-10W and -50, respectively. These extreme lubricants usually show a very slight OFT increase with decreasing temperature. Interestingly, the rough 30 cSt is the same threshold viscosity after which the fired cases decrease as well. The OFTs of SAE-50 for both low temperatures are usually higher than the other measurements especially for the OC segments.

Although the dominant effect of viscosity is not as pronounced as the fired cases, the OFT-viscosity relationship for all the motored cases is shown in Figure 4-27 and is compared with numerical model predictions from the *FRICTION-OFT* model. Not surprisingly, predictions sharply diverge eventually by more than a factor of two soon after 30 cSt -- the threshold viscosity for both fired and motored trends. Even the high OFT measurements from SAE-50 still fall short of the model predictions.

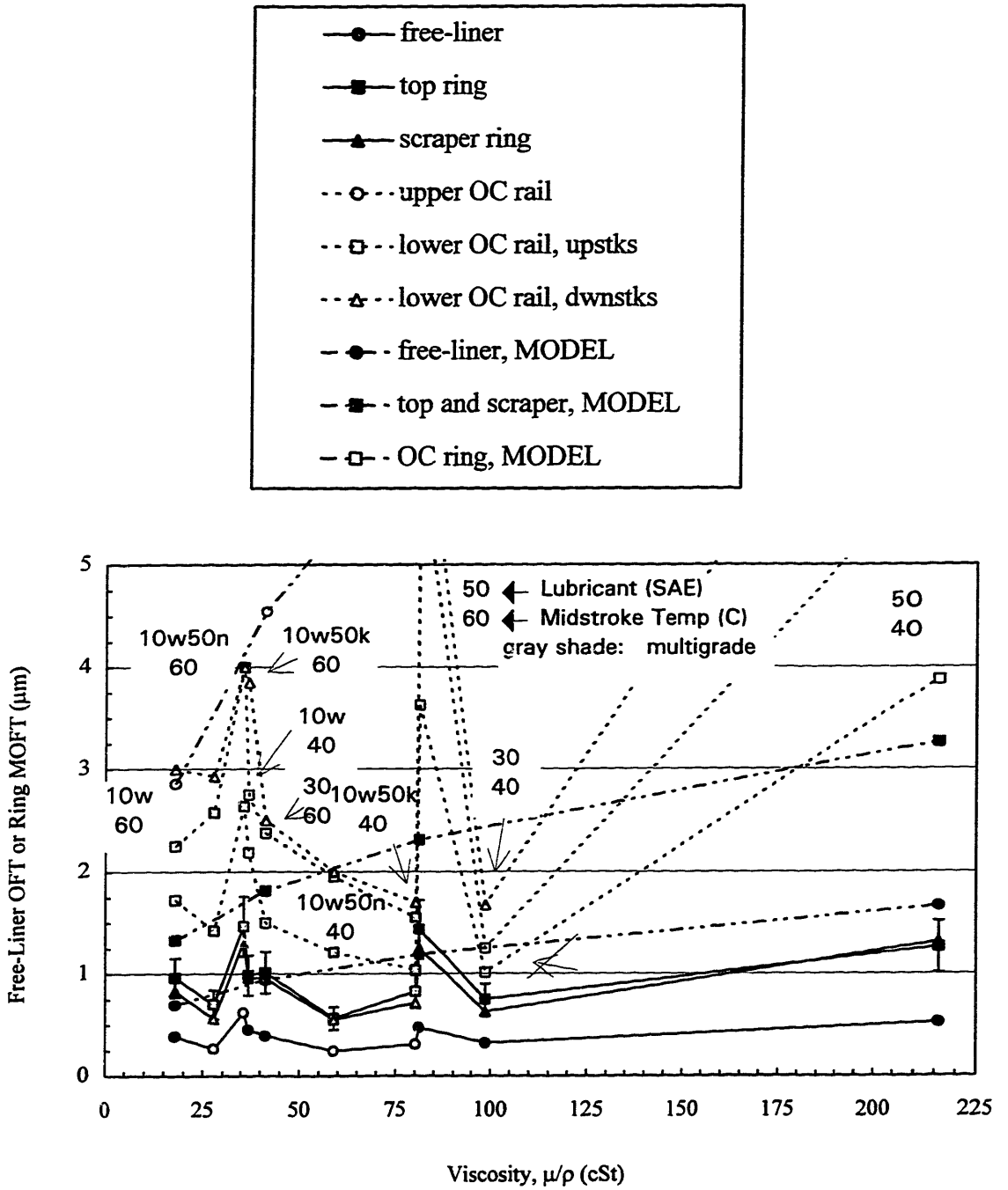

Figure 4-27 Free-Liner OFT and Ring MOFTs for the Viscosity for the Five Lubricants for Liner Temperatures of 40 and 60°C
(Window 1, Motored WOT at 2500 rpm)

4.4 EFFECT OF PISTON SPEED

Influencing hydrodynamic lubrication shown in equations G.1 and G.8, the sliding speed of the rings is determined by the piston speed and, thus, may change in two ways. First, overall piston speed increases with engine speed (rpm). Engine speeds of 1800 and 2500 rpm and their effects on OFT are observed from each of the four windows. (Acquisition of oil film data for 3500 rpm was originally taken but found to be no good.) Secondly, instantaneous sliding speed changes along a stroke for a constant engine speed shown in Figure D-6. A comparison of measurements from midstroke (window 1) and near-BC (window 6) captures this type of speed effect along a stroke. Shown in this section, both types of speed effects are noticeable in the measurements and are consistent with theory and numerical model predictions.

4.4.1 Engine Speeds at 1800 and 2500 rpm

As the Kohler engine speed increases from 1800 to 2500 rpm, mean piston speed ($\bar{S}_P = 4aN$) changes from 4.02 to 5.58 m/s -- an increase of 39%. The instantaneous piston speed is related to mean piston speed from differentiating equation D.2 resulting in the following equation

$$S_P = \bar{S}_P f(\theta) \qquad (4.6)$$

where $f(\theta)$ is a function of engine geometry and crank angle [1]. Therefore, any ring will experience an increased speed by 39 percent at any point along the liner by increasing engine speed from 1800 to 2500 rpm. From an order-of-magnitude analysis shown in Appendix G, an increase in MOFTs scales with the square root of speed (eqn. G.8) -- an increase of roughly 20 percent. (Providing confirmation, a more exact numerical correlation for a fully-flooded ring at midstroke has the speed raised to the power of 0.53 [19].) Unfortunately, this rough MOFT increase of 20 percent is approximately the same magnitude as the MOFT COV determined in section 4.1; Therefore, obtaining large significant MOFT differences between speeds is unlikely, and, at best, trends may be observed. Because MOFT differences are expected to be small

between the two speed conditions, comparing cases from the test matrix which have the highest calibration accuracy is imperative. (Calibration accuracies are noted with the calibration coefficients in Table D.1.)

Additionally at midstroke, $f(\theta)$ and, thus, the instantaneous speeds of the different rings differ less than 2% when the rings pass by the midstroke window locations at maximum piston speed -- roughly 6.5 and 9 m/s at 1800 and 2500 rpm, respectively. Therefore, for the same sliding speed, MOFT comparisons between different rings are legitimate at midstroke windows. (The exact crank angles where the rings pass at midstroke and near-BC windows are shown in Figure D-2.)

Having high calibration accuracies at window 1, the cases for SAE-10W, -10W/50n, and -50 are presented in Figures 4-28 (a) - (c), respectively, in terms of stroke-averaged MOFTs and free-liner OFT for engine speeds of 1800 and 2500 rpm. Model predictions from the *FRICTION-OFT* model are also displayed with the data. The predicted MOFTs are all stroke-averaged over a cycle even for the OC ring. (Predicted individual stroke MOFTs did not differ from predicted stroke-averaged MOFTs by more than 1 percent for the free liner and compression rings and 5 percent for the OC ring.)

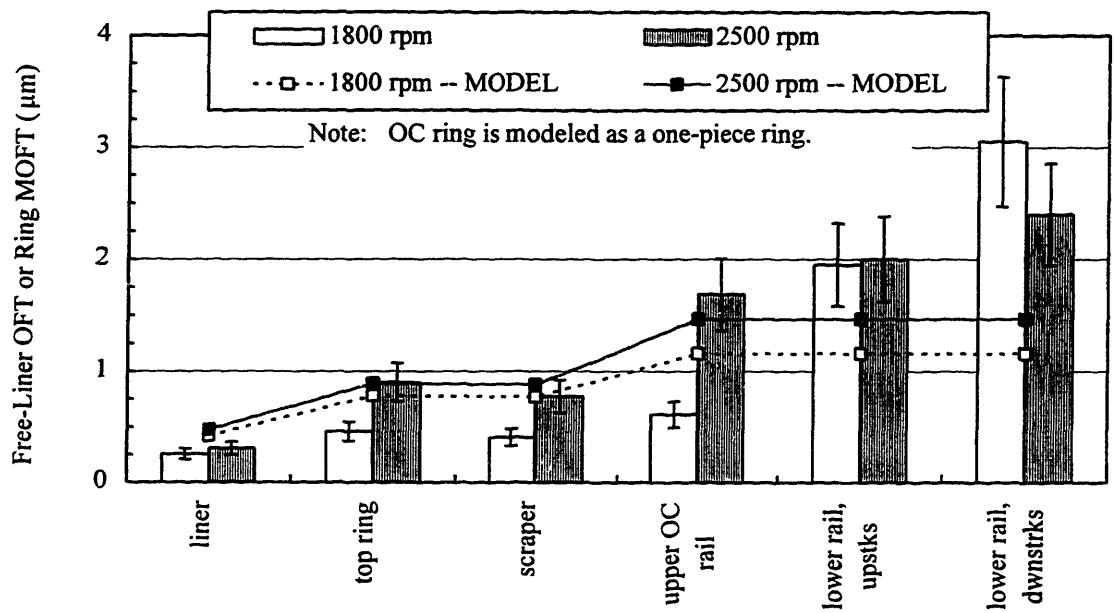

(a) SAE-10W

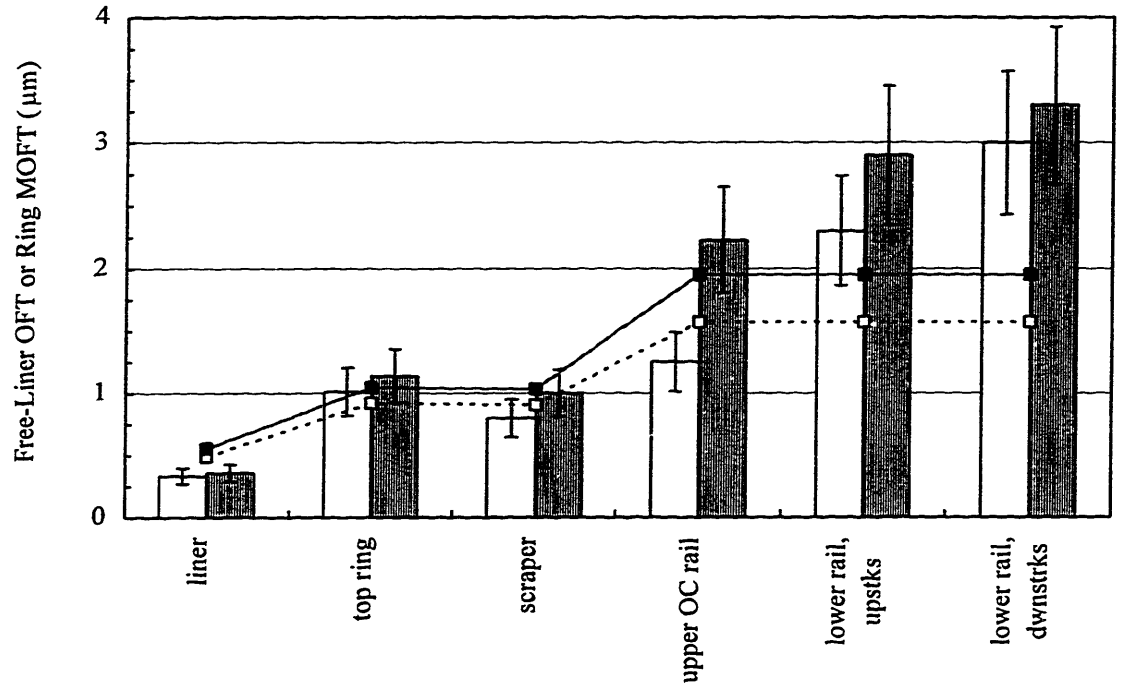

(b) SAE-10W/50n

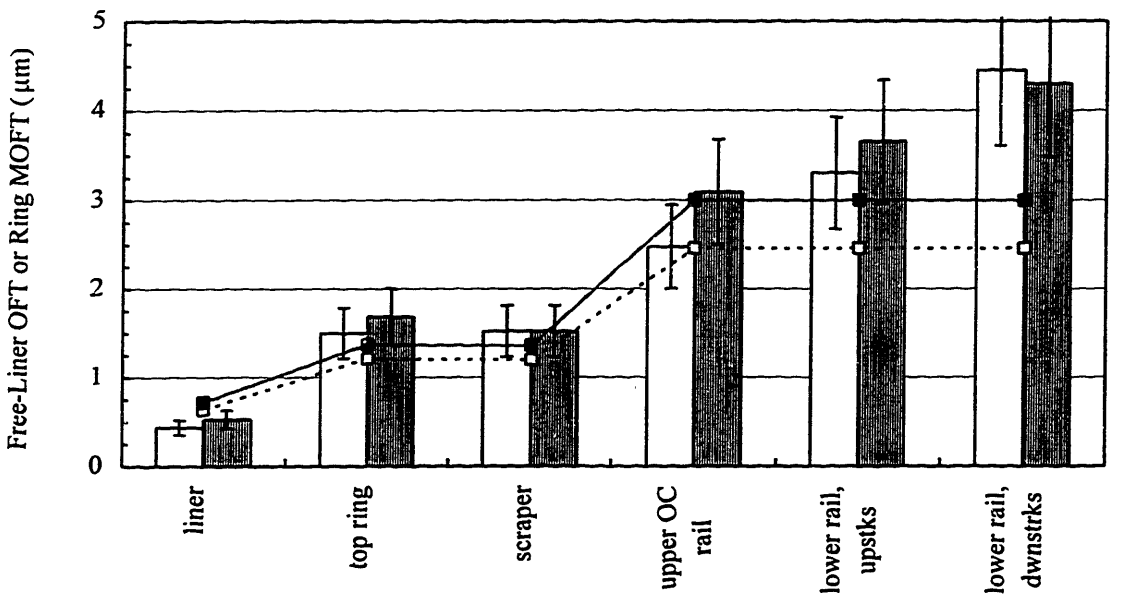

(c) SAE-50

Figure 4-28 Engine Speed Effect from 1800 to 2500 rpm Measured from Window 1 for (a) SAE-10W, (b) -10W/50n, and (c) -50.
(2/3 Load, 100°C Midstroke Liner Temperature)

Both the measurements and numerical predictions show an increasing trend with engine speed -- a trend characteristic of hydrodynamic lubrication. For the measured OFTs of the free liner and under the rings, an increase is always observed with the exception of the lower OC rail during its downstrokes for SAE-10W and -50. These rare exceptions aren't that significant because their the uncertainty bars heavily overlap which is typical for the lower OC rail; less uncertainty overlap and greater differences are observed for the free-liner OFT and the remaining rings and upper OC rail.

The upper OC rail always has the greatest percent increase. Most likely, this high increase results from an accompanying large increase in oil accumulation within the third land region for the same increase in speed. (For the three lubricants studied here, oil volume within the third land region has the greatest increase among the different regions as engine speed is increased shown in section 5.5.) Therefore, it's plausible that the large upper wedge of the upper OC rail has access to a larger oil supply as speed increases, moreso than the other rings. This explanation implies that some of the oil within the third land region does not solely remain on the third land but is transported to supply the upper OC rail sliding along the liner.

The percent increase becomes greater for thinner oils supported by the fact that uncertainty bars overlap less for the less-viscous lubricants. Although the average percent increase over the OFTs for SAE-10W and -50 is approximately 60 and 10 percent, respectively, the percent increase averaged over the three lubricants is 32 percent -- not too far off the rough expectation of 20 percent from theoretical scaling.

Overall, the numerical predictions agree fairly well with the measurements in terms of the OFT trends and magnitudes. MOFT predictions are within the uncertainty bars of the measurements except for the low measured magnitudes of SAE-10W at 1800 rpm, the slightly lower free-liner OFTs, and the higher MOFTs of the lower OC rail for the rest of the lubricants. However, all predictions are within a factor of two of the measurements.

Accurate predictions for the OC rails were not expected because the model does not capture three-piece OC ring behavior. Nevertheless, accurate predictions for the

upper OC rail is captured by the model which also shows the greatest percent increase compared to the other rings. Part of this greatest percent increase is due to the additional oil supply from the second ring's scraping function. Accounted for in the model, during the downstroke the scraper does scrape more oil for the higher engine speeds and the scraped oil is evenly supplied along the subsequent upstroke to the upper wedge of the OC ring.

Lastly, the increasing trends fairly agree as well. Although not as extreme as the data, the model also predicts a lesser percent increase for the thicker lubricants -- 17, 19, and 20 percent for SAE-50, -10W/50n, and -10W; these magnitudes are roughly equal to the 20 percent increase from scaling arguments. Additionally, since the MOFT is related to speed to some power, the calculated power constants range from 0.36 to 0.71 for the five lubricants. Averaging the power constants for each OFT results in a power constant of 0.52 -- impressively close to the numerical correlation and the scaling analysis which have power constants of 0.53 and 0.5, respectively.

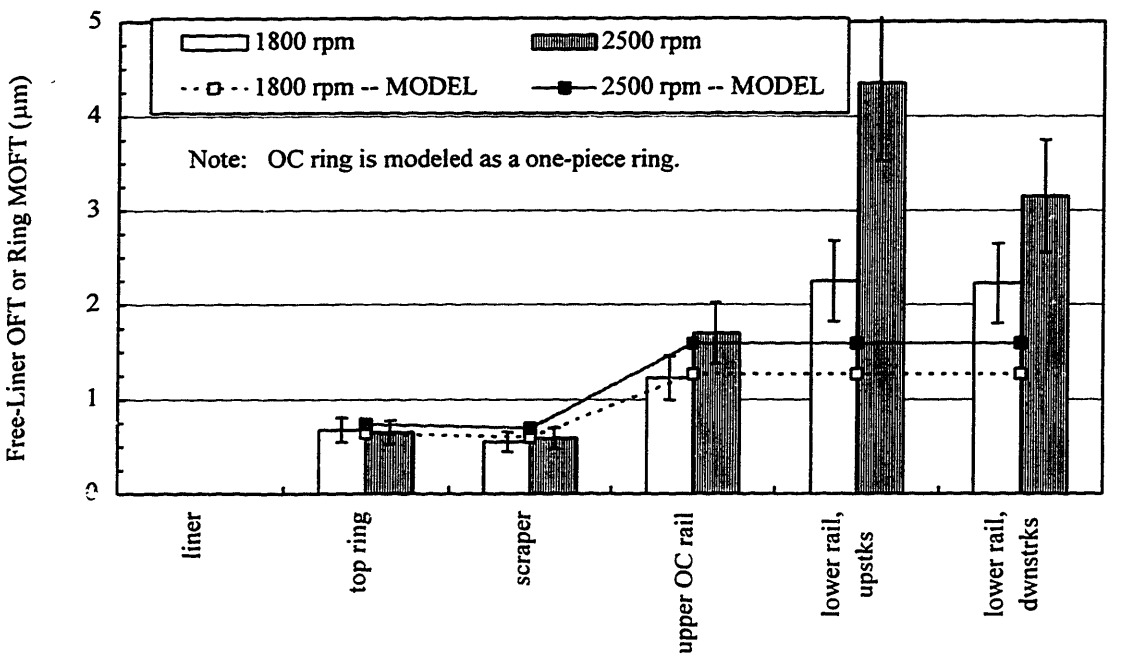

Figure 4-29 Engine Speed Effect from 1800 to 2500 rpm Measured from Window 6 for SAE-10W/50n
(2/3 Load, 100°C Midstroke Liner Temperature)

Since window 6 is located near BC, the piston is decelerating during a downstroke and accelerating during an upstroke in this region. Consequently, the sliding speeds of the rings are considerably different as each ring passes the window. For instance, as the piston decelerates through a downstroke at 2500 rpm, the lower OC rail is followed by the top ring, and they are traveling at speeds of 6.19 m/s and 1.89 m/s, respectively -- a 70 percent decrease in sliding speed. Therefore, although the MOFTs for the rings are in the same figure, Figure 4-29, comparing MOFTs for the same sliding speed is illegitimate. (Further analysis for how MOFTs change along a stroke is continued in the next section, section 4.4.2.)

Although squeezing terms in equation G.3 are have a greater influence at BC than midstroke, scaling arguments discussed in Appendix G show that these time-dependent squeezing terms are still negligible even at window 6 for the top ring; only for speeds of one meter per second or less should these terms become a concern.

Displaying MOFTs from window 6 at the two engine speeds for SAE-10W/50n, Figure 4-29 reveals the same increasing trend with engine speed as seen at midstroke although there isn't much difference between the MOFTs of the top and scraper rings. Perhaps the gaining influence, although still small, of the squeezing effects are slightly mitigating the effects of sliding speed for the lower speeds of the top and scraper rings compared to the OC segments or rings at midstroke. (The free-liner OFT could not be measured because the top of the crown land did not pass the window.)

Again, the model fits the data remarkably well. Especially for the compression rings and the upper OC segment, predictions are within the uncertainty of the measurements -- a trend seen at midstroke except for the low-viscous lubricant SAE-10W at 1800 rpm. All measurements agree with model predictions within a factor of two except for the high upstroke MOFTs of the lower OC segment at 2500 rpm.

Low confidence in high calibration accuracies for the remaining cases at window 2, 4, and 6 precludes further accurate comparisons of absolute magnitudes with engine speed. Nevertheless, from knowledge of the LIF system and how the data was acquired

by the experimenter, useful information from these remaining cases addressing engine speed effects can still be extracted.

Two conditions must be met in order to extract information from the less accurate data. First, cylinder liner temperature was strictly controlled at 100°C between the two engine speeds. Consequently, although friction and, thus, viscous dissipation increases with engine speed, the lubricant temperature along the liner should remain the same. So the fluorescent efficiency of a particular lubricant should not change with engine speed. Secondly, between the different speeds for a particular lubricant, the experimenter did not disturb the system in any way such as temporarily detach the system from window to window or even adjusting the LIF probe or PMT voltage.

Since lubricant fluorescent efficiency and the experimental apparatus remains the same during an engine speed change, relative effects for changes in engine speed can be detected even for poor calibration accuracy -- contingent on one important condition; different cases for the same lubricant must be reduced with the same calibration coefficient. Further proof of the credibility of this approach may be found in comparing the calibration coefficients found for the cases with high calibration accuracy at windows 1 and 6 from Table D.1. For every lubricant for both engine speeds, the calibration coefficients are the same. Conversely, for lubricants for cases with low confidence in high calibration accuracy, the calibration coefficients deviated from equality, further confirming poor calibration accuracy at these conditions.

In conclusion, useful information on MOFT trends for different engine speeds may be extracted from the same-lubricant cases provided that the same calibration coefficient, regardless of the degree of accuracy, is used between them. Although the absolute magnitudes may be uncertain, the trends are meaningful.

However, despite this effort, results from the cases with less certain calibrations at window 2, 4, and 6 shown in Appendix I provide little confirmation to the clear trends found for the highly accurate cases at windows 1 and 6; in fact, a very slight decreasing trend with engine speed is observed for the free-liner OFT and MOFTs of the compression rings and upper OC segment but is highly questionable due to heavy standard deviation overlap. (Two drastically different exceptions include SAE-10W at

windows 2 and 6 and SAE-50 at window 6. Significant decreasing trends exist for SAE-10W at windows 2 and 6, but significant increasing trends exist for SAE-50 at window 6.)

Perhaps the slightly decreasing MOFT trend is actually occurring because of a slight difference in lubricant and measured liner temperatures. As engine speed increases, increased friction and viscous dissipation may slightly increase lubricant temperature although the liner temperature measured several millimeters from the liner surface doesn't change. Even a slight increase in lubricant temperature can have compounding effects; both fluorescent efficiency (and, thus, the LIF signal) and lubricant viscosity decrease with increased temperature. Consequently, the measurements would decrease even if sliding speed alone had no significant hydrodynamic effect on film thickness. In view of this argument and the general trends observed from the cases of poor calibration uncertainty, results from calibration correction are inconclusive, and engine speed effects on increasing OFT are, at best, less influential off the major-thrust side at midstroke corresponding to window locations 2 and 4.

4.4.2 Instantaneous Piston Speed Along a Stroke

As mentioned in the last section, the rings are approximately traveling at their maximum sliding speeds at midstroke. From midstroke windows to near BC along a stroke, ring speeds decrease by 31, 39, 51, and 79 percent as the lower OC segment, upper rail, and scraper and top rings passes window 6, respectively. Therefore, the larger changes in MOFT should be experienced by the rings closer to the top of the piston, and this effect from speed reduction on the MOFTs is indeed what is observed in the data and is described below in detail.

Comparing different instantaneous piston speeds along a stroke from window 1 to 6, Figures 4-30 (a) - (c) include SAE-10W, -10W/50n, and -50 for engine conditions of 2/3 load, 2500 rpm, and 100°C liner temperature. Additional cases are presented in Figures 4-31 (a) - (c) for different liner temperatures of 80°C and 60°C and an engine speed of 1800 rpm, respectively. Accompanying both sets of figures are model predictions for the ring MOFTs. (Again, the free-liner OFT was unable to be measured at

window 6, and the predictions only model a one-piece OC ring.) As in the engine speed analysis in the previous section, only cases with high calibration accuracies are compared against one another.

In view of the experimental data in the figures, all MOFTs (except for the lower OC segment on the upstrokes for half of the cases) decrease as the instantaneous sliding speed decreases along a stroke from window 1 to 6. From ring to ring, the top and scraper rings decrease more than the upper or lower OC segments as expected except for the case at 80°C where the percent decreases are more comparable. A good typical example is SAE-10W/50n at the baseline condition in Figure 4-30 (b). The percent decreases include 43, 41, 23, -50, and 4.5, corresponding to the rings and rails, respectively. From equation G.8, the MOFT is roughly proportional to the square of the sliding speed for a particular lubricant when squeezing effects are neglected. For the top and scraper rings and the upper OC rail, the experimental percent decreases are very comparable to the estimated decreases from analytical scaling including 54, 30, and 22 percent, respectively.

Roughly, 17 percent is expected for the OC segment but drastically differs from the lower OC rail results due to the trend reversal between upstrokes and downstrokes from windows 1 and 6. Also mentioned in section 4.2.3.1, in many cases the lower OC segment has a greater MOFT for the upstrokes than the downstrokes at 2500 rpm at window 6; this trend is opposite to what is usually observed at midstroke windows for 1800 and 2500 rpm and at window 6 for 1800 rpm. From this instantaneous sliding speed analysis, the lower OC rail also may not be as sensitive to sliding speed but may even increase from window 1 to 6.

One possible explanation for less sensitivity of the lower OC segment with instantaneous speed is the influence from the piston motion through lower rail contact with the groove. As the piston reverses direction moving through BC, the piston moves away from the major-thrust side towards the minor-thrust side during the upstrokes. Since inertial forces are down during the upstrokes and greater with increased speed, the increased contact of the lower rail and its groove may be enough for piston motion to draw the lower OC segment slightly away from the major-thrust side causing greater

upstroke MOFTs reversal. (Cylinder and land pressures relatively don't have much influence on behavior of the OC ring or lubricant around the OC compared to the high inertial and frictional forces between the OC ring and liner and groove.) Takashi *et al.* found piston motion to influence the OC ring behavior [17]; their findings are consistent with this explanation of stroke-by-stroke behavior for the lower OC segment described above.

Although the percent decreases of the experimental MOFTs are higher than numerical predictions -- typical for the *FRICTION-OFT* model -- numerical predictions for the top and scraper rings as well as the upper OC segment are usually within the standard deviations of the measurements except for the unusually low MOFTs from SAE-10W at window 6. Additionally, the model predicts less MOFT decreases for the OC ring than the compression rings -- also consistent with the data.

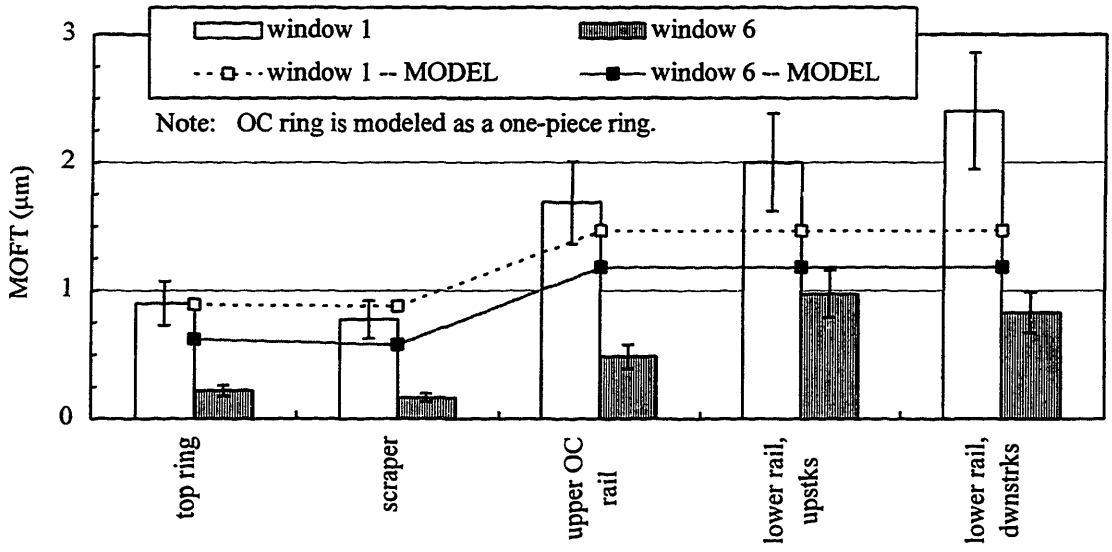

(a) SAE-10W

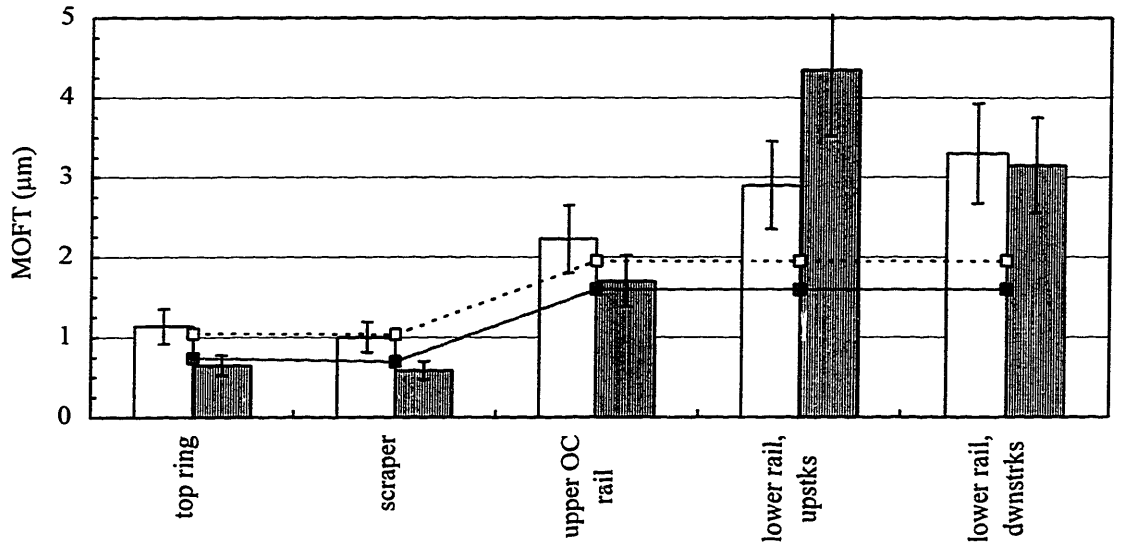

(b) SAE-10W/50n

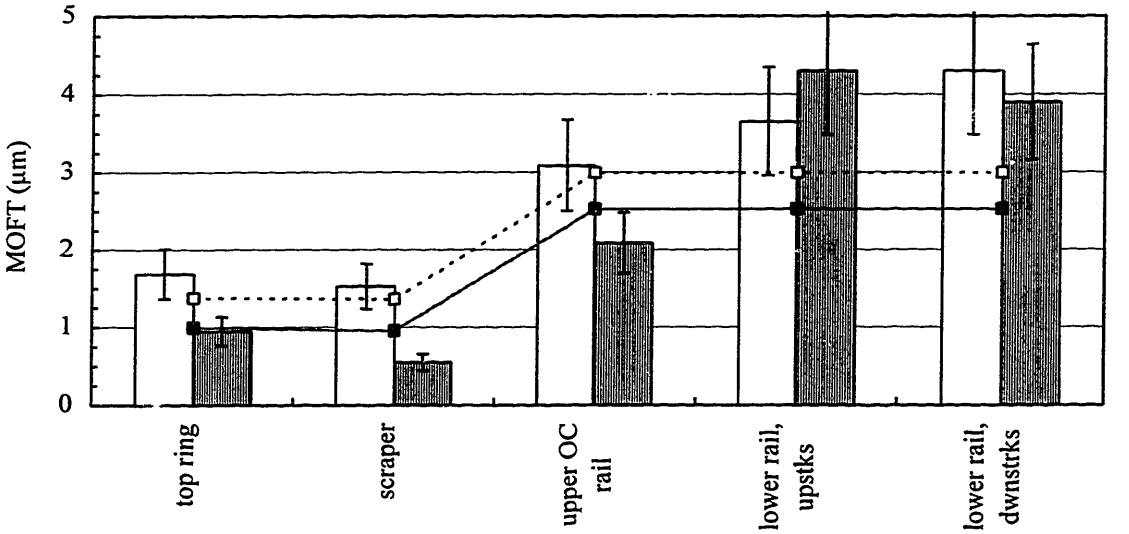

(c) SAE-50

Figure 4-30 Instantaneous Speed Effect along a Stroke from Window 1 to Window for (a) SAE-10W, (b) -10W/50n, and (c) -50.
(2/3 Load, 2500 rpm, 100°C)

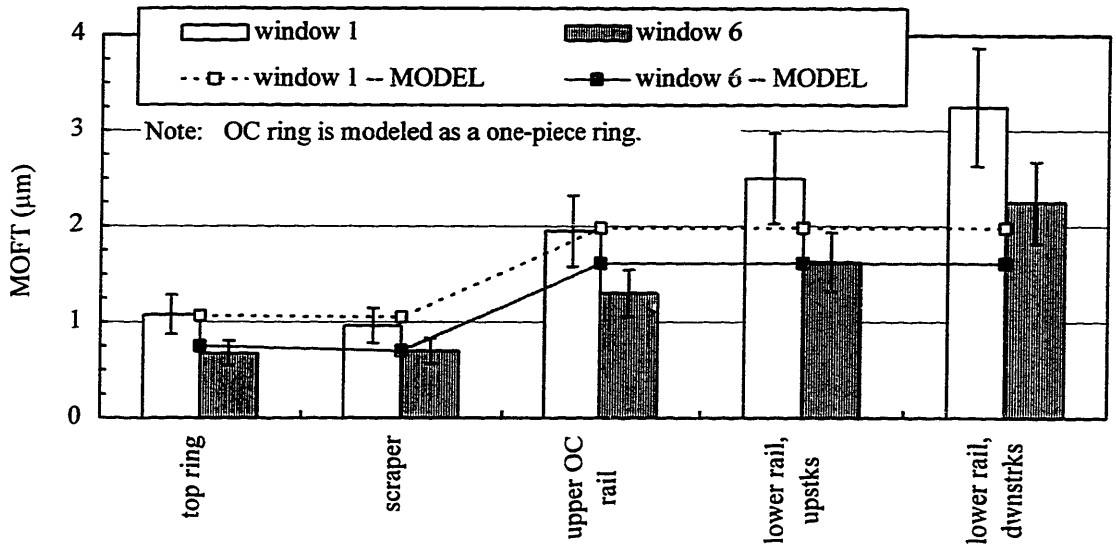

(a) SAE-10W at 80°C (2/3 load at 2500 rpm)

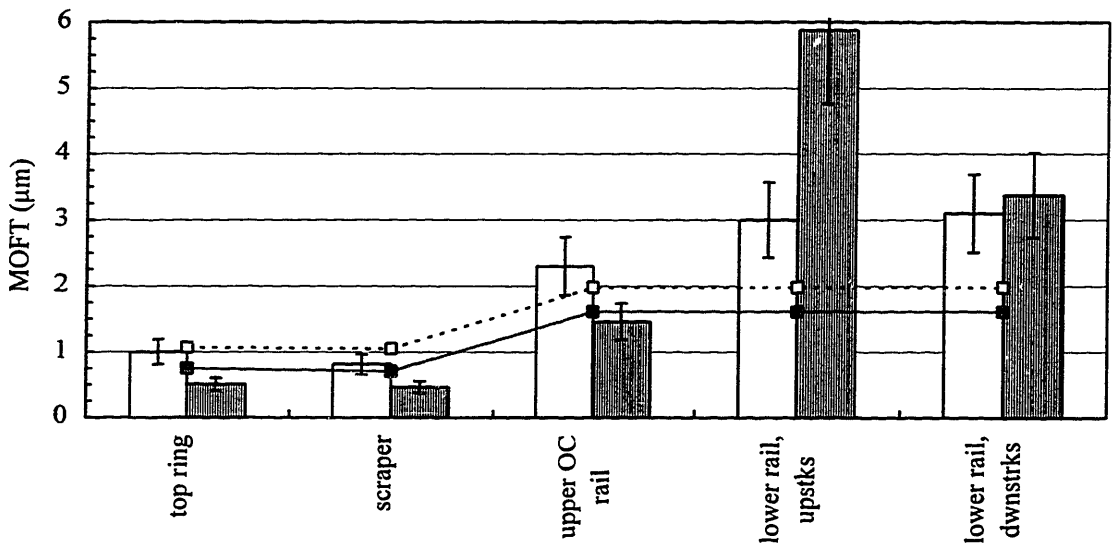

(b) SAE-10W at 60°C (2/3 load at 2500 rpm)

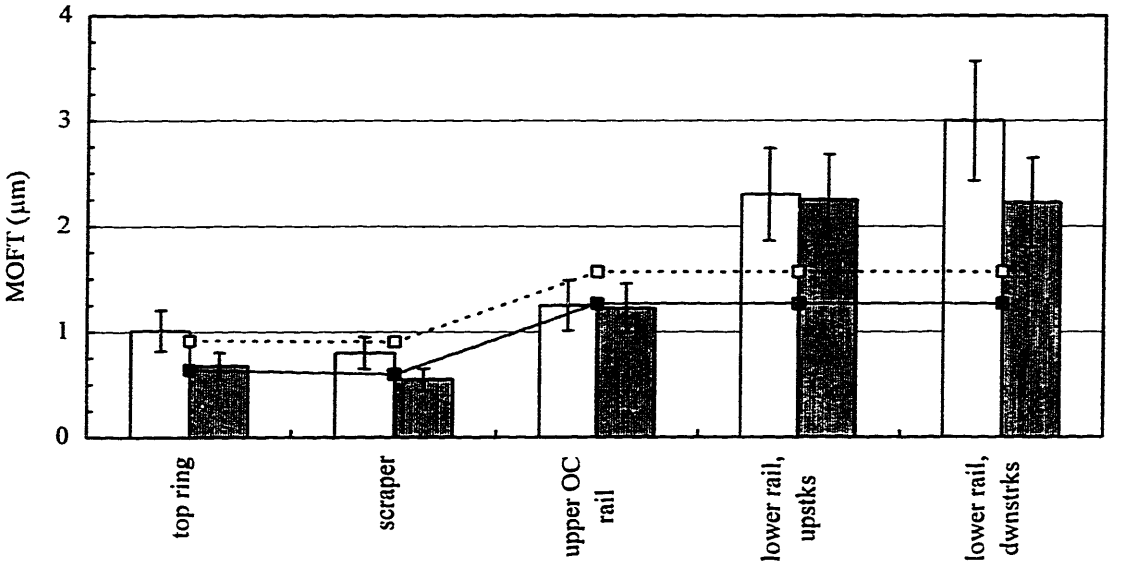

(c) SAE-10W/50n at 1800 rpm (2/3 load at 100°C)

Figure 4-31 Instantaneous Speed Effect along a Stroke from Window 1 to 6 for (a) SAE-10W (80°C, 2500 rpm), (b) -10W (60°C, 2500 rpm), and (c) -10W/50n. (1800 rpm, 100°C)

As a last note, when the time-dependent squeezing terms do become significant and dominate at very low piston speeds past window 6, MOFT hierarchy of the rings and segments can become vastly different. CA-resolved model predictions in Figure 4-19 show that at BC for -180° CA the MOFT of the OC ring can experience MOFTs much less than the compression rings. Compared to the compression rings, the high OC ring tension of five bars (typical of an OC ring) and its very sharp ring profile contribute to severe squeezing conditions. Especially for the OC ring around endstrokes, in addition to the low MOFTs and severe wear, the dynamic behavior is often very different than around midstroke [17].

4.5 SHEAR THINNING AND THICKENING OF MULTIGRADE LUBRICANTS

As mentioned in section 2.2, one characteristic of multigrade lubricants is their viscosity dependence upon the shear rate. For the Kohler engine as the piston reciprocates from midstroke to endstrokes, shear rates range from orders of 10^7 to zero 1/s, respectively. With critical shear rates of 10^4 or 10^5 1/s, multigrades experience high and low shear viscosities. At midstroke, by means of comparing the MOFT differences of monograde and multigrade lubricants, an argument can be made that shear thinning occurs before midstroke. However, this section shows that direct observation of shear thickening at window 6 cannot be observed and is not seen in the data.

At midstroke, multigrade lubricants flowing under the piston rings are experiencing high shear rates well above their critical shear rates and, thus, have high-shear viscosities (see section 2.2). The multigrade, SAE-10W/50n, has a high-shear viscosity of 8.4 cSt -- fairly close to the monograde SAE-10W with 6.3 cSt. The low-shear viscosity of this multigrade is about 17 cSt -- much closer to the thick lubricant, SAE-50, with 19.4 cSt. Since the MOFTs are roughly proportional to the square root of viscosity for a given sliding speed (eqn. G.7), at midstroke MOFTs from SAE-10W/50n are closer to MOFTs from SAE-10W than -50. Therefore, shear-thinning must be occurring earlier during the stroke. MOFTs from the top ring from these three lubricants are shown in Figures 4-32 (a) and (b) for engine speeds of 1800 and 2500 rpm, respectively. For 2500 rpm, the top ring MOFT from SAE-10W/50n is closer to SAE-10W. For 1800 rpm, although its hard to say whether the top ring MOFT of SAE-10W/50n is closer to SAE-50 in view of the uncertainty, the MOFT from SAE-10W/50n is approximately 35 percent lower than SAE-50's MOFT -- exactly the rough estimate from scaling predicts from high-shear viscosities. Therefore, these results suggest that shear thinning of SAE-10W/50n occurs.

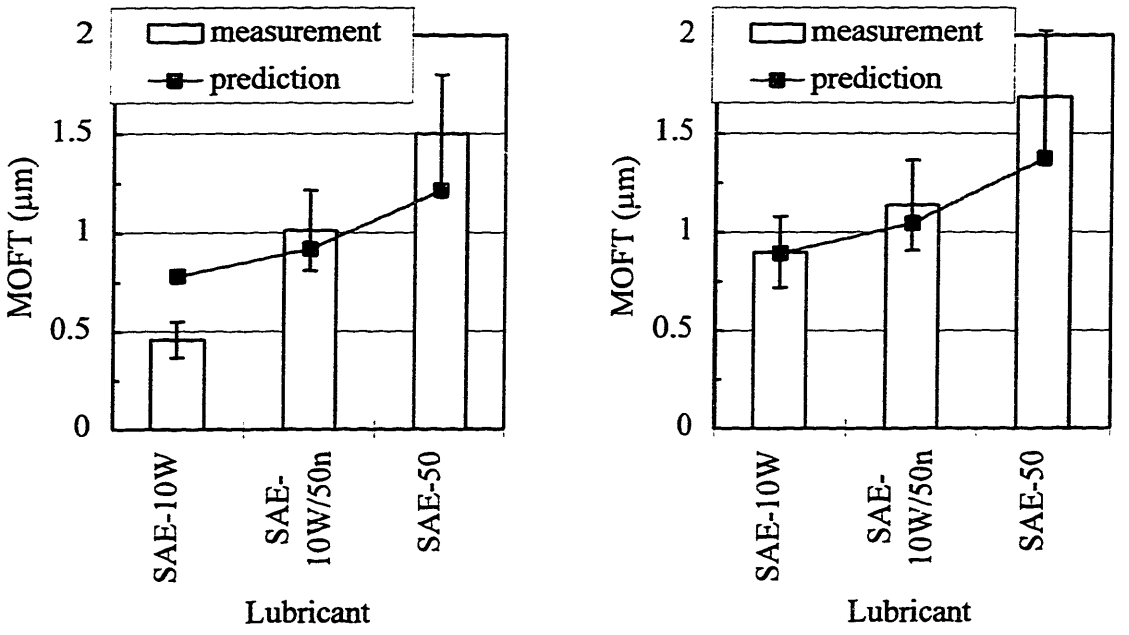

(a) 1800 rpm

(b) 2500 rpm

Figure 4-32 Top Ring MOFT for SAE-10W, -10W/50n, and -50 at Midstroke for (a) 1800 and (b) 2500 rpm
(Window 1, 2/3 Load, 100°C)

However, window 6 near BC is not far enough down the liner to detect shear thickening for multigrades. Since the top ring travels the slowest among the rings at window 6, the top ring generates the lowest shear rate within the lubricant -- approximately $2x10^6$ and $3x10^6$ at 1800 and 2500 rpm, respectively, for a liner temperature of 100°C. These shear rates are still well above the critical shear rate 40,730 1/s of SAE-10W/50n. Therefore, highly-viscous effects from shear thickening are not occurring and, thus, not inducing a MOFT effect at window 6. Figure 4-33 highlights the top ring MOFTs and how they change for the lubricants from midstroke at window 1 to near BC at window 6. All lubricants undergo a decrease in MOFT from the decrease in the instantaneous piston sliding speed along a stroke. However, SAE-10W/50n has the potential to have less of a MOFT decrease if the viscosity shear thickens.

Despite this possibility, the MOFT percent decreases in Figure 4-33 are very comparable from lubricant to lubricant -- especially SAE-10W/50n and -50 having

decreases of 43 and 44 percent, respectively. Therefore, there is no measured effect of shear thickening. From the viscosity-shear rate relation in Figure 2-2, any small amount of shear thickening corresponds to less than a one percent increase in the high-shear viscosity of SAE-10W/50n from window 1 to 6. Therefore, the shear-thickening effect from this small change in high-shear viscosity would not be detected in view of the precision of the LIF system which is consistent with the measured results.

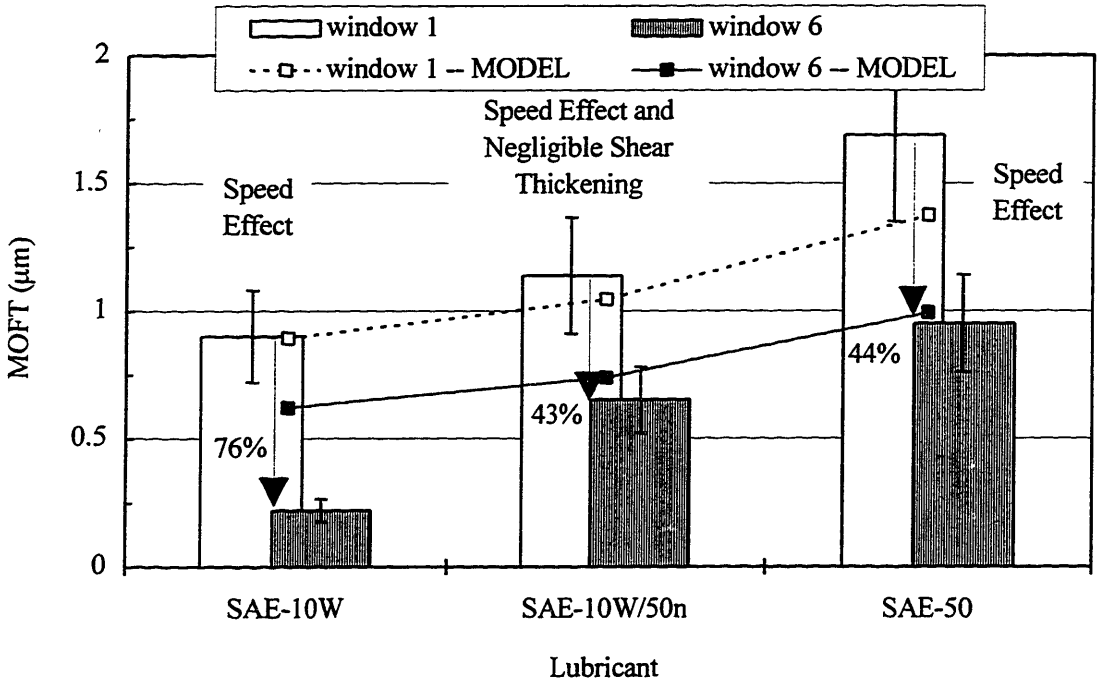

Figure 4-33 Top Ring MOFT for SAE-10W, -10W/50n, and -50 from Midstroke to near BC
(Window 1 Versus Window 6, 2/3 Load, 2500 rpm, 100°C)

4.6 AZIMUTHAL EFFECTS AT MIDSTROKE FROM BORE DISTORTION

The compression and OC rings must provide minimum levels of local surface pressure around the entire circumference of the bore to maintain their complex sealing function. One of the most important factors to affecting sealing is cylinder bore out-of-

roundness (OOR). The shape of the bore distortion as well as magnitude are important to whether the piston rings can adequately conform and seal properly. Studying the azimuthal differences of OFT along the free liner and under the rings can help determine the range of acceptability of bore OOR dependent on adequate sealing.

Having the best calibration accuracies at the three midstroke windows 1, 2, and 4, several lubricants shown in Table 4.1 are compared azimuthally around the bore's circumference at midstroke to these window locations. (However, the calibration accuracies of these cases do not all have calibration uncertainties better than +/- 5 percent Refer to Table D.1 for more details.)

Lubricant Number	*Lubricant Name*	*Operating Condition (f-fired, m-motored)*	*Kinematic Viscosity (cSt)*
1	SAE-10W/50n	f-2500 rpm, 100°C	8 (17)
2	SAE-30	f-2500 rpm, 100°C	12
3	SAE-10W	m-2500 rpm, 60°C	18
4	SAE-10W/50n	f-2500 rpm, 60°C	28 (56)

Table 4.1 Numbering Assignments for Lubricants
(Note: High-shear viscosities are in parentheses.)

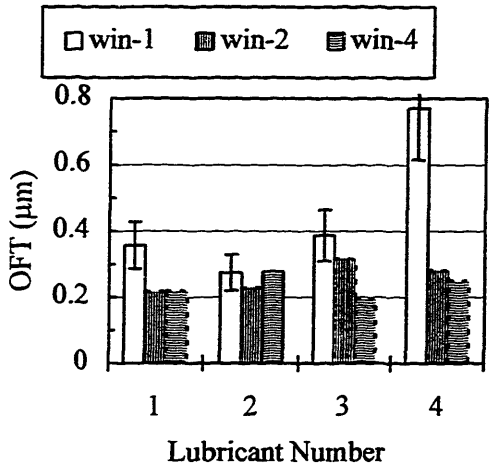

(a) Free Liner

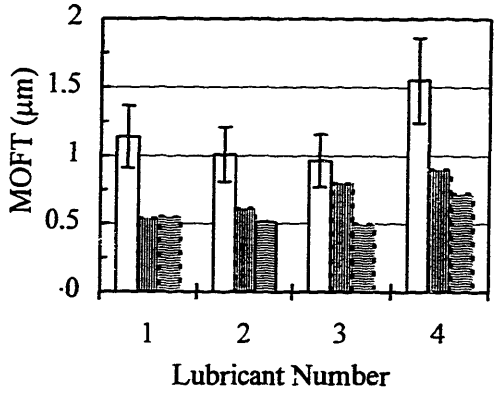

(b) Top Ring

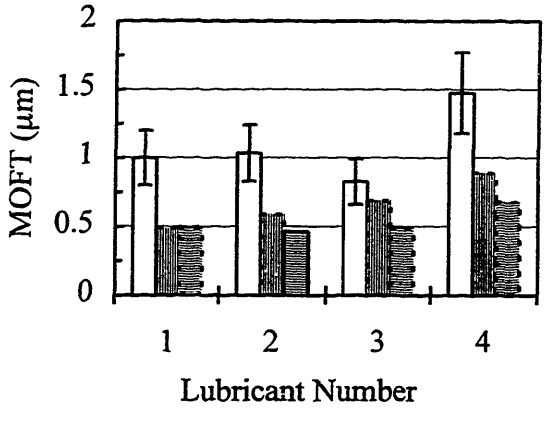

(c) Scraper Ring

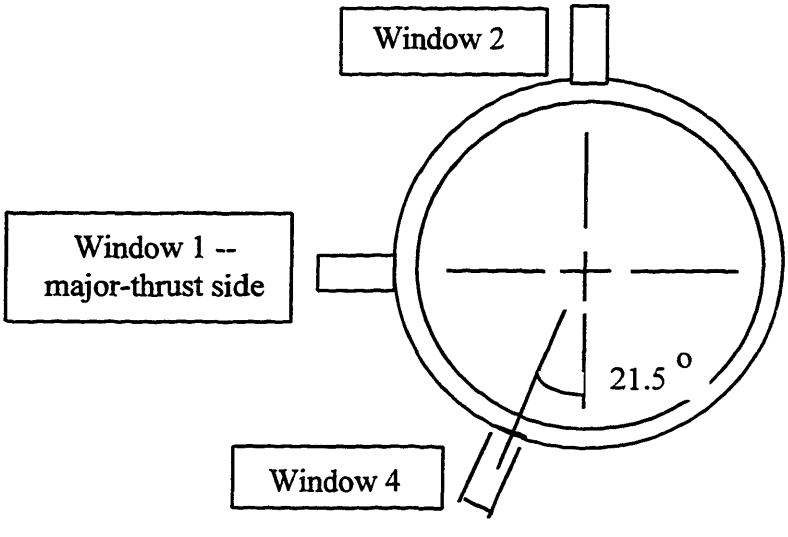

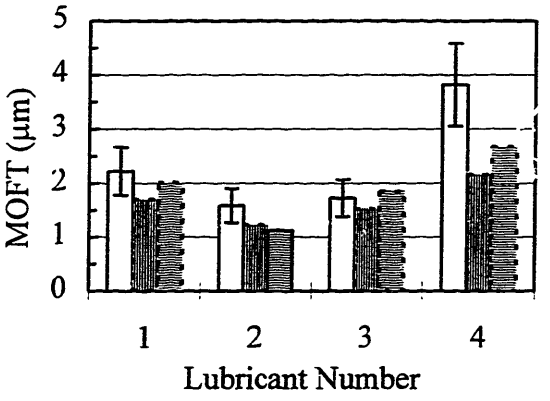

(d) Upper OC Segment

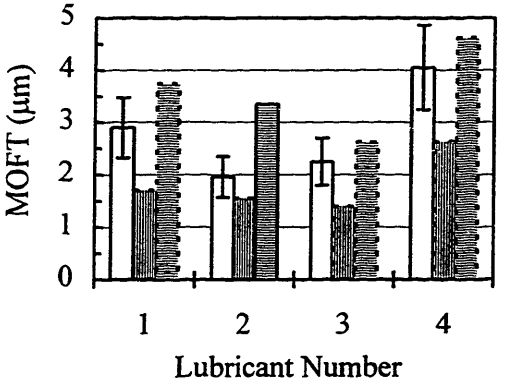

(e) Lower OC Segment, Upstrokes

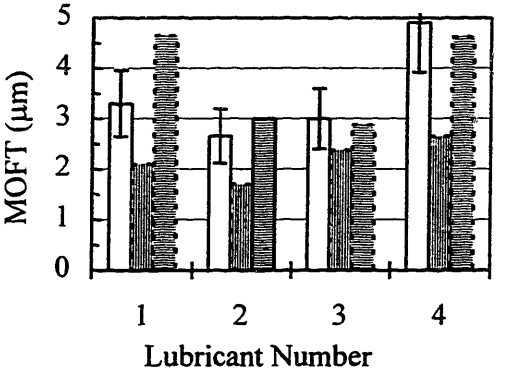

(f) Lower OC Segment, Downstrokes

Figure 4-34 Azimuthal OFT Measurements at Windows 1, 2, and 4 for Selected Lubricants and Operating Conditions for (a) Free Liner, (b) Top Ring, (c) Scraper Ring, (d) Upper OC Segment, (e) Lower OC Segment, Upstrokes, and (f) Lower OC Segment, Downstrokes.

OFTs for the free liner and under the top and scraper rings shown in Figures 4-34 (a) - (c) are always greater at window 1 by a half to three-fourths of a micron -- a factor of two greater than windows 2 and 4 in more than half of the cases. When OFTs at window 2 exceed those at window 4, the differences are marginal.

Since the scraper's lower wedge is always fully-flooded and scraping during the downstrokes, both the scraper and top rings have adequate oil supplies regardless of

azimuthal window locations. In view of the small differences in azimuthal OFT relative to the maximum radial difference between the windows of 16 μm (addressed in Appendix C), proper ring conforming and sealing is occurring. Arguing that proper ring sealing occurs, Schneider *et al.* [20] howed that reducing radial bore distortion from 50 to 30 μm does not substantially affect OC -- however, radial bore distortion of 100 μm does. vertheless, the small OFT differences but large percent decreases can be explained by differences in local ring pressure from bore distortion.

Illustrated in Figure 4-35, a non-conformed ring is shown within the worn bore profile. (Note the change in scale from millimeters within the O.D. of the ring to orders of microns outside the O.D. of ring.) As seen in the figure, the ring is perfectly rigid. Relaxing this restriction and allowing for ring conformability to the bore, sealing and OFTs as measured and shown above can be realized where every azimuthal location of the ring can be in contact with the thin oil film close to the bore. However, the local pressure distributed azimuthally may be far from uniform as shown by a qualitative possibility in Figure 4-36. Therefore, the local ring pressure on the lubricant film is most likely much less at window 1 than windows 2 and 4 based on the cold bore geometry in Figure 4-35. The less ring pressure on the lubricant at window 1 allows greater hydrodynamic lift of the rings and, thus, greater OFTs than windows 2 and 4.

For the oil control (OC) ring, OFT differences shown in Figures 4-34 (d) - (f) are a little different compared to the free liner and compression rings. The upper rail differences are much less between the windows and have very comparable MOFTs. The lower OC rail has equal or slightly greater MOFTs at window 4 compared to window 1. Window 2 always has significantly less MOFTs. Differences between windows are less pronounced for the OC ring. This result may be attributed to less differences in local OC ring pressures due to its greater flexibility and ring tension.

Additionally, at window 2 less oil exists immediately below the lower OC segment (see Chapter 5) and this less oil availability may contribute to less lift reflected in the lower MOFTs of the lower OC segments at window 2. (This is one of the reasons why calibration to the piston machining marks was not possible for window 2.) Although

the OFT trace appears to be fully-flooding the ring, starving is a still a possibility because of the decreased oil availability.

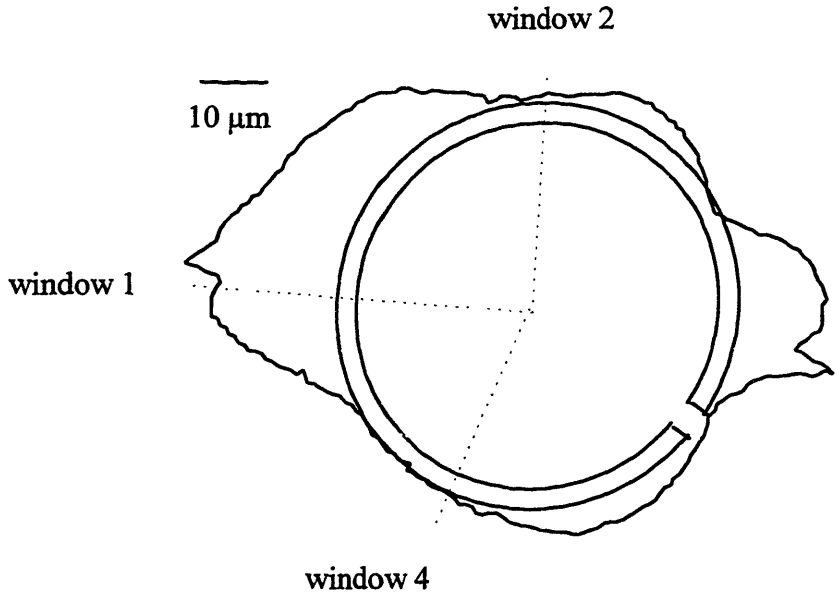

Figure 4-35 Bore Distortion with Non-Conformed Ring
(note: scale changes to orders of microns outside O.D. of ring.)

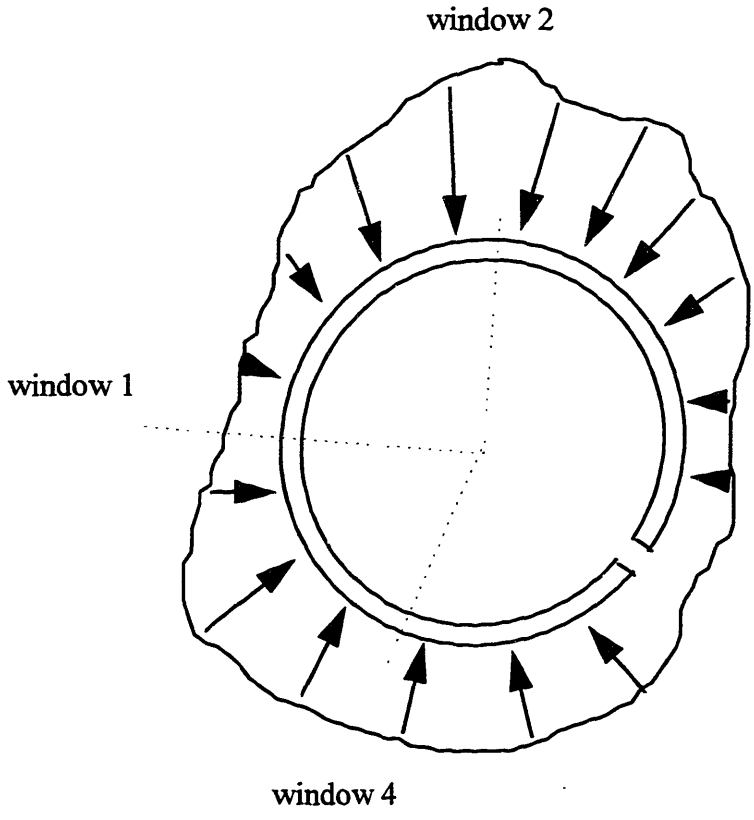

Figure 4-36 Possible Local Ring Pressure Load on Lubricant Film

4.7 OFT SUMMARY

This last section of Chapter 4 briefly summarizes the important OFT findings into two subsections. The first subsection primarily highlights the magnitudes and trends of the experimental OFT findings which, in most cases, are consistent with analytical and numerical analyses except for those cases which are explicitly addressed. In the second subsection, a comprehensive summary of the accuracy and range of applicability of the *FRICTION-OFT* model applied to the entire database is shown in a chart.

4.7.1 Experimental Findings

Careful and accurate calibration and data reduction resulted in extracting as much information from the current database as possible. Three different levels of calibration accuracy were found among the lubricant cases. Category I qualifies cases to have better than a +/- 5 percent calibration uncertainty and accounts for about 40 percent of the cases within the test matrix (see Tables 3.1 and D.1). (Most of the data used in this chapter are categorized with calibration levels of I or II.) The most accurate calibration method proved to be fitting the OFT trace to the upper skirt machining marks during the upstrokes when upper-skirt flooding is most reliable.

To help determine whether differences in ring minimum oil film thicknesses (MOFTs) among strokes, rings, and lubricant cases are significant or not, a covariance correlation from the manually-fitted MOFTs was determined from two independent databases resulting in a Coefficient of Variation (COV) of 18 percent. Typical COVs for the automated free-liner OFT measurements are roughly half this value.

The stroke-by-stroke differences (or lack thereof) for the OFT under the rings and along the free liner were investigated to justify using a stroke-averaged representation of the OFT measurements used throughout the majority of the study and to confirm and improve understanding of stroke-by-stroke ring behavior and its relation to OFT throughout a cycle. For the MOFTs of the top, scraper, and OC rings, differences and trends are only significant for the lower OC segment between the upstrokes and downstrokes in view of the rough 20 percent COV. At midstroke for a majority of the

cases, the lower OC MOFTs are greater during the downstrokes than upstrokes. For some random cases, the upper OC segment also shows this stroke-by-stroke trend, even near BC at window 6. (A simplistic conceptual model for this three-piece OC ring was described and explained this behavior.) Although trends of the lower OC MOFTs at window 6 for 1800 rpm are the same as midstroke but less pronounced, the MOFT trend of the lower OC segment reverses at 2500 rpm; the upstroke MOFTs are greater than downstroke MOFTs at this axial liner location and engine speed.

Having greater precision and a COV about half of the MOFT COV, the free-liner OFTs show some significant and consistent stroke-by-stroke differences and consistent trends. The intake and compression OFTs are approximately the same as well as the OFTs for the expansion and exhaust strokes. However, for the major-thrust side at midstroke, the latter two strokes (the expansion and exhaust) are significantly greater than the former two strokes (the intake and compression). Plausible explanations include effects from piston tilt and land pressures on scraper ring dynamics and are further supported with numerical calculations from *RINGPACK-OC* and *FRICTION-OFT* models. Compared to the effects of land pressures on the major-thrust side, the relative contribution of piston tilt on the scraper ring profile relative to the liner has a greater influence on free-liner stroke-by-stroke behavior.

For any single lubricant case within the entire database, an OFT hierarchy along the ring pack to the free liner is as follows. The free-liner OFT is about half of the MOFTs of the top and second rings which are approximately equal. The OC rails always have the greatest MOFTs with the lower OC rail always having the highest. This OFT hierarchy is explained and shown both experimentally and theoretically.

For the fired cases at moderate cylinder liner temperatures of 60, 80, and 100°C, the results on and off the baseline condition for the windows around midstroke and along a stroke near bottom center (BC) at the constant engine speed of 2500 rpm suggest that both the temperature and lubricant effects primarily translate into a viscosity effect; the OFT magnitudes and trends predominantly depend upon lubricant viscosity regardless of liner temperature or chemically-formulated differences between the lubricants. With the exclusion of the strong exception of SAE-50 (from 100 to 80 to 60°C) and the weak

exception of SAE-10W/50n (at 60°C from windows 2, 4, and 6) whose OFTs decrease starting in the neighborhood of 30 cSt, ring MOFT and free-liner OFTs increase with lubricant viscosity and agree with rough analytic scaling and the more exact numerical predictions from the *FRICTION-OFT* model. Although predicting the MOFTs of the upper OC rail quite well, the *FRICTION-OFT* model representing the OC ring as a single piece is still inadequate for describing the lower OC MOFT.

This trend reversal of the OFT-viscosity relationship for highly-viscous lubricants such as the fired behavior of SAE-50 have been observed in past works. Moore [18] argues that oil pumping difficulties through gap-and-groove oil flow pathways exist for the highly viscous lubricants. However, this claim has been ruled out for this engine based upon the oil distribution study in the Chapter 5, and any proven explanation has yet to be found.

After approaching the motored data similar to the fired data by evaluating the temperature and lubricant effects, an OFT-viscosity relationship is less clear. However, from 60 to 40°C, OFTs within the entire ring pack and free liner definitely decrease between 30 and 100 cSt for the three moderate lubricants not including the thinnest and thickest lubricants corresponding to SAE-10W and -50, respectively. These extreme lubricants usually show a very slight OFT increase with decreasing temperature. Interestingly, the rough 30 cSt is the same threshold viscosity after which the fired cases decrease as well. The OFTs of SAE-50 for both low temperatures are usually higher than the other measurements especially for the OC segments. Although the dominant effect of viscosity is not as pronounced as the fired cases, numerical predictions sharply diverge by more than a factor of two soon after 30 cSt -- the threshold viscosity for both fired and motored trends. Even the high OFT measurements from SAE-50 still fall short of the model predictions.

Because the different load conditions were tested between different temperature ranges, it's difficult to say whether the differences in lubricant behavior are due to the different loads or viscosity regimes. However, the fired trend reversal of the OFT-viscosity relationship including the strong and weak trends of SAE-50 and SAE-10W/50n, respectively, whose OFTs decrease starting in the neighborhood of 30 cSt and

the decreasing motored OFT trend starting soon after 30 cSt seem to support the argument that the trend reversal is governed predominantly by viscosity.

Speed effects on OFT due to engine speeds from 1800 to 2500 rpm (which originally included 3500 rpm as well) and the instantaneous piston speed along a stroke from window 1 to 6 at a constant engine speed are detected along the major-thrust side windows. Characteristic of hydrodynamic lubrication, measured OFT increases with speed comparable to analytical scaling with the square root of speed and more exact numerical calculations. However, results off the major-thrust side around midstroke corresponding to window locations 2 and 4 were inconclusive and, at best, less influenced by speed.

Although shear thinning and thickening are experienced by multigrade lubricants at some point throughout an engine stroke, only shear thinning is detected from windows 1 and 6. Empirically calculated shear rates on the order of 10^6 1/s are well above the critical shear rate of 40,730 1/s for SAE-10W/50n, and OFTs (including the free liner) at midstroke and near-BC windows only depend only upon the high-shear viscosity (insensitive to the low-shear viscosity) and, thus, are not affected by shear thickening.

Lastly, bore distortion affects azimuthal variations in OFT shown by the free liner and the top and scraper rings which have greater OFTs at window 1 by a half to three-fourths of a micron -- a factor of two greater than windows 2 and 4 in more than half of the cases. In view of the small differences in azimuthal OFT relative to the maximum radial difference between the windows of 16 microns, proper ring conforming and sealing is occurring. Nevertheless, the small OFT differences (but large percent differences) can be explained by differences in local ring pressure from bore distortion. Differences between windows are less pronounced for the OC ring. This result may be attributed to less differences in local OC ring pressures due to its greater flexibility and ring tension.

4.7.2 Extent of Agreement between OFT Measurements and Predictions from the *FRICTION-OFT* Model

Table 4.2 charts how well the OFT predictions from the *FRICTION-OFT* model agree with the experimental data. A complete legend and a description of the symbolisms

accompany the chart. Comparisons between the cases with poor accuracy (category III) and the model were not generally considered, indicated by the dark-shaded cells.

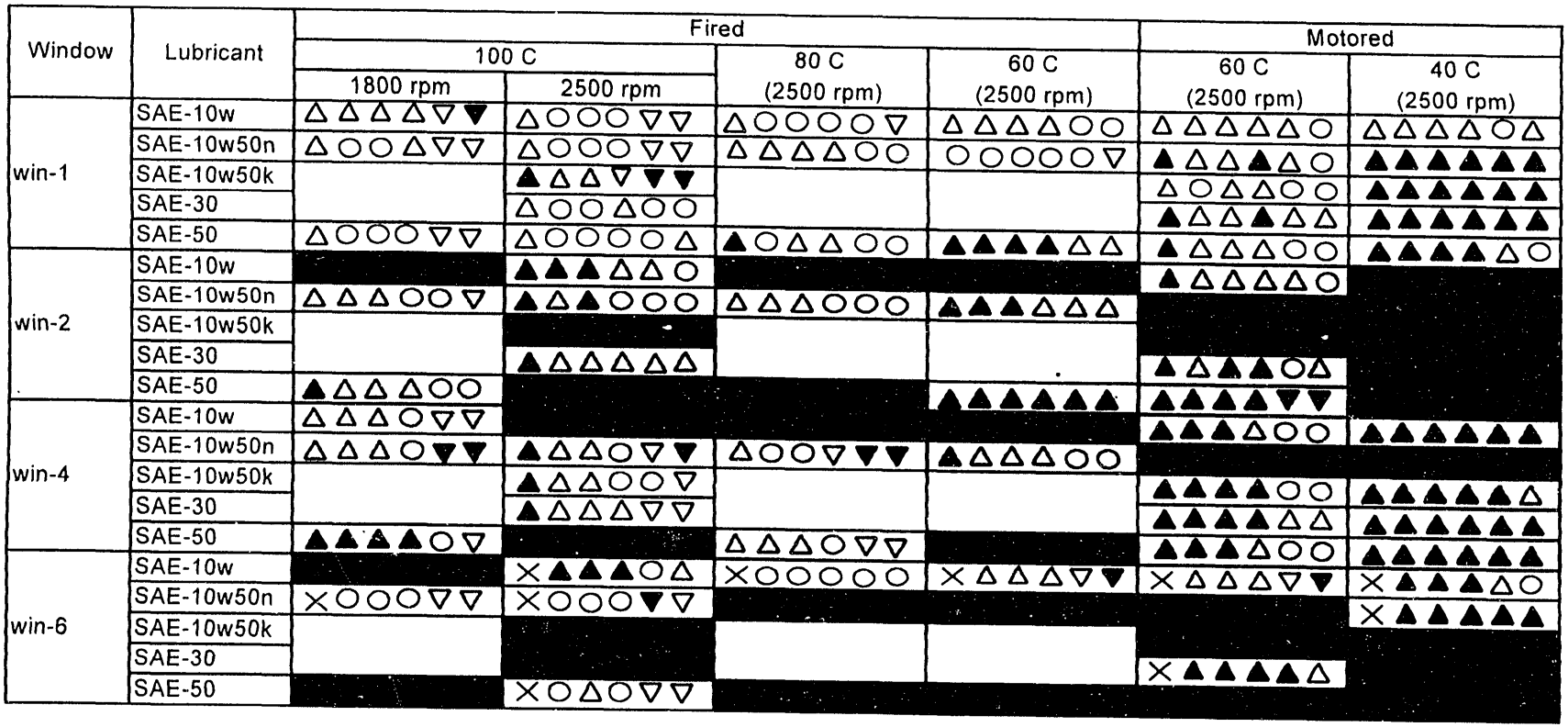

Legend:
- +/-5% calibration uncertainty or less.
- +/-5% is questionable .
- worse than +/- 5% calibration uncertainty.

Note: At window 4, all light-shaded cases have better accuracy than other light-shaded cases at other windows except for SAE-10w and -50 at 1800rpm and SAE-50 at 80 C.

Table 4.2 Extent of Agreement between OFT Measurements and Predictions from the *FRICTION-OFT* Model

Symbols:

Model prediction is

- ○ - within standard deviation of the OFT measurement
- △ - outside standard deviation, greater than the OFT measurement but within a factor of two
- ▽ - outside standard deviation, less than the OFT measurement but within a factor of two
- ▲ - greater than a factor of two (and outside standard deviation)
- ▼ - less than a factor of two (and outside standard deviation)

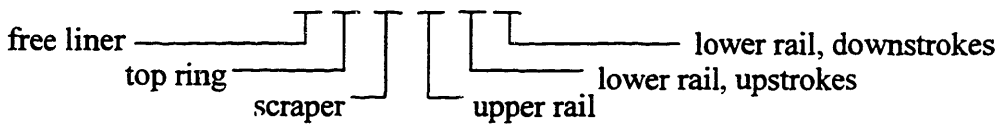

For the highly-accurate fired cases at moderate cylinder liner temperatures of 60, 80, and 100°C, OFT predictions on and off the baseline condition for the windows around midstroke and along a stroke near bottom center (BC) at the engine speeds of 2500 rpm and 1800 rpm (only at 100°C) usually fall within a factor of two of the data if not within its standard deviation. The OFT magnitudes and trends predominantly increase with lubricant viscosity. However, the trends of the model and measurements start to diverge for SAE-50 (from 100 to 80 to 60°C) and SAE-10W/50n (at 60°C from windows 2, 4, and 6) whose measured OFTs decrease starting in the neighborhood of 30 cSt. Within the chart, this divergence is indicated by the dark upward arrows for SAE-50 at 60°C which indicate gross overpredictions by greater than a factor of two for the free liner, the top and second rings, and the upper OC rail. Although predicting the upper OC MOFT quite well, the *FRICTION-OFT* model representing the OC ring as a single piece is still inadequate for describing the lower OC MOFT.

For the motored cases, predictions continue to overpredict the magnitudes and contradict the trends especially between 30 and 100 cSt for the three moderate lubricants not including the thinnest and thickest lubricants corresponding to SAE-10W and -50, respectively. This viscosity range includes many cases from 40°C, and model divergence

by more than a factor of two is indicated by the black upward arrows dominating the right side of the chart.

Once accurate OFTs have been predicted as shown in the chart, accurate friction predictions may follow. Although no friction measurements from the Kohler were taken, measurements from a diesel engine at Shell including the same five lubricants in this thesis are predicted quite well from the *FRICTION-OFT* model. Friction results were summarized in the lubrication meeting for the MIT Lubrication Consortium [21]. Although the model only calculates ring-pack friction, predicted fmeps by the model range from 40 to 55 percent of experimental fmeps -- typical percentages of the ring-pack contribution to total piston assembly friction.

(This page is intentionally left blank.)

CHAPTER 5:
OIL DISTRIBUTION WITHIN THE RING PACK AND ALONG THE PISTON SKIRT

Oil transport within the piston ring pack and along the piston skirt is the least understood area in PRL lubrication. However, understanding oil transport within the PRL system is most important for understanding and predicting oil consumption, and no comprehensive oil transport model for predicting oil consumption has proven accurate to date.

To help confirm current understanding of the oil behavior and further characterize oil transport within the ring pack and along the piston skirt, the measured oil distribution patterns within the ring pack and along the skirt are studied in this chapter. The approach is similar to the OFT study in the last chapter but starts with a detailed chapter summary which presents the major findings and refers to the appropriate subsections which follow. First, quantification of the oil in different regions along the piston assembly is described and dependent upon azimuthal and axial window location. Secondly, all of the baseline results from the four windows are shown and represented by stroke as well as a justified stroke-averaged representation. From case to case, the effects of the different lubricants are investigated. Additionally, any stroke-to-stroke differences (or lack thereof) within the cycle are shown and interpreted.

Thirdly, results off the baseline condition are investigated including effects from different lubricants, liner temperatures, loads, and speeds. Azimuthal differences from bore distortion at midstroke are shown and interpreted as well.

Lastly, some dominant oil transport mechanisms and parameters are directly observed throughout the chapter and are highlighted in the last subsection. In addition to influences from inertia, scraping, and oil squeezing between the top ring and its groove and the piston skirt and liner, oil dragging from gas flows and viscosity restriction on oil flow are shown to affect oil transport as well.

During this study when appropriate, both the *RINGPACK-OC* and *FRICTION-OFT* models are applied to assist in the interpretation. Although the *RINGPACK-OC* model generates land pressures for the *FRICTION-OFT* model, the predicted ring lifts within the grooves provides insight to the stroke-by-stroke trends of oil squeezing between the rings and grooves. Also, predicted gas flows help interpret the oil distribution trends along the upper lands.

As for the *FRICTION-OFT* model, oil transport physics captured by the model are confirmed and validated from the measurements. Although the *FRICTION-OFT* was solely developed to predict free-liner OFT and ring MOFT, it does predict one form of oil transport -- ring scraping. During a downstroke as the scraper scrapes oil from its fully-flooded lower wedge called down-scraping, oil accumulates within the third land region. Additionally, ring dynamic twist and its effects on top and scraper scraping which affects OFT are also predicted by the model and are especially important for diesels but less important for gasoline engines with lower cylinder and land pressures like the Kohler [22].

5.1 A DETAILED OIL DISTRIBUTION SUMMARY

This first section of Chapter 5 summarizes the important findings from the oil distribution study. The first subsection highlights the experimental findings to which predictions from the *RINGPACK-OC* and *FRICTION-OFT* models were applied when appropriate to help assist in the interpretation. First, stroke-by-stroke differences within different regions exist only for the regions between the OC rails and below the OC ring. In addition to ring oil squeezing from interaction of the top ring and its groove, oil transport along the piston skirt on the major-thrust side is significant. Then, stroke-averaged average region thickness (ART) magnitudes and trends (or lack thereof) are summarized for fired and motored cases which include the different lubricants for different cylinder liner temperatures. Implications of oil film thickness (OFT) behavior with an emphasis on SAE-50 and oil pathways through gaps and grooves between different regions are addressed. Thirdly, other engine operating effects on ARTs and oil

distributions from loads and speeds are studied, and results show evidence of oil dragging from gas flows consistent with numerical predictions of gas-flow and ring dynamics from the *RINGPACK-OC* model. Measured and calculated oil travel from inertial influences along the third land region compare fairly well for both engine speeds of 1800 and 2500 rpm. Lastly, azimuthal differences and randomness of ART data for the upper lands are briefly addressed in view of the bore distortion, OFT, and recent findings from two-dimensional (2-D) visualization.

The second subsection addresses model verification of ring boundary conditions such as scraping (fully-flooded) and starved (unflooded) conditions in the *FRICTION-OFT* model and quantitative verification of predicted scraper down-scraping along a stroke from the *FRICTION-OFT* model and predicted top ring lift within a cycle from the *RINGPACK-OC* model.

5.1.1 Experimental Findings

Stroke-By-Stroke Differences (from Section 5.3.2)

Within the ring pack, stroke-by-stroke differences in average region thicknesses (ARTs) are significant between the rails of the OC ring and along the second land region only when oil squeezing between the top (and rarely second) ring and its groove is exceptionally high (especially for SAE-50 which typically has the most oil on the second land compared to the other lubricants). Between the OC rails (region 4), ART downstrokes are often higher than the upstrokes. At midstroke, this stroke-by-stroke trend is rather independent of azimuthal location which suggests that the mechanism for this stroke-by-stroke behavior may have more to do with the OC ring behavior than the influence of piston secondary motion. In part, this occurrence may be due to the higher downstroke MOFTs of the lower OC segment. Conversely, opposite ART trends exist for the motored cases for 40°C and 60°C at window 1 but are more random and less clear and significant at the remaining windows.

Since oil squeezing between the top (and rarely second) ring and its groove depends upon relative ring lift which may differ from stroke to stroke (i.e., expansion and

intake), oil squeezing between the top ring lower channel is greatest during the expansion stroke and mostly nonexistent in the intake stroke. The compression and exhaust strokes exhibit less squeezing than the expansion stroke with compression squeezing a little higher than the exhaust. This stroke-by-stroke oil squeezing hierarchy is explained by top ring lift relative to its groove and is confirmed by predicted ring lift and contact pressures from the *RINGPACK-OC* model for both the midstroke and near-BC window locations throughout the cycle.

Lastly, for the regions below the OC ring, stroke-by-stroke differences are shown to be significant for the groove/chamfer and upper piston skirt regions (corresponding to regions 5 and 6, respectively). (Refer to section 5.2 for region assignments.) For region 5 on the major-thrust side, the expansion is greater than the intake with the upstrokes having the lowest ARTs. However, along region 6 the upstrokes are greater than the downstrokes. These stroke-by-stroke trends are caused by piston skirt interactions with the cylinder liner which develop highly dynamic lubricant environments on the major-thrust side from piston secondary motion; oil transport mechanisms including inertial, squeezing, and scraping are accompanied by the hydrodynamic lubrication characterized along the lower portion of the piston skirt (region 7). Oil transport up the groove/chamfer region and azimuthally around the skirt as the piston reciprocates through top center during the gas exchange strokes as well as the power strokes is shown to significantly occur.

Fired Cases at 2/3 Load for 2500 and 1800 RPM for Moderate Cylinder Liner Temperatures of 60, 80, and 100°C (from Section 5.4.1)

For all of the fired cases, negligible oil exists on the top crown land. The absence of oil is probably due to evaporation, burning, and downward gas flows through the top ring gap and groove which drag oil into the second land region. (One exception is for SAE-10W/50n at 60°C. This case is atypical and is recommended to be ignored based upon reasons in section 5.4.1.1.2). Quite unlike any other regions, ring scraping does not directly contribute to oil on the top and second lands -- only gap and groove oil transport

-- and is one of many reasons why no oil and very little oil exist on the crown and second lands, respectively.

Ranging from 0.5 to 2.25 microns, oil on the second land is shown to be significant. Relative to the top land, less evaporation from lower piston land temperature, greater lubricant partial pressure within the second land vapor, and absence of burning contribute to more oil. Additionally, downward gas flows from the top land from high fired cylinder pressures hold back oil along the second land, and the second land also has direct access (through the second ring gap and groove) to large quantities of oil supply within the third land region which are an order of magnitude higher and accumulate, in part, from the down-scraping of the taper-faced second ring. Although no clear trend is observed for small viscosity scales (~ 1 cSt) within the second and third land regions, ARTs tend to increase for large viscosity scales (>10 cSt) except for the drop in SAE-50 at 60°C.

Except for the increase of SAE-50 at 60°C for region 4 -- the region between the upper and lower segments, ARTs do not change much over large viscosity scales (>10 cSt. For small viscosity scales (~ 1 cSt) the pattern is rather random, and no clear trend is evident.

The lower OC segment is observed to always be fully-flooded, and its scraping contributes to the highest ARTs along the entire piston assembly within the groove/chamfer region (region 5) especially for the downstrokes resulting in ARTs which range from 70 to 90 microns on the major-thrust side. ARTs increase with decreasing temperature (or increasing viscosity) especially for the upstrokes. The oil scraped is supplied from the lower piston-skirt regions.

Because the regions below the OC ring include piston geometries and piston tilt effects which are greatly different between azimuthal windows around midstroke, results from the major-thrust and non-major-thrust locations are summarized separately. For the major-thrust side, ARTs for region 5 increase slightly with viscosity over the entire viscosity range with the upstrokes increasing at a faster rate. However, the downstroke ARTs of region 6 (which are lower than the upstrokes) reveal the same trend as that along region 7 which strongly resemble the OFT trends for hydrodynamic lubrication; ART (or

OFT from the OFT analysis under the rings and along the free liner) increases with viscosity except for SAE-50 which decreases with viscosity corresponding to cylinder liner temperatures of 100 to 80 to 60°C. Hydrodynamic lubrication is most likely predominant in region 7 which includes the skirt's largest diameter. Regions 5 and 6 are governed by inertia, OC ring scraping, and piston oil squeezing and are supplied by the hydrodynamic flow from the lower portion of the skirt -- region 7.

Interestingly, the free-liner OFT below the piston skirt -- region 8 (captured by window 6 near BC) -- ranges from 3 to 6 microns. However, no trends are evident in view of the large standard deviations.

For the non-major-thrust window locations below the OC ring, ARTs from window 4 increase with increasing viscosity for regions 5 and 6. Along region 7 where there is no piston skirt, it is hard to describe a trend in view of the large standard deviations. (Having similar piston geometry as window 4, window 2 had cases with worse calibration accuracies due to the starved region 6 where the calibrating tool marks exist.)

Motored (WOT) at 2500 RPM for Low Cylinder Liner Temperatures of 40 and 60°C (Major-Thrust Side at Midstroke) (from Section 5.4.2)

Unlike the fired cases, a small amount of oil now exists on the crown land ranging from 0.25 to 1.75 microns. However, no clear ART-viscosity trend for lubricants at the same temperature is evident, and SAE-50 always has more oil than the other lubricants.

Having a greater amount of oil than the crown land by a factor of two, the second land reveals the same random patterns for the lubricants with SAE-50 having more oil whose relative amount is less pronounced at 60°C.

Although the magnitudes are an order of magnitude higher compared to the second land region and, again, reveal no clear trends for the same temperature, ARTs from the third land region have the same lubricant patterns as the oil on the crown and second lands (with one weak exception for SAE-10W at 60°C).

However, region 4 has a decreasing ART-viscosity trend at 40°C except for SAE-50 and the remaining regions between the OC ring from 5 - 7 hint at this decreasing ART-viscosity relationship in region 4 (except for SAE-50) but is certainly less clear.

For the same lubricant subjected to a decrease in temperature (or viscosity) from 60 to 40°C, the ARTs decrease. The oil on the crown and second lands and along third land region typically decreases with temperature except for SAE-10W/50n on the crown land and SAE-10W in the third land region which do not change significantly between the two temperatures. This ART-temperature trend strongly reverses for SAE-50 for regions 4 and greater. The ARTs from region 7 and downstroke ARTs from region 6 are very comparable and characterize the ART-viscosity pattern found in hydrodynamic lubrication under the rings from the OFT analysis; ARTs along the piston (and OFTs under the rings) definitely decrease with decreasing temperature between 30 and 100 cSt for the three moderate lubricants not including the thinnest and thickest lubricants corresponding to SAE-10W and -50, respectively. (From the OFT analysis, SAE-50 shows an slight increase with decreasing temperature while SAE-10W remains relatively the same.)

Important Insights and Implications to Fired and Motored ART Results (from Sections 5.4.1 and 5.4.2)

In addition to the ART trends (or lack thereof) in individual regions along the piston assembly, other important information concerning oil transport may be extracted including inter-region lubricant flow through the gaps and grooves and the relationship between oil distribution and OFT behavior under the rings and along the free liner.

Although the magnitudes along the third land region are an order of magnitude higher, the oil on the second land (as well as the oil on the top land during motoring) shows patterns (not trends) very similar to the ART patterns from the third land region -- a recurring and universal result independent of liner location, lubricant, and engine operating condition. (A pattern is the figure resulting from ARTs versus viscosity and is independent of any viscosity trends.) Since ring scraping is absent along the crown and second land regions, pattern similarity among the first three land regions suggests that

gap-and-groove oil pathways are significant within these regions. The high oil accumulation scraped within the third land region acts as a finite reservoir supplying the second land region with oil via the second ring gap and groove; a greater oil supply within third land region allows more oil to seep through these non-hydrodynamic pathways. The different magnitudes between the regions provide support to the fact that other oil transport physics are at work besides solely a gap-and-groove pathway such as second ring down-scraping within the third land and downward gas flows through the second gap and groove to retain oil below the second ring.

On the contrary, regions 3 and 4 exhibit quite contradictory ART patterns especially for SAE-50 at 60°C falling from 80°C by almost half in region 3 and rising in region 4. This finding may imply that oil transport between the third land region and the region between the OC rails are not strongly linked through ring gaps and grooves.

However, region 4 and those regions immediately below the OC ring typically do not exhibit contradictory patterns and, at best, resemble each other. This finding provides evidence to the argument that, despite a fully-flooded lower OC rail, regions immediately below the OC ring may contribute to and feed other oil transport routes via the OC ring gaps and groove.

ART behavior of SAE-50 lends some insight to its OFT behavior. Actually, studying the ART behavior of SAE-50 helps to understand what is NOT happening to its OFT under the rings and along the free liner. From the OFT analysis for SAE-50, the OFT for the top ring decreases from 100 to 80°C (or with increasing viscosity). However, in view of the ARTs for SAE-50 for the second and third land regions, the ARTs increase. Therefore, for this engine, the decrease in top ring OFT is NOT due to oil pumping difficulty for the highly-viscous SAE-50 through the second ring gap and groove.

Additionally for SAE-50, oil behavior related to hydrodynamic lubrication (including oil flow under the rings as well as along the piston skirt for regions 6 and 7) experiences a decrease in OFT (or ART for the regions) with viscosity. For this trend reversal of the OFT-viscosity relationship for the highly-viscous lubricant SAE-50, a better explanation may be a change in the viscosity only during engine operation. One

mechanism may be due to increased local oil film temperature from excessive viscous dissipation especially between the piston skirt and the liner. The ART trend-reversal is definitely evident along region 7 where the maximum skirt diameter is located. Another mechanism for viscosity change may be chemical changes in viscosity due to contamination of the fuel which escapes combustion and is left on the cylinder walls. Having the thickest viscosity, SAE-50 may be the most sensitive to a viscosity change with fuel contamination. However, the latter explanation is unlikely because the lubricants were tested before and after the experiments for viscosity changes, and none were found.

Other evidence for independent and uncoupled behavior of oil on the lands and OFT under the rings include some motored counter-examples. Top and scraper MOFTs do not significantly decrease for SAE-10W and -50 with temperature (or viscosity). However, oil on the crown and second lands decrease for SAE-10W and 50. If the ring MOFTs were strongly linked to oil on the lands, the MOFTs should experience a marked decrease as well.

In retrospect, although oil accumulation does not affect the top and scraper MOFTs, oil accumulation along the lands does result, in part, from ring and rail scraping and may only affect the possibly unflooded upper OC rail MOFT. Gas flow on oil dragging (soon to be summarized for the load and speed effects), oil squeezing between rings and grooves and the piston skirt and liner, inertial forces, and viscosity restriction are influential to accumulation as well.

Fired Versus Motored (WOT) at 2500 RPM for Cylinder Liner Temperature of 60°C (from Section 5.4.3)

The top land is not completely dry for the motored cases, and the second land typically has more oil than the fired cases. Comparisons of the motored and fired oil distributions show that oil does not only increase due to accumulation of oil on the lands but from oil squeezing between the top and scraper rings and their grooves characterized by the sharp spikes along the relatively uniform oil distributions. (With the greatest percent increase of oil along the lands within the ring-pack, SAE-50 has the greatest

amount of oil squeezing.) ARTs increase within the regions 3 and 4 as well in the ring pack. Additionally within the ring pack, the percent increase in ART slightly increases with viscosity for the monogrades SAE-10W and -50, and the ART percent increase for SAE-10W/50n is less than the monogrades.

Since the regions below the OC ring provide vast but finite oil reservoirs which supply the ring-pack regions, the ART increase within the ring-pack may indicate that less oil is held back in these lower regions from reduced downward gas flows resulting in lesser ARTs observed within these lower regions. As a global measure, predicted blowby decreases by almost half from 3.03 to 1.75 l/minute from fired to motored, respectively, reduced by the fired and motored cylinder pressures corresponding to peak pressures of 31 and 18 bars, respectively.

Ring dynamics and gas flows through gaps and grooves are affected by the different loads caused by the cylinder pressures and affects how much of the oil is dragged by the gas flows. Although no drastic change in the predicted ring dynamics is evident, instantaneous mass flow rates through gaps and grooves of the top two rings decrease significantly especially through the gaps. Because gas flow rates significantly decrease and gap-and-groove oil pathways are significant, less oil is dragged down towards the third land region resulting in a greater amount of oil along the crown and second lands and within the channels between the rings and their grooves indicated by increased oil squeezing as well.

Although the lower channel of the top ring and the upper channel of the second ring are adjacent to the second land which directly connects any oil transport between the two, the amount of oil squeezing differs greatly between the two channels caused by channel gas flow in addition to the shape of the oil distribution on the land which is caused by changes in channel and gap gas flows from the different load conditions.

The gap flows contribute significantly to oil transport as well. Two-dimensional (2-D) visualization employed by the MIT Lubrication Consortium [23] confirms this result. For the top ring, the lower channel gas flows are negligible compared to the high positive gap gas flows which drag lubricant to the second land region. Conversely, less downward oil dragging potential exists for the second ring gap due to the lower gas flows

differing by an order of magnitude. More insightful though is the second ring upper channel gas flows which are greater than the gap flows by at least a factor of two because of second ring flutter.

In addition to oil dragging from gas flows, a host of other factors contribute to load effects on oil distribution particularly within the upper lands. Temperatures of the piston and rings are certainly lower resulting in less evaporation. In the vicinity of the crown land, oil burning is avoided compared to the fired condition. Relative to the top land, less evaporation in the second land region from greater lubricant partial pressure within the second land vapor contributes to more oil. Another effect from decreased temperatures result in changes in ring and groove clearances and their relative angles affecting gas flows and ring dynamics. For regions lower along the piston assembly, the intensity and timing of piston slap changes with load and may affect oil feeding of the OC ring as well on the major- and minor-thrust sides. All these factors probably have some degree of influence on the oil distribution between different loads but are very difficult to quantify.

Engine Speed Effects -- 1800 Versus 2500 RPM at 100°C (from Section 5.5)

Substantial enough to affect OFT in chapter 4, an engine speed change from 1800 to 2500 rpm affects the oil distribution even more in terms of percent increase for most regions and is detected from all windows.

Along the major-thrust side at midstroke (window 1) and near BC (window 6), the average region thicknesses (ARTs) significantly increase with speed for all the regions within the ring pack and along the piston skirt. Although the crown land has negligible oil under these fired conditions, the small amount of oil on the second land increases significantly.

Nevertheless, the greatest increases occur in regions with high oil masses -- regions 3 - 7 (and 8) -- with the third land region, the space between the OC rails, and regions below the OC ring (and the free-liner below skirt) having the greatest percent increases, typically soaring well over 100 percent -- much greater than MOFT increases of roughly 30 percent from hydrodynamic lubrication. Additionally, engine speed effects

between different lubricants are greater for the less-viscous lubricants which is probably caused by less viscosity restriction on oil flow. The percent increases for SAE-10W are much greater than the percent increases for SAE-10W/50n and -50 which show comparable percent increases. Lastly, upper OC ring MOFTs experience the greatest percent increase, probably resulting from its possibly starved upper wedge which is fed by the large increase in oil accumulation along the third land region.

Off the major-thrust side at midstroke for windows 2 and 4, the increasing ART trend with speed isn't as strong. The crown and second land regions show no marked increase in view of the standard deviation. Still, other regions significantly increase with engine speed but not as much as the major-thrust side. From the OFT study, no changes in MOFT are observed at windows 2 and 4 for SAE-10W/50n except for marginal increases for the OC ring segments at window 4 (see Appendix I). These results further conclude that oil transport pathways through the gaps and grooves (other than under the rings and ring oil scraping) and oil transport mechanisms such as lubricant dragging from gas flows and inertial forces play a significant role.

One mechanism for increased oil accumulation is inertial forces. As oil masses and acceleration increase from 1800 to 2500 rpm, the oil experiences greater inertial forces which shear and cause greater oil flow back and forth along the regions or lands resulting in greater inertial driving potential to move oil along the lands and force lubricant through gaps and grooves between different regions. As expected, oil travel along the land increases with speed. The average oil displacement along a land during half a stroke scales with engine speed (N) and the square of the local oil thickness (h) and inversely with its viscosity (ν). Measured and calculated oil displacements along the third land agree fairly well as shown in Table 5.1 and are typically undetectable at 1800 rpm and on the order of 0.5 mm at 2500 rpm. Even SAE-10W with lower third land ARTs compared to SAE-10W/50n and -50 has similar oil displacement because its viscosity restriction is less.

A second mechanism is oil dragging by gas flows. Since oil transport to the crown and second lands must occur only through the second ring gap and groove, second

ring dynamics and gas flows through its gap and groove are extremely important. Predicted ring flutter at 1800 rpm is all but eliminated with only a marginal relative lift resulting in lower groove gap flow. However, higher second land pressure develops for 1800 rpm due to the slower engine speed and more gap flow compensates for the lower groove flow resulting in about the same blowby at 3 l/minute for both speeds.

Although the cumulative effect of groove and gap gas flow on lubricant dragging results in lesser oil on the second land for lower speeds, the spatial distribution of oil indicates that less groove gas flow develops if gas flow is indicative of oil dragging. The damped second ring flutter at 1800 rpm accompanied by less groove gas flow through the lower channel results in less lubricant dragging from the second groove to the third land, and, consequently, more oil exists for second ring oil squeezing and along the lower portion of the second land as seen in the data. The decreased gas flow through the second ring gap from 1800 to 2500 rpm and increased oil supply within the third land region accompanied by the increased inertial driving forces are predominant for increasing the amount of oil on the second land.

Oil squeezing and scraping and inertial influences on oil transport increase and compound with engine speed, and, therefore, increase the ARTs. This increase allows more oil availability for oil to escape into the combustion chamber especially from the upper land regions. Interestingly, this finding is consistent with oil consumption studies which typically correlate an increase in oil consumption with engine speed [20, 24]. Additionally, recent results in the MIT Lubrication Consortium simultaneously correlate increased oil distribution and oil consumption with speed [25].

Azimuthal Effects around Midstroke (from Section 5.6)

For the ring-pack regions, no strong trends exist for azimuthal effects, contrary to the clear OFT trends for the free liner and the top and scraper rings found in the OFT analysis. However, considering one highly-accurate case, local ring tension differences from azimuthal bore distortion is a plausible explanation for greater ARTs along the second and third land off the major-thrust side. The greater local ring tensions at

windows 2 and 4 result in greater second ring scraping, greater third land (and second land) oil accumulation, and less oil flow under the ring observed from the OFT analysis.

For regions below the OC ring, the large amount of oil at the major-thrust side is probably due to the thrust-side oil transport which moves oil up the upper piston skirt to the piston chamfer region. Window locations off the major-thrust side at windows 2 and 4 lack the large piston skirt regions which contact and transport oil along the liner.

Despite the large differences from window to window within the regions below the OC ring, a majority of the differences within the ring pack are smaller especially between the OC rails. Largely caused by different skirt geometries and piston motion on oil behavior, the large ART differences (from window to window) below the OC ring do not drastically affect the azimuthal oil behavior for the regions within the piston ring-pack mostly caused, in part, by local radial ring pressure differences on the lubricant film from bore out-of-roundness.

Lastly, azimuthal randomness in the data as well as the lack of ARTs trends along the crown, second, and third lands mentioned in other sections are consistent with latest results from 2-D visualization of oil distribution employed in the MIT Lubrication Consortium [23]. With the gas flows having greater influence within the upper lands of the piston ring pack, 2-D measurements show that circumferential gas flows through the gaps induce complex fluid flows heavily dependent upon relative top and second ring gap orientations. These complex flows drag lubricant resulting in different azimuthal distributions which may change as the relative gap orientations change even for a single steady-state operating condition. Gas flow effects are less significant within lower regions of the ring pack reflected in the more-consistent and less-random oil distribution trends found in the current database.

5.1.2 Model Verification of Ring Boundary Conditions and Predicted Scraper Down-Scraping from the *FRICTION-OFT* Model and Predicted Top Ring Lift from the *RINGPACK-OC* Model

Ring Boundary Conditions

Ring boundary conditions in the *FRICTION-OFT* model are confirmed by the entire database and include a starved top ring, a flooded (scraping) and unflooded (starved) second ring during the downstrokes and upstrokes, respectively, a flooded OC ring during the downstrokes, and during an upstroke an OC ring fed by the oil accumulated within the third land region scraped by the second ring during the previous downstroke. However, the manner in which the scraped oil is fed to the OC ring needs further investigation in addition to an accurate three-piece OC ring instead of the one-piece currently employed in the model.

Scraper Down-Scraping from Midstroke (Window 1) to Near-BC (Window 6) (from Section 5.7.2)

Predicted down-scraping of oil scraped by the second ring is validated from ART measurements within the third land region as the scraper scrapes oil from midstroke (window 1) to near-BC (window 6) on the major-thrust side. Since the relative profile of the scraper ring with the liner is affected by the piston tilt effects which are greatest for the major- and minor-thrust sides, both predictions and a majority of the measurements show greater scraping for the intake stroke than the expansion stroke. This finding is consistent with the stroke-by-stroke OFT results especially for the free-liner OFT which indicates higher OFT for the expansion stroke than the intake stroke. (However, model predictions overpredicted the tilt effects on oil scraping and OFT.)

Predicted Top Ring Lift from the RINGPACK-OC Model (from Section 5.3.2.1.1)

Also at midstroke and near-BC, predicted top ring lift within its groove from the *RINGPACK-OC* model is verified from the top ring oil squeezing in its groove which results from the top ring contact with the top or bottom of the ring's groove. Top channel

or bottom channel oil squeezing occur throughout a cycle as the ring move axially up and down against the top and bottom portions of its groove. Found at all window locations, top ring contact with the bottom of its groove (or bottom channel oil squeezing) occurs during the compression, expansion, and exhaust strokes with the expansion stroke having the greatest oil squeezing. For top ring contact with the top of its groove, oil squeezing is evident only for the intake stroke.

5.2 DATA REDUCTION ALONG DIFFERENT REGIONS OF THE PISTON ASSEMBLY FOR DIFFERENT AZIMUTHAL AND AXIAL WINDOW LOCATIONS

Unlike the MOFT analysis which employs manual ring fitting, the quantification of oil along different regions of the ring pack and below the OC ring is automated via a FORTRAN program developed by the author. Once a calibration coefficient is manually obtained, the program integrates the OFT trace along each specified region and divides this oil volume by the region's length, L, resulting in an average region thickness, ART. This region averaging process continues for each stroke of each cycle within a 10-cycle data file. Ultimately, final results include a 10 cycle average of each region's thickness within a stroke, the actual standard deviation from each 10 cycle average of the particular region, and the corresponding coefficient of variation (COV).

For each window location, the different regions were carefully selected by observing the oil behavior along the piston assembly from stroke to stroke. Of course, the free liner is above the piston crown region and averaged over the first five millimeters. For the ring pack, boundaries to each region are naturally obvious -- a region beginning and ending at ring locations corresponding to the different lands. Therefore, the free liner, top land, second land, third land, and the space between the upper and lower OC segments correspond to regions f, 1, 2, 3, and 4, respectively, and are shown in Figure 5-1. These region assignments are universal for every window location.

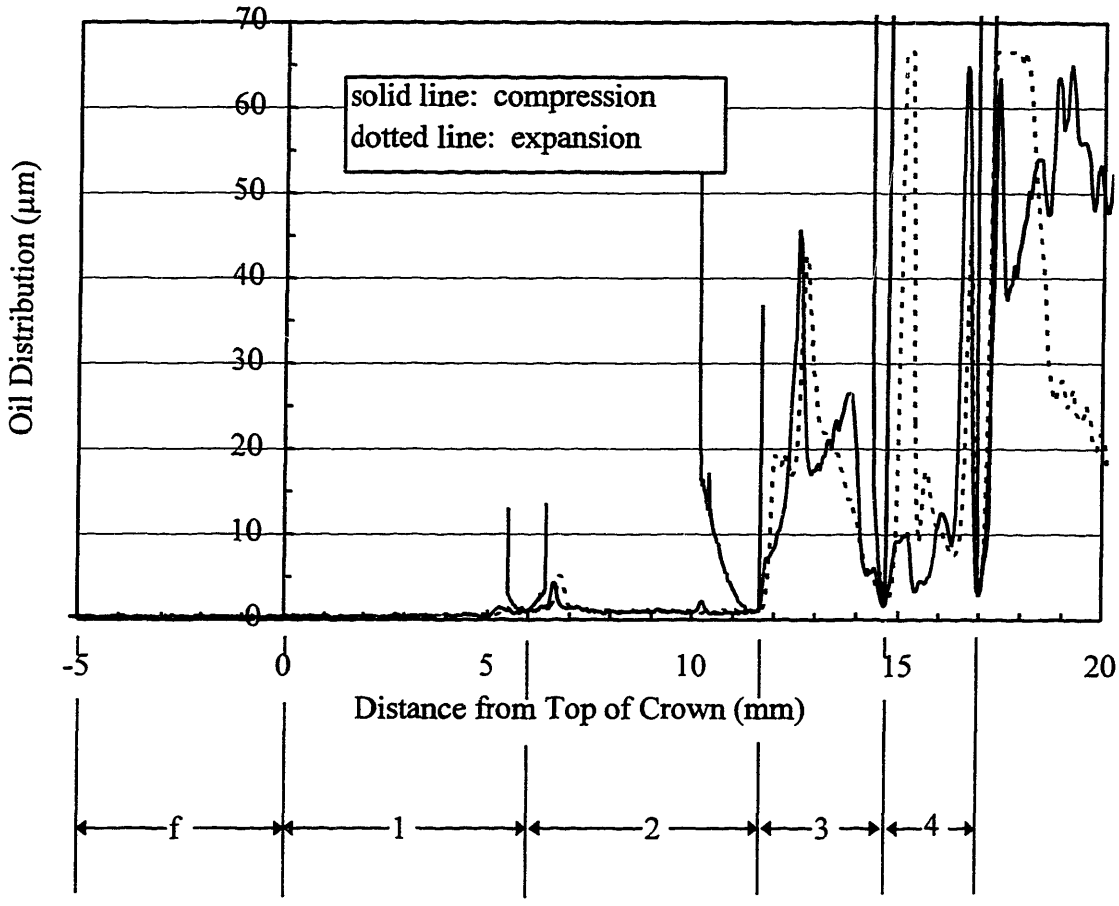

Figure 5-1 Region Assignments for the Free Liner and Ring Pack

However, because of the different oil behavior below the OC ring and the different geometrical features of the piston for different window locations, region assignments below the OC ring are different from window to window -- both azimuthally and axially. The region assignments for window 1, 4 (and 2), and 6 are presented in Figures 5-2 (a), (b), and (c), respectively. Within each figure, some geometric feature from the piston is shown with the oil distribution pattern. Since windows 1 and 6 see most of the skirt, if not all, qualitative hand-drawn skirt profiles are drawn with possible orientations roughly fit to the oil film trace. It is important to keep in mind that these profiles represent one possible orientation for a particular instant (or CA) in time; whereas, the OFT along the skirt region is taken over a range of crank angles over a finite

period of time. The order of magnitude of the distance between the piston skirt (both upper and lower portions) and liner are reasonably justified by gap sensor measurements made by Ryan within using the same type of Kohler engine and piston assembly [26]. Additionally, upper piston machining marks which are used for calibration during the upstrokes are shown with the compression and expansion traces. The piston during the expansion stroke is usually against the major-thrust side of the bore as shown in the figures. The maximum skirt diameter is located roughly 40 millimeters from the top of the piston -- the piston's lowest location at window 1. Lastly, piston tilt corresponding to the drawn skirt orientations don't exceed 10 minutes.

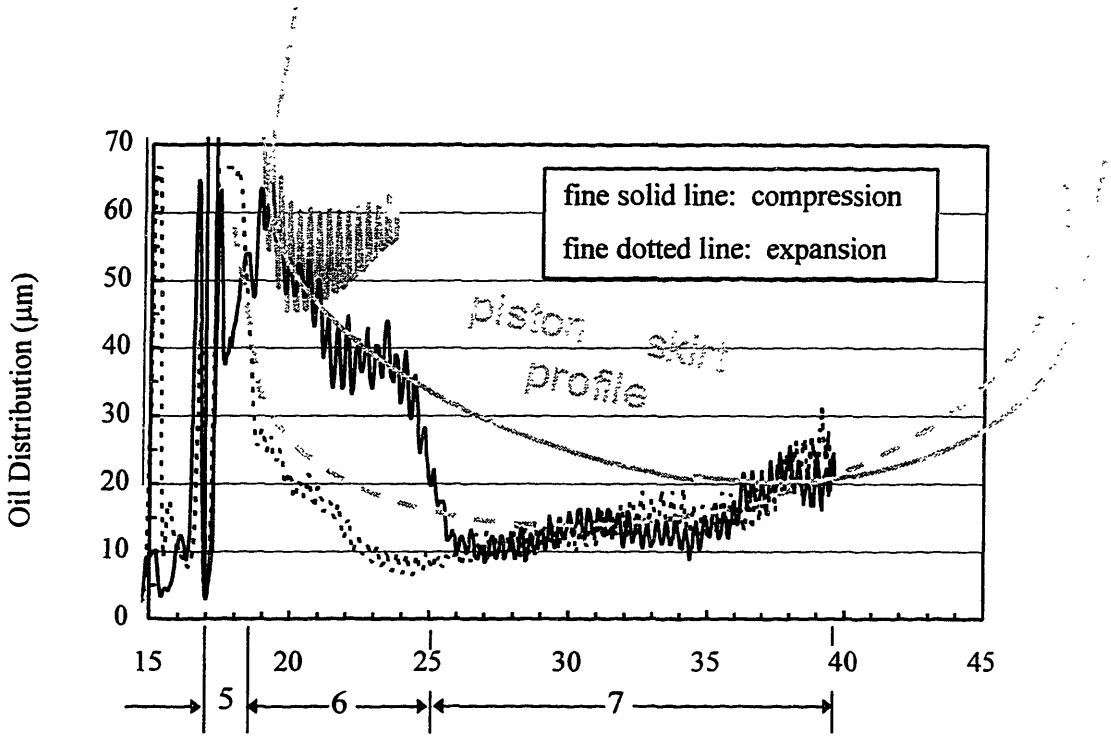

(a) Window 1

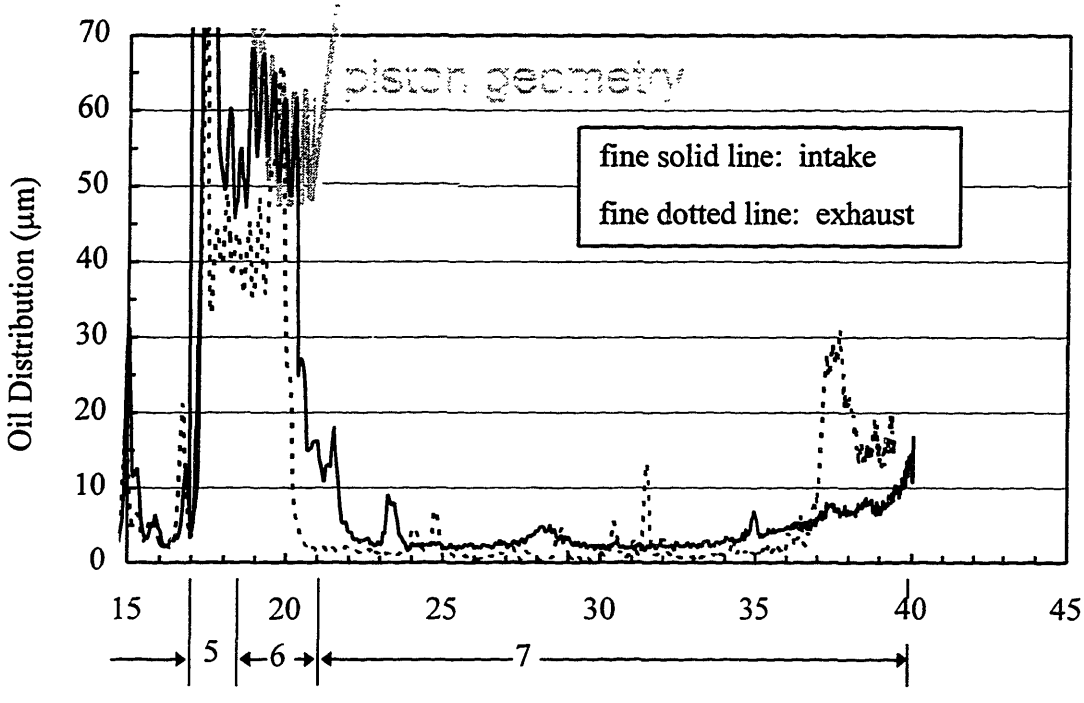

(b) Window 4 (and 2)

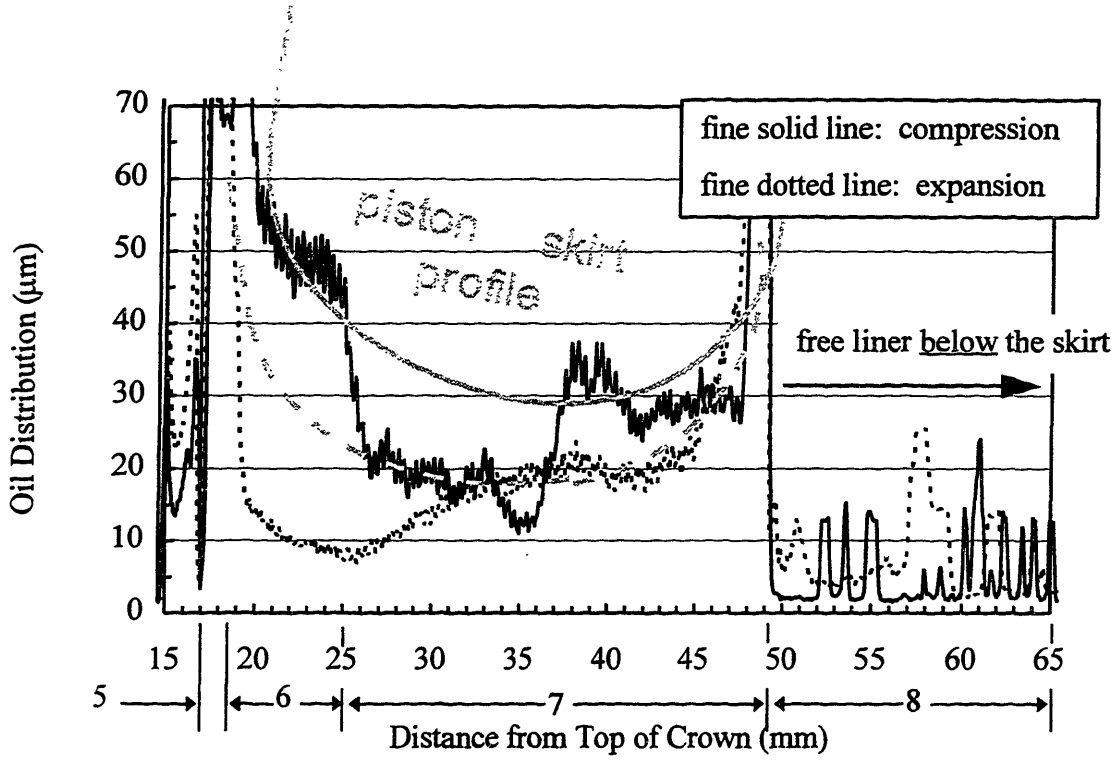

(c) Window 6

Figure 5-2 Region Assignments below the OC Ring for the Azimuthal Locations at (a) Windows 1, (b) 4 (and 2), and the Near-BC Location at (c) Window 6.

As the piston passes by windows 2 and 4, however, no geometry below the OC ring passes close to these windows except for a very short extension from the skirt as shown in Figure 5-2 (b); the wrist pin and surrounding regions are very far away from the liner. Distribution from window 2 never has fully-flooded machining marks in region 6 as shown in the figure from window 4 which is important for accurate calibration.

In addition to the free-liner OFT above the piston, another free liner exists below the piston closer to the sump. This region, called region 8, is measured from window 6 shown in Figure 5-2 (c).

In retrospect, in view of the different piston geometries below the OC ring viewed from different window locations and after a careful study of the oil distribution patterns

from many cases, region boundaries below the OC ring were assigned differently from window to window both azimuthally and axially.

5.3 BASELINE RESULTS

All of the ART measurements for the baseline condition addressed within the test matrix in Chapter 3 are shown in this section. The five lubricants were tested within the engine operating at 2/3 load, 2500 rpm, and 100°C at midstroke, and LIF measurements were acquired from the four window locations -- three azimuthally around midstroke corresponding to windows 1, 2, and 4 and one window (6) near BC on the major-thrust side of the bore. In this order, the data corresponding to these windows are shown by figures (a), (b), (c), and (d), respectively, within each figure number. First, the stroke-by-stroke averaged ARTs for regions 3 - 7 (or 8) are shown in Figures 5-3 (a) - (d). Because the magnitudes are an order of magnitude lower, the stroke-averaged ARTs of the free liner and the crown and second lands are shown in separate figures, Figures 5-4 (a) - (d). Secondly, results for each of the four strokes starting at the intake are shown corresponding to Figures 5-5 and -6, 5-7 and -8, 5-9 and -10, and 5-11 and -12, respectively.

For each window (or figure) there are five clusters of data corresponding to the five lubricants. Each lubricant cluster displays ARTs sequentially along the ring pack outlined by thick lines followed by regions below the OC ring outlined by thin lines.

Additionally, as in the OFT analysis, each lubricant cluster represents one calibrated case and, thus, one calibration coefficient. These calibration coefficients have three different levels of calibration accuracies, and, consequently, each cluster falls within one of three categories of calibration accuracy. These categories, their symbolism in the figures, and their importance may be reviewed in section 4.2. (Actual calibration coefficients and calibration accuracies for the entire test matrix are presented and explained in further detail in Appendix D.)

The first subsection (section 5.3.1) highlights the magnitudes and trends of the highly accurate cases for regions within the ring pack and below the OC ring. Since the

different lubricant cases are compared with one another at the same engine operating condition, this type of effect on oil behavior is called the lubricant effect. To provide a clear and succinct presentation, results are stroke-averaged -- a process justified by section 5.3.2 which follows the stroke-avg results. In section 5.3.2, stroke-by-stroke differences (or lack thereof) are shown and interpreted.

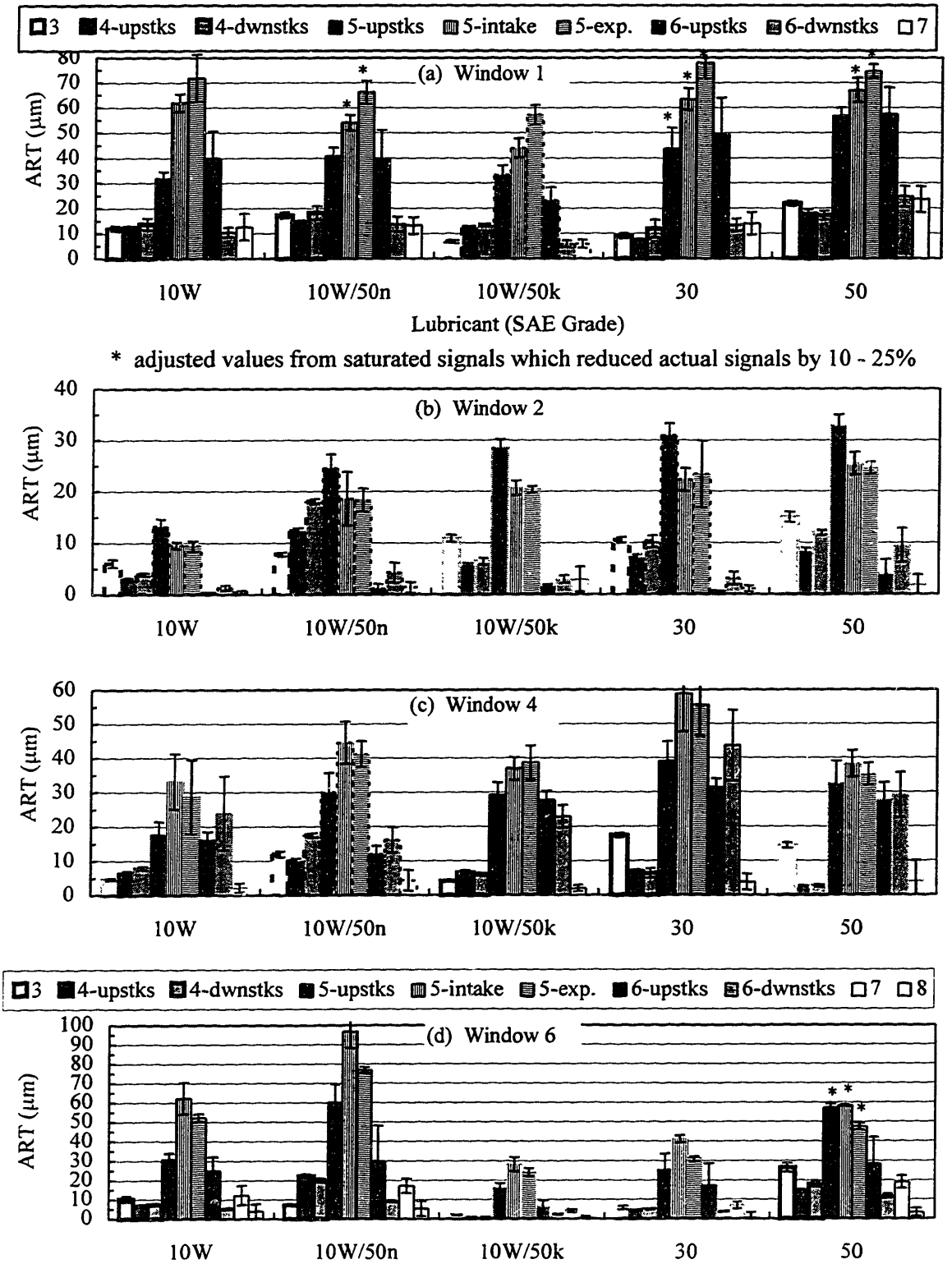

Figure 5-3 Baseline Average Region Thicknesses (Stroke-Averaged) for Regions 3 - 8 from Windows (a) 1, (b) 2, (c) 4, and (d) 6.
(2/3 Load, 2500 rpm, 100°C)

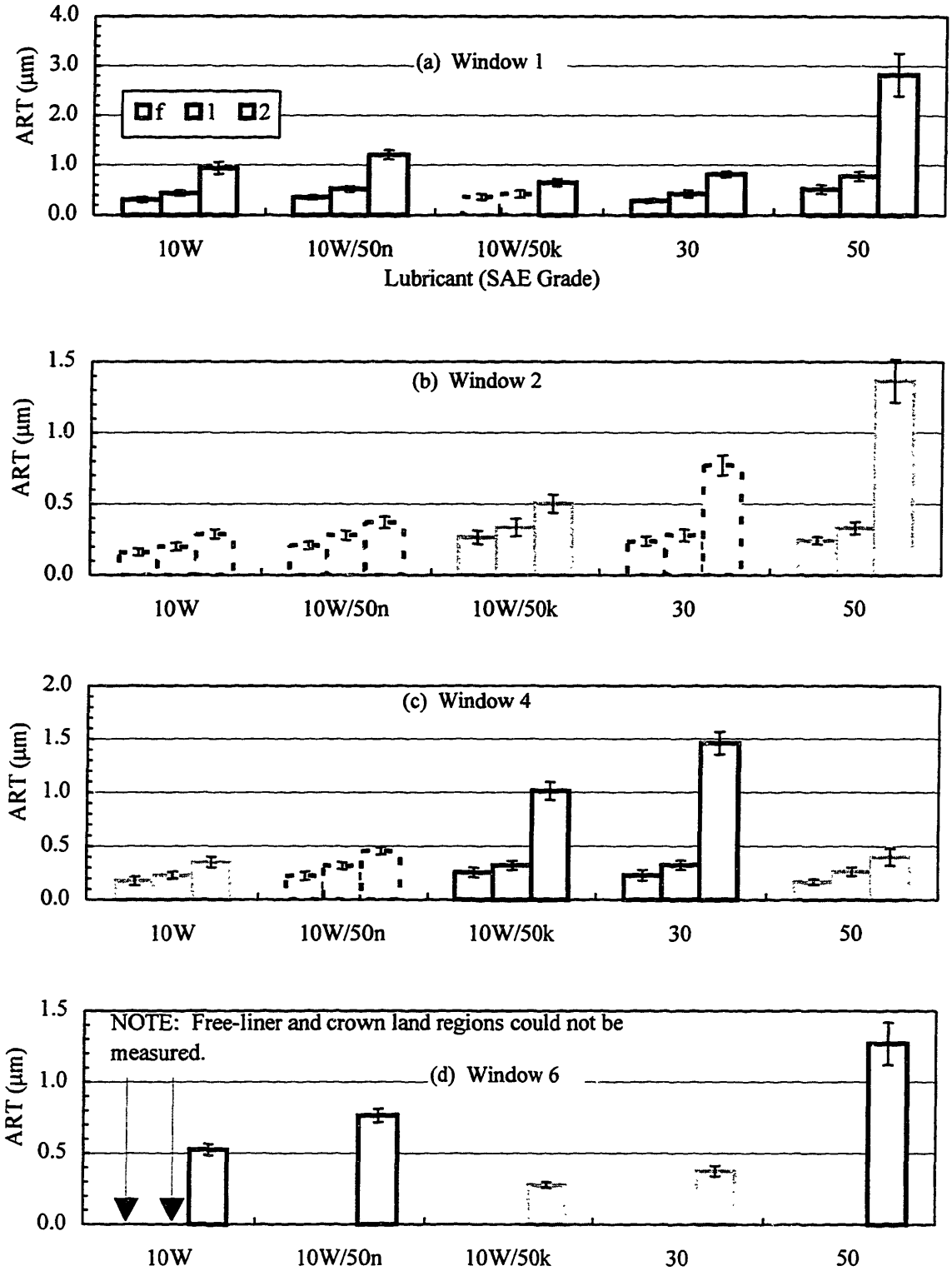

Figure 5-4 Baseline Average Region Thicknesses (Stroke-Averaged) for Free Liner and First and Second Land Regions from Windows (a) 1, (b) 2, (c) 4, and (d) 6. (2/3 Load, 2500 rpm, 100°C)

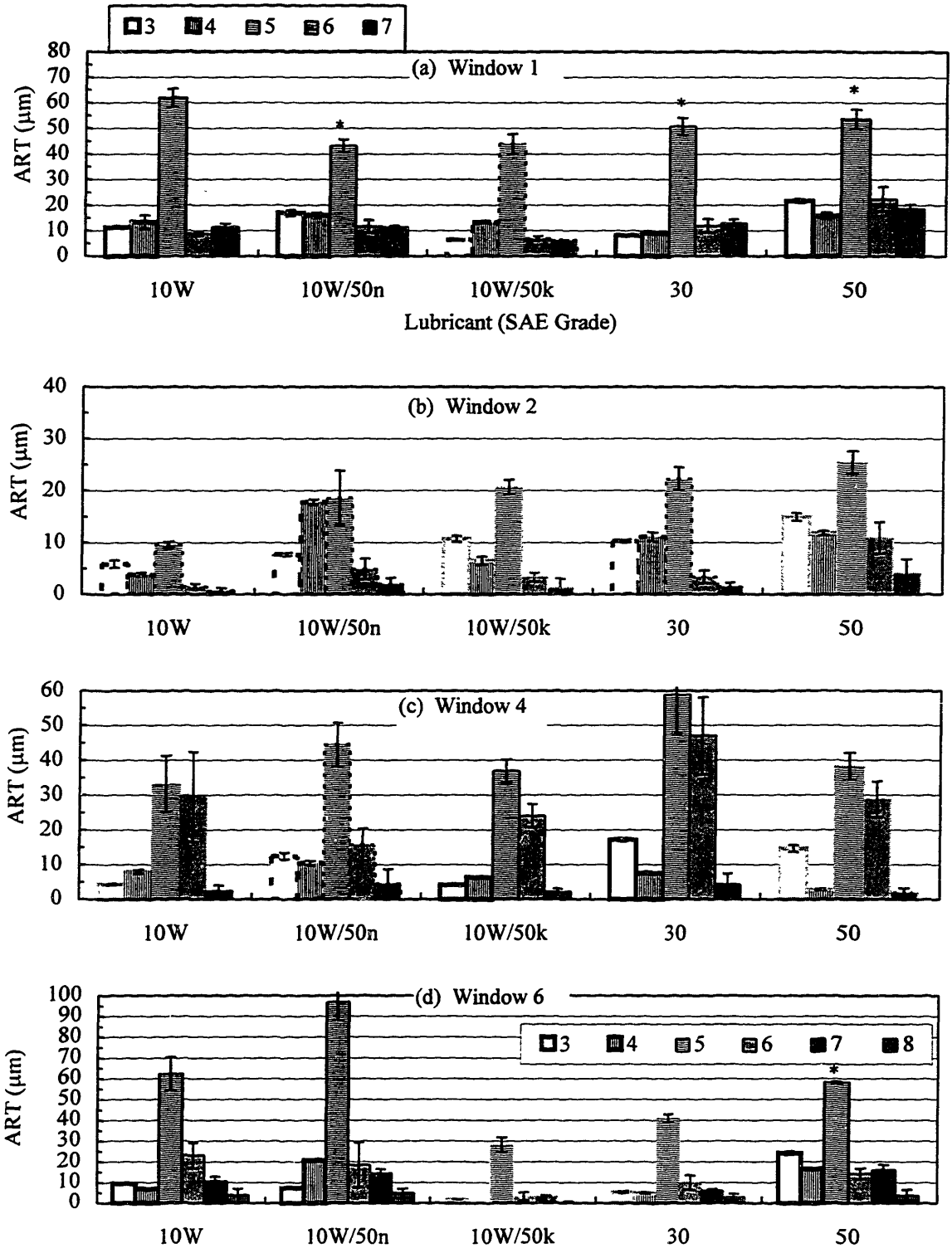

Figure 5-5 Baseline Average Region Thicknesses for the Intake Stroke for Regions 3 - 8 from Windows (a) 1, (b) 2, (c) 4, and (d) 6.
(2/3 Load, 2500 rpm, 100°C)

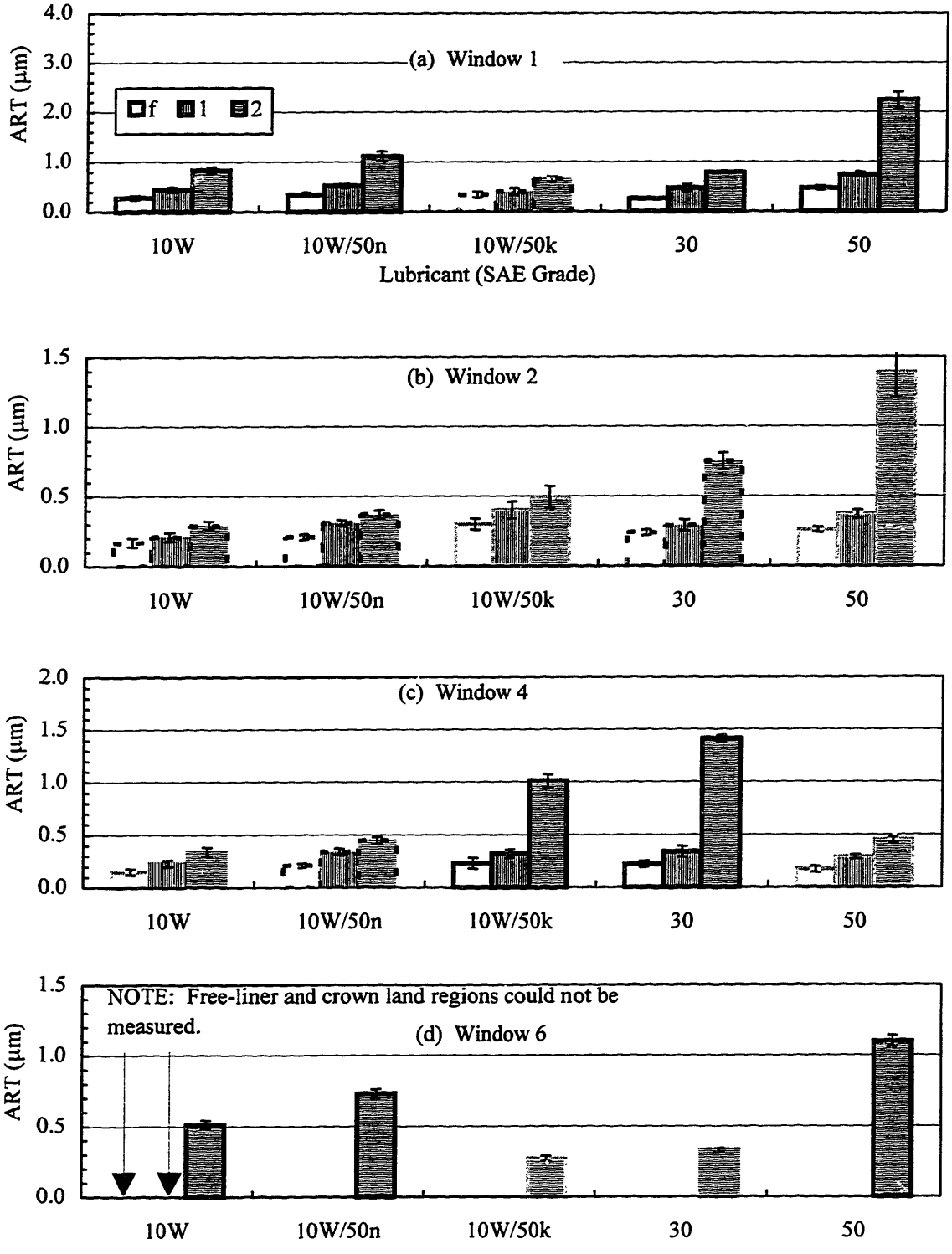

Figure 5-6 Baseline Average Region Thicknesses for the Intake Stroke for Free Liner and First and Second Land Regions from Windows (a) 1, (b) 2, (c) 4, and (d) 6. (2/3 Load, 2500 rpm, 100°C)

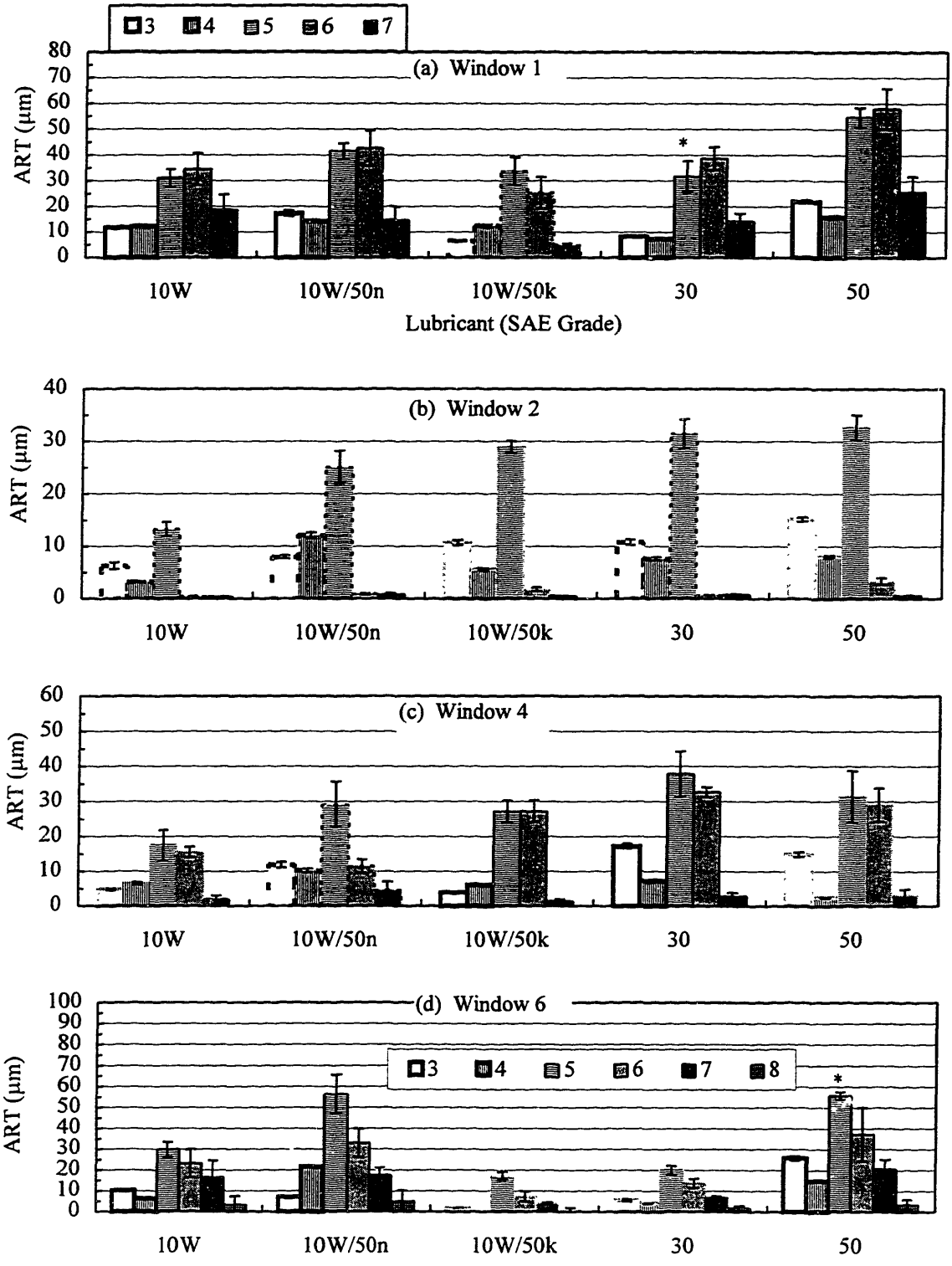

Figure 5-7 Baseline Average Region Thicknesses for the Compression Stroke for Regions 3 - 8 from Windows (a) 1, (b) 2, (c) 4, and (d) 6.
(2/3 Load, 2500 rpm, 100°C)

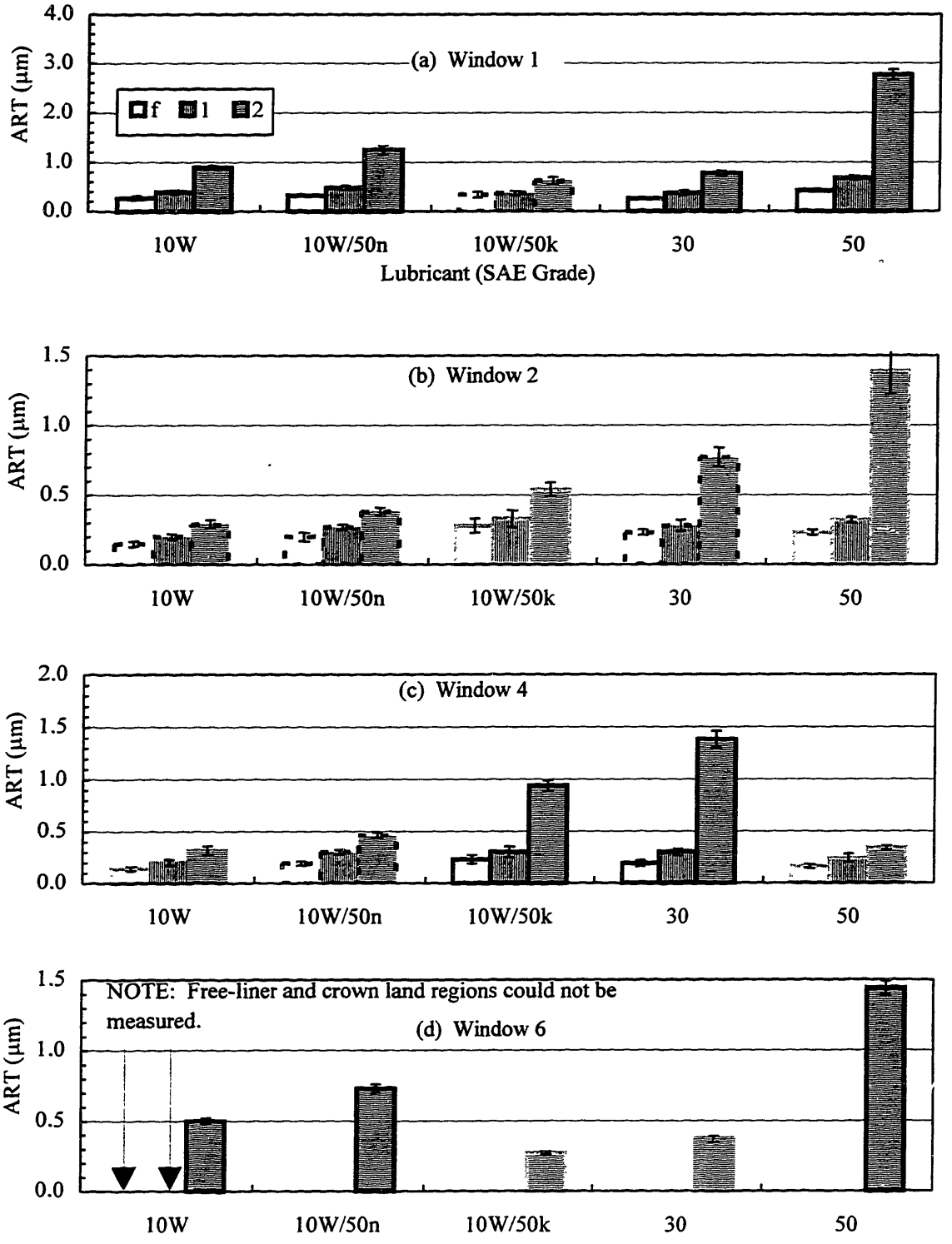

Figure 5-8 Baseline Average Region Thicknesses for the Compression Stroke for Free Liner and First and Second Land Regions from Windows (a) 1, (b) 2, (c) 4, and (d) 6. (2/3 Load, 2500 rpm, 100°C)

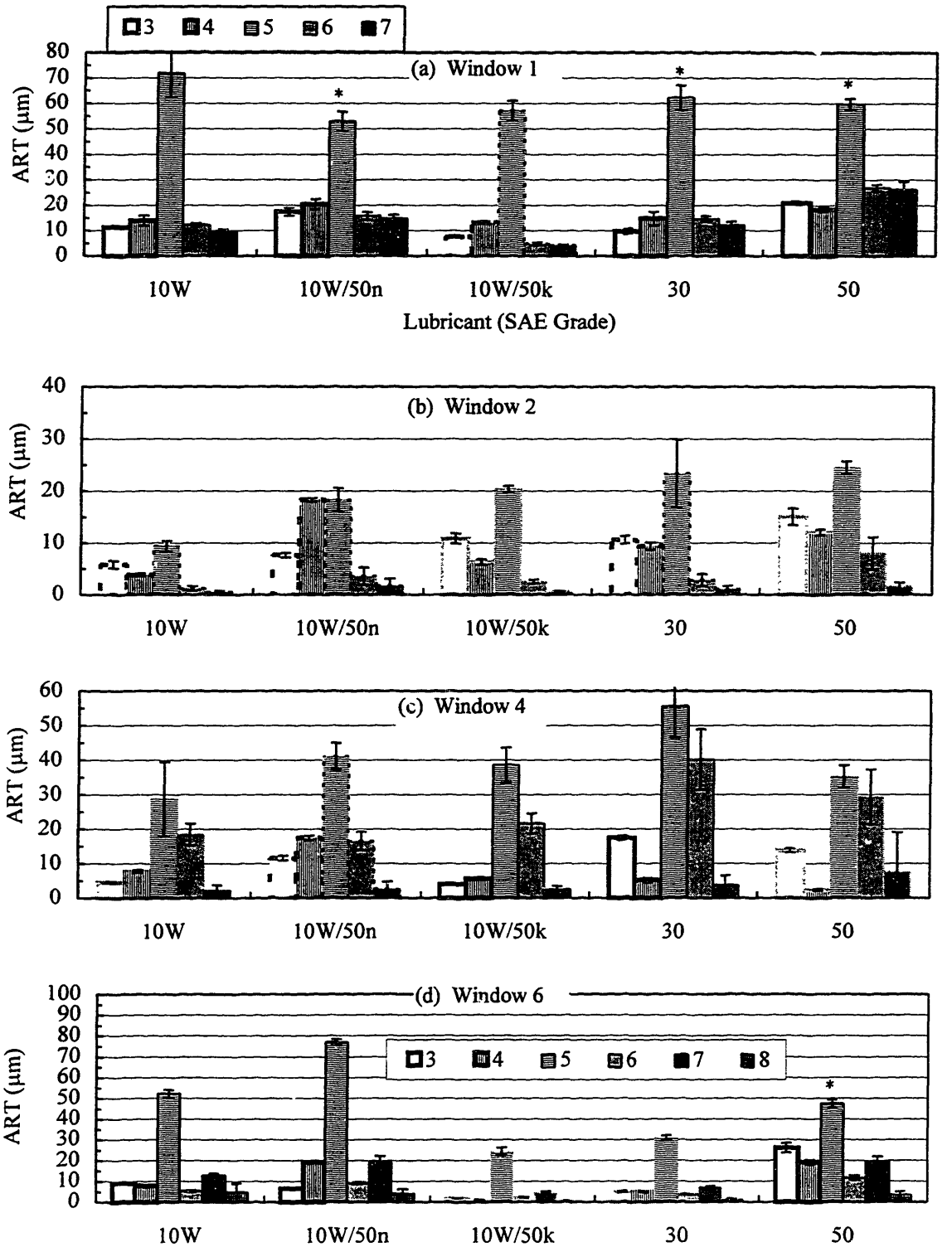

Figure 5-9 Baseline Average Region Thicknesses for the Expansion Stroke for Regions 3 - 8 from Windows (a) 1, (b) 2, (c) 4, and (d) 6.
(2/3 Load, 2500 rpm, 100°C)

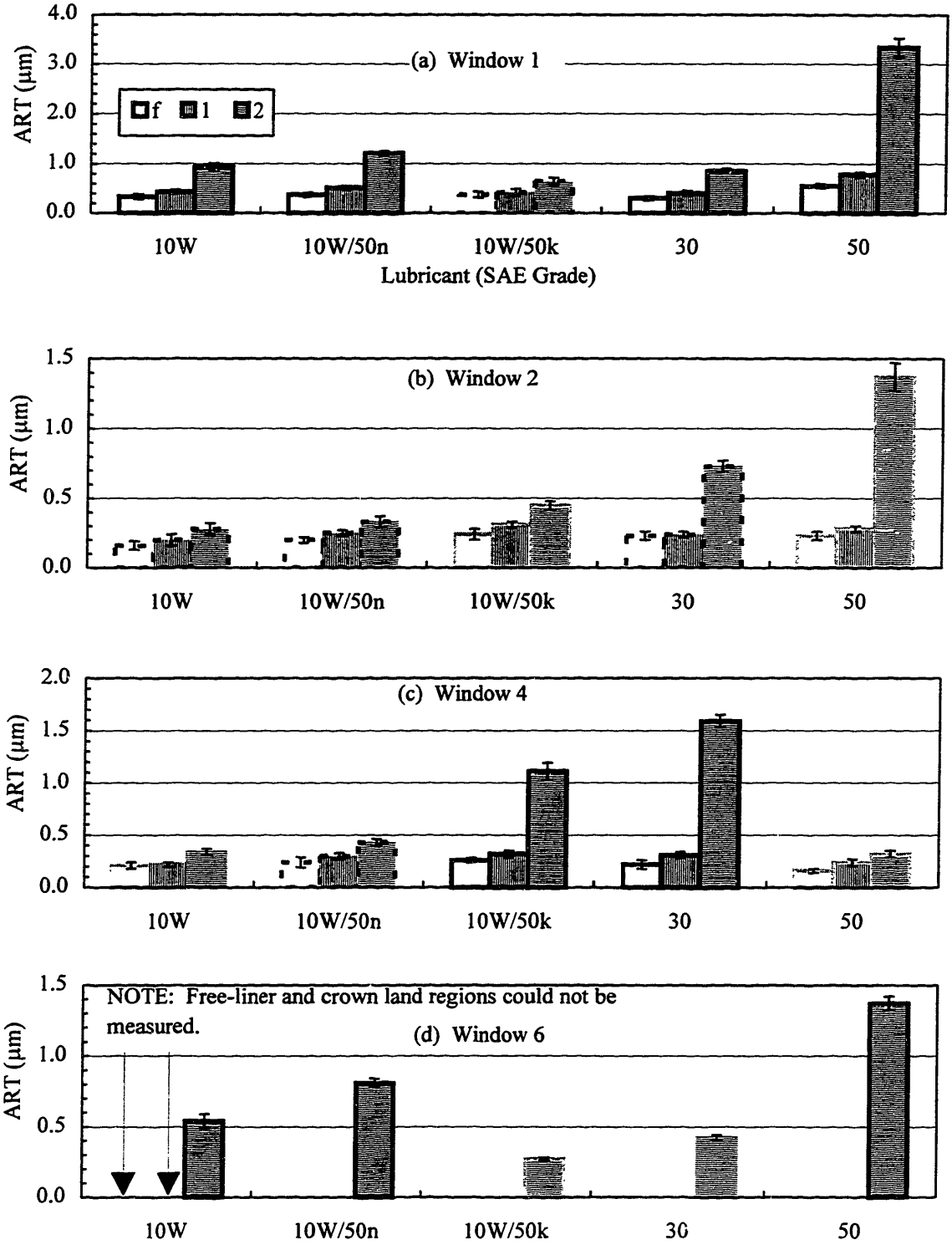

Figure 5-10 Baseline Average Region Thicknesses for the Expansion Stroke for Free Liner and First and Second Land Regions from Windows (a) 1, (b) 2, (c) 4, and (d) 6. (2/3 Load, 2500 rpm, 100°C)

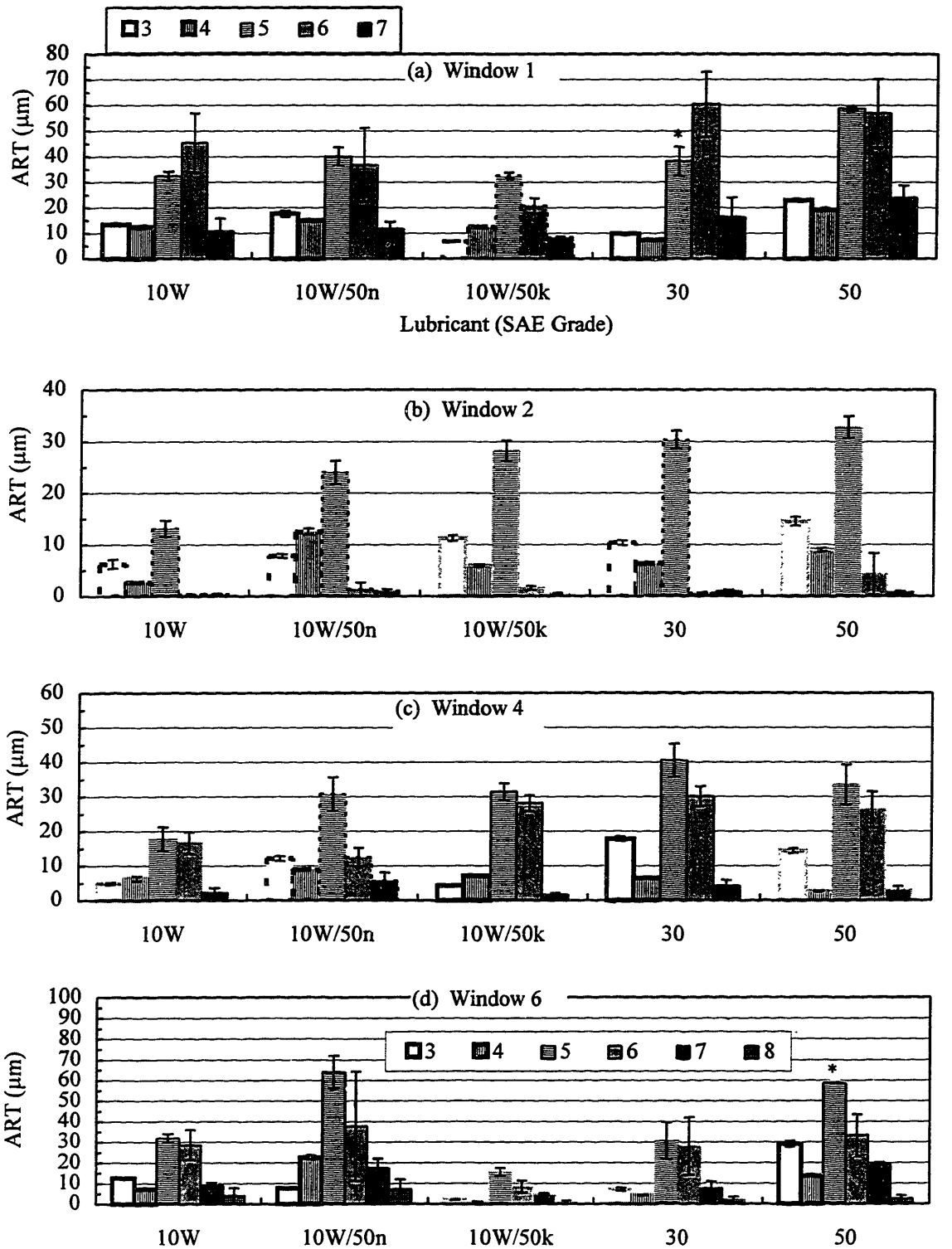

Figure 5-11 Baseline Average Region Thicknesses for the Exhaust Stroke for Regions 3 - 8 from Windows (a) 1, (b) 2, (c) 4, and (d) 6.
(2/3 Load, 2500 rpm, 100°C)

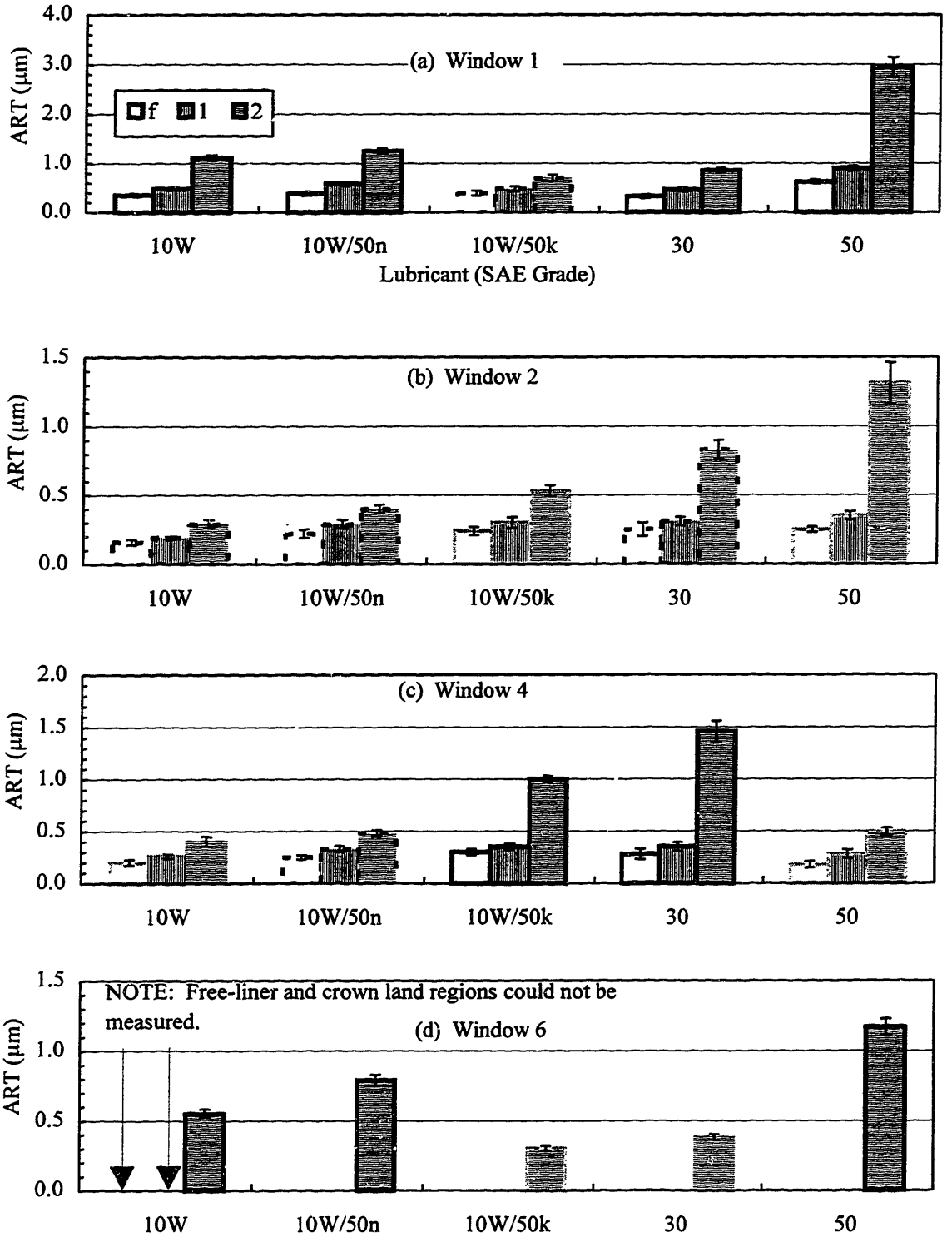

Figure 5-12 Baseline Average Region Thicknesses for the Exhaust Stroke for Free Liner and First and Second Land Regions Windows (a) 1, (b) 2, (c) 4, and (d) 6. (2/3 Load, 2500 rpm, 100°C)

5.3.1 The Lubricant Effect

Since viscosity should play a role in oil flow among the lands and regions of the piston and has a predominant effect in the OFT analysis shown in the last chapter, ART results are presented with the same representation. At the baseline condition, stroke-averaged ARTs from the different lubricant cases with high calibration accuracy are plotted as a function of kinematic viscosity. For the same load condition, liner temperature, and speed, the resulting effect from different lubricants on ART magnitudes and trends is called the lubricant effect.

Figures 5-13, -14, and -15 correspond to ART results from windows 1, 4, and 6, respectively. (Window 2 doesn't have any cases with high calibration accuracy.) Each figure letter corresponds to one of the regions along the ring pack or piston skirt. Along the abscissa, lubricant viscosities correspond to the 100°C midstroke liner temperature and are the high-shear values[1] for the multigrade lubricants. The hollow and solid symbols correspond to the multigrade and monograde lubricants, respectively, and the actual standard deviations were calculated from the ten cycles within a lubricant case.

[1] One may argue against using the high-shear viscosities for the multigrade lubricants to investigate behavior of the oil along the lands because oil flowing along them is probably not subjected to shear rates high enough to shear thin. However, while shear thinning of lubricant flow along the lands probably does not occur, much of the oil on the lands is transported there through ring scraping from the scraper and rails of the OC ring . (This oil may then flow through ring gaps and grooves to other regions.) The scraped oil is from the oil supply from the liner which is left from hydrodynamic lubrication under the rings or piston skirt subjecting the lubricant to high-shear rates. Therefore, oil accumulation along the lands may be directly affected by shear thinning, although oil flow along the lands, per se, most likely does not shear thin. It is difficult to determine what shear viscosity to use (whether high- or low-shear values or somewhere in between) since both arguments are reasonable.

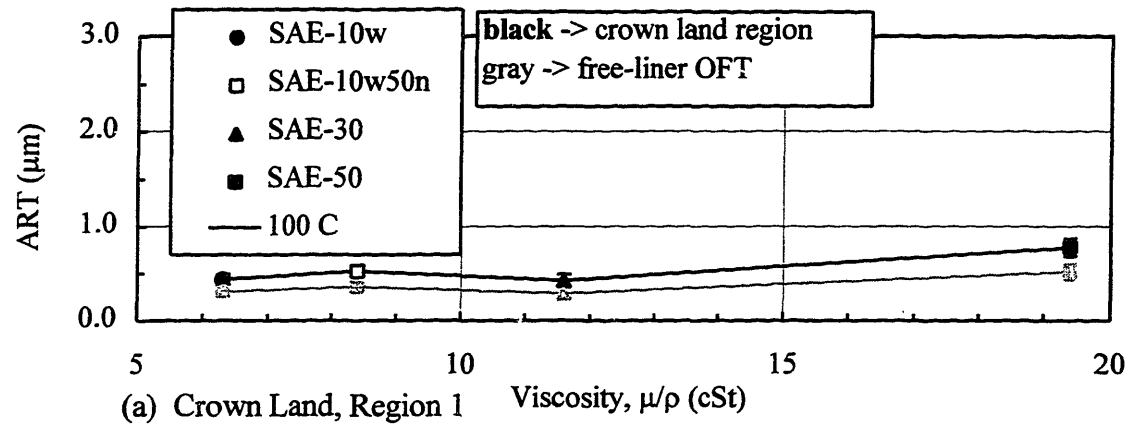

(a) Crown Land, Region 1

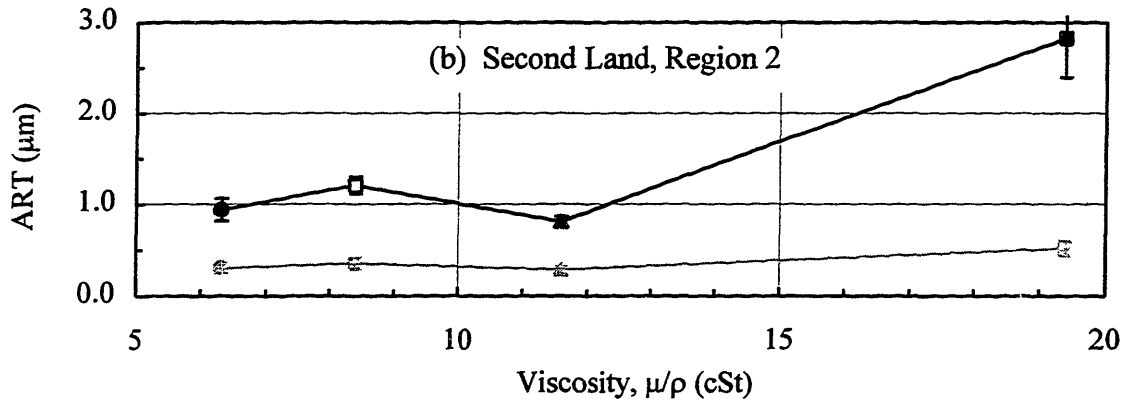

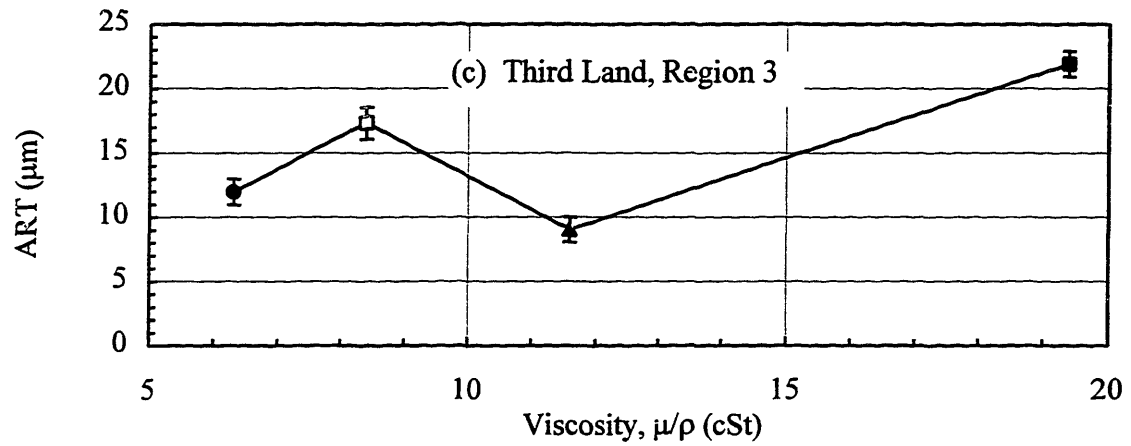

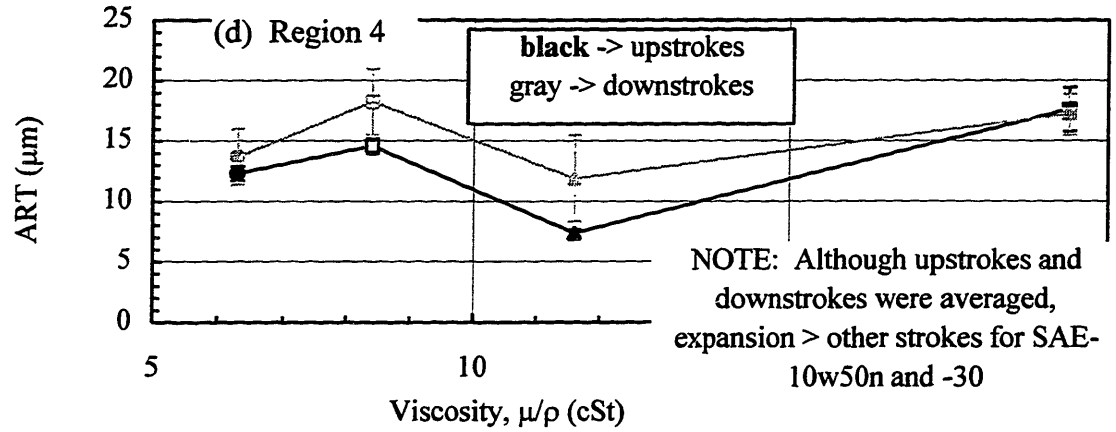
(d) Region 4
black -> upstrokes
gray -> downstrokes
ART (μm)
25
20
15
10
5
0
5
10
Viscosity, μ/ρ (cSt)
NOTE: Although upstrokes and downstrokes were averaged, expansion > other strokes for SAE-10w50n and -30

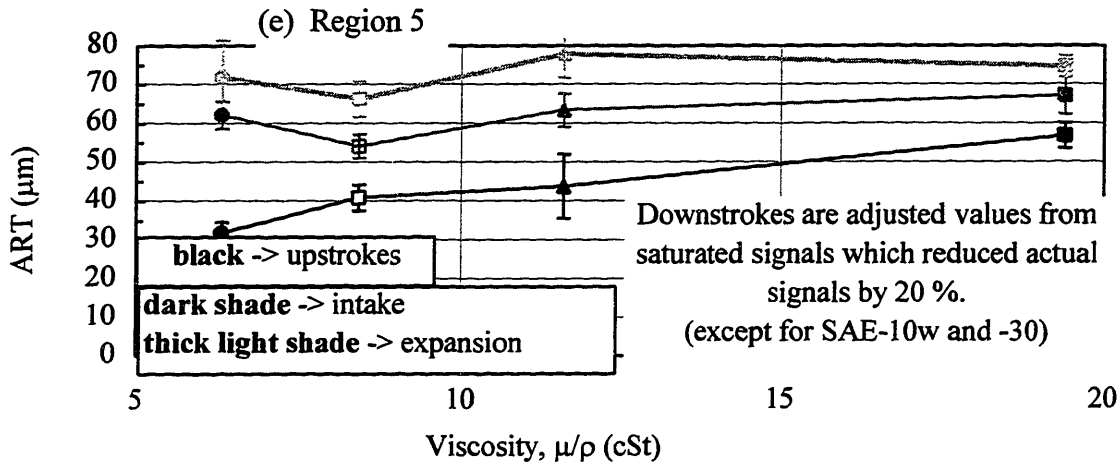
(e) Region 5
ART (μm)
80
70
60
50
40
30
20
10
0
black -> upstrokes
dark shade -> intake
thick light shade -> expansion
Downstrokes are adjusted values from saturated signals which reduced actual signals by 20 %.
(except for SAE-10w and -30)
5
10
15
20
Viscosity, μ/ρ (cSt)

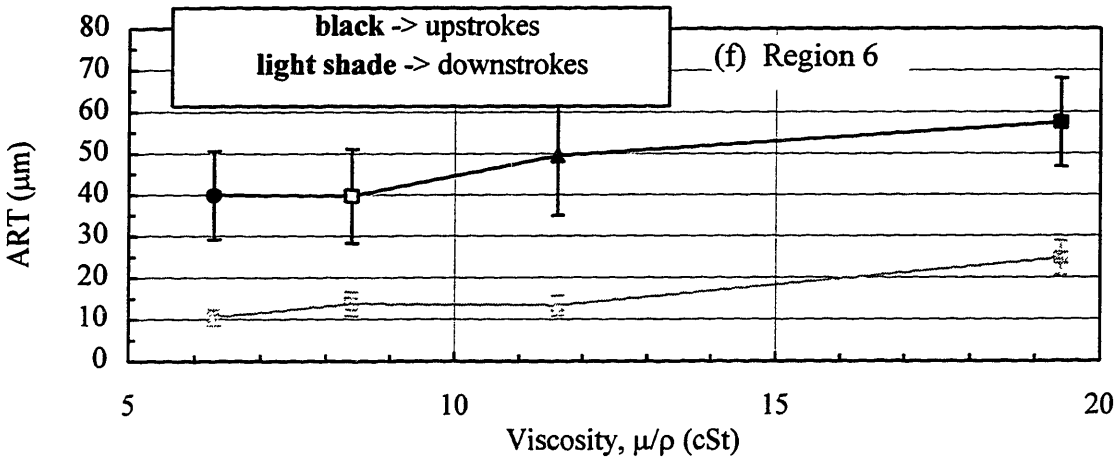
black -> upstrokes
light shade -> downstrokes
(f) Region 6
ART (μm)
80
70
60
50
40
30
20
10
0
5
10
15
20
Viscosity, μ/ρ (cSt)

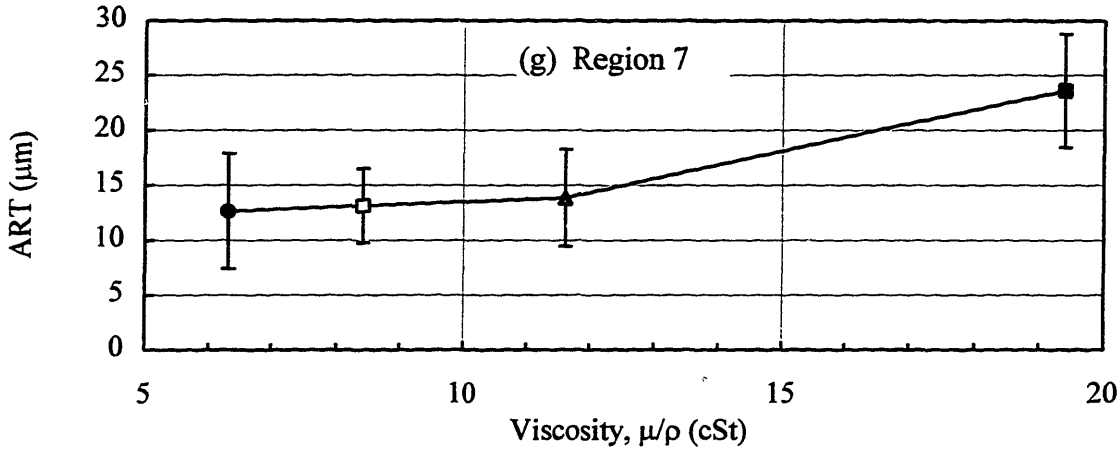

Figure 5-13 Baseline Average Region Thicknesses (Stroke-Averaged) from Window 1 for Regions (a) 1, (b) 2, (c) 3, (d) 4, (e) 5, (f) 6, and (g) 7.
(2/3 Load, 2500 rpm, 100°C)

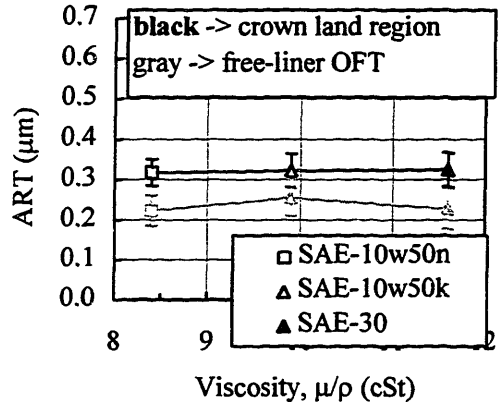

(a) Crown Land, Region 1

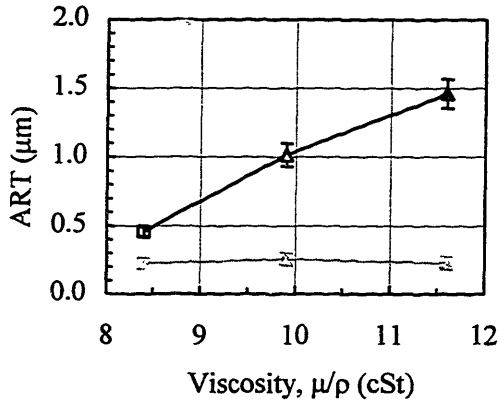

(b) Second Land, Region 2

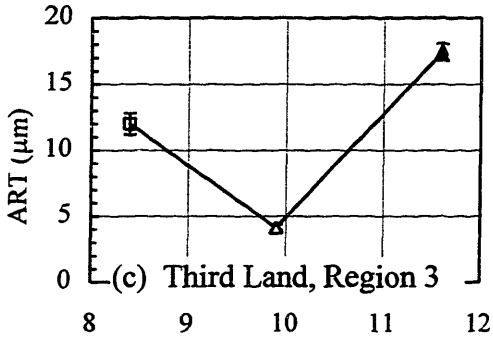

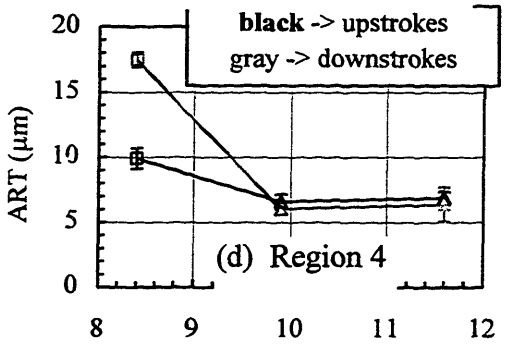

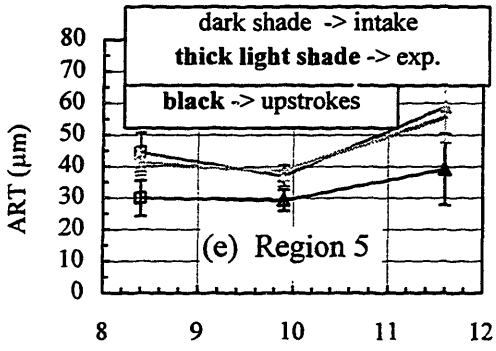

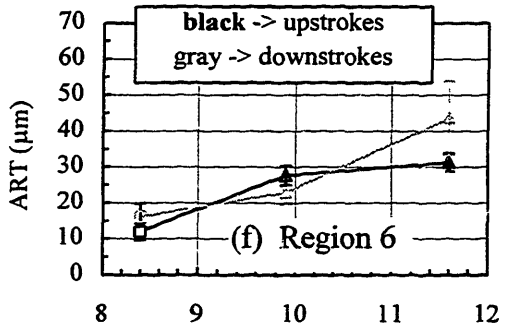

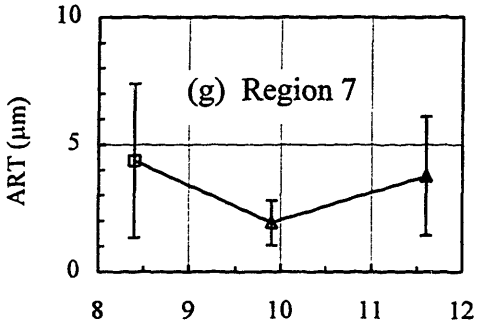

Figure 5-14 Baseline Average Region Thicknesses (Stroke-Avg) from Window 4 for Regions 1 - 7.
(2/3 Load, 2500 rpm, 100°C)
(NOTE: SAE-10W/50n has category II calibration accuracy.)

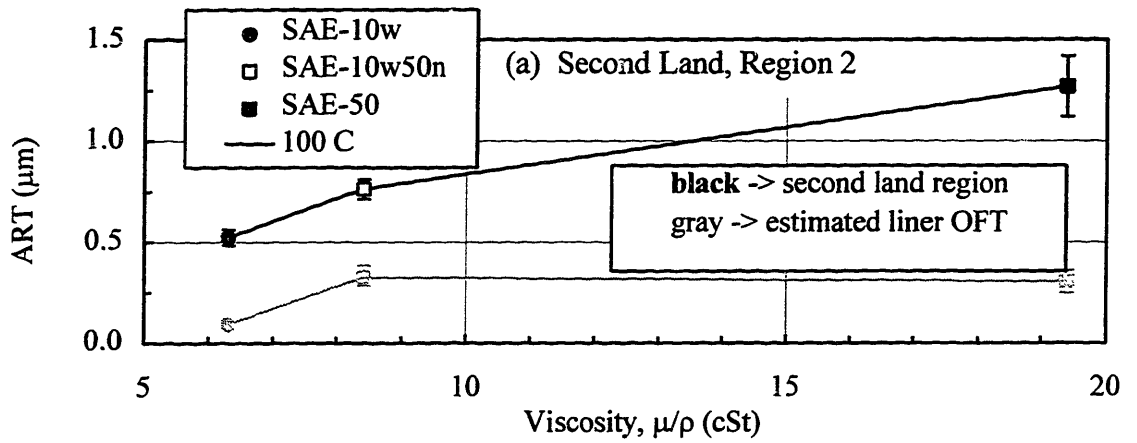
SAE-10w
SAE-10w50n
SAE-50
100 C
(a) Second Land, Region 2
black -> second land region
gray -> estimated liner OFT
ART (μm)
1.5
1.0
0.5
0.0
5
10
15
20
Viscosity, μ/ρ (cSt)

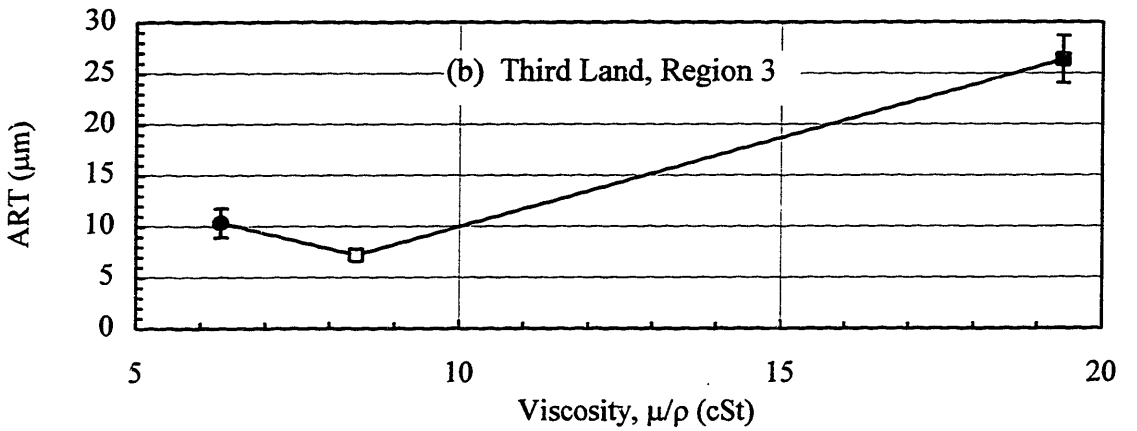
(b) Third Land, Region 3
ART (μm)
30
25
20
15
10
5
0
5
10
15
20
Viscosity, μ/ρ (cSt)

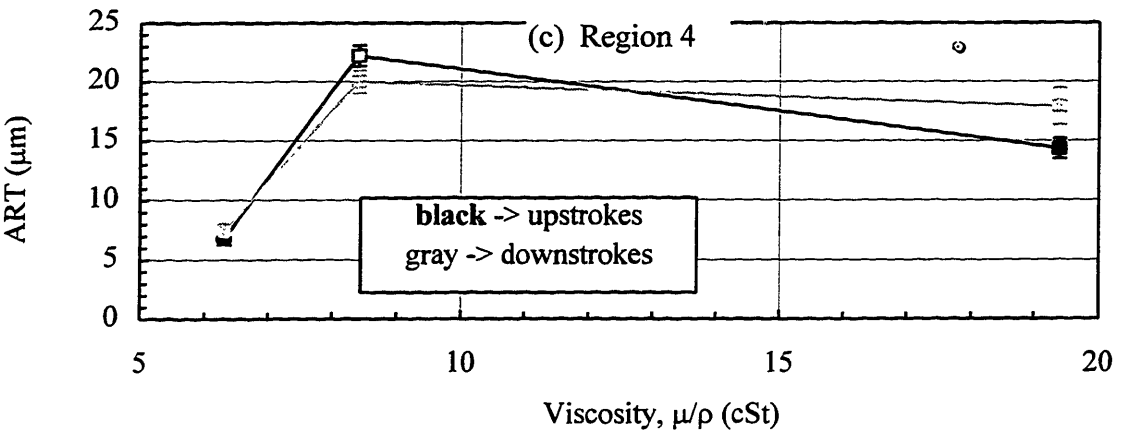
(c) Region 4
black -> upstrokes
gray -> downstrokes
ART (μm)
25
20
15
10
5
0
5
10
15
20
Viscosity, μ/ρ (cSt)

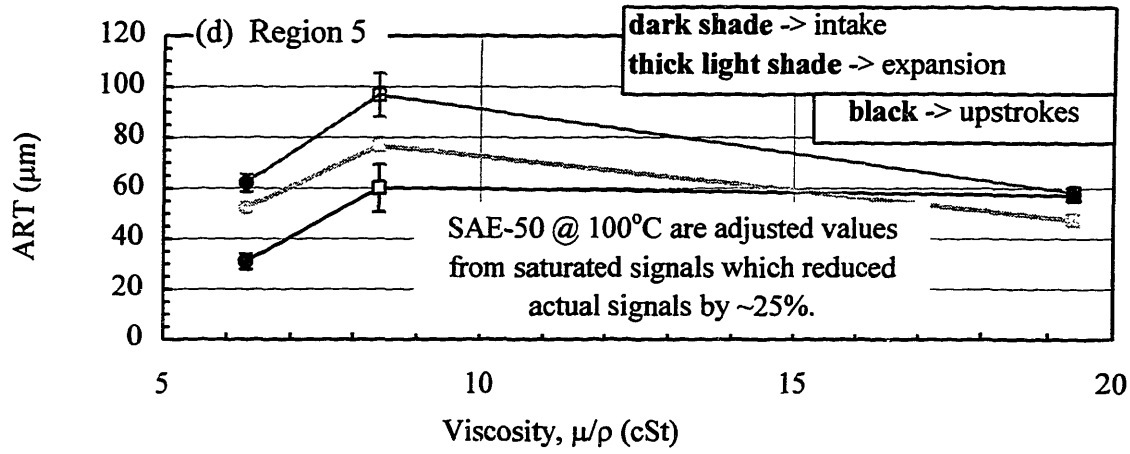
(d) Region 5
dark shade -> intake
thick light shade -> expansion
black -> upstrokes
SAE-50 @ 100°C are adjusted values
from saturated signals which reduced
actual signals by ~25%.
ART (μm)
120
100
80
60
40
20
0
5
10
15
20
Viscosity, μ/ρ (cSt)

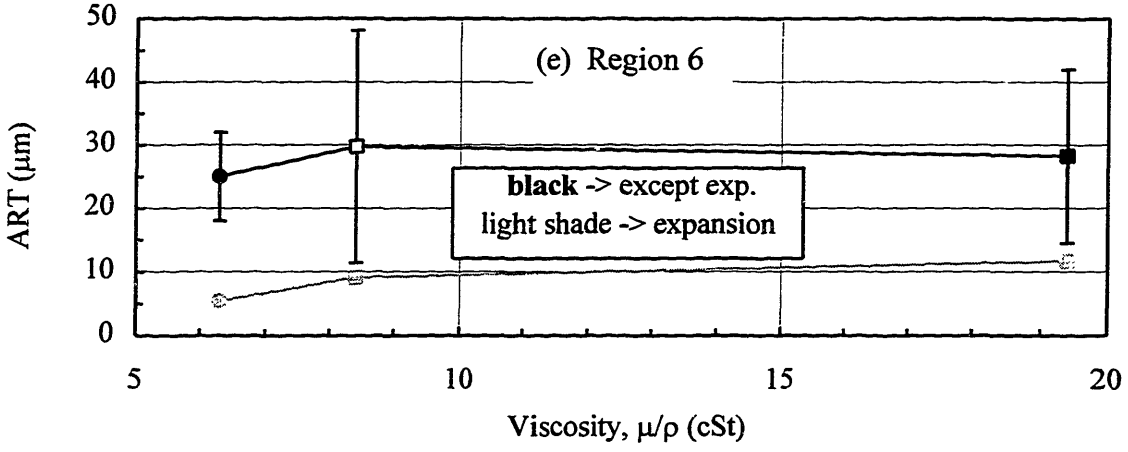
(e) Region 6
black -> except exp.
light shade -> expansion
ART (μm)
50
40
30
20
10
0
5
10
15
20
Viscosity, μ/ρ (cSt)

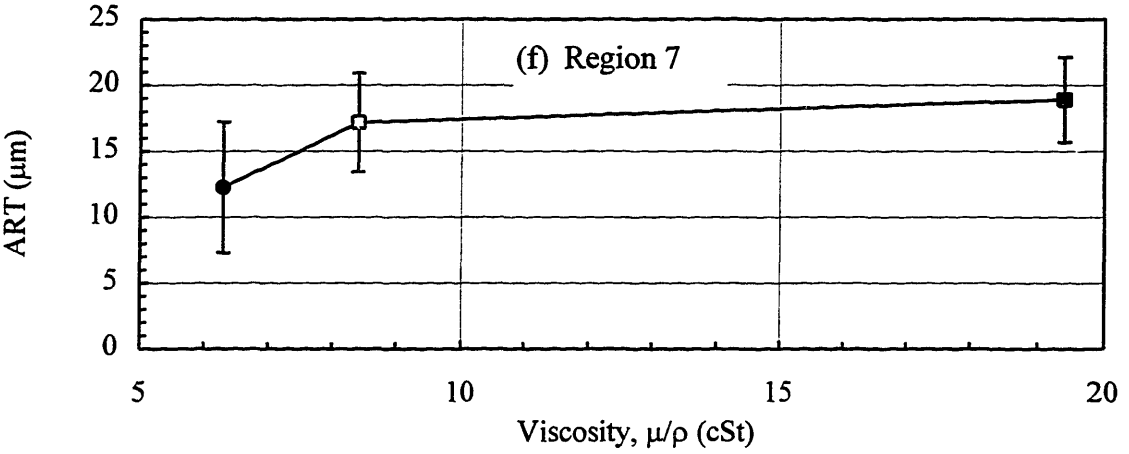
(f) Region 7
ART (μm)
25
20
15
10
5
0
5
10
15
20
Viscosity, μ/ρ (cSt)

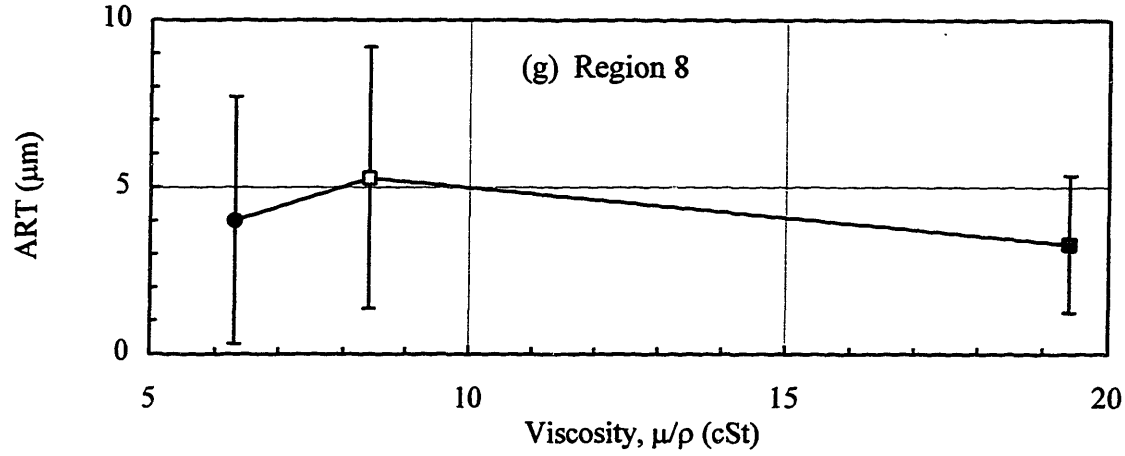

Figure 5-15 Baseline Average Region Thicknesses (Stroke-Averaged) from Window 6 for Regions (a) 2, (b) 3, (c) 4, (d) 5, (e) 6, (f) 7, and (g) 8.
(2/3 Load, 2500 rpm, 100°C)

Major-Thrust Side at Midstroke -- Window 1

Most of this section focuses on the results of window 1 on the major-thrust side of the bore because it contains the most accurate cases. In Figures 5-13 (a) and (b) for the crown and second lands, the free-liner OFT left by oil flow under the rings is included so the reader may mentally subtract out the free-liner OFT from the total ART. The subtracted result is the actual oil on the land since the free-liner OFT is the same as the liner OFT left by the top and scraper rings (see section 4.2.1). The crown land has negligible oil, and, consequently, its ART follows the free-liner OFT magnitudes and trends. The absence of oil is probably due to evaporation, burning, and blowby. In Figure 4-18 (a), the pressure drop over the top ring is always positive throughout the cycle (except for the small pressure rise during the intake stroke) providing blowing or dragging of any oil on the crown land through the gap and groove of the top ring. During the intake stroke the low pressure rise reversing the blowby is relatively small because of the high load.

After subtracting the free-liner OFT from the second land ARTs, although small, the second land oil is shown be significant ranging from 0.5 to over 2.0 microns shown in Figure 5-13(b). Relative to the top land, less evaporation from lower second land

temperature, greater lubricant partial pressure within the second land vapor, and the absence of any burning contribute to more oil. Quite unlike any other regions, no ring scraping or oil squeezing (besides ring and groove squeezing) contribute to oil on the top and second land -- only gap and groove oil transport. As seen in Figure 5-13 (c) and (d), ARTs from the third land and region 4 are an order of magnitude larger than the top and second lands largely due to scraper and segments scraping in addition to oil dragging down through gaps and grooves.

For these regions 1-4 within the ring pack, the same ART pattern among the different lubricant cases exists although the magnitudes are different; SAE-10W/50n is higher than SAE-10W and SAE-30 but lower than SAE-50. SAE-30 is usually quite lower than the other lubricants. The highly comparable patterns suggest that these ring-pack regions are linked through gap-and-grooves oil pathways; however, the different magnitudes provide support to the fact that other oil transport physics are at work such as gas flows and ring scraping.

These same patterns aren't the same as the OFT trends from the last chapter which increase with lubricant viscosity. This finding suggests that oil transport from lands to oil under the rings may not be strongly coupled. However, comparing with Figure 4-8 (a), OFT trends do indicate some subtle similarities of these same ART patterns and don't blatantly contradict them which may imply a weak link at best. Although it's hard to say that the SAE-30 OFTs are the lowest in view of the standard deviation, often they are slightly lower than SAE-10w/50n and substantially lower than SAE-50 except for the scraper ring. Especially for the starved wedges of the top ring and upper OC segments, increased oil on lands may provide some additional oil supply than what's solely on the liner for lubrication under the rings. Oil on the top and/or second lands may supply a unilateral link to the top compression rings since there is no ring scraping. Although more difficult to discern from the oil distribution, often the upper OC rail is starved as well and may receive oil supply from the vast amount of oil in the third land region in addition to the oil on the liner. This argument for the upper rail behavior is also supported by the engine speed affect addressed in sections 4.4 and 5.5.

One may hastily argue that this consistent ART pattern between the ring-pack regions is probably due to slight arbitrary errors in calibration. However, the ART patterns along the piston skirt regions are quite different and, thus, disproves this argument.

Although there seems to be no strong trend of ART with viscosity for the piston-ring pack, along the piston-skirt regions, ARTs increase very gradually with increasing viscosity as shown in Figures 5-13 (e) - (g). In addition to other transport mechanisms described in section 5.3.2.2.1, scraping largely contributes to these regions. The lower OC segment is observed to always be fully-flooded, and its scraping contributes to the highest ARTs along the entire piston assembly within the groove/chamfer region (region 5) especially for the downstrokes which range from 55 to 80 microns and greater for conditions off the baseline. The oil scraped is supplied from the lower piston-skirt regions.

Region 7 along the piston includes the largest skirt diameter, experiences hydrodynamic lubrication when sliding against the liner, and results in a ART trend characteristic of hydrodynamic lubrication found from the OFT analysis. Since OFT increases with viscosity, the oil accumulated from scraping this oil within regions 5 and 6 will consequently increase as well as seen in the figures.

In addition to refuting the calibration argument above, these piston-skirt trends also suggest that the regions along the piston-skirt are not strongly coupled to those within the piston-ring pack; the lubricant patterns below the OC ring are opposite to those within the ring pack with the exception of SAE-50 still having the highest ARTs.

Large stroke-by-stroke differences exist for the region between the OC segments and especially for those regions along the upper piston skirt. A more comprehensive investigation of these differences and others, and the reasons for stroke-by-stroke behaviors are studied in section 5.3.2.

Off Major-Thrust Side -- Window 4

Oil distribution results from window 4 are very comparable to those from window 1 in terms of the lubricant effect within each region. (SAE-10W/50n has questionable

high accuracy for calibration -- category II.) In Figures 5-14 (a) - (d), oil on the crown land is negligible, and there is no strong trend of ART with viscosity for the piston-ring pack. However, along the piston-skirt regions, ARTs increase with increasing viscosity for regions 5 and 6 as shown in Figures 5-14 (e) - (f). Along region 7 where there is no piston skirt, it is hard to describe a trend in view of the large standard deviations.

Differing from window 1, the lubricant patterns between regions in the ring pack are different and don't suggest that these ring-pack regions are strongly linked through gap-and-grooves oil pathways.

Near Bottom Center (BC) -- Window 6

On this note, region-by-region patterns between regions 3 and 4 from window 6 also differ and don't support strong linking between them. After subtraction of the free-liner OFTs from the total ARTs from the second land region, lubricant patterns from region 2 do not necessarily contrast those within the third land region.

However, although there seems to be no strong trend of ART with viscosity for the piston-ring pack, ARTs along the piston-skirt regions do increase with increasing viscosity as shown in Figures 5-15 (d) - (f). (ARTs for SAE-50 in region 5 are questionable because they are estimated due to signal saturation. Figure 5-15 (g) shows region 8, the free-liner OFT below the piston skirt, and any trends are suspect due to the high standard deviations.) Also, in agreement with all windows for the high-accuracy lubricant cases, over a large viscosity scale for SAE-10W and -50, the ARTs increase within every region, even within the ring pack.

5.3.2 Stroke-by-Stroke Differences

This section investigates the stroke-by-stroke differences and trends for the average region thicknesses (ARTs) within the ring pack. Measured from a 10 cycle-trace average, the stroke-by-stroke differences in ARTs are measured by comparing the ART from a particular window location along a stroke to other strokes in the cycle.

Results will show the differences and trends, first, for the regions within the ring pack including the region between the OC rails for the upstrokes and downstrokes and justification for the four-stroke average of the ARTs for the crown, second, and third land regions in view of the standard deviation. Not only affecting some of the stroke-by-stroke ARTs within the second land, stroke-by-stroke oil squeezing between the top and second rings and their grooves contribute to peaks within the otherwise uniform oil distributions within the crown and second land regions. Predictions of ring relative lift within ring grooves from the *RINGPACK-OC* model are validated from the stroke-by-stroke oil squeezing at midstroke and near BC and help interpret oil squeezing trends throughout the cycle.

Lastly, stroke-by-stroke differences for the regions below the OC ring are shown to be significant for the upper piston skirt and groove/chamfer regions (regions 6 and 5, respectively). In addition to the hydrodynamic lubrication characterized along the lower portion of the piston skirt, oil transport mechanisms including inertial forces and oil squeezing and scraping are clearly observed. Oil transport up the groove/chamfer region and azimuthally around the skirt as the piston reciprocates through top center during the gas exchange strokes as well as the power strokes is shown to significantly occur.

All results highlight the baseline measurements but also include some data off of the baseline to further substantiate findings and point out the rare exceptions to the general and consistent trends found within the entire database.

5.3.2.1 Within the Ring Pack

Figures 5-16 (a), (b), and (c) show the stroke-by-stroke ARTs for the crown, second, and third land regions, respectively, for each lubricant case corresponding to high calibration accuracy from window 1 for the baseline. The stroke-by-stroke patterns

within a region for each lubricant case are typical for the entire database excluding the exceptions which are explicitly addressed for the particular region.

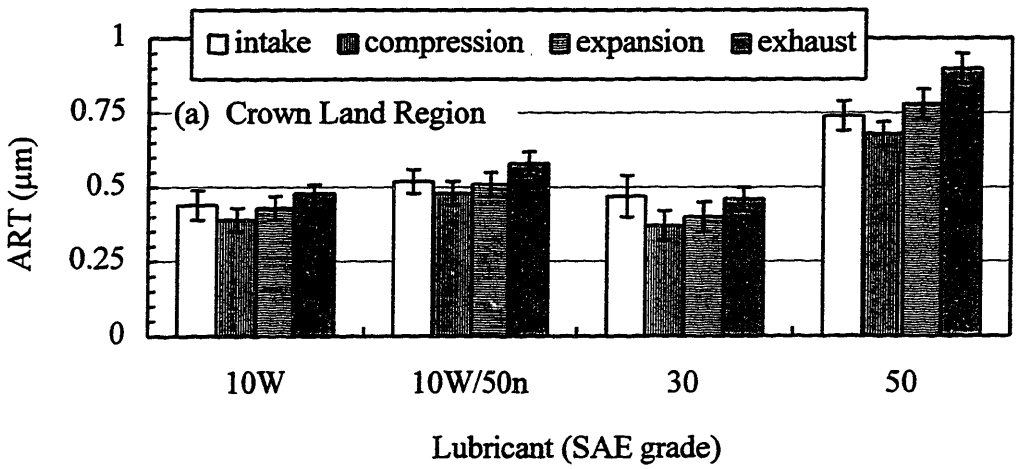

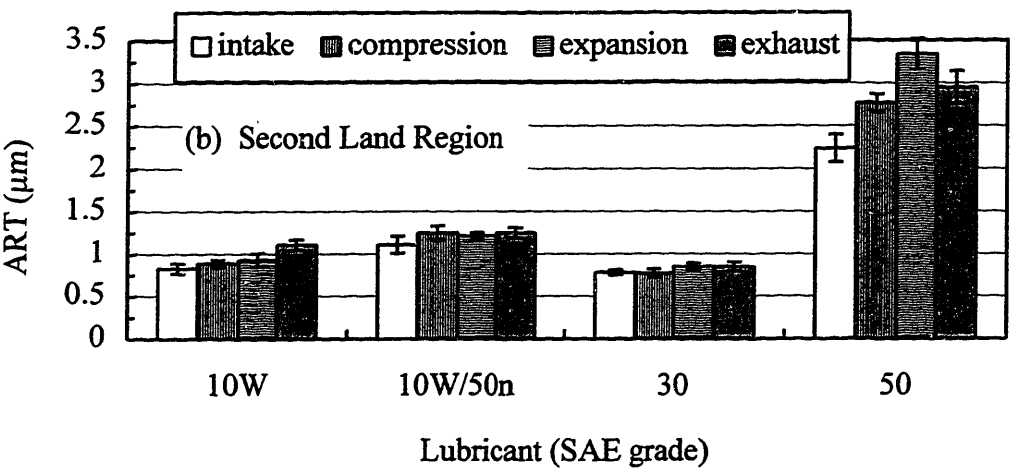

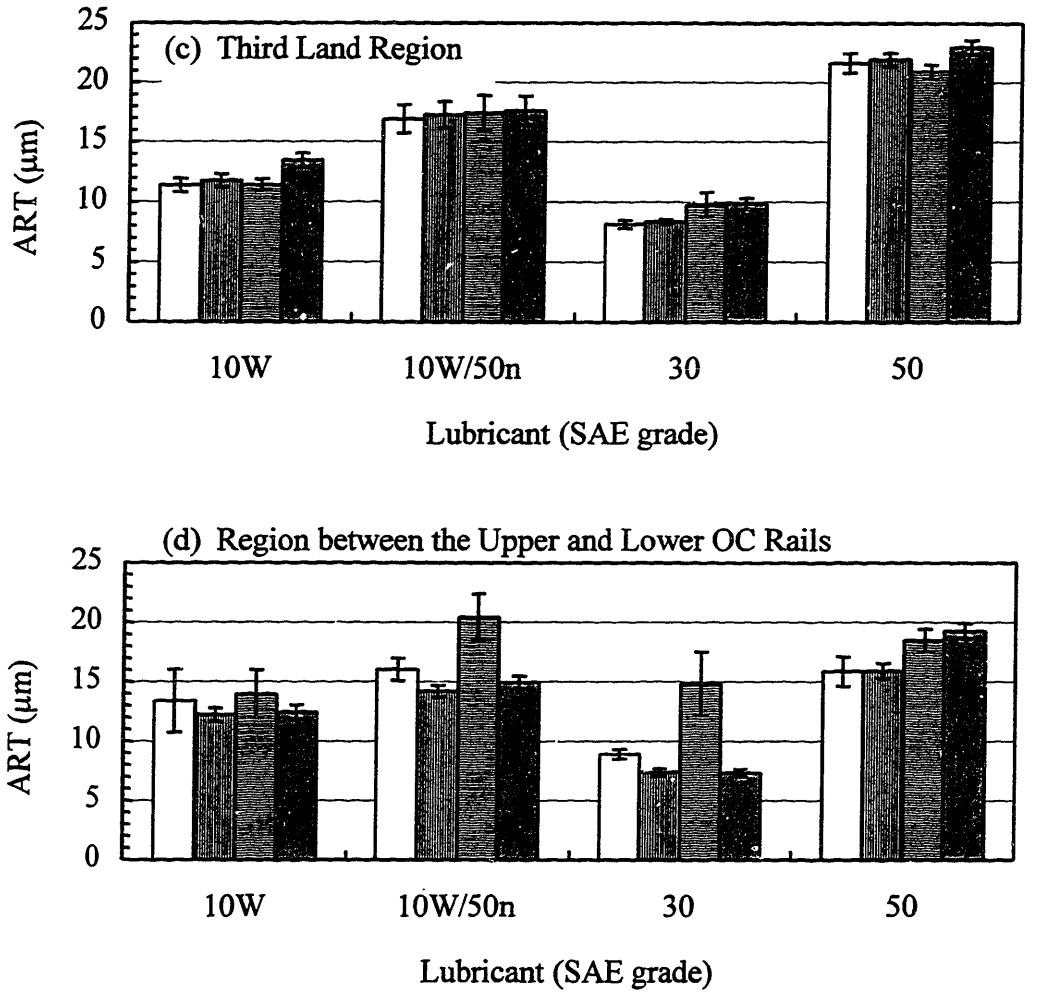

Figure 5-16 Stroke-By-Stroke, Average Region Thicknesses from the Ring Pack for the (a) Crown Land Region, (b) Second Land Region, (c) Third Land Region, and (d) Region between the Upper and Lower OC Rails.
(Window 1, 2/3 Load at 2500 rpm, 100°C)

5.3.2.1.1 Crown and Second Land Regions -- ARTs and Oil Squeezing in Grooves

Since the crown land typically has negligible oil for the fired cases as shown in section 5.3.1, the ARTs along the crown land region tend to follow the stroke-by-stroke patterns for the free-liner OFTs found and explained in the OFT analysis in section 4.2.3.3. (For the motored cases addressed in sections 5.4.2 and 5.4.3, oil does exist on the

crown land but the amount is very little. The stroke-by-stroke differences are negligible for the motored cases as well.)

The small amount of oil along the second land region does not vary from stroke to stroke except when oil squeezing between the rings and their grooves becomes significant. For example, for the SAE-50 case, the intake stroke is the lowest while the expansion stroke is the highest with the compression and exhaust strokes in between these extremes. This result can be attributed to oil squeezing. For the fired cases, oil squeezing is only detected in the lower channel between the top ring and its groove as shown for SAE-50 in Figure 5-17 (a) depicted by the sharps peaks. (For certain motored cases, enough oil exists within the upper channel between the second ring and its groove because of reduced lubricant dragging from reduced groove gas flow shown in section 5.4.3.) When oil availability on the second land is low such as for SAE-10W, oil squeezing is much less and barely detected shown in Figure 5-17 (b). Additionally, with the exception of any oil squeezing peaks, the distribution of oil along the region is fairly uniform like the crown land region -- a characteristic uncommon to lower regions of the ring pack.

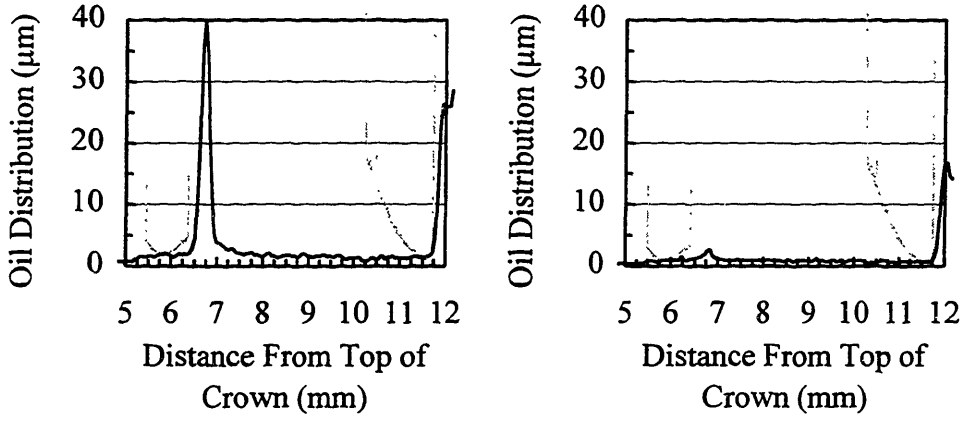

Figure 5-17 Oil Distribution Along Second Land Region During the Expansion Stroke for (a) SAE-50 and (b) -10W.
(Window 1, 2/3 Load at 2500 rpm, 100°C)

This mechanical oil squeezing between the ring and the top and bottom of its groove can transport oil both radially inward and outward. The outward flow which may attach to the lands and/or travel down the ring flank towards the liner is directly observed by the LIF system for the top ring between both the top flank of the ring and top of the groove and bottom flank and bottom of the groove. (Some motored cases reveal squeezing between upper channel between second ring and its groove in sections 5.4.3. Oil squeezing between rings and grooves in other regions is obscured by the massive oil masses in the ring vicinity.) Since ring squeezing is contingent upon ring lift within the groove, the predicted ring lift from the *RINGPACK-OC* model will be verified shortly.

Actual measured top and bottom channel squeezing from oil distribution traces for the top ring are shown in Figures 5-18 (a) - (c) for every stroke within a cycle. For the LIF system to detect the channel squeezing from ring lift and contact with its groove, sufficient oil must exist within the channels. Figure 5-18 (a) shows bottom channel squeezing at midstroke and only enough oil exists within the bottom channel to observe any squeezing as opposed to the top channel. Only for rare cases (mostly motored) where oil along the second land region is substantial (and equivalent to more than a few microns in ART along the region) does enough oil exist within the top channel to reveal top channel squeezing in Figure 5-18 (b). Opposite to bottom channel squeezing, top channel squeezing only occurs during the intake stroke at midstroke.

The radially long flat surfaces of the ring flanks and top and bottom parts of the groove provide a channel through which lubricant can flow. Top channel and bottom channel squeezing occur throughout a cycle as the ring move axially up and down against the top and bottom portions of its groove. Figures 5-19 (a) and (b) schematically illustrate bottom and top channel squeezing, respectively, of the top ring during the latter half of the expansion and intake strokes, respectively. (The latter half of the stroke is when the piston is decelerating and inertial forces are down corresponding to crank angles greater than 74.2° ATC.) During bottom channel squeezing net downward pressure and inertial forces dominate any upward friction forces driving the ring down making contact with the bottom of the groove. Bottom channel squeezing also occurs during the compression and exhaust strokes at the axial window positions within the Kohler. During

top channel squeezing for the intake stroke, upward net pressure forces and ring-liner friction forces compete against the downward inertial forces and drive the ring upward, making contact with the top of the groove.

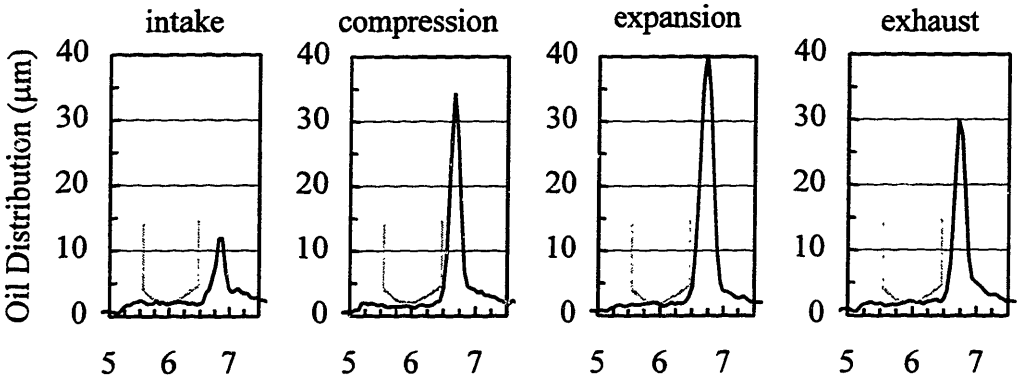

(a) Bottom Channel Squeezing at Midstroke
(Window 1, SAE-50, 2/3 load at 2500 rpm, 100°C)

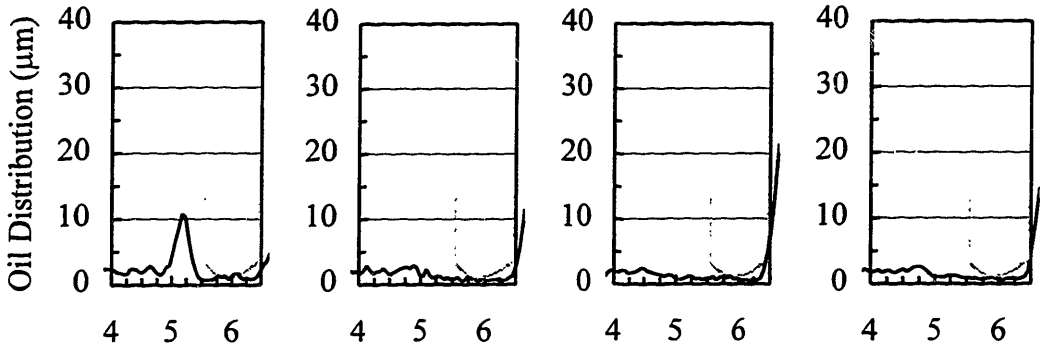

(b) Top Channel Squeezing at Midstroke
(Window 4, SAE-50, Motored WOT at 2500 rpm, 100°C)

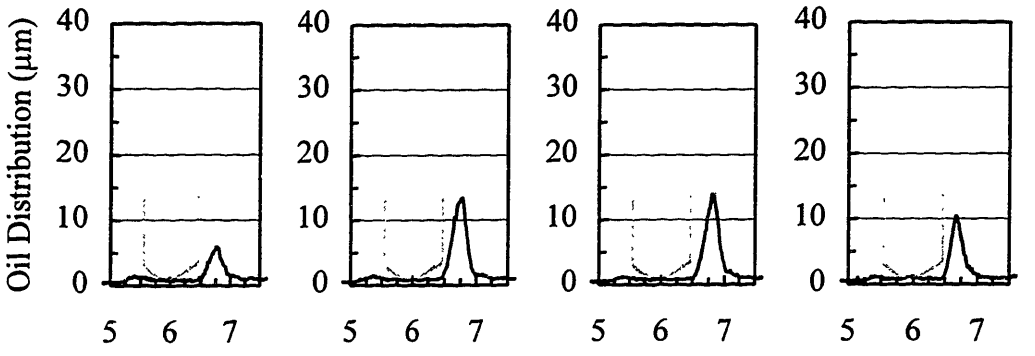

(c) Bottom Channel Squeezing near BC
(Window 6, SAE-50, 2/3 Load at 2500 rpm, 100°C)

Figure 5-18 Stroke-by-Stroke Top Ring Squeezing at Midstroke for (a) Bottom and (b) Top Channel Squeezing and near BC for (c) Bottom Channel Squeezing

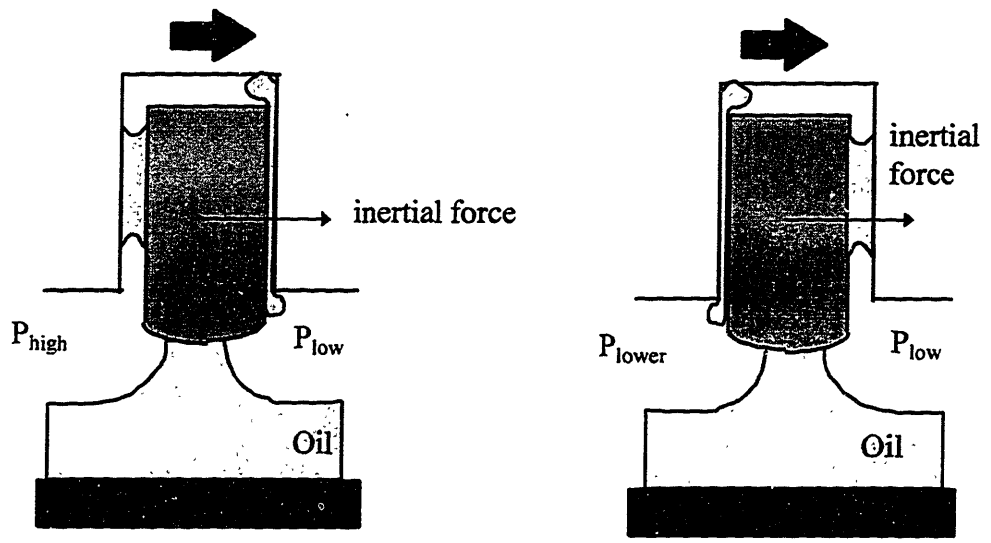

(a) Bottom Channel Squeezing during Latter Half of Expansion Stroke

(b) Top Channel Squeezing during Latter Half of Intake Stroke

Figure 5-19 Schematic of Oil Squeezing within Channels during an Latter Half of an (a) Expansion Stroke and (b) Intake Stroke

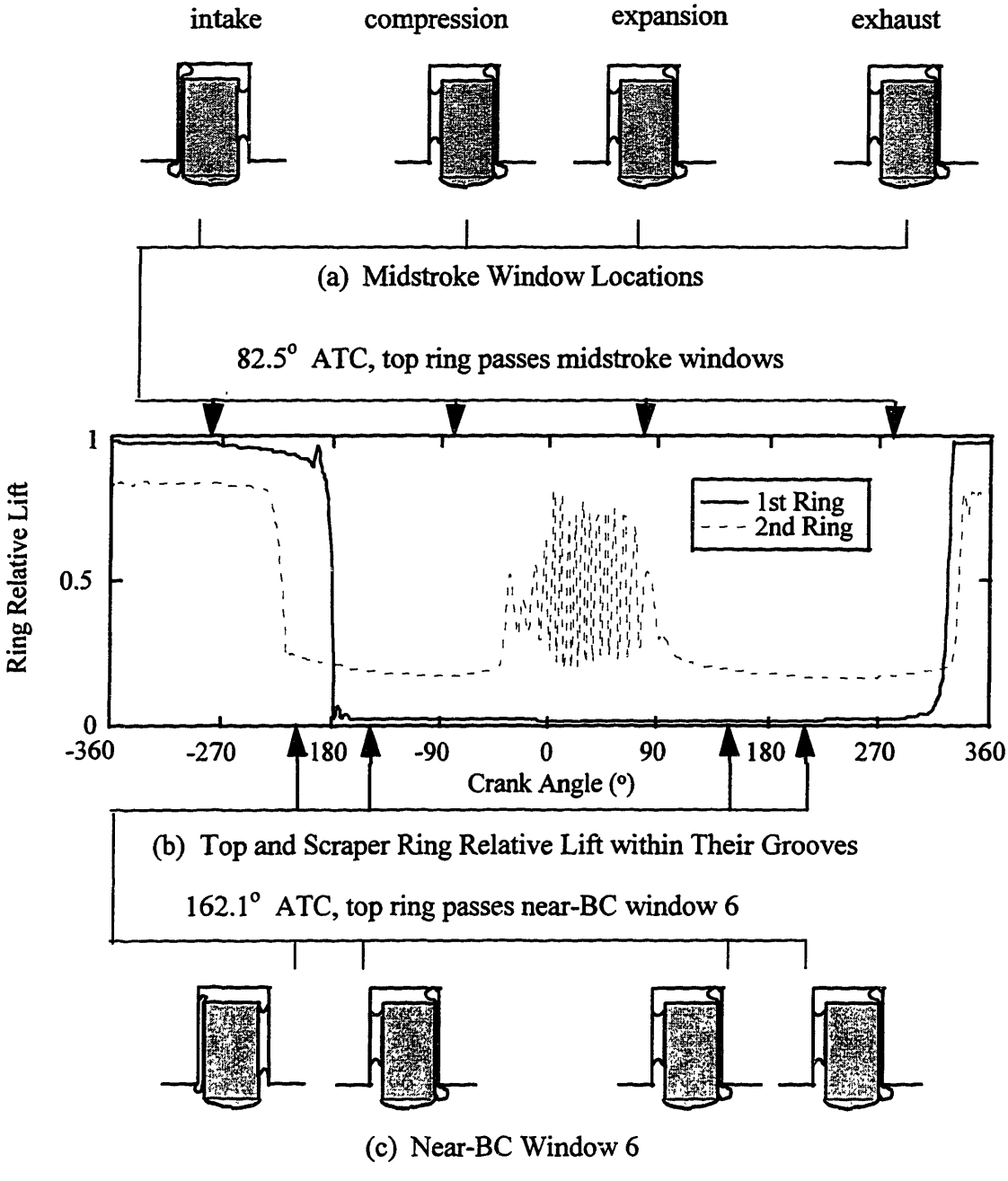

Figure 5-20 Top Ring Position within Its Groove at (a) Midstroke Windows, from (b) Predicted Top and Scraper Ring Lift from *RINGPACK-OC*, and at (c) Near-BC Window 6.

To add more credibility to this interpretation of channel squeezing, Figure 5-20 (b) provides numerical predictions of relative ring lift for the top and scraper rings within their grooves versus CA over a complete cycle. Arrows along the absisca denote the exact window locations when the top ring passes during the cycle and are accompanied by schematic top ring positions relative to its groove at midstroke and near BC in Figures 5-20 (a) and (c), respectively. (The measured cylinder pressure trace and predicted land pressures used in the *RINGPACK-OC* model were shown earlier in Figure 4-18 (a)). Even for the near-BC window 6, both the predictions and measurements show top channel squeezing during the intake stroke indicating that inertial ring forces throughout a stroke must be relatively low.

During the expansion stroke, contact pressures between the lower ring flank and bottom groove are the greatest from the high cylinder pressures and cause the greatest squeezing shown in the measurements at midstroke and near-BC windows in Figures 5-18 (a) and (c), respectively. The compression stroke shows a little less squeezing from lower compressive cylinder pressures followed by the exhaust stroke. This stroke-by-stroke squeezing hierarchy is consistent with the model predictions implied by the amount of ring lift and contact pressures. Although the differences between the compression and exhaust lifts are hard to discern, predicted CA-resolved contact pressures between the ring and groove are greater for the compression than exhaust.

5.3.2.1.2 Third Land Region

In view of the standard deviation, stroke-by-stroke differences for the third land region shown in Figure 5-16 (c) are consistently negligible although the ARTs for the third land region are an order of magnitude higher than those for the second land region. In addition to scraping, downward gas flows through the second ring grooves and gaps particularly during the expansion stroke, hold back lubricant from being transported to the second land region. (Gas flows are discussed in further detail in section 5.4.3 addressing the load effect.) Despite the large stroke-by-stroke differences of gas flows through the second ring gap and groove shown in Figures 5-31 (b) and -32 (b) which may drag lubricant (especially for expansion stroke accompanied by second ring flutter), no

stroke-by-stroke differences in oil distribution are detected around the scraper ring for the third land region and the second land region. Perhaps the steady-state running condition of the engine is not extreme enough to cause a stroke-by-stroke affect. However, over long time scales, effects of different gas flows on oil distribution and ARTs induced by different engine running conditions including the different loads and speeds are found and shown in sections 5.4.3 and 5.5, respectively.

5.3.2.1.3 Region Between the Upper and Lower OC Rails

Although no stroke-by-stroke differences are detected within the third land region, the downstrokes for region 4 are often higher than the upstrokes shown in Figure 5-16 (d) in view of the standard deviations. This trend is even more pronounced from window 2 in Figure 5-21 (a) but less clear from window 4 in Figure 5-21(b) and window 6. (Although the absolute magnitudes for some cases are suspect due to the different levels of calibration accuracies, the relative stroke-by-stroke trends with standard deviations within a lubricant case are real.) This stroke-by-stroke trend is rather independent of azimuthal location which suggests the mechanism for this stroke-by-stroke behavior may have more to do with the OC ring behavior than the influence of piston secondary motion. In part, this occurrence may be due to the higher downstroke MOFTs of the lower OC segment addressed in section 4.2.3.1.

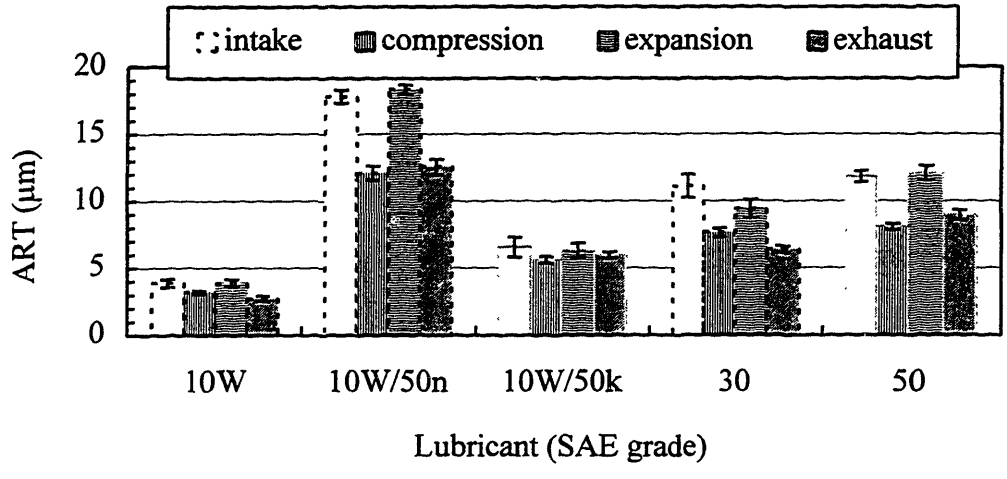

(a) Window 2

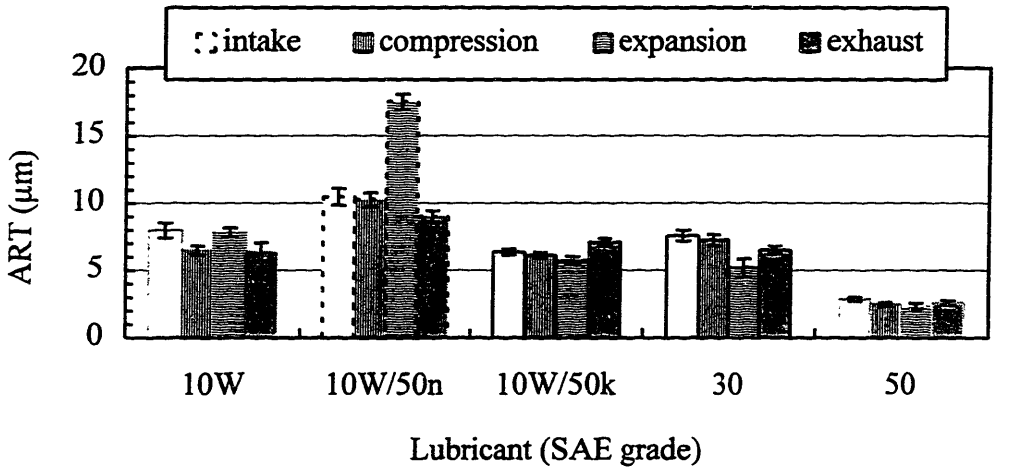

(b) Window 4

Figure 5-21 Stroke-By-Stroke, Average Region Thicknesses for Region 4 from (a) Window 2 and (b) Window 4.
(2/3 Load at 2500 rpm, 100°C)

However, compared to the fired cases shown above, an opposite trend exists for the motored cases. Typical cases are shown in Figure 5-22 from window 1 for 60°C. At 40°C, these trends also hold. But these motored trends are more random and less clear at the remaining windows.

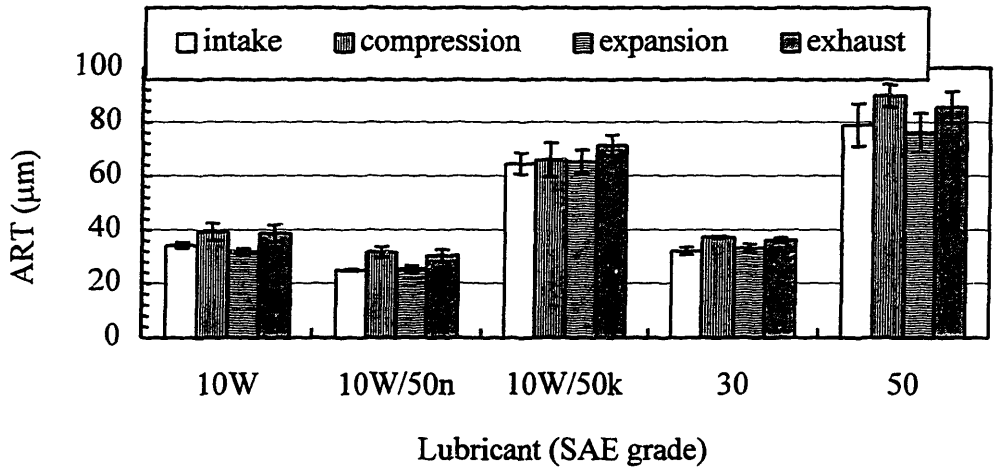

Figure 5-22 Motored Stroke-By-Stroke, Average Region Thicknesses for Region 4 from Window 1.
(Window 1, Motored (WOT) at 2500 rpm, 60°C)

5.3.2.2 Below the OC Ring Including Oil Transport Along Skirt on Major-Thrust Side

Since oil behaves very differently off the major-thrust side below the OC ring, stroke-by-stroke oil behavior is first characterized along the major-thrust side at midstroke and near bottom center (BC) corresponding to windows 1 and 6, respectively, considering the first three regions assigned along the piston skirt in Figures 5-2 (a) and (c). In addition to hydrodynamic lubrication, clear influences of oil transport mechanisms are observed including oil scraping and squeezing and driving from inertial forces. Calculated ARTs from stroke to stroke reflect the oil behavior seen in the oil distributions. Oil transport up the groove/chamfer region and azimuthally around the skirt as the piston reciprocates through top center during the gas exchange strokes as well as the power strokes is shown to significantly occur. Lastly, different ART trends from windows 2 and 4 are briefly shown based on the three region assignments in Figure 5-2 (b).

5.3.2.2.1 Major-Thrust Side -- Midstroke and Near Bottom Center (Windows 1 and 6)

Since the experimental setup enables optical access at midstroke and near bottom center (BC) corresponding to window 1 and 6, respectively, along the major-thrust side, development of the oil distribution along a stroke and from stroke to stroke as the piston reciprocates throughout a cycle may be observed as shown in the typical example in Figures 5-23 (a) - (g). Oil distributions along the skirt measured from window 1 correspond to upward inertial forces while those from window 6 correspond to downward inertial forces. (Further details concerning the inertial forces and crank angles for different regions of the piston assembly may be found in Appendix D.)

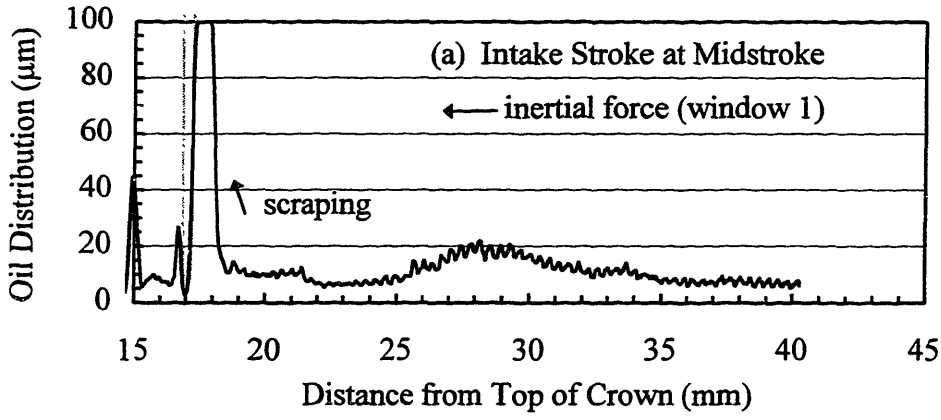

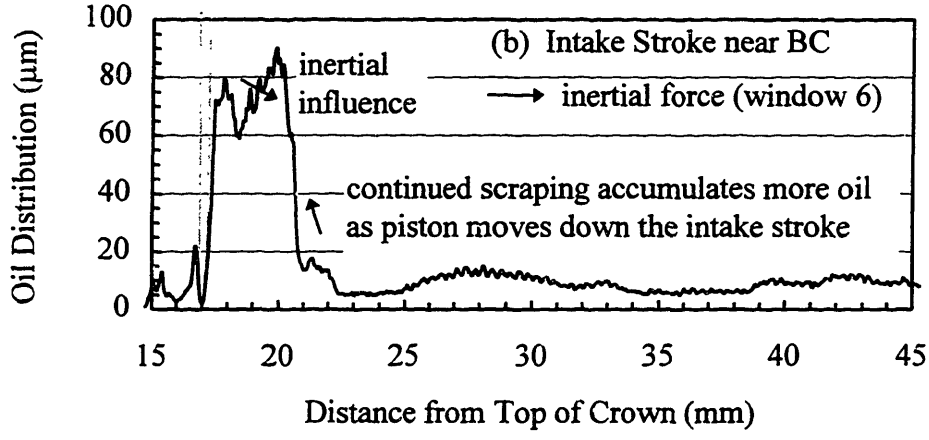

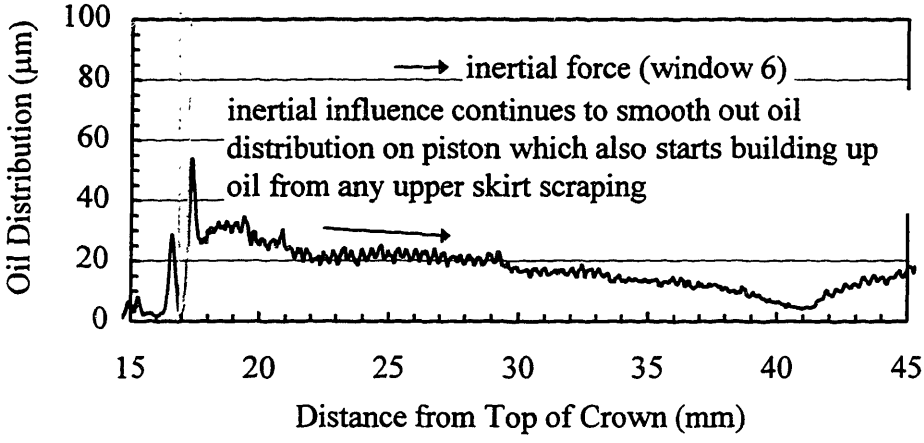

(c) Compression Stroke near BC

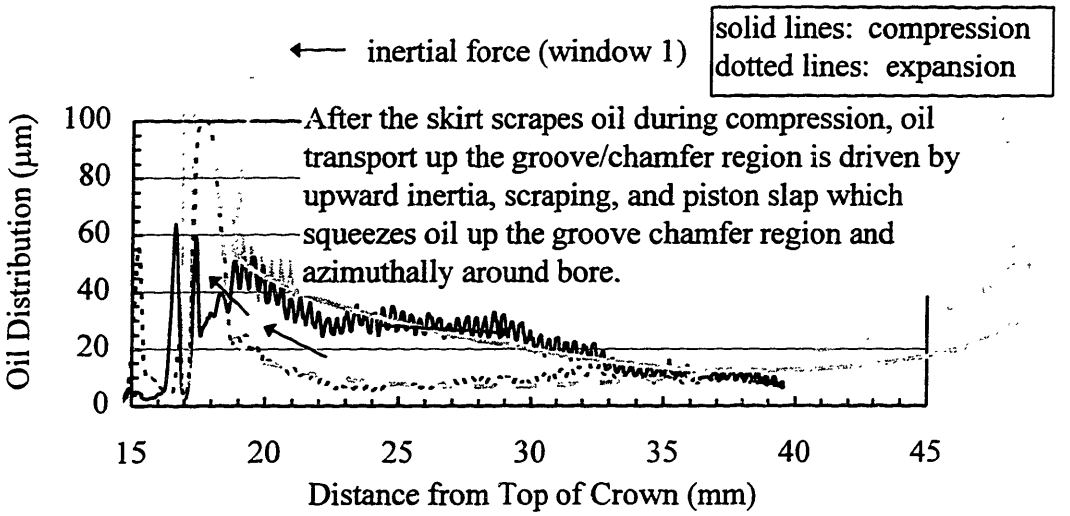

(d) Compression and Expansion Stroke at Midstroke

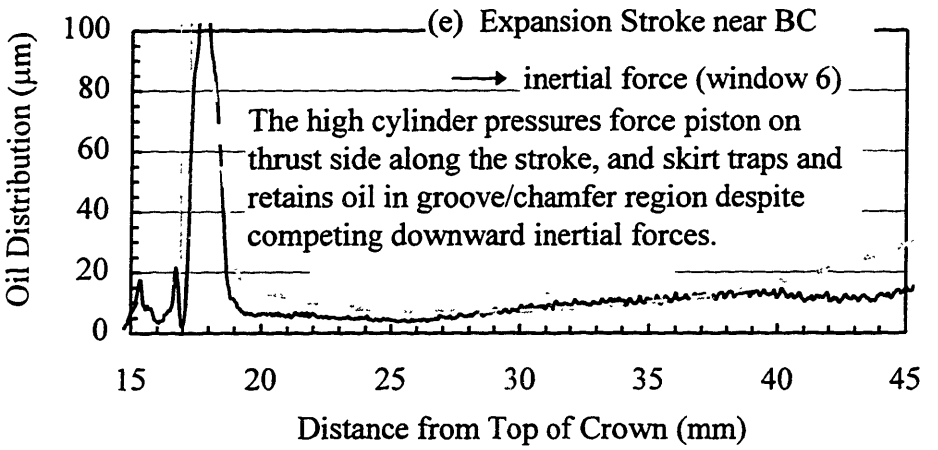

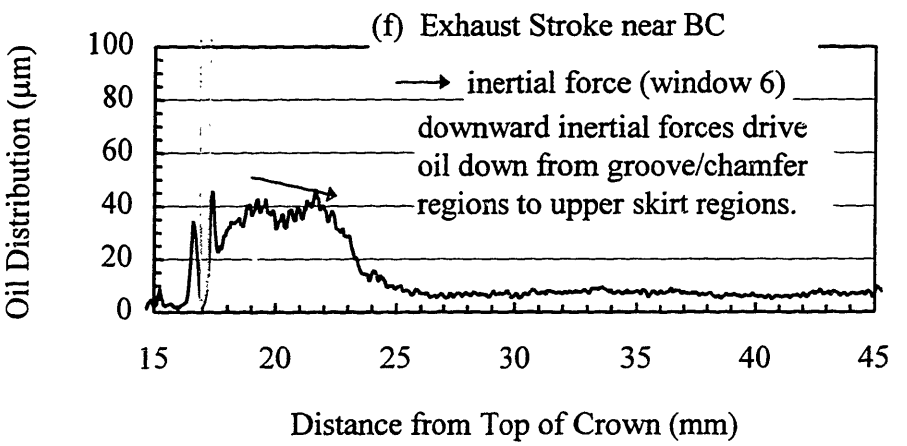

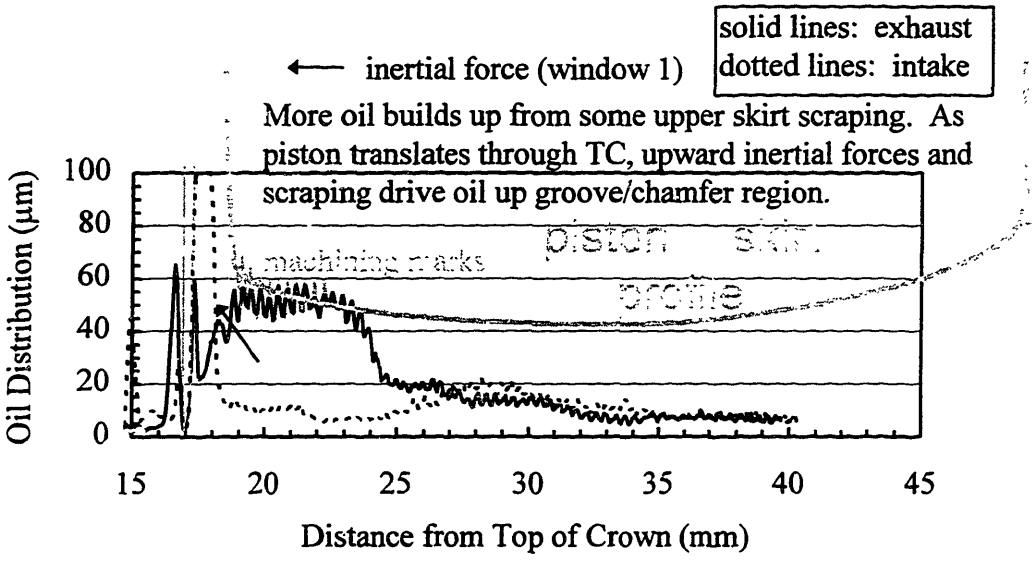

(g) Exhaust and Intake Strokes at Midstroke

Figure 5-23 Oil Distribution along the Skirt as the Piston Translates throughout a Cycle for (a) Intake Stroke at midstroke, (b) Intake Stroke near BC, (c) Compression Stroke near BC, (d) Compression and Expansion Stroke at Midstroke, (e) Expansion Stroke near BC, (f) Exhaust Stroke near BC, and (g) Exhaust and Intake Strokes at Midstroke (SAE-10W, 2/3 Load, 2500 rpm, 100°C)

As the piston travels through midstroke during its intake stroke in Figure 5-23 (a), the lower OC rail scrapes oil in the groove/chamfer region and has a fully-flooded converging wedge. The upward inertial forces help retain the large oil masses up against the lower OC rail within the groove/chamfer region. However, although oil scraping continues to accumulate oil within the groove chamfer region as the piston reciprocates completely through midstroke towards BC, inertial forces change direction and drive some of the large oil masses out of the groove/chamfer region to the upper skirt regions shown in Figure 5-23 (b).

On the following upstroke during compression, the downward inertial forces continue to smooth out the large oil masses resulting in a more uniform oil distribution along the piston skirt as shown in Figure 5-23 (c). Although there is no further oil

accumulation through lower OC ring scraping, any scraping from the skirt during skirt and liner contact starts to contribute to further accumulation.

Oil build up during the compression stroke continues along the upper skirt region from piston scraping as the piston translates past the midstroke window shown in Figure 5-23 (d). Clear machining marks are detected within the oil distribution trace, and an accompanying overlay of a schematic of the piston skirt is shown along with a few actual machining marks. As the piston reciprocates through top center (TC) and passes by the midstroke window during the expansion stroke, oil transport up the groove/chamfer region is driven by lower OC rail scraping, upward inertial forces, and piston slap which squeezes the oil up towards the groove/chamfer region and azimuthally around the bore. Additionally, while the piston slides along the liner especially for the portion of the skirt with the maximum diameter around 40 millimeters from the top of the crown land, hydrodynamic lubrication (also characterized in sections 5.3.1 and 5.4) is occurring along the lower piston skirt region, region 7. The oil distribution between 33 and 40 millimeters exactly overlap indicating that the piston pivots around this location changing tilt angles during compression and expansion strokes.

As the piston continues to translate throughout the expansion stroke towards BC, it continues to reside against the major-thrust side shown in Figure 5-23 (e). Despite the competing downward inertial forces, this piston position physically traps and retains oil accumulation within the groove/chamfer region as opposed to the intake stroke for this window.

Only when the piston pulls away liner are the downward inertial forces allowed to drive oil into the upper skirt region as for the exhaust stroke near BC in Figure 5-23 (f). As the piston continues through the exhaust stroke passing by the midstroke window, additional oil builds up from any upper skirt scraping from contact with the liner shown in Figure 5-23 (g). As the piston reciprocates through TC, upward inertial forces and scraping during the downstroke during intake drive oil up the groove/chamfer region.

Oil flow from inertial forces is not instantaneous from one location to another. Contrasting the expansion (exhaust) and intake (compression) strokes in Figures 5-23 (e) and (b) ((f) and (c)) shows that movement of oil along the upper skirt region takes time to

develop. No inertial influence confines oil accumulation within the groove/chamfer region during the expansion stroke as shown in Figure 5-23 (e). However, when inertial forces do influence the oil flow as in the following exhaust stroke, oil flowing out of the groove/chamfer region moves slowly to the top portion of the upper piston skirt region and is not instantaneously distributed uniformly over the entire piston skirt. As more time passes, the oil gradually distributes itself more uniformly under the continual influence of downward inertial forces. Figure 5-23 (c) for the compression stroke near BC is another good example.

Since the influence of inertial forces start much later starting during the exhaust stroke due to oil entrapment within the groove/chamfer region during expansion, oil travel is not as far as shown in Figure 5-23 (f).

The study of oil behavior below the OC ring is important because large quantities of oil exist along these regions and supply oil to regions above the lower OC rail. Additionally, the regions along the groove/chamfer and upper piston skirt experience the highest dynamic transport environments especially at top center when the OC ring is lifted within its groove because of the upward inertial forces from the heavy OC ring and small pressure influences. (OC ring lift within its groove has just recently been numerically calculated within the MIT Lubrication Consortium under the initiative for OC ring model development.) OC ring lift around TC provides a great opportunity for oil to be transported from the groove/chamfer region to behind the OC ring as oil is driven up the groove/chamfer region from the upper piston skirt region shown in Figures 5-23 (d) and (g). Therefore, in addition to oil flow from hydrodynamic lubrication under the lower OC rail, other oil pathways include the groove (and also the gap) through which the OC ring may be fed from regions below the OC ring.

By integrating the oil distributions below the OC ring and taking the difference between the compression and expansion strokes or intake and exhaust stokes, significant volumetric flows are shown to occur in Figures 5-24 for other lubricants as well at the baseline and other engine liner temperatures. Oil behavior for other engine conditions and lubricants is qualitatively similar to the example for SAE-10W shown above. The volumetric flows are always positive, and, for almost all of the cases, the actual standard

deviations do not bracket zero which indicates that the oil transport up the groove/chamfer region and azimuthally around the bore is significant.

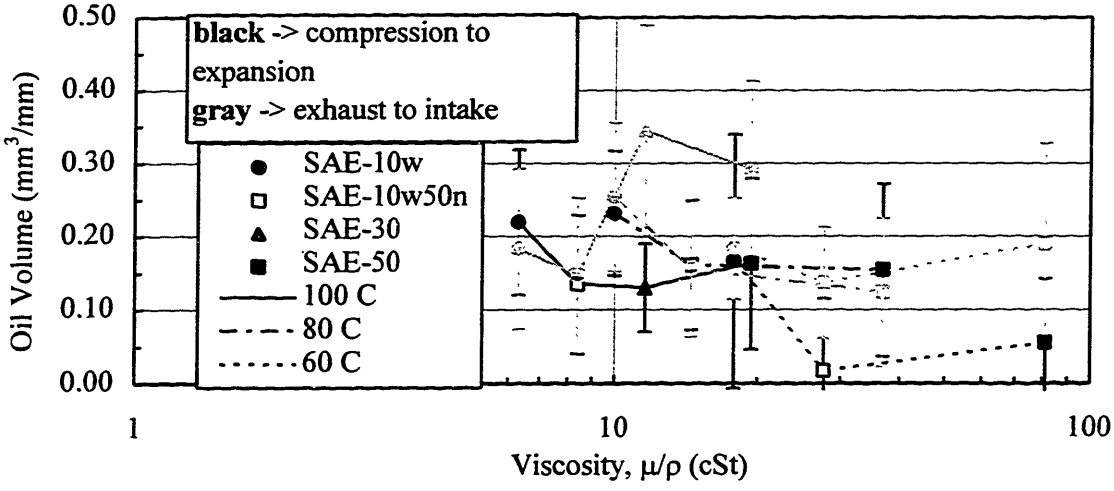

Figure 5-24 Volumetric Oil Transport along Piston Skirt as Piston Reciprocates through TC from compression to expansion and exhaust to intake strokes.

Although the exhaust-to-intake flows tend to have values higher than the compression-to-expansion flows for a small minority of cases, the heavy overlap of standard deviations marginalizes this difference. However marginal the difference, one might expect the opposite because of the additional oil squeezing from compression-to-expansion strokes compared to the exhaust-to-intake strokes (during which squeezing is much less, if it exists at all). The data shows that the additional oil squeezing does not have an affect on the volumetric oil flow.

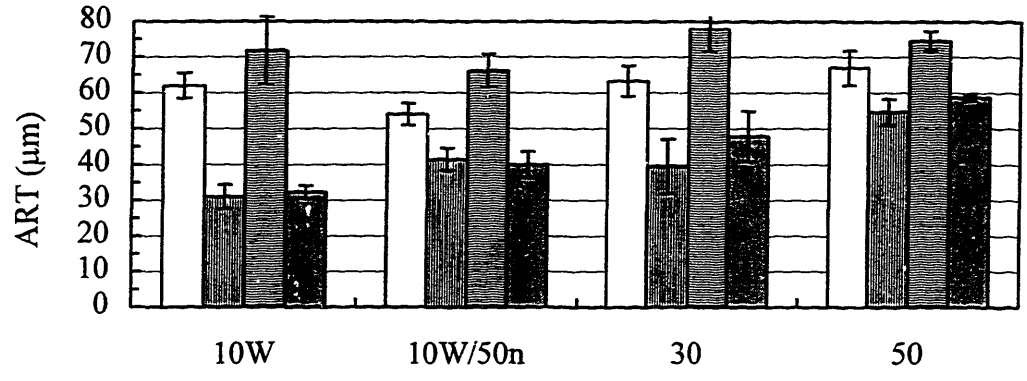

Downstrokes are adjusted values from saturated signals which reduced signals by 10 - 20 % (except for SAE-10W).

(a) Groove/Chamfer Region -- Region 5

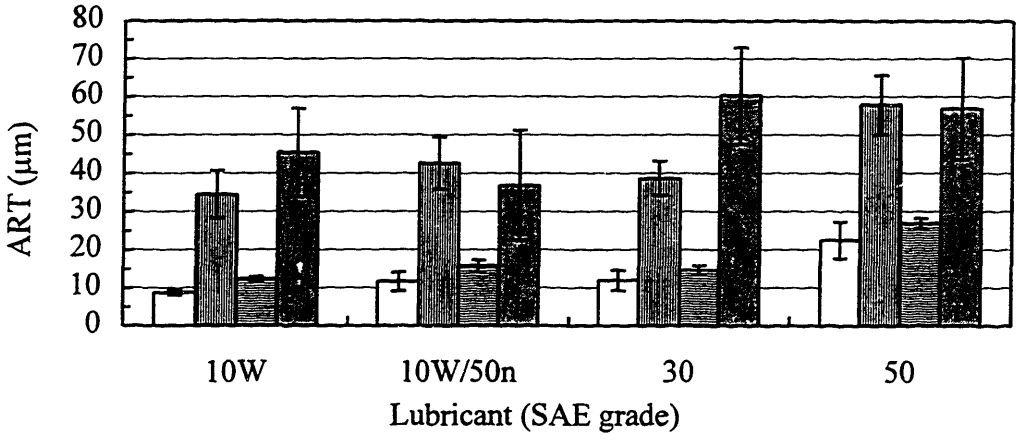

(b) Upper Piston Skirt Region -- Region 6

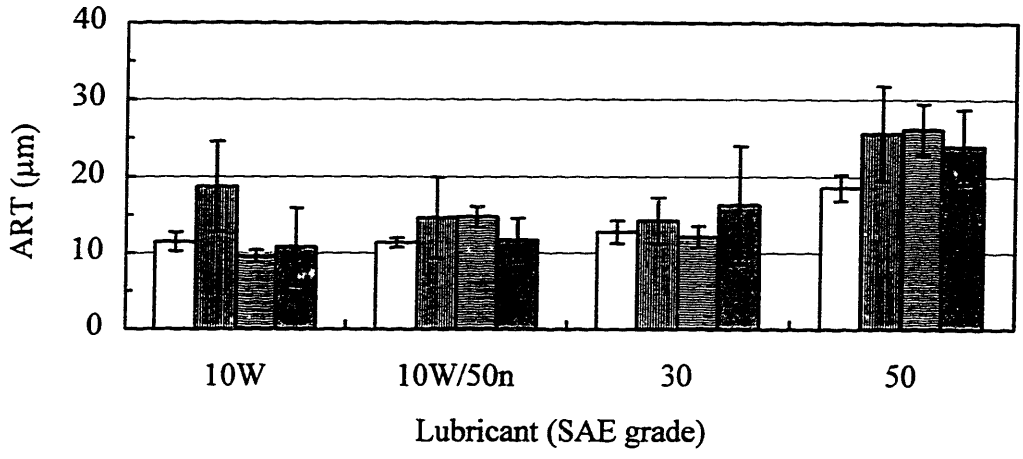

(c) Lower Piston Skirt Region -- Region 7

Figure 5-25 ARTs for Regions below the OC Ring on the Major-Thrust Side for (a) Groove and Chamfer Region -- Region 5, (b) Upper Piston Skirt Region -- Region 6, and (c) Lower Piston Skirt Region -- Region 7
(Window 1, 2/3 Load at 2500 rpm, 100°C)

Still, oil squeezing does seem to have an influence when comparing strokes within the groove/chamfer region shown in Figure 5-25 (a). The expansion stroke always has a higher ART than the intake stroke. Also, the upstrokes always have higher ARTs than the downstrokes. Again, this ART hierarchy between strokes reflect the scraping, inertial, and oil squeezing mechanisms of oil transport.

Conversely, the downstrokes are always less than the upstrokes along the upper piston skirt region (or region 6) shown in Figure 5-25 (b). These results are predominantly caused by inertia forces with some skirt scraping described earlier in this section.

No significant differences between strokes for the lower portion of the piston (or region 7) occurs as shown in Figure 5-25 (c). Along this region which includes the maximum skirt diameter, hydrodynamic lubrication is predominant.

ARTs from window 6 near BC show exactly the same stroke-by-stroke trends as those from window 1 except for the upper piston skirt region shown in Figure 5-26. Unlike midstroke during the intake stroke, a large portion of the oil distribution from

inertial forces has moved into this region (Figure 5-23 (b)). Therefore, instead of the downstrokes having less ARTs than the upstrokes, the expansion has much less than all of the other strokes typically having comparable magnitudes. (ARTs from the free-liner below the piston regions (or region 8) do not vary significantly from stroke to stroke.)

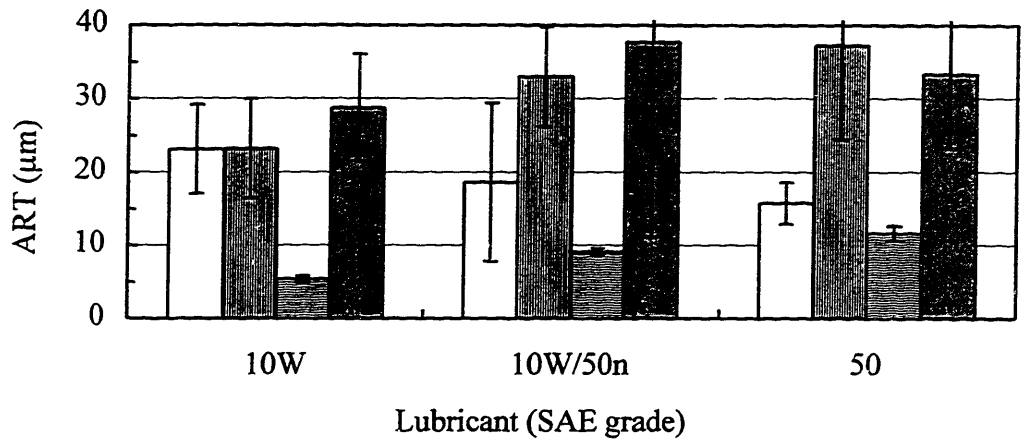

Figure 5-26 ARTs along the Upper Piston Skirt Region -- Region 6 -- from Window 6 (Window 6, 2/3 Load at 2500 rpm, 100°C)

These ARTs along the skirt quantitatively reflect the oil transport physics described in the first half of this subsection. Furthermore, this ART study justifies the stroke-averaged ARTs represented within the other sections of this chapter from the insignificant differences between the strokes in view of the standard deviation.

5.3.2.2.2 Off the Major-Thrust Side at Midstroke (Windows 2 and 4)

(See Appendix K.)

5.4 RESULTS OF PARAMETRIC STUDIES -- EFFECTS OF LUBRICANTS, LINER TEMPERATURE, AND LOAD

Cylinder liner temperature not only affects lubricant properties such as viscosity, volatility [27], and diffusion coefficients for fuel absorption/desorption studies[28], but thermal expansion of engine geometry. Enough thermal expansion especially incurred by

ring gaps and ring and groove clearances may cause changes to gaseous flow patterns and land pressures affecting lubricant flow and supply to different piston regions and, in turn, even affect ARTs within the ring-pack and along the piston. Results by Linna [29] show significant changes in blowby for different cylinder liner temperatures. Different loads including heavy loads and motored WOT conditions also affect gas pressures as well as piston secondary motion and, consequently, induce different lubrication environments.

This section investigates how the lubricants behave within different regions when subjected to different cylinder liner temperatures and engine loads off the baseline shown in the test matrix in Figure 3-2. As in the OFT analysis, two different loads are investigated separately and include the following:

- Fired conditions at 2/3 load include moderate liner temperatures of 60, 80, and 100°C.
- Motored conditions at WOT and 2500 rpm correspond to low cylinder liner temperatures of 40 and 60°C.

For each load condition, two different effects are studied. First, as a continuation from the baseline, the lubricant effects (the behavior between different lubricants at the same operating conditions) on average region thicknesses (ARTs) are studied off the baseline condition including 1800 rpm and the three moderate temperatures at 2500 rpm. Secondly, for the same lubricant, load condition, and speed, the cylinder liner temperature is varied, and the magnitudes and trends of average region thicknesses (ARTs) are investigated. The resulting effect on ARTs is defined as the temperature effect.

Finally, the ARTs from the fired and motored load conditions are directly compared at 2500 rpm and 60°C. Results from the oil distributions and ARTs especially for the top and second lands are interpreted with the help of predicted gas flows from the *RINGPACK-OC* model using the measured fired and motored cylinder pressures.

5.4.1 Fired Cases for Different Lubricants at Moderate Liner Temperatures – 60, 80, and 100°C

Fired at 2/3 load, the engine is operated at moderate cylinder liner temperatures of 60, 80, and 100°C. SAE-10W, -10W/50n, and -50 were tested at 2500 rpm at each temperature and 1800 rpm only at 100°C. Additionally at 2500 rpm and 100°C, SAE-10W/50k and -30 were tested as well. The lubricant and cylinder liner temperature effects provide the opportunity to observe the OFT measurements in two different ways.

5.4.1.1 Lubricant Effects off the Baseline

For the same cylinder liner temperature, load condition (and fired for this section), and speed, the lubricant is varied from very thin to thick lubricants ranging from SAE-10W to -50, respectively. This lubricant study is an extension from the baseline investigation in section 5.3.1. The condition at 1800 rpm and 100°C is studied first followed by engine operation at 2500 rpm for the moderate liner temperatures of 60, 80, and 100°C.

5.4.1.1.1 1800 rpm at 100°C

Using the exact format as the baseline cases in Figures 5-13, -14, and -15 but for a different engine operating condition off the baseline, Figures 5-27 (a) - (g) display ART results for this same midstroke liner temperature but at 1800 rpm and only at window 1. Again, monogrades and multigrades correspond to the solid and hollow symbols respectively.

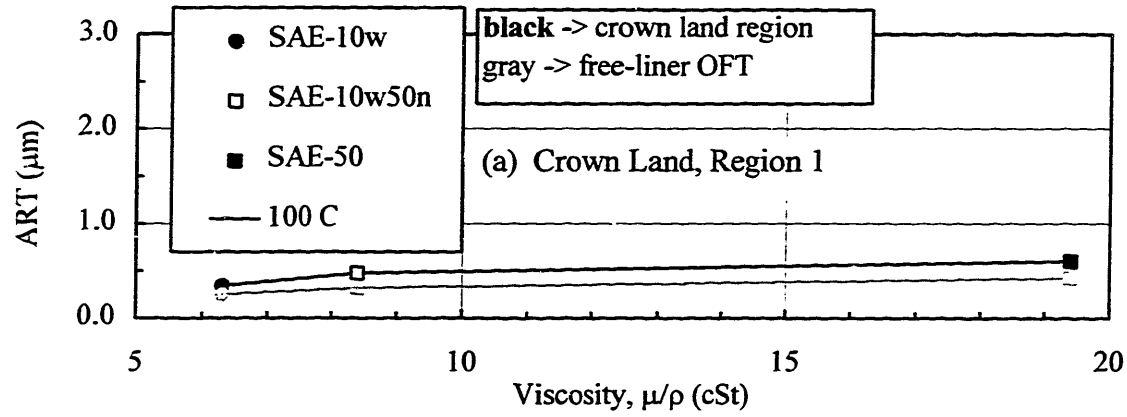
SAE-10w
SAE-10w50n
SAE-50
100 C
black -> crown land region
gray -> free-liner OFT
(a) Crown Land, Region 1
ART (μm)
3.0
2.0
1.0
0.0
5
10
15
20
Viscosity, μ/ρ (cSt)

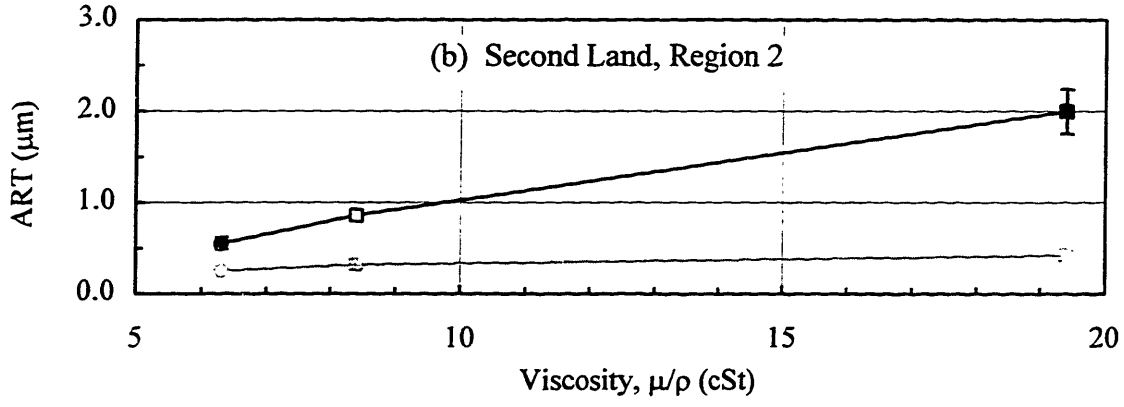
(b) Second Land, Region 2
ART (μm)
3.0
2.0
1.0
0.0
5
10
15
20
Viscosity, μ/ρ (cSt)

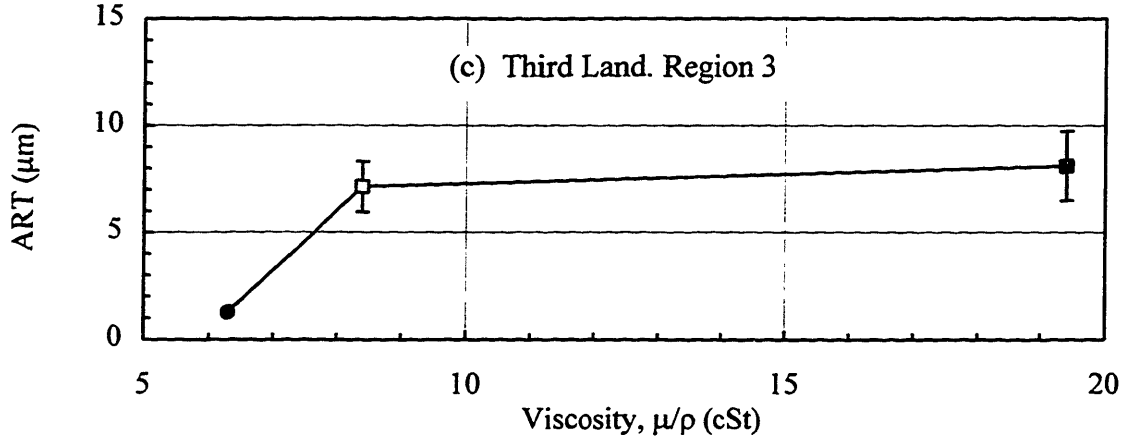
(c) Third Land. Region 3
ART (μm)
15
10
5
0
5
10
15
20
Viscosity, μ/ρ (cSt)

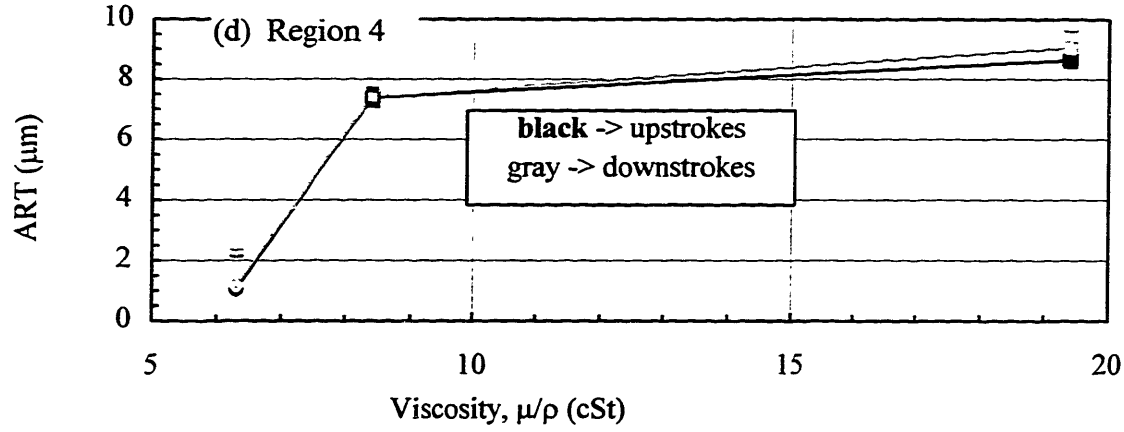

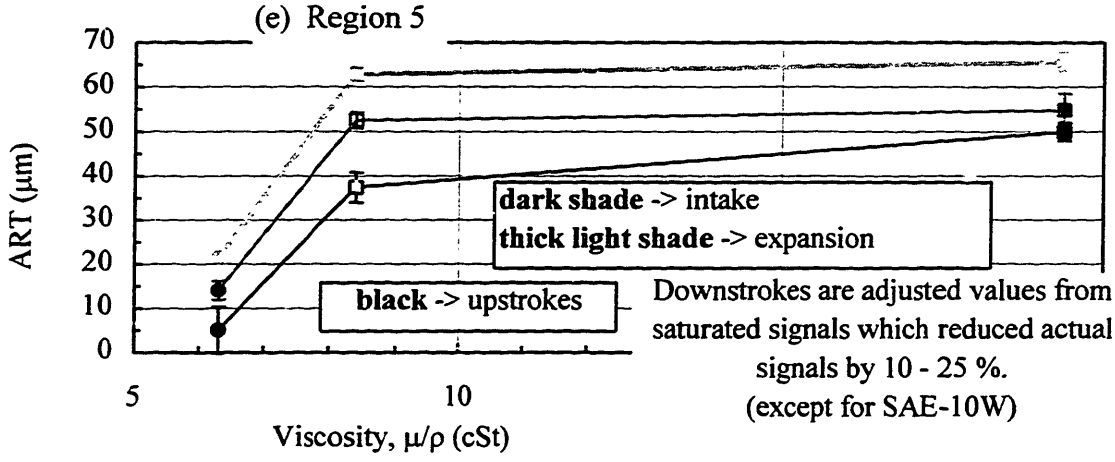

Downstrokes are adjusted values from saturated signals which reduced actual signals by 10 - 25 %. (except for SAE-10W)

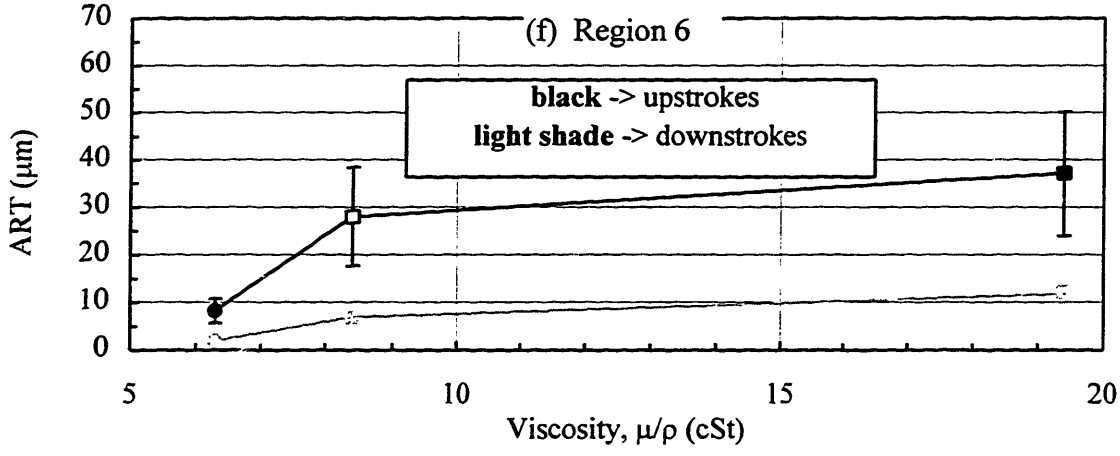

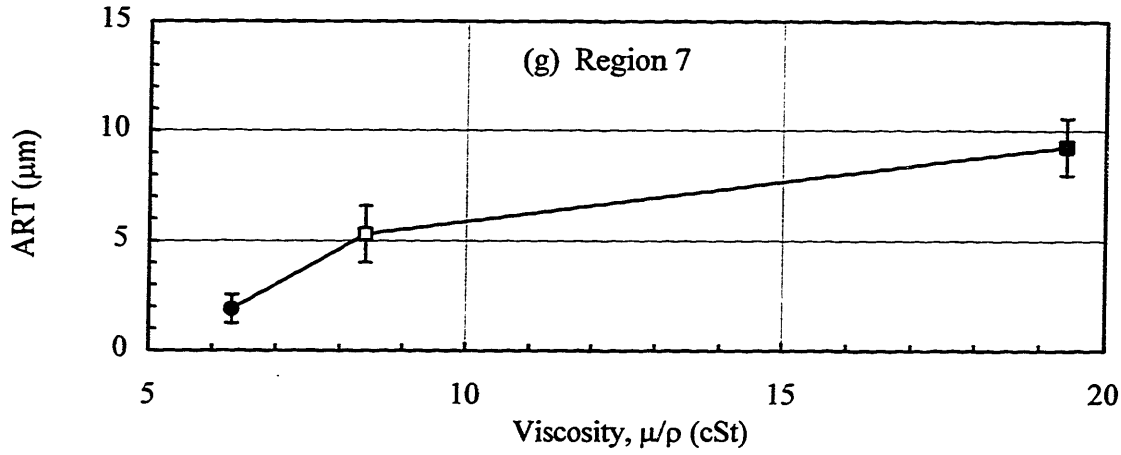

Figure 5-27 Average Region Thicknesses (Stroke-Averaged) at 1800 rpm from Window 1 for Regions (a) 1, (b) 2, (c) 3, (d) 4, (e) 5, (f) 6, and (g) 7.
(Window 1, 2/3 Load at 1800 rpm, 100°C)

Again the crown land has negligible oil as shown in Figure 5-27 (a). However, for all other regions, the ARTs within the ring pack and along the piston skirt increase with viscosity for the three lubricants. If SAE-30 was removed from the baseline results in Figure 5-13 for this same window, both the baseline (at 2500 rpm) and running condition at 1800 rpm have increasing ARTs with viscosity.

5.4.1.1.2 Moderate Liner Temperatures at 2500 rpm

Extending the ART analysis from the 100°C baseline in section 5.3.1 for window 1, this section studies the lubricant effect as liner temperatures decrease to 80 and 60°C. As in the OFT analysis, overlaying lubricant mappings corresponding to the different temperatures onto one figure provides further insight to the overall lubricant behavior for different liner temperatures and are shown in Figures 5-28 (a) - (g) for ARTs. Lines are used to connect the different lubricants at the same temperature. Additionally, monogrades and multigrades correspond to the solid and hollow symbols respectively. Again, as a reminder, the uncertainty is the actual ART standard deviation calculated from ten consecutive cycles.

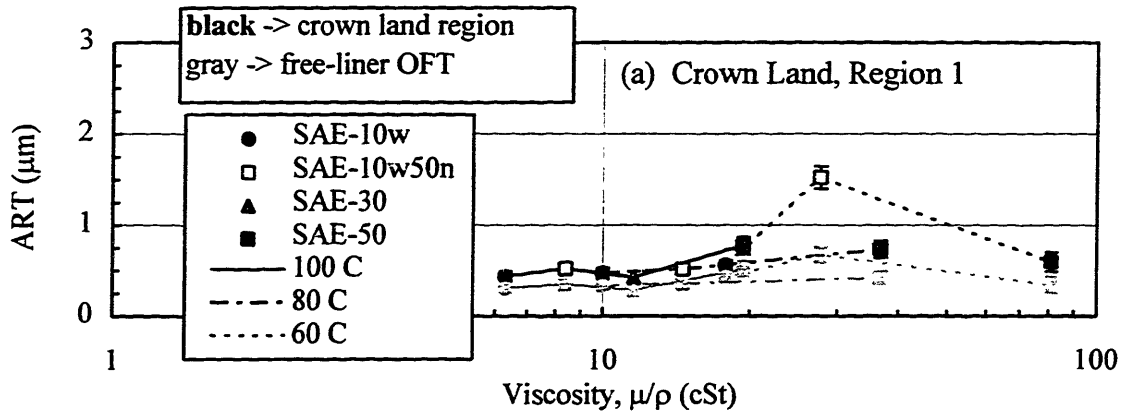
black -> crown land region
gray -> free-liner OFT
(a) Crown Land, Region 1
SAE-10w
SAE-10w50n
SAE-30
SAE-50
100 C
80 C
60 C
ART (μm)
Viscosity, μ/ρ (cSt)

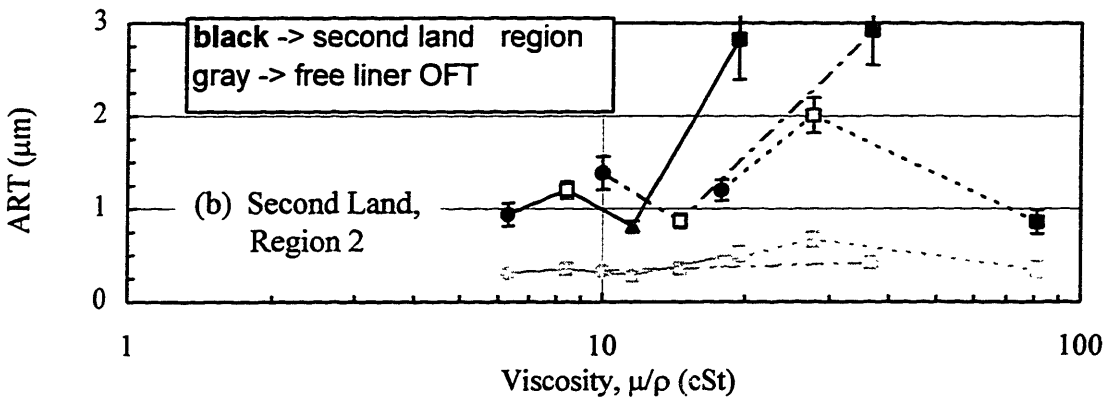
black -> second land region
gray -> free liner OFT
(b) Second Land,
Region 2
ART (μm)
Viscosity, μ/ρ (cSt)

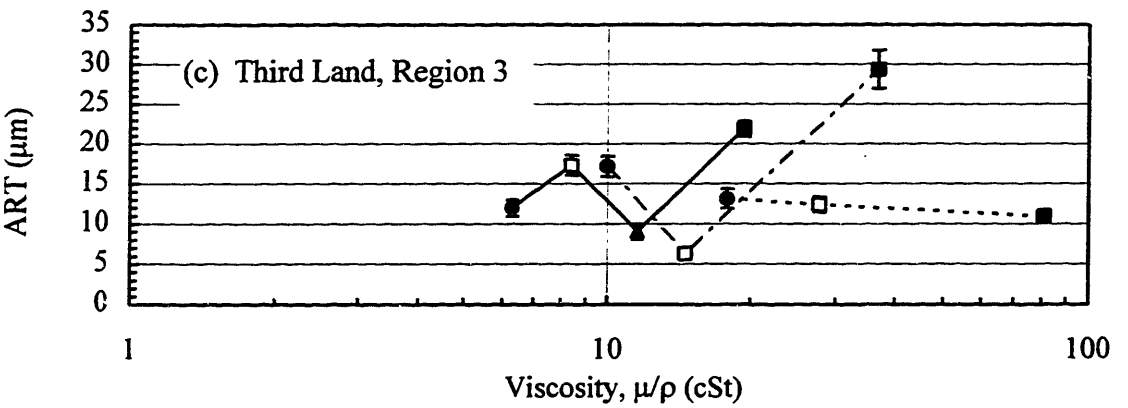
(c) Third Land, Region 3
ART (μm)
Viscosity, μ/ρ (cSt)

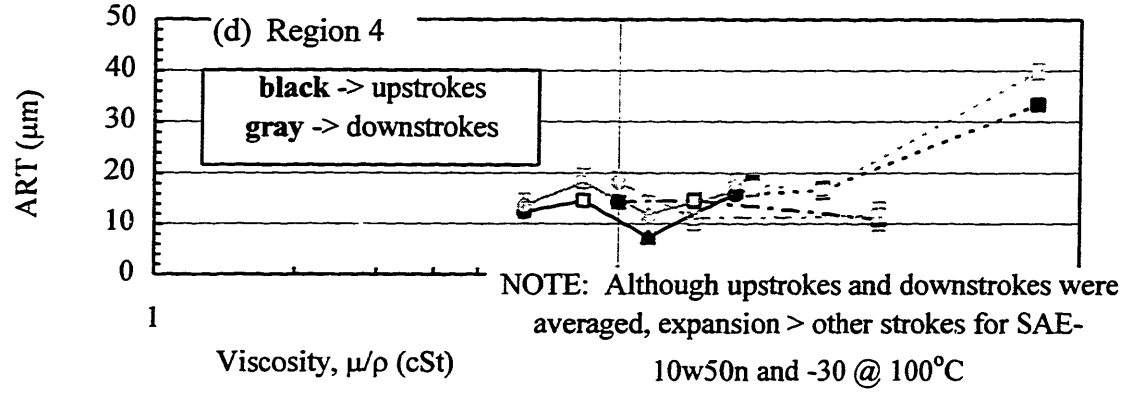

NOTE: Although upstrokes and downstrokes were averaged, expansion > other strokes for SAE-10w50n and -30 @ 100°C

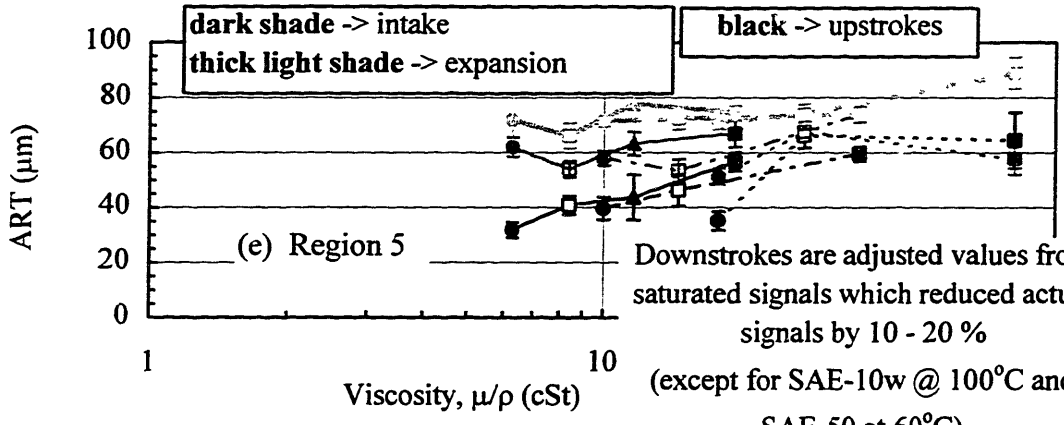

Downstrokes are adjusted values from saturated signals which reduced actual signals by 10 - 20 % (except for SAE-10w @ 100°C and SAE-50 at 60°C)

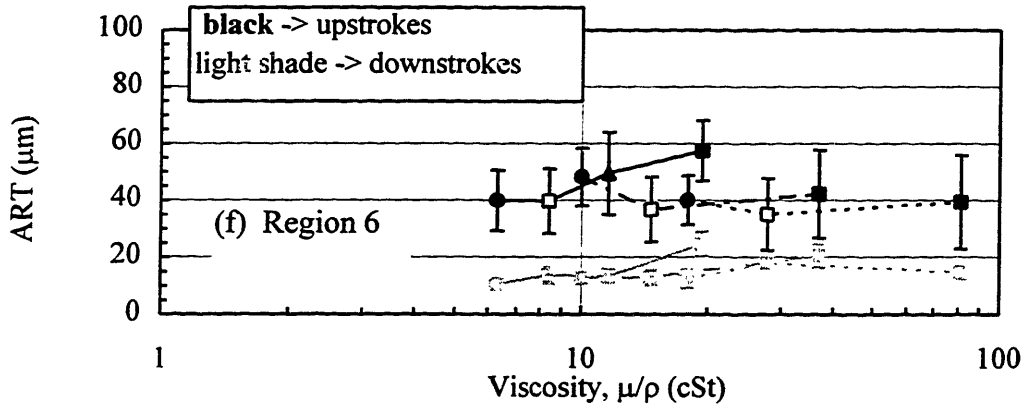

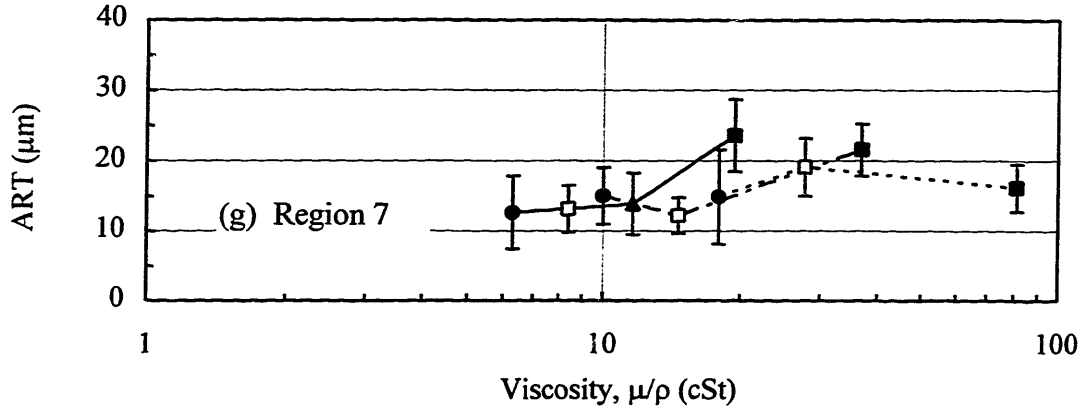

Figure 5-28 Average Region Thicknesses (Stroke-Averaged) at Moderate Temperatures of 60, 80, and 100°C from Window 1 for Regions (a) 1, (b) 2, (c) 3, (d) 4, (e) 5, (f) 6, and (g) 7.
(Window 1, 2/3 Load at 2500 rpm)

Because the lubricant viscosities at a particular temperature span great widths but overlap viscosity ranges corresponding to other temperatures, ARTs may be directly compared. Shown in Figure 5-28 (a) and consistent with baseline findings, negligible oil exists on the top crown land except for SAE-10W/50n at 60°C. For this atypical case, the oil distribution is not uniform along the crown land (see Figure 5-35) -- an abnormal characteristic; a disproportionate amount of oil exists for the first 20 percent of the crown land while the remainder of the land is dry. It's possible that this oil was scraped from the liner if the top of the piston made contact with the liner sometime during the cycle. Or this lump may be due to some random deposit buildup which is saturated with oil.

Ranging from 0.5 to 2.25 microns, oil on the second land is shown to be significant after subtracting the liner OFT from the total ART. Relative to the top land, less evaporation from lower piston land temperature, greater lubricant partial pressure within the second land vapor, and the absence of any burning contribute to more oil. Additionally, the second land has direct access to large quantities of oil supply within the third land region via the second ring gap and groove. Although no clear trend is observed

for small viscosity scales (~ 1 cSt), ARTs tend to increase for large viscosity scales (>10 cSt) except for SAE-50 at 60°C.

Although there are no clear ART-viscosity trends along the second land, the ART-viscosity patterns on the second land after subtraction of the liner OFT closely resemble those within the third land region shown in Figure 5-17 (c). Pattern similarity between the second and third land regions suggests that these regions are linked through gap-and-groove oil pathways although the magnitudes between the regions are different. The different magnitudes between the regions provide support to the fact that other oil transport physics are at work besides gap-and-groove transport such as gas flows and second ring down-scraping within the third land region.

Lastly, quite unlike any other regions, no ring scraping directly contributes to oil on the top and second land -- only gap and groove oil transport originally supplied from the third land region. Lack of ring scraping within the top two regions is a primary reason why pattern similarity between the second and third land regions is so clear providing evidence for gap and groove oil transport.

ARTs for Region 4 -- the region between the upper and lower segments -- do not increase over large viscosity scales except for SAE-50 at 60°C. For small viscosity scales the pattern is rather random, and no clear trend is evident.

Although the lubricant pattern for the 100°C baseline is comparable to that of the third land region, the other patterns at 80 and 60°C contrast the third land patterns especially for SAE-50 at 60°C which rises instead of falls. This finding contradicts the earlier claim from the baseline that the third and fourth regions may be strongly coupled via the lower OC rail gaps and groove.

The ARTs along the piston skirt regions are shown in Figures 5-28 (e) - (g). ARTs for region 5 increase slightly with viscosity over the entire viscosity range with the upstrokes increasing at a faster rate. Because of the high standard deviation for the upstrokes of region 6, it is difficult to determine a clear trend. However, the lower downstroke ARTs reveal the same trend as that along region 7 and strongly resemble OFT trends for hydrodynamic lubrication (see Figures 4-21 (a) - (f)); ART (or OFT)

increases with viscosity except for SAE-50 at 60°C. Hydrodynamic lubrication is most likely predominant in region 7 which includes the skirt's largest diameter.

No more highly accurate cases in addition to the baseline are found at window 4. For window 6, the few additional cases with high accuracy are better studied in the next section addressing the temperature effect.

5.4.1.2 Cylinder Liner Temperature Effect at 2500 rpm

To further study the ART behavior on and off the baseline for the moderate liner temperatures of 60, 80, and 100°C at 2500 rpm, the measurements may be presented in a different way. For the same lubricant, load, and engine speed, ring-pack and skirt ARTs vary with liner temperature. The resulting effect is called the temperature effect. The results for each lubricant including SAE-10W, -10W/50n, and -50 may be overlaid as shown in Figures 5-29 (a) - (g) for window 1. The single case for SAE-30 is also included.

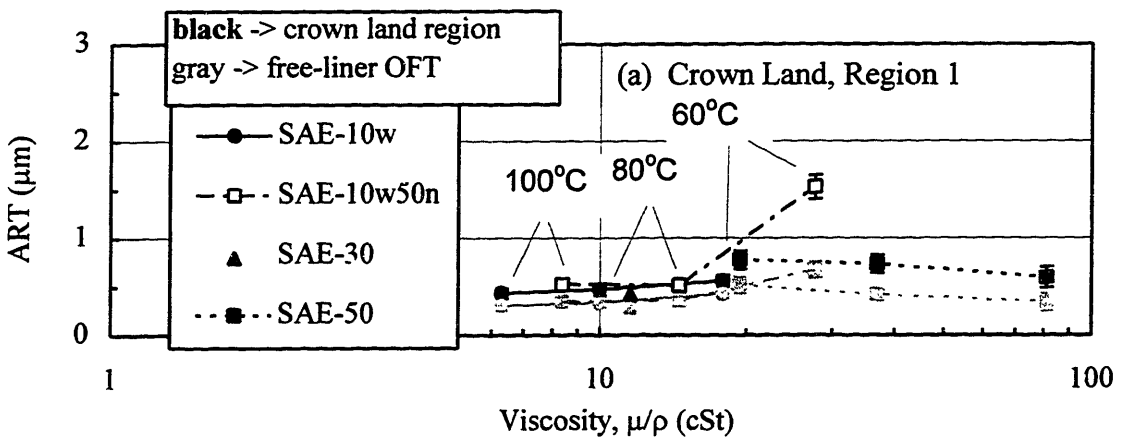

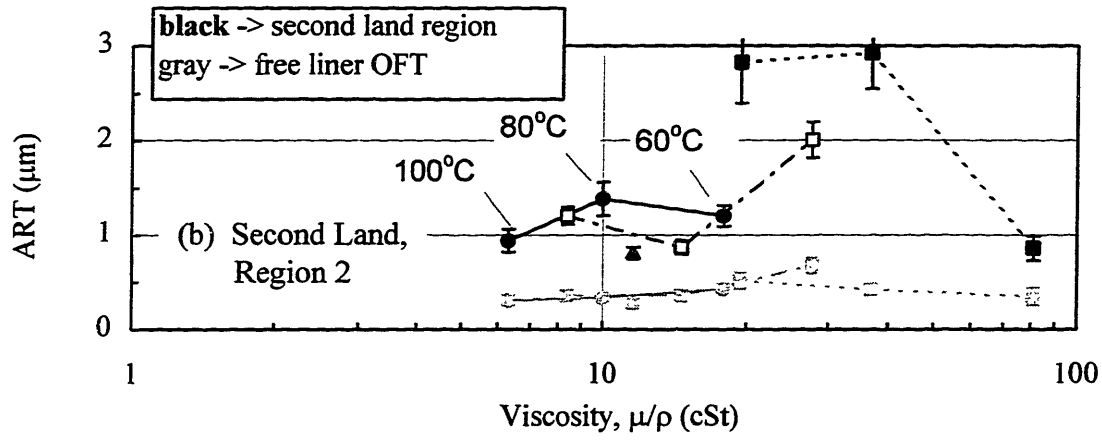

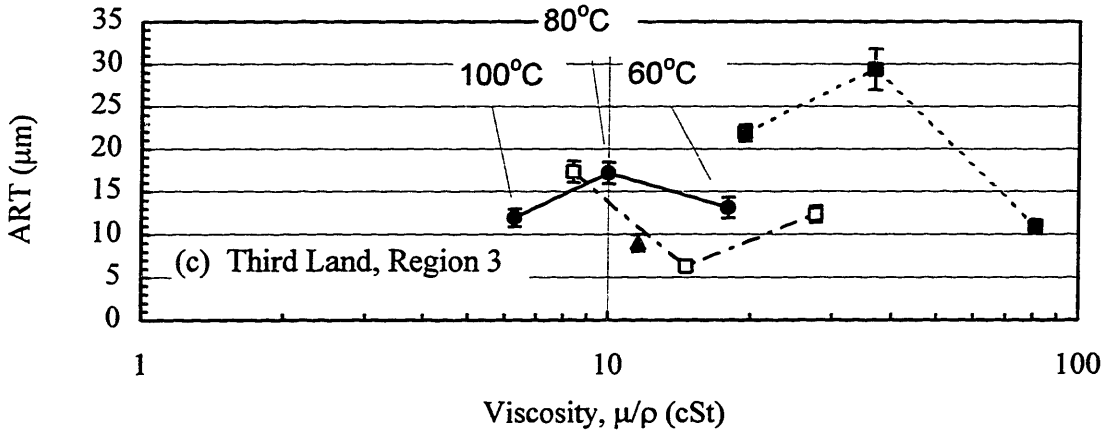

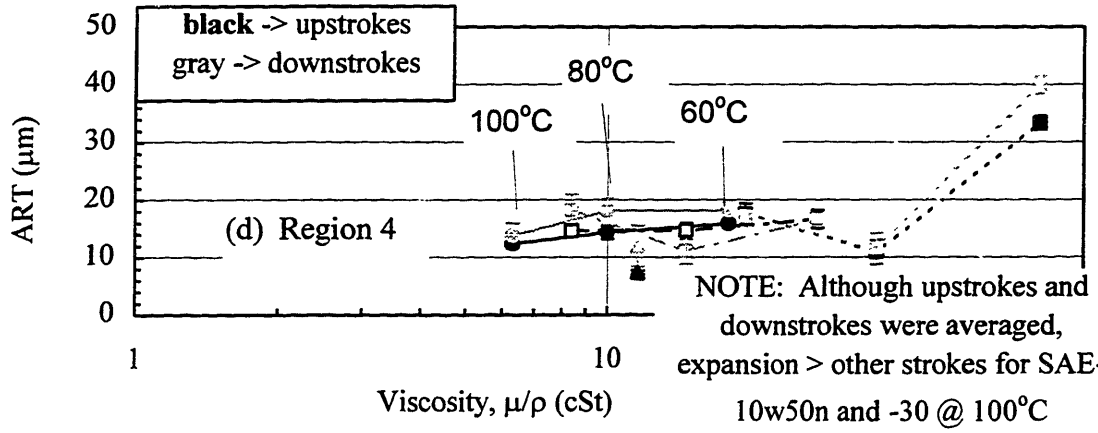

NOTE: Although upstrokes and downstrokes were averaged, expansion > other strokes for SAE-10w50n and -30 @ 100°C

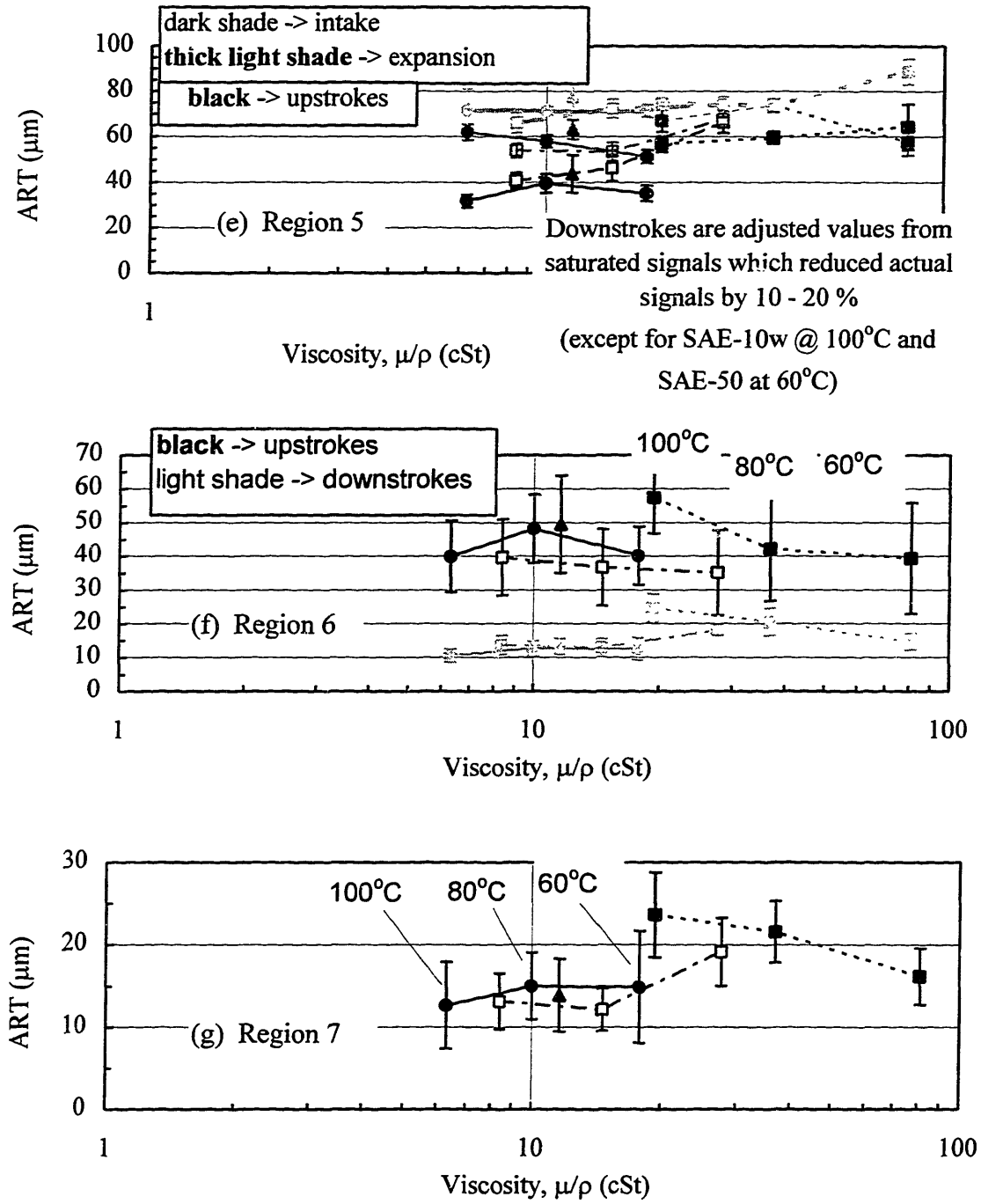

Figure 5-29 ARTs (Stroke-Averaged) for the Temperature Effect (Fired) at Moderate Temperatures of 60, 80, and 100°C from Window 1 for Regions (a) 1, (b) 2, (c) 3, (d) 4, (e) 5, (f) 6, and (g) 7.
(Window 1, 2/3 Load at 2500 rpm)

As usual, the crown land is completely dry except for the anomaly of SAE-10W/50n at 60°C explained in the last section. Individually, the second and third land regions show no consistent viscosity trends. However, although the magnitudes along the third land region are an order of magnitude higher, the oil on the second land after the liner OFT subtraction shows patterns very similar to those of the third land. Consistent with all other findings to this point, this observation further supports the claim that these ring-pack regions are linked through gap-and-groove oil pathways. The oil accumulation within the third land region acts as a finite reservoir supplying the second land region with oil via the second ring gap and groove; a greater oil supply within third land region allows more oil to seep through these non-hydrodynamic pathways. The different magnitudes between the regions provide support to the fact that other oil transport physics are at work such as gas flows and second ring down-scraping within the third land.

Additionally, the ART behavior of SAE-50 lends some insight to its OFT behavior. From the OFT analysis for SAE-50 shown in Figure 4-22 (c), the OFT for the top ring decreases for each decrease in temperature. Moore [18] find this result as well for highly-viscous lubricants for the top ring. He claims that this decrease in OFT with viscosity is due to a decrease in oil supply within the land regions supplied from the lower regions of the piston via the gaps and grooves; with highly-viscous lubricants, the pumping of oil through these oil pathways is more difficult and further starves the top ring. However, in view of the ARTs for SAE-50 in Figures 5-29 (b) and (c) for the second and third land regions, the ARTs increase from 100 to 80°C. Therefore, if the second land (supplied by the third land region) is supplying oil to the starved top ring, more oil would be supplied, not less, and the top ring and free-liner OFTs would increase, not decrease. Therefore, for this engine, the decrease in top ring OFT is not due to oil pumping difficulty for the highly-viscous SAE-50 via the second ring gap and groove.

Additionally, oil behavior related to hydrodynamic lubrication including oil flow under the rings as well as along the piston skirt for regions 6 and 7 experiences a decrease in OFT (or ART for the regions) with viscosity shown in Figures 4-22 and 5-29 (f) and (g). For this trend reversal of the OFT-viscosity relationship for the highly-viscous

lubricant SAE-50, a better explanation may be a change in the viscosity. One mechanism may be due to increased local oil film temperature from excessive viscous dissipation especially between the piston skirt and the liner. The trend reversal is definitely evident along region 7 where the maximum skirt diameter is located. Another mechanism for viscosity change may be chemical changes in viscosity due to contamination of the fuel which escapes combustion and is left on the cylinder walls. Having the thickest viscosity, SAE-50 may be the most sensitive to a viscosity change with fuel contamination. However, the latter explanation is unlikely because the lubricants were tested before and after the experiments for viscosity changes, and none were found.

ARTs for Region 4 -- the region between the upper and lower segments -- do not increase over large viscosity scales (>10 cSt) except for SAE-50 at 60°C. For small viscosity scales (~ 1 cSt) the pattern is rather random, and no clear trend is evident. Although the lubricant pattern for the 100°C baseline is comparable to that of the third land region, the other patterns for 80 and 60°C contrast the third land patterns especially for SAE-50 at 60°C which rises instead of falls. This finding contradicts the earlier claim from the baseline which suggests that the third and fourth regions are linked.

Overall ART behavior within region 5 increases slightly with viscosity. Although no strong trends for the upstrokes along region 6 are clear, the ARTs for the downstrokes of region 6 and the cycle-averaged ARTs for region 7 increase with viscosity except for the decreasing trend of SAE-50. Highly resembling the OFT patterns, these ART patterns are, therefore, characteristic of hydrodynamic lubrication.

Figures 5-30 (a) - (f) show the ARTs for regions 2 - 7, respectively, from window 6. From knowledge of the liner OFT approaching 0.56 (1/1.8) of the MOFT of the passing ring mentioned in section 4.2.1, a liner OFT is estimated from the scraper MOFT shown in Figure 5-19 (a) because the free-liner OFT above the piston cannot be measured from this window location. However, because of the near-BC location of window 6, the free-liner OFT below the piston is measured shown in Figure 5-30 (g).

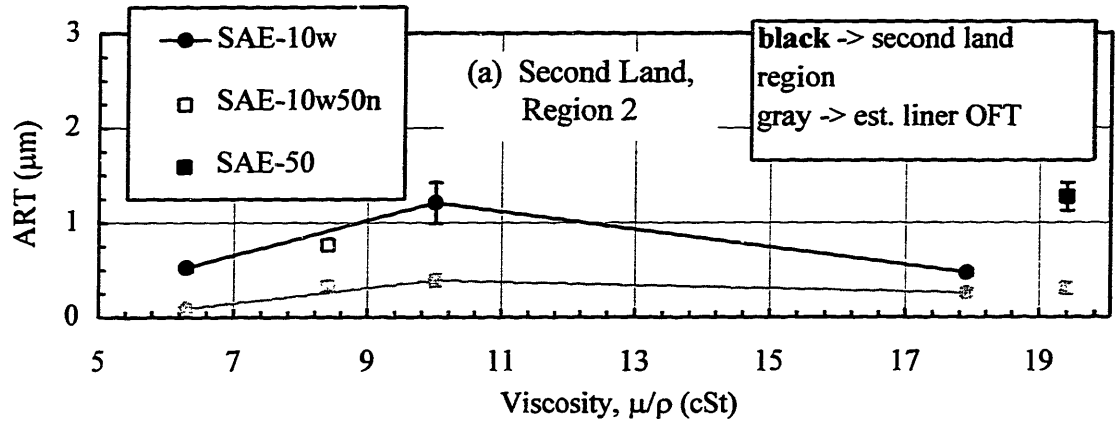
SAE-10w
SAE-10w50n
SAE-50
(a) Second Land, Region 2
black -> second land region
gray -> est. liner OFT
ART (μm)
Viscosity, μ/ρ (cSt)

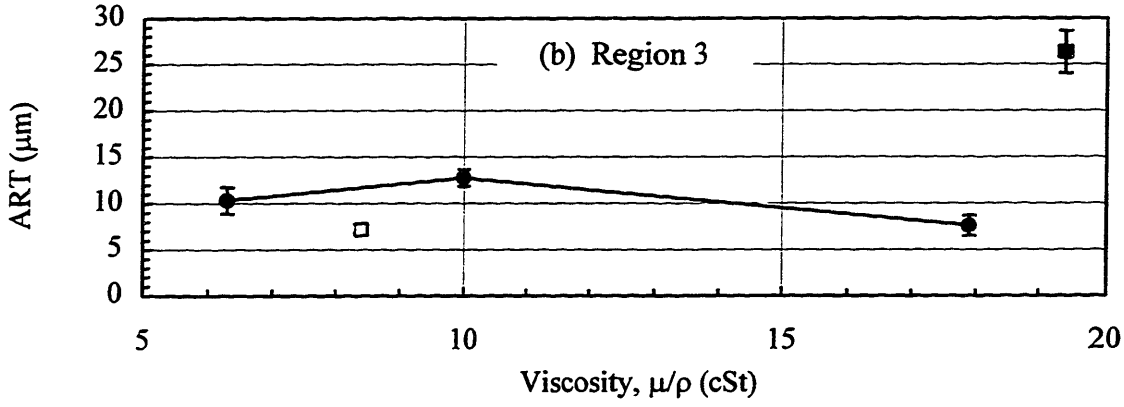
(b) Region 3
ART (μm)
Viscosity, μ/ρ (cSt)

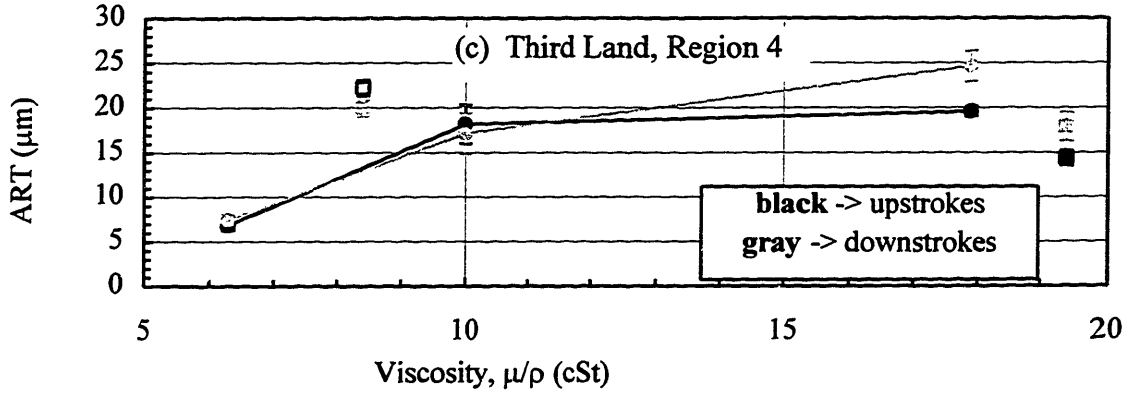
(c) Third Land, Region 4
black -> upstrokes
gray -> downstrokes
ART (μm)
Viscosity, μ/ρ (cSt)

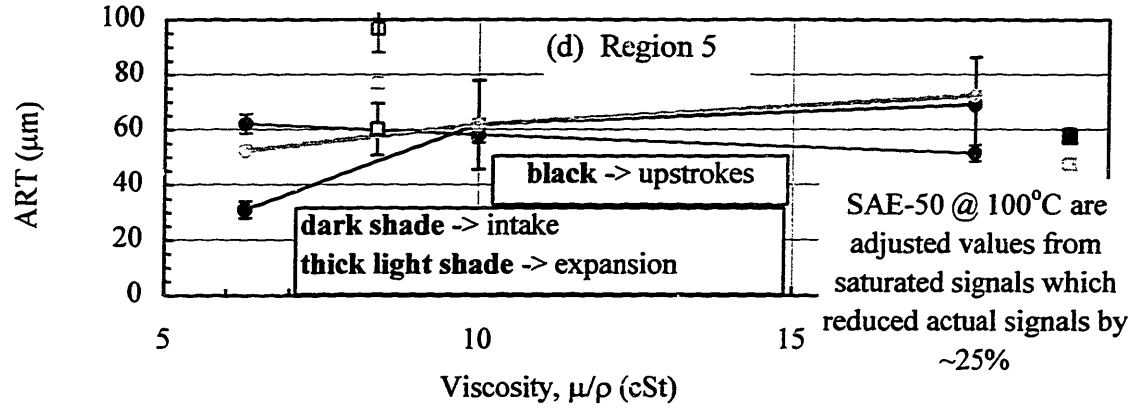
(d) Region 5
ART (μm)
100
80
60
40
20
0
5
10
15
Viscosity, μ/ρ (cSt)
black -> upstrokes
dark shade -> intake
thick light shade -> expansion
SAE-50 @ 100°C are adjusted values from saturated signals which reduced actual signals by ~25%

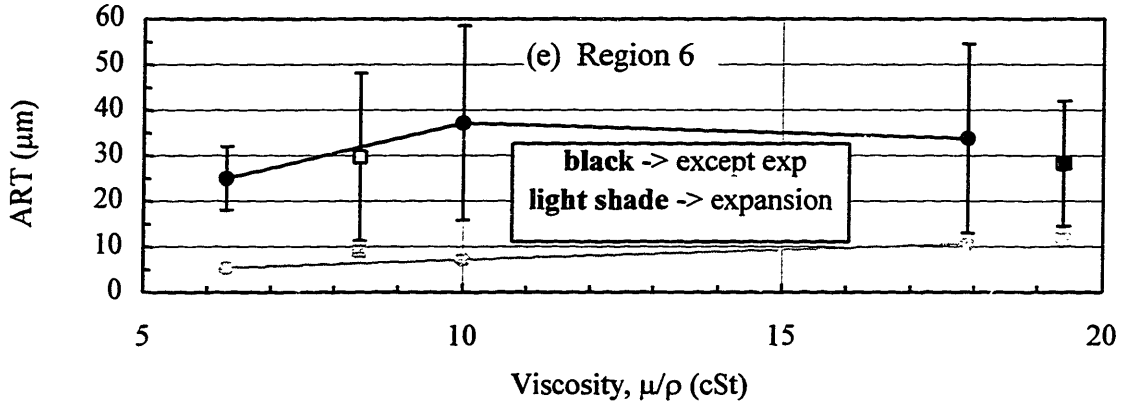
(e) Region 6
ART (μm)
60
50
40
30
20
10
0
5
10
15
20
Viscosity, μ/ρ (cSt)
black -> except exp
light shade -> expansion

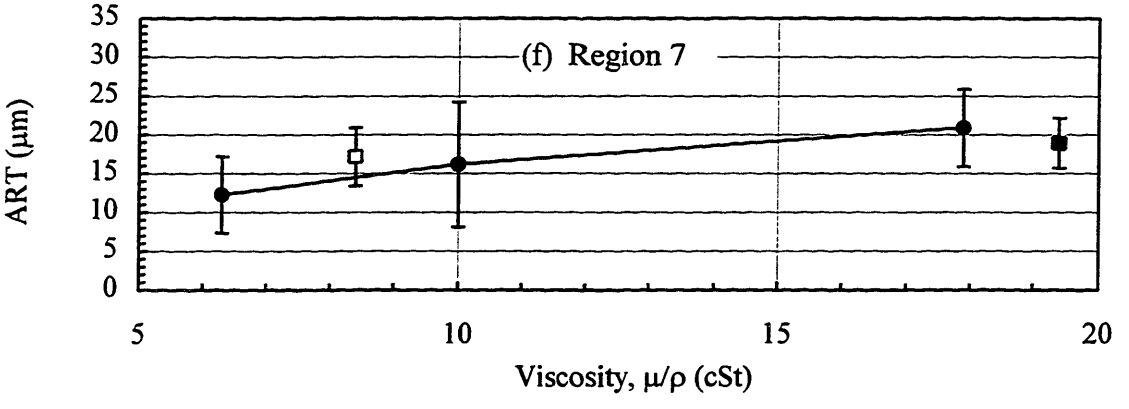
(f) Region 7
ART (μm)
35
30
25
20
15
10
5
0
5
10
15
20
Viscosity, μ/ρ (cSt)

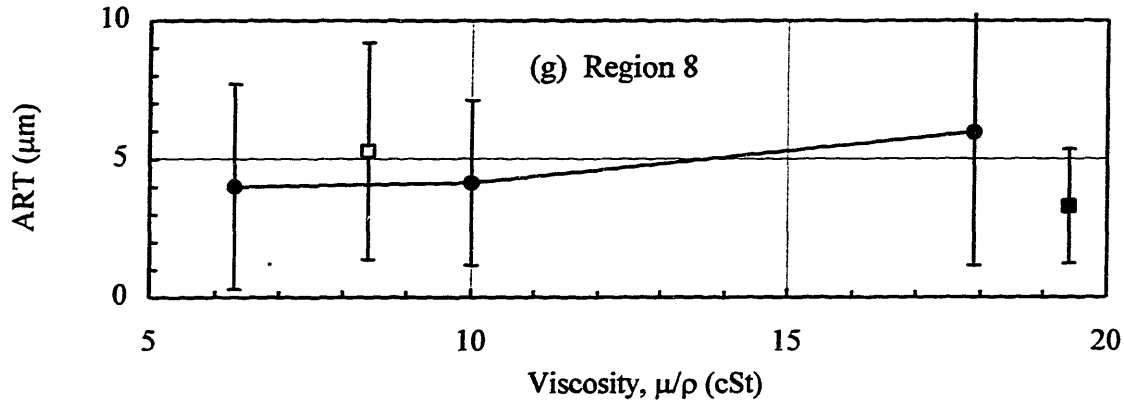

Figure 5-30 ARTs (Stroke-Averaged) for the Temperature Effect (Fired) at Moderate Temperatures of 60, 80, and 100°C from Window 6 for Regions (a) 2, (b) 3, (c) 4, (d) 5, (e) 6, (f) 7, and (g) 8.
(Window 6, 2/3 Load at 2500 rpm)

Individually, the second and third land regions show no consistent ART-viscosity trends for these highly accurate cases; ARTs from SAE-10W rises and then falls from 100 to 60°C, and the other two lubricants do not fall along this curve. However, after subtraction of the liner OFTs from the average region thicknesses in region 2, the second land thicknesses and ARTs from region 3 have similar patterns which are comparable to those from window 1.

Although lubricant patterns are similar between the second and third land regions, the magnitudes along the third land region are an order of magnitude higher. Consistent with all other findings to this point, this observation further supports the claim that these ring-pack regions are coupled through gap-and-groove oil pathways. The different magnitudes between the regions provide support to the fact that other oil transport physics are at work besides gap-and-groove transport such as gas flows and second ring down-scraping within the third land region.

ARTs of SAE-10W for Region 4 -- the region between the upper and lower segments -- from window 6 increase more than the very slight increase from window 1. Again, as in window 1, this pattern from region 4 contrasts that from region 3 especially for SAE-10W at 60°C falling from 80°C by almost half in region 3 and rising in region 4.

Consistent with all other findings to this point (except the weak baseline patterns), this observation further supports the claim that these ring-pack regions are not strongly linked through gap-and-groove oil pathways.

Overall ARTs within region 5 increase with viscosity except for the slight decrease for the intake strokes. Comparable to window 1, although no strong trends for the intake/compression/exhaust strokes along region 6 are clear, the ARTs for SAE-10W for the downstrokes of region 6 and the cycle-averaged ARTs for region 7 and 8 increase with viscosity.

5.4.2 Motored Cases for Different Lubricants at Low Liner Temperatures -- 40 and 60°C at 2500 rpm

The motored cases at wide-open-throttle (WOT) for the low liner temperatures of 40 and 60°C at 2500 rpm include all five lubricants. Since almost all of the accurate motored cases are at window 1, results are only shown from this window. The approach for analyzing the motored data is comparable to the approach used for the fired measurements which include analyzing the lubricant and cylinder liner temperature effects from overlaying lubricant mappings from different temperatures.

5.4.2.1 Lubricant Effect

The overall motored behavior of different lubricants at the same low temperatures of 40 and 60°C are shown in Figures 5-31 (a) - (g). Each figure containing measurements from different lubricants corresponds to a particular region within the ring-pack or along the skirt. Lines are used to connect the different lubricants at the same temperature. Additionally, monogrades and multigrades correspond to the solid and hollow symbols, respectively.

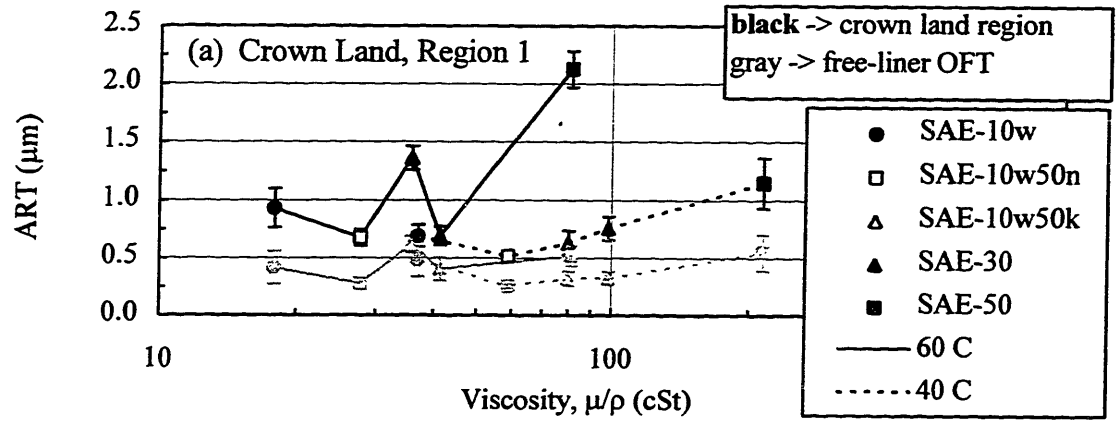
(a) Crown Land, Region 1
black -> crown land region
gray -> free-liner OFT
SAE-10w
SAE-10w50n
SAE-10w50k
SAE-30
SAE-50
60 C
40 C
ART (μm)
Viscosity, μ/ρ (cSt)

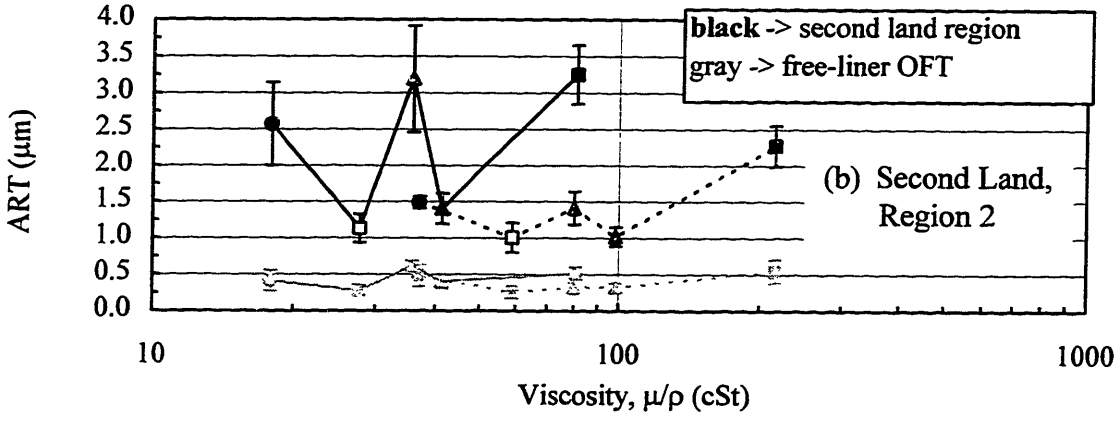
black -> second land region
gray -> free-liner OFT
(b) Second Land, Region 2
ART (μm)
Viscosity, μ/ρ (cSt)

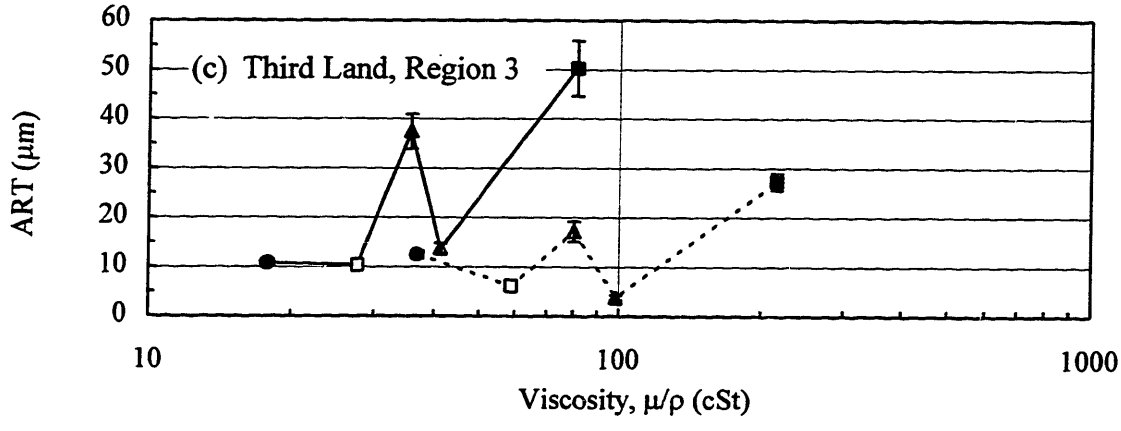
(c) Third Land, Region 3
ART (μm)
Viscosity, μ/ρ (cSt)

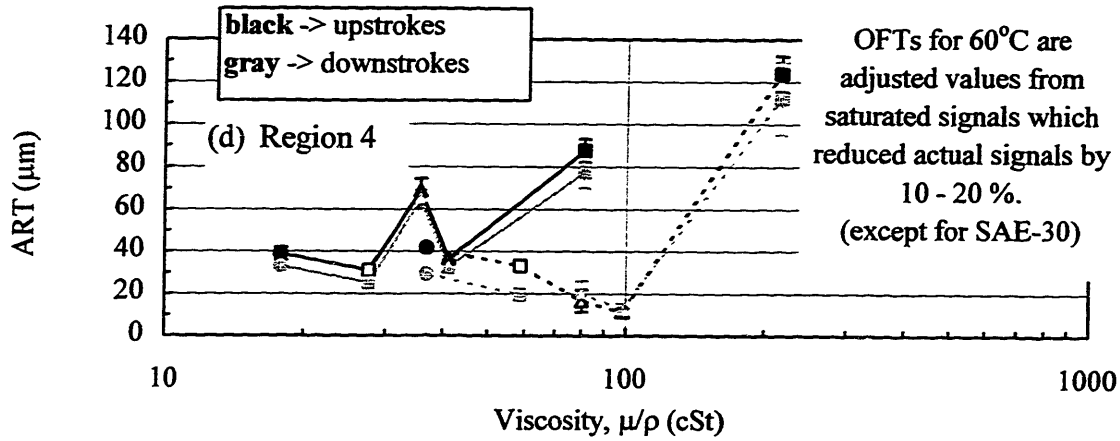
black -> upstrokes
gray -> downstrokes
(d) Region 4
OFTs for 60°C are adjusted values from saturated signals which reduced actual signals by 10 - 20 %. (except for SAE-30)
ART (μm)
140
120
100
80
60
40
20
0
10
100
1000
Viscosity, μ/ρ (cSt)

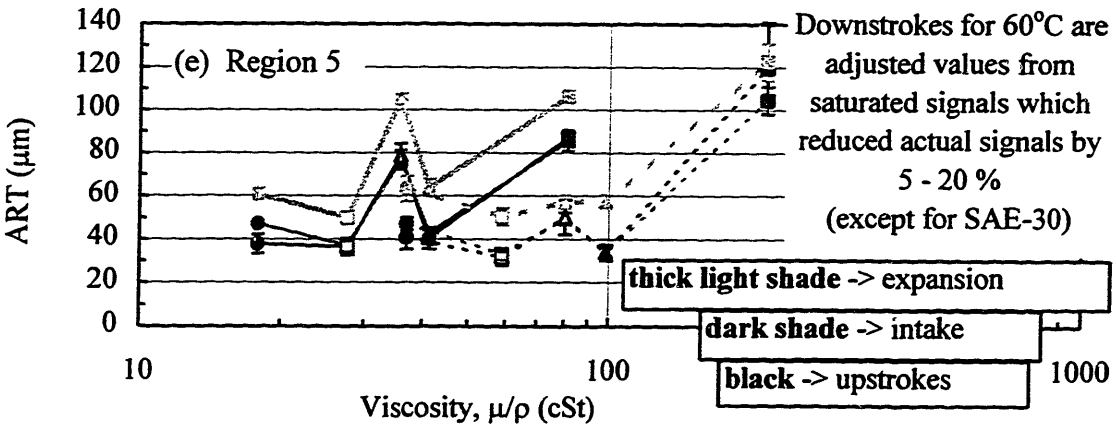
(e) Region 5
Downstrokes for 60°C are adjusted values from saturated signals which reduced actual signals by 5 - 20 % (except for SAE-30)
thick light shade -> expansion
dark shade -> intake
black -> upstrokes
ART (μm)
140
120
100
80
60
40
20
0
10
100
1000
Viscosity, μ/ρ (cSt)

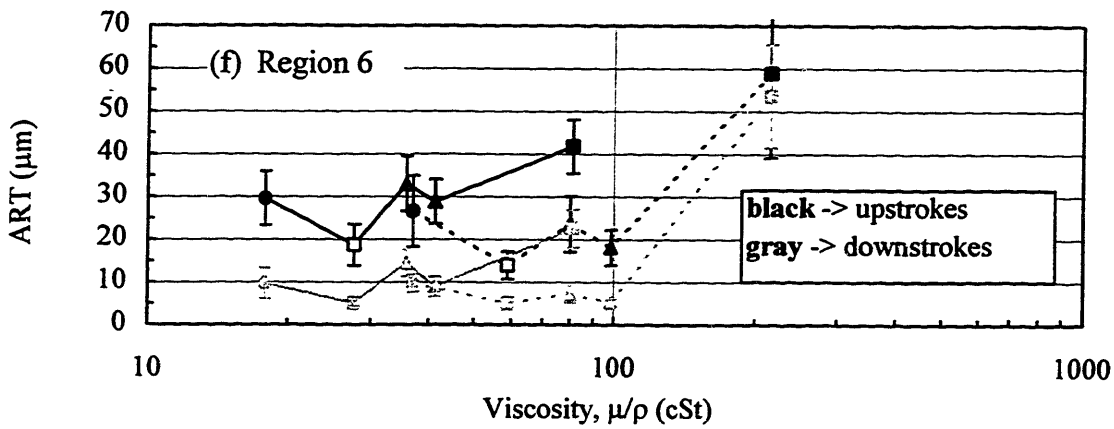
(f) Region 6
black -> upstrokes
gray -> downstrokes
ART (μm)
70
60
50
40
30
20
10
0
10
100
1000
Viscosity, μ/ρ (cSt)

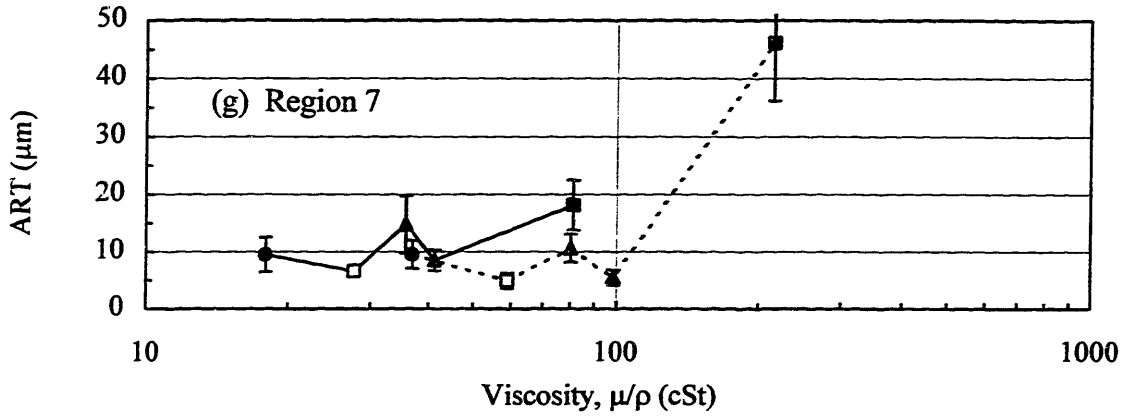

Figure 5-31 Average Region Thicknesses (Stroke-Averaged) for the Lubricant Effect (Motored) at Low Temperatures of 40 and 60°C from Window 1 for Regions (a) 1, (b) 2, (c) 3, (d) 4, (e) 5, (f) 6, and (g) 7.
(Window 1, Motored WOT at 2500 rpm)

Unlike the fired cases, a small amount of oil now exists on the crown land after the liner OFT is subtracted from the total ART in Figure 5-31 (a). (A direct comparison of ARTs between the motored and fired cases is presented in section 5.4.3 addressing the effects of load.) However, no clear ART-viscosity trend is apparent and SAE-50 is always higher than the other lubricants for the same temperature.

Having ARTs greater than a factor of two compared to the top land, the second land reveals the same random patterns for the lubricants with SAE-50 having high ART which, however, is less pronounced at 60°C. With the exception of SAE-10W at 60°C, these random patterns are very comparable to those in region 3 although magnitudes are an order of magnitude higher. Again, consistent with findings up to this point, this pattern similarity between the crown and second lands and the third land region further confirms the argument claiming significant oil transport routes via the top and second ring gaps and grooves.

The different magnitudes reflect each region's characteristics subjected to different environmental conditions. Unlike the other regions, the top land is open to the combustion chamber and, driven by inertia and gas flows, oil attached to the land is not constrained by any physical boundary (i.e., another ring) but only by its viscosity. Under

motored conditions, the high inertial forces which can through oil off the land and the relatively low vapor partial pressure within the chamber contribute to less oil compared to the second land. Although differing by factors of two or three and bounded by the top and second rings, the second land has oil which was not supplied by scraping but through ring gaps and grooves just like the crown land. Having ARTs greater by an order of magnitude, the third land region is accompanied by scraping and positive gas flow through the second ring groove and gap primarily contributing to the order of magnitude difference.

Shown in Figure 5-31 (d), region 4 reveals a decreasing ART-viscosity trend at 40°C with SAE-50 as an exception. In fact, if SAE-50 is ignored, ARTs decrease with viscosity continuing from the cases at 60°C having a less consistent trend.

From a glance, regions 3 and 4 seem to have comparable patterns; however, a closer look reveal some differences which support the argument that oil transport within these regions are not strongly linked via ring gap and grooves. Taking SAE-10W and 10W/50n as a reference at 60°C, the ARTs of these two lubricants is much lower than SAE-10W/50k in region 3 but much higher in region 4. Also, although SAE-50 remains high, the relative difference between the two temperatures of 40 and 60°C is reversed between the two regions. This reversed difference is then apparent throughout the remainder of the regions from region 4 - 7.

The remaining regions from 5 - 7 hint at this decreasing ART-viscosity relationship in region 4 at 40°C (except for SAE-50) but is certainly less clear.

5.4.2.2 Motored Liner Temperature Effect

The data representation used to investigate the liner temperature effects isolates the different lubricants from one another and provides additional insight to the motored trends. Shown in Figures 5-32 (a) - (c), oil on the crown and second lands after subtraction of the liner OFT and the ARTs within the third land region typically decrease with temperature except for SAE-10W/50n on the crown land and SAE-10W in the third land region which do not change significantly between the two temperatures. Except for

these mild exceptions to the general trend, the pattern similarity between these regions is consistent with findings in earlier sections.

However, this ART-viscosity trend strongly reverses for SAE-50 for regions 4 and greater. The ARTs from region 7 and downstroke ARTs from region 6 are very comparable and characterize the ART-viscosity pattern found in hydrodynamic lubrication under the rings from section 4.3.2.2; ARTs and OFTs along the piston definitely decrease with decreasing temperature between 30 and 100 cSt for the three moderate lubricants not including the thinnest and thickest lubricants corresponding to SAE-10W and -50, respectively. From the OFT analysis, SAE-50 shows an slight increase with decreasing temperature while SAE-10W remains relatively the same.

Although the ART patterns here and in many other sections support linked oil transport pathways between the top, second, and third lands via gaps and grooves, the decreasing ART-viscosity relationship may be caused by lesser clearances from less thermal expansion of engine components. The lesser clearances in the gaps and between rings and their grooves and greater viscosity from the temperature change constructively interfere with oil flow. For SAE-50, this restriction on oil flow to the upper lands retains greater oil in lower regions from 60 to 40°C.

Again, the oil on the lands do not account for the OFT trends in section 4.3.2.2. Top and scraper MOFTs do not significantly decrease for SAE-10W and -50 with viscosity as shown in Figures 4-26 (d) and (e). However, oil on the crown and second lands decrease for SAE-10W and 50. If the ring MOFTs were strongly linked to oil on the lands, the MOFTs should experience a marked decrease as well.

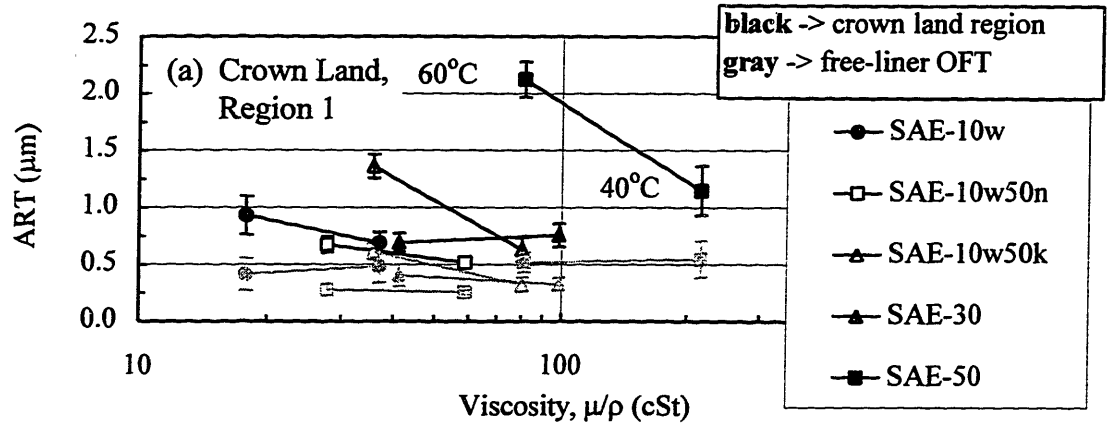
(a) Crown Land, Region 1
60°C
40°C
black -> crown land region
gray -> free-liner OFT
SAE-10w
SAE-10w50n
SAE-10w50k
SAE-30
SAE-50
ART (μm)
Viscosity, μ/ρ (cSt)

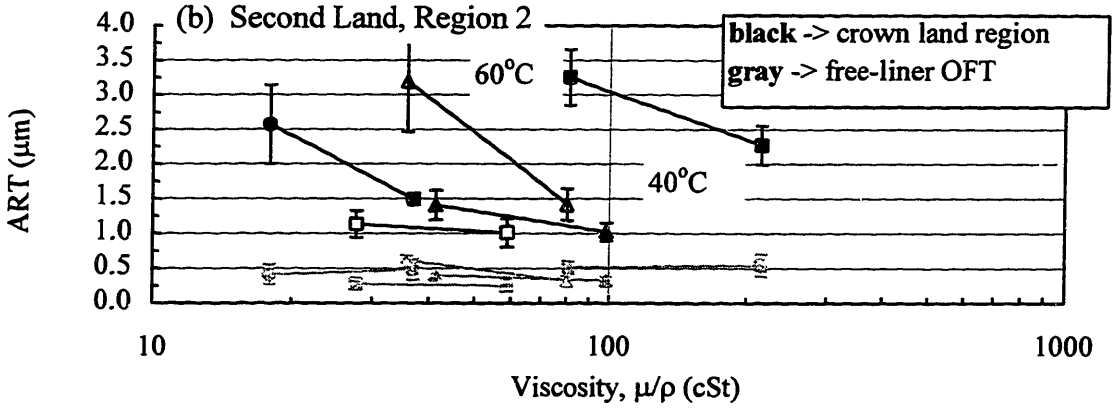
(b) Second Land, Region 2
60°C
40°C
black -> crown land region
gray -> free-liner OFT
ART (μm)
Viscosity, μ/ρ (cSt)

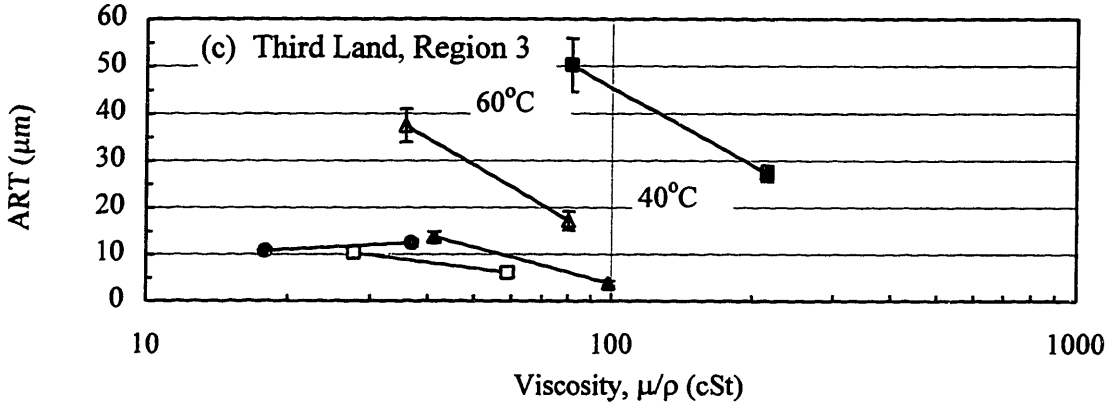
(c) Third Land, Region 3
60°C
40°C
ART (μm)
Viscosity, μ/ρ (cSt)

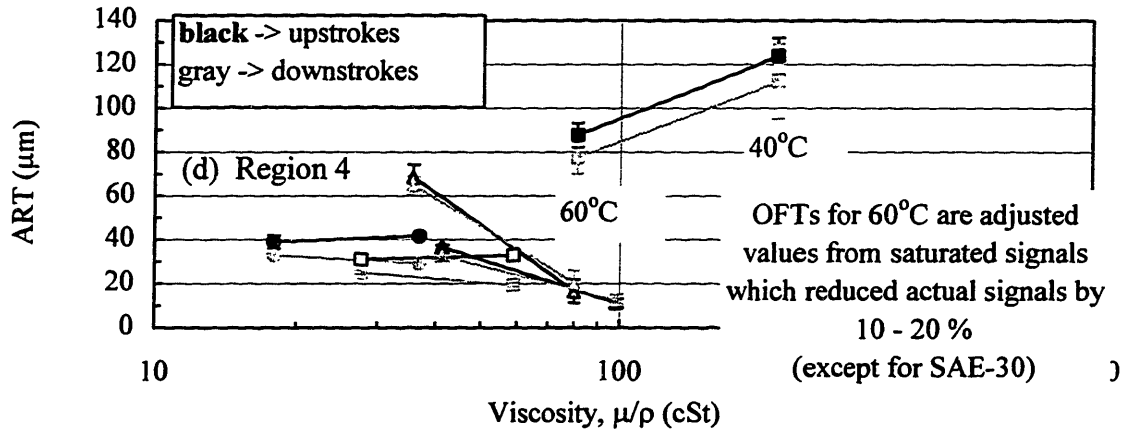
black -> upstrokes
gray -> downstrokes
(d) Region 4
40°C
60°C
OFTs for 60°C are adjusted values from saturated signals which reduced actual signals by 10 - 20 % (except for SAE-30)
ART (μm)
Viscosity, μ/ρ (cSt)

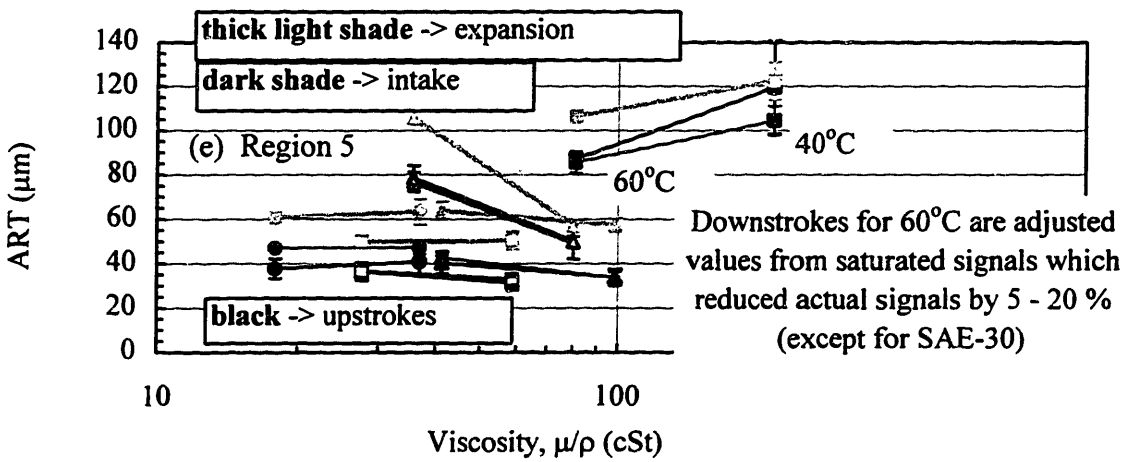
thick light shade -> expansion
dark shade -> intake
(e) Region 5
40°C
60°C
black -> upstrokes
Downstrokes for 60°C are adjusted values from saturated signals which reduced actual signals by 5 - 20 % (except for SAE-30)
ART (μm)
Viscosity, μ/ρ (cSt)

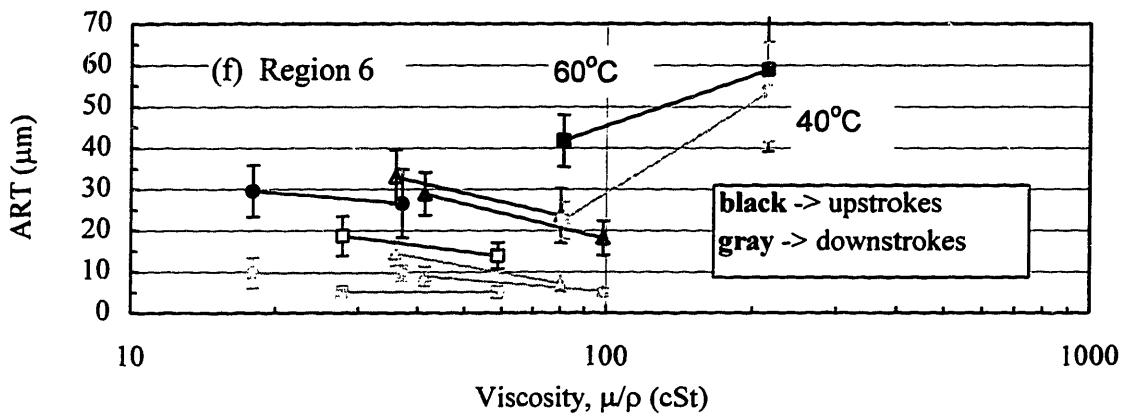
(f) Region 6
60°C
40°C
black -> upstrokes
gray -> downstrokes
ART (μm)
Viscosity, μ/ρ (cSt)

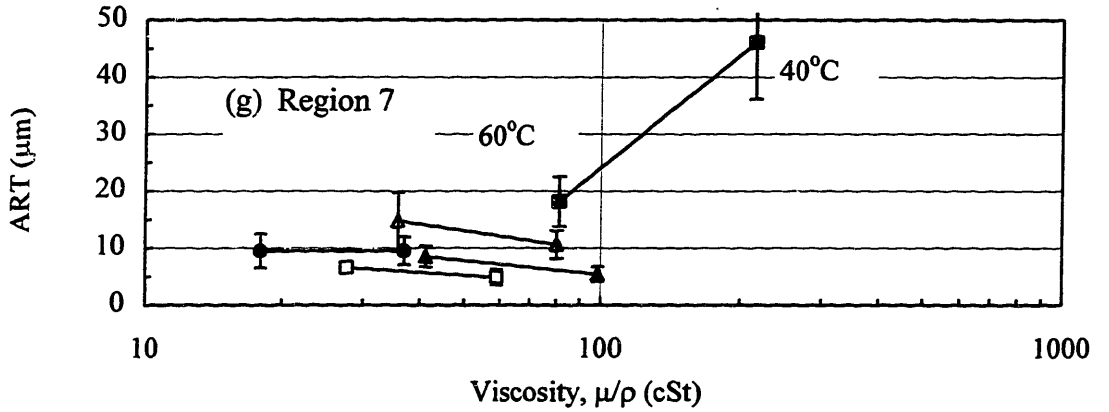

Figure 5-32 ARTs (Stroke-Averaged) for the Temperature Effect (Motored) at Low Temperatures of 40 and 60°C from Window 1 for Regions (a) 1, (b) 2, (c) 3, (d) 4, (e) 5, (f) 6, and (g) 7.
(Window 1, Motored WOT at 2500 rpm)

5.4.3 The Load Effect -- 2/3 Load Versus Motored (WOT) at 60°C

As seen in the last section and unlike the fired cases, the top land is not completely dry for the motored cases, and the second land typically has more oil than the fired cases after subtraction of the liner OFTs from the total ARTs. This load effect on ARTs is shown directly in Figures 5-33 (a) - (g) for all regions along the piston assembly. (After the liner OFT subtraction for the second land, SAE-10W/50n's change is negligible in view of the standard deviation.)

Accompanying the ARTs in Figures 5-33 (a) and (b), the actual oil distribution from which the ARTs were calculated for the crown and second lands are shown in Figures 5-34, -35, and -36 for SAE-10W, -10W/50n, and -50, respectively. Each set of figures compare the motored and fired conditions for each of the four strokes within the cycle. (As noted in section 5.4.1.1.2, SAE-10W/50n at 2/3 load only for the crown land is an atypical case; the oil distribution is not uniform along the crown land -- an abnormal characteristic. A disproportionate amount of oil exists for the first 20 percent of the crown land while the remainder of the land is relatively dry. It's possible that this oil was scraped from the liner if the top of the piston made contact with the liner sometime during the cycle. Or this lump may be due to some random deposit buildup

which is saturated with oil. Omission of the ART for the crown land for SAE-10W/50n under fired condition is recommended for studying the load effect.)

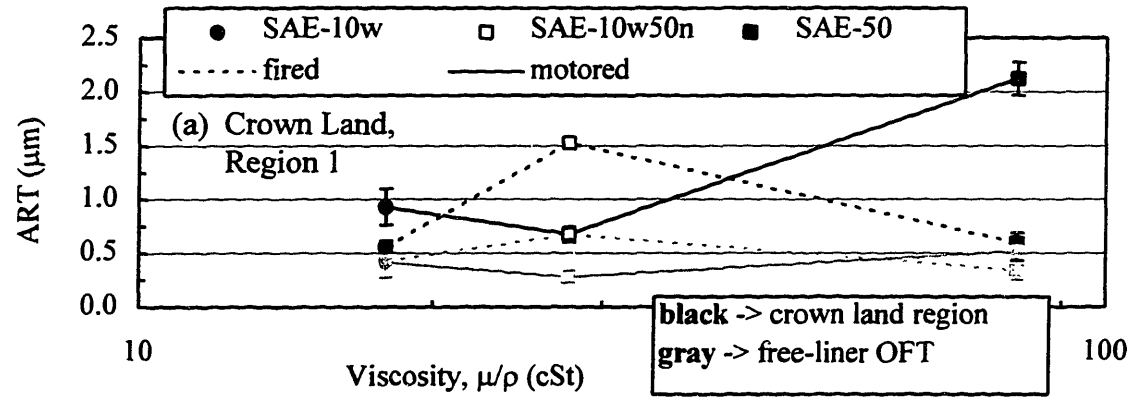

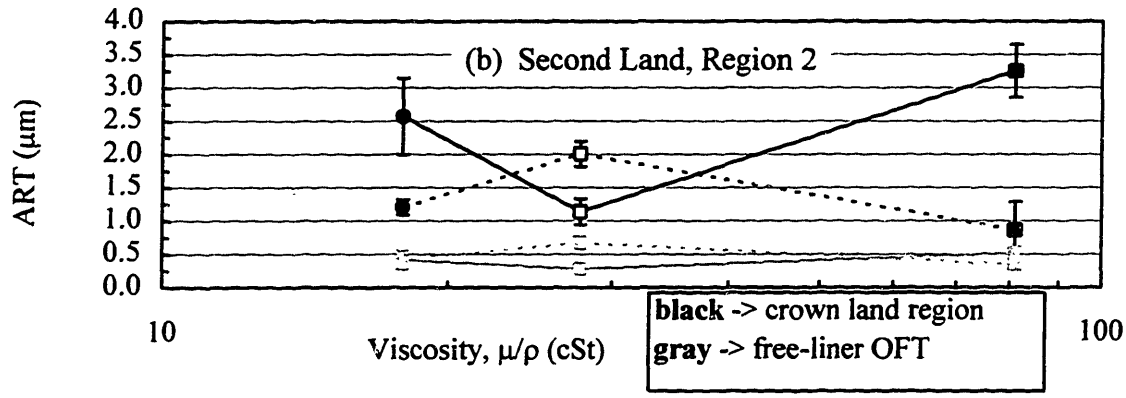

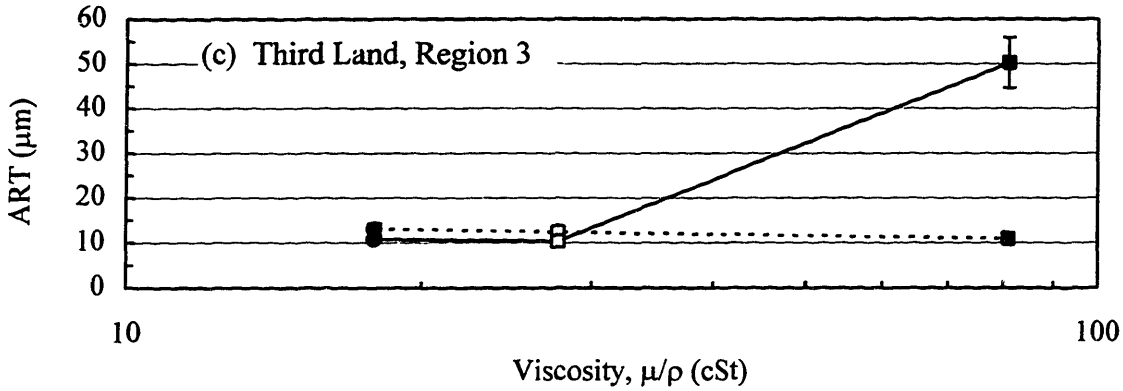

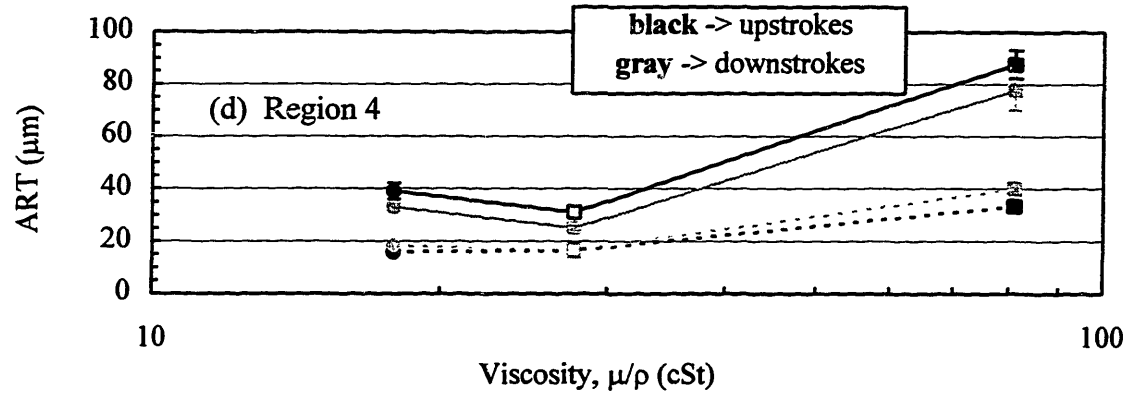
black -> upstrokes
gray -> downstrokes
(d) Region 4
ART (μm)
100
80
60
40
20
0
10
100
Viscosity, μ/ρ (cSt)

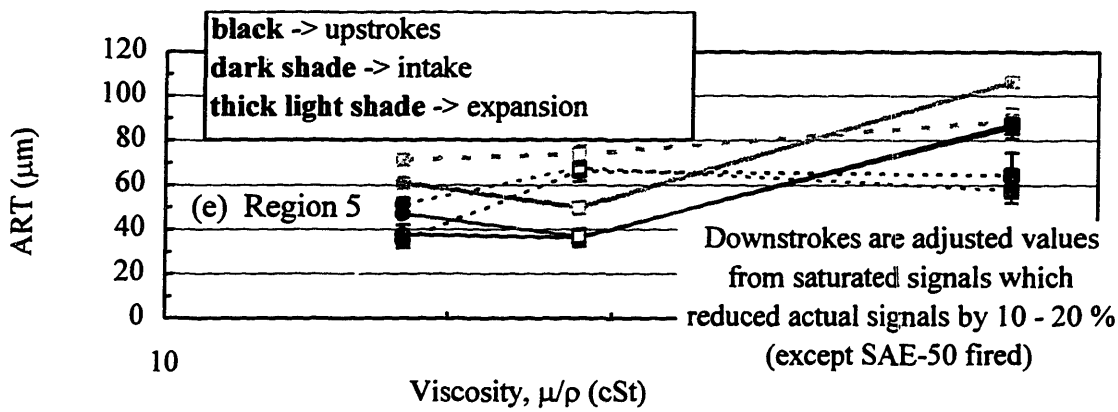
black -> upstrokes
dark shade -> intake
thick light shade -> expansion
(e) Region 5
ART (μm)
120
100
80
60
40
20
0
10
Viscosity, μ/ρ (cSt)
Downstrokes are adjusted values
from saturated signals which
reduced actual signals by 10 - 20 %
(except SAE-50 fired)

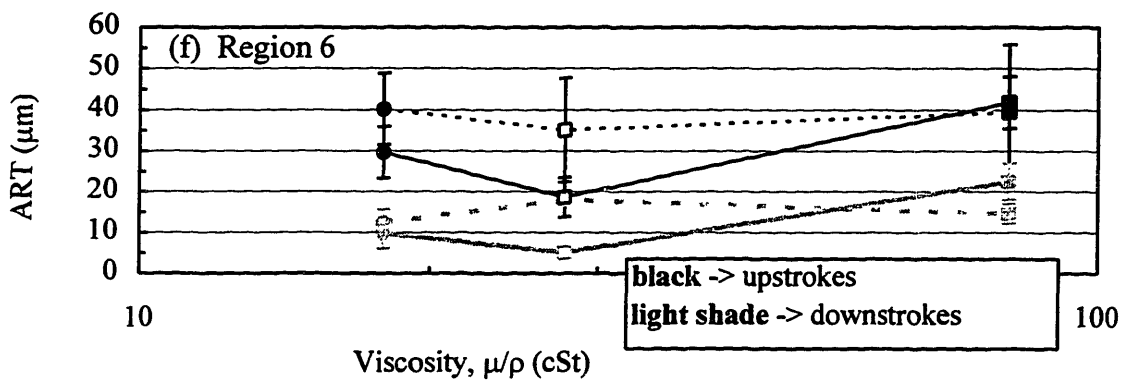
(f) Region 6
ART (μm)
60
50
40
30
20
10
0
10
100
Viscosity, μ/ρ (cSt)
black -> upstrokes
light shade -> downstrokes

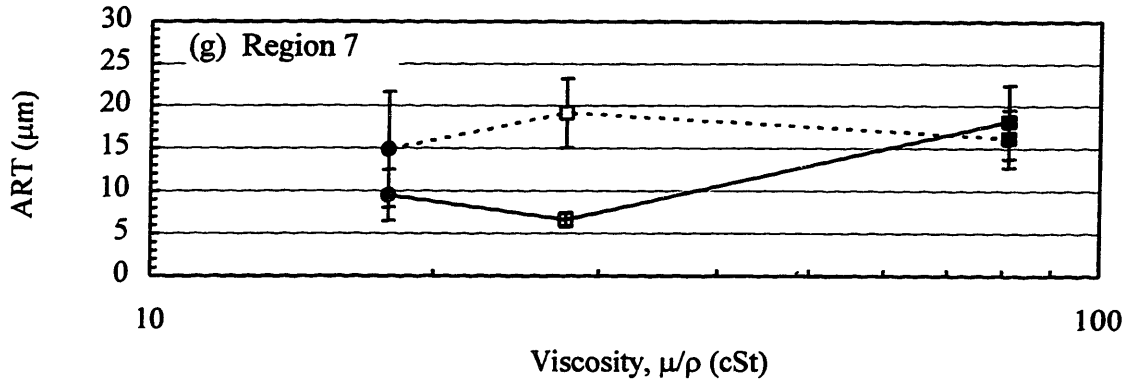

Figure 5-33 ARTs (Stroke-Averaged) for the Load Effect (Fired Versus Motored) from Window 1 for Regions (a) 1, (b) 2, (c) 3, (d) 4, (e) 5, (f) 6, and (g) 7.
(2/3 Load Versus Motored WOT, 2500 rpm, 60°C)

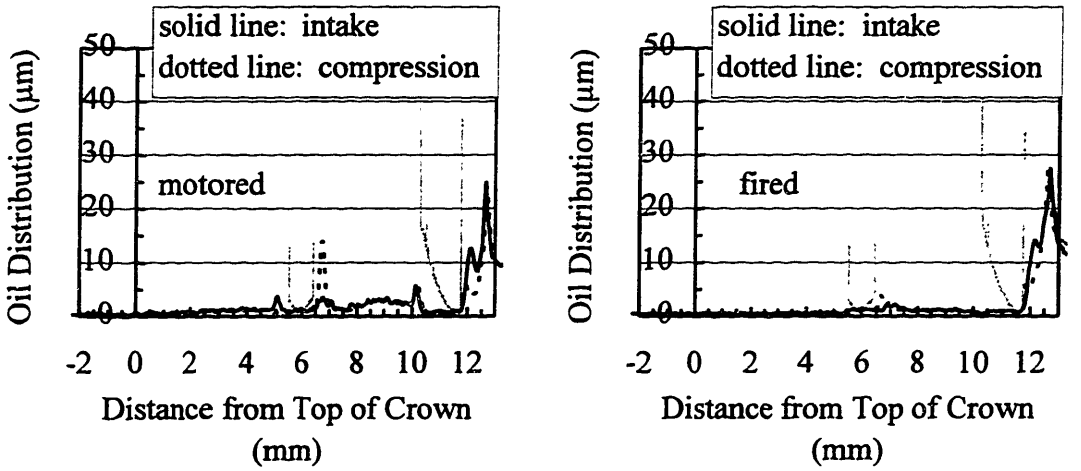

(a) Intake and Compression Strokes (Motored Versus Fired)

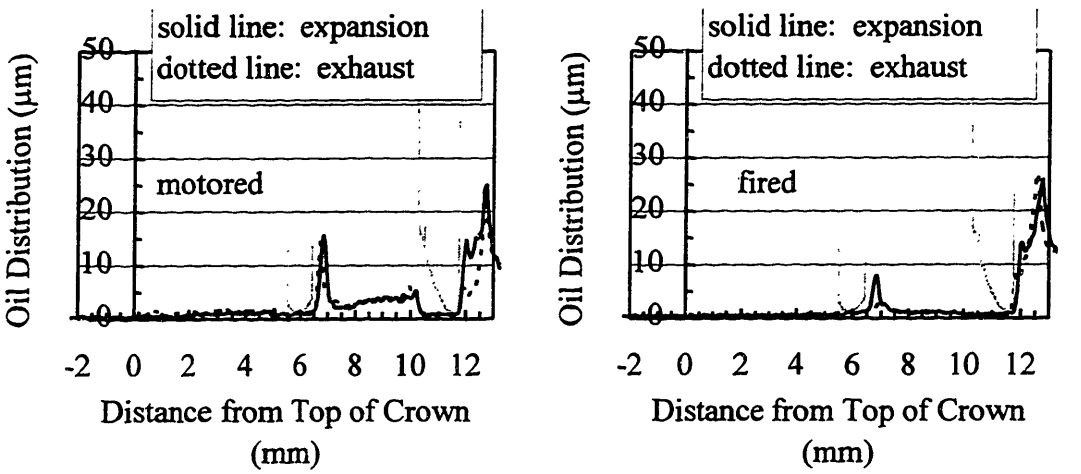

(b) Expansion and Exhaust (Motored Versus Fired)

Figure 5-34 Ring-Pack Oil Distribution for SAE-10W for the Load Effect (Fired Versus Motored) for the (a) Intake and Compression Strokes and (b) Expansion and Exhaust Strokes.
(Window 1, 2500 rpm, 60°C)

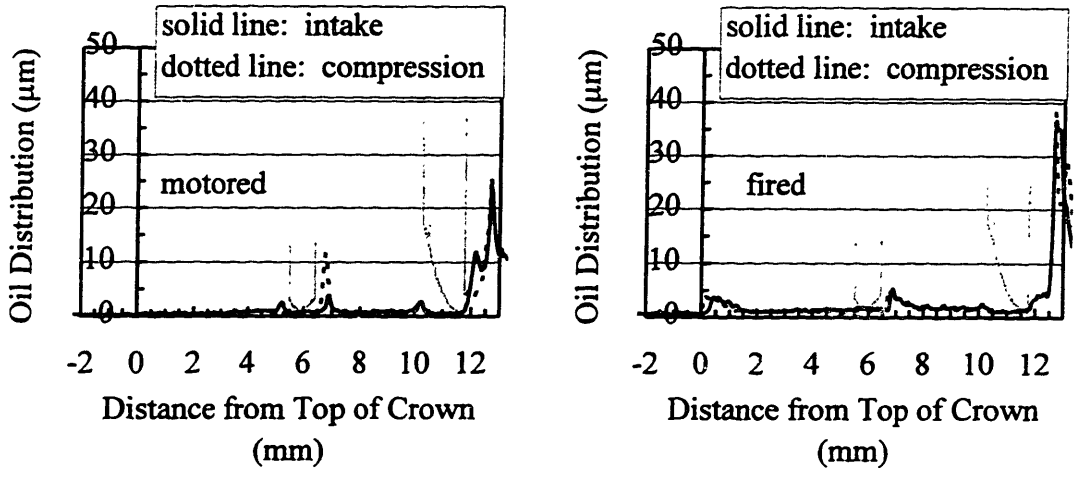

(a) Intake and Compression Strokes (Motored Versus Fired)

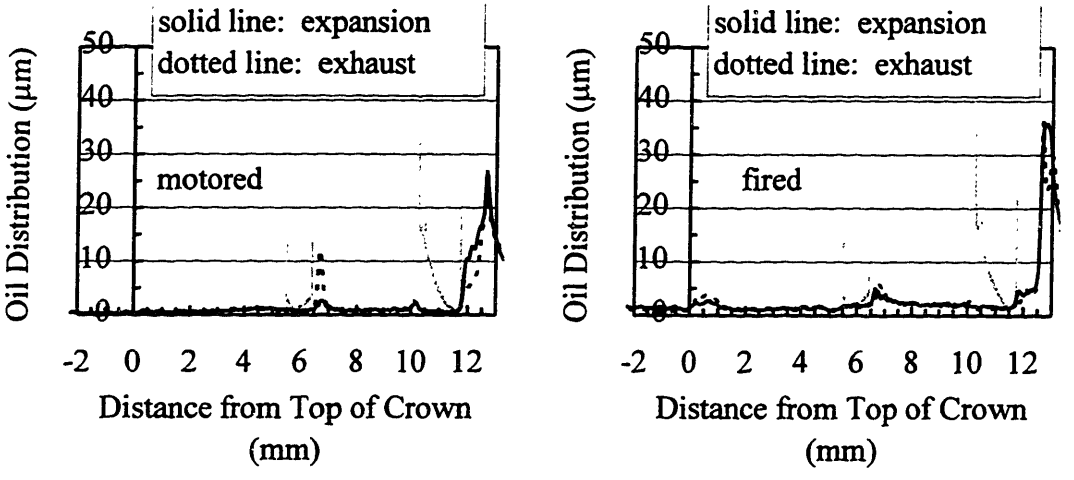

(b) Expansion and Exhaust (Motored Versus Fired)

Figure 5-35 Ring-Pack Oil Distribution for SAE-10W/50n for the Load Effect (Fired Versus Motored) for the (a) Intake and Compression Strokes and (b) Expansion and Exhaust Strokes.
(Window 1, 2500 rpm, 60°C)

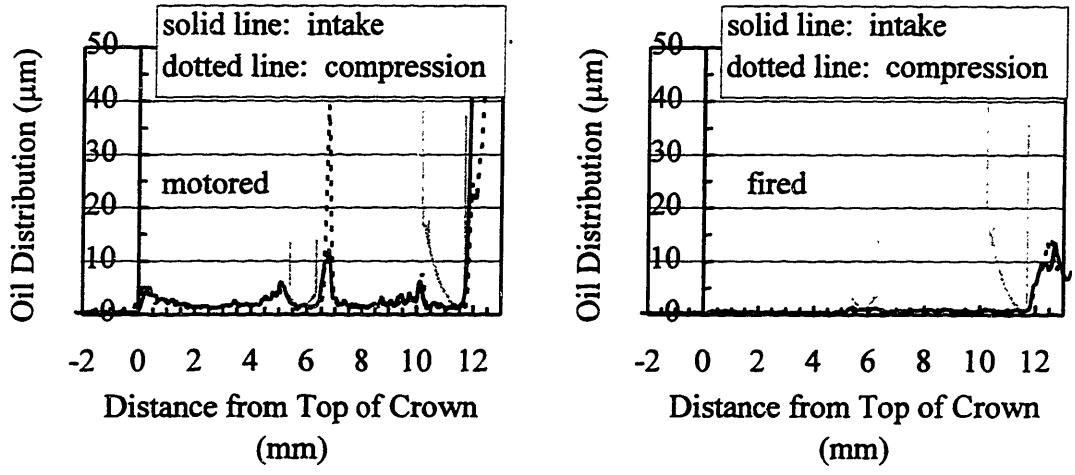

(a) Intake and Compression Strokes (Motored Versus Fired)

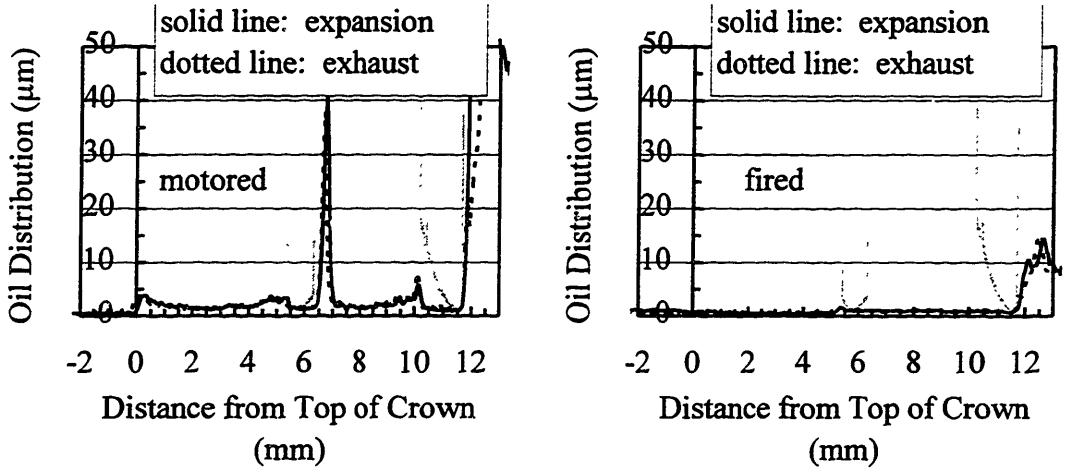

(b) Expansion and Exhaust (Motored Versus Fired)

Figure 5-36 Ring-Pack Oil Distribution for SAE-50 for the Load Effect (Fired Versus Motored) for the (a) Intake and Compression Strokes and (b) Expansion and Exhaust Strokes.
(Window 1, 2500 rpm, 60°C)

Comparisons of oil distribution reveal that the ARTs not only increase from fired to motored conditions due to accumulation of oil on the lands but from oil squeezing between the top and scraper rings and their grooves characterized by the sharp spikes along the relatively uniform oil distributions. More oil on the lands and, most likely, behind the rings within the grooves allows oil squeezing to be detected from the LIF system. With the greatest percent increase of oil along the lands within the ring-pack, SAE-50 has the greatest amount of oil squeezing as well. (The stroke-by-stroke differences in oil squeezing is explained by ring lift within its groove in the stroke-by-stroke section, section 5.3.2.1.1.)

ARTs increase along the third and fourth regions as well except for the negligible change for SAE-10W and -10W/50n in the third region. Additionally within the ring pack, the percent increase in ART slightly increases with viscosity for the monogrades SAE-10W and -50, and the ART percent increase for SAE-10W/50n is less than the monogrades. (Any ring-and-groove oil squeezing within these regions are masked by the large amounts of oil within these regions.)

For the regions below the OC ring shown in Figures 5-22 (e) - (g), the ARTs typically decrease from fired to motored -- the ART-load trend reverses except for the negligible change in SAE-50 for regions 6 and 7 and the slight increase for region 5. Since the regions below the OC ring provide vast but finite oil reservoirs which supply the ring-pack regions, the ART increase within the ring-pack may indicate that less oil is held back in these lower regions from reduced downward gas flows resulting in lesser ARTs within these lower regions. Gas flows are reduced because of the lower cylinder pressure under motored conditions compared to the fired condition. Blowby and gas flows through the ring pack are mostly the study of the remainder of this section.

The increasing trend of ARTs within the ring-pack as the load changes from fired to motored may be caused by a host of different factors whose influence on oil distribution is very difficult to determine due to the lack of understanding of oil transport. The intensity and timing of piston slap certainly changes from high to low loads found by Ryan [26]. As a result, the oil squeezing between the piston skirt and liner, suggested

from section 5.3.2.2, may behave differently influencing the manner in which oil is supplied behind the OC ring and above regions.

Also, temperatures of the piston and rings are certainly lower. One result from decreased temperature is less evaporation. In the vicinity of the crown land, the absence of hot gases as well lessens evaporation and avoids any burning compared to the fired condition. Relative to the top land, less evaporation from greater lubricant partial pressure within the second land vapor contributes to more oil. Another effect from decreased temperatures result in changes in ring and groove clearances and their relative angles affecting gas flows and ring dynamics.

Just as influential on the load effect, if not more, are the gas flows and ring dynamics which are affected by the different loads caused by the cylinder pressures. The motored peak cylinder pressure of 18 bars is much lower than the fired peak pressure of 31 bars, and, of course, the peak is shifted back to exactly top center (TC) under motored conditions. For the motored WOT condition, measured cylinder and predicted land pressures as well as the relative ring lifts of the top and scraper rings from the *RINGPACK-OC* model are shown in Figures 5-37 (a) and (b), respectively. Additionally, gas flows through grooves and gaps are shown in Figures 5-38 and -39, respectively, comparing fired and motored conditions. (For the fired condition at 2/3 load, the fired cylinder and land pressures and ring lifts are shown in Figures 4-18 (a) and (b), respectively. Between the fired and motored conditions, the only change in the model input is the measured cylinder pressure[2].) Besides the second ring flutter occurring slightly later than in the fired condition, no drastic change in the ring dynamics is evident.

[2] Although some accuracy is probably lost due to actual geometric changes from thermal distortion caused by the difference between motored and fired temperatures mentioned in the last paragraph, the substantial cylinder pressure decrease from fired to motored conditions should provide a rough model prediction of the actual magnitudes and trends of the pressures and gas flows along the lands and through ring gap and grooves. Decreased temperatures result in changes in ring and groove clearances and ring gap spacing. Additionally, groove angles change relative to the rings and their relative angles affect gas flows and ring dynamics. Unfortunately, these exact geometric changes from thermal distortion are unknown.

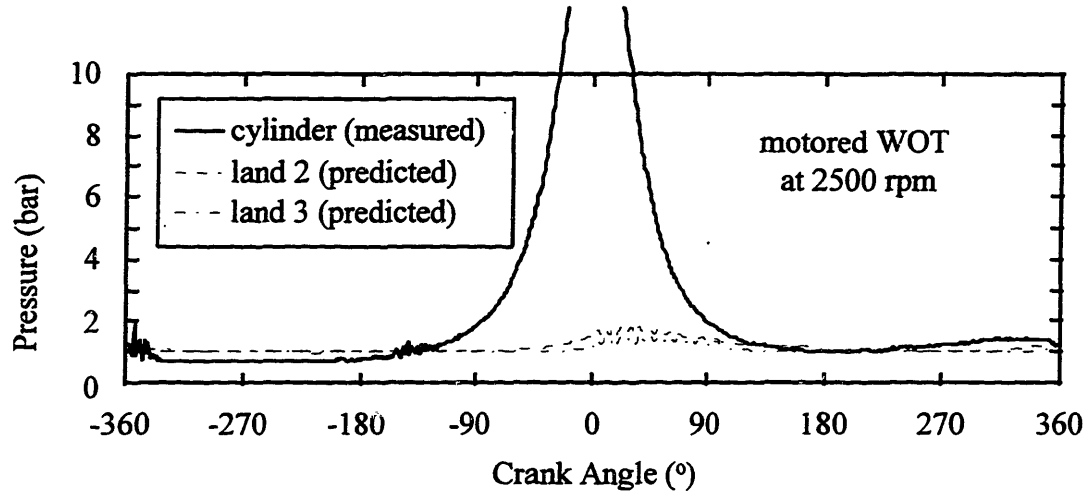

(a) Measured Cylinder and Predicted Second and Third Land Pressures

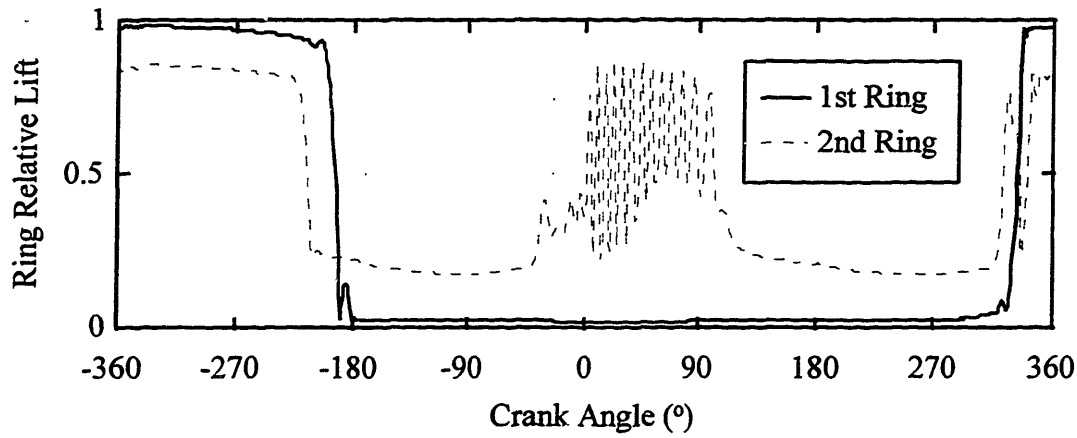

(b) First and Second Ring Relative Lift within Their Grooves

Figure 5-37 Motored (WOT) *RINGPACK-OC* Results for (a) Land Pressure Predictions and (b) Top and Scraper Ring Relative Lift within Their Grooves (2500 rpm , 60°C)

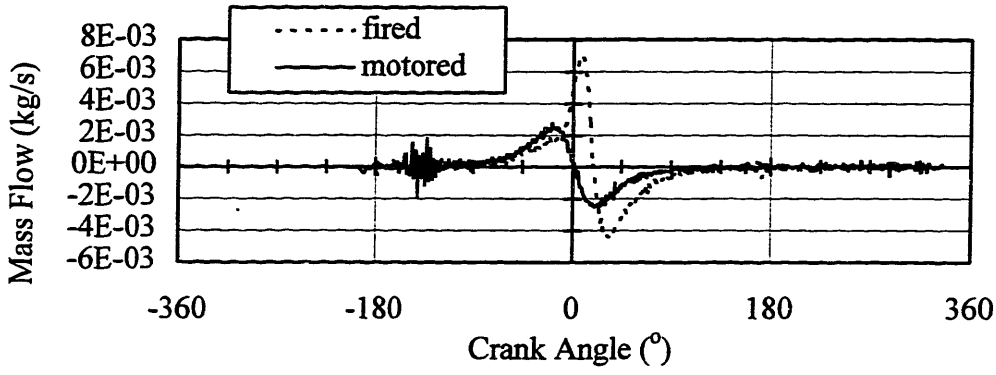

(a) Crown Land to Region Behind Top Ring

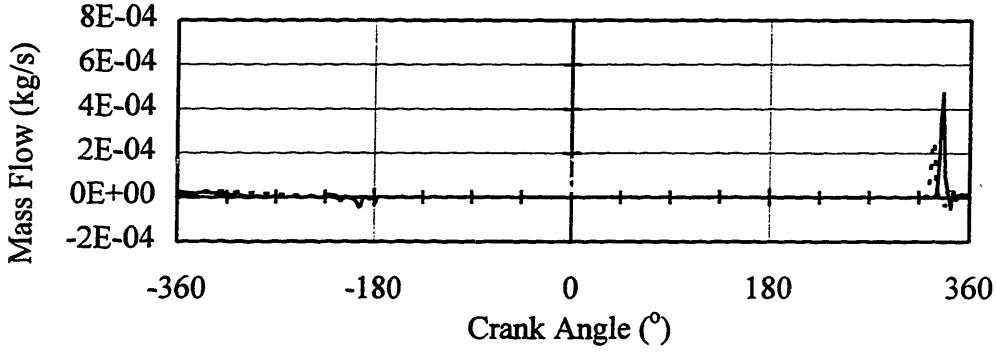

(b) Region Behind Top Ring to Second Land

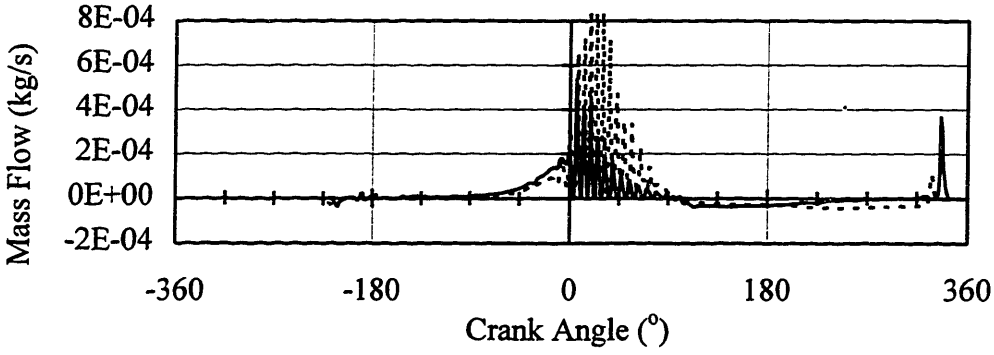

(c) Second Land to Region Behind Second Ring.

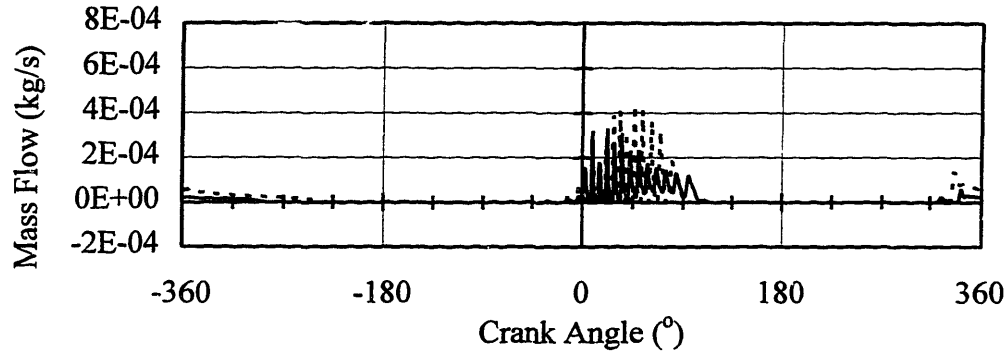

(d) Region Behind Second Ring to Third Land

Figure 5-38 Predicted Mass Flow Rates through Channels between Rings and Grooves During a Cycle for Fired and Motored Conditions from (a) Crown Land to Region Behind Top Ring, (b) Region Behind Top Ring to Second Land, c) Second Land to Region Behind Second Ring, and (d) Region Behind Second Ring to Third Land (Fired Versus Motored at 2500 rpm, 60°C)

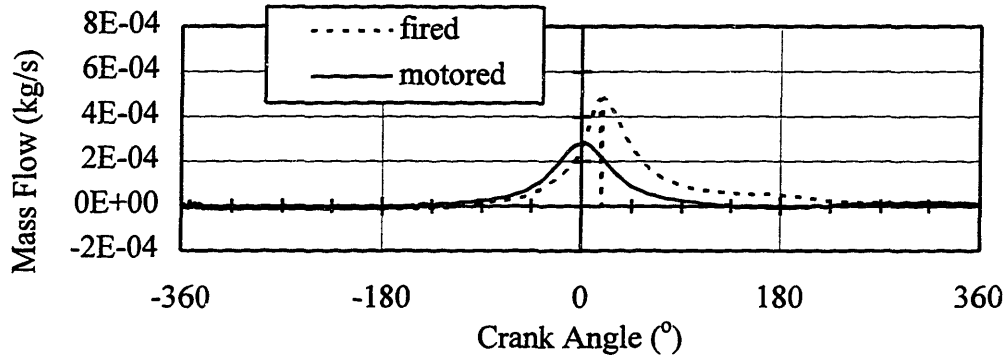

(a) Top Ring Gap

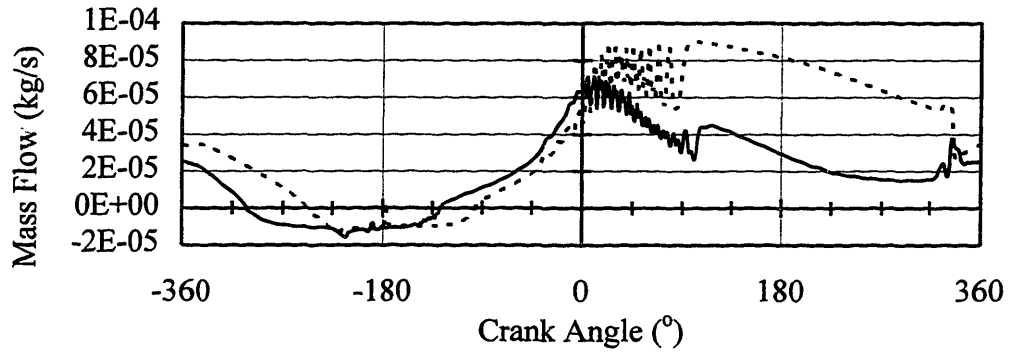

(b) Second Ring Gap

Figure 5-39 Predicted Gap Mass Flow Rates During a Cycle for Fired and Motored Conditions for the (a) Top and (b) Second Rings.
(Fired Versus Motored at 2500 rpm, 60°C)

Nevertheless, the gas flows significantly change. As a global measure, predicted blowby decreases by almost half from 3.03 to 1.75 l/minute from fired to motored, respectively. For the top two rings, instantaneous mass flow rates through gaps and grooves shown in Figures 5-38 and -39, respectively, decrease significantly especially through the gap.

Any oil within these narrow channels between the rings and their grooves and small gap spacings is especially sensitive to gas flows and their changes between conditions. Since the crown and second land regions are linked between ring gaps and grooves, oil along the lands is directly affected as well. Because gas flow rates significantly decrease, less oil is dragged down towards the third land region resulting in a greater amount of oil along the crown and second lands and within the channels between the rings and their grooves.

The amount of oil squeezing between the top and bottom channels of the top ring (shown in Figures 5-34, -35, and -36) differ because of two reasons. One, gas flows through the lower channel shown in Figure 5-38 (b) are relatively negligible (due to good lower ring sealing from lack of top ring lift throughout most of the cycle) compared to the high flows in and out of the upper channel shown in Figure 5-38 (a). Thus, much less oil is dragged out of the lower channel than the upper channel and, consequently, more oil resides within the lower channel for oil squeezing. Two, ring lift is always down except for the intake stroke resulting in high contact pressures for oil squeezing between the ring and its lower groove. These stroke-by-stroke differences from ring lift are studied in more detail in the stroke-by-stroke section, section 5.3.2.1.1, where measurements from both midstroke windows and window 6 are used to validate the predicted top ring lift in the *RINGPACK-OC* model.

Although the lower channel of the top ring and the upper channel of the second ring are adjacent to the second land which directly connects any oil transport between the two, the amount of oil squeezing differs greatly between the two channels which is probably caused by the difference in channel gas flows. The gas flows within the lower channel of the top ring are negligible compared to the second ring where ring flutter

causes less ring sealing, allows much higher gas flows, and, thus, provides greater lubricant dragging out of this channel resulting in less oil squeezing.

In retrospect, these results show that oil squeezing between the rings and their grooves can be significant and is greatly affected by gas flows for different regions and clearances along the piston especially for the top and second rings as well as for different operating conditions. Since the ring gaps and grooves link the crown and second lands, oil along the lands is directly affected by the ring and groove gas flow conditions dragging lubricant. Quite unlike any of the other regions, no ring scraping contributes to oil on the top and second land -- only gap and groove oil transport.

The gap flows probably contribute significantly to oil transport as well. For the top ring, the lower channel gas flows are negligible compared to the high positive gap gas flows which drag lubricant to the second land region. Conversely, less downward oil dragging potential exists for the second ring gap due to the lower gas flows differing by an order of magnitude. More insightful though is the second ring upper channel gas flows which are greater than the gap flows by at least a factor of two compared between Figures 5-38 (c) and -39 (b), respectively.

5.5 ENGINE SPEED EFFECTS -- 1800 VERSUS 2500 RPM

The engine speed effects from 1800 to 2500 rpm on oil distribution were measured on the major-thrust side at windows 1 and 6 and azimuthally off the major-thrust side at windows 2 and 4 while the cylinder wall temperature was maintained at 100°C at midstroke. Stroke-averaged region thicknesses are used to compare different cases, and the actual standard deviation accompanies the measurements. (The data presented here correspond to high calibration accuracies tabulated in Table D.1, or, as for the measurements from window 2 and 4, the calibration coefficients for these cases at 1800 rpm are adjusted my means of the procedure explained in section 4.4.1 for the OFT study. Acquisition of oil film data for 3500 rpm was taken but found to be no good.)

Substantial enough to affect OFT in section 4.4, this speed change affects the oil distribution even more in terms of percent increase for most regions and is detected from all windows. Along the major-thrust side at midstroke (window 1) and near BC (window 6), the average region thicknesses (ARTs) significantly increase with speed for all the regions shown in Figures 5-40 and 5-41, respectively.

Engine speed effects between different lubricants are greater for the less-viscous lubricants. The percent increases for SAE-10W are much greater than the percent increases for SAE-10W/50n and -50 which show comparable percent increases. (Possibly affected by its high low-shear viscosity along the lands for this speed effect, SAE-10W/50n behaves more like SAE-50 than -10W.) Oil flow for less-viscous lubricants along the lands and through the gaps and grooves is easier and has less viscosity restriction than the highly-viscous lubricants. Therefore, SAE-10W is more sensitive to changes in speed reflected in greater percent increases. (Viscosity restriction is discussed in detail in section 5.6.)

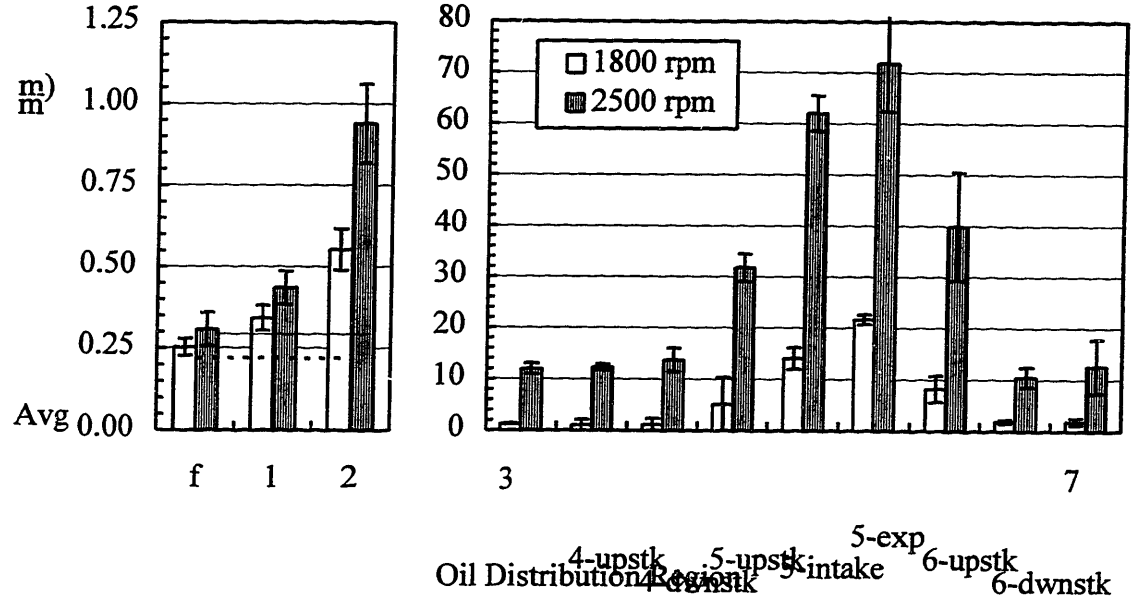

(b) SAE-10W

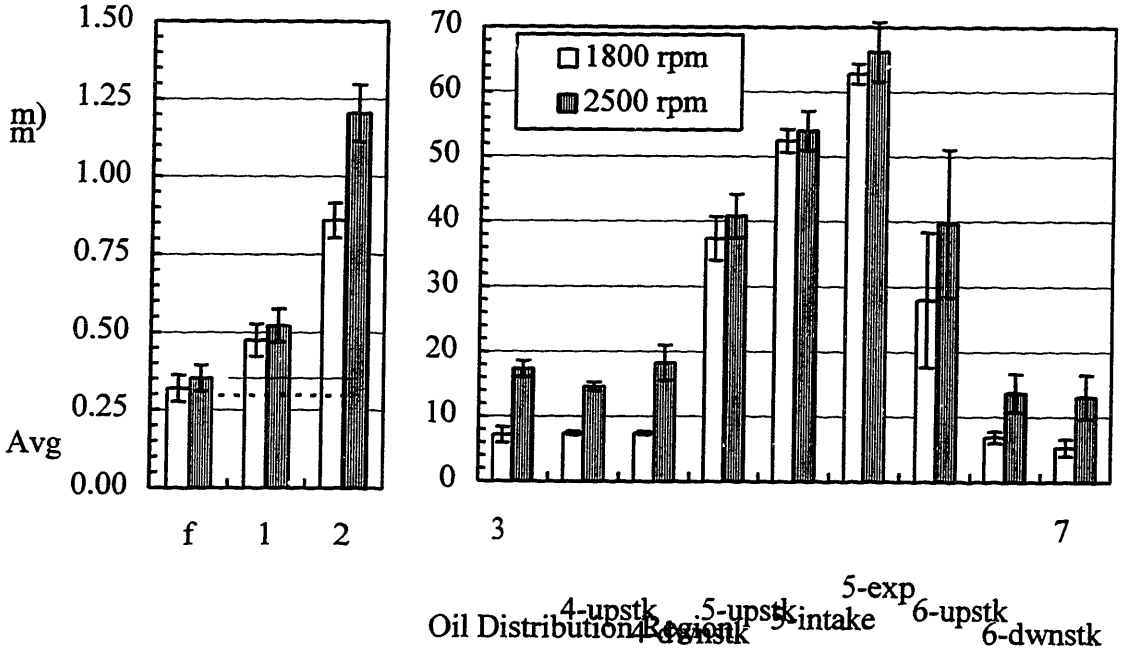

(b) SAE-10W/50n

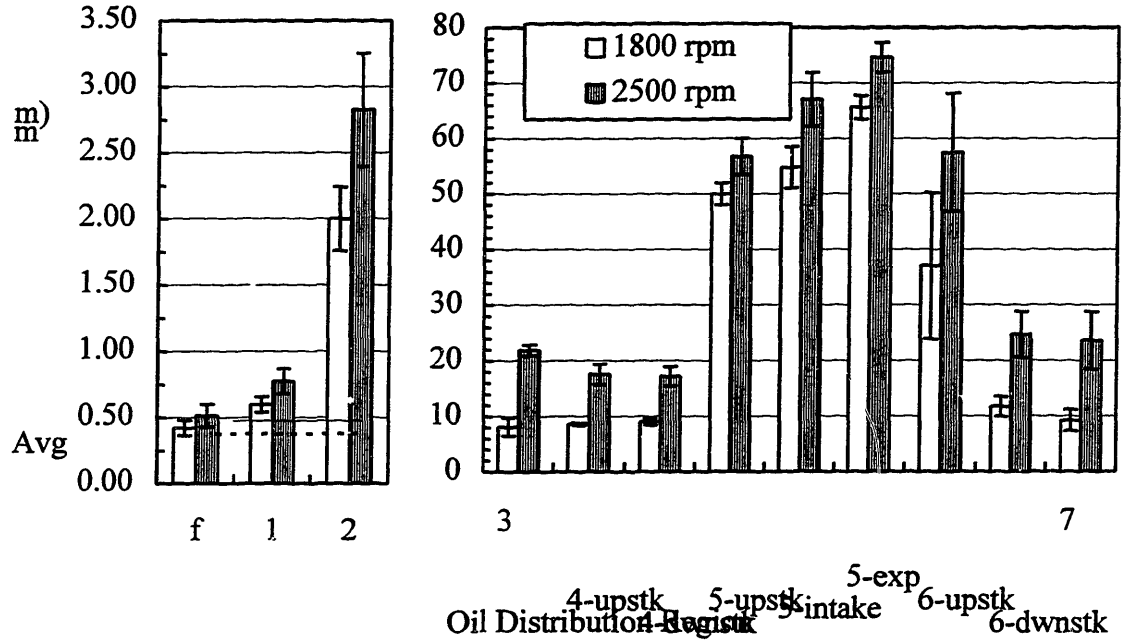

(c) SAE-50

Figure 5-40 Engine Speed Effect (1800 Versus 2500 rpm) at Midstroke on Major-Thrust Side (Window 1) for (a) SAE-10W, (b) -10W/50n, and (c) -50. (Window 1, 2/3 Load, 100°C)

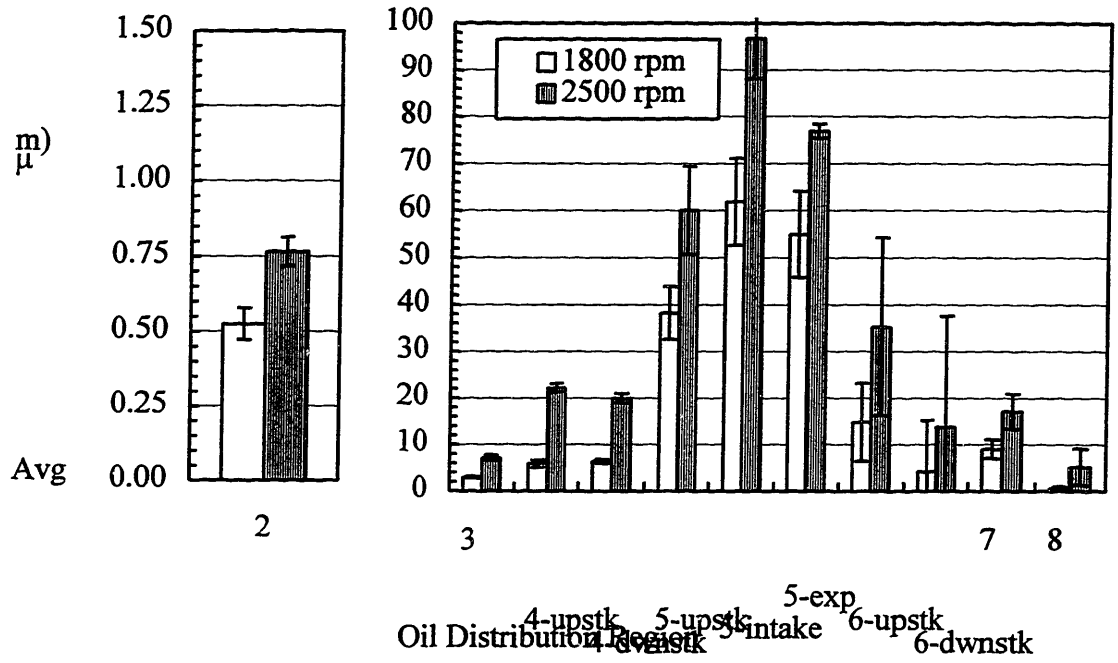

Figure 5-41 Engine Speed Effect (1800 Versus 2500 rpm) near BC on Major-Thrust Side (Window 6) for SAE-10W/50n. (Window 6, 2/3 Load, 100°C)

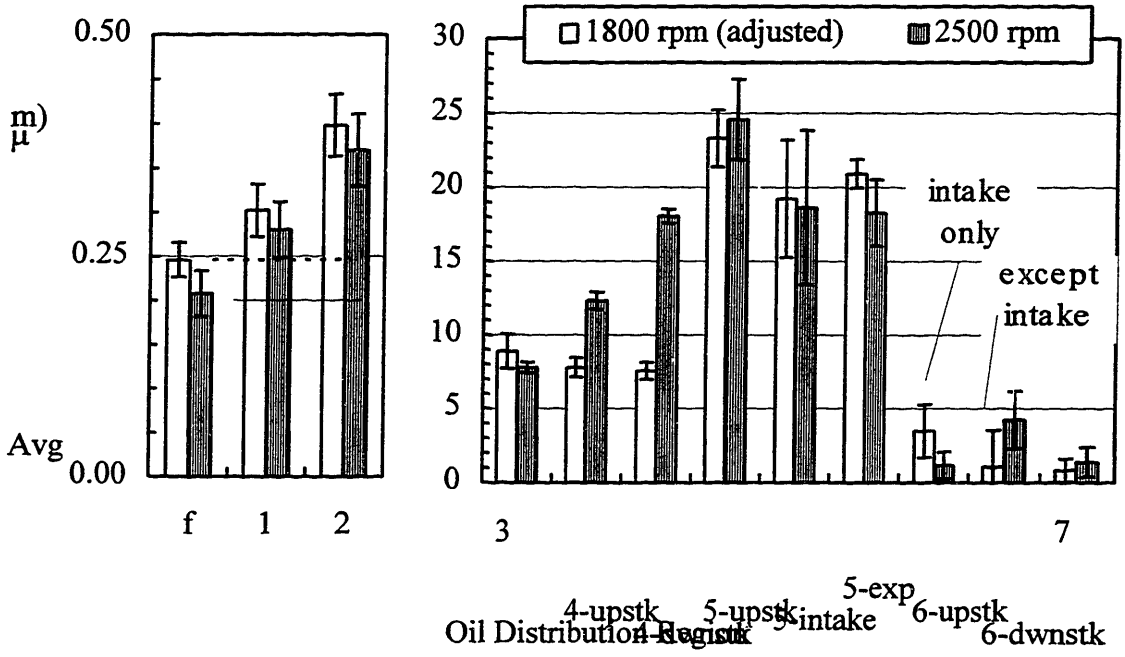

(a) Window 2

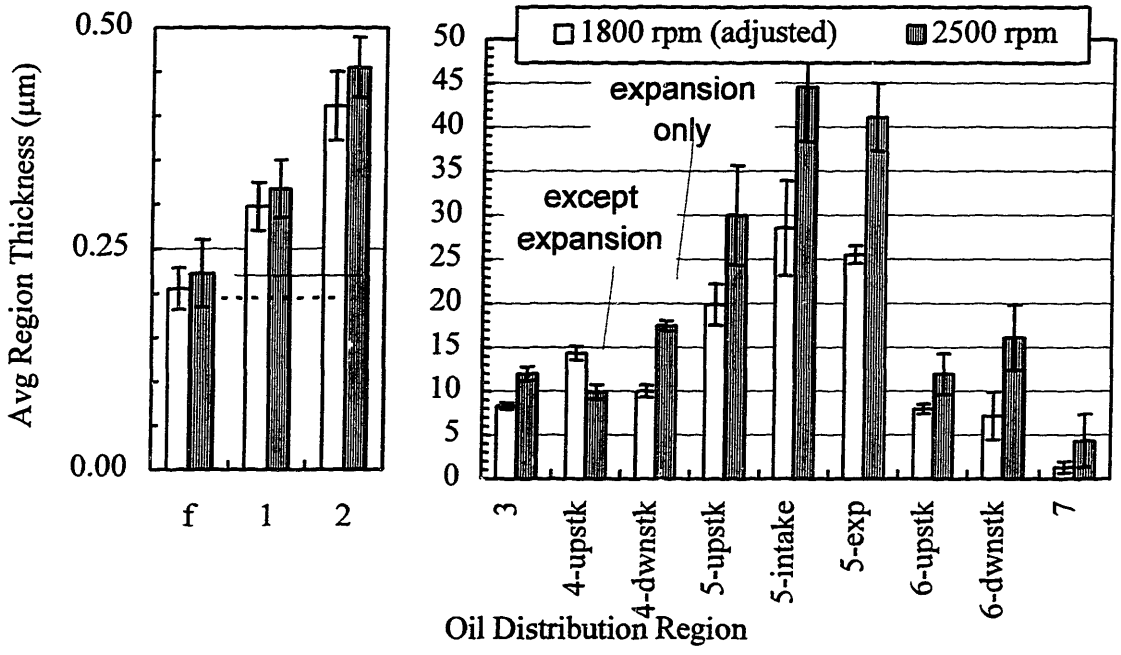

(b) Window 4

Figure 5-42 Engine Speed Effect (1800 (adjusted) Versus 2500 rpm) at Midstroke Off Major-Thrust Side for SAE-10W/50n at (a) Window 2 and (b) 4.
(2/3 Load, 100°C)

Off the major-thrust side at windows 2 and 4 shown in Figures 5-42 (a) and (b), respectively, the increasing ART trend with speed isn't as strong. The crown and second land regions show no marked increase in view of the standard deviation. Still, other regions significantly increase with engine speed but not as much as the major-thrust side. From the OFT study, no changes in MOFT are observed at windows 2 and 4 for SAE-10W/50n except for marginal increases for the OC ring segments at window 4 (see Appendix I). These results further conclude that oil transport pathways through the gap and grooves of the OC ring (besides oil flow under the rings and scraping) play a significant role.

For each lubricant at each window, small ARTs exist for the crown and second land. Under these fired conditions, the crown land has negligible oil, and its ART behaves in accordance with the liner OFT from hydrodynamic lubrication of the top ring. Any small amount of oil that is transported through the top ring gap and groove to the top

land probably evaporates and/or burns quickly due to the hot piston and gases from firing. However, much greater than the free-liner increase, the second land ARTs on the major-thrust side in Figures 5-40 and -41 increase significantly with speed having no overlapping standard deviations between the two speed conditions. Since both the top and scraper rings do not scrape oil from the liner, any oil transport to these upper lands must occur only through the second ring gap and groove.

The ART increase with speed along the second land is often accompanied by oil squeezing between the top ring and its groove at 2500 rpm shown in Figures 5-43, -44, and -45 for SAE-10W, -10W/50n, and -50, respectively. Typically, 1800 rpm does not have any oil squeezing due to the small amounts of oil which exist on the upper lands (except for SAE-50 for the second ring during the upstroke).

With the only source of oil transport occurring through the second ring gap and groove in the absence of scraping, the oil transported to the crown and second lands is heavily dependent upon the gas flows and ring dynamics of the scraper ring. Figures 5-46 (a) and (b) show the measured cylinder and predicted land pressures and the relative ring lifts of the top and second rings within their grooves for the engine speed of 1800 rpm. (For the engine speed of 2500 rpm, Figure 4-18 (a) and (b) shows the pressures and ring lift, respectively.) Higher second land pressure develops for 1800 rpm because the slower engine speed allows more time for the second land to approach the cylinder pressure. Consequently, accompanied by the lower inertial forces from lower engine speed, the higher land pressures dominate more than inertial forces, and the scraper ring flutter is all but eliminated resulting in low relative lift.

Although the predicted blowby is about the same at 3.03 l/minute between the two speeds, gas flows through grooves and gaps may change as shown in Figures 5-47 and -48. The cumulative effect of gas flows through both the groove and gap on oil dragging results in higher ARTs for the second land for higher speeds. The damped second ring flutter at 1800 rpm is accompanied by relatively small predicted ring and groove gas flow through the lower channel shown in Figure 5-47 (d) compared to 2500 rpm. Consequently, lubricant dragging from the gas flows through the second groove to the third land is less, and more oil exists for second ring squeezing and along the lower

portion of the second land shown in Figures 5-45 (a) and (b) for SAE-50. (This effect for SAE-10W and -10W/50n is undetected due to the small amount of oil.) However, at this low speed, the second ring gap flow is relatively high compared to 2500 rpm in Figure 5-48 (b) and over-compensates for the lack of lubricant dragging through the lower second ring groove to the third land.

At 2500 rpm, substantial second ring flutter is induced and is accompanied by much higher second groove gas flows but less second ring gap flows and more oil within the third land resulting in greater inertial driving forces. The decreased gas flow within the second ring gap and increased oil supply within the third land region accompanied by the increased inertial driving forces are responsible for increasing the ARTs for the second land. Not only does the ART increase with speed but the spatial distribution along the land is altered from the change in gas flows and second ring dynamics. Now, much of the oil around the second ring in the second land region is drawn through the groove to the third land resulting in no second ring oil squeezing within the top channel and relatively small amounts of oil on the second land near the scraper ring shown in Figures 5-43, -44, and -45 for 2500 rpm. Much of the oil on the second land accumulates along the upper portion of the second land which supplies enough oil to the top ring groove for oil squeezing. (The stroke-by-stroke differences on oil squeezing from ring lift are studied in more detail in the stroke-by-stroke section, section 5.3.2.1.1, where measurements from both midstroke windows and window 6 are used to validate the predicted top ring lift from the *RINGPACK-OC* model.)

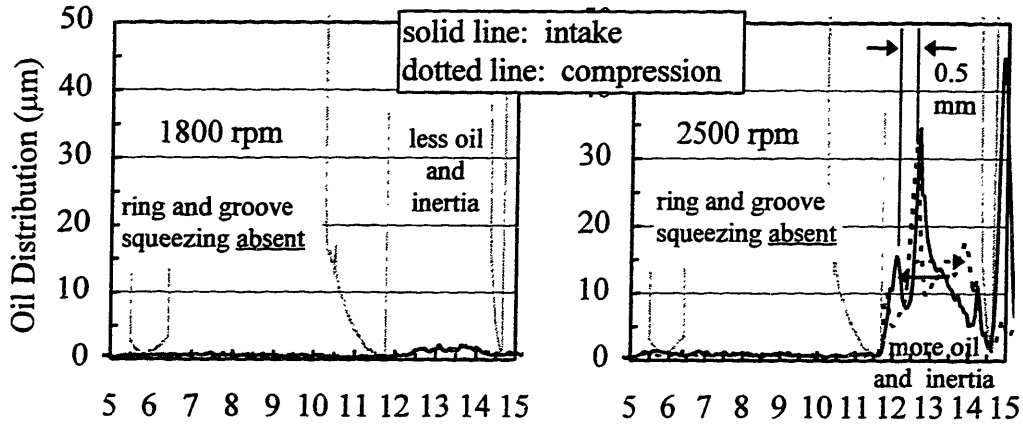

(a) Intake and Compression Strokes (Motored Versus Fired)

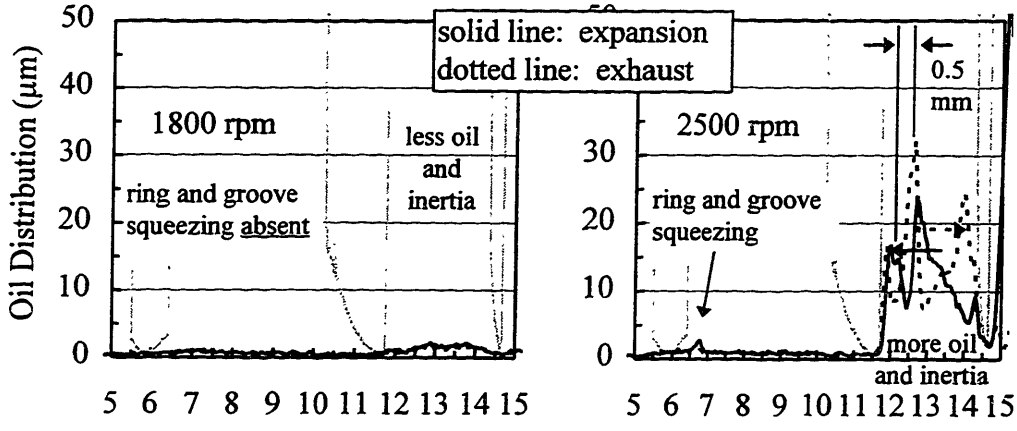

(b) Expansion and Exhaust (Motored Versus Fired)

Figure 5-43 Ring-Pack Oil Distribution for SAE-10W for the Speed Effect (1800 Versus 2500 rpm) for the (a) Intake and Compression Strokes and (b) Expansion and Exhaust Strokes.
(Window 1, 1800 Versus 2500 rpm, 100°C)

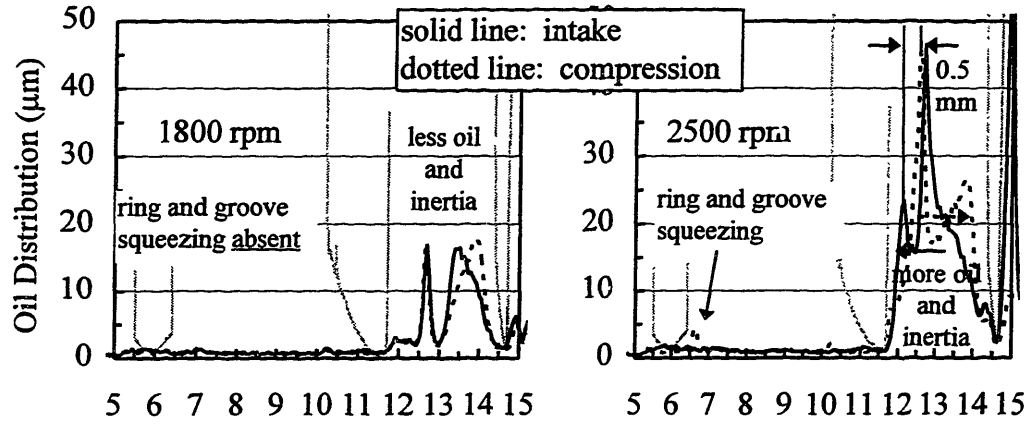

(a) Intake and Compression Strokes (Motored Versus Fired)

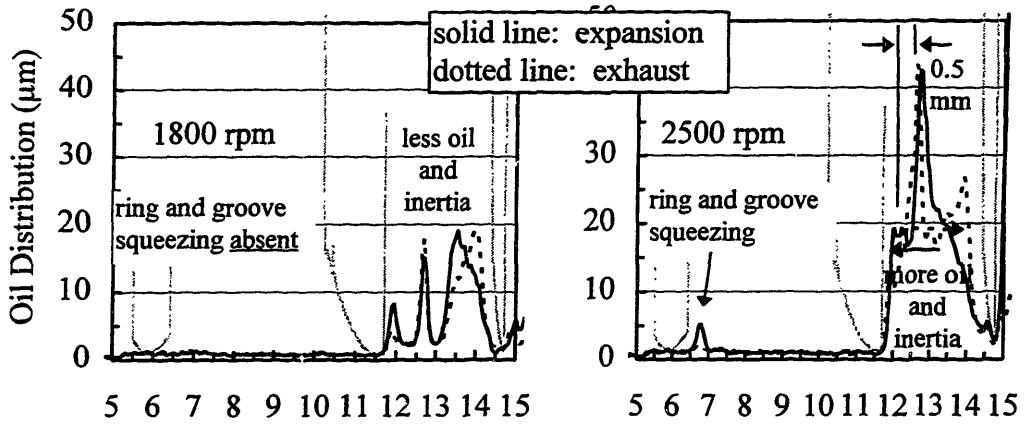

(b) Expansion and Exhaust (Motored Versus Fired)

Figure 5-44 Ring-Pack Oil Distribution for SAE-10W/50n for the Speed Effect (1800 Versus 2500 rpm) for the (a) Intake and Compression Strokes and (b) Expansion and Exhaust Strokes.
(Window 1, 1800 Versus 2500 rpm, 100°C)

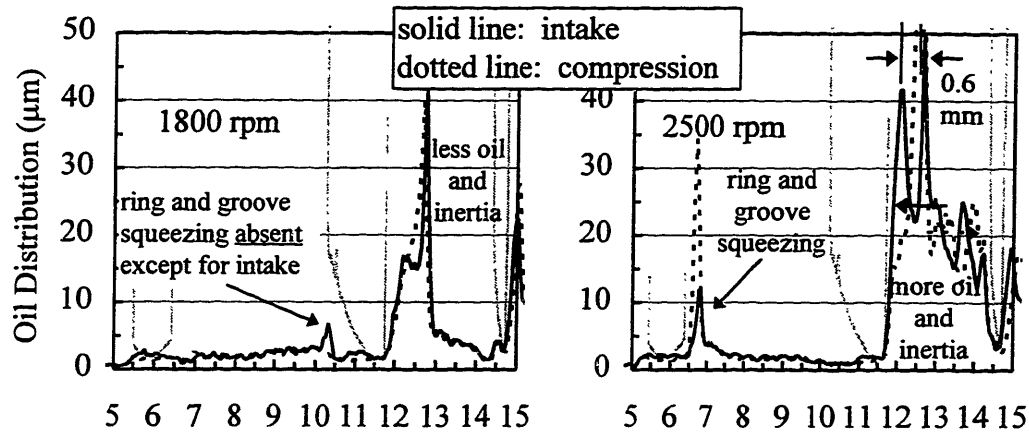

(a) Intake and Compression Strokes (Motored Versus Fired)

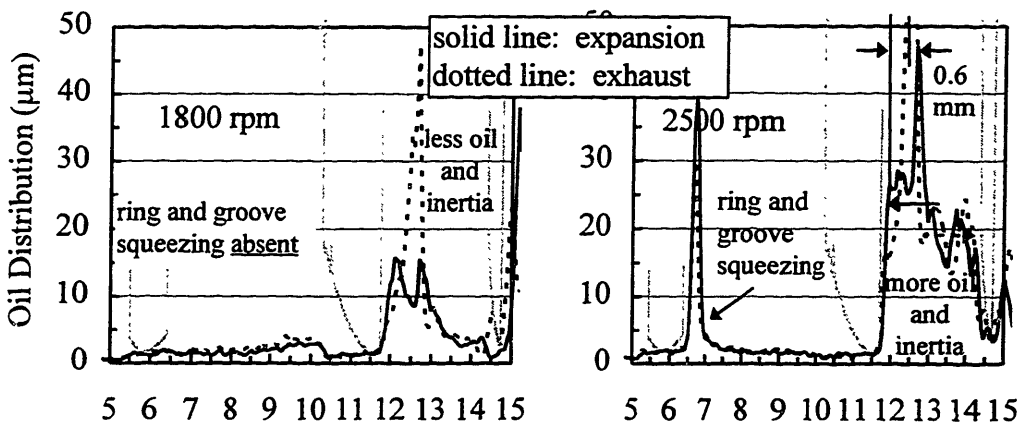

(b) Expansion and Exhaust (Motored Versus Fired)

Figure 5-45 Ring-Pack Oil Distribution for SAE-50 for the Speed Effect (1800 Versus 2500 rpm) for the (a) Intake and Compression Strokes and (b) Expansion and Exhaust Strokes.
(Window 1, 1800 Versus 2500 rpm, 100°C)

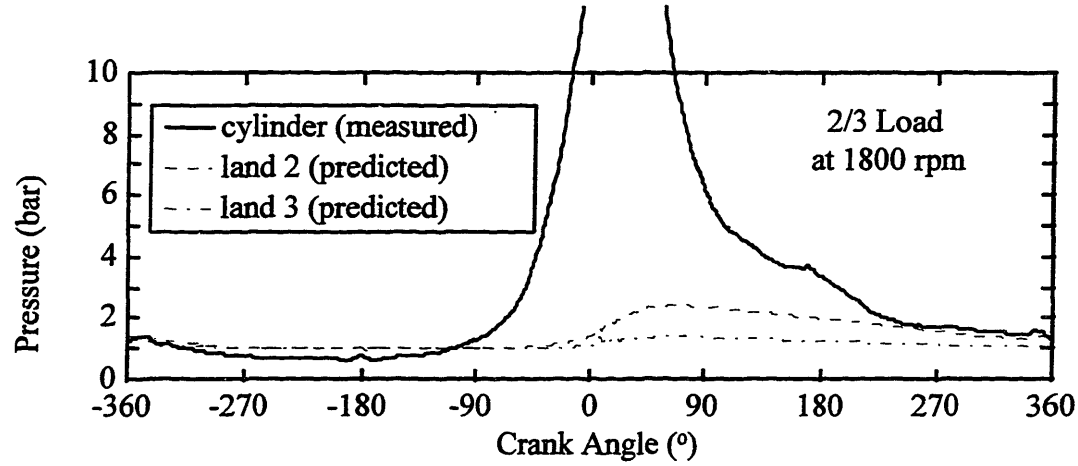

(a) Measured Cylinder and Predicted Second and Third Land Pressures

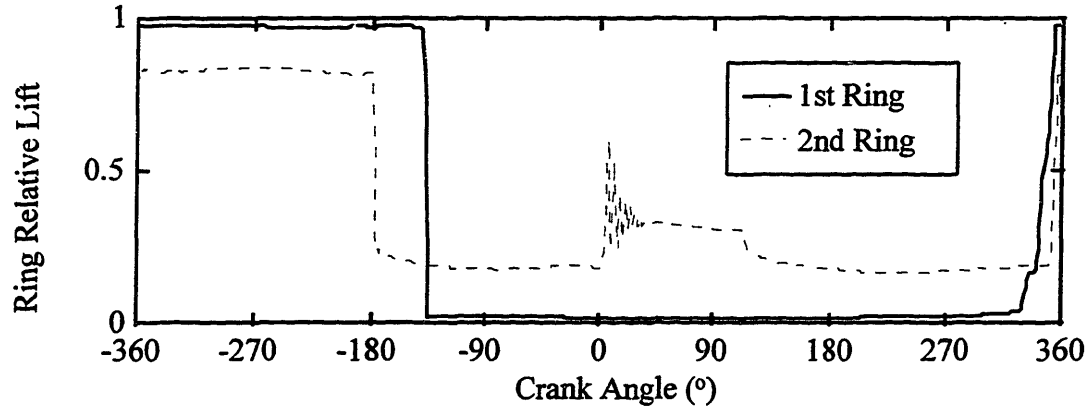

(b) First and Second Ring Relative Lift within Their Grooves

Figure 5-46 *RINGPACK-OC* Results at 1800 RPM for (a) Land Pressure Predictions and (b) Top and Scraper Ring Relative Lift within Their Grooves (1800 rpm , 2/3 Load, 100°C)

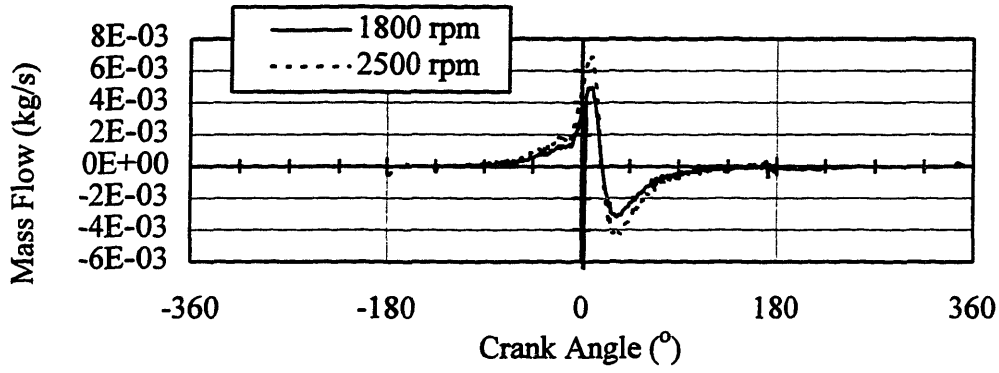

(a) Crown Land to Region Behind Top Ring

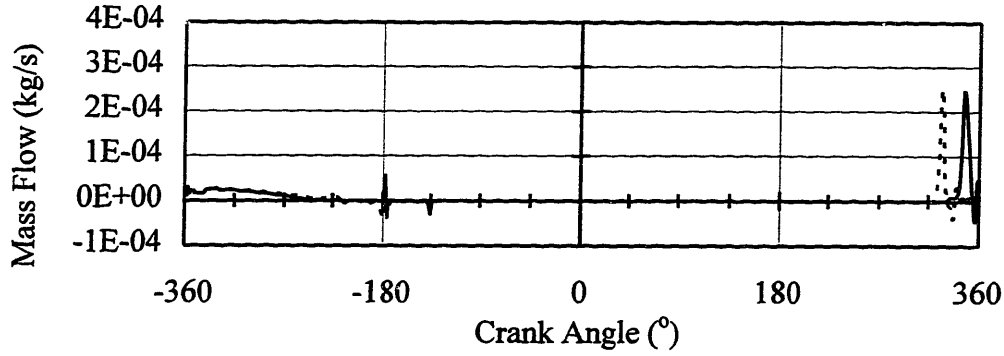

(b) Region Behind Top Ring to Second Land

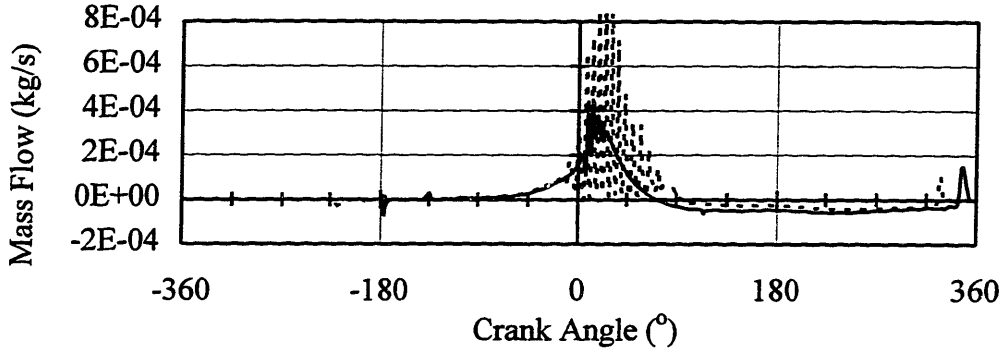

(c) Second Land to Region Behind Second Ring.

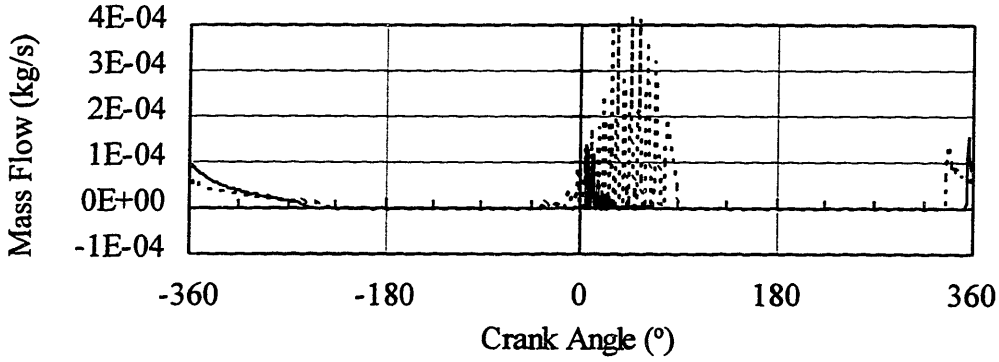

(d) Region Behind Second Ring to Third Land.

Figure 5-47 Predicted Mass Flow Rates through Channels between Rings and Grooves During a Cycle for 1800 and 2500 RPM from (a) Crown Land to Region Behind Top Ring, (b) Region Behind Top Ring to Second Land, (c) Second Land to Region Behind Second Ring, and (d) Region Behind Second Ring to Third Land.
(Fired Versus Motored at 2500 rpm, 60°C)

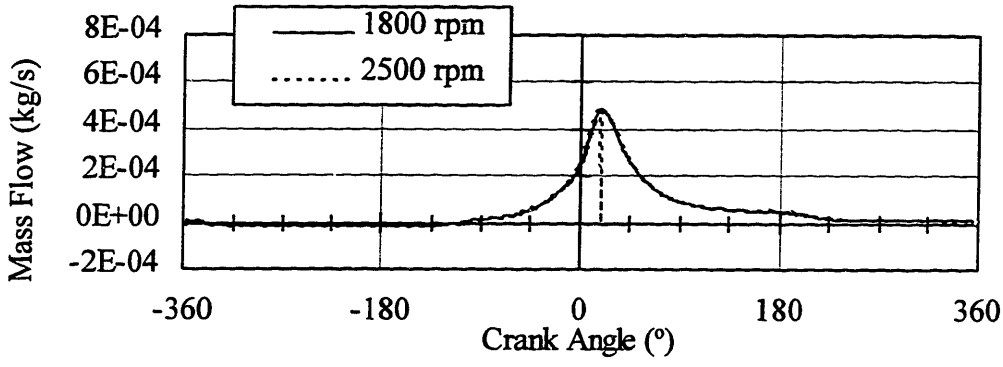

(a) Top Ring Gap

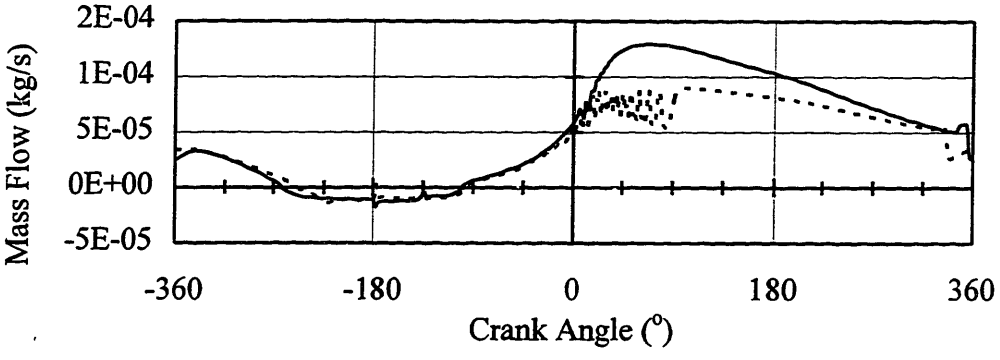

(b) Second Ring Gap

Figure 5-48 Predicted Gap Mass Flow Rates During a Cycle for 1800 and 2500 RPM for the (a) Top and (b) Second Rings.
(1800 Versus 2500 rpm, 2/3 Load, 100°C)

Nevertheless, the greatest increases occur in regions with high oil masses -- regions 3 - 7 (and 8). Unquestionably, the largest percent increases occur along the third land region, between the OC rails, and along the lower piston skirt (and free-liner below skirt), region 7 (and 8). Typically for these regions, percent increases soar well over 100 percent -- much greater than MOFT increases of roughly 30 percent from hydrodynamic lubrication in section 4.4.1. Even region 7, which includes the maximum skirt diameter and experiences hydrodynamic lubrication (see section 5.3.1), has percent increases over 100 percent. Observed from window 6, this large increase is probably due to the large increase in lubricant availability from the free-liner below the skirt along region 8; the

ART of region 8 increases by roughly 700 percent from 1800 to 2500 rpm for SAE-10W/50n.

As mentioned in section 4.4.1, the OFTs under the rings and along the free-liner theoretically scale with the square root of engine speed, $\sqrt{N}$, resulting in a rough predicted increase of ~ 20 percent from 1800 to 2500 rpm which is consistent with the typical empirical increase of ~ 30 percent. However, oil velocity along the lands scales with engine speed to the second power, N^2, from the following equation proposed by Tian [30].

$$V = \frac{ah^2}{\nu} \tag{5.1}$$

V, a, h, and ν are the velocity, acceleration, local oil height, and oil kinematic viscosity respectively. By approximating the average acceleration, it can be shown that the average oil velocity along a land is

$$\bar{V} \approx \frac{8}{9}\frac{(\pi Nh)^2 L}{\nu} \tag{5.2}$$

$$\bar{V} \sim N^2 \tag{5.3}$$

where L is the length of a stroke. Therefore, the average oil displacement along a land during half a stroke scales with N and the square of the local oil thickness and inversely with its viscosity.

$$\bar{x} = \bar{V}\Delta t = \bar{V}/_{2N} \approx \frac{8}{18}\frac{(\pi h)^2 NL}{\nu} \tag{5.4}$$

$$\bar{x} \sim \frac{Nh^2}{\upsilon} \tag{5.5}$$

Displacement increases with speed by roughly 40 percent for a fixed oil height and lubricant viscosity. This increase is a lower limit because the local oil thickness increases with speed as well.

Table 5.1 shows rough oil displacement measurements with calculations along the third land which compare fairly well. As expected, the oil displacement along the land increases with speed. Even SAE-10W with lower third land ARTs compared to SAE-10W/50n and -50 has similar oil displacement because its viscosity restriction is less.

Lubricant (viscosity, cSt)	Speed, N (rpm)	Distance Traveled (mm)	
		Measured	Calculated
SAE-10W (6 cSt)	1800	0.0	0.0
	2500	0.5	0.5
SAE-10W/50n (17 cSt)	1800	0.5	0.2
	2500	0.5	0.3
SAE-50 (19 cSt)	1800	0.3	0.2
	2500	0.6	0.4

Table 5.1 Measured and Calculated Oil Travel along the Third Land for 1800 and 2500 rpm for SAE-10W, -10W/50n, and -50.

There are several pathways for oil transport to different regions and are listed below:

1) One pathway is passage of oil under the rings. This type of oil passage from hydrodynamic lubrication is dominant along the crown land region where the crown land is dry. As observed earlier for the crown land region (and in the OFT analysis in both the measurements and model), the ARTs (and OFTs) increase with speed due to increased liner OFT from greater hydrodynamic lift of the rings. (Recall that the total ART measured by the LIF system measures oil on the land and along the liner.)
2) A second pathway includes ring gaps and grooves. An isolated example is the second land region which reveals a combination of two pathways: liner OFT from under the rings and oil flow through the ring gaps and grooves. However, the absence of scraping in the second land region precludes any contribution from oil on the liner to oil on the second land.

3) In addition to oil transport through ring gaps and grooves, a third route comes from ring oil scraping off the liner experienced by the scraper during its downstrokes and the upper and lower OC segments. Since the amount of oil scraping is contingent upon the amount of oil on the liner which increases with speed from greater MOFTs, the amount of oil scraped will increase with speed as well.

These oil pathways and the scraping mechanism for oil transport are discussed in further detail in section 5.7. However, inertial mechanisms must be mentioned in this section as well because their influence increases dramatically due to increased piston acceleration and oil masses. For example, Figures 5-43, -44, and -45 shows oil masses along the third land region for 1800 and 2500 rpm. As oil masses and acceleration increase from 1800 to 2500 rpm, the oil experiences greater inertial forces which shear and cause greater oil travel along the regions or lands. Therefore, more inertial driving potential exists to force lubricant through gaps and grooves between different regions. The gap and groove pathways between the second and third land regions are good examples and are the only oil transport links to the crown and second lands. The increase in ARTs for the second land results from increased oil transport through these pathways caused by changes in gas flows and the drastic increase in oil supply and inertial forces within the third land region.

In retrospect, oil squeezing and scraping and inertial influences on oil transport increase and compound with engine speed, and, therefore, increase the ARTs. This increase allows more oil availability for oil to escape into the combustion chamber especially from the upper land regions. Interestingly, this finding is consistent with oil consumption studies which typically correlate an increase in oil consumption with engine speed [20, 24, 25].

5.6 AZIMUTHAL EFFECTS AROUND MIDSTROKE

From the OFT analysis in section 4.6, proper ring conforming and sealing is found at midstroke. Nevertheless, large percent decreases in OFT (but small OFT differences

relative to the maximum radial difference of 16 mm between the windows) occur between the major-thrust and other midstroke windows. This section investigates the midstroke azimuthal differences in terms of average region oil thicknesses (ARTs) along the ring-pack and piston skirt and explains these differences in view of the OFT findings and piston geometry.

Having the best calibration accuracies at the three midstroke windows 1, 2, and 4, several lubricants which were also used in the OFT analysis are again shown in Table 5.2 with low- and high-shear viscosities for the multigrade. Average Region Thicknesses (ARTs) from the ring-pack and below the OC ring in Figures 5-49 and -50, respectively, are compared azimuthally around the bore's circumference at midstroke from these window locations. (However, the calibration accuracies of these cases do not all have calibration uncertainties better than +/- 5 percent. The lubricant cases with questionable calibration accuracy are outlined with a dashed line. Refer to section 4.2 or Table D.1 for more details.)

Lubricant Number	*Lubricant Name*	*Operating Condition (f-fired, m-motored)*	*Kinematic Viscosity (cSt)*
1	SAE-10W/50n	f-2500 rpm, 100°C	8 (17)
2	SAE-30	f-2500 rpm, 100°C	12
3	SAE-10W	m-2500 rpm, 60°C	18
4	SAE-10W/50n	f-2500 rpm, 60°C	28 (56)

Table 5.2 Numbering Assignments for Lubricants
(Viscosity values in parenthesis are low shear.)

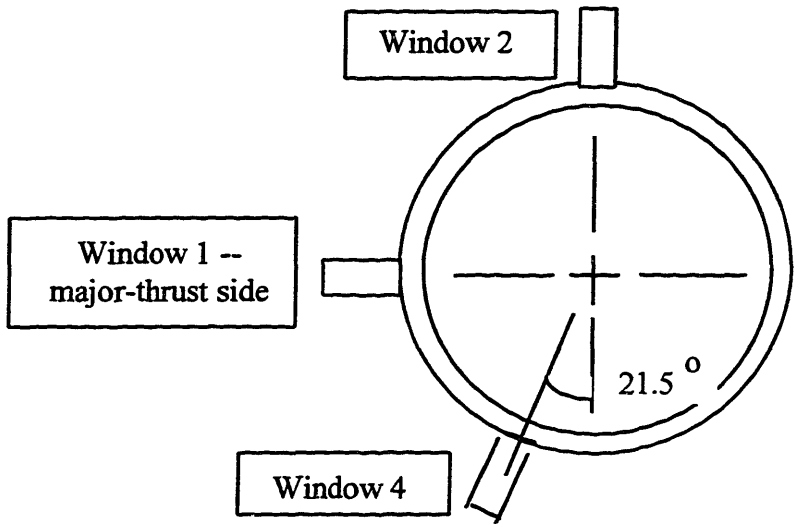

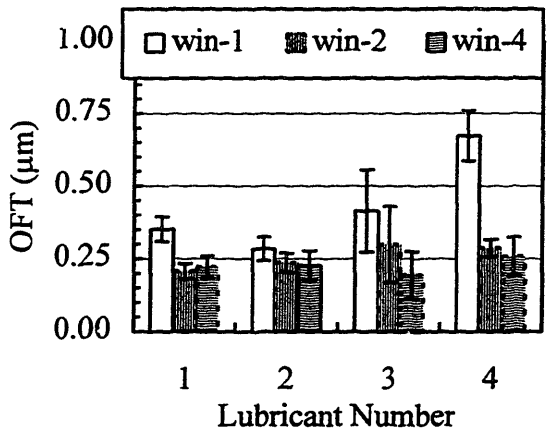

(a) Free Liner (reference)

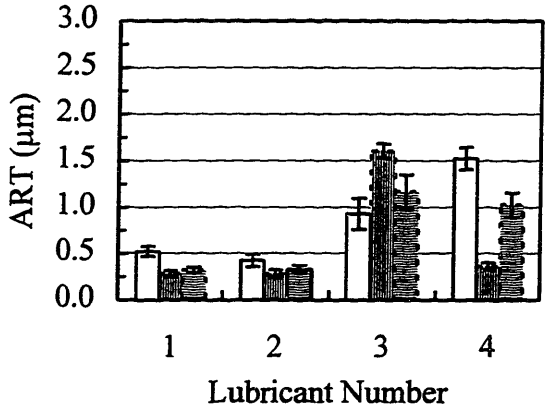

(b) Crown Land Region

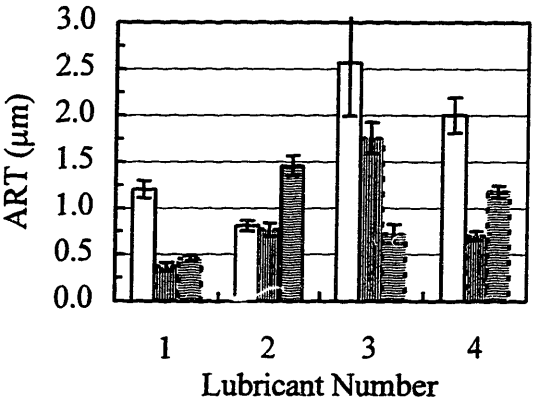

(c) Second Land Region

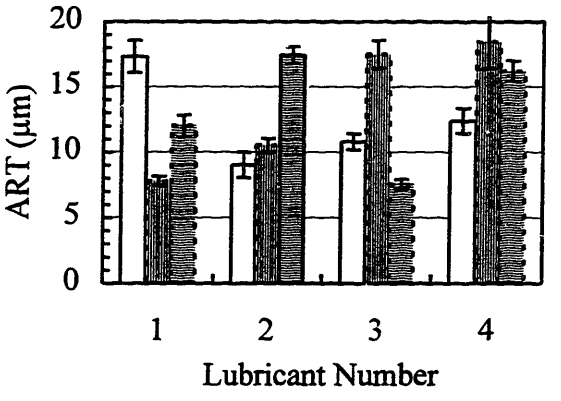

(d) Third Land Region

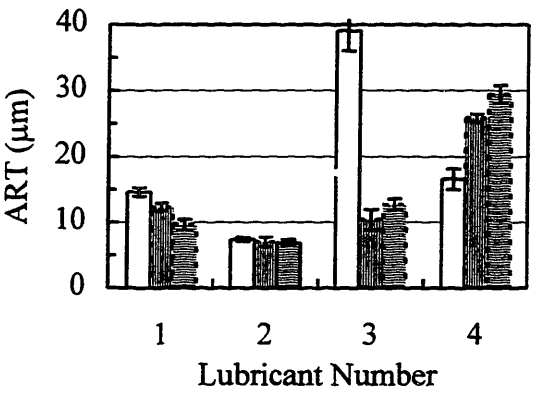

(e) Between OC Rails -- Upstrokes

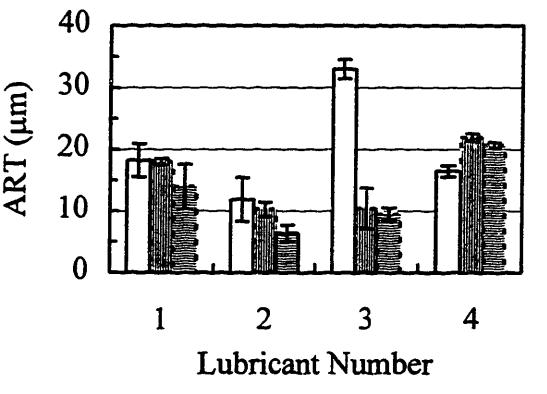

(f) Between OC Rails -- Downstrokes

Figure 5-49 Azimuthal ARTs at Windows 1, 2, and 4 for Selected Lubricants and Operating Conditions for the Ring Pack Including the (a) Free Liner (reference), (b) Crown Land Region, (c) Second Land Region, (d) Third Land Region, (e) Region between OC Rails -- Upstrokes, and (f) Region between OC Rails -- Downstrokes.

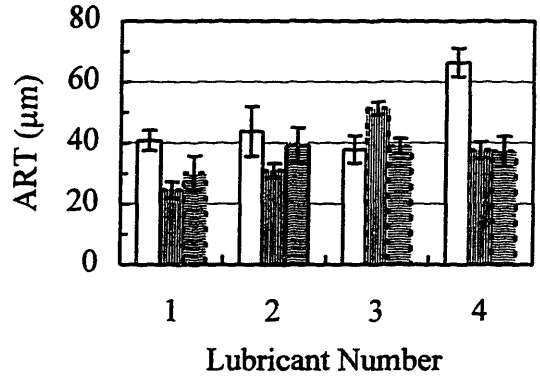

(a) Piston Chamfer Region, Region 5 -- Upstrokes

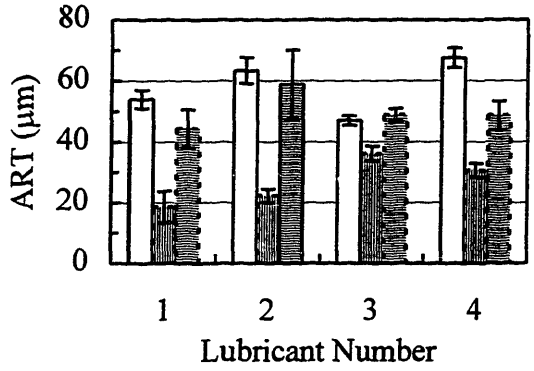

(b) Piston Chamfer, Region 5 -- Intake

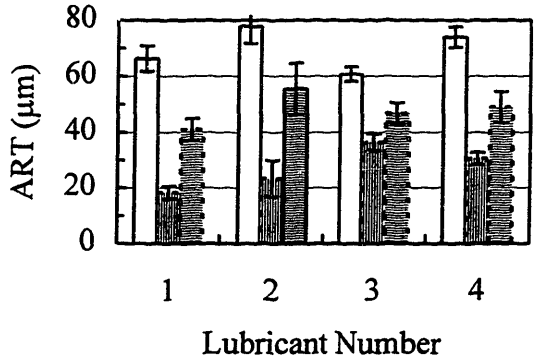

(c) Piston Chamfer, Region 5 -- Expansion

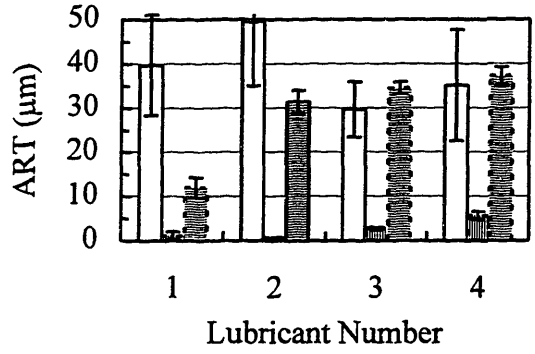

(d) Region 6 -- Upstrokes

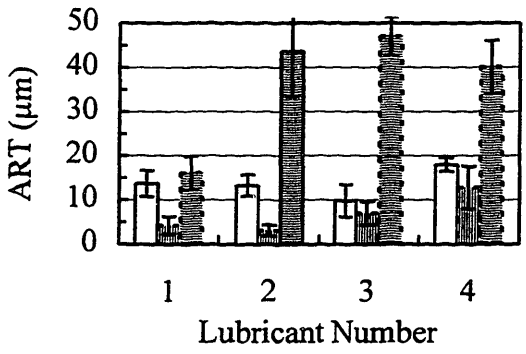

(e) Region 6 -- Downstrokes

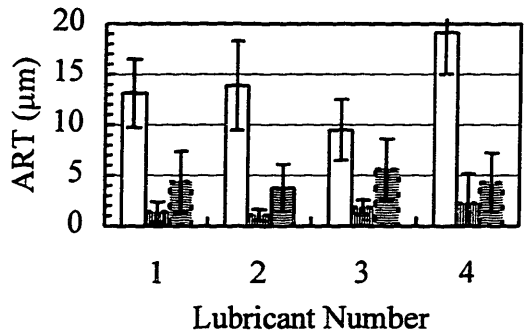

(f) Region 7 (Lower Piston Skirt Region for Major-Thrust Side)

Figure 5-50 Azimuthal ARTs at Windows 1, 2, and 4 for Selected Lubricants and Operating Conditions for Regions Below the OC Ring Including the (a) Chamfer Region (Region 5) -- Upstrokes, (b) Region 5 -- Intake, (c) Region 5 -- Expansion, (d) Region 6 (Upper Piston Skirt for Major-Thrust Side) -- Upstrokes, (e) Region 6 -- Downstrokes, and (c) Region 7 (Lower Piston Skirt for Major-Thrust Side).

For the ring-pack regions in Figures 5-49 (a) - (f), no strong trends exist for azimuthal effects, contrary to the clear OFT trends for the free liner and the top and scraper rings found in section 4.6. After subtracting the free liner OFTs from the crown region ARTs, negligible oil exists except for the motored case (lubricant 3) for all windows and the anomaly for lubricant 4 at window 1 (as explained in sections 5.4.3). As found in many other sections, the ART patterns on the second land (after subtraction of the liner OFT) resemble the third land patterns although the magnitudes between the two regions are an order of magnitude different. Again, this result suggests a strong oil transport links between the regions via the gaps and grooves.

If one restricts the study to only the most accurate cases for all the windows, only SAE-30 (lubricant 2) provides the highest accuracy with only window 2 having questionable high accuracy. For this lubricant, ARTs increase for the second land and third land region as measurements are compared off the major-thrust side referenced to window 1, especially for window 4. This trend is opposite to the OFT trend for the free liner and top and scraper rings which can help explain this ART trend. From section 4.6, the local radial ring pressure changes azimuthally on the lubricant film due to bore distortion. Higher local ring pressure is exerted at windows 2 and 4 compared to window

1. Thus, compared to window 1, less oil is allowed to pass by the scraper ring resulting in reduced OFTs but increased second ring scraping contributing to greater ARTs within the third land. Since the second and third land regions are strongly linked, the oil on the second land reflects the increased oil within the third land region.

ARTs for regions below the OC ring are shown in Figures 5-50 (a) - (f). Not only does the piston below the OC ring have different geometries from window to window around midstroke (except for region 5), but region assignments are different as shown in Figures 5-2 (a) - (c) and addressed at the beginning of this chapter. These differences must be kept in mind when comparing and interpreting the data from different windows.

However, the piston chamfer region (region 5) is the same geometrically and has the same region assignment from window to window. Although the upstroke ARTs are fairly comparable with slightly lower ARTs at window 2 and 4, the intake and expansion strokes have very low ARTs at window 2 (by roughly a factor of two compared to the thrust-side at window 1) followed by window 4. The large amount of oil at the major-thrust side is probably due to the thrust-side oil transport which moves oil up the upper piston skirt to the piston chamfer region mentioned in section 5.3.2. Window locations off the major-thrust side at windows 2 and 4 lack the large piston skirt regions which contact and transport oil along the liner.

Region 6 includes the upper piston skirt for the major-thrust side and a very small portion of the piston resembling part of the piston skirt at windows 2 and 4. From Figures 5-50 (d) and (e), window 2 is extremely starved compared to windows 1 and 4. ARTs within these regions reflect the oil supply from region 7 shown in Figure 5-50 (f) which shows window 2 having the lowest ART along the liner (absent of the skirt) followed by window 4. Window 1 on the major-thrust side shows higher ARTs by, at least, factors of two and four for windows 4 and 2, respectively. Since the piston skirt passes by window 1 and not 2 and 4 for region 7, the major-thrust side observes greater ARTs from the hydrodynamic lubrication between the lower portion of the piston and the liner.

Despite the large differences from window to window within the regions below the OC ring, a majority of the differences within the ring pack are smaller especially

between the OC rails. Largely caused by different skirt geometries and piston motion on oil behavior, the large ART differences (from window to window) below the OC ring do not drastically affect the azimuthal oil behavior for the regions within the piston ring-pack mostly caused, in part, by local radial ring pressure differences on the lubricant film from bore out-of-roundness.

5.7 DIRECT OBSERVATION OF OIL TRANSPORT MECHANISMS

Oil Squeezing between rings and their grooves and the piston skirt and the liner, ring scraping, oil dragging from gas flows, inertial forces on oil oil masses, and viscosity restriction on oil flow are all significant mechanisms related to oil transport, and their effects are directly observed in the oil distribution traces.

5.7.1 Oil Squeezing Between Top Ring and Groove

Top ring oil squeezing between both the top flank of the ring and top of groove and bottom flank and bottom of groove is directly observed for most lubricants and operating conditions. However, oil Squeezing between the second ring and its groove is detected for certain conditions under such as motoring or low engine speeds and may be explained by gas flow behavior which drags oil. Oil Squeezing for the OC ring is obscured by the massive oil masses in the ring which accumulate, in part, from oil scraping. This section references the sections in this chapter that relate to oil squeezing for the ring interactions with their grooves.

Section 5.3.2.1.1 addresses the stroke-by-stroke behavior of oil squeezing for the top and second rings within their grooves which is heavily contingent upon ring dynamics throughout a cycle. The *RINGPACK-OC* model which numerically predicts ring relative lift within the grooves is validated for the top ring lift throughout a cycle against the oil squeezing data from midstroke windows as well as near bottom center at window 6.

Section 5.4.3 addresses the oil squeezing dependence on engine load between firing at 2/3 load and motoring at WOT. Unlike the fired cases, the top land is not completely dry for the motored cases, and the second land typically has more oil than the

fired cases. The increased oil availability accompanies greater oil squeezing. Both the difference in piston and gas-flow temperatures and gas flows through gaps and grooves between the fired and motored conditions account for these different oil distributions.

Section 5.5 includes the oil squeezing dependence on engine speed from 1800 to 2500 rpm between the top and scraper rings and their grooves under the fired conditions. Not only does the oil distribution on the second land significantly increase with speed, but the spatial oil distribution along the second land region changes from changing gas flows which drag oil.

5.7.2 Down-Scraping of Scraper Ring Along a Stroke

In addition to squeezing with its groove, a ring may scrape oil along the liner with a fully-flooded convergent wedge. The worn taper-faced second ring scrapes throughout a downstroke with its fully-flooded convergent wedge shown in a schematic and oil distribution trace in Figures 5-51 and 5-52, respectively. An example of down-scraping from the model predictions is shown in Figure 5-51 (b). Relative to the ring, the approaching oil film on the liner within the third land region is sufficient enough to fully flood the narrow convergent wedge of the scraper ring during a downstroke. A fraction of this approaching oil is scraped and carried by the scraper ring while the remaining oil passes underneath it. Accompanying the predicted oil on the liner in the figure are the thrust-side window locations -- window 1 and 6 at midstroke and near BC, respectively.

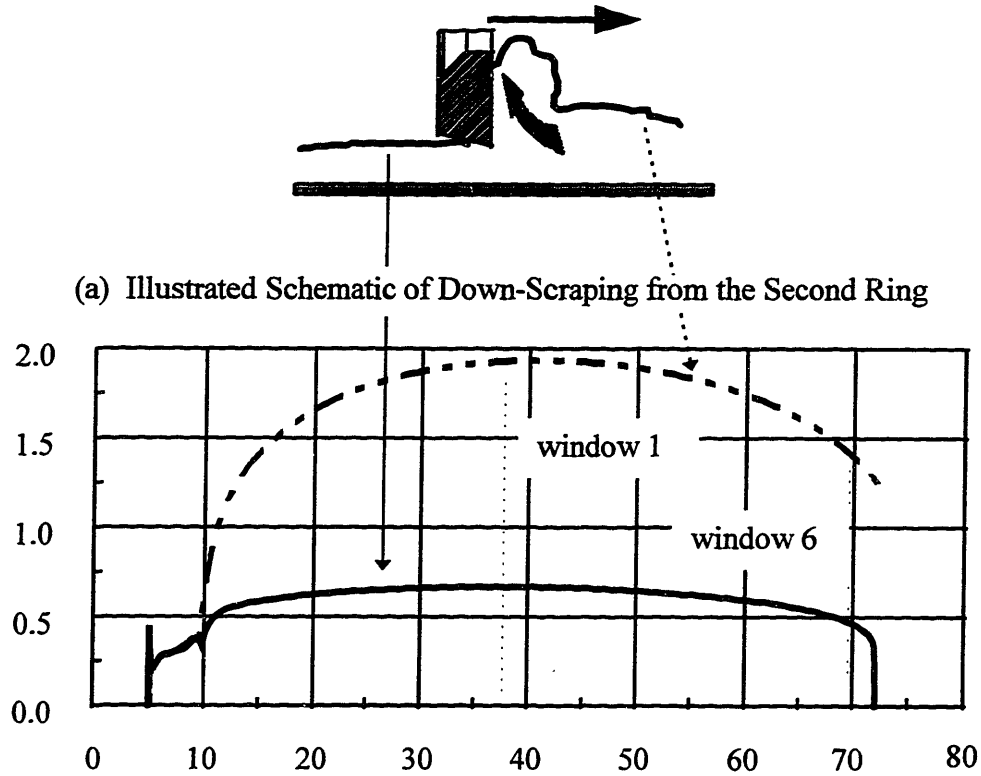

(a) Illustrated Schematic of Down-Scraping from the Second Ring

(b) Model Predictions of Approaching and Existing Liner Oil Films

Figure 5-51 Down-Scraping of the Second Ring from (a) an Illustrated Schematic and (b) Model Predictions of Approaching and Exiting Liner Oil Films

With the 1-D LIF system and multi-window access along a stroke, the amount of down-scraping can be measured. Figure 5-52 (a) shows two oil distribution traces within the piston ring pack during a downstroke. The solid trace corresponds to the measured oil film from window 1 at midstroke. The dotted trace is from window 6. Shown in Figure 5-52 (b) averaging each oil distribution trace within the third land region as described in section 5.1, results in average region thicknesses (ARTs) correspond to near BC and midstroke. In this order, the difference represents the amount of measured down-scraping in terms of an average height shown in Figure 5-52 (c).

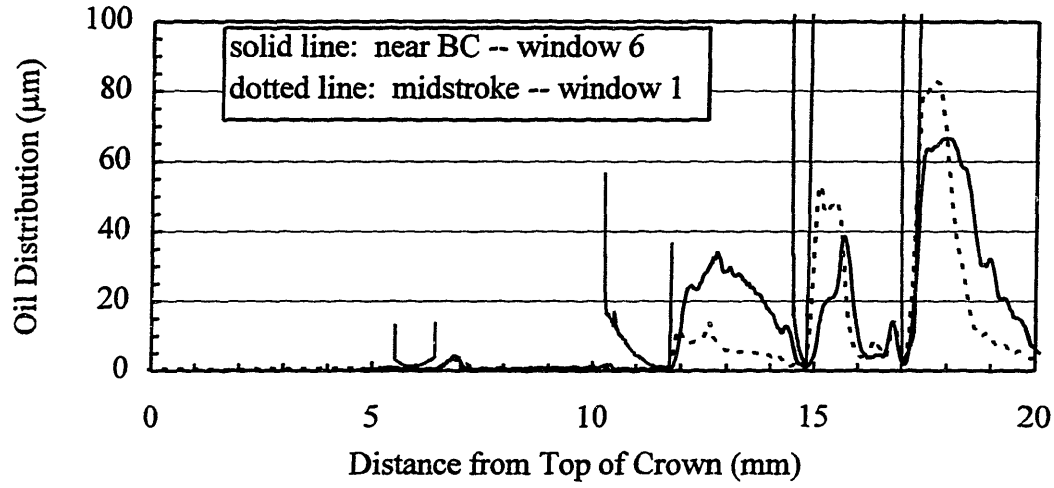

(a) Entire Oil Distribution Traces

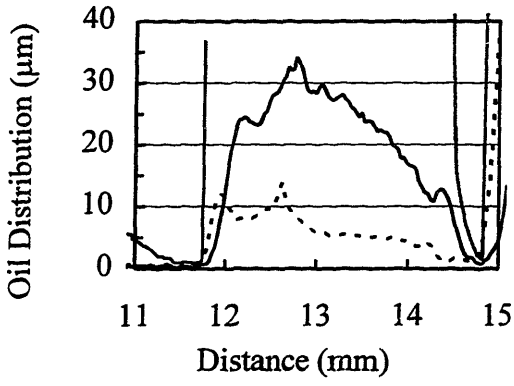

(b) Third Land Region

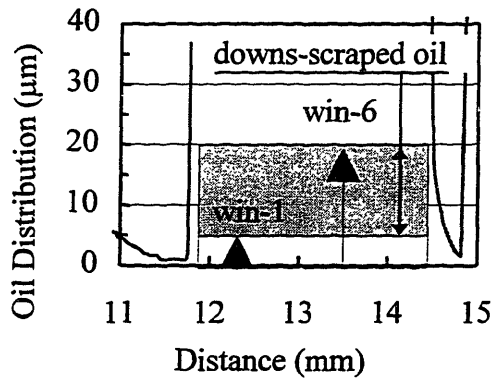

(c) ART in Third Land Region

Figure 5-52 Measured Oil Down-Scraping Shown by (a) an Entire Oil Distribution Traces, (b) the Third Land Region, and (c) the ART in Third Land Region from Window 1 to Window 6 (SAE-10W/50n, 2500 rpm, Motored WOT at 40°C)

It is important to note that not all the oil in the third land region is due to down-scraping during one stroke; this is why a difference between the windows was employed. Some oil on the land may have accumulated from the previous stroke or built up over many cycles over a much larger time scale than for a single stroke. So it's important to take the difference in order to subtract off the oil accumulated from previous strokes or cycles.

Lubricant cases with large amounts of measured down-scraped oil are tabulated along with down-scraping predictions from the *FRICTION-OFT* model in Table 5.3. In fact, the exact model output files from the OFT analysis in Chapter 4 were used for the down-scraping calculations, and, thus, no input parameters were tampered with. Only cases with high calibration accuracy are used from Table D.1.

Lubricant (SAE-Grade)	Condition (temp - f/m)	Downstroke	Down-Scraped Oil in Average Region Thickness, ART (μm)		
			Data	Model - no tilt	Model - tilt
10W	40°C - m	intake	5.76	18.60	18.60
		expansion	3.40	18.66	11.90
10W/50n	40°C - m	intake	16.68	24.38	24.38
		expansion	13.93	24.45	16.31
30	60°C - m	intake	1.68	19.83	19.83
		expansion	0.17	19.90	12.84
50	100°C - f	intake	2.58	12.38	12.38
		expansion	5.15	12.44	7.20

Table 5.3 Scraper Down-scraping from Window 1 to 6 -- Measurements and Predictions with and without Expansion Tilt

Measurements show significant amounts of oil scraped by the scraper and transported downward. Only at low temperatures did the thinner lubricants such as SAE-10W and -10W/50n show substantial scraping. This result is probably due to the lower OFTs under the rings. As the OFT under the rings is lower for less-viscous lubricants, the amount of oil that's left on the liner approaching the scraper in the third land region from the upper OC rail is much less. This decreased oil supply results in less oil scraping.

When the piston tilt is neglected, the model predictions overpredict the data -- typically over a factor of two. However, the model still predicts the general trend from

lubricant to lubricant. For instance, SAE-10W has less down-scraping than 10W/50n but comparable down-scraping with SAE-30 for both the measurements and predictions.

As in the free-liner OFT analysis in section 4.2.3.3.1, negative piston tilt effects during the expansion stroke on the major-thrust side may affect the oil down-scraping within the third land and account for the higher intake height compared to expansion. Piston tilt can affect the orientation of the narrow fully-flooded convergent wedge shown in Figures 4-15 (a). Along the major-thrust side, less down-scraping will occur during the expansion stroke because more oil will be allowed to pass under the ring and, thus, less down-scraping in the third land region. This effect is observed in most of the data from down-scraping from window 1 to 6 shown in Table 5.3 (except SAE-50).

Again, the predicted tilt can account for the measured intake and expansion differences but grossly overpredicts this difference by a rough factor of three for SAE-10W and -30 and less for the other two cases. Other effects may account for these differences such as ring tilt within its groove as explained in section 4.2.3.3.1 and oil transport from lubricant dragging from the different gas flows for the motored and fired conditions.

5.7.3 Lubricant Dragging from Gas Flow

High velocity gas flows through narrow passages such as ring gaps and between rings and their grooves may drag and transport oil residing in these areas. Predicted and designed to be occurring within this Kohler engine, second ring flutter is intended to help retain oil below the scraper ring keeping the first and second lands dry [10] -- highly favorable for low oil consumption. Oil distributions along the second land and gas flow predictions show definite signs that oil transport from lubricant dragging from gas flows is occurring. The small amounts of oil on the second land especially compared to other gasoline engines [31, 32, 33] further supports this argument as well as a close look at the oil distributions and ring-and-groove oil squeezing within the second land region discussed below.

The large positive pressure drop across the scraper as shown in Figure 4-18 (a) for 2500 rpm at 2/3 load during expansion induces high gas flows through the narrow second

ring gap and groove which drag oil residing in the vicinity and transports the oil downward as the second ring flutters as shown in Figures 4-18 (a). The gas flows are substantial enough to leave relatively little oil near the second ring on the lower portion of the second land and in the second ring's groove precluding oil squeezing despite the vast oil accumulated very close by within the third land region as shown in the oil distributions in Figures 5-43, -44, and -45 for 2500 rpm (section 5.5 for the speed effect) and Figures 5-34, -35, and -36 for the fired (section 5.4.3 for the load effect).

Although the lower channel of the top ring and the upper channel of the second ring are adjacent to the second land which directly connects any oil transport between the two, the amount of oil squeezing differs greatly between the two channels probably caused by the difference in channel gas flows. For the fired condition at 2500 rpm, the predicted gas flows within the lower channel of the top ring are negligible shown in Figures 5-38 (b) compared to the second ring shown in Figures 5-38 (c) where ring flutter causes less ring sealing (Figure 4-18 (b)) , allows much higher gas flows (Figures 5-38 (c) and (d)), and, thus, provides greater lubricant dragging out of this channel resulting in less oil squeezing. So, for the baseline condition, oil distribution on the second land, if not uniform, has greater proportion of oil on the upper portion of the second land ompared to the lower portion near the second ring groove where higher gas flows exist. A good example is shown in Figures 5-17 (a) and (b)for SAE-50 and -10W, respectively, under the fired baseline condition. Also insightful though, is the second ring upper channel gas flows which are greater than the gap flows by at least a factor of two compared between Figures 5-38 (c) and -39 (b), respectively. This difference in groove and gap flows is found in other works as well [10].

However, as gas flows change as engine operating conditions change, the amount of lubricant dragging changes as well. Although ring dynamics don't show a large difference between the motored and fired conditions comparing Figures 5-37 (b) and 4-18 (b), respectively, gas flows via ring grooves and gaps change dramatically and are contrasted in Figures 5-38 and -39 (section 5.4.3 for the load effect). Because gas flow rates significantly decrease, less oil is dragged down towards the third land region resulting in a greater amount of oil along the crown and second lands and within the

channels between the rings and their grooves shown in Figures 5-34, -35, and -36 comparing the motored and fired conditions.

The amount of oil squeezing between the top and bottom channels of the top ring (shown in Figures 5-34, -35, and -36) differ because of two reasons related to gas-flow oil dragging. One, gas flows through the lower channel shown in Figure 5-38 (b) are relatively negligible (due to good lower ring sealing from lack of top ring lift throughout most of the cycle) compared to the high flows in and out of the upper channel shown in Figure 5-38 (a). Thus, much less oil is dragged out of the lower channel than the upper channel and, consequently, more oil resides within the lower channel for oil squeezing. Two, top ring relative lift is always down except for the intake stroke resulting in high contact pressures for oil squeezing between the ring and its lower groove.

For changes in engine speed from 1800 rpm to 2500 rpm addressed in section 5.4, both ring dynamics especially for the scraper ring and gas flows change as well and, consequently, oil dragging.

Despite the large stroke-by-stroke differences of gas flows through the second ring gap and groove shown in Figures 5-31 (b) and -32 (b) which drags lubricant (especially for expansion stroke accompanied by second ring flutter), no stroke-by-stroke differences in oil distribution are detected around the scraper ring for the third land region and the second land region. Additionally, in view of standard deviation, no more oil is accumulated within the third land region during the expansion and exhaust strokes compared to the compression stroke. Nevertheless, the lack of stroke-by-stroke differences does not disprove an absence of oil dragging; perhaps the steady-state running condition of the engine is not extreme enough to cause a stroke-by-stroke affect. However, over long time scales, effects of different gas flows on oil distribution and ARTs induced by different engine running conditions including the different loads and speeds are shown in sections 5.4.3 and 5.5, respectively.

5.7.4 Inertial Forces and Viscosity Restriction on Oil Flow

The largest oil masses exist along the third land region, between the OC ring segments, and along the region of the upper piston skirt largely due to scraping of the

second ring and OC rails. As the piston speeds up and slows down, these large oil masses experience enough inertial forces to drive the lubricant back and forth within the regions and provide opportunity for oil transport between rings and through their grooves and gaps. Lubricant properties such as density and viscosity take a significant role as well. Viscosity allows thinner oils to move more freely and thicker oils less freely.

The restricting effect of viscosity for thicker oils or lubricants which transition to higher viscosities at lower temperatures is directly observed as well as inertial effects from oil distribution patterns particularly in the region between the OC rails. Since the rails are relatively symmetric around the expander, the inertial and viscous effects may be seen clearly during the upstrokes and downstrokes on the oil accumulated from rail scraping.

Figures 5-53 (a) and (b) show the oil distributions from region 3 and 4 for the gas exchange and power strokes, respectively. Inertial and scraping effects are predominant with the restriction of viscosity relatively low due to the low viscosity. Therefore, oil especially between the OC rails is able to move back and forth rather freely and up against the rails. During the downstrokes in Figure 5-53 (a) and (b), upper OC rail down-scraping builds up oil against its lower flank with help from inertial forces which are up (see Appendix D) during the former portion of the downstroke. For the former half of the upstrokes, inertial forces are down with the lower OC rail up-scraping and, consequently, most of the oil banks up against its upper flank. This same inertial effect can be observed within the third land regions in the figures.

However, the forces on the oil masses are not very high because these regions are around midstroke, and lubricant viscosity resists and retards the inertial force effects especially for higher viscosities. With approximately the same amount of oil between the OC rails, the oil distribution for a much lower temperature or higher viscosity is shown in Figures 5-54 (a) and (b). As the temperature is decreased from 100 to 60°C and the lubricant's viscosity increases over 200 percent from 8.4 to 27.7 cSt, the increased viscosity restriction on oil flow is directly observed, and inertial forces loose its dominant role as seen in regions 3 and 4. Although scraping still occurs, shifting of the oil is much less and arbitrarily favors a greater proportion against the upper OC rail in region 4.

Since the oil accumulation between the two cases corresponding to Figures 5-53 and -54 are approximately the same (see section 5.3.1), the inertial forces don't change from case to case in this instance.

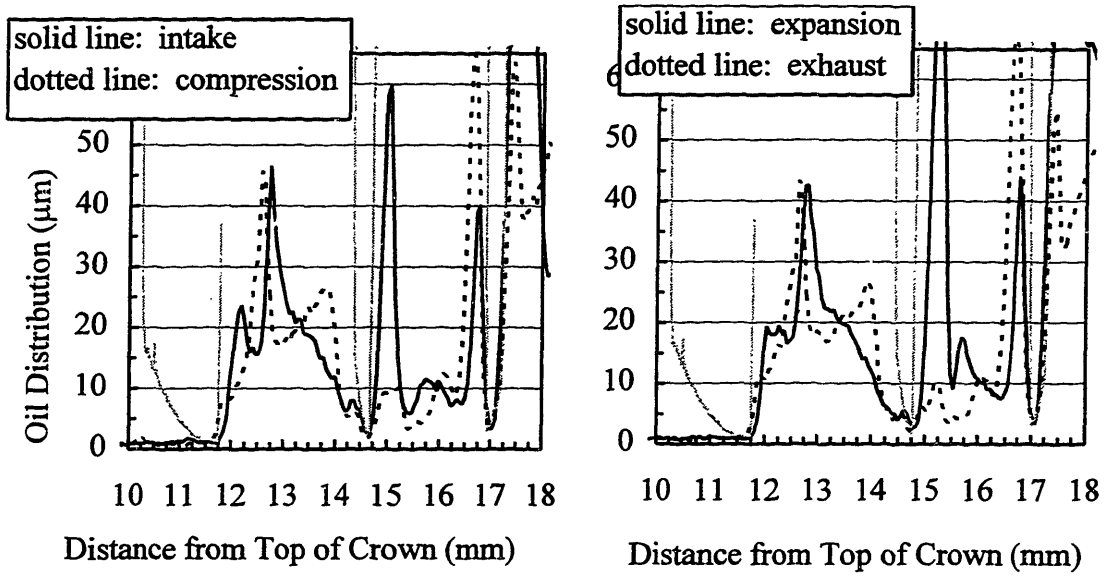

(a) Intake and Compression Strokes (b) Expansion and Exhaust Strokes

Figure 5-53 Oil Distribution Comparison at Midstroke Downstrokes (solid line) Versus Upstrokes (dotted line) for 8.4 cSt at 100°C
(SAE-10W/50n, Window 1, 2/3 load)

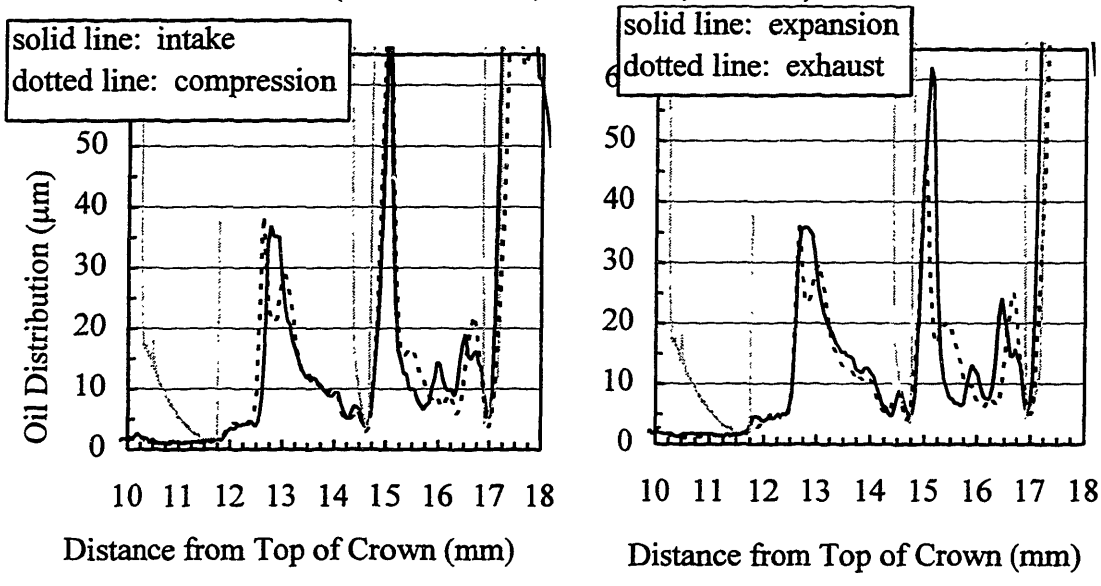

(a) Intake and Compression Strokes (b) Expansion and Exhaust Strokes

Figure 5-54 Oil Distribution Comparison at Midstroke -- Downstrokes (solid line) Versus Upstrokes (dotted line) for 27.7 cSt at 60°C
(SAE-10W/50, Window 1, 2/3 load)

Since piston accelerations increase as the piston moves away from midstroke to near BC (from window 1 to 6), inertia forces increase their dominance over viscosity reluctance on oil flow. For the thin SAE-10W at midstroke, the inertial forces accompanied by scraping dominate over relatively weak restriction in viscosity shown in Figures 5-55 (a) and (b) from midstroke. As inertial forces grow from increasing accelerations off midstroke towards window 6 near BC, inertial forces move a large proportion of the oil up against the lower OC ring even during the downstrokes while the upper OC rail is down-scraping shown in Figures 5-56 (a) and (b). Again, the oil masses between midstroke and near BC are roughly the same and may be qualitatively verified (see section 5.3.1).

Comparing midstroke and near-BC measurements but for the thickest SAE-50, Figures 5-57 and -58 show the reduced influence from inertial forces mitigated by the restriction of high viscosity. As with SAE-10W/50n at 60°C in the first example, shifting of the oil for the thick SAE-50 is much less compared to the thin SAE-10W. However, for SAE-50, greater proportion of the oil distribution arbitrarily favors residing against the lower OC rail in Figures 5-57 (a) and (b). While inertial influences are relatively low compared to the viscous restriction, the scraping effects are more visible in Figures 5-58 (a) and (b).

In summary, it has been shown that both inertial forces (dependent upon oil volume and density) and lubricant viscosity must be taken into when developing the physical mechanisms inherent to any complete oil transport model.

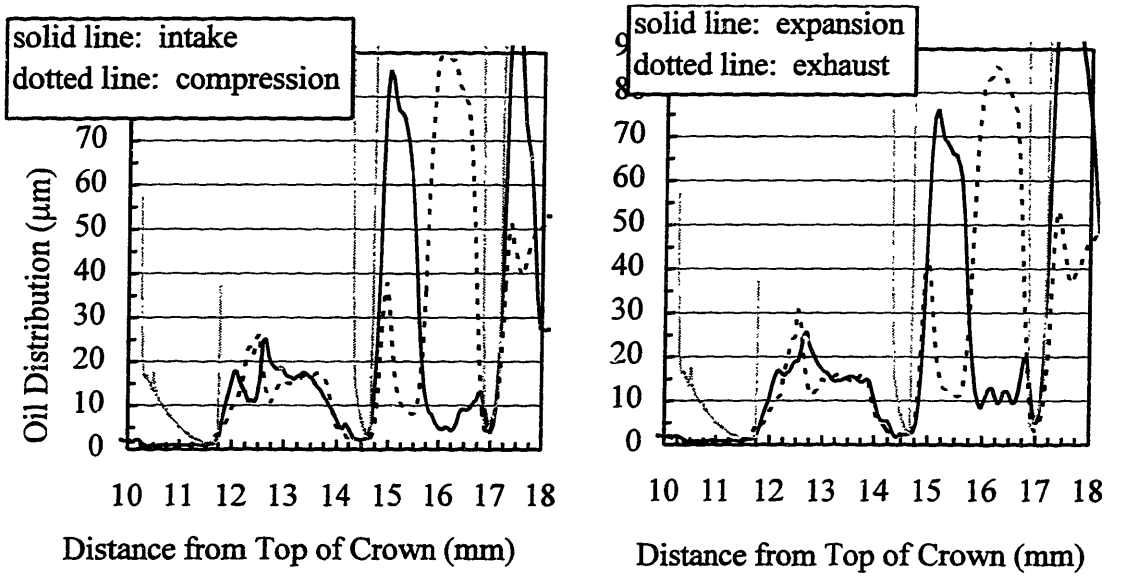

(a) Intake and Compression Strokes (b) Expansion and Exhaust Strokes

Figure 5-55 Oil Distribution Comparison at Midstroke -- Downstrokes (solid line) Versus Upstrokes (dotted line)
(SAE-10W, Window 1, Motored (WOT), 40°C)

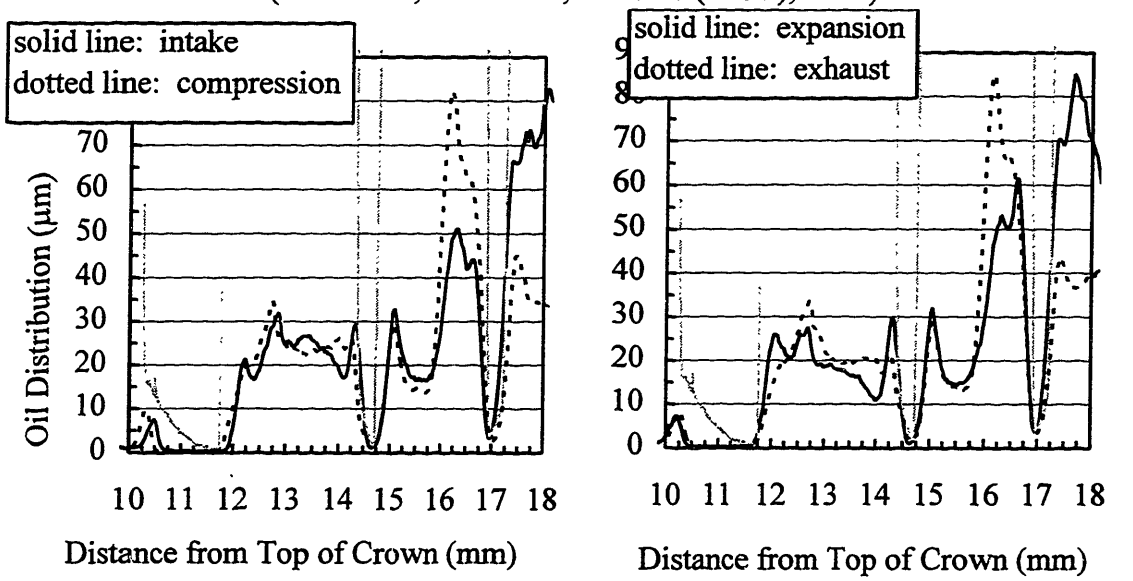

(a) Intake and Compression Strokes (b) Expansion and Exhaust Strokes

Figure 5-56 Oil Distribution Comparison near BC-- Downstrokes (solid line) Versus Upstrokes (dotted line)
(SAE-10W, Window 6, Motored (WOT), 40°C)

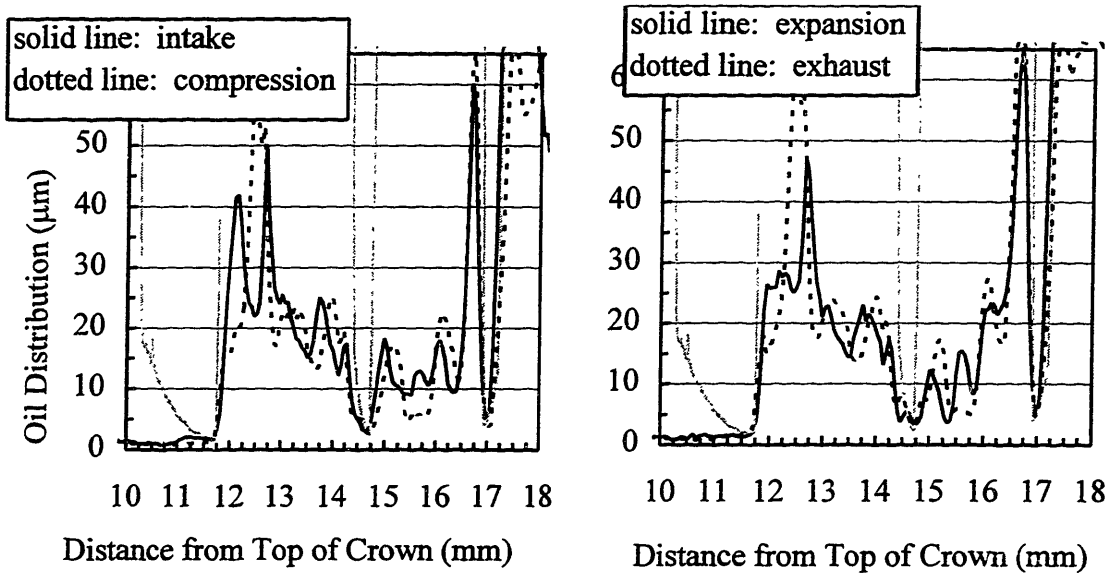

(a) Intake and Compression Strokes (b) Expansion and Exhaust Strokes

Figure 5-57 Oil Distribution Comparison at Midstroke -- Downstrokes (solid line) Versus Upstrokes (dotted line)
(SAE-50, Window 1, 2/3 load, 100°C)

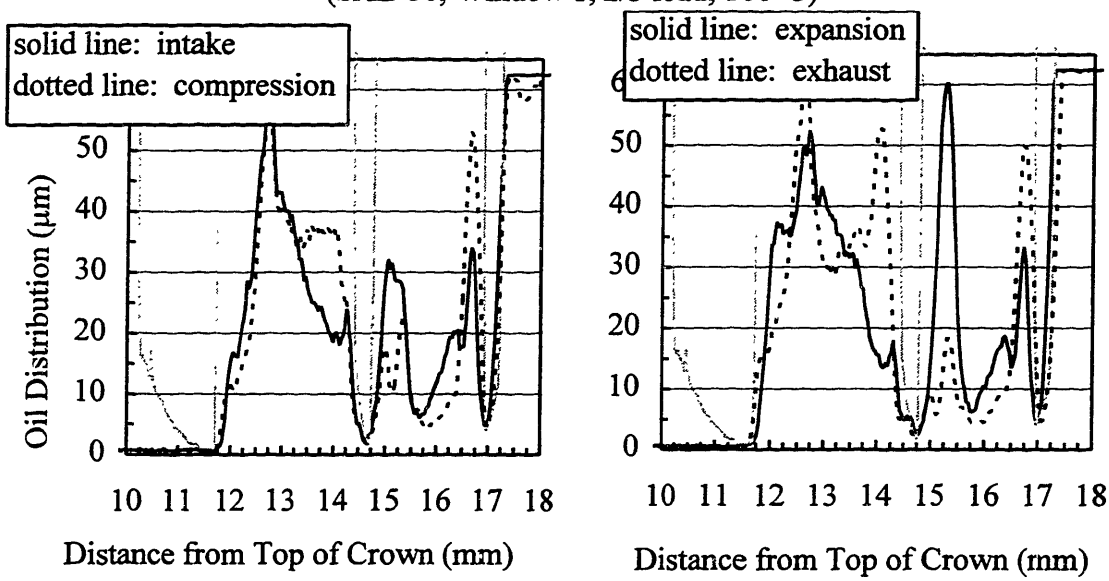

(a) Intake and Compression Strokes (b) Expansion and Exhaust Strokes

Figure 5-58 Oil Distribution Comparison near BC -- Downstrokes (solid line) Versus Upstrokes (dotted line)
(SAE-50, Window 6, 2/3 load, 100°C)

5.7.5 Oil Behavior Along Piston Skirt – Thrust-Side Oil Transport

Section 5.3.2.2.1 directly characterizes the stroke-by-stroke oil behavior of the oil distribution below the OC ring on the major-thrust side from both midstroke and near-BC windows and shows that thrust-side oil transport up the groove/chamfer region (region 5) and azimuthally around the skirt is occurring as the piston reciprocates through top center during both the gas exchange and power strokes. In addition to hydrodynamic lubrication, clear influences of oil transport mechanisms are observed including oil scraping and squeezing and driving from inertial forces. Because the regions below the OC ring supplies the upper regions with oil and experience the highest dynamic transport environments especially at top center when the OC ring is lifted, OC ring lift around TC provides a great opportunity for oil to be transported from the groove/chamfer region to behind the OC ring as oil is driven up the groove/chamfer region from the upper piston skirt region. Therefore, in addition to oil flow from hydrodynamic lubrication under the lower OC rail, other oil pathways include the groove (and also the gap) through which the OC ring may be fed from regions below the OC ring.

(This page is intentionally left blank.)

CHAPTER 6: CONCLUSIONS AND RECOMMENDATIONS

Careful and accurate calibration and quantitative data reduction resulted in extracting as much information from the current database as possible including oil film thickness (OFT) under the rings and along the free liner as well as the oil distribution within the ring pack and along regions below the oil control (OC) ring. The most accurate calibration method proved to be fitting the OFT trace to the upper skirt machining marks during the upstrokes when upper-skirt flooding is most reliable.

OFT Analysis for the Ring Pack and Along the Free Liner

- In view of a correlated Coefficient of Variation (COV) of 18 percent determined from two independent databases, no stroke-by-stroke differences are evident for the ring-pack except for the OC ring where the lower OC MOFTs are greater during the downstrokes than upstrokes. This MOFT trend reverses at 2500 rpm near BC (at window 6). The free-liner on the major-thrust side has greater OFTs for the latter two strokes (the expansion and exhaust) than the former two strokes (the intake and compression). Plausible explanations include effects from piston tilt and land pressures on scraper ring dynamics and are further supported with numerical calculations indicating that the relative contribution of piston tilt on the major-thrust side is much greater (approximately 97 percent) than land pressure effects.
- Shown both experimentally and theoretically, an OFT hierarchy for any single lubricant case within the entire database is as follows. The free-liner OFT is about half of the MOFTs of the top and second rings which are approximately equal. The OC rails always have the greatest MOFTs with the lower OC rail always having the highest.
- For the fired cases at moderate cylinder liner temperatures of 60, 80, and 100°C, the results on and off the baseline condition suggest that the OFT magnitudes and trends

predominantly depend upon lubricant viscosity regardless of liner temperature or chemically-formulated differences between the lubricants. With the exclusion of the strong exception of SAE-50 (from 100 to 80 to 60°C) and the weak exception of SAE-10W/50n (at 60°C from windows 2, 4, and 6) whose OFTs decrease starting in the neighborhood of 30 cSt, ring MOFT and free-liner OFTs increase with lubricant viscosity and agree with rough analytic scaling and the more exact numerical predictions from the *FRICTION-OFT* model. However, the *FRICTION-OFT* model representing the OC ring as a single piece is still inadequate for describing the lower OC MOFT.

- For the motored data, an OFT-viscosity relationship is less clear. However, from 60 to 40°C, OFTs within the entire ring pack and free liner definitely decrease between 30 and 100 cSt for the three moderate lubricants not including the thinnest and thickest lubricants corresponding to SAE-10W and -50, respectively, which usually show a very slight OFT increase with decreasing temperature. SAE-50 is usually higher than the other lubricants especially for the OC segments. Although the dominant effect of viscosity is not as pronounced as the fired cases, numerical predictions sharply diverge by more than a factor of two soon after 30 cSt -- the threshold viscosity for both fired and motored trends. Both the fired trend reversal of the OFT-viscosity relationship including the strong and weak trends of SAE-50 and SAE-10W/50n, respectively, whose OFTs decrease starting in the neighborhood of 30 cSt and the decreasing motored OFT trend starting soon after 30 cSt support the argument that the trend reversal is governed predominantly by viscosity.
- Speed effects on OFT due to engine speeds from 1800 to 2500 rpm (which originally included 3500 rpm as well) and the instantaneous piston speed along a stroke from window 1 to 6 at a constant engine speed are characteristic of hydrodynamic lubrication where measured OFT increases with sliding speed comparable to analytical scaling with the square root of speed and more exact numerical calculations.

- Empirically calculated shear rates on the order of 10^6 1/s are well above the critical shear rate of 40,730 1/s for SAE-10W/50n, and OFTs (including the free liner) at midstroke and near-BC windows only depend upon the high-shear viscosity (insensitive to the low-shear viscosity from shear thinning) and, thus, are not affected by shear thickening.
- Lastly, bore distortion affects azimuthal variations in OFT shown by the free liner and the top and scraper rings. Nevertheless, in view of the small differences (< 1 μm) in azimuthal OFT relative to the maximum radial difference (16 μm) between the windows, proper ring conforming and sealing is occurring. The small OFT differences (but large percent differences) can be explained by differences in local ring pressure from bore distortion. Differences between windows are less pronounced for the OC ring probably attributed to less differences in local OC ring pressures due to its greater flexibility and ring tension.

Oil Distribution Analysis for the Regions along the Ring pack and the Rest of the piston Below the OC Ring

- Within the ring pack, stroke-by-stroke differences in average region thicknesses (ARTs) are significant between the rails of the OC ring and along the second land region only when oil squeezing between the top (and rarely second) ring and its groove is exceptionally high (especially for SAE-50). Between the OC rails (region 4) and independent of azimuthal location, ART downstrokes are often higher than the upstrokes except for the motored cases where the opposite trend exists although less clear for windows other than window 1.
- For the regions below the OC ring, stroke-by-stroke differences are shown to be significant for the groove/chamfer and upper piston skirt regions (regions 5 and 6, respectively) which are caused by piston skirt interactions with the cylinder liner which develop highly dynamic lubricant environments on the major-thrust side from piston secondary motion; oil transport mechanisms including inertial, squeezing, and

scraping are accompanied by the hydrodynamic lubrication characterized along the lower portion of the piston skirt (region 7). Oil transport up the groove/chamfer region and azimuthally around the skirt as the piston reciprocates through top center during the gas exchange strokes as well as the power strokes is shown to significantly occur.

- Since oil squeezing between the top (and rarely second) ring and its groove depends upon relative ring lift which differs from stroke to stroke (i.e., expansion and intake), predicted top ring relative lift (in conjunction with contact pressures) from the *RINGPACK-OC* model is verified by the empirical stroke-by-stroke oil squeezing hierarchy from the top ring and its groove for both the midstroke and near-BC window locations throughout the cycle.
- For all of the fired cases, negligible oil exists on the top crown land due to evaporation, burning, and downward gas flows through the top ring gap and groove which drag oil into the second land region. Oil on the second land ranges from 0.5 to 2.25 microns due to less evaporation from lower piston land temperature, greater lubricant partial pressure within the second land vapor, and absence of burning contribute to more oil. Quite unlike any other regions, ring scraping does not directly contribute to oil on the top and second lands -- only gap and groove oil transport.

Additionally, downward gas flows from the second land (through the second ring gap and groove especially during ring flutter) hold back oil in the third land region which has large quantities of oil -- an order of magnitude higher than the second land -- accumulating, in part, from the down-scraping of the taper-faced second ring. (Pattern (not trend) similarity between the two regions -- a recurring and universal result independent of liner location, lubricant, and operating condition -- further suggests that gap-and-groove pathways are significant within these regions.) Although no clear trend is observed for small viscosity scales (~ 1 cSt) within the second and third land regions, ARTs tend to increase for large viscosity scales (>10 cSt) except for the drop in SAE-50 at 60°C.

Except for the increase of SAE-50 at 60°C for region 4 -- the region between the upper and lower segments, ARTs do not show any clear trends and, although small, variation is random.

From scraping of the lower OC segment having access to a large oil supply below the OC ring, oil within the groove/chamfer region (region 5) is greatest along the entire piston assembly especially for the downstrokes resulting in ARTs which range from 70 to 90 microns on the major-thrust side. ARTs for region 5 increase slightly with viscosity over the entire viscosity range with the upstrokes increasing at a faster rate. However, the downstroke ARTs of region 6 (which are lower than the upstrokes) reveal the same trend as that along region 7 which includes the skirt's largest diameter and strongly resembles the OFT trends for hydrodynamic lubrication; ART (or OFT from the OFT analysis under the rings and along the free liner) increases with viscosity except for SAE-50 which decreases with viscosity corresponding to cylinder liner temperatures of 100 to 80 to 60°C. Although no trends are evident in view of the large standard deviations, the free-liner OFT below the piston skirt -- region 8 (captured by window 6 near BC) -- ranges from 3 to 6 microns. (For the non-major-thrust window locations, results below the OC ring differ from the major-thrust side due to different skirt (or lack thereof) geometries and piston tilt effects but are less interesting and useful.)

- For this engine, the decrease in top ring OFT for SAE-50 is NOT due to oil pumping difficulty for the highly-viscous SAE-50 through the second ring gap and groove supported by ART behavior on the second land. In fact, oil behavior of SAE-50 related to hydrodynamic lubrication (including oil flow under the rings as well as along the piston skirt for regions 6 and 7) experiences a decrease in OFT (or ART for the regions) with viscosity which may suggest that change in viscosity only during engine operation may cause such behavior. However, the cause of viscosity change during engine operation needs yet to be determined.
- Although oil accumulation does not affect the top and scraper MOFTs, oil accumulation along the lands does result, in part, from ring and rail scraping and may

only affect the possibly unflooded upper OC rail MOFT. The empirical oil down-scraping from the scraper ring along a stroke is reasonably predicted by the *FRICTION-OFT* model.

- Gas flow on oil dragging, oil squeezing between rings and grooves and the piston skirt and liner, inertial forces, and viscosity restriction are shown to be influential to accumulation as well.
- Like the fired cases, the motored cases exhibit no general sweeping ART-viscosity trends. However, unlike the fired cases, a small amount of oil ranging from 0.25 to 1.75 microns exists on the crown land for the motored cases. In fact, comparisons of the motored and fired oil distributions show that oil does not only generally increase within the ring pack due to accumulation of oil on the lands but from oil squeezing between the top and scraper rings and their grooves characterized by the sharp spikes along the relatively uniform oil distributions.

Since the regions below the OC ring provide vast but finite oil reservoirs which supply the ring-pack regions, the ART increase within the ring-pack may indicate that less oil is held back in these lower regions from reduced downward gas flows resulting in lesser ARTs observed within these lower regions. As a global measure, predicted blowby from fired to motored decreases by almost half from 3.03 to 1.75 l/minute, respectively, reduced by the fired and motored cylinder pressures corresponding to peak pressures of 31 and 18 bars, respectively.

Although no drastic change in the predicted ring dynamics evident, instantaneous mass flow rates through gaps and grooves of the top two rings decrease significantly especially through the gaps which cause less dragged oil is down towards the third land region and results in a greater amounts of oil along the crown and second lands and within the channels between the rings and their grooves indicated by increased oil squeezing as well. Nevertheless, in addition to oil dragging from gas flows, a host of other factors (i.e., temperatures, thermal expansion, and piston slap) may contribute to load effects on oil distribution to some degree but are very difficult to quantify.

- Along the major-thrust side at midstroke (window 1) and near BC (window 6), the average region thicknesses (ARTs) significantly increase with speed from 1800 to 2500 rpm for all the regions within the ring pack (skirt except for the crown land which has negligible oil) and along the piston. Off the major-thrust side at midstroke for windows 2 and 4, the increasing ART trend with speed isn't as strong. These results along with OFT results further conclude that oil transport pathways through the gaps and grooves (other than under the rings and ring oil scraping) and oil transport mechanisms such as lubricant dragging from gas flows and inertial forces play a significant role.

  One mechanism for increased oil accumulation is inertial forces. Oil travel along the land increases with speed. The average oil displacement along a land during half a stroke scales with engine speed (N) and the square of the local oil thickness (h) and inversely with its viscosity (ν). Measured and calculated oil displacements along the third land agree fairly well and are typically undetectable at 1800 rpm and on the order of 0.5 mm at 2500 rpm.

  A second mechanism is oil dragging by gas flows through the ring gaps and grooves. Predicted ring flutter at 1800 rpm is all but eliminated with only a marginal relative lift resulting in lower groove gap flow. Consequently, the spatial distribution of oil indicates that less groove gas flow develops if gas flow is indicative of oil dragging although the cumulative effect of groove and gap gas flow on lubricant dragging results in lesser oil on the second land for lower speeds.

  Oil squeezing and scraping and inertial influences on oil transport increase and compound with engine speed, and, therefore, increase the ARTs. Allowing more oil to escape to the combustion chamber, this finding is consistent with oil consumption studies which typically correlate an increase in oil consumption with engine speed.
- For the ring-pack regions, no strong trends exist for azimuthal effects, contrary to the clear OFT trends for the free liner and the top and scraper rings found in the OFT analysis. For regions below the OC ring, the large amount of oil at the major-thrust side is probably due to the thrust-side oil transport which moves oil up the upper

piston skirt to the piston chamfer region. Window locations off the major-thrust side at windows 2 and 4 lack the large piston skirt regions which contact and transport oil along the liner.

- Azimuthal randomness in the data as well as the lack of ARTs trends along the crown, second, and third lands are consistent with latest results of complex azimuthal 2-D fluid flows from 2-D visualization of oil distribution employed in the MIT Lubrication Consortium [41]. Gas flow effects are less significant within lower regions of the ring pack reflected in the more-consistent and less-random oil distribution trends found in the current database.

Recommendations

- To fully complete the one-dimensional *FRICTION-OFT*, an accurate model of the three-piece OC ring needs to be developed in place of the one-piece OC ring which is currently employed in order to predict upper and lower rail MOFTs.
- In view of OFT decreasing with viscosity greater than ~30 cSt for SAE-50 (and -10W/50n at 60°C) during firing and most cases during motoring, a more focused investigation is needed to understand this behavior.
- A numerical deflection analysis on the rings may be performed in conjunction with hydrodynamic lubrication to quantify and confirm the azimuthal OFT differences from bore distortion.
- For the LIF system, the experimenter may want to reconsider using coumarin 6 instead of 523. Coumarin 6 fluoresces greater than Coumarin-523 and could possibly increase the S/N ratio.

REFERENCES

[1] Heywood, J.B. (1988). Internal Combustion Engine Fundamentals, New York: McGraw-Hill.

[2] Coy, R.C., Y. Michopoulos, and J.P.T. Wilkinson (1994). "Environmental Impact of Lubricants", *Proceedings of the 21st Leeds/Lyon Symposium of Tribology "Lubricants and Lubrication".*

[3] Tian, T., R. Rabute, V. Wong, and J.B. Heywood (1997). "Effects of Piston-Ring Dynamics on Ring/Groove Wear and Oil Consumption in a Diesel Engine", *SAE Technical Paper 970835.*

[4] Coy, R.C., L.J. Kirsch, T.W. Bates, and P.J. Burnett (1994). "Automotive Lubrication Studies," Presentation at Austrib, Shell Research Thornton.

[5] Stephen H. Hill and Steven J. Sytsma (1991). "A Systems Approach to Oil Consumption" *SAE Technical Paper 910743.*

[6] Peralta, Norman (1997). "The Process of Fuel Transport in Engine Oil", MIT Master's Thesis, Dept. of Mechanical Engineering, May.

[7] Tamai, Goro (1995). "Experimental Study of Engine Oil Film Thickness Dependence on Liner Location, Oil Properties, and Operating Conditions", MIT Master's Thesis, Dept. of Mechanical Engineering, August.

[8] Deutsch, Eric (1992). "Piston Ring Friction Analysis from Oil Film Thickness Measurements", MIT Master's Thesis, Dept. of Mechanical Engineering, February.

[9] Tian, T., V.W. Wong, and J.B. Heywood (1996). "A Piston Ring-Pack Film-Thickness and Friction Model for Multigrade Oils and Rough Surfaces", *SAE Technical Paper 962032.*

[10] Tian, T., B. Noordzij, V.W. Wong, and J.B. Heywood (1996). "Modeling Piston-Ring Dynamics, Blowby, and Ring-Twist Effects", *ASME ICE Fall Technical Conference*, October.

[11] Wu, C.S.P, T. Melodick, S.C. Lin, J.L. Duda, and E. Klaus (1990) , "The Viscous Behavior of Polymer Modified lubricating Oils Over a Broad Range of Temperature and Shear Rate", Journal of Tribology. Vol. 112, July.

[12] Taylor, R.I., T. Kitahara, T. Saito, and R.C. Coy (1995). "Piston Assembly Firction and Wear: the Influence of Lubricant Viscometry", *Proceedings of the International Tribology Conference*, Yokohama.

[13] Internal Study for the MIT Lubrication Consortium, Dr. Tian Tian.

[14] Coyne, J.C., and H.G. Elrod (1970). "Conditions for the Rupture of a Lubricating Film. Part I: Theoretical Model", Journal of Lubrication Technology, July.

[15] Taylor, John R. (1982). An Introduction to Error Analysis, The Study of Uncertainties in Physical Measurements. Mill Valley, California: University Science Books.

[16] Hoult, D. P., V. W. Wong, and J. H. Azzola (1991). "Direct Observation of the Friction Reduction of Multigrade Lubricants", *SAE Technical Paper 910742.*

[17] Noda, T., Y. Masago, C. Yasuhiro, J. Kawamoto, and N. Masahiko (1989). "Analysis of Oil Consumption Mechanism by Measuring Ring Radial Movement", *SAE Technical Paper 892104.*

[18] Moore, S. L. (1985), "Piston Ring Oil Film Thickness -- The Effect of Viscosity", *SAE Technical Paper 950439.*

[19] Tian, Tian (1994). "A Note on Hydrodynamic Friction Coefficient and Minimum Film Thickness of a Piston Ring". Internal Report for the MIT Lubrication Consortium, July.

[20] Schneider, E. W., D.H. BlossFeld, D.C. Lechman, F.H. Hill, R.F. Reising, and J.E. Brevick (1993). "Effect of Cylinder Bore Out-of-Roundness on Piston Ring Rotation and Engine Oil Consumption", *SAE Technical Paper 930796.*

[21] Casey, Steve (1996). "Comparison Against Existing Data and Status Report of Film Thickness and Friction", Presentation at the MIT Lubrication Consortium Meeting, June.

[22] Tian, T. (1997). "Oil Transport Processes in the Ring-Pack: The Scraping Mechanism", Presentation at the MIT Consortium on Lubrication in Internal Combustion Engines, June.

[23] Thirouard, Benoist (1997). "Two-Dimensional Laser-Induced Fluorescence Measurements of Lubricant Behavior in the Ring-Pack", Presentation at the MIT Consortium on Lubrication in Internal Combustion Engines, June.

[24] Hiruma, M., H. Yoshida, S. Furuhama, and K. Shin (1983). "Effect of Piston Ring Movement upon Oil Consumption", JSME, March.

[25] Rae, Jon (1997). "Concurrent Experimental Data on Oil Distribution and Oil Consumption from a Single-Cylinder Diesel Engine", Presentation at the MIT Consortium on Lubrication in Internal Combustion Engines, October.

[26] Ryan, Jim (1993), "Impact Analysis of Piston Slap in a Spark Ignition Engine", MIT Master's Thesis, September.

[27] Furuhama, S, M. Hiruma, and H. Yoshida (1981). "An Increase of Engine Oil Consumption at High Temperature of Piston and Cylinder", *SAE Technical Paper 810976.*

[28] Linna, J.R. (1997). "Contribution of Oil Layer Mechanism to the Hydrocarbon Emissions from Spark-Ignition Engines", MIT Ph.D. Thesis, Dept. of Mechanical Engineering, May.

[29] Linna, J.R. (1997). "Contribution of Oil Layer Mechanism to the Hydrocarbon Emissions from Spark-Ignition Engines", MIT Ph.D. Thesis, Dept. of Mechanical Engineering, May.

[30] Tian, T. (1995). "Modeling Oil-Transport and Oil-Consumption Mechanisms and the Influence of Piston and Ring Dynamics", Presentation at the MIT Consortium on Lubrication in Internal Combustion Engines, June.

[31] Artzner, Denis (1996). "Investigation of Oil Consumption Mechanisms in a Spark-Ignition Engine", MIT Master's Thesis, May.

[32] Lusted, R. M. (1994). "Direct Observation of Oil Consumption Mechanisms in a Production Spark Ignition Engine Using Fluorescence Techniques", MIT Master's Thesis, May.

[33] Mulgrave, P. M. (1997). "Development of a Laser Induced Fluorescence System for Measuring Oil Film Thickness in Two Dimensions in a Reciprocating Engine", MIT Master's Thesis, June.
[34] Tian, Tian (1997). "Modeling the Performance of the Piston Ring-pack in Internal Combustion Engines", Ph.D. Thesis, Dept. of Mechanical Engineering, June.
[35] Hoult, D.P., J.P. Lux, V.W. Wong, and S.A. Billian (1988). "Calibration of Laser Fluorescence System", *SAE Technical Paper 881587.*
[36] Bronchtein, Leon (1993). "Diagnostic Enchancements for the Laser-Induced Fluorescence System", MIT Consortium of Lubrication in Internal Combustion Engines, October.
[37] Lee, M.J. (1993). "Film Thickness Measurements in a Production Spark Ignition Engine", B.S. Thesis, Department of Mechanical Engineering, May.
[38] Hoult and Masaaki Takiguchi (1991), "Calibration of the Laser Fluorescence Technique Compared with Quantum Theory", Tribology Transactions,Volume 34.
[39] Shaw, B.T. (1992). "Direct Observation of the Oil Consumption Mechanism of a Production Single-Cyliner Diesel Engine", MIT Master's Thesis, Dept. of Mechanical Engineering, February.
[40] Hill, S.H., and S.J. Sytsma (1991), "A Systems Approach to Oil Consumption", *SAE Technical Paper 910743.*
[41] Li, Chin-Hsiu (1982). "Piston Thermal Deformation and Friction Considerations", *SAE Technical Paper 820086.*
[42] Tada, T. and S. Furuhama (1964). "On the Heat Flow from the Pistons in a Farm Type Gasoline Engine", Bulletin of JSME, Volume 7, July.
[43] French, C.C.J. and K.A. Atkins (1973). "Thermal Loading of a Petrol Engine", Proceedings of the Institution of Mechanical Engineers, Volume 187, London.
[44] Furuhama, S. and E. Yoshiteru (1973). "Piston Temperature of Automobile Gasoline Engine in Driving on the Road", Bulletin of JSME, Volume 16, September.

(This page is intentionally left blank.)

APPENDICES

APPENDIX A:
OVERVIEW OF THE PISTON/RING/LINER (PRL) SYSTEM AND GOVERNING MECHANISMS OF LUBRICANT BEHAVIOR

This section describes a typical PRL assembly shown in Figure A-1 within a SI engine and the basic functions of its different components in context of the governing mechanisms of lubricant behavior -- lubrication between rings and liner, ring axial and angular dynamics, oil squeezing between rings and their grooves, gas-flow oil dragging, piston secondary motion, and inertia. As the PRL system and lubricant behavior are described, definitions and terminology are established that will be used consistently throughout the remainder of the thesis.

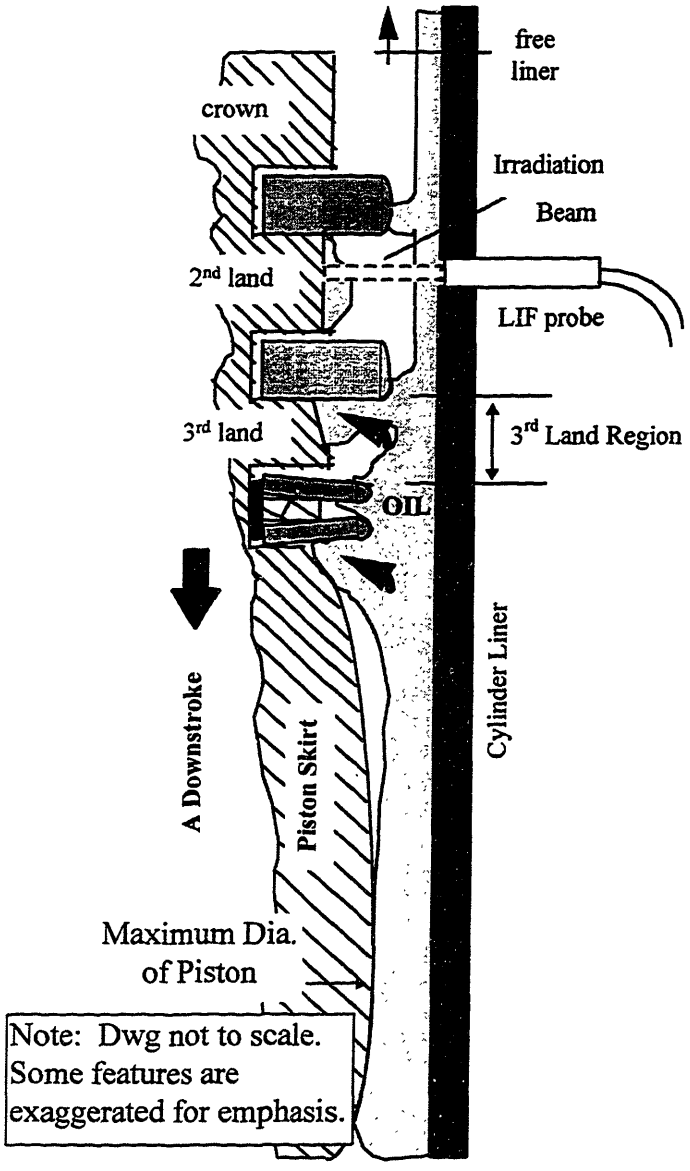

Figure A-1 The PRL System -- the Ring Pack and Piston.

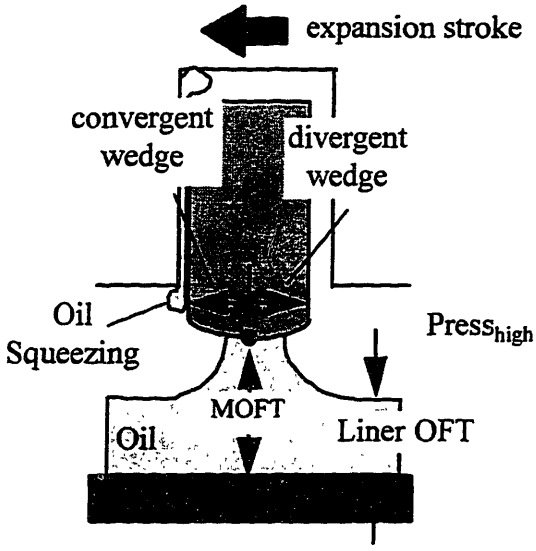

Figure A-2 Top Compression Ring

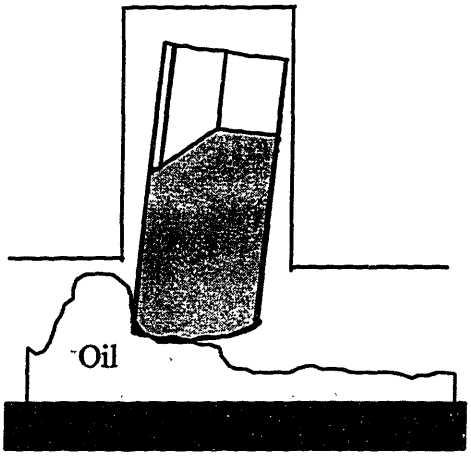

Figure A-3 Scraper Ring -- Scraping and Negative Twist

A.1 LUBRICATION BETWEEN RINGS AND LINER

Lubrication between the rings and liner accounts for about half of the total piston assembly friction and is, of course, responsible for wear. The typical ring pack within an SI engine consists of three rings -- the top compression, scraper, and oil control (OC) rings.

Shown in Figure A-2 the top compression ring is primarily responsible for controlling the high-pressure gas within the combustion chamber. As with most rings, it has adjacent convergent and divergent wedges -- each starting from the lowest point of the ring called the minimum point; the convergent wedge is portion of the ring where the approaching film on the liner attaches itself, and, likewise, the divergent wedge is that portion where the exiting lubricant flow from under the ring detaches. A convergent wedge on a downstroke becomes the divergent wedge on an upstroke. If the lubricant doesn't wet the full width of the wedge, this is an unflooded (or starved) condition. Complete wetting of a wedge constitutes a fully-flooded condition, and ring scraping of oil then occurs. The oil film under the ring at the minimum point is called the minimum oil film thickness (MOFT). After the ring passes, it leaves a film on the liner (or liner OFT). The OFT left after the piston passes during a downstroke is called the free-liner OFT.

On the downstrokes, oil is supplied to the top ring from what liner OFT the scraper ring leaves behind. Shown in Figure A-3, the scraper ring has a relatively small, fully-flooded convergent wedge which down-scrapes oil in the third land region. During an upstroke the starved convergent wedge (which was the divergent wedge in the downstroke) allows all liner oil supplied from the top ring to pass underneath the scraper ring contributing no oil to the second land and, thus, leaving the second land relatively dry. (However, in the present work and others some significant amount of oil has been found on the second land due to gap-and-groove oil transport as mentioned in the next section, A.2.)

Also characteristic of the scraper ring is the negative static twist caused by the chamfer cut into the bottom side of the inside diameter. This negative static twist is

designed to induce ring flutter during late compression and expansion strokes and help blow-down oil from the second to third land to reduce oil consumption [10]. (Further explanation on scraper ring flutter is provided in section A.2.) Aiding the top ring, the scraper ring also helps control gas leakage from the combustion chamber.

The oil scraped by the scraper ring is supplied by an oil control (OC) ring. In the case of a three-piece OC ring, the ring consists of two segments (or rails) and an expander between the two. Often, the rails are not exactly flush with the groove and expander but angled with respect to them. The OC ring's primary function, as the name suggests, is to control the oil flow into the piston ring pack and onto the liner. Supplied with a vast amount of oil from the lower parts of the piston, the OC ring really acts as the first barrier to oil flow. Within the ring pack, its behavior is the least understood.

A.2 RING AXIAL AND ANGULAR DYNAMICS, GAS-FLOW OIL DRAGGING, AND INERTIA OF OIL MASSES

As the piston reciprocates, the PRL system accelerates during the first part of a stroke and decelerates during the last portion of the stroke. Because of the high accelerations and decelerations, inertial forces as well as friction between the rings and liner and gas flow among the lands and piston cylinder play a significant role in the ring dynamics [34] -- both axially and angularly -- which may squeeze oil in and out of ring grooves. Additionally, large oil masses on the piston incur enough inertial force to drive oil back and forth within the lands, up against rings, and through grooves and gaps. These governing motions are probably the most critical understanding for lubricant control and transport.

The forces contributing to ring dynamics -- friction, gas pressures, and inertia -- determine how a ring axially sits in its groove. During most of the cycle, the rings are forced up or down against the ring grooves; for only a small fraction of the cycle is the ring experiencing a transition. Large pressures generated between the ring flanks and the groove squeezes oil out of this channel such as during an expansion stroke shown in Figure A-2. Additionally, if large enough pressures exist, especially for diesels,

significant dynamic twist results, changing the ring's contact distribution within the groove and its relative face profile to the liner causing a normally starved ring to fully flood and scrape oil with its converging wedge.

A special case was mentioned in the previous section for a the scraper ring with negative static twist. A rapid succession of many transitions up and down within the groove due to competing effects of inertia and gas pressures during early- to mid-expansion stroke result in ring flutter whereby significant gas is now allowed to flow between the ring and groove from the second to third land. This mass flow is usually at least as much as regular blowby rates which occurs mostly through ring gaps within the ring pack [10]. This fluttering and gas flow process is good for oil consumption; any oil which happens to be near the scraper ring and groove can be dragged down further into the piston ring pack away from the combustion chamber. Therefore, in addition to the oil pathways between the rings and liner, oil passage may also occur between the rings and grooves and their gaps shown in Figure A-4.

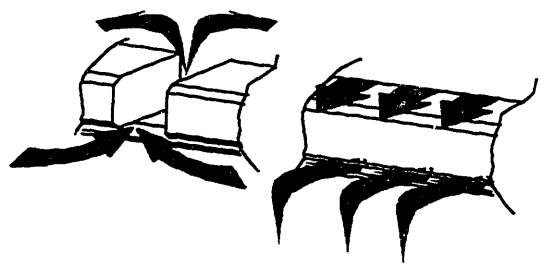

Figure A-4 Gap and Groove Oil Transport

Lastly, large oil masses are present along the third land region, between the OC ring segments, and along the region of the upper piston skirt. As the piston speeds up and slows down, these large oil masses experience enough inertial forces to drive the lubricant back and forth within the regions and provide opportunity for oil transport between rings and through their grooves and gaps. Lubricant properties such as density and viscosity take a significant role here. Viscosity, the property that is a measure of resistance to change shape, allows thinner oils to move more freely and thicker oils less freely.

It is important to note that the oil measured between the OC ring and the scraper does not all directly reside on the third land. As shown in Figure A-1, the nature of the LIF system measures all the oil volume encountered by the incident laser beam. Some oil is on the liner. Because the scraper is scraping on the downstroke, there is most likely some oil on the lower flank of the scraper as well. Therefore, when talking about measured oil, care has been taken to describe its existence as "oil in the third land region" and not "oil on the third land". Taking this thought one step further, in order to quantify oil in these regions, it is helpful to take an average region thickness (or height) of the oil distribution measured along the region denoted by the acronym ART. The general calculation is as follows

$$ART = \frac{\int_{region} OFT(x) \bullet dx}{L} \qquad (A.1)$$

where OFT(x) is the actual measured trace of the oil film along the region and L is the region's length. Complete region assignments are given later in Chapter 5 addressing oil distribution.

A.3 PISTON SECONDARY MOTION

Piston secondary motion involving piston tilt and slap affects lubricant behavior as well. Within the ring pack, piston tilt is enough to significantly change the rings' relative profile to the liner. At major- and minor-thrust sides, tilt effects on ring relative profiles are greatest and, thus, may cause azimuthal variations as well as stroke-to-stroke variations.

The interaction of the piston skirt and cylinder liner accounts for 20 - 30 percent of total engine friction and much of the engine noise. Piston slap provides a fluid dynamic environment for oil along the piston to be forced up along the piston towards the OC ring and azimuthally around the skirt from oil scraping and squeezing, inertial forces, and hydrodynamic lubrication along the skirt's largest diameter (refer to Figure A-1).

APPENDIX B:
EXPERIMENTAL APPARATUS

The experimental set-up consists of three main parts: the one-dimensional LIF system, the modified engine, and the data acquisition system. A schematic of all of the components of the experimental apparatus is shown in Figure B-1.

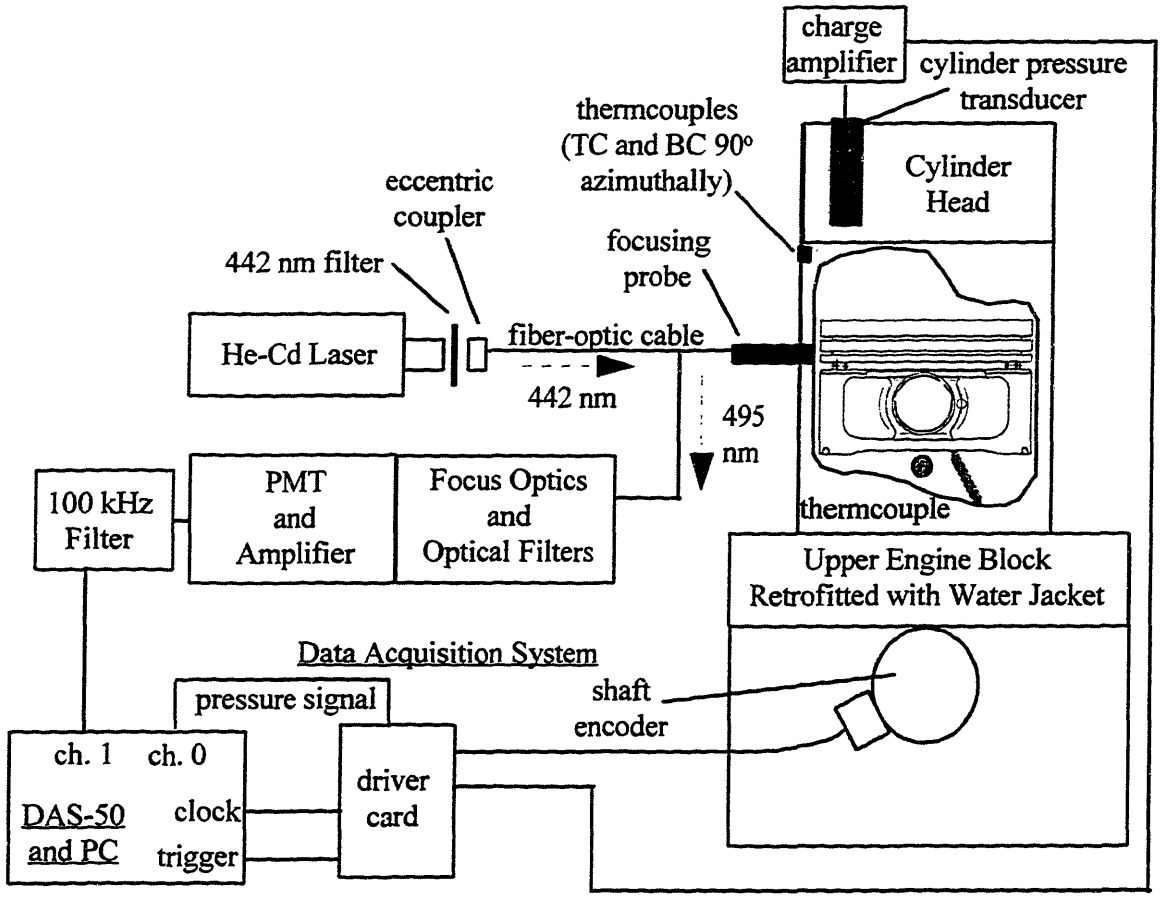

Figure B-1 Schematic of the LIF System, Configured Engine, and Data Acquisition System

B.1 THE MODIFIED ENGINE

General engine specifications and modifications are listed in Table B.1, and drawings for the LIF probes and engine block are given by Deutsch [8].

Engine	Kohler CH-14 single-cylinder spark-ignition. Cast aluminum block with iron cylinder liner.
Displacement	398 cc, bore x stroke = 87 mm x 67 mm.
Connecting Rod Length	112.9 mm
Power	10.5 kW @ 3600 rpm.
Torque	28.9 N-m @ 2600 rpm.
LIF Windows	Six: four at midstroke, one near each endstroke on major-thrust side.
Cooling	Retrofitted water jacket around head, city water @ 4°C.
Thermocouples	Omega K-type, Two: one near top center on thrust side, and one near bottom center 90° offset azimuthally from major-thrust side (clockwise from top view).
Pressure Transducer	One Kistler 6051A with Kistler 503D amplifier mounted in the cylinder head next to spark plug.
Shaft Encoder	Model H25 (Interpolation T2) mounted on the crank shaft. (Bei Motion Systems Company)

Table B.1 Kohler Engine Specifications and Modifications

B.1.1 Window Location and Installation Procedure

Placing multiple windows in these strategic locations as shown in Figure 3-1 allows the experimentalist to capture different effects. First, axial placement at midstroke and near dead centers was chosen to study OFT behavior during a stroke. The tradeoff between high-speed midstroke friction and low-speed endstroke wear may be investigated. Near the endstrokes, the rings are all traveling slower than at midstroke (and at different speeds) due to the slower piston sliding speed. At the midstroke windows, all of the rings approximately pass at maximum piston speed -- about 9 m/s. At near bottom center (BC), the rings pass at different speeds; the lower OC segment and

top ring pass at approximately 6.5 and 2 m/s, respectively. Since the ring MOFTs are governed by hydrodynamic lubrication and dependent upon speed, a comparison of MOFTs of the rings is legitimate at midstroke but not valid near the endstroke. (The relationship between window location and piston kinematics and dynamics are discussed in detail in Appendix D.1.)

In addition to a speed effect, other axial effects along a stroke may be observed such as down-scraping of rings, inertial effects within the different regions, and oil behavior during piston motion reversal.

Secondly, the azimuthal placement of multiple windows at midstroke provides insight to 1) magnitudes and comparison of MOFTs of the different rings all approximately traveling at the maximum piston speed and oil distribution within different regions and 2) azimuthal variations of these measurements. Cylinder bore distortion, window protrusion, piston geometry especially around the skirt, piston secondary motion including tilt and slap, and ring gap location may influence these variations.

Although six windows were installed, two windows were inoperable -- one at TC and the other on the minor-thrust side at midstroke. For the top window, its high transmissivity (normally over 90 percent) dropped to very poor levels because of combustion residue which built up in a matter of minutes. The top window is located within the top five millimeters of the liner where the top ring does not pass. The cause of the failure of the other inoperable window on the minor-thrust side is not clear [7].

The overall goal of successful window installation is the window-to-liner flushness and because an exact flushness isn't possible, a very slight protrusion is more favorable than a recess. (A slight recess could allow air gaps between the oil on the window and the passing ring and, thus, giving an erroneous LIF signal for the MOFT; a further explanation of this is given in section C.3.2, Window-to-Liner Flushness.)

With this goal in mind, the window installation process is as follows. Initially, the windows are carefully installed by hand as flush as possible. Since the silicone adhesive takes several hours to cure, careful adjustments to accurate window seating can be made. A recess of less than 25 microns (which can be felt by hand) is acceptable for subsequent honing. Honing is performed to ensure that the liner-to-window interface is

as smooth as possible. Since the quartz window is harder than the iron liner, more material will be radially removed from the liner than the window. Sufficient honing should then result in flushness or a small protrusion on the order of a micron. (Detailed micro-geometry of the window-to-liner flushness is presented in section C.3.2, Window-to-Liner Flushness.)

Lastly, several precautions were taken during this procedure. To simulate residual pressure loads from a fully-assembled engine during the honing procedure, most of the engine was assembled and a torque plate made out of aluminum was custom built to imitate the cylinder head load. After honing, if the measured bore diameter exceeds the maximum allowable bore diameter, over-sized pistons and ring sets must be selected and are available from Kohler. However, this was not the case for this modified engine, and standard components were used.

B.1.2 Retrofitted Water Jacket

Because of the necessity to flexibly regulate the cylinder liner temperature, engine cooling was changed from air-cooled to water-cooled. Originally, convective cooling fins exposed to the air were cast into the upper engine block and around the cylinder head. A thick aluminum band was stitch welded onto the tips of the fins, and aluminum-based epoxy was used to fill the remaining gaps.

Precautions were taken to avoid the effects of residual stresses on bore distortion by keeping the bore relatively cool during the welding by applying cool wet rags within the cylinder [7].

B.1.3 Thermocouples

In order to monitor cylinder temperature accurately, two thermocouples were imbedded in the liner. Near TC on the major-thrust side, one thermocouple was installed next to the top window (window 5). Another was installed near BC approximately 90° offset (clockwise with respect to the top view) from the major-thrust side. To ensure that the temperature measurements were as close to the liner surface temperature in contact

with the lubricant, the thermocouples were embedded about 60 percent through the iron liner.

By careful control of the water flow within the cooling jacket, the thermocouples can be held within five degrees Celsius of each other. Thus, the midstroke temperature is assumed to be the average of these measurements.

B.1.4 Cylinder Pressure Transducer

Monitoring cylinder pressure was performed by a Kistler pressure transducer mounted in the cylinder head next to the spark plug. The charge amplifier delivers an amplified voltage signal to the driver card which is then recorded by the data acquisition system. (Pressure calibration is addressed in Appendix D on Data Processing.)

B.1.5 Shaft Encoder

In order for the data acquisition system to be clocked at a particular sampling rate, the H25 crank shaft encoder outputs a squarewave at 4000 cycles/revolution and has frequency response of 200 kHz. (The upper limit for its operation is discussed in Appendix D on Data Processing.)

B.2 ONE-DIMENSIONAL LIF DIAGNOSTIC SYSTEM

In-situ measurements of the oil film thicknesses on the cylinder liner and between the liner and piston assembly are acquired using the one-dimensional, LIF system. The LIF technique is widely used for measuring oil films due to its nonintrusive nature and accuracy and is described in depth in other works [7, 8, 35].

B.2.1 Precision and Accuracy

Components inherent to the current LIF system at MIT ensure the system's precise and accurate performance. By incorporating fiber-optic technology, now beam widths of irradiation are on the order of 50 μm; a width acceptable to even detect OC rail

face profiles of the OC ring which typically have face widths of about 250 μm. Accuracy of calibration from ring profiles and piston skirt machining marks are, thus, enhanced as well. (Calibration is discussed in Appendix D.)

In addition, the enclosed fiber-optic cables limit extraneous signals and noise from the environment. Also helping to maximize S/N ratio are the optical and electrical filters.

But there are simple tasks the user can perform to help improve the S/N ratio which are not inherent to the LIF system. The user should adjust the focusing probe to maximize the signal on the oscilloscope before acquiring data for each test cases. Secondly, if the PMT voltage is set above about 700 volts, the PMT S/N ratio increases dramatically [36]; therefore, the user should not exceed this upper limit. One other reason to limit the PMT voltage setting is due to the upper voltage limit that our data acquisition system can process; if the system receives higher voltage than the voltage range specified by the user, the large parts of the signal will be cut off or "saturated". Lastly, selecting the proper fluorescent dye to dope the lubricant is important as well. Some dyes have better fluorescent efficiencies than others; the greater fluorescence given by a dye for a given irradiation, the greater the S/N ratio.

Because light typically attenuates exponentially in a thick medium, the absorption (and emission) is only linear for very thin mediums. The lubricant's fluorescent intensity is only linearly proportional to the oil film thickness up to about 80 microns [35]. Lee found linear proportionality for up to 125 microns [37]. So, as a worst case, any OFTs above 80 microns is suspect regarding its scaling.

B.2.2 Viscosity and Temperature Effects on Fluorescent Efficiency

Both the temperature and viscosity of the lubricant has an effect on the fluorescent efficiency and, thus, fluorescent intensity for a given irradiation beam. It has been shown theoretically by Hoult and Takiguchi from quantum theory and experimentally through bench experiments that the fluorescent efficiency is directly related to the viscosity and inversely related to the temperature [38]. For ensuring proper data acquisition, these

effects are primary reasons why the experimentalist should make adjustments to the data acquisition voltage range, the PMT voltage, and the focusing probe for every test case.

B.3 THE DATA ACQUISITION SYSTEM

Once the LIF signal in the form of voltage reaches the Keithley Metrabyte DAS-50 board installed in an IBM clone, the analog signal is digitized and recorded in the computer. On a separate channel, the same is done to the cylinder pressure signal delivered by the driver card.

The purpose of the driver card is two-fold. First, using the measured cylinder pressure and the five-volt pulse supplied from the shaft encoder at every top center (TC), the driver card delivers only one five-volt pulse during a cycle -- TC of the intake stroke -- to the digital trigger of the DAS-50. So when the user starts taking data from the computer, data acquisition will always start at the beginning of the intake stroke.

Since the DAS-50 board clocks the two channels sequentially (not simultaneously), it would use two encoder pulses for one LIF measurement and one pressure measurement. Therefore, doubling the encoder pulses would result in the sampling frequency of the LIF signal equal to the pulse frequency of the shaft encoder. This pulse doubling is the second function of the driver card and is delivered to the DAS-50 clock [39]. The two pulses from the driver for every one encoder pulse are two microseconds apart which is half of 1 MHz, the maximum sampling rate of the DAS-50 board.

The DAS-50 has a 12 bit resolution. For an acquisition voltage range of 0 - 10 volts, the 12 bit resolution implying 2^{12} increments means that the smallest discernible voltage difference is 0.00244 volts. In oil film thickness, assuming the lowest calibration coefficient of 30 mV/μm (refer to section 6.3 on OFT Calibration) -- a worst case for OFT resolution, the smallest discernible film thickness difference is about 0.08 μm; this value is an order of magnitude less than even the measured free-liner OFT.

APPENDIX C:
MEASUREMENTS OF ENGINE COMPONENTS

Both geometric dimensions and features for the piston, rings, skirt, and bore are highlighted in this section. Macro-geometric dimensions and features of the piston as well as the relative window locations with respect to the piston are helpful to orient the reader on the azimuthal LIF measurements and may prove as a helpful reference throughout the remainder of the report. The micro-measurements of the piston lands, piston skirt, bore, and rings show roughnesses, wear patterns, and important profiles related to the physics of lubricant behavior.

C.1 THE PISTON

Figure C.1 is a piston schematic showing macro-geometric dimensions and features. Accompanying the drawing are the azimuthal locations of the operable windows at midstroke. Window 1 is on the major-thrust side of the piston and sees the oil under the rings, along the land regions, along the chamfer region below the OC ring, and along the full skirt as the piston translates axially. However, windows 2 and 4 do not have the opportunity to see the full skirt because these locations are close to the azimuthal location of the wrist pin. There is a slim region immediately below the OC ring groove which can be viewed as part of the skirt with machining marks; although available for calibration, these machining marks were only partially flooded for a minority of cases at window 4 and none at window 2.

Both the first and second lands have machining marks as well and on the same order of magnitude -- 20 μm peak-to-peak shown in subsequent sections. However, machining marks on the third land are absent.

The dimensions and features should prove helpful for reference later within the report. The way OFT distribution is presented along the ring pack and skirt is relative to the top of the crown land as the dimensions are shown here.

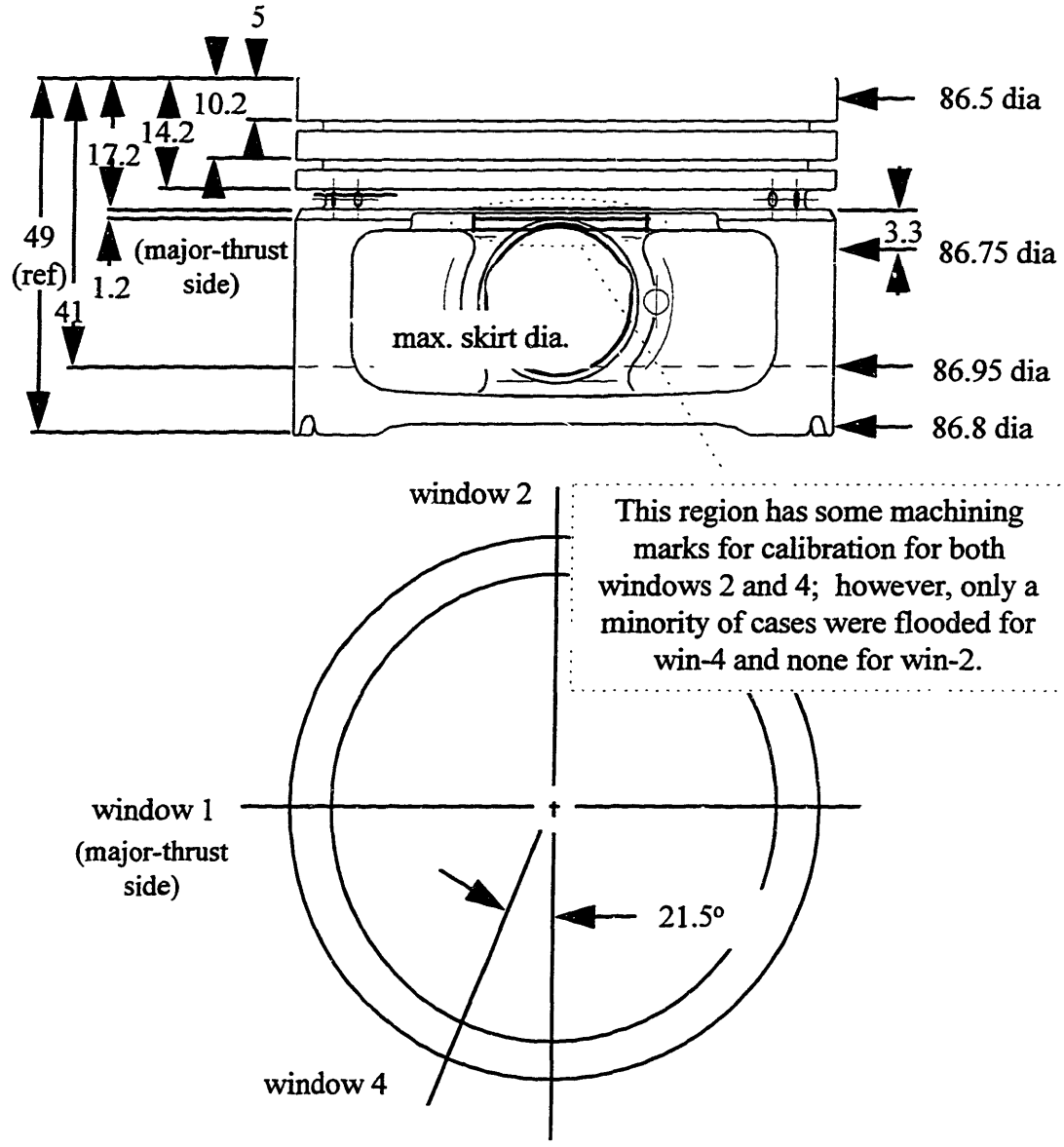

Figure C-1 Selected Piston Dimensions and Window Locations Relative to Skirt. (All dimensions in mm. Although the piston is slightly oval in shape, the piston dimensions are from the major axis of the piston.)

C.2 MICRO-MEASUREMENTS -- THE BORE AND PRL SYSTEM

The micro-measurements of the piston lands, piston skirt, bore, and rings show roughnesses, wear patterns, and important profiles related to the physics of lubricant behavior such as the scraper ring and deposits on the crown land. Quite distinct changes in micro-geometry take place throughout extended periods of engine operation including wear of rings, skirt, and bore, and the deposit build-up on the crown land. Measurements were taken before and after the experiments; however, the first set of measurements were taken at least 50 operating hours before the lubricants were tested. So the micro-geometry measured after all the tests are more representative of the actual geometry during the tests for these lubricants. (The stylus of the profilometer has a tip radius of approximately ten microns with an included angle of 60°.)

C.2.1 The Rings

Accurate profilometer measurements were taken of new and worn ring profiles. The rings were worn considerably during engine operation enduring over 100 hours of use. Figure C-2 shows the worn and unworn ring face profiles measured 90° off of the ring gap location in their free states. (The ring's free state describes the state of the ring when the ring isn't under tension and not closed to it's nominal diameter; conversely, when a ring is closed to its nominal diameter and, thus, under tension, the ring is in a tensioned state.) The horizontal and vertical scales are different to amplify ring face profiles. Surface roughness of the rings didn't exceed 0.1 μm (R_a); even the new top and scraper rings exhibit only slightly higher surface roughnesses when compared to the worn rings.

Although surface roughnesses did not change much during ring use, the ring profiles sure did. The top ring shown in Figure C-2(a) wore into a profile similar to the scraper -- having a large upper wedge and a smaller lower wedge but still large enough to avoid scraping. Significant lower flank wear was experienced as well -- more than any of the other rings. These wear patterns are primarily due to significant dynamic twist during

the expansion stroke; the high cylinder pressure creates a dynamic negative twist moving the minimum point up the ring and high asperity contact between the lower flank and groove [3]. The flank measurements support this explanation as well.

Originally, the unworn scraper ring had no lower converging wedge during a downstroke and was very sharp shown in Figure C-2(b). Wear flattened this point and also developed a small lower wedge when considering the ring's negative static twist. Because the second ring in its tensioned state has negative static twist, the twist must be considered when examining the face profile in the ring's free state shown in the figure. Although not affecting the actual face profile, the twist affects the profile's angular relation to the liner, and, therefore, how it scrapes along the liner. For example, the negative static twist at this location was measured to be approximately 0.005 radians (or about 0.3°) providing a small lower wedge about 0.1 mm shown in Figure C-3.

Compared to a non-twisted or positively-twisted ring designs, the taper face, reverse-twisted second ring generally results in superior oil control characteristics [40]. During late compression stroke and early-to-mid expansion stroke, upward inertia forces and downward forces generated from high second land pressures compete and contribute to second ring flutter allowing oil to be dragged in downward gas flow between the ring and groove [3].

The segments from the OC ring are sharp and have segment widths of 0.5 mm. (The vertical scale changes between the rings and segments by a factor of 1/5.) Only a little curvature is evident, and the segments have worn rather linearly; for this azimuthal ring location, the approximate linear profiles for the upper and lower segments have angles of 2.9 and 3.8°, respectively, with respect to the liner. This result possibly suggests that the segments within the tensioned OC ring assembly are angling with respect to the expander and groove similar to typical segment orientation within the OC ring shown in Figure 5-4. For this configuration, geometric calculations of cold OC ring and groove geometries still result in face angles of approximately 1.6 and 2.5° with respect to the liner. Piston tilt on the order of 0.5° doesn't fully account for this difference. (The equipment used to acquire these accurate profile measurements could

not measure the segment faces in the OC assembly while in tension within the piston groove.)

If the segments aren't considered symmetric with respect to the expander with only one segment angled, this segment's profile is now approximately flush to the liner; but then the other segment assumes its position as measured in its free state in Figures C-2(c) or (d).

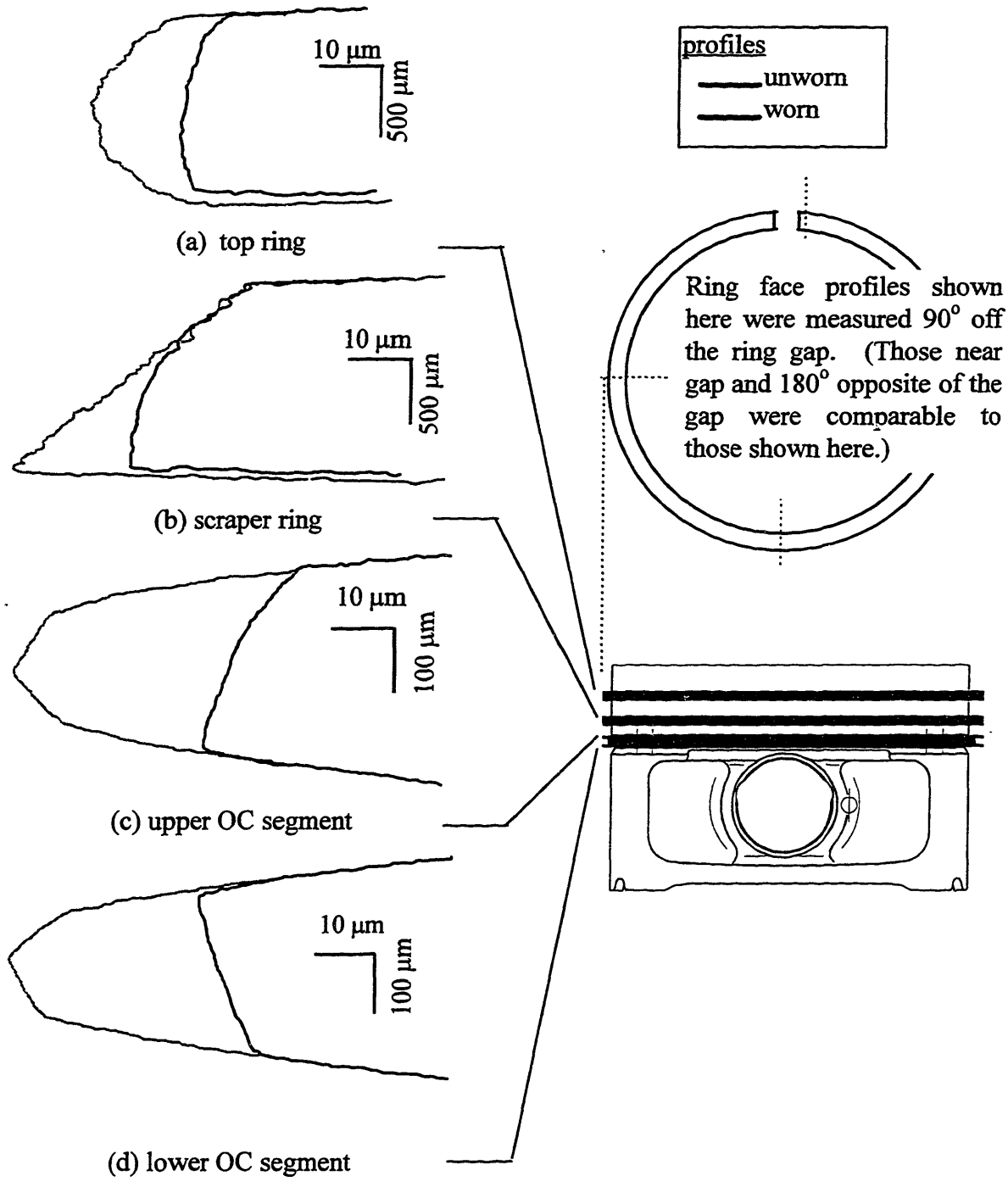

Figure C-2 Micro-geometry of Ring Face Profiles.
(Ring Profiles Were Measured in their Free State; Negative Static Twist Angle is Absent as well as the Segment Angles in their Sprung State within the Three-Piece OC Ring.)

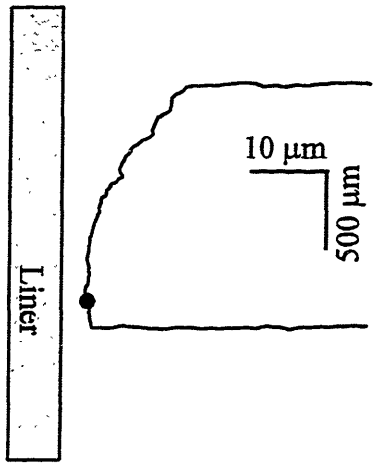

Figure C-3 Scraper Ring with Negative Static Twist under Tension with Minimum Point

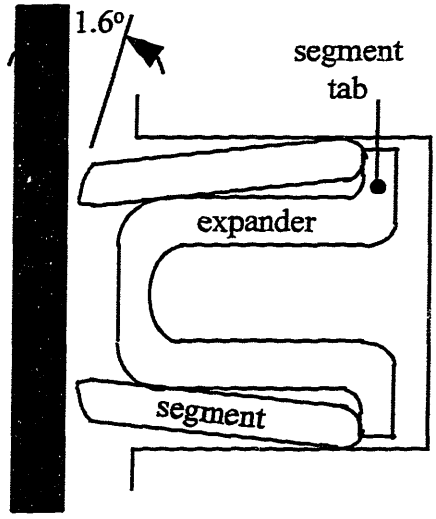

Figure C-4 One Possible Configuration of the OC Ring Assembly Under Tension within Its Groove

In retrospect, it's difficult to conclude how the segments are positioned with respect to its expander and groove when subjected to engine operation based on its cold geometry and wear patterns. Perhaps the segment-expander-groove interaction changes considerably throughout a stroke. The behavior at the endstrokes where most of the wear usually occurs may be quite different than at midstroke. Not knowing how the segments precisely position themselves within the OC ring during engine operation implies that calibrating from the upper OC segment [7] may not be reliable as once thought.

C.2.2 The Piston

Particular regions along the piston where measured for surface roughness and machining mark profiles for the lands and upper piston skirt. Measurements on the thrust-side were taken after initial break-in -- about 20 hours -- and after the experiments extending over 100 hours of engine operation. A sample of the results are shown in Figure C-5.

C.2.2.1 Land Machining Mark Profiles on Major-Thrust Side

As for all of the machining marks, the top land machining marks have an amplitude of about 10 μm and cycle every 350 μm. After the experiments, no machining marks shown in Figure C-5(a) were detectable. One possible reason for this absence could be due to the substantial carbon deposits which fill in the troughs. Another reason may be wear somewhere during the cycle.

Wear is more evident on the second land shown in Figure C-5(b). Notice how the peaks of the tool marks are sheared off and the troughs remain. Minimal deposits were found in this region and the second land was very clean.

The third land had no machining marks; its roughness was negligible compared to the machining mark magnitudes.

C.2.2.2 Upper Piston Machining Mark Profiles on Major-Thrust Side

Upper piston tool marks were measured and shown to wear shown in Figure C-5(c). However, immediately below the chamfer, the first three peaks did not wear. This region was used extensively for accurate LIF calibration; further calibration details are reported in Appendix D on data processing.

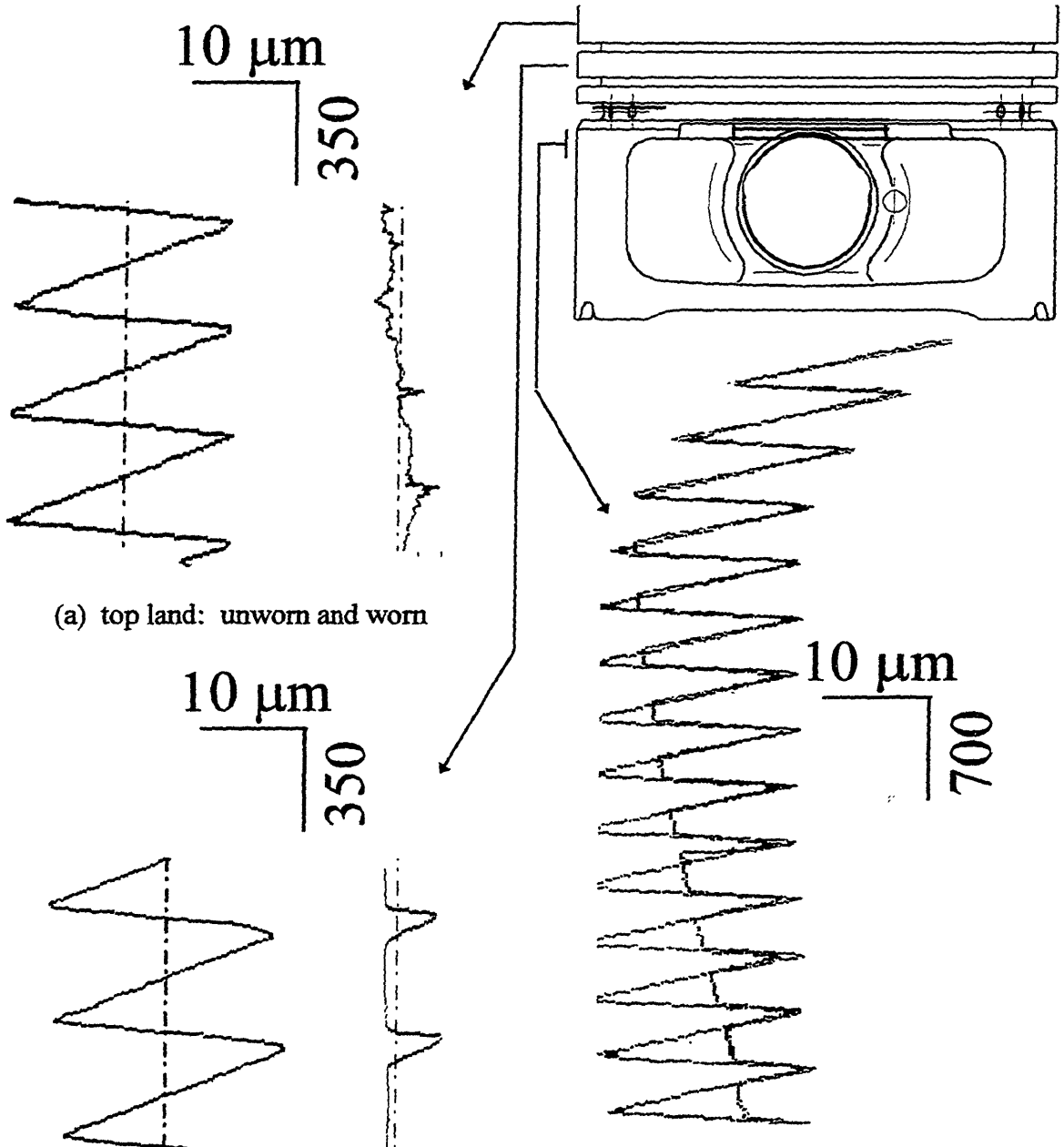

(a) top land: unworn and worn

(b) second land: unworn and worn

(c) Upper piston skirt below the chamfer. The two profiles are overlapped; the worn profile is the darker.

Figure C-5 Micro-Measurements of Selected Piston Regions on Major-Thrust Side -- Top and Second Lands and Upper Piston Skirt (first five millimeters). Worn profiles are to the right of the unworn profiles.

C.2.3 Bore and Window-to-Liner Flushness

Measurements along the liner at midstroke and near dead centers at the window locations were taken and include bore distortion and window-to-liner flushness. And again, measurements on the thrust-side were taken after initial break-in -- about 20 hours -- and after the experiments extending over 100 hours of engine operation. As in the cylinder liner honing procedure, the engine was assembled as much as possible to represent residual loads on the engine structure as much as possible; however, all measurements were conducted at room temperature.

C.2.3.1 Bore Distortion

Since in-situ bore distortion measurements during engine operation are extremely difficult, the cold bore measurements from before and after the experiments can only provide a qualitative distribution of which regions wore more than others. Exact relative magnitudes from location to location should be viewed as questionable because at running temperatures of 100°C thermal deformations of the block are inevitable.

Figure C-6 shows a bore distortion distribution around midstroke measured after the experiments. Measured around the circumference, it shows the bore's actual roundness and its deviation from a perfectly round bore. The dotted lines with their window designations give the location of the windows. The maximum radial difference azimuthally around the liner is approximately 20 μm, while the maximum radial difference between windows is about 16 μm. This distribution is also fairly representative of others near the dead centers at windows 5 and 6 except that at the location of window 3 the depression is only a third as severe. These bore patterns are substantially different than those measurements conducted before the experiments which showed very little azimuthal variation in comparison. Circumferential variations in micro-geometry are important because of their effect on OFT azimuthal variations.

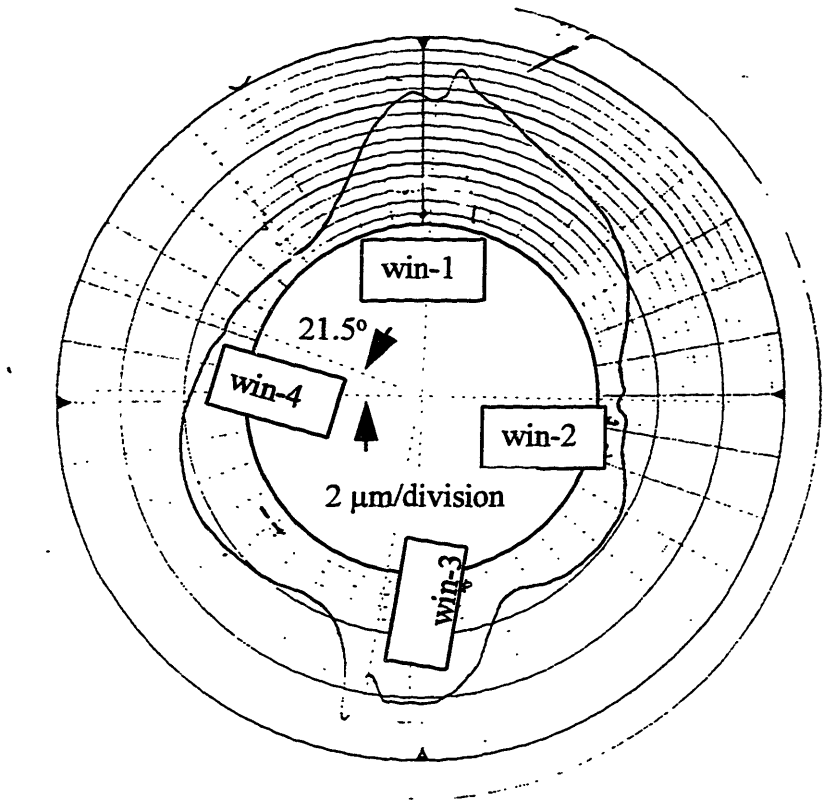

Figure C-6 Bore Distortion at Midstroke after Experiments.
(Scale: 2 μm per minor division.)

C.2.3.2 Window-to-Liner Flushness

Detailed axial micro-measurements of the window and adjacent liner highlighting the window-to-liner flushness and surface roughness were taken for the four operable windows. Since the components were at room temperature, these measurements, at best, only approximate the actual window-to-liner flushness during normal engine operation up to liner temperatures of 100°C.

The micro-geometry of window four and its immediate adjacent liner is shown in Figure C-7, and comparisons may be made between (a) before and (b) after the experiments. Even at midstrokes off the major-thrust side at window four, wear has taken

its toll. Before the experiments(a), the window is slightly recessed into the liner. During the experiments, the softer liner wore more than the hard silica/quartz window and left a window protrusion of one micron.

Also clearly evident is the reduction in surface roughness from about 0.5 μm to 0.12 μm in terms of the arithmetic roughness average, R_a. Even though there are several deceptively large troughs in the profilometer measurement (b), these troughs are extremely narrow and don't add much to the surface roughness calculation. Lastly, the roughnesses of the window and liner in each case have about the same roughness.

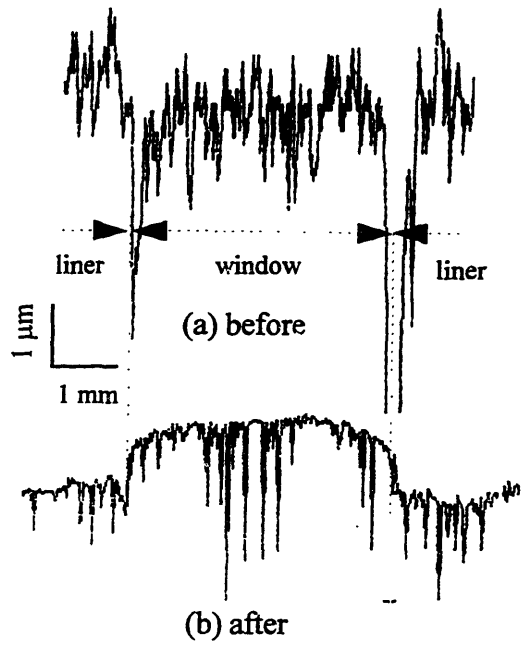

Figure C-7 Window 4 and Its Adjacent Liner (b) Before and (c) After Experiments.

Qualitatively, window four is representative of windows one, two, and six -- an initially flush or slightly recessed window, greater wear of the liner lending to slight window protrusion, a decrease in surface roughness, and approximate equality between liner and window surface roughness. Worn measurements most closely representing those during normal engine operation are quantitatively summarized in Table C.1.

Window	Surface Roughness, R_a (μm)	Protrusion (μm)
1	0.06	2
2	0.14	2
4	0.12	1
6	0.08	0

Table C.1 Surface Roughness and Protrusion of Operable LIF Windows Measured After the Experiments

These measurements are important and favorable in view of LIF OFT measurements especially for the free-liner, top ring, and scraper MOFTs whose magnitudes are on the order of a micron referring to Chapter 4. First, although a perfectly flush window and liner is ideal, a slight window protrusion is favorable over a recessed one. When a ring slides along the bore, fluid hydrodynamic pressure pushes against the ring and supports it while the lubricant passes between the ring and running surface. As the ring passes a window, this running surface also includes a small fraction (about 6 percent at midstroke for the four windows) of window running surface in addition to the liner. If a window is recessed, the amount of oil between it and the passing ring may not be enough to contribute any hydrodynamic pressure to the ring, and, thus, may not even be in contact with the ring; in this case, a LIF MOFT reading would be erroneous and simply measure the oil puddle sitting on the window.

Secondly, a protrusion's effect on ring tension is simply negligible for a deflection on the order of a micron for typical ring tensions of 150,000 pascals (Pa).

Finally, with both the ring face, window, and liner surface roughnesses less than 0.15 μm, LIF signals reading magnitudes on the order of 0.5 μm or greater can be considered actual OFTs, provided that the dynamic resolution of the system is high enough. In these experiments, this later criterion is fulfilled and was investigated in the Appendix B.3 on the data acquisition system.

(This page is intentionally left blank.)

APPENDIX D:
DATA PROCESSING

To extract useful information from the data, it must first be converted from a LIF digitized signal over a 12 bit range (or 4096 points) to an actual OFT trace and then transformed from OFT versus CA to OFT versus distance along the piston. The latter representation allows the piston and rings to be overlaid and their geometric features to be fitted and aligned with the OFT trace resulting in Figure D-1. OFT behavior under the rings and along regions with respect to the piston may then be measured and interpreted. For proper conversion, transformation, and interpretation of the signal, an adequate understanding of the engine kinematics and dynamics in view of window placement, the method and accuracy of calibration, and the quantification of variations is needed.

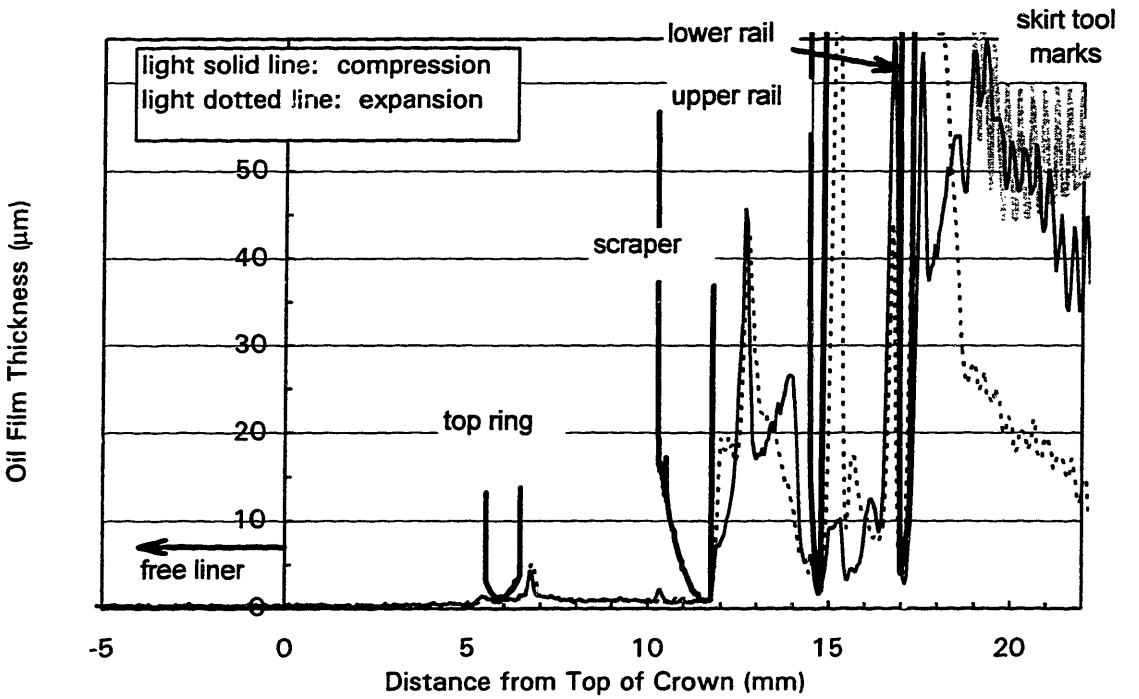

Figure D-1 Oil Film Thickness within the Ring Pack and Partially Along the Upper Skirt and Free Liner at Window 1.
(SAE-50, motored WOT @ 2500 rpm and 60°C, 30 mV/µm, 5 V)

D.1 ENGINE KINEMATICS AND DYNAMICS

As the piston reciprocates throughout a cycle, different rings and regions along the piston assembly pass a particular window at different times or crank angles and different speeds. Figure D-2 provides a geometric layout of the PRL system with connecting rod and crank accompanied by the widow locations. The CA position for the passing of each ring or OC segment by a midstroke or BC window is also shown. In addition, equation D.1 in the figure describes the kinematic relationship between distance from the piston's top land and the crank angle for a particular window and is used in the signal transformation (resulting in Figure D-1).

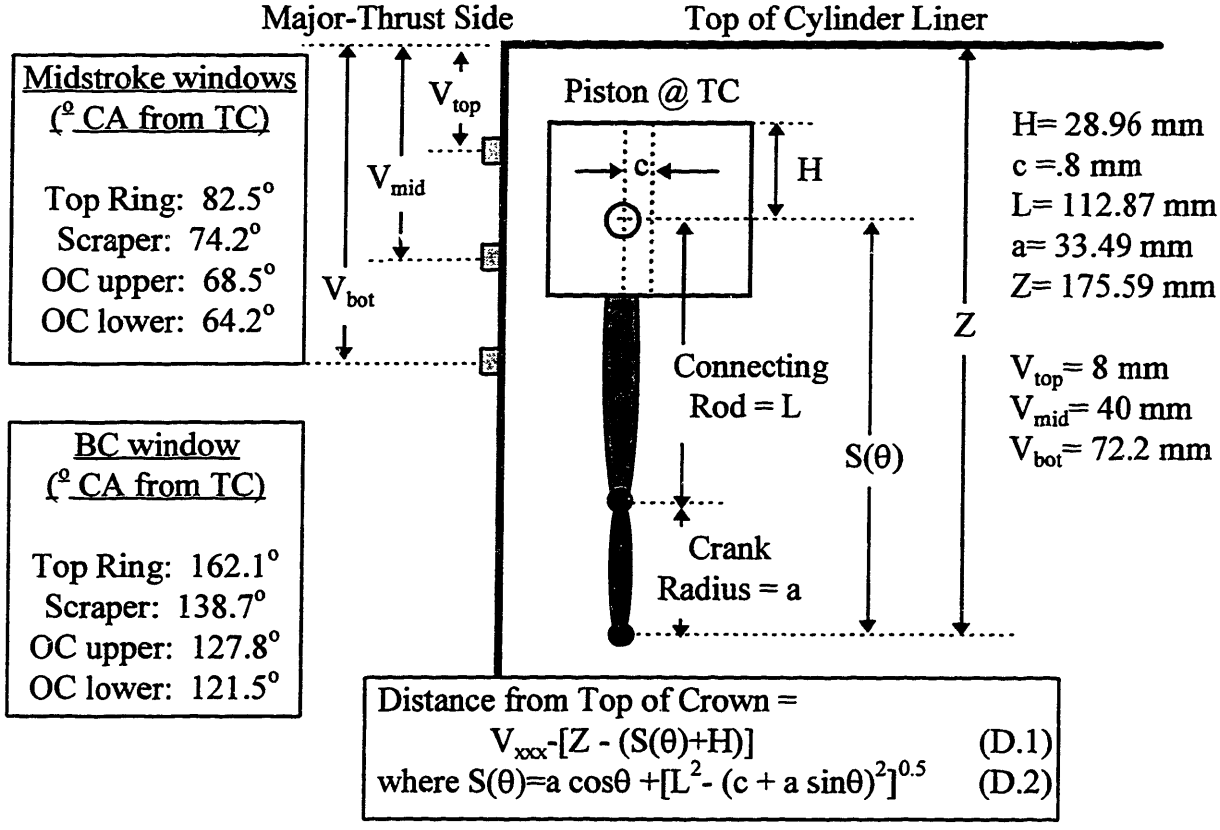

Figure D-2 Schematic of PRL System with Window Locations for Kinematic Evaluation.

With knowledge of the piston's position (equation D.2) throughout the cycle, the liner location of any region or point along the piston at any instant in a cycle is also

known. Figure D-3 (blown up from Figure D-5) shows the liner location of any point of the piston during the first half of a stroke as well as the midstroke windows 40 mm down the liner. At TC the midstroke window on the major-thrust side is only about two-thirds down the piston skirt. As the piston reciprocates downward, the OFT along the upper piston skirt is measured followed by the OC segments, the rings, and lastly the free liner above the top of the crown. Maximum piston speed of about 9 m/s at 2500 rpm (also shown in Figure D-4 and D-6) occurs at 74.2° CA -- exactly when the scraper ring passes.

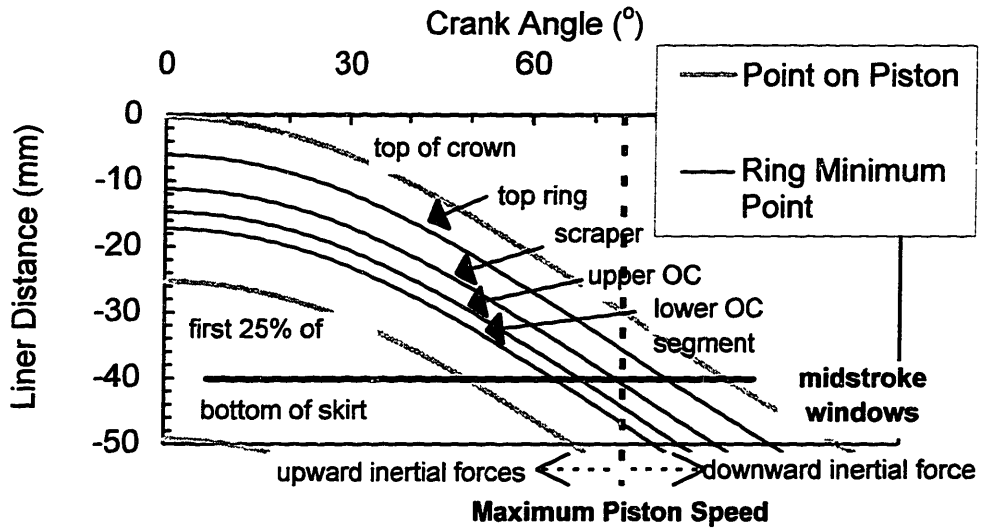

Figure D-3 Piston Region and Ring Position Versus Crank Angle with Reference To Midstroke Windows Along the Liner

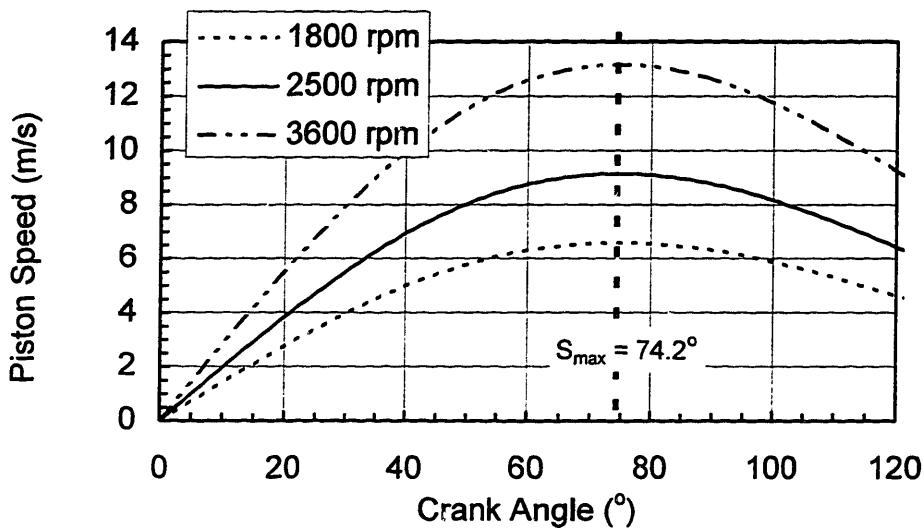

Figure D-4 Instantaneous Piston Speed versus CA

Several features from Figure D-3 are worth noting. First, the speeds of the rings and OC segments are within five percent of each other at approximately the maximum piston speed. Since the MOFTs are governed by hydrodynamic lubrication and dependent upon speed, a comparison of MOFTs is legitimate at midstroke windows.

Secondly, accelerating and decelerating along a stroke, the piston assembly experiences inertial forces as well. During a downstroke before 74.2° where the scraper passes the midstroke windows, the piston is accelerating and inertial forces are towards the combustion chamber for all OC segments and regions along the piston below the scraper ring. For example in Figure D-1 during the expansion downstroke indicated by the dotted line, inertial forces along the third land, between the OC segments, and immediately below the OC ring gravitate the oil masses towards the combustion chamber. During the compression upstroke indicated by the solid OFT trace, inertial forces are reversed and away from the combustion chamber for regions below the scraper; therefore, oil is forced in the opposite direction compared to the expansion downstroke. Above the scraper ring, oil volumes for this case are not large enough to experience movement from inertial forces. Shown in section 5.5, for oil masses to experience enough inertial force for movement depends not only on their density, oil height, and engine speed but their viscosity -- resistance of the lubricant to shear.

In addition to the oil masses in the piston regions, inertial forces are experienced by the rings which cause them to move axially up and down within their grooves throughout a cycle and affecting lubricant squeezing and flow between the ring and groove. These dynamics and their effects on lubricant behavior will be discussed further within Chapter 5.

Meanwhile near BC, OFT is measured from window six about 72 mm down the liner. Shown in Figure D-5 as the piston reciprocates through a downstroke, window six has access to the free liner below the piston skirt, then the skirt, and followed by the rings. However, the piston stops just after the top ring passes the window.

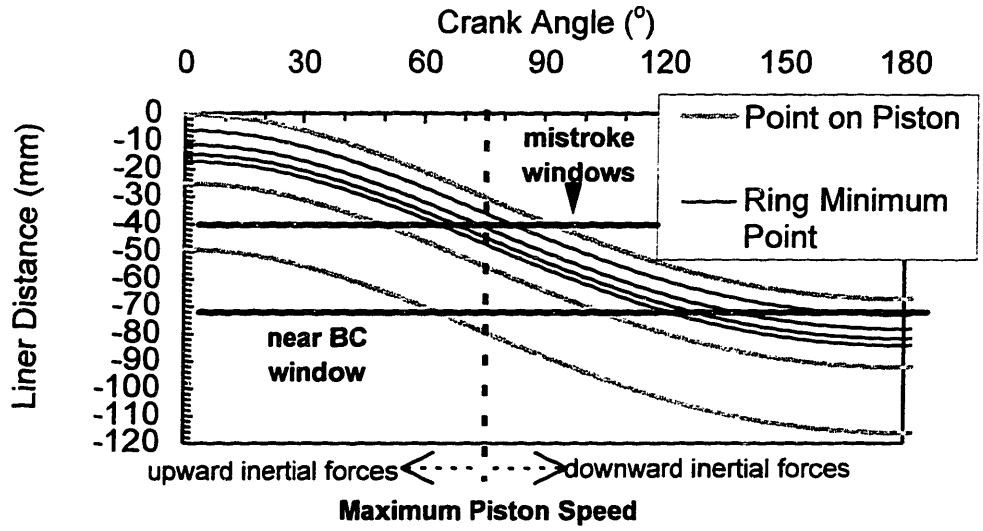

Figure D-5 Piston Region and Ring Position Versus Crank Angle with Reference To Window Location Along the Liner

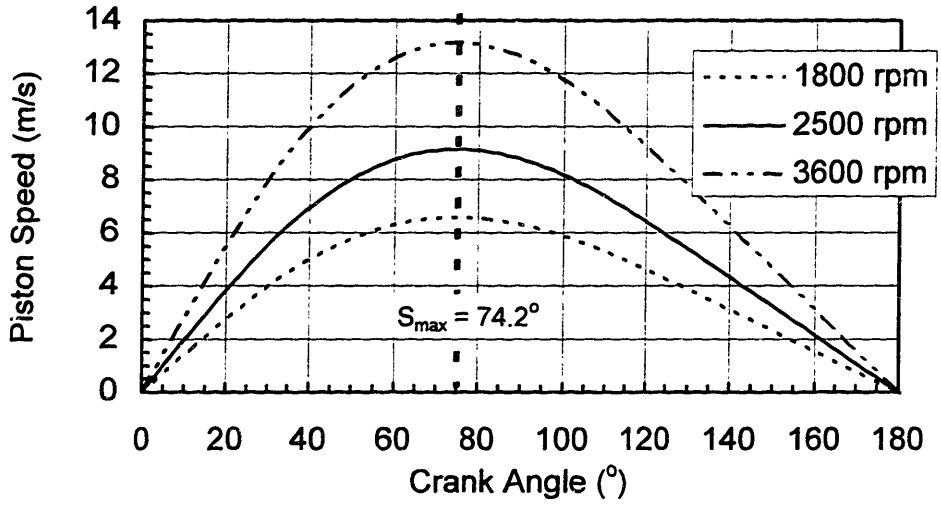

Figure D-6 Instantaneous Piston Speed versus CA for an Entire Stroke

Unlike the midstroke windows, the near-BC window measures the MOFTs of the rings which travel at significantly different speeds; the lower OC segment and the top ring pass the window at approximately 6.5 and 2 m/s, respectively. Therefore, comparison of ring MOFTs this far down the liner is not valid. However, ring MOFT comparisons between window one, which is a midstroke window, and window six is

valid if the objective is to capture a speed effect along the stroke; for instance, a greater speed effect on MOFTs should be experienced by our top ring than our OC segments.

Additionally, as the piston passes by the window, inertial forces are mostly away from the combustion chamber for the downstrokes and upstrokes as the piston decelerates and accelerates, respectively.

These different features, which are characteristic of window six near BC, may be seen in Figure D-7 (a) and (b) showing the ring pack and along the skirt and free liner below the skirt. It is important to note that the skirt profiles in Figure 6-7 (b) have been hand-drawn to only give the reader a sense of the length of the piston. The semi-oval profile is qualitative. The skirt's tilt is only one possible angular orientation at one crank angle position during a stroke.

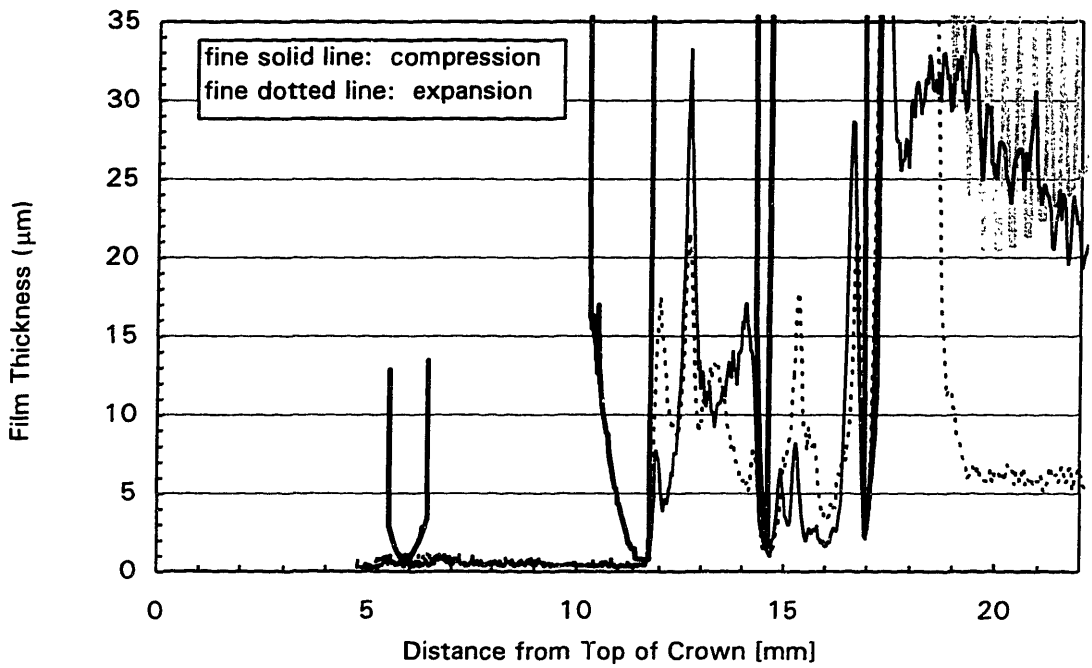

(a) OFT Within the Ring Pack and Partially Along the Upper Skirt

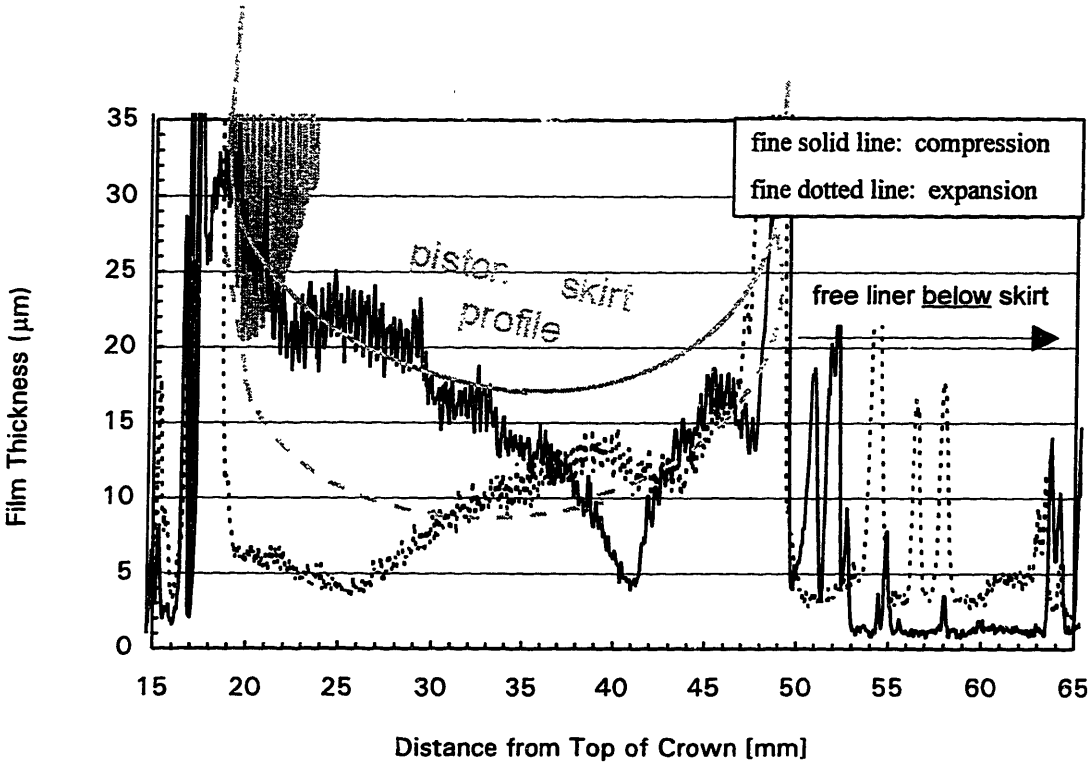

(b) Along Entire Skirt and Free Liner Below Skirt

Figure D-7 Oil Film Thickness near BC at Window 6. (a) Within the Ring Pack and Partially Along the Upper Skirt (b) Along Entire Skirt and Free Liner Below Skirt (SAE-10W, 2/3 load @ 2500 rpm and 100°C, 50 mV/µm, 10 V)

D.2 CALIBRATION OF THE LIF SYSTEM

In-situ calibration of the LIF system involves converting the OFT voltage signal to an actual OFT trace in microns and requires fitting micro-geometry of certain areas of the piston assembly to the OFT trace by adjusting a calibration coefficient. Calibration accuracy depends upon which geometry within the assembly is used.

D.2.1 Method of Calibration

Once the OFT representation in Figure D-1 is obtained using any arbitrary calibration coefficient, an accurate in-situ calibration requires adjusting this coefficient to

match certain micro-geometric profiles of the piston assembly. Two methods of in-situ calibration are employed for this project.

The first method requires fitting the OFT trace to the machining marks on the upper portion of the piston skirt. A typical example is shown in Figure D-8, and several observations are worth noting. (Please refer to section C.2.2.1 for detailed skirt geometry.) First, not all of the machining marks along the piston are fully-flooded with oil. In fact, out of the ten cycles acquired for each data file, usually only a minority have fully-flooded regions comparable to this example and, thus, a strong OFT fingerprint of the machining marks. However, when this method was implemented, a strong print was found in at least three of the ten cycles.

Secondly, only the compression and/or exhaust strokes have these strong prints. One reason is inertial forces. As mentioned in section D.1, during the upstrokes for this region along the piston, inertial forces are directed away from the combustion chamber; therefore, any oil downscraped by the lower OC segment along the piston chamfer region by the previous downstroke will now be forced down the piston, away from the combustion chamber, and into the tooth troughs. It's possible that some scraping on the upstrokes in this region may also occur.

Thirdly, since only several of the ten cycles had clear fully-flooded machining marks during the compression and/or exhaust strokes, calibration fitting to a 10 cycle-trace average would be erroneous; Because only three or more matches can be made per data file and no one fitting is exact, manual iterations were performed between them by making small adjustments to the calibration coefficient resulting in a fine-tuned calibration coefficient for the entire data file.

Lastly, since the fluorescent efficiency of the doped lubricant changes with temperature, it is important to have the upper piston skirt temperature very close to the liner temperature in the vicinity of MOFT measurements. From two independent studies, Tamai concluded that this is approximately the case for this engine [7].

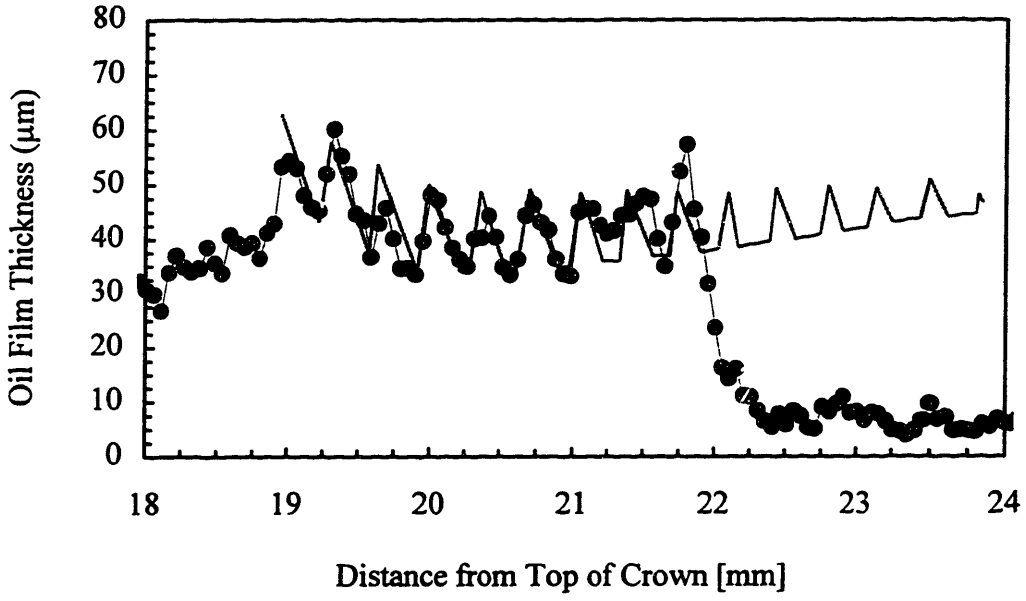

Figure D-8 Calibration to Upper Skirt Machining Marks During Compression Stroke
(Window 1, SAE-10W, Motored WOT @ 2500 rpm and 60°C, Cycle 6, 80mV/mm, 5 V)

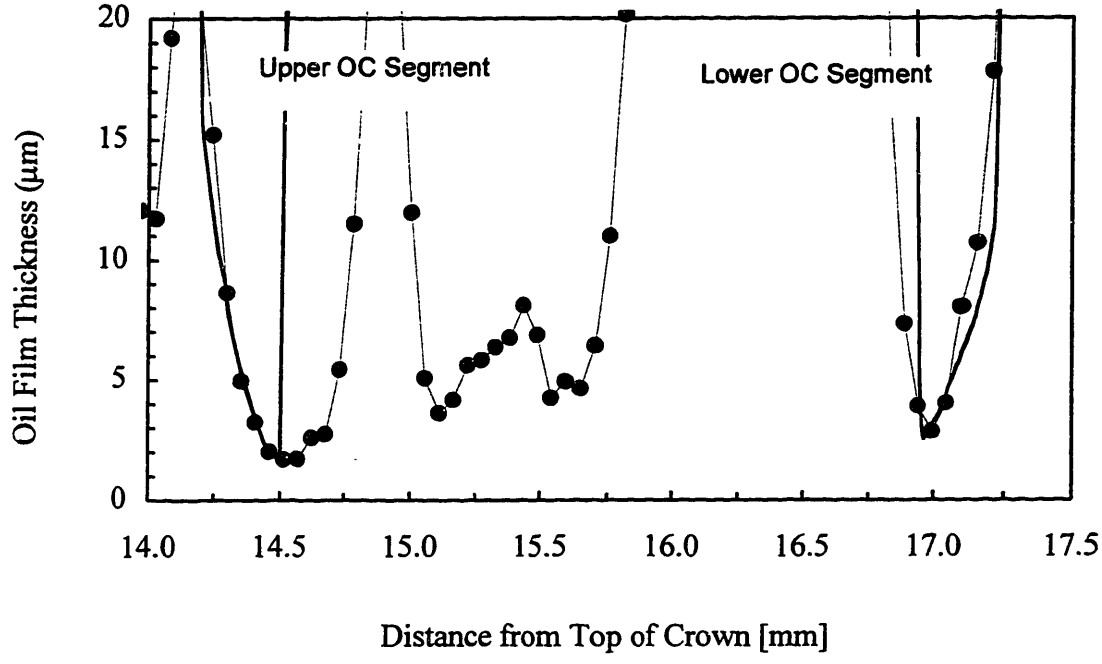

Figure D-9 Calibration to Upper OC Rail During Exhaust Stroke
(Window 1, SAE-10W, Motored WOT @ 2500 rpm and 60°C, Cycle 6, 80mV/mm, 5 V)

The second method involves fitting the face profile of the upper OC segment to the OFT trace shown in Figure D-9. Because the rings and segments always have sufficient wetted-widths along their faces, contact of the oil film and the segment geometry is guaranteed unlike the unflooded problems incurred by the first method. This reasoning is exactly why Tamai [7] and Deutsch [8] described this method to be the most reliable. However, the accuracy of this approach falls short because this arrangement assumes the OC segments aren't angled with respect to its expander or groove like typical OC rings and implied by the worn face profiles. No one really knows how the three-piece oil control ring actually behaves dynamically within an actual engine; thus, any calibration coefficient from this method is uncertain. (For more detailed explanation on the OC ring geometry, please refer to section C.2.1 and Figures C-2(c), C-2(d), and C-4.)

In retrospect, if a clear OFT print of the tool marks can be detected along the region of the upper piston skirt, calibration to the skirt machining marks is far more accurate than the latter method because no wear occurs for the first four tool peaks, and the piston flooding affords greater exposure to the oil than any wetted-width of the upper OC segment. Lastly, and most convincingly, the dynamic behavior and, therefore, the angular positions of the OC segments are unknown throughout an engine cycle.

D.2.2 Calibration Coefficients for Cases Within the Test Matrix

Since Tamai's thesis [7], 96 of the 108 data files corresponding to the test matrix presented in Chapter 4 have been calibrated and reduced and are shown in Table D.1. (The remaining twelve data files correspond to the cases at 3500 rpm -- a speed too fast for the frequency response of 200 kHz of the shaft encoder; the fastest speed for proper operation of the encoder is 3000 rpm for 4000 samples/rev.) Even the fraction of data files Tamai reduced were reduced again to confirm accurate calibration and MOFT fits.

Confidence in manual iterative calibration fits in terms of percent accuracy are shown by a shaded color scheme. The unshaded cells correspond to a +- 5% or better calibration fit, and the cases are calibrated from the skirt machining marks and some from the upper OC rail. All of the remaining cases have questionable coefficients greater than

+-5% accuracy due to unclear skirt machining marks and/or using the upper OC segment method only.

Window	Lubricant	Fired				Motored	
		100 C		80 C	60 C	60 C	40 C
		1800 rpm	2500 rpm	(2500 rpm)	(2500 rpm)	(2500 rpm)	(2500 rpm)
win-1	SAE-10w	50	50	75	75	80	50
	SAE-10w50n	75	75	75	60	85	60
	SAE-10w50k		30			50	60
	SAE-30		65			55	40
	SAE-50	75	75	75	67	50	30
win-2	SAE-10w		68			60	
	SAE-10w50n	80	100	70	100		
	SAE-10w50k						
	SAE-30		45			35	
	SAE-50	80			40	55	
win-4	SAE-10w	30				85	75
	SAE-10w50n	70	80	45	70		
	SAE-10w50k		40			40	50
	SAE-30		45			45	30
	SAE-50	60		45		55	45
win-6	SAE-10w		50	90	90	95	90
	SAE-10w50n	75	75				70
	SAE-10w50k						
	SAE-30					110	
	SAE-50		80				

Legend: Unshaded cells correspond to +/- 5% calibration uncertainty or less, and cases are calibrated from machining marks on skirt and most from upper OC rail.

Light-shaded cases are calibrated from upper OC rail and a few with the lower OC rail. However, +/- 5% calibration uncertainty is questionable due to unknown rail angle wrt liner.

Shaded cells correspond to worse than +/- 5% calibration uncertainty.

Note: At window 4, all light-shaded cases have better accuracy than other light-shaded cases at other windows *except for* SAE-10w and -50 @1800rpm and SAE-50 at 80 C.

Table D.1 Calibration Coefficients (mV/μm)

D.3 PISTON TEMPERATURE EFFECTS ON FLUORESCENT EFFICIENCY AND MEASURED OIL

Because local piston temperatures may be different from stroke to stroke and axially along the different piston lands, the fluorescent efficiency (which depends upon temperature) of the oil directly on the piston may differ stroke by stroke and axially along the piston, providing imprecise measurements of the actual amount of oil.

Stroke to stroke throughout an engine cycle, temperature fluctuations for the crown land and top piston surface only affect a piston surface layer up to 2 mm thick, slightly changing with engine speed and load [41]. These thermal transients diminish along lower regions of the piston which are less affected by the different stroke-by-stroke gas temperatures and convective flows. While no oil exists on the top land (for the fired cases for the current engine), oil on the second land shows no stroke-by-stroke differences and, thus, no temperature transient effects on oil fluorescence. If surface temperature fluctuations did affect the oil fluorescence, the expansion and exhaust strokes would have less measured oil than the intake and compression strokes. (Not caused by any temperature fluctuations on oil fluorescence, the only stroke-by-stroke differences in the amount of oil on the second land occurs when enough oil exists for oil squeezing between the rings and groove.) For regions below the second land, the diminishing temperature fluctuations have a negligible effect on oil fluorescence.

However, local temperatures axially along the lands and skirt of the piston significantly differ and affect the oil fluorescence and, thus, the measured signal axially along the piston. Although the piston temperature is generally higher than the temperature of the cylinder bore [41], Tamai [7] references works which argue that the upper piston skirt temperature is not more than 5°C above the temperature of the cylinder bore at top center (TC). Since the temperatures of the bore at top center (TC) and bottom center (BC) were maintained within 5°C of each other for the current engine, the upper skirt temperature where in-situ calibration is performed is very close to the actual measured liner temperature.

However, the piston land temperatures are considerably higher and decrease the oil fluorescent efficiency which is proportional to

$$\frac{1}{T^{2.5}} \qquad \text{(D.3)}$$

described by Hoult and Takiguchi [38]. A number of works [41, 42, 43, 44] record the crown land temperatures ranging from 40 to 100°C above the upper piston skirt temperature depending upon the engine operating condition.

For a cylinder liner temperature of 100°C (a best case where oil fluorescence is less sensitive to temperature at higher temperatures) and a typical crown land temperature of 170°C, the second and third lands may be estimated at 147 and 123°C, respectively. Therefore, for oil on the crown (which typically has no oil), second, and third lands, measured values may possibly be 73, 62, and 41 percent lower, respectively, than the actual amount of oil. Although the measured amounts of oil reported in this thesis are not corrected using equation D.3, the reader may correct them from these rough percentages.

APPENDIX E:
NUMERICAL MODELS USED FOR DATA ANALYSIS AND INTERPRETATION

Two numerical models developed within the MIT Lubrication Consortium are used to help analyze and interpret the magnitudes and trends of the LIF measurements. One complete mixed-lubrication model called *FRICTION-OFT* predicts OFT and friction within the piston ring-pack including crank-angle (CA) resolved and gross cycle results [9, 34]. Generating important predictions such as second and third land pressures used as input to *FRICTION-OFT*, *RINGPACK-OC* is a ring-dynamics and gas-flow model for studying the interactions between rings and their grooves, blowby, and the influence of other ring and piston parameters such as keystone ring/groove configurations and static twist.

Generally, both of these models are appropriate for applying to measurements in this thesis. Both models have been validated against SI engine measurements for both land pressures [10] and OFT [9] and diesel measurements for wear [3] and friction.

Brief model descriptions in view of their applications to the LIF measurements in this thesis are presented below. Further details of the models may be found in the references cited above.

E.1 *FRICTION-OFT* MODEL

The 1-D *FRICTION-OFT* model predicts oil film thickness and friction of the piston ring-pack. Pure boundary and hydrodynamic lubrication as well as the mixed regimes take part in crank-angle (CA) resolved predictions over an entire cycle. Temperature dependence as well as shear dependence of multigrade lubricants are taken into account.

Some of the most important input and output parameters are summarized as follows:

Primary Inputs

- macro-geometry -- ring dimensions, tensions, and properties; piston lands, bore, connecting rod, and crank shaft
- micro-geometry -- surface roughnesses of rings and liner; accurate ring face profiles
- engine operating conditions -- liner temperatures; engine speed; measured cylinder pressure and predicted land pressures from *RINGPACK-OC* (described in Section 7.2)
- lubricant properties in terms of Vogel and Cross equations

Primary Outputs

- CA-resolved OFT and friction for all rings and free liner
- asperity contact between rings and liner
- ring down-scraping oil transport

Because no one knows exactly how the three-piece OC ring behaves, the modeling of the three-piece OC ring is oversimplified to a one-piece ring shown in Figure E; its geometrical description is treated in the same manner as a single-piece ring. The actual upper and lower rail profiles are used for the profiles of the upper and lower wedges of the single-piece, respectively, and a typical OC ring pressure of five bars is assumed.

The predictions of both models are 1-D or line calculations. However, azimuthal input such as piston tilt effects on ring face profiles relative to the liner can quick change results into 2-D.

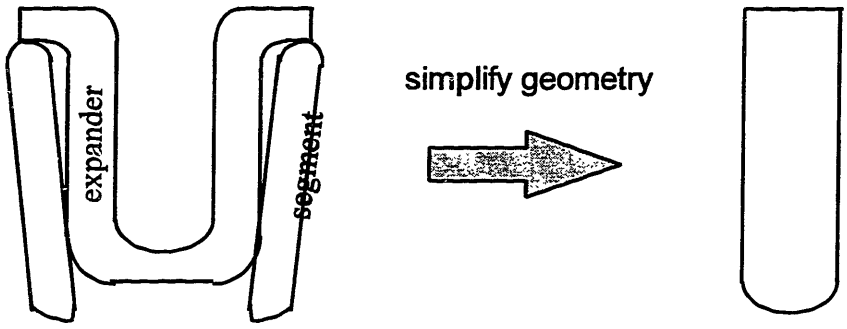

Actual Kohler OC Ring
(Three-Piece)

Model OC Ring
(Single-Piece)

Figure E Single-Piece Model Simplification of the Actual Three-Piece OC Ring

E.2 *RINGPACK-OC* MODEL

The ring-dynamics and gas-flow model has inputs comparable to those for *FRICTION-OFT*, less the predicted land pressures; however, the cylinder pressure trace is needed.

The ring dynamics and gas flows are intimately coupled in the formulation. Specifically, among other CA-resolved outputs throughout a complete cycle, relevant predictions for this thesis are as follows:

- gas flows and pressures through gaps and grooves and among the lands
- ring dynamics -- static and dynamic ring twist, detailed ring and groove contact, ring lift within the groove, and ring flutter

APPENDIX F:
STANDARD DEVIATION AND UNCERTAINTY FORMULAS

This section describes how standard deviations were directly calculated from the measurements as well as indirectly determined from averaging, multiplying, adding, and subtraction.

STANDARD DEVIATION FROM MEASUREMENTS

The mathematical definition of standard deviation used in this thesis is defined as

$$\sigma_s = \sqrt{\frac{1}{(N-1)}\sum (x_i - \bar{x})^2} .$$

where N, $x_i, \bar{x}$ are the number of data points, the values of the data points, and the average of these values, respectively. Statistically, if our measurements are normally distributed, then about 70 percent of our measurements would lie within a distance of the calculated standard deviation on either side of the average.

Determining standard deviations and uncertainty indirectly from formulas described by Taylor [15].

COMBINING DIFFERENT TYPES OF UNCERTAINTY

Combining different types of uncertainty proposed by Taylor [15], total uncertainty may be calculated from these different components

$$\sigma_t = \sqrt{\sigma_s^{\,2} + \sigma_c^{\,2}}$$

where σ_t, σ_s, and σ_c correspond to the different uncertainties and refer to the total, standard deviation, and calibration, respectively. Relative to their corresponding magnitudes, a total coefficient of variation may then be calculated. For the MOFTs, σ_s / MOFT = COV which is roughly 20 percent. From the calibration accuracy, σ_c/(calibration coefficent) is about 0.05. Since 0.05^2 is much less than 20^2, σ_t / MOFT $\approx$ 20 percent.

APPENDIX G:

ANALYTICAL ARGUMENT FOR MEASURED OFT HIERARCHY WITHIN ANY LUBRICANT CASE AND CRITERIA FOR LOCALLY FULLY-DEVELOPED FLOW, NEGLIGIBLE ENTRANCE LENGTH AND SQUEEZING, AND MOFT DEPENDENCE ON VISCOSITY AND SPEED FOR MIDSTROKE AND NEAR-BC LOCATIONS WITHIN THE KOHLER ENGINE

This appendix provides an explanation of the measured OFT hierarchy found within each lubricant case by an analytical argument applied to the piston and ring parameters and operating conditions of this specific Kohler engine. As an additional outcome of the order-of-magnitude analysis, the OFT dependence upon viscosity and speed is derived.

INTER-RING AND FREE LINER DEPENDENCE VIA LUBRICANT BEHAVIOR RESULTING IN MEASURED OFT HIERARCHY

An analytically theoretical argument can be made as follows and is accompanied by Figure G-1 for terminology. The Navier-Strokes equation in the x-direction

$$\rho\left(\frac{\partial u}{\partial t}+u\frac{\partial u}{\partial x}+v\frac{\partial u}{\partial y}\right)=-\frac{\partial P}{\partial x}+\mu\left(\frac{\partial^2 u}{\partial x^2}+\frac{\partial^2 u}{\partial y^2}\right) \qquad (G.1)$$

simplifies under highly-viscous, inertia-free laminar flow under the ring justified by the satisfied criteria at the end of this appendix. Consequently, G.1 reduces to an equation representing locally fully-developed flow even at window 6, near BC.

$$0\approx-\frac{\partial P}{\partial x}+\mu\frac{\partial^2 u}{\partial y^2} \qquad (G.2)$$

Satisfying the criteria for locally fully-developed flow also satisfies negligible entrance length relative to the ring width. Then an integral form of the mass conservation may be written as

$$Uh_\infty + \frac{dx_1}{dt}\left[h(x_1) - h_\infty\right] - (x - x_1)\frac{dh_o}{dt} = \frac{Uh}{2} - \frac{h^3}{12\mu}\frac{\partial p}{\partial x} \qquad \text{(G.3)}$$

taken from a control volume which cuts the flow at the free-liner entrance and the cross flow underneath the ring at position x.

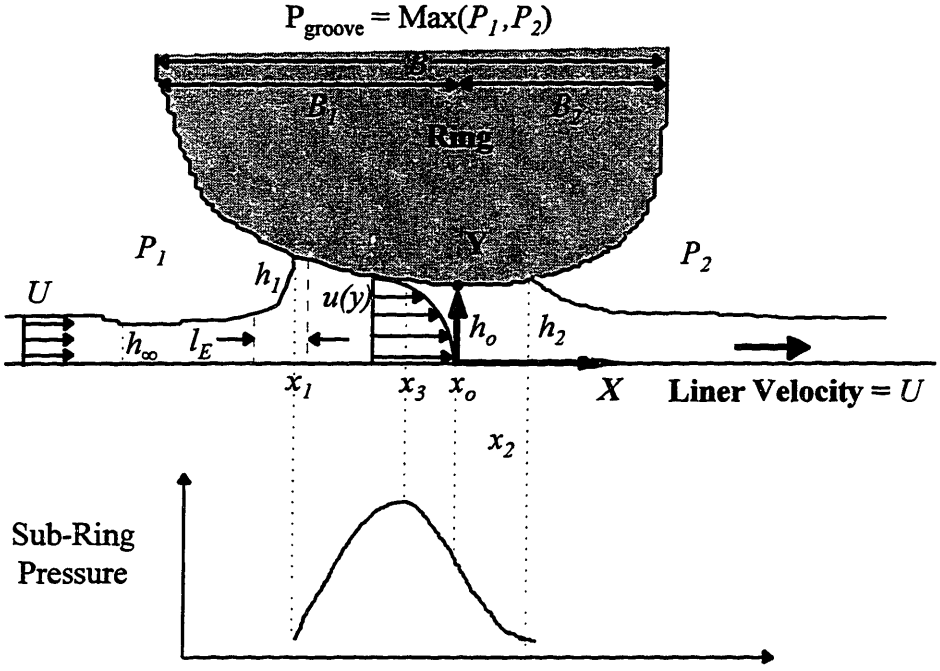

Figure G-1 Ring-Liner Lubrication with Sub-Ring Pressure Profile

At the end of this appendix, an order-of-magnitude scaling shows that, at midstroke and near-BC window locations, the terms involving the time derivatives are negligible. At x_o, our simplified equation becomes

$$\frac{h_o^2}{6\mu U}\frac{\partial p}{\partial x}\bigg|_o \approx \left(1 - 2\frac{h_\infty}{h_o}\right) \qquad \text{(G.4)}$$

Continuing with worst case magnitudes given at the end of this appendix, the left side is of the order 0.04 and much less than 1; therefore, for a ring with a starved converging wedge, its MOFT is roughly twice the free-liner OFT. More exactly, allowing equation G.4 to be evaluated at x_3 corresponding to the peak pressure and the zero pressure gradient, h_3 is twice the liner OFT. The MOFT (or h_o) is a little below h_3 and, thus, the

MOFT is slightly less than twice the liner OFT. This result agrees with a more general numerical study by Tian [13] where the MOFT is approximately 1.8 times the free-liner OFT.

When piston sliding speed becomes slow (U ~ 0.1 m/s from the end of this appendix), unsteady behavior in the lubricant flow under the rings -- the time-dependent squeezing and varying inflow conditions -- become significant. Even for a liner speed of zero, pressure within the lubricant can still exist from ring pressure and squeeze oil in the positive and/or negative X-direction as the MOFT decreases.

MOFT DEPENDENCE ON VISCOSITY AND SPEED

In order to determine how MOFT scales with viscosity and speed, the terms from equation G.4 governing locally fully-developed flow can be given orders of magnitude where

$$\frac{h_o^2}{6\mu U}\left.\frac{\partial p}{\partial x}\right|_o \sim \frac{H_o^2 P}{6\mu U B} \qquad (G.5)$$

$$h_\infty \sim H_o$$

Also, the instantaneous piston speed $U = 4aNf(\theta)$ reduces to $U \propto N$ for a fixed crank radius and particular liner location. So for a particular ring having a fixed ring tension (or unit pressure P) and width (B), equation G.4 scales to

$$H_o \sim \sqrt{6\frac{\mu N B}{P}} \qquad (G.6)$$

And taking the ratios at different conditions 1 and 2 reduces the scaling further to

$$H_{o2} = MOFT_2 \sim MOFT_1\sqrt{\frac{\mu_2 N_2}{\mu_1 N_1}} \qquad (G.7)$$

This order-of-magnitude relationship is the MOFT dependence upon both viscosity and speed for a particular ring having the same ring tension and width at different conditions 1 and 2. For the speed effect in section 4.4, the midstroke cylinder liner temperature is fixed from 1800 to 2500 rpm. Assuming that this liner temperature is the same as the

lubricant temperature, this rough relationship reduces further if the same lubricant is used the different conditions 1 and 2. Then, the viscosities cancel, and the MOFT scales with the speed

$$MOFT_2 \sim MOFT_1\sqrt{\frac{N_2}{N_1}} \tag{G.8}$$

CRITERIA FOR LOCALLY FULLY-DEVELOPED FLOW

For locally fully-developed flow represented by the simplified form in equation 8.3, the following criteria need to be satisfied,

$$\frac{\partial u}{\partial t} << \nu\frac{\partial^2 u}{\partial y^2} \tag{G.9}$$

$$u\frac{\partial u}{\partial x} << \nu\frac{\partial^2 u}{\partial y^2} \tag{G.10}$$

$$v\frac{\partial u}{\partial y} << \nu\frac{\partial^2 u}{\partial y^2} \tag{G.11}$$

$$\frac{\partial^2 u}{\partial x^2} << \frac{\partial^2 u}{\partial y^2} \tag{G.12}$$

From order-of-magnitude scaling,

$$\frac{\partial u}{\partial t} \sim \frac{U}{\tau} \tag{G.13}$$

$$v \sim \frac{U}{B}H \quad \text{from continuity equation} \quad v = -\int_0^y \frac{\partial u}{\partial x}dy \tag{G.14}$$

$$u\frac{\partial u}{\partial x} \sim \frac{U^2}{B} \tag{G.15}$$

$$v\frac{\partial u}{\partial y} \sim \frac{U}{B}H\frac{U}{H} = \frac{U^2}{B} \tag{G.16}$$

$$\frac{\partial^2 u}{\partial x^2} \sim \frac{U}{B^2} \tag{G.17}$$

$$\frac{\partial^2 u}{\partial y^2} \sim \frac{U}{H^2} \qquad \text{(G.18)}$$

If τ is on the order of the time it takes to complete a stroke, then

$$\tau U \sim \text{stroke} \qquad \text{(G.19)}$$

and the criteria of the scaled inequalities is now represented by

$$\text{Re}\frac{H}{\text{stroke}} << 1 \qquad \text{(G.20)}$$

$$\text{Re}\frac{H}{B} << 1 \qquad \text{(G.21)}$$

and $$\left(\frac{H}{B}\right)^2 << 1 \qquad \text{(G.22)}$$

where $\text{Re} = \frac{HU}{\nu}$ is the Reynolds number. For our application, worst case values are chosen for parameters and are the following:

H = on the order of film thickness of top or scraper ring ~ 1 μm

U = " " piston speed at win-6 for the top ring ~ 1 m/s

ν = " " kinematic viscosity ~ 0.01 St (or $1\text{x}10^{-6}$ m^2/s or $0.820\text{x}10^{-3}$ Pa-s for a lubricant density of 820 kg/ m^3)

B = on the order of ring width ~ 1 mm

stroke = on the order of a stroke ~ 0.1 m

Therefore, Re = 1 implying highly-viscous, laminar flow, and ,with H/B = 0.001, the locally fully-developed criteria is easily satisfied even at window 6, near BC .

NEGLIGIBLE ENTRANCE LENGTH

One of the criterion for locally fully-developed flow, $\text{Re}\frac{H}{B} << 1$, also implies that the entrance length, l_E, has negligible length relative to the ring width, B.

$$\frac{l_E}{B} = \text{Re}\frac{H}{B} << 1 \qquad \text{(G.23)}$$

This relationship allows an integral form of mass conservation to be written as in equation G.3.

NEGLIGIBLE SQUEEZING AND ENTRANCE WETTING FOR EQUATION G.3

To see if the terms involving the time derivatives in equation G.3 are significant at midstroke and near BC, same method of scaling needs to be applied.

$$\frac{dx_1}{dt}\left[h(x_1)-h_\infty\right] << Uh_\infty \qquad \text{(G.24)}$$

$$(x-x_1)\frac{dh_o}{dt} << Uh_\infty \qquad \text{(G.25)}$$

and

$$Uh_\infty \sim UH \qquad \text{(G.26)}$$

$$\frac{dx_1}{dt}\left[h(x_1)-h_\infty\right] \sim \frac{B}{\tau}H \qquad \text{(G.27)}$$

$$(x-x_1)\frac{dh_o}{dt} \sim B\frac{H}{\tau} \qquad \text{(G.28)}$$

Therefore, the criterion for negligible inflow due to varying inlet and squeezing under the ring is

$$\frac{B}{\tau U} << 1 \qquad \text{(G.29)}$$

For $\tau U \sim$ stroke, which is typically the case away from the endstrokes, this criterion is satisfied. However, when piston speed gets very slow (U ~ 0.1 m/s), then this criterion becomes violated and squeezing and varying inlet flow at the entrance cannot be ignored.

RELATION OF MOFT AND LINER OFT

From equation G.5, the following criterion must hold for the MOFT to roughly equal twice the liner OFT.

$$\frac{h_o^2}{6\mu U}\left.\frac{\partial p}{\partial x}\right|_o << 1 \qquad \text{(G.30)}$$

Scaling suggests

$$\frac{h_o^2}{6\mu U}\left.\frac{\partial p}{\partial x}\right|_o \sim \frac{H^2 P}{6\mu UB} \tag{G.31}$$

where

P = order of magnitude of ring tension (Pa) ~ 200,000 Pa

Therefore,

$$\frac{H^2 P}{6\mu UB} \sim 0.04 << 1 \tag{G.32}$$

So, roughly, MOFT $\approx$ 2 * OFT(liner). (G.33)

(This page is intentionally left blank.)

APPENDIX H:

OFT-VISCOSITY EFFECT AT WINDOW 4 FOR THE FIRED CASES

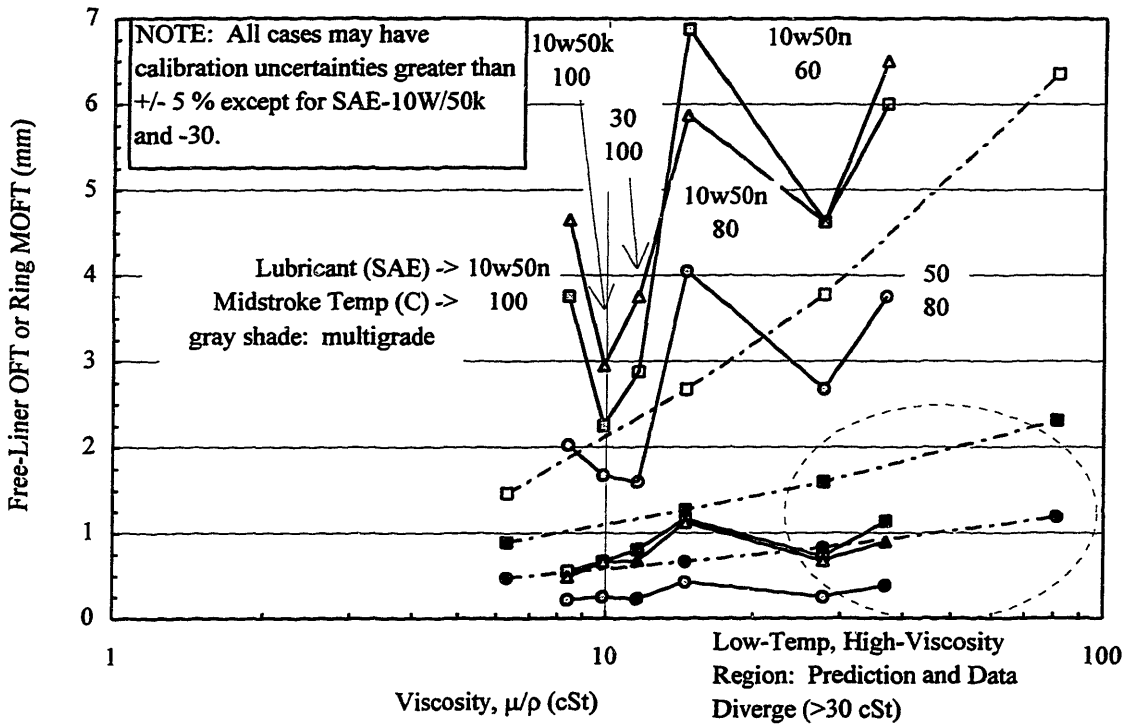

Free-Liner OFT and Ring MOFTs from Window 4 for the Viscosity Effect of SAE-10W, -10W/50n, -30, and -50 for Liner Temperatures of 100, 80, and 60°C (2/3 load at 2500 rpm)

APPENDIX I:

ENGINE SPEED EFFECTS FOR CASES WITH LOW CALIBRATION ACCURACIES AT MIDSTROKE AND NEAR-BC

For the cases at windows 2, 4, and 6 having calibration coefficients with poor accuracy, the calibration coefficient corresponding to the case with greater calibration accuracy was chosen and applied to the second case. If cases have roughly the same calibration accuracy, the case at 2500 rpm was arbitrarily chosen and used in the case for 1800 rpm. The calibration coefficients and their accuracies are presented in Table D.1. Model predictions are not shown because the magnitudes of the measurements are questionable; however, the trends are real. Since relative magnitudes between the cases are compared for trends using equal calibration coefficients, the uncertainty component corresponding to calibration uncertainty was neglected in calculating the uncertainty; therefore, just the standard deviation from the MOFT COV correlation is shown -- roughly 20 percent.

MEASUREMENTS FROM WINDOW 2

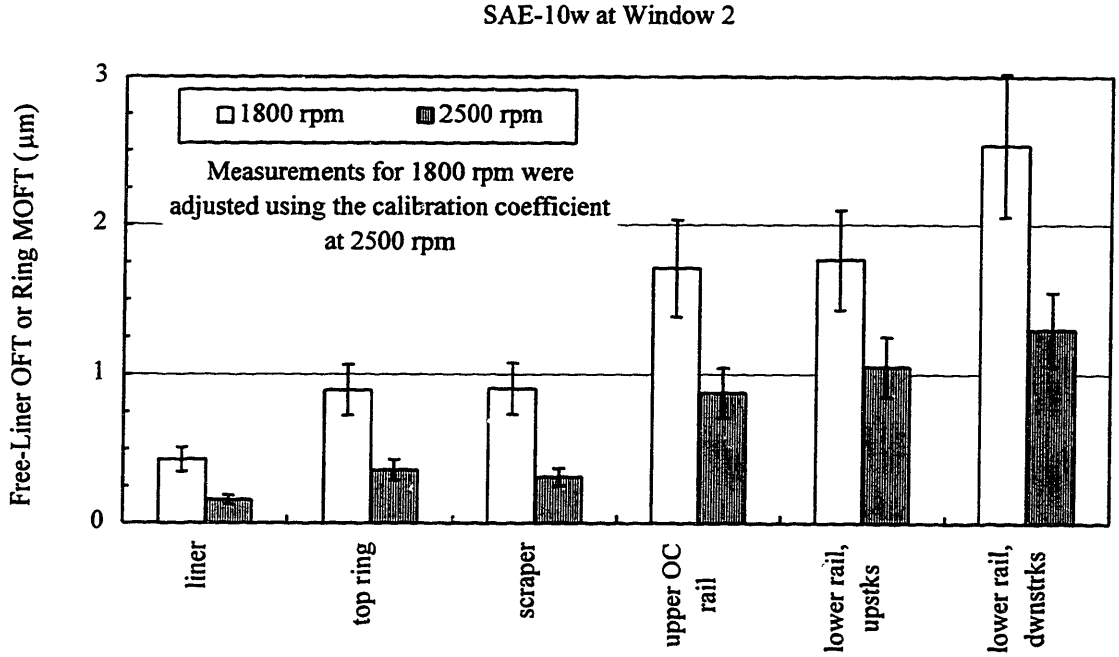

SAE-10w50n at Window 2

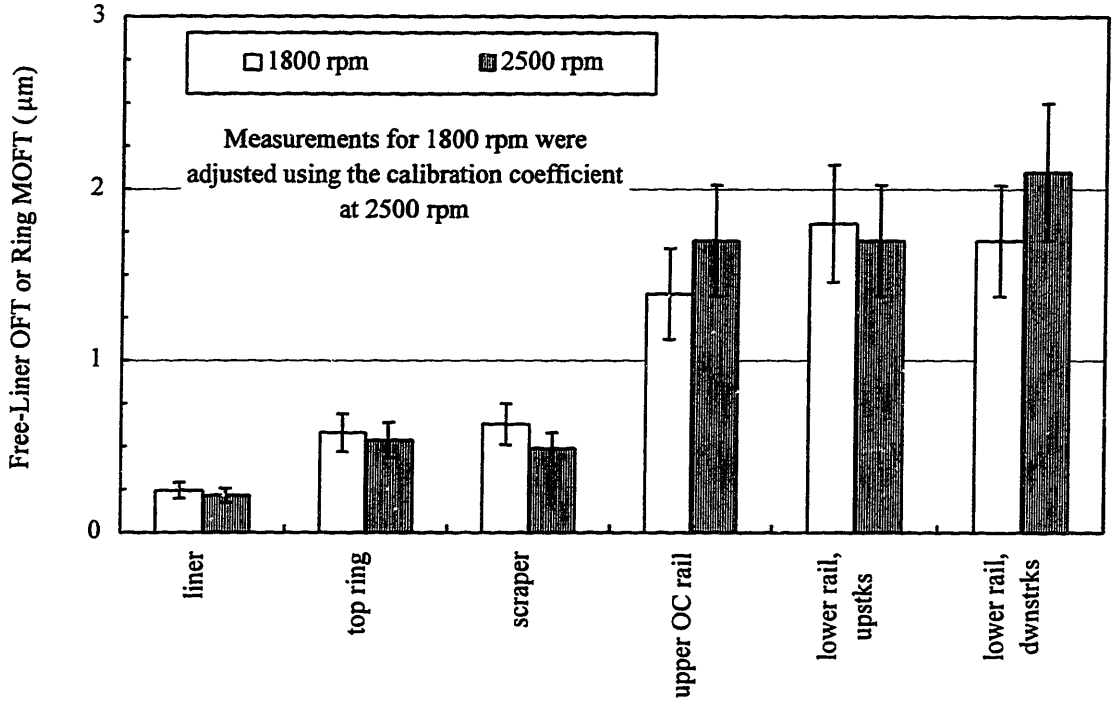

SAE-50 at Window 2

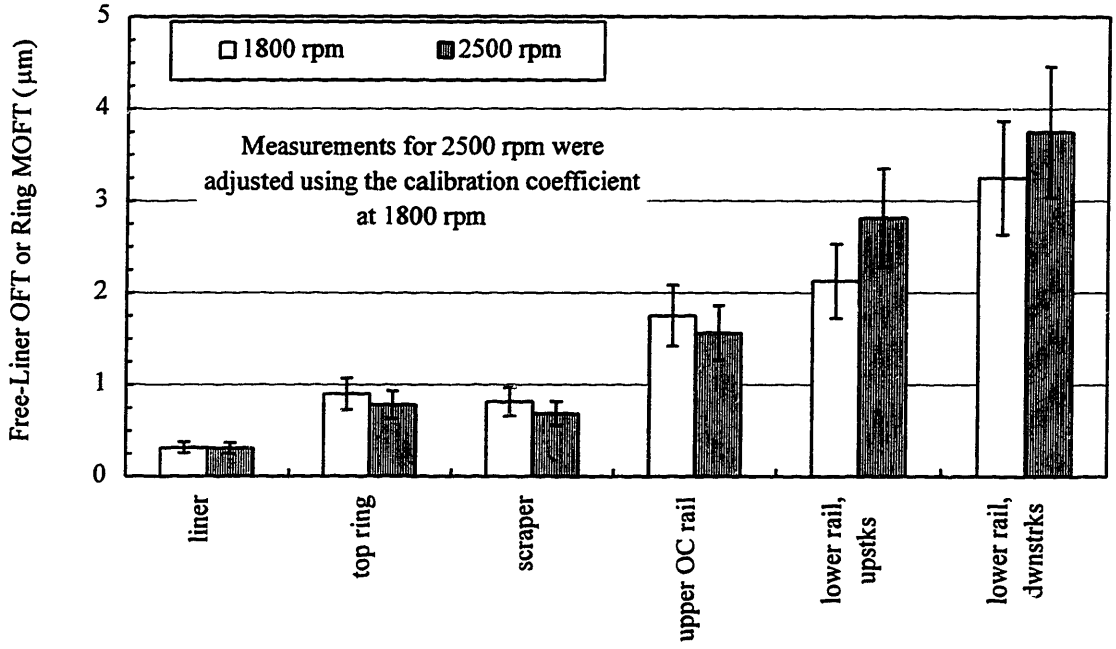

MEASUREMENTS FROM WINDOW 4

SAE-10w at Window 4

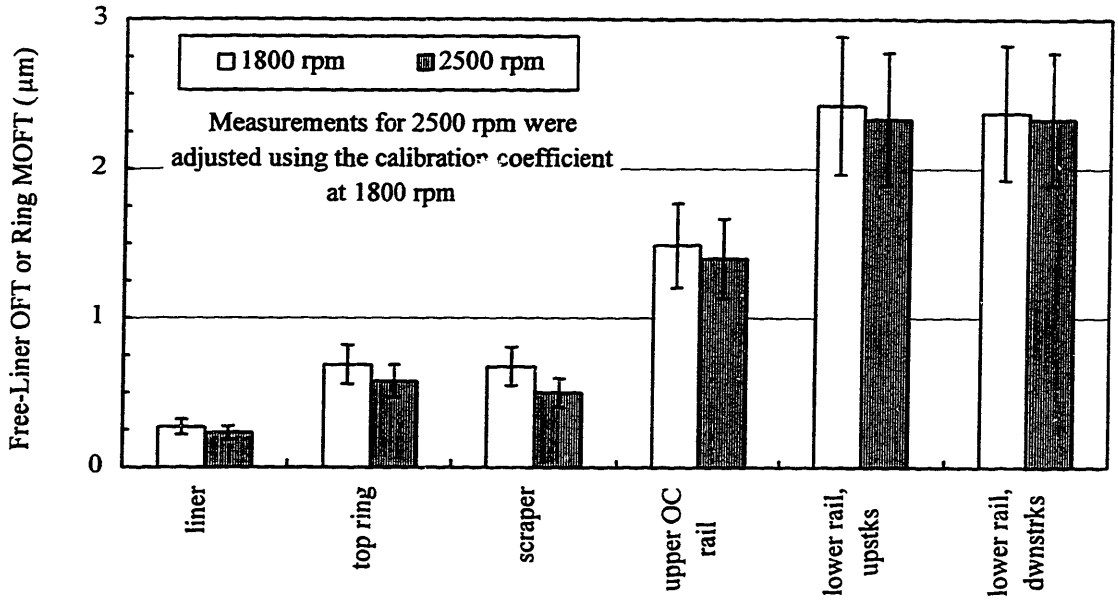

SAE-10w50n at Window 4

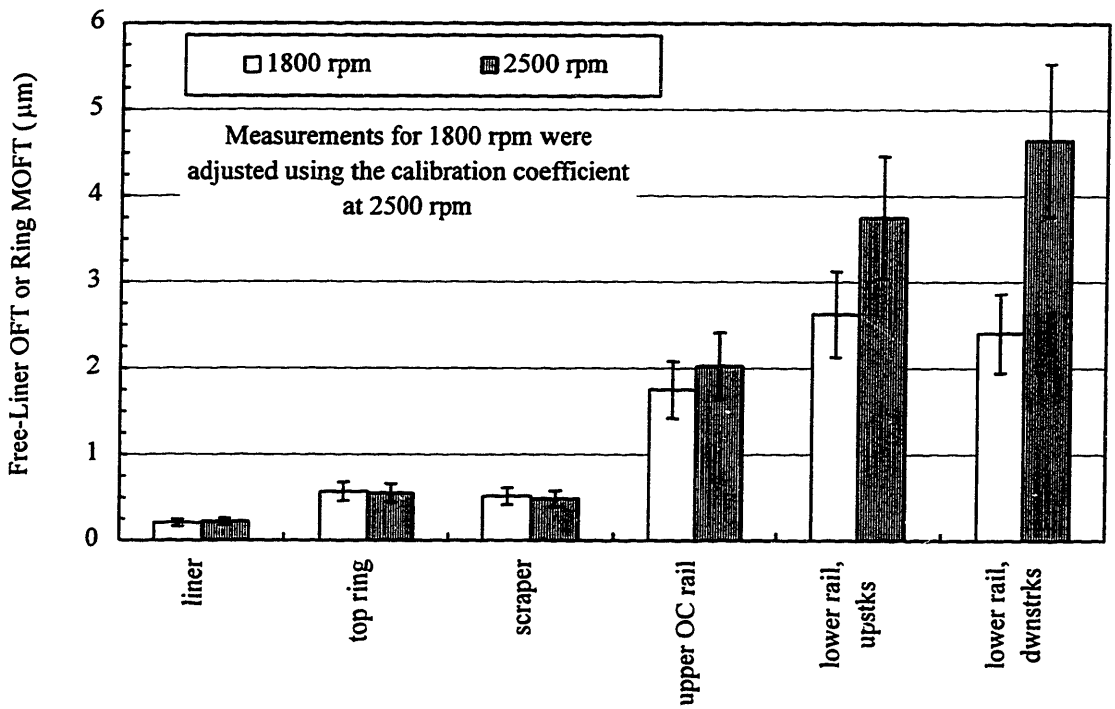

SAE-50 at Window 4

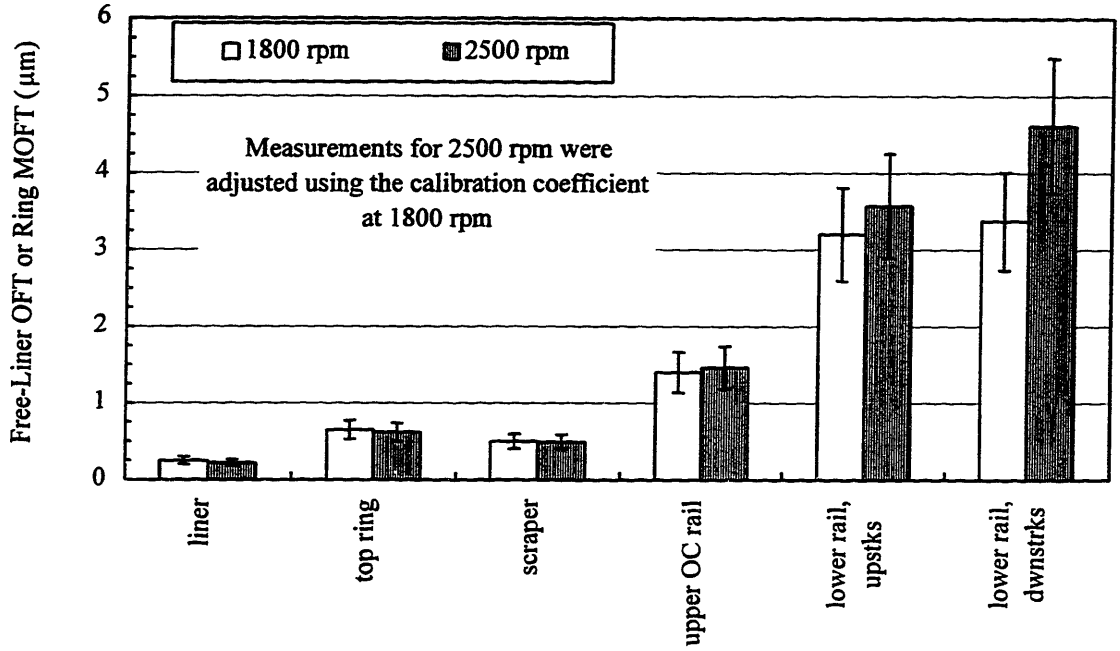

MEASUREMENTS FROM WINDOW 6

SAE-10w at Window 6

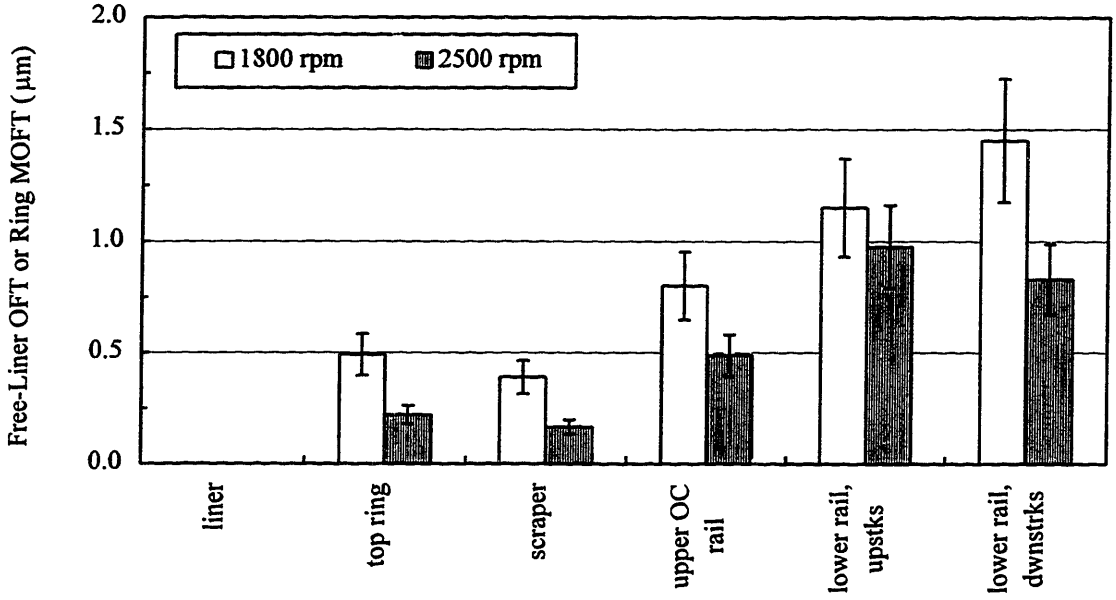

SAE-50 at Window 6

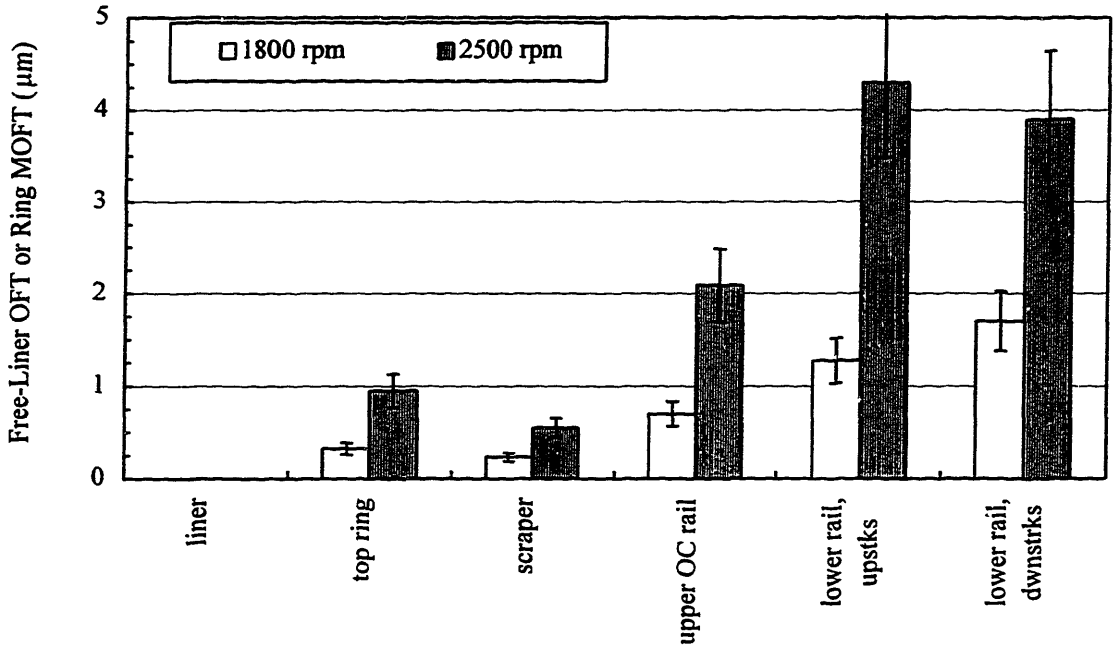

BRIEF SUMMARY

For midstroke window 2, SAE-10W shows a significant MOFT decrease with increased engine speed. However, for all the other cases at midstroke windows 2 and 4, it's hard to say if engine speed has an effect. If at all, there's a slight decreasing MOFT trend with speed; however, standard deviations heavily overlap.

On the major-thrust side at window-6, SAE-10W again experiences a significant MOFT decrease with engine speed. However, for the remaining two lubricants, SAE-10W/50n and -50, MOFT increases with speed especially for SAE-50.

In retrospect, results from calibration correction are inconclusive, and engine speed effects on increasing OFT are, at best, less influential off the major-thrust side at midstroke corresponding to window locations 2 and 4.

APPENDIX J:
REFUTED ARGUMENTS FOR FREE-LINER STROKE-BY-STROKE TRENDS

In addition to scraper ring behavior, other possible reasons for the higher expansion/exhaust OFTs for the free liner than the intake/compression strokes observed in section 4.2.3.3 are related to combustion and varying temperatures throughout the cycle. Three arguments are presented here and refuted. After being refuted, two of the three arguments support the claim that the measured free-liner OFT trends are less pronounced than what's actually occurring.

ARGUMENT #1: During the expansion and exhaust strokes, the free-liner oil temperature is exposed to the hot gases from combustion. Since thermal penetration is extremely fast due to the very thin free-liner OFT, the free-liner oil is probably hotter during the expansion and exhaust strokes. After the piston travels up and then down into the intake stroke, the oil has been given the opportunity to refresh and cool resulting in lower free-liner oil temperatures and additionally exposed to cooler intake and compression gases. The hotter oil probably fluoresces greater than the cooler oil during the intake and compression strokes, resulting in higher measured OFT during expansion/exhaust than intake/compression strokes.

The problem with this argument is the last sentence. The fluorescent efficiency decreases with temperature (see Appendix B) which would result in lower free-liner OFTs during the expansion/exhaust strokes than the intake/compression strokes. Assuming that the temperature increase is enough to affect the oil's fluorescent efficiency, these measured free-liner OFT trends are less pronounced than what is actually occurring.

ARGUMENT #2: OK, if temperature variations of free-liner oil do not contribute to the consistent free-liner trends, failing to calibrate from stroke to stroke could possibly explain the observed trends. Temperatures can affect the calibration as well.

Since the upper piston tool marks were used to calibrate the OFT trace during the compression and/or exhaust strokes (see Appendix D), the temperature of the upper piston tool marks may be different during other strokes and necessitate using stroke calibration coefficients instead of one calibration coefficient for the entire stroke. Although the temperature variations at this piston location are probably low enough not to have an effect on the lubricant's fluorescent intensity, let's assume that it does. Assigning a higher upper piston temperatures during the expansion/exhaust strokes than the intake and compression strokes results in a lower calibration coefficient K (mV/μm). (A greater signal would result in greater voltage from the PMT.) For any LIF voltage signal, it is divided by the calibration coefficient to convert to micrometers. So for a given free-liner LIF signal, it would be higher for the expansion/exhaust strokes compared to the intake/compression stroke. So again, the measured free-liner OFT trends are probably less pronounced than what is actually occurring.

ARGUMENT #3: During expansion and exhaust strokes, hot combustion gases emit radiation which adds an additional component to the regular LIF oil fluorescent signal and, consequently, results in a higher expansion and exhaust measurements. Let alone oil fluorescent effects.

In addition to oil fluorescence, an added component to the LIF signal from the hot combustion gases and flows within the chamber during the expansion and exhaust strokes is highly unlikely. For gasoline engines, significant burning of the air-fuel mixture ends well before the piston completely passes the midstroke windows. For mixtures close to stoichiometric with reasonable burn rates, the mass fraction burned approaches about 95 percent around 35 - 40 $^{\circ}$ ATC [1]. Thus, any visible radiation from combustion is mostly long past by the time the top of the crown land has passed the midstroke windows at 92° ATC (see Appendix D). Of course, infrared radiation is of no concern because it has wavelengths well below that acquired from and filtered by the LIF system.

APPENDIX K:
STROKE-BY-STROKE DIFFERENCES IN OIL DISTRIBUTION BELOW THE OC RING OFF THE MAJOR-THRUST SIDE AT MIDSTROKE (WINDOWS 2 AND 4)

Although the geometric feature of the chamfer is similar between the major-thrust side of the piston and off the major-thrust side, lower regions are not and are assigned differently as shown in Figure 5-2 (b).

For window 2, the groove/chamfer region has, by far, the most oil compared to the other lower regions shown in Figures K-1 (a) and (b). As opposed to the major-thrust side, upstrokes have more oil in this region than the downstrokes. This is probably due to upper skirt scraping at the very beginning of the machining marks during the upstrokes only, and, consequently, oil buildup is observed on the lower portion of the groove/chamfer region during upstrokes as shown in the figures by the dotted lines. The downstrokes show lower OC rail scraping.

Because of the lack of a full skirt to induce good hydrodynamic lubrication and skirt scraping, relatively small oil films exist below the groove/chamfer region. ARTs for these regions are shown in Figures K-2 (a) - (c). Lower ARTs exist in region 6 for the upstrokes shown in Figure K-2 (b) because the partial skirt is contacting the liner and scraping that contributes to the increased scraped oil during upstrokes within the groove/chamfer region in Figure K-2 (a). No scraping occurs from the partial skirt during the downstrokes because the piston is not as close as the upstrokes and, thus, allows oil to pass.

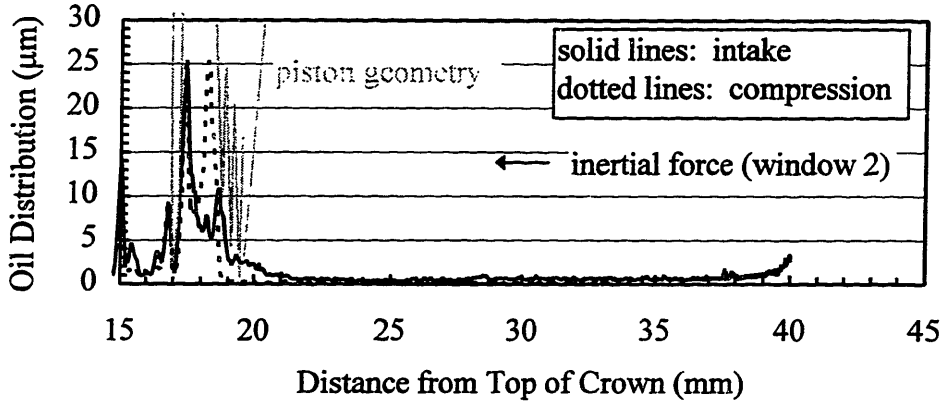

(a) Intake and Compression Strokes

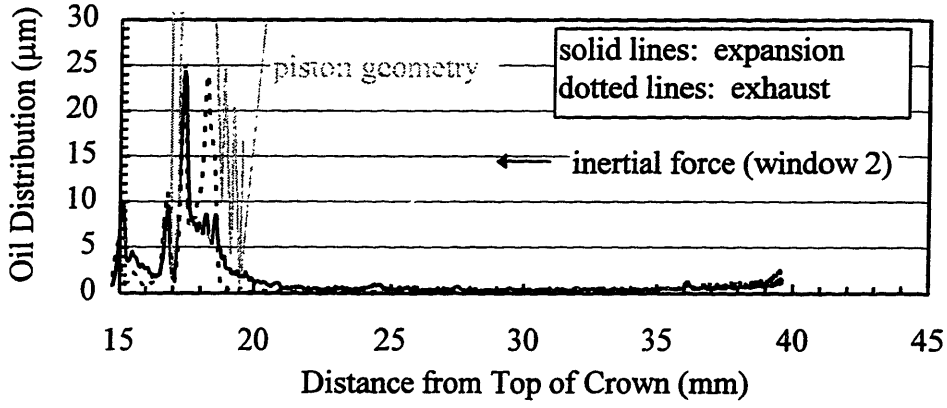

(b) Expansion and Exhaust Strokes

Figure K-1 Oil Distribution below the OC Ring from Window 2 for (a) Intake and Compression and (b) Expansion and Exhaust Strokes.
(SAE-10W, Window 2, 2/3 Load at 2500 rpm, 100°C)

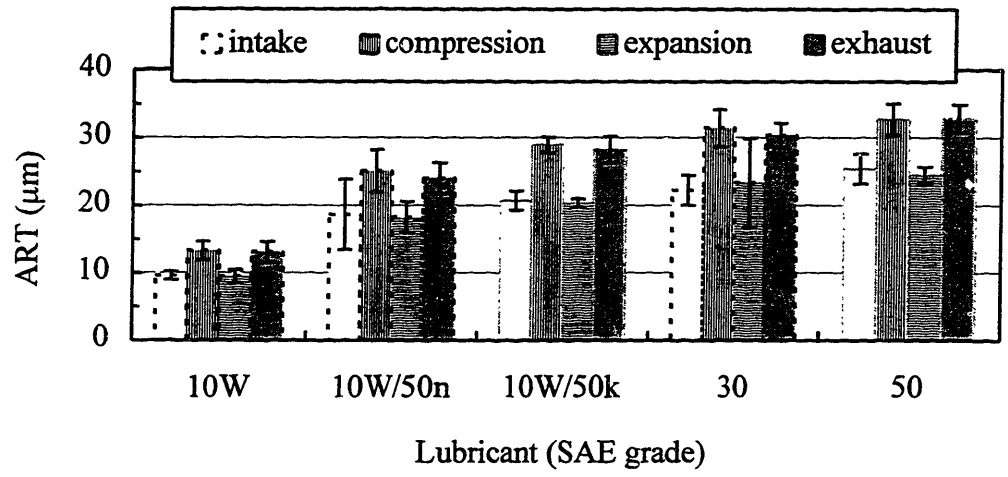

(a) Groove and Chamfer Region -- Region 5

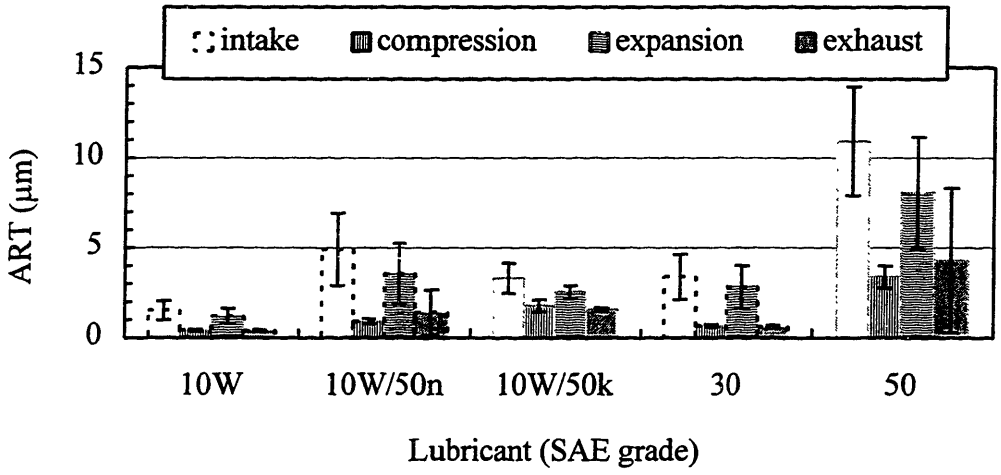

(b) Upper Piston Region -- Region 6

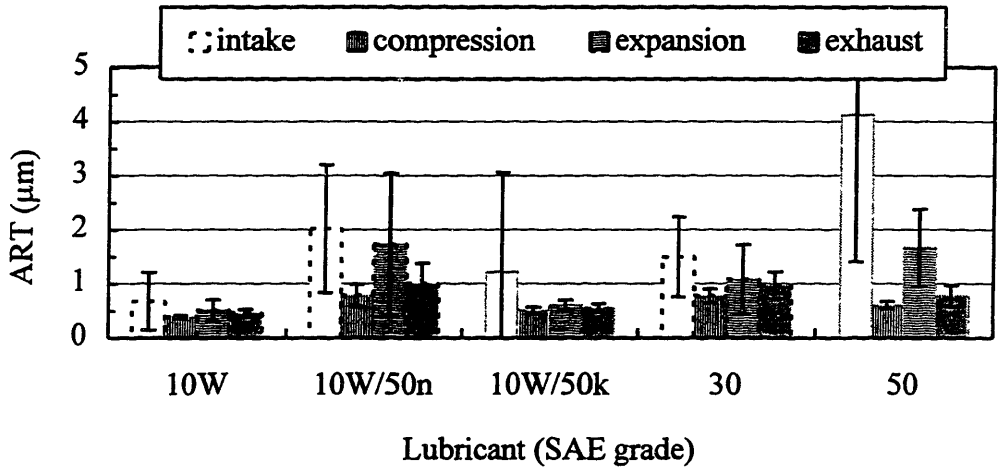

(c) Lower Piston Region -- Region 7

Figure K-2 ARTs for Regions below the OC Ring from Window 2 for (a) Groove and Chamfer Region -- Region 5, (b) Upper Piston Region -- Region 6, and (c) Lower Piston Region -- Region 7
(Window 2, 2/3 Load at 2500 rpm, 100°C)

For window 4 shown in Figures K-3 (a) and (b), no heavy partial skirt scraping occurs which allows comparable ARTs between regions 5 and 6 shown in Figures K-4 (a) and (b), respectively, except that region 5 has higher ARTs because of lower OC rail scraping. However, below the partial skirt region along region 7 is still very small as shown in the figures.

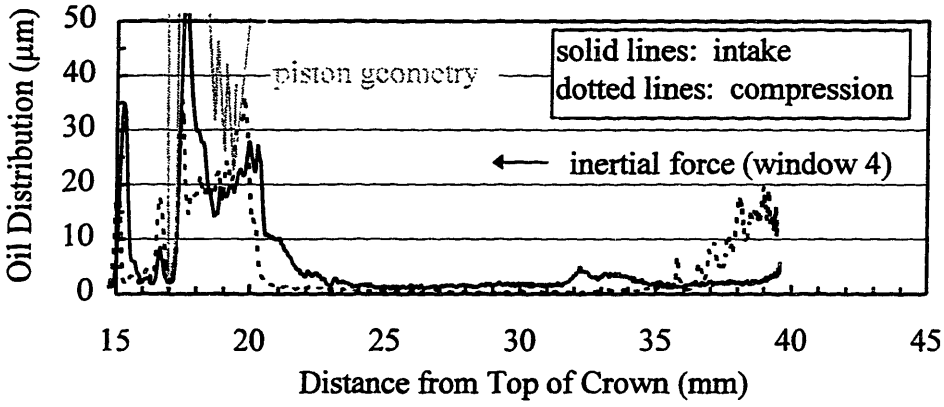

(a) Intake and Compression Strokes

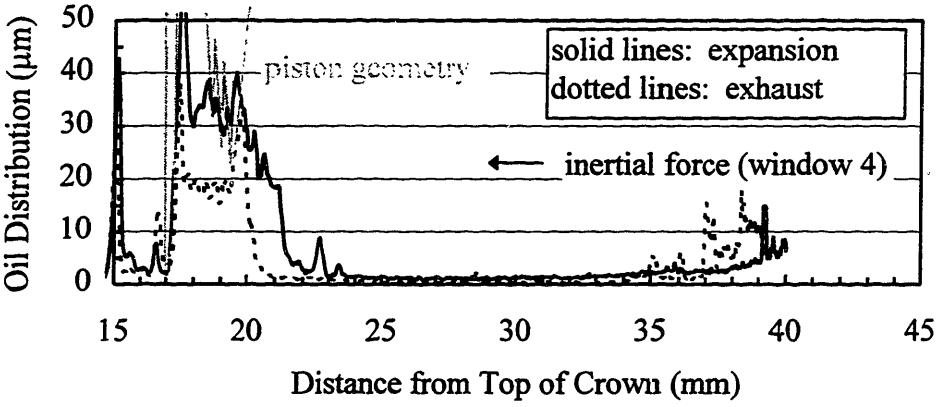

Figure K-3 Oil Distribution below the OC Ring from Window 4 for (a) Intake and Compression and (b) Expansion and Exhaust Strokes.
(SAE-10W, Window 4, 2/3 Load at 2500 rpm, 100°C)

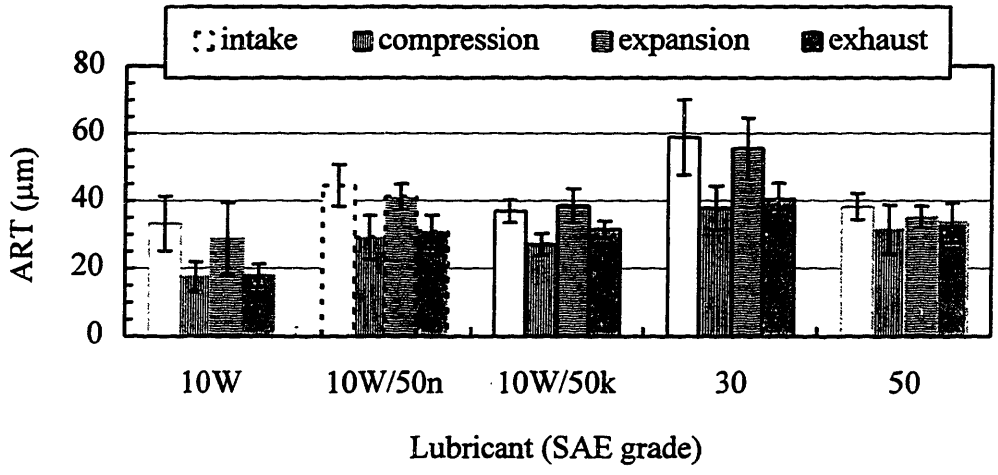

(a) Groove and Chamfer Region -- Region 5

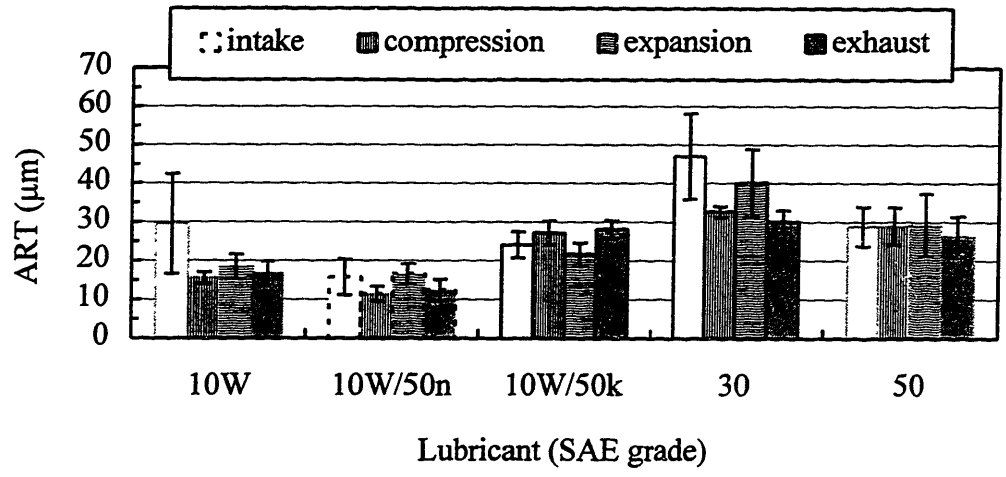

(b) Upper Piston Region -- Region

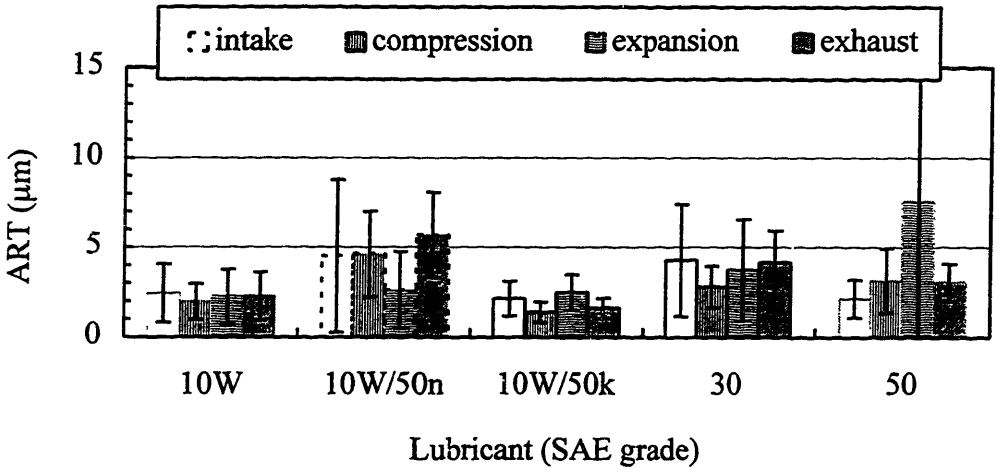

(c) Lower Piston Region -- Region 7

Figure K-4 ARTs for Regions below the OC Ring from Window 4 for (a) Groove and Chamfer Region -- Region 5, (b) Upper Piston Region -- Region 6, and (c) Lower Piston Region -- Region 7.
(Window 4, 2/3 Load at 2500 rpm, 100°C)

THESIS PROCESSING SLIP

FIXED FIELD: ill. _____ name _____

index _____ biblio _____

▶ COPIES: (Archives) Aero Dewey (Eng) Hum

Lindgren Music Rotch Science

TITLE VARIES: ▶☐ _____

NAME VARIES: ▶☑ Michael

IMPRINT: (COPYRIGHT) _____

▶ COLLATION: 356p

▶ ADD. DEGREE: _____ ▶ DEPT.: _____

SUPERVISORS: _____

NOTES:

cat'r: date:

page: F38

▶ DEPT: M.E.

▶ YEAR: 1998 ▶ DEGREE: M.S.

▶ NAME: CASEY, Steven M.